DATE LABEL

30 MAR 1971 11

14 APR 1971

JUN 1971

Call No. 540.03 H3961 Date 31.3.56.

Account N. 14390

J. & K. UNIVERSITY LIBRARY

This book should be returned on or before the last stamped above. An overdue charges of 6 nP. will be levied for each day. The book is kept beyond that day.

THE INTERPRETATION OF X-RAY DIFFRACTION PHOTOGRAPHS

THE INTERPRETATION OF X-RAY DIFFRACTION PHOTOGRAPHS

BY

N. F. M. HENRY, PH.D.
DEPARTMENT OF MINERALOGY AND PETROLOGY, UNIVERSITY OF CAMBRIDGE

H. LIPSON, D.Sc.
COLLEGE OF TECHNOLOGY, UNIVERSITY OF MANCHESTER

AND

W. A. WOOSTER, Sc.D.
DEPARTMENT OF MINERALOGY AND PETROLOGY, UNIVERSITY OF CAMBRIDGE

MACMILLAN AND CO., LIMITED
ST. MARTIN'S STREET, LONDON
1953

This book is copyright in all countries which are signatories to the Berne Convention

First Edition 1951
Reprinted with corrections 1953

548.83
H396I
ST-01
RG1

JAMMU & KASHMIR UNIVERSITY
LIBRARY
No. 14398
Date 31.3.56
SRINAGAR

ALLAMA IQBAL LIBRARY
14398

PRINTED IN GREAT BRITAIN

PREFACE

THE study of crystalline matter by means of X-rays has developed rapidly in the last twenty years and has become of great importance in chemistry, physics, metallurgy and mineralogy. The primary purpose of this book is to help students and research workers to understand the theory and practice of the interpretation of X-ray diffraction photographs. Although ionisation-spectrometer methods are discussed as auxiliary techniques, it is with photographic methods that this book is essentially concerned. Discussion is confined to the study of the crystalline state proper ; the liquid and semi-crystalline states are not touched upon.

The essentials of the theory of crystal symmetry have been included in order to permit the adequate presentation of the various X-ray methods. The theory of space groups has not, however, been included, although examples have been given to show how space groups can be determined from the consideration of systematically-absent reflections. The large subject of crystal-structure determination has not been touched upon, although the experimental basis for it, namely the fundamentals of the measurement and calculation of intensities of X-rays diffracted from crystals, is included.

Much of the material is presented in a geometrical way, as it has been found that this is the most suitable method of teaching crystallography. Analytical methods have been used only where they were considered to be the most convenient for the purpose. In order to make it possible for the photographs and charts to be used by students for practice, these have been reproduced to scale. All the diagrams, with the exception of those acknowledged below, have been specially drawn. A sufficient number of tables has been included to facilitate calculations without the necessity of a reference book.

The authors are indebted to various writers and to several of their colleagues, past and present, for their contributions to the methods of teaching crystallography used in this book. In particular they wish to thank Dr. A. J. Bradley, Dr. F. C. Phillips and Dr. R. C. Evans. Dr. Phillips and Dr. Evans, along with Dr. Nora Wooster and Dr. A. Hargreaves, have given unstinted help with the typescript and with the correction of the proofs. The authors also wish to express their thanks to Mr. A. J. V. Gale for much help and advice, and to Mr. H. C. Waddams of Messrs. Emery Walker, Ltd., who has contributed much to the production of the the drawings in this book.

Thanks are due also to Professor J. D. Bernal for permission to reproduce Figs. 50 and 51 ; to Professor H. W. Fairbairn for permission to reproduce one of his diagrams in modified form for Fig. 23 ; to the author and to Messrs. Longmans Green and Co. Ltd. for the loan of a number of diagrams from " An Introduction to Crystallography " by F. C. Phillips which have been used for Figs. 2, 5, 7, 8, 17, 18.1, 19.1, 20.1 ; and to the author and the Oxford University Press for the loan of a diagram from " Chemical Crystallography " by C. W. Bunn, which has been used for Fig. 188.

N. F. M. HENRY
H. LIPSON
W. A. WOOSTER

CONTENTS

CHAP. PAGE

1. INTRODUCTION TO THE GEOMETRY AND SYMMETRY OF CRYSTALS
   1. The Study of Crystal Faces 3
   2. The Classification of Crystals 7
   3. Crystal Lattices 9
   4. Twin Crystals 16
   5. Crystallographic Projections 17

2. X-RAYS
   1. Nature of X-rays 25
   2. Production of X-rays 27
   3. X-ray Wave-lengths 28
   4. Refraction of X-rays 29
   5. Absorption of X-rays 29
   6. Crystal-reflected Radiation 32
   7. Precautions against Harmful Effects of X-rays 33

3. GEOMETRY OF X-RAY REFLECTIONS
   1. Diffraction of X-rays by Crystalline Matter 34
   2. The Reciprocal Lattice 37
   3. Interpretation of Bragg's Law in terms of the Reciprocal Lattice . . 40

4. SINGLE-CRYSTAL AND FIBRE PHOTOGRAPHS
   1. Introduction 41
   2. Types of Photograph 41
   3. Some Practical Details 45

5. INTERPRETATION OF OSCILLATION PHOTOGRAPHS
   1. Geometry of X-ray Reflection 48
   2. Indexing the Reflections 58

6. INTERPRETATION OF LAUE PHOTOGRAPHS
   1. Geometry of X-ray Reflection 71
   2. Symmetrical Laue Photographs 75
   3. Non-symmetrical Laue Photographs 84

7. INTERPRETATION OF WEISSENBERG PHOTOGRAPHS
   1. Introduction 87
   2. Geometry of X-ray Reflection 87

CHAP. PAGE

3. Indexing of Equatorial Photographs 92
4. Other Types of Weissenberg Photograph 94
5. Principal Uses of Weissenberg Photographs 100

8. STUDY OF ORIENTATION IN SINGLE CRYSTALS AND TWINS

1. Introduction 101
2. Geometry of X-ray Reflection for Various Orientations . . . 102
3. Determination of Orientation from X-ray Photographs . . . 107
4. Determination of Orientation by the Ionisation Spectrometer . . 115
5. Orientation in Twin Crystals 116

9. STUDY OF PREFERRED ORIENTATION IN POLYCRYSTALLINE AGGREGATES

1. Introduction 122
2. Fibre Texture in Wires 122
3. Preferred Orientation in Metal Sheets 125
4. Study of Fibre Photographs of Organic Materials 130

10. FURTHER STUDY OF THE GEOMETRY AND SYMMETRY OF CRYSTALS

1. Further Study of Crystal Lattices 132
2. Symmetry of Crystal Classes 146
3. Examples of the Study of Trigonal Crystals 161

11. METHODS OF TAKING POWDER PHOTOGRAPHS

1. Introduction 168
2. Preparation of Powder Specimens 170
3. Measurement of Bragg Angles 170
4. Powder Cameras 173

12. INTERPRETATION OF POWDER PHOTOGRAPHS

1. Introduction 177
2. Interpretation when the Unit Cell is known 177
3. Interpretation when the Unit Cell is unknown . . . 178
4. Interpretation by Graphical Methods 184
5. Comparison of Analytical and Graphical Methods 187

13. ACCURATE DETERMINATION OF CELL DIMENSIONS

1. Introduction 189
2. Elimination of Systematic Errors in Powder Photographs . . . 189
3. Procedure for Powder Photographs of Cubic and of Uniaxial Specimens . 191
4. Procedure for Single-crystal Photographs 193
5. Applications 196

CONTENTS

CHAP.		PAGE
14.	MEASUREMENT OF THE INTENSITIES OF X-RAY REFLECTIONS	198
	1. Photographic Methods	201
	2. Ionisation Method	
15.	CALCULATION OF THE INTENSITIES OF X-RAY REFLECTIONS	204
	1. Introduction	204
	2. Intensity Formulae	207
	3. The Structure Factor	210
	4. Applications	
16.	MEASUREMENT OF CRYSTAL GRAIN SIZE IN POLYCRYSTALLINE AGGREGATES	212
	1. Introduction	212
	2. The ' Spottiness ' of Powder Photographs	213
	3. The Broadening of Powder Lines	217
	4. Applications	
17.	IDENTIFICATION OF CRYSTALLINE MATERIALS BY MEANS OF POWDER PHOTOGRAPHS	219
	1. Introduction	220
	2. General Methods of Identification	222
	3. Identification within a Limited Range of Possibilities	
	APPENDIXES	
	1. Calculations for Calcite	227
	2. Some Equations for the Various Lattices	228
	3. Instructions for Electro-plating Targets	229
	4. Solutions to Problems	230
	TABLES	
	1. Data for X-ray Targets and Filters	233
	2. Some Data for the Elements	234
	3. Mass Absorption Coefficients, μ_m, for $K\alpha$-Radiations	236
	4. Gram-atomic Absorption Coefficients	238
	5. Values of $(h^2+k^2+l^2)$, (h^2+k^2) and (h^2+hk+k^2) up to 100	240
	6. Values of $\sin^2\theta$	242
	7. Values of $\cos 2\pi x$ and $\sin 2\pi x$	244
	8. Values of $(1+\cos^2 2\theta)/\sin 2\theta$	245
	9. Values of $(1+\cos^2 2\theta)/\sin^2\theta\cos\theta$	246
	10. Values of $\frac{1}{2}\left(\frac{\cos^2\theta}{\sin\theta}+\frac{\cos^2\theta}{\theta}\right)$	248
	SUBJECT INDEX	251
	REFERENCES AND NAME INDEX	255

NOTE

EACH chapter is divided into sections and sub-sections. The number and title of the chapter are given at the head of each left-hand page, while the number and title of the section are given at the head of each right-hand page. In the text a reference to a particular topic in the book is given by means of the chapter number in bold type, followed by the number of the section or sub-section ; for example, **1**, 4.2.

The Figures are not numbered consecutively ; each Figure carries the number of the page on which it occurs. When two or more Figures occur on the same page, they are distinguished by a second number placed after a full point ; for example, 17.2. When there is more than one part in a particular Figure, the letters (*a*), (*b*), etc., are used to identify the different parts ; for example, 17.2 (*b*).

The Appendixes contain some information of general importance, along with the working-out of some calculations and the solutions to certain problems given in the text. They are numbered separately from 1 to 4. Following these come the Tables, which contain numerical data found to be of particular usefulness. These also are numbered separately, from 1 to 10. The tables which appear in the text are not given a number.

All works referred to in the text are given under the name of the first author in the References and Name Index, along with all additional proper names mentioned. In the Subject Index, wherever there is a main reference, this is printed in bold type.

During the preparation of this book, the change from kilo-X units (kX.) to Angström units proper (A.) has been officially made by international agreement (**2**, 3.2). In chapters 1 to 10, inclusive, the old values of spacings and wave-lengths have been retained ; but they have been called Angström units, except where the number of figures given requires that the name kilo-X units should be used. In chapters 11 to 17, however, in which the question of accuracy is very important, all values have been recalculated into Angström units proper.

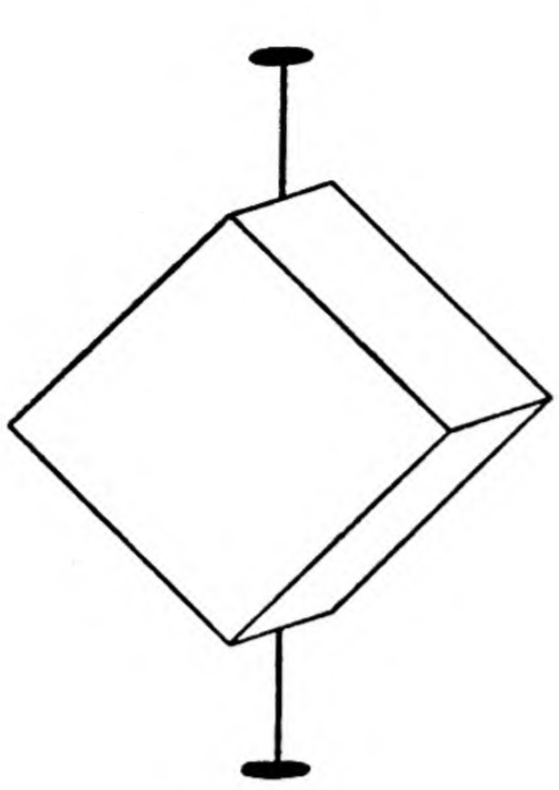

(a)

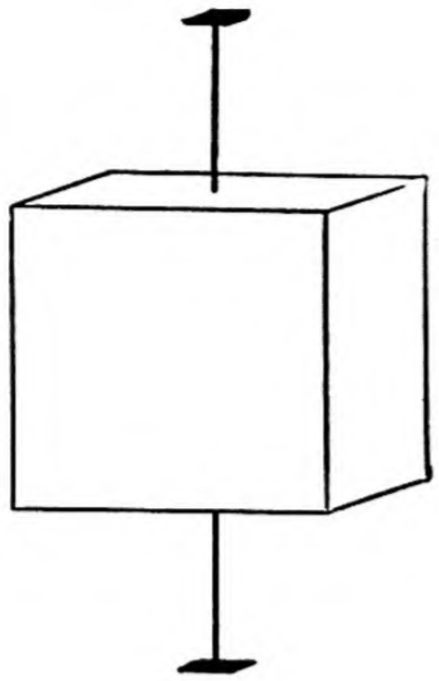

(b)

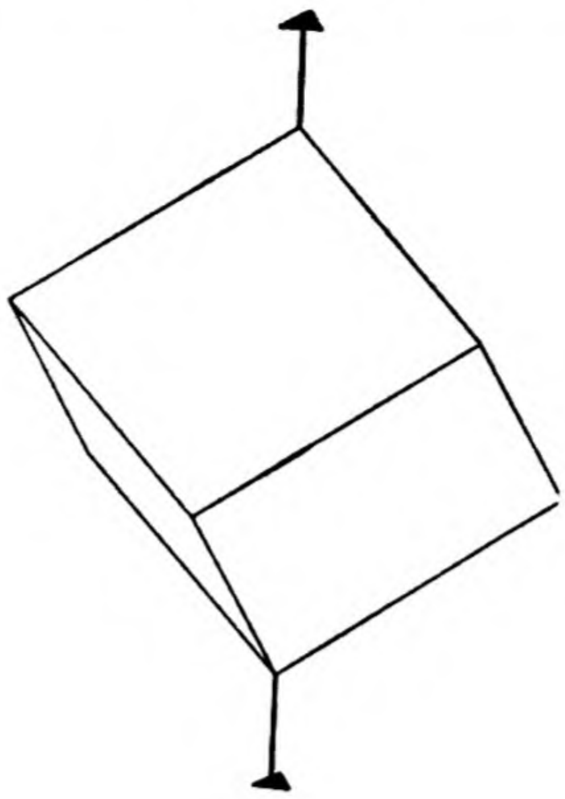

(c)

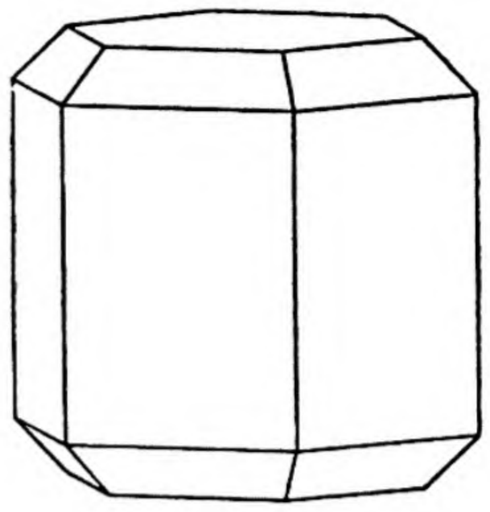

(d)

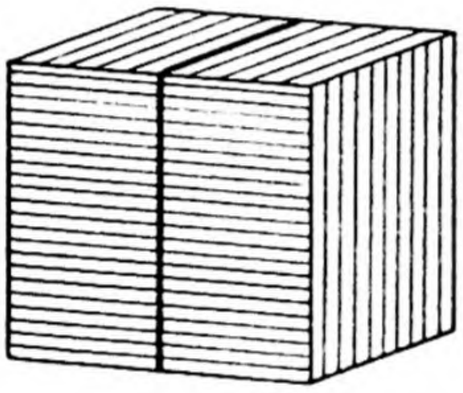

(e)

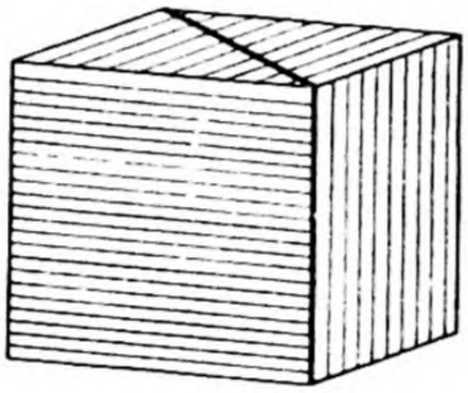

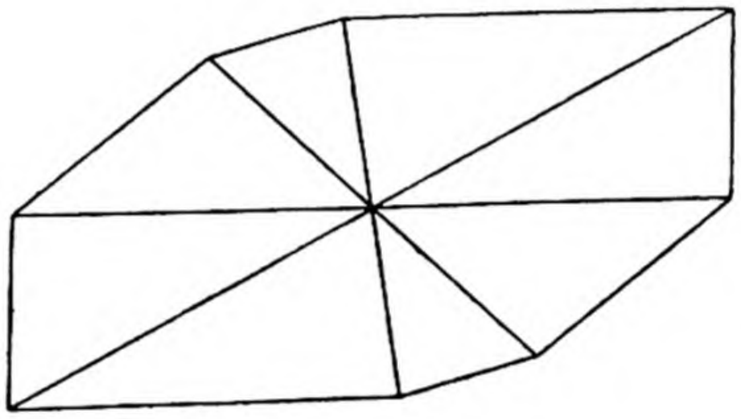

(f)

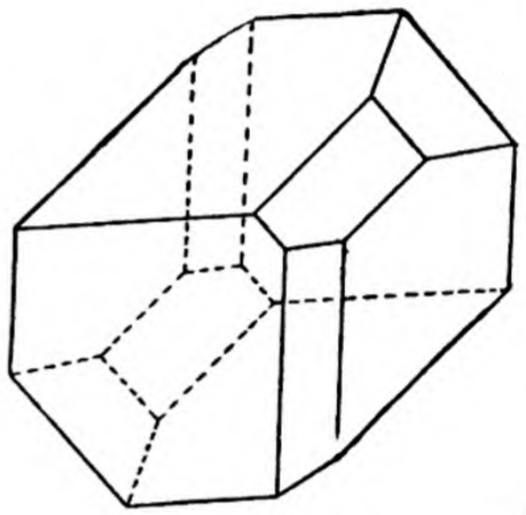

(g)

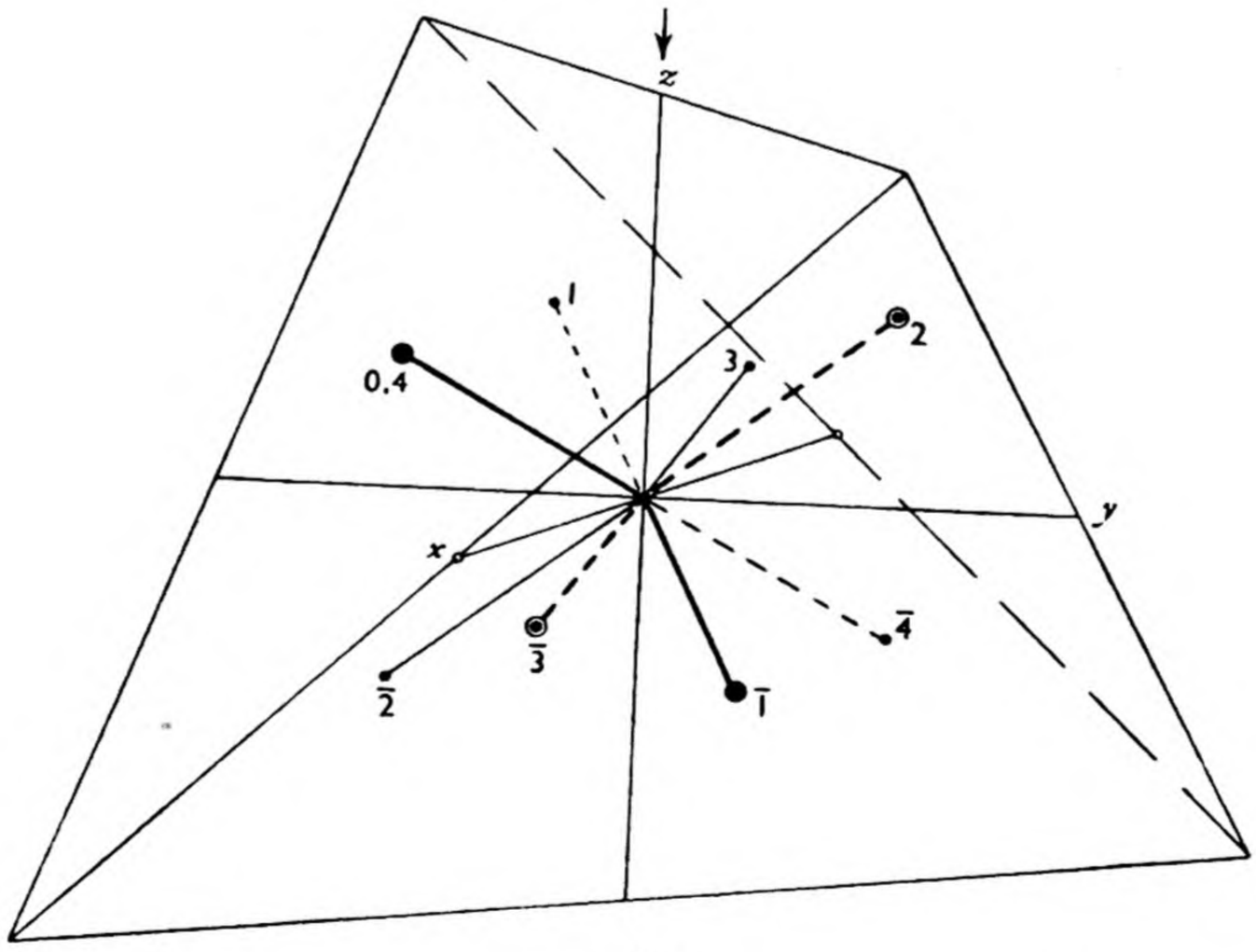

(h)

FIG. 2. Diagrams illustrating symmetry elements of crystals

CHAPTER 1

INTRODUCTION TO THE GEOMETRY AND SYMMETRY OF CRYSTALS

1. The Study of Crystal Faces

1.1 Faces of crystals. When a single crystal grows under favourable conditions, it is generally bounded by plane faces. As these faces are the external manifestation of the internal regularity of atomic arrangement, they bear a definite geometrical relationship to each other. Although there are numerous crystalline substances which never develop visible faces, faces are, nevertheless, the most obvious characteristic of a great many crystals. It is therefore natural to begin the study of crystalline matter by examining the arrangement of the faces on well-developed crystals. This study of the external shape and symmetry of crystals is called Crystal Morphology.

1.2 External symmetry elements of crystals. We shall study first the axes of symmetry of a crystal. If we rotate an unsymmetrical body about any line through it, the body does not pass through any position congruent with its initial position until this is reached again after a rotation of 360°. But if we rotate a cube about a line joining the centres of a pair of opposite edges, the cube reaches a position congruent with its initial position after rotation through an angle of 180° (Fig. 2 *a*). Such an axis is called an *axis of two-fold*, or *diad*, *symmetry*, and the body is said to possess a two-fold axis of symmetry in the direction specified. If we rotate the cube about an axis through the centre and perpendicular to a pair of faces, it comes to a congruent position after a rotation of 90° (Fig. 2 *b*). Such an axis is called an *axis of four-fold*, or *tetrad*, *symmetry*. If we rotate the cube about an axis joining a pair of opposite corners, it comes to a congruent position after a rotation of 120° (Fig. 2 *c*). Such an axis is called an *axis of three-fold*, or *triad*, *symmetry*. If we select a right prism with a regular hexagon as its base and rotate it about an axis normal to the base and passing through the centre, the prism comes to a congruent position after a rotation of 60° (Fig. 2 *d*). Such an axis is called an *axis of six-fold*, or *hexad*, *symmetry*.

In Fig. 2 (*e*) a cube is shown with markings on the faces. A plane through the centre parallel to one pair of faces divides the crystal into two parts, each of which is the mirror image of the other. Such a plane is called a *symmetry plane* (*reflection plane*, or *mirror plane* of symmetry), and the body is said to possess a symmetry plane in the direction shown ; on the other hand, it possesses no symmetry plane in the diagonal position (perpendicular to one pair of faces only).

The next type of symmetry is most easily demonstrated first in a two-dimensional figure. If inside the figure there is a point such that for any line drawn through the point the intersections with the periphery are at equal distances on opposite sides of the point, the figure is said to possess a *centre of symmetry*. In Fig. 2 (*f*) is shown a centro-symmetrical figure in which each edge has an exactly similar edge parallel to it on the other side of the figure. When this condition holds for a solid body, the body is said to possess a centre of symmetry, or to be *centro-symmetrical*. The symmetry operation is called *inversion*. The cube and the hexagonal prism are centro-symmetrical bodies, as is the crystal in Fig. 2 (*g*). It should be noted that in two dimensions a centre is the same as a diad axis normal to the plane of the figure.

One more kind of symmetry operation must be considered at this point. In Fig. 2 (*h*) the axis indicated on the tetrahedron is something more than a two-fold rotation axis ; it is an *inverse tetrad axis*. In the figures this axis is vertical, and we shall consider its operation on the face-normal marked 0 or 4. The normal is rotated through 90° to position 1 ; but, instead of being left there, it is inverted through the origin to position $\bar{1}$ as if a centre of symmetry were acting on it ; the normal in position $\bar{1}$ is then rotated through 90° in the same direction to position $\bar{2}$; and again, instead of being left there, it is inverted through the origin to position 2 : finally, the normal in position 2 is rotated through 90° to position 3 and inverted through the origin to position $\bar{3}$. Thus by the operation of an inverse tetrad axis on a face, we derive the tetrahedron with four faces ; whereas by the operation of a diad we would obtain only two faces. It should be noted that, although inversion through the origin is part of the complex symmetry operation, the resultant form does not necessarily possess a centre of symmetry, as is obvious in the case of the tetrahedron. It follows that the operation of an inverse tetrad is not equal to the combination of a tetrad axis plus a centre, because from the latter operations only centro-symmetrical forms would result.

The symmetry elements which we have discussed above are given in the table on p. 4. With combinations of these it is possible to produce all the groups of elements of external symmetry which occur

in crystals. In the systematic classification of crystals, however, use is made of inversion axes of two-, three-, and six-fold symmetry as well as of the inverse four-fold axis. A complete table of elements of external symmetry, with conventional symbols, is given in **10**, 2.1. In this table it can be seen that there is no symmetry axis of five-fold or of more than six-fold symmetry in crystals, and a note on this is given in **1**, 3.3.

Symmetry Element	Operation
	Rotation about the axis through an angle of :
Two-fold (diad) axis	$2\pi/2$
Three-fold (triad) axis	$2\pi/3$
Four-fold (tetrad) axis	$2\pi/4$
Six-fold (hexad) axis	$2\pi/6$
Symmetry (mirror or reflection) plane	Reflection across the plane.
Centre	Inversion through the centre.
Inverse four-fold (tetrad) axis	Rotation about the axis through an angle of $2\pi/4$ followed by inversion through a point on the axis

1.3 Miller symbols or indices of faces. In order to define the relative orientation of the various faces on a crystal, we select a set of co-ordinate axes of reference which are called *crystallographic axes*. In general, these axes may be selected in several ways, but it is necessary that they should be chosen parallel to important directions in the crystal in order to exhibit the simple relations which exist between different faces. When the crystal shows good faces, the edges between them define some of the important directions in the crystal. Three non co-planar edges between prominent faces may be chosen as the crystallographic axes. The next step is to define the relative lengths of the unit intercepts, a, b and c, on the three axes, and this is done by selecting as the parametral plane a prominent face which cuts all the axes (*ABC* in Fig. 4). It should be pointed out that the magnitude of the actual intercepts is unimportant, and the plane can always be moved along its normal because we are concerned only with the ratios of the intercepts of planes to the corresponding intercepts of the parametral plane. The three intercepts of the plane *ABC* are,

$$a/1 : b/1 : c/1.$$

We now take a second plane such as *AB'C'* with intercepts $a/1$, $b/2$ and $c/3$. The *Miller symbols*, or *Miller indices*, or more usually the *indices*, of the face *AB'C'* are the integers (123). It should be specially noted that the indices are proportional to the reciprocals of the intercepts and are not proportional to the intercepts themselves. In general, if a/h, b/k, c/l are the intercepts cut off by a face on the selected set of crystallographic axes of reference, then the indices of the face are (hkl). The indices (hkl) can always be expressed as integers, commonly small integers, for the reason given in **1**, 3.6 ; they are properly enclosed in round brackets, as shown, when they denote a particular face. In the diagrams the brackets are omitted, but they should always be used if there is risk of confusion with any other symbol (**1**, 1.5 and **1**, 1.7). The indices of the parametral plane, such as

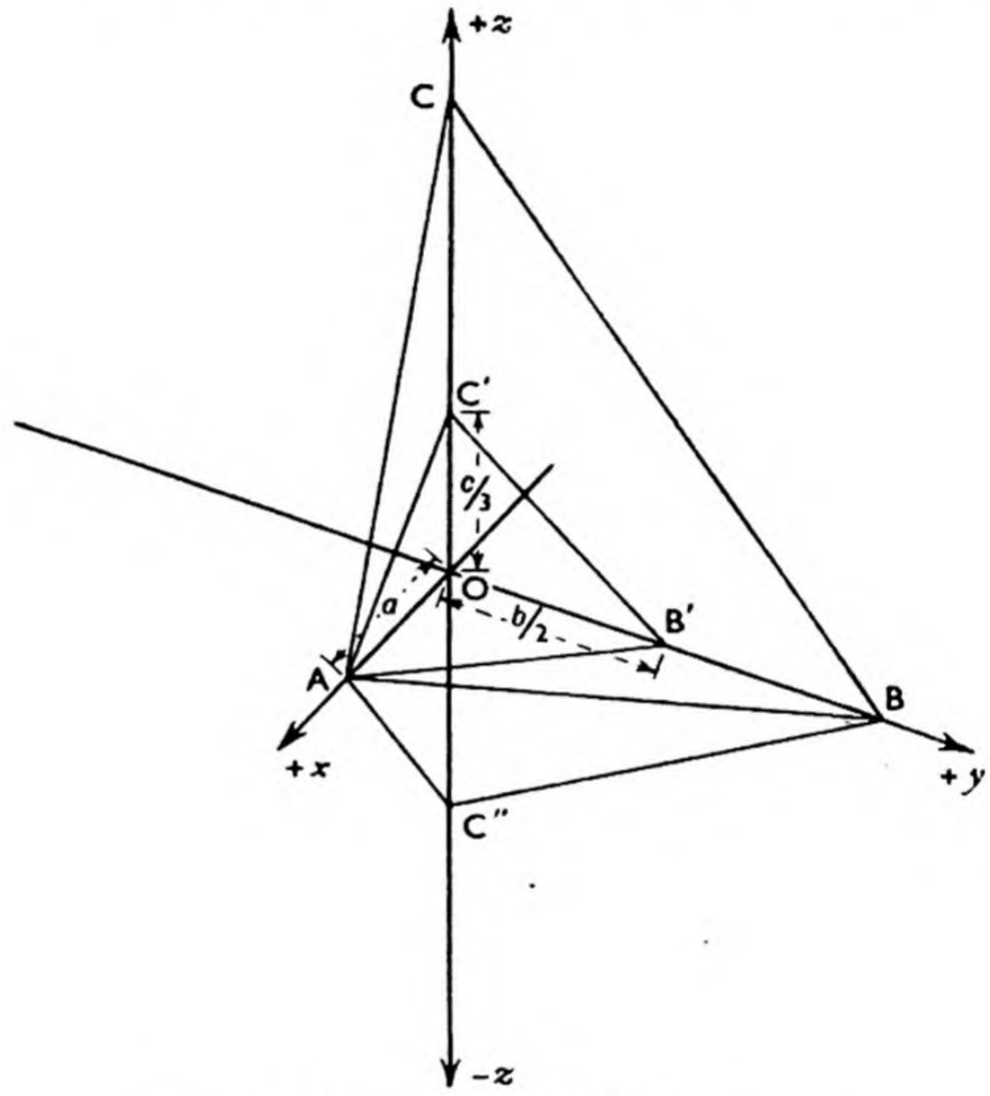

Fig. 4. Intercepts of planes on axes

ABC in Fig. 4, are always (111), since this is the plane selected to define the unit lengths along the respective axes. Indices corresponding to intercepts on the negative side of the origin of the axes have a minus sign placed above the symbol in question; for example the particular indices of the face *ABC''* are $(11\bar{2})$. When a face is parallel to a crystallographic axis, its intercept on that axis is infinity, and the corresponding index is zero. For example, if a face cuts off one unit of the x-axis, half a unit of the y-axis and is parallel to the z-axis, its intercepts are $a/1$, $b/2$, c/∞ and its indices are (120). When a double-figure appears in the indices, two commas are inserted as in (11,1,5).

1.4 Crystallographic axes. When the crystal possesses axes or planes of symmetry, the symmetry must be taken into account in the selection of the particular edges to be used as crystallographic axes of reference. If this is not done, two faces which are related by symmetry elements may have quite different

integers in their Miller symbols, and hence their relation may be obscured. Thus it is desirable to have certain conventions about the selection of crystallographic axes so that the symmetry of the crystal may be exhibited. It is found that every crystal possesses one of seven main types of symmetry, on the basis of which all crystals are allocated to one or other of the seven symmetry systems. For each of these symmetry systems there is one set of crystallographic axes which best exhibits the symmetry of the particular type. Each set is distinguished by the characteristic angular and linear relations which exist between the axes of the set. These relations and the connection between them and the corresponding symmetry type are discussed later for all seven sets (**1**, 2.2 and **1**, 2.3).

In crystallography use is also made of other kinds of axes: ellipsoid axes (**1**, 2.4), symmetry axes, and zone axes. It is therefore unfortunate that the term 'crystallographic axes' has come to be applied in particular to the kind of axes described in the above section, but this usage is of long standing.

1.5 Crystal forms, special and general. It has been seen (**1**, 1.2) that, depending on the symmetry possessed by the crystal, a face may be repeated on the same crystal. We can imagine the operation of the symmetry elements being performed on an initial face to produce a number of similar faces, as in Fig. 2 (*h*). The number of times a face is repeated and the relationship of all the similar faces depend both on the symmetry possessed by the crystal and on the relation of the faces to the symmetry elements.

Now consider the group of symmetry elements which has one axis of four-fold symmetry perpendicular to a plane of symmetry. If we begin with a face which is inclined to both the axis and the plane, the operation of these two symmetry elements produces the eight-faced shape shown below. When

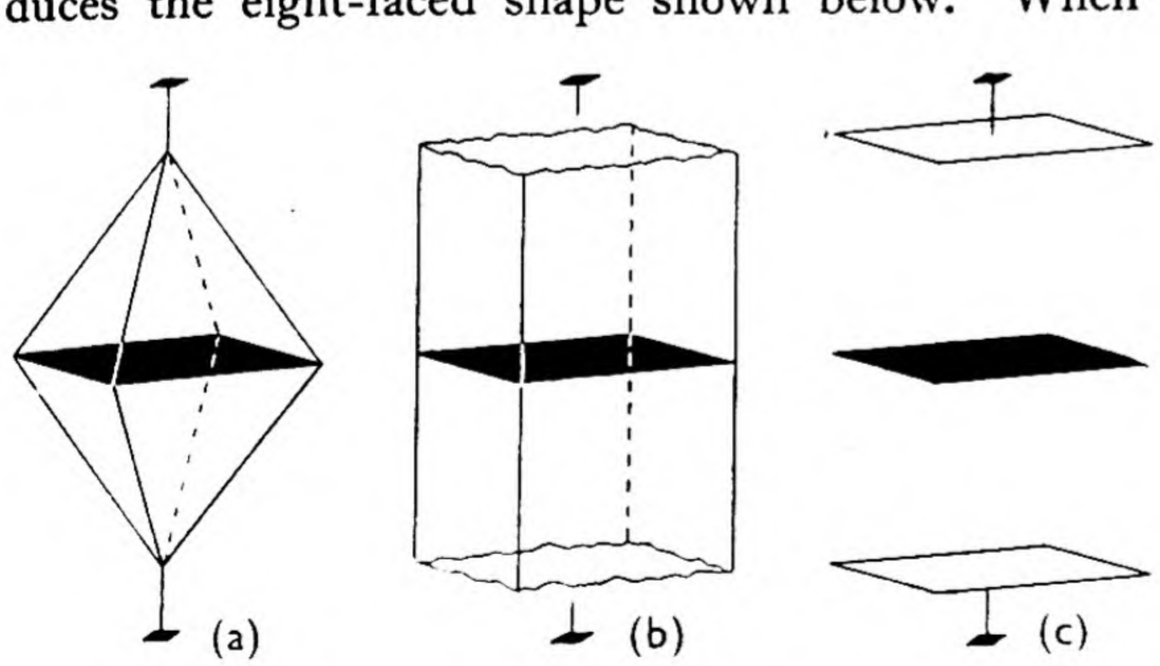

FIG. 5.1. Three types of crystal form

the initial face is perpendicular to the symmetry plane, the result is a four-sided figure of square cross-section (*b*) which extends parallel to the single four-fold axis, because the symmetry plane cannot give rise to any new faces in this case. When the initial face is perpendicular to the four-fold axis, this axis cannot give rise to any new faces and the result consists only of the two parallel faces shown in (*c*). Each such group of exactly similar faces resulting from the operation of a given group of symmetry elements on an initial face is called a *form*. A form which encloses space and hence can exist by itself is called a *closed form* (for example, Fig. 5.1, *a*). A form which does not enclose space and hence cannot exist by itself is called an *open form* (for example, Fig. 5.1, *b*). When the faces of a form bear a special relationship to the symmetry elements, the form is called a *special form*. All the faces of Fig. 5.1 (*b*) are parallel to the four-fold axis and perpendicular to the symmetry plane: both the faces of Fig. 5.1 (*c*) are perpendicular to the four-fold axis and parallel to the symmetry plane; both these forms are special forms. When the faces of a form bear a quite general relation to the symmetry elements, the form is called a *general form* (for example, Fig. 5.1, *a*). A form is indicated by placing the indices of any face of the form in curly brackets; thus {132} or, in general, {*hkl*}.

1.6 Enantiomorphism. Sometimes two crystals of the same substance have faces which are related to

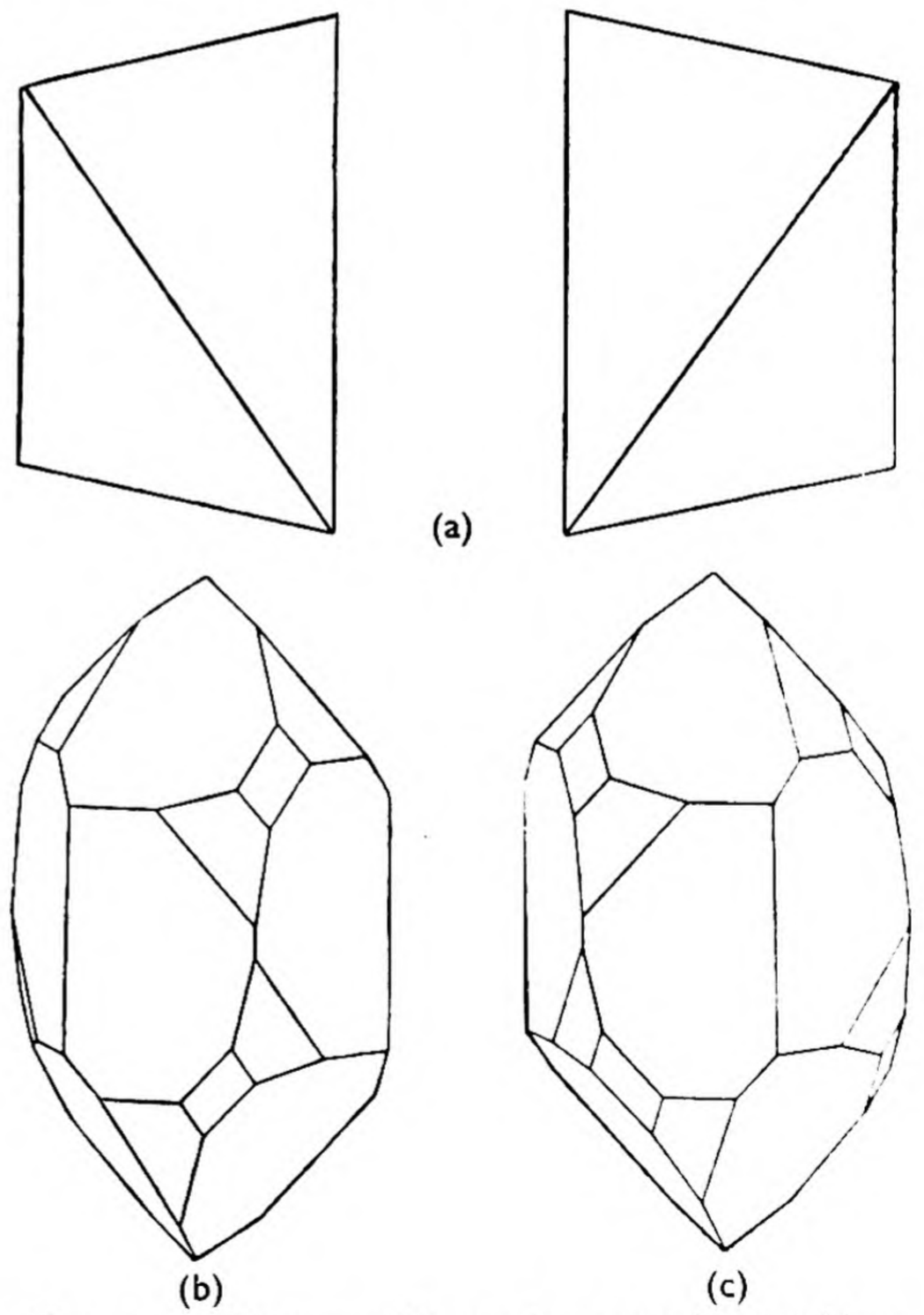

FIG. 5.2. Diagrams illustrating enantiomorphism
(*a*) Sphenoids of class 222
(*b*) Right-handed crystal of quartz
(*c*) Left-handed crystal of quartz

each other as a right hand is to the left hand : that is, one can be brought into congruence with the other only by reflection across a mirror plane between them and not by any rotational operation. Such crystals are said to be *enantiomorphous*, and good examples of this type of crystal are shown in Fig. 5.2. Enantiomorphous crystals lack all elements of symmetry which would produce a right-handed arrangement from a left-handed one, and vice versa. These elements of symmetry are the *symmetry plane*, *inversion axis*, and *centre of symmetry*. If any one of these elements is present, then to each face of the crystal there will correspond a similar face related to the first as a right hand to a left hand, and no such crystal can be enantiomorphous to another. If an enantiomorphous crystal shows certain combinations of special forms, as in quartz, it may be impossible to detect enantiomorphism by study of the arrangement of the faces, and other methods are required (**10,** 2.5 to **10,** 2.7). Enantiomorphism is an important property because of its connection with optical activity, and because of its occurrence in substances of great biological and technical importance. A list of enantiomorphous classes of symmetry is given in **10,** 2.7.

1.7 Zones and zone axes. Faces on a crystal often lie in groups so that each face of a group is parallel to a particular line. The faces of such a group are said to lie in a *zone*, and the direction to which they are parallel is called the *zone axis*. When two faces in a zone meet, the edge between them, because it is a line common to both planes, is parallel to the direction of the zone axis, and it is this feature of parallel edges which enables the eye to pick out the zones in a well-developed crystal. It is clear that any two faces, provided that they are not parallel to each other, are sufficient to define a zone. Examples of zones on a crystal are shown in Fig. 5.2 (*b*, *c*).

The direction of a particular zone axis in the crystal is defined in the following manner. The selection of the crystallographic axes and of the parametral plane fixes the ratios of the unit lengths on the axes. For the reason discussed in **1,** 3.8 it is always possible to choose a point on the zone axis so that it has integral co-ordinates on the crystallographic axes. In Fig. 6 the co-ordinates of the point P are : two units along the x-axis, one unit along the y-axis (negative), three units along the z-axis ; that is, $2a$, $\bar{1}b$, $3c$. As the zone axis passes through the origin of the axes, any other point on it fixes its direction ; and so we can use the co-ordinates of any such point as the *zone symbol.* The symbol of the zone axis shown in Fig. 6 is therefore $[2\bar{1}3]$, the square brackets always being used to distinguish a zone symbol from face indices. We could equally well have taken the point on the other side of the origin of the axes, and the zone symbol would then have been $[\bar{2}1\bar{3}]$, so that changing the sign of each index of a zone symbol does not alter the direction specified.

In general terms, if the co-ordinates on the crystallographic axes of a point on the zone axis are Ua, Vb, Wc, then $[UVW]$ is the zone symbol. Where a common factor occurs it is usually eliminated from the indices of the zone axis. The particular zone axis selected as the x crystallographic axis has the zone symbol [100], while for the y- and z-axes the zone symbols are respectively [010] and [001]. It should be noted that the zone axis [*hkl*] is not normal to the face (*hkl*), except in the cubic system, and in some special cases in other systems, excluding the triclinic. The relation between the zone symbol and the indices of faces lying in the zone is studied in **1,** 3.8.

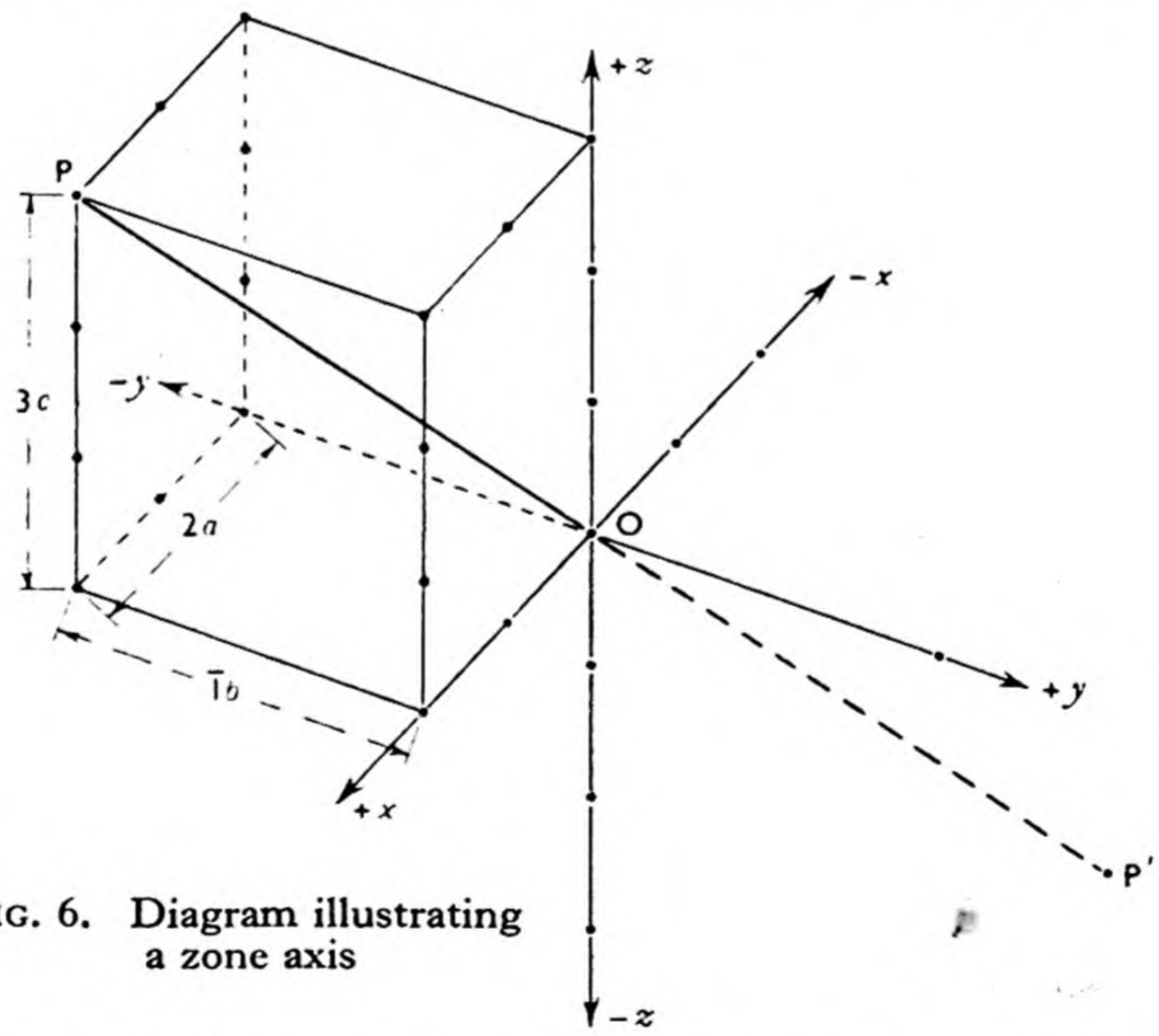

FIG. 6. Diagram illustrating a zone axis

2. The Classification of Crystals

2.1 The thirty-two crystal classes (point groups). The primary divisions of crystalline matter are the thirty-two crystal classes, each of which is characterized by the possession of a particular group of symmetry elements. Let us ascertain the total number of symmetry elements of all kinds possessed by five examples.

1. HEXAGONAL CRYSTAL (FIG. 2, *d*)	2. TRICLINIC CRYSTAL (FIG. 2, *g*)
1 hexad (vertical) axis 6 diad (horizontal) axes 1 plane (horizontal). 6 planes (vertical) centre	centre only

POSSIBLE SYMMETRY ELEMENTS IN CUBIC SYSTEM	3. TETRAHEDRON (FIG. 2, *h*)	4. STRIATED CUBE (FIG. 2, *e*)	5. CUBE (FIG. 7)	
4 triad axes	4 triads	4 triads	4 triads	
3 two- or four-fold axes (mutually perpendicular)	3 inverse tetrads	3 diads	3 tetrads	
6 diad axes (diagonal)	none	none	6 diads	
3 planes	none	3 planes	3 planes	9 planes
6 planes (diagonally)	6 planes	none	6 ,,	
centre	none	centre	centre	

Each of these five bodies belongs to a different class of symmetry because each has a different set of symmetry elements from all of the others. In each group of symmetry elements all the symmetry elements intersect at a single point and form what is called a *point group*, to distinguish them from other groups of symmetry with which we are not concerned here. It can be shown mathematically that all possible combinations of these symmetry elements give rise to only thirty-two different arrangements. Thus there are thirty-two crystallographic point groups, and hence thirty-two sub-divisions of crystalline matter which we call *classes*. A complete table of all the thirty-two point groups and the international symbolism is given in **10**, 2.1.

2.2 The seven sets of crystallographic axes and axial ratios. In **1**, 1.4 it was shown that crystallographic axes are co-ordinate axes of reference and we chose the most convenient set for dealing with the faces of a particular crystal. The thirty-two classes of crystals can be grouped into seven *crystal systems* each of which is characterized by a particular, most convenient, set of crystallographic axes.

Three of the classes illustrated above possess four triad axes equally inclined to three mutually perpendicular axes of symmetry (either tetrad, diad or inverse tetrad axes). The most convenient set of reference axes consists of three mutually perpendicular axes coincident with the three tetrad, diad or inverse tetrad axes. The unit lengths of these must all be equal, because the axes are interchanged by the symmetry operation of the triad. These three classes, plus two others not illustrated, fall into the *cubic*, or *isometric*, *system* in which all crystals have four equally inclined triad axes. Since the unit lengths along the three mutually perpendicular crystallographic axes are equal, the angle between any two faces of indices $(h_1k_1l_1)$ and $(h_2k_2l_2)$ is the same for all cubic crystals, whatever the substance is.

If we take the axes of the cubic system and alter the length of the vertical axis, this becomes the only tetrad axis, no matter what other symmetry elements are still present. This is the symmetry characteristic of crystals of the tetragonal system, in which the three crystallographic axes are still mutually perpendicular but the vertical unit length, c, differs from the unit length, a, of the two horizontal axes. The ratio c/a is different for each crystalline substance in the tetragonal system, but is a constant characteristic of all specimens of the same material. The ratio c/a is called the *axial ratio* and has to be specified for each tetragonal crystalline substance.

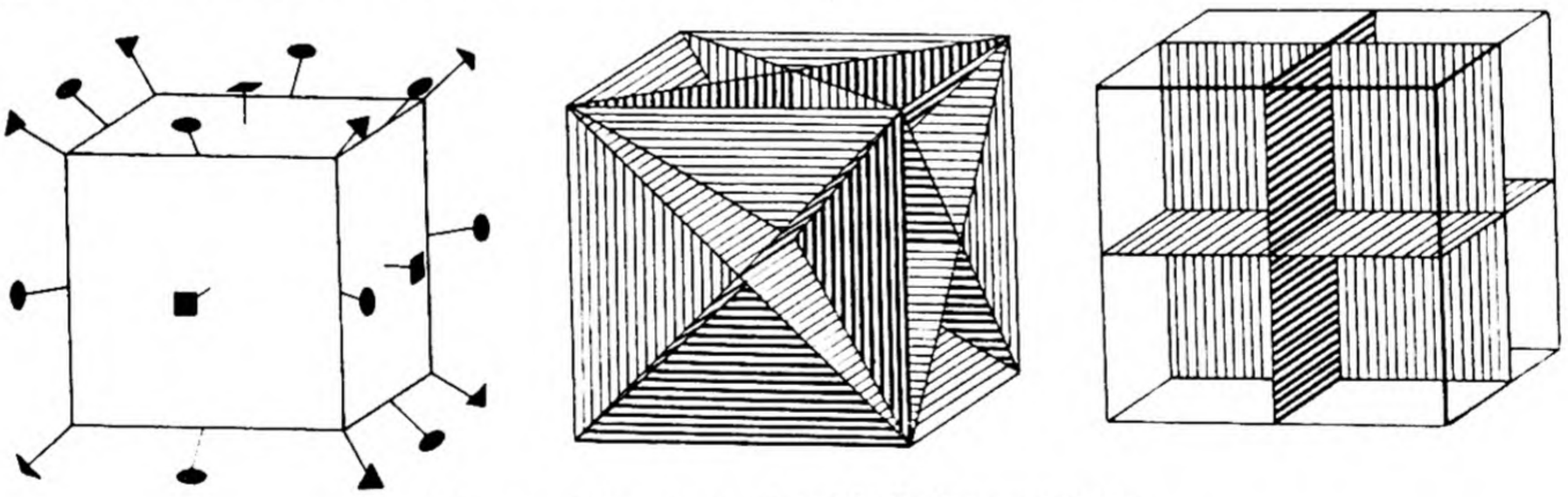

FIG. 7. Elements of cubic holosymmetry

If the unit lengths of the two horizontal axes are made unequal and different from the vertical one, we get the set of crystallographic axes most convenient for crystals of the orthorhombic system (Fig. 8, *a*). Crystals of this system possess no axes of symmetry of higher degree than two-fold. When, in addition, one of the angles is not a right angle, we get the set of crystallographic axes suitable for the monoclinic system in which crystals can have a diad axis as their only symmetry axis. Conventionally the diad axis is

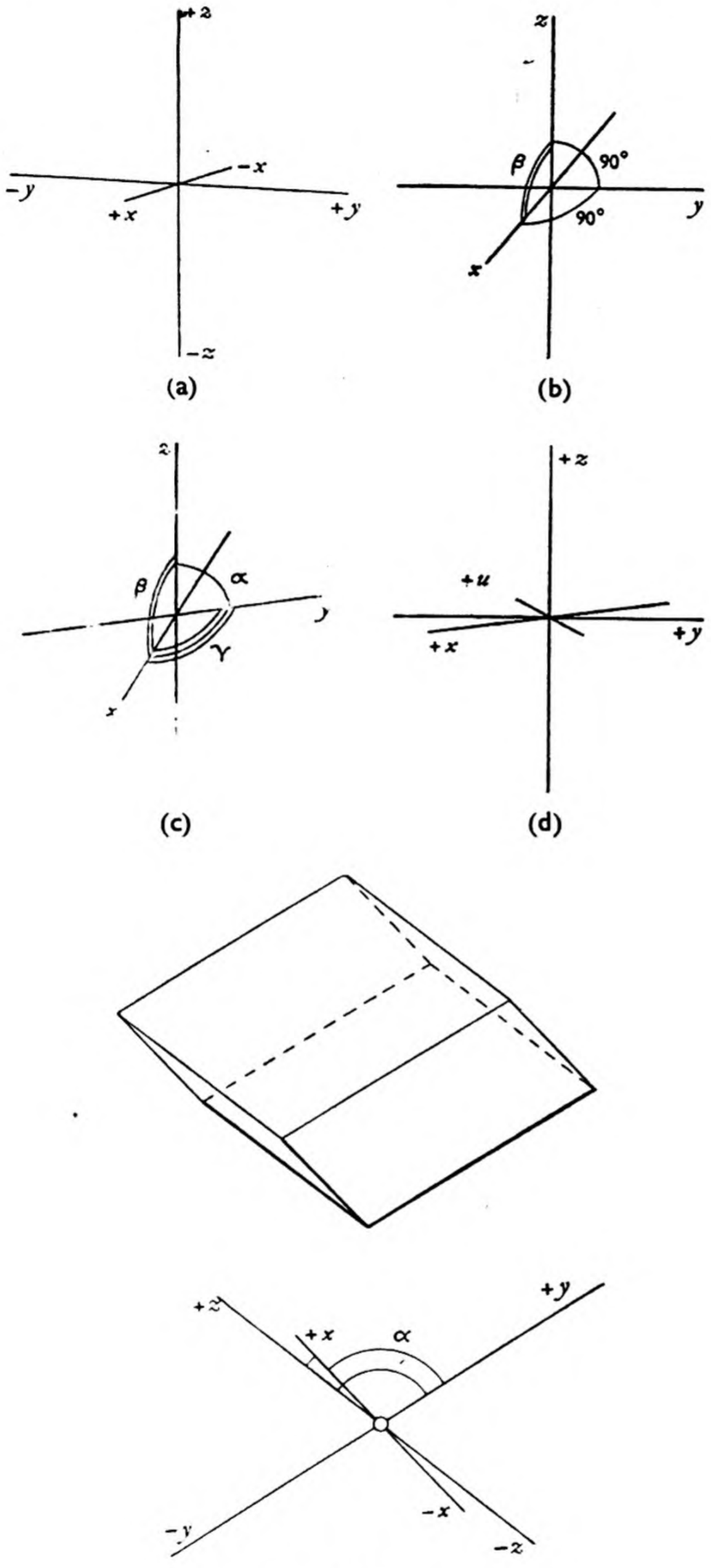

FIG. 8. Crystallographic axes
(*a*) orthorhombic (*b*) monoclinic (*c*) triclinic
(*d*) hexagonal (*e*) rhombohedral

taken as the crystallographic *y*-axis, so that the angle β between $+x$ and $+z$ has to be specified for each crystalline substance of this system; this angle β is usually expressed as an obtuse angle, so that the *x*-axis slopes downward from the back (negative) towards the front (positive) (Fig. 8, *b*). If we make two of the angles unequal and different from 90°, then the possibility of any symmetry axis is destroyed, and we get the set of crystallographic axes most suitable for the triclinic system in which none of the three angles is a right angle (Fig. 8, *c*).

For a hexagonal crystal it is inconvenient to use only three axes of reference, because different faces of the same form would have a different relationship to the three crystallographic axes. A fourth axis is therefore introduced (Fig. 8, *d*). The three horizontal axes are inclined to each other at an angle of 120° and are of equal unit length, while the vertical axis is perpendicular to the three horizontal axes and is of different unit length. It is clear that the intercepts of a plane on any two of the horizontal axes determine the intercept on the third horizontal axis and hence the indices of the plane. The relationship of the first three of the indices, *hki*, is $h+k+i=0$. Some authors omit the index *i* and insert a dot, for example (21.1) for $(21\bar{3}1)$, but in this book we shall use a small asterisk, as in (21*1), wherever it is inconvenient to use all four indices.

If a cube is either extended or compressed along one of the triad axes, the resulting solid is a rhombohedron (Fig. 8, *e*). The edges of the rhombohedron which meet at either end of the unique triad axis are called the *polar edges*. These polar edges, which are of equal length and are inclined to each other at the same angle (not a right angle), give the directions of the three crystallographic axes *x*, *y* and *z*. Owing to the special relationship between the trigonal and the hexagonal systems, trigonal crystals can be studied with hexagonal axes of reference (**10**, 1.4). This is often done in morphological work, because the indexing of faces on hexagonal crystallographic axes is simpler than on rhombohedral axes. When the three polar edges of a rhombohedron are used as axes, these are referred to either as *rhombohedral axes* or as *Miller axes*; but when the four axes of the hexagonal set are used, these are called either *hexagonal axes* or *Miller-Bravais axes* because their use was first suggested by Bravais.

The orientation of the crystallographic axes used in Fig. 8 is conventional in morphological crystallography. In the three orthogonal systems positive *x* points towards the observer, positive *y* is to his right, and positive *z* points vertically upwards. In the *monoclinic system* the *x*-axis slopes downwards from the back (negative) towards the front (positive); while, in the *triclinic system*, the *y*-axis also usually slopes downwards from the left (negative) towards the right (positive). In *rhombohedral axes* positive *x* slopes upwards towards the observer, while positive *y* and *z* slope upwards to his right and left respectively (Fig. 8, *e*). In the *hexagonal axes* positive *x* points over the left shoulder of the observer, positive *y*

points to the right and the negative u axis points over his right shoulder ; in this way, starting from positive x, the 120° angle is measured anticlockwise (looking down) to positive y and then to positive u ; positive z points vertically upwards as in all other systems (Fig. 8, *d*).

2.3 The seven crystal systems. In discussing the most convenient set of crystallographic axes of reference, we have seen that the general symmetry characteristics of a particular crystal determine the particular set of crystallographic axes to be selected. We can therefore group together symmetry classes into symmetry systems either by allocating them to the most convenient set of crystallographic axes, or by stating the essential symmetry characteristic which determines that allocation. The relationship is shown in the table on p. 10. The question of symmetry systems is also approached in another way in **1**, 3.2.

2.4 Isometric, uniaxial and biaxial systems. In the study of the physical properties of crystals, use is made of *representation surfaces*. Each radius vector of a representation surface is proportional to the coefficient of the physical property measured in that direction of the crystal. The equations of surfaces such as the sphere and the ellipsoid contain no terms of higher order than the second, and so are called *surfaces of the second order*. In a crystal, the variation with direction of the coefficients of certain physical properties, such as refractive indices and thermal conductivity, can be expressed by representation surfaces of the second order. Such properties are therefore called *second-order properties*.

In the study of such physical properties, it is found that the representation surface for the systems of lowest symmetry is always a *general* (*triaxial*) *ellipsoid*. It is called ' triaxial ' because it has three unequal principal axes, each of which is a two-fold symmetry axis of the ellipsoid. The three systems of lowest symmetry (triclinic, monoclinic and orthorhombic) have no axes of symmetry higher than two-fold, and so the general ellipsoid is necessarily associated with them. Such an ellipsoid possesses two special directions, each normal to a circular section ; and in crystal optics these directions are called *optic axes*. With reference to these two optic axes of the general ellipsoid, the three systems, triclinic, monoclinic and orthorhombic, are called the *biaxial systems*. When we pass to the three systems, trigonal, tetragonal and hexagonal, which possess a unique axis of symmetry higher than two-fold, we find that the corresponding properties are represented by an ellipsoid of revolution ; this has only one optic axis, and so these systems are called the *uniaxial systems*. Finally, in the cubic system the properties can only be represented by a sphere, and this system is called the *isoaxial system*. This grouping of systems is important in several aspects of crystallography.

Isotropic	Isoaxial—Cubic (or Isometric).
Anisotropic	Uniaxial—Hexagonal, Tetragonal, Trigonal.
	Biaxial—Orthorhombic, Monoclinic, Triclinic.

2.5 The eleven Laue symmetry groups. In much of the field of X-ray crystallography we are concerned with diffraction effects which behave as if they were produced by a centro-symmetrical crystal, whether the actual specimen possesses a centre of symmetry or not. By adding a centre of symmetry to each of the twenty-one crystal classes which do not possess one, we can produce in each case one of the eleven centro-symmetrical classes. Thus the thirty-two classes can be divided into eleven Laue symmetry groups (**10**, 2.5) which are shown on p. 161. The symmetry of these Laue symmetry groups is, of course, identical with that of the corresponding centro-symmetrical class. Each of the seven systems has at least one such class, but four systems—the cubic, tetragonal, trigonal and hexagonal systems—have two. In each of the uniaxial systems one of the two centro-symmetrical classes lacks the vertical planes and horizontal diad axes of the full-symmetry (holosymmetric) class. In the cubic system the class with two-fold symmetry lacks the diagonal planes and the diagonal diad axes of the full-symmetry class.

3. Crystal Lattices

3.1 Repetition of a unit by translation. In all truly crystalline matter there is a regular repetition in three dimensions of a particular atomic, or molecular, grouping. In order to study the operation of this regular repetition, we shall take a two-dimensional pattern such as might be found on wallpaper or linoleum. In Fig. 11 a motif, which is a scalene triangle and hence has no symmetry, is repeated at regular intervals in the plane of the paper. The lines marked are those along which the six shortest repeat distances occur. The whole infinitely extended pattern can, in this simple case, be produced by the repeated translation of the motif along a pair of suitable directions, provided that the repeat distance is given for each of these directions. But the motif is not the unit of pattern, because knowledge of the size and shape of the motif alone does not enable us to develop the whole pattern.

In order to determine the true unit of pattern, we first consider the repetition by translation, neglecting the shape and size of the motif. If we select any point in the pattern as at A in Fig. 11 (*a*), and place a dot at this point and at every exactly similar position in the pattern, the array of points of Fig. 11 (*b*) is obtained.

Characteristic Symmetry and Crystallographic Axes of the Seven Systems

System	Crystallographic Axes	Angles and Axial Ratios to be specified for each substance	Characteristic symmetry
Cubic	Three orthogonal axes of equal unit length. $a=b=c$ $\alpha=\beta=\gamma=90°$	none	Four triad axes each inclined at 54° 44′ to each crystallographic axis
Tetragonal	Three orthogonal axes, two of equal unit length and the third of different unit length—the z axis. $a=b\neq c$ $\alpha=\beta=\gamma=90°$	$c:a$	Only one tetrad or inverse tetrad axis
Orthorhombic	Three orthogonal axes all of unequal unit lengths. $a\neq b\neq c$ $\alpha=\beta=\gamma=90°$	$a:b$ and $c:b$	No axes of higher symmetry than two-fold. Three mutually perpendicular two-fold axes, any of which can be rotation or inverse
Monoclinic	Two axes inclined to each other, with the third—the y-axis—normal to the plane of the first two : all unit lengths unequal. $a\neq b\neq c$ $\alpha=\gamma=90°\neq\beta$	$a:b$, $c:b$, β	No axes of higher symmetry than two-fold. Only one (two-fold) axis, rotation and/or inverse. *Note* : an inverse diad in a given direction is equivalent to a plane of symmetry perpendicular to that direction
Triclinic	Three axes of unequal unit lengths inclined at different angles to each other. $a\neq b\neq c\quad\alpha\neq\beta\neq\gamma\neq90°$	$a:b$, $c:b$, α, β, γ	Neither axes nor planes of symmetry
Trigonal (on rhombohedral axes)	Three axes of equal unit length inclined at the same angle to each other $a=b=c\quad\alpha=\beta=\gamma\neq90°$	α	Only one triad or inverse-triad axis
Hexagonal, and Trigonal (on hexagonal axes)	Three co-planar axes of equal unit length inclined at 120° to each other, with a fourth—the z-axis—of different unit length perpendicular to the plane of the first three. $a=b\neq c$ $\alpha=\beta=90°,\quad\gamma=120°$	$c:a$	Only one hexad or inverse hexad axis

Note : The third horizontal axis—the u-axis—has the same unit length as the x- and y-axes, and the positive ends of these three co-planar axes make angles of 120° with each other.

This regular array of points is called a *lattice*, and gives a complete representation of the geometry of the repetition by translation in the original pattern. The first point was arbitrarily selected relative to the motif, but when this has been fixed, a lattice point must be placed in every exactly similar position; consequently, each lattice point has exactly the same environment in the same orientation as every other point, both in the pattern and in the lattice itself.

The lattice is specified by a suitable pair of vectors which define a parallelogram. This parallelogram is

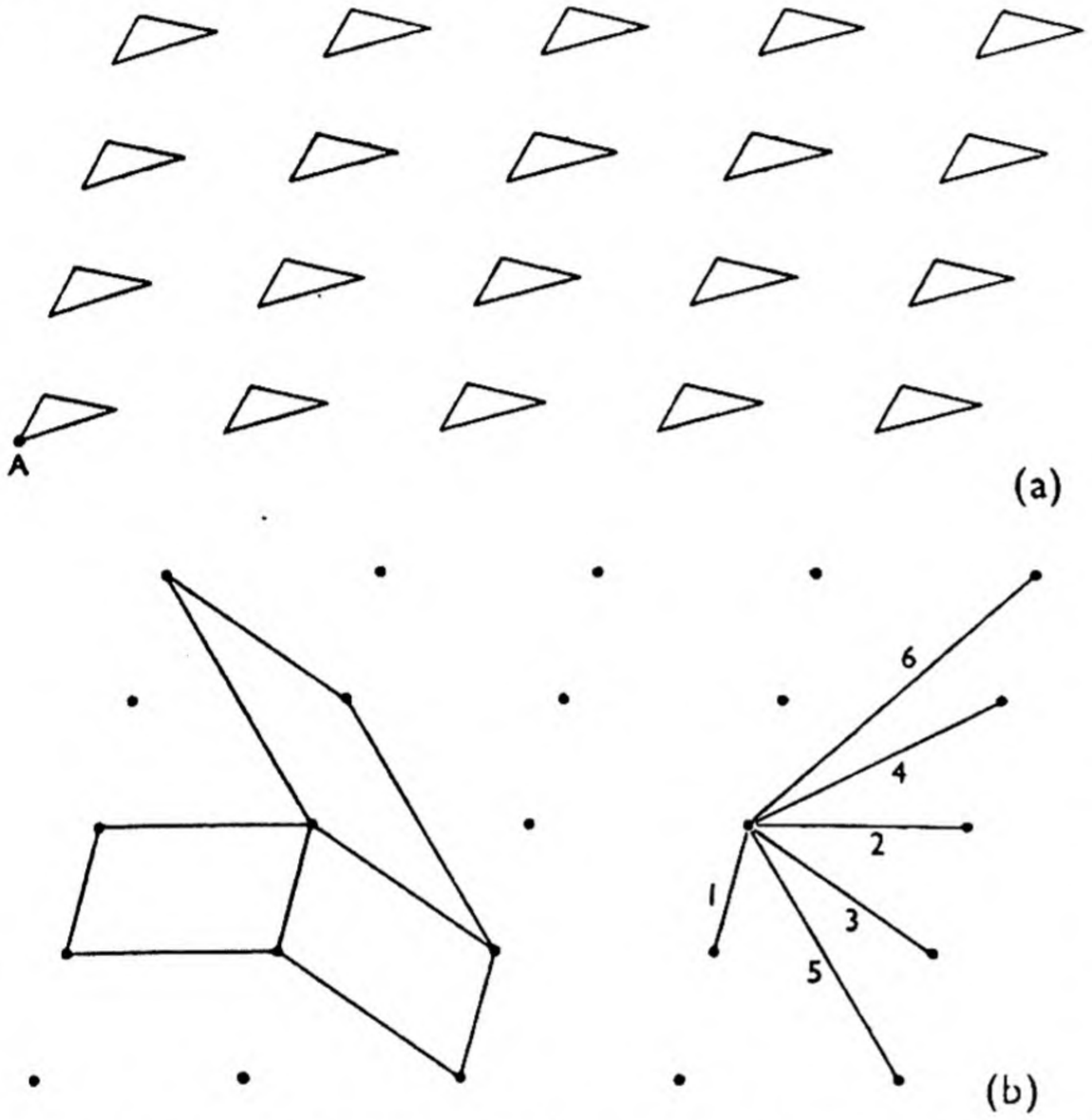

FIG. 11. Diagram showing (*a*) a two-dimensional pattern (*b*) the lattice of this with the six shortest vectors and three alternative ways of selecting the unit mesh

the *unit mesh* of the lattice. In the example under consideration, different pairs of vectors can be chosen to give parallelograms of the same area; three of the possible choices are shown in the figure. It is usual to select the two vectors, or *axes* as they can be called, so that the parallelogram will be one of the alternatives with the smallest area. If one of the motifs is restored and repeated by the translations of the lattice, the original pattern is obtained. It can be seen that the true unit of pattern consists of the contents of the unit mesh.

We can consider a crystal as a three-dimensional pattern, and in such patterns the unit cell is a parallelepiped. The unit of pattern consists of the unit cell plus the atomic or molecular grouping which it contains. As the thorough understanding of the concepts of the crystal lattice and the unit cell are very important, they are studied further in **10**, 1.1.

3.2 Types of unit cell and the fourteen Bravais lattices. The crystal lattice can be defined as an infinite three-dimensional array of regularly-spaced points such that all points have identical environments in similar orientation.

From this definition it is clear that each point can be considered to be a centre of symmetry, and the points in the lattice form a centro-symmetrical arrangement. It is also clear that the vectors defining the lattice may have particular values or angular relationships which result in the arrangement of points acquiring elements of symmetry additional to the centres. For example, if the three non co-planar vectors are mutually perpendicular but of unequal magnitudes, the resulting lattice has two-fold axes of symmetry parallel to each vector and planes of symmetry perpendicular to each vector. A lattice with this arrangement of points is easily visualised, and it is clear that it has full orthorhombic symmetry. Similarly, by giving the appropriate values to the three vectors, we can construct a lattice which has the full symmetry of each of the other crystal systems in turn (**10**, 1.1).

In the study of an actual crystal specimen, we select the directions of the three vectors of the lattice so that the unit cell has the full symmetry of the crystal system of the specimen; also, the magnitudes of these vectors are taken to be proportional to the repeat distances in the corresponding directions within the actual crystal. When this is kept in mind, the reason for the existence of the seven crystal systems becomes clear. The unit cells of Fig. 136 represent all possible symmetries in a lattice. It has been shown (**1**, 2.2) that in the choice of the crystallographic axes it is necessary to take into account the symmetry of the crystal in order to obtain the simplest indices for the faces. We can now connect this with the concept of the unit cell of the lattice and the symmetry which it possesses. In order to obtain the simplest indices and to exhibit the relations between faces, the unit cell is chosen to be the smallest possible which conforms to the symmetry conventions; the vectors of this unit cell are taken as defining the directions and the relative unit lengths of the crystallographic axes.

Consideration of the lattices given in Fig. 136 shows that for each system, except the trigonal, there is a single characteristic shape of unit cell:

Isometric (cubic)	cube
Tetragonal	square-based right prism
Orthorhombic	rectangle-based right prism
Monoclinic	parallelogram-based right prism
Triclinic	parallelogram-based oblique prism

Hexagonal	60° - rhombus - based right prism
Trigonal	either a 60°-rhombus-based right prism or a rhombohedron.

If systems are defined on the morphological basis, either the trigonal has full status or is included as a sub-division of the hexagonal. But in actual crystals which belong to one of the five point groups listed in **10,** 2.1 as trigonal, the lattice may be found by X-ray methods to be either the hexagonal lattice or the rhombohedral lattice. Therefore, if the trigonal is considered as a separate system, as in this book, it has to be said that it does not have a single characteristic shape of the unit cell. If it is included in the hexagonal system, as is the usage in the United States of America, then the hexagonal system does not have a single characteristic shape of unit cell. This difficulty results from the close relationship between the rhombohedral and the hexagonal lattices and is further discussed later (**10,** 1.4). In this book the term ' rhombohedral ' will always be used to indicate the lattice or the axes, and the term ' trigonal ' will be used to indicate the symmetry system which includes the five crystal classes with a single triad or inverse triad axis (**10,** 2.1).

But caution is necessary at this point. While in the great majority of crystals it is true that the shape of the unit cell is characteristic of the particular system, this is not a strictly correct way of defining a system. In any given case, a crystal of lower-symmetry system might have crystal constants which simulated the unit-cell shape of the higher-symmetry system. It is the symmetry elements which define a system, although in most cases a distinctive shape of unit cell results from these.

The seven types of primitive unit cell all have lattice points only at the corners. It is possible to add other lattice points to some of these without breaking any of the conditions which we have laid down. For example, to the cube we can add a point at the middle of each face as in Fig. 12 (*a*) without destroying the lattice or changing its symmetry. Similarly, we can add a point at the intersections of the body diagonals of the cube, as in Fig. 12 (*b*). In both the face-centred cubic and the body-centred cubic lattices, we can select the vectors in such a way that the unit cell has lattice points only at the corners. But such a unit cell obscures the real symmetry of the lattice and is never chosen. When the possible types of *centred lattices* are added to the original seven, the total becomes fourteen. These fourteen types of crystal lattice are called *Bravais lattices*, and the development of the centred types is discussed further in **10,** 1.1.

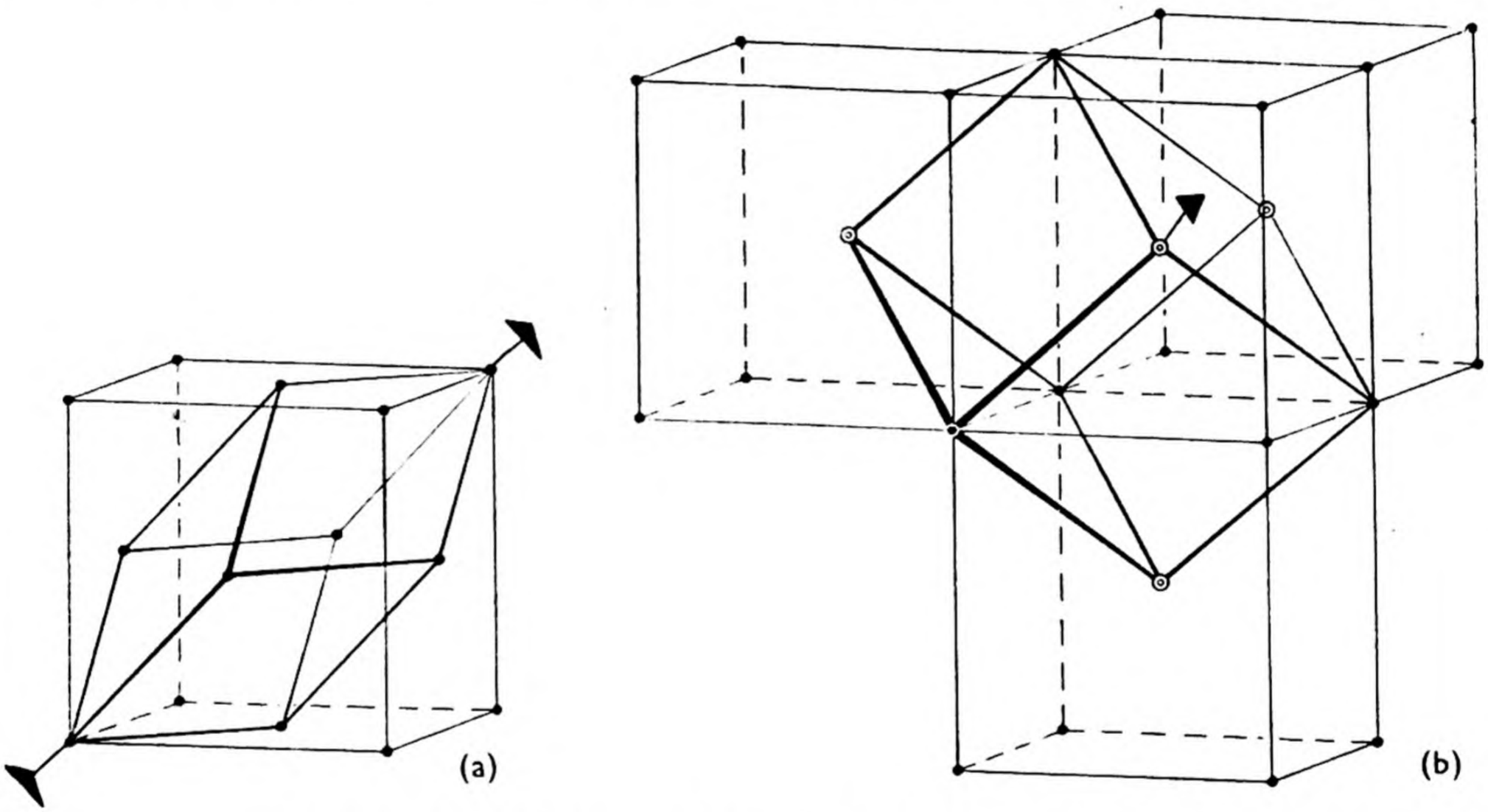

FIG. 12. Centred cubic unit cells with rhombohedral cells outlined
(*a*) Face-centred cubic (*b*) Body-centred cubic

3.3 Absence of five-fold or more than six-fold axes of symmetry. It is easily understandable that the unit cells must be parallelepipeds because only these, of the simplest units, can be stacked in three dimensions without interstices between them. The possible varieties of shape of the parallelepipeds are, as we have seen, associated with axes of 2-, 3-, 4- or 6-fold symmetry. It is, however, impossible to select

and stack together identical units in such a way as to produce axes of 5-, or more than 6-fold symmetry. Hence such axes are absent from crystals, although they may occur in finite patterns which do not have to obey the lattice condition of being infinitely repeated.

3·4 Conventional choice of unit cell. From the study of the angular relations of external faces on a well-developed crystal, it is possible to make a choice of the directions and relative unit lengths of the crystallographic axes; any choice is permissible which conforms to the symmetry and does not violate any accepted rule or convention. The constants which result are called *morphological constants*, and consist in general of the axial ratios $a : b : c$ and the inter-axial angles α, β, γ. For nearly all substances with well-recorded data, there is general agreement on the choice of morphological constants; and the practice has been to follow the choice of the first investigator unless its unsuitability is revealed by further knowledge.

By means of X-ray measurements, however, the absolute lengths, a, b, c can be found, and these, along with the angles α, β, γ are properly called the *crystal-lattice constants*.† The introduction of absolute lengths further restricts our freedom of choice of unit cell, because it is conventional to select the smallest cell unless there is some special reason for not doing so. We now have the possibility that the choice of unit cell made by the X-ray crystallographer differs from that which corresponds to the choice of axes and axial ratios made by the crystal morphologist. This has happened in several cases, but it is surprising how often the morphological choice corresponds to the smallest unit cell. It is necessary for the crystallographer, when comparing data, to be on the alert for such differences of choice, and some examples of this are given below.

Example 1. Beryl is hexagonal, so that the direction of the vertical z-axis is fixed by symmetry, but the three horizontal axes of equal unit length can be in either of two positions inclined to each other at an angle of 30°. The axial ratio chosen by morphologists is:

$$c : a = 0{\cdot}498 : 1.$$

X-ray measurements give for the smallest unit cell,

$$c = 9{\cdot}17 \text{ A.}, \quad a = 9{\cdot}21 \text{ A.},$$

which gives an axial ratio of:

$$c : a = 0{\cdot}996 : 1.$$

Fig. 13.1 shows that, although the orientation of the axes is the same in both cases, the face indexed as $(11\bar{2}1)$ by the morphologists should be $(11\bar{2}2)$ when we use the true unit cell of smallest volume.

† The use of the word *constants* is perhaps unfortunate because these vary with temperature.

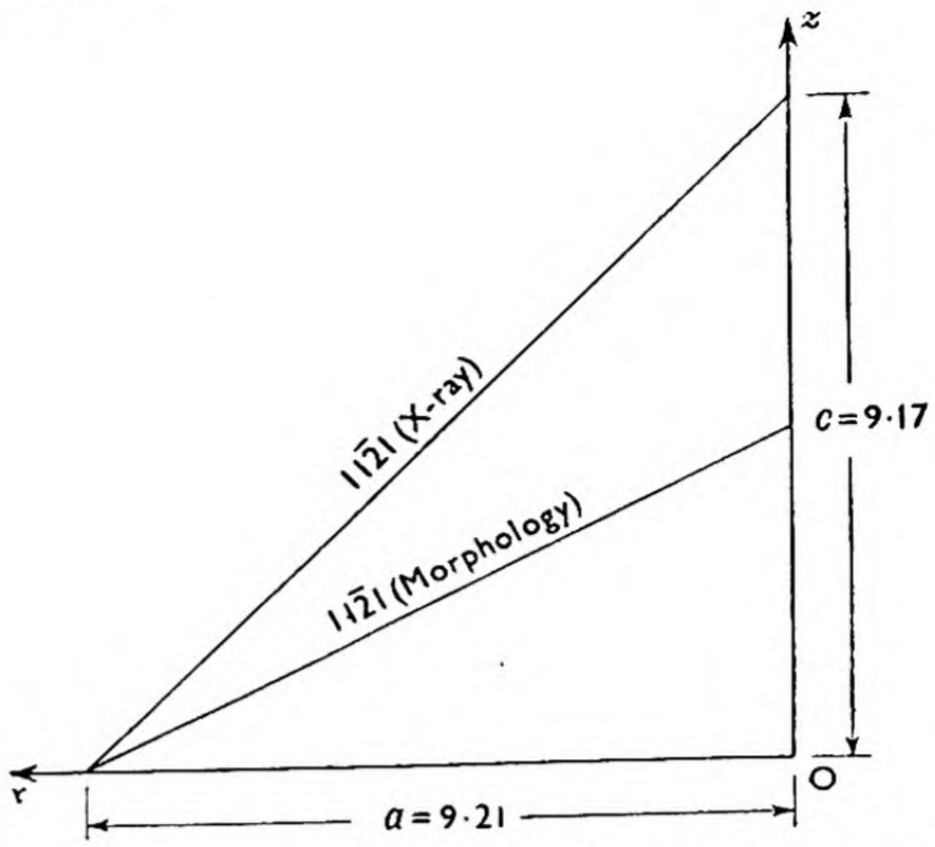

FIG. 13.1. Diagram showing choice of parametral plane in beryl

Example 2. Scheelite is tetragonal, so that the direction of the z-axis is fixed by symmetry; but the two mutually perpendicular horizontal axes of equal length can be in either of two positions inclined at 45° to each other. The axial ratio chosen by morphologists is:

$$c : a = 1{\cdot}536 : 1.$$

Measurement by X-rays gave the unit length along the tetrad axes as $c = 11{\cdot}38$ A., while the shortest unit length in a horizontal direction was found to be $a = 5{\cdot}24$ A. These values give an axial ratio of:

$$c : a = \sqrt{2} \times 1{\cdot}536 : 1.$$

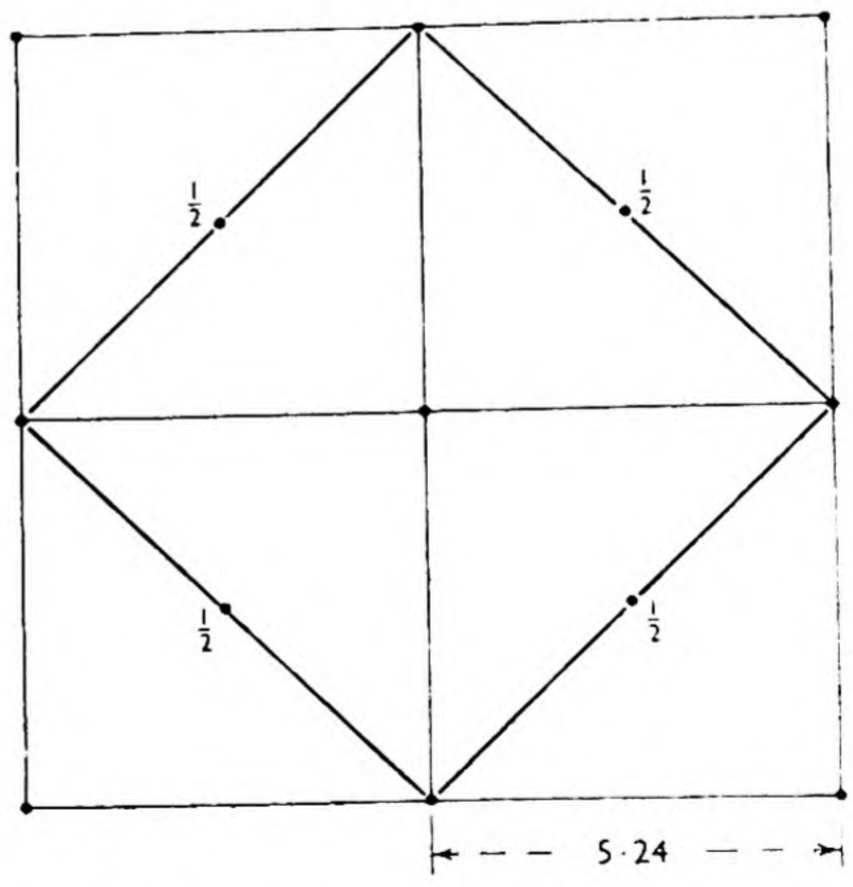

FIG. 13.2. Lattice of scheelite projected on (001)

Fig. 13.2 shows that the latter choice gives the smaller unit cell. Since this smaller unit cell is body-centred in this substance, the unit cell which corresponds to the choice made by the morphologists would be an

all-face-centred one of twice the volume of the smaller cell.

Example 3. Muscovite (white mica) is monoclinic so that the direction of the y-axis is fixed by symmetry, but a choice has to be made of the directions and unit lengths (relative or absolute) of the x- and z-axes, which lie in a plane perpendicular to the y-axis. The orientation usually found in mineralogical text-books gives

$$a : b : c = 0{\cdot}577 : 1 : 3{\cdot}313, \ \beta = 90^\circ\ 6'.$$

Measurement by X-rays showed that of all possible choices of the smallest unit cell, none corresponded

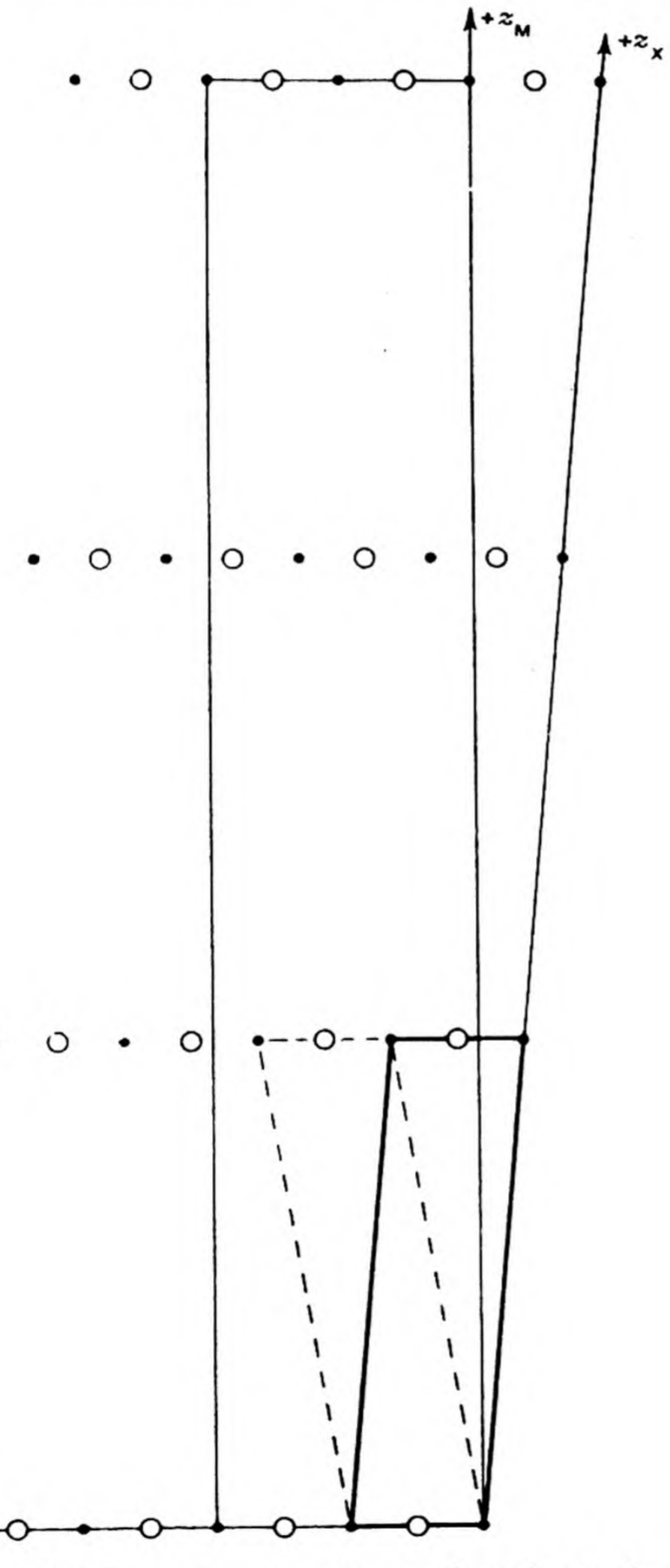

FIG. 14. Lattice of muscovite projected on (010). Points at height zero are shown by dots, and points at height one-half by circles. The morphological unit cell is shown by a thin line, the X-ray unit cell by a heavy line, while the dashes outline an alternative unit cell

to the morphological constants. The investigators (Jackson & West, 1931) selected the unit cell which gives the crystal constants as

$$a = 5{\cdot}18 \text{ A.}, \ b = 9{\cdot}02 \text{ A.}, \ c = 20{\cdot}04 \text{ A.}, \ \beta = 95^\circ\ 30',$$

and this gives axial ratios of :

$$a : b : c = 0{\cdot}574 : 1 : 2{\cdot}222, \ \beta = 95^\circ\ 30'.$$

Fig. 14 shows the X-ray unit cell and that which corresponds to the morphological choice of axes and parametral plane. The unit length a of the X-ray unit cell is the shortest repeat distance, and the unit length c is the second shortest in the plane (010). The z-axis of the morphological cell is one with a large repeat distance of about 59·5 A., and in order to preserve the morphological axial ratio given above, it is necessary to double the true unit lengths of both the a- and the b-axes. This gives a cell corresponding to the morphological choice, which has

$$a = 10{\cdot}36 \text{ A.}, \ b = 18{\cdot}04 \text{ A.}, \ c = 59{\cdot}50 \text{ A.}, \text{ and } \beta = 90^\circ\ 06'.$$

The morphological cell has a volume which is twelve times that of the X-ray unit cell. There is a small discrepancy between the axial ratios 0·577 : 1 and 0·574 : 1 given by the optical and the X-ray measurements. The discrepancy is sometimes greater than this, and it is not usually possible to decide which is the more accurate value. Although X-ray measurements are capable of great accuracy, unless precision methods such as are described in **13**, 4 are used, the angles and axial ratios derived from optical goniometry may be more accurate. This will be likely if the substance develops good faces giving sharp optical reflections, and if a considerable number of measurements of these have been made.

3·5 Lattice planes and their relation to external faces. In X-ray crystallography we are concerned with the diffraction of X-rays by the crystal, which acts as a three-dimensional grating. As is shown in Chapter 3, we can consider diffracted rays as being 'reflected' from planes of lattice points, as this makes the process easier to understand. We cannot, of course, consider only one plane of lattice points, but must take into account the whole set of equally-spaced lattice planes parallel to the first. When the shape and size of the unit cell of the lattice is known, it is easy to determine the spacing between successive planes of any set. In Fig. 15 the trace PB of a plane is shown, its intercepts being $a/2$ and $b/1$; planes parallel to this are drawn through the other three corners of the unit cell $OBAM$: the spacing of this set of planes, d, is then the perpendicular distance between successive members of the set. It should be noted that every lattice point lies on one plane in each family of parallel planes.

External faces of crystals are developed parallel to planes of lattice points, and, in general, parallel to

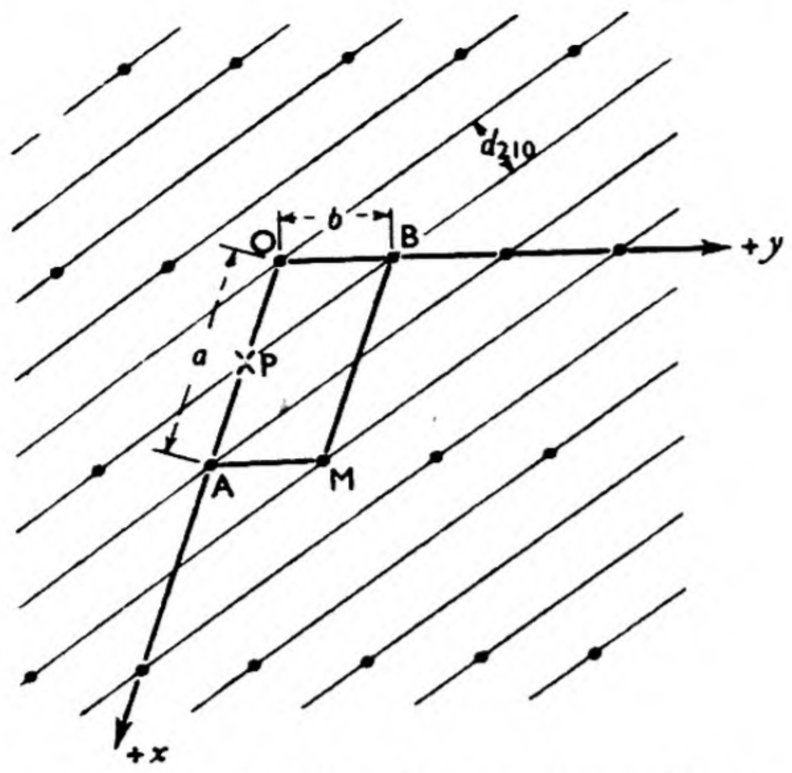

FIG. 15. Diagram showing the spacing of lattice planes

those planes which have a high density of lattice points. The method of defining planes of lattice points is exactly the same as for external faces, that is by means of indices (**1**, 1.3). The relationships given in the next two sections were derived from the study of external faces but are more easily demonstrated by means of the lattice.

3.6 The law of rational indices. All planes of lattice points must, from the nature of the lattice, have rational intercepts on reference axes, which are themselves rows of lattice points; the indices of all planes can therefore be expressed as integers. When the lattice planes are densely populated with lattice points, the fractional intercepts have small denominators, and the indices are, accordingly, small integers. Hence the external faces have, in general, small integers as indices. In X-ray work it is often necessary to consider reflections from lattice planes with indices higher than those which usually occur in morphological work.

3.7 The law of constancy of angle. All crystals of the same crystalline material have the same shape and size of unit cell. Hence the angle between the corresponding pair of planes is constant for all crystals of the same material. In crystallography the angle between planes is always stated as the angle between normals to the planes. Alteration of the unit-cell dimensions may be effected by change of temperature or pressure, or by the replacement of some atoms by others in isomorphous mixture; this alteration may produce a change in interfacial angles in non-cubic crystals.

3.8 Zone-axis symbols and the zone law. In **1**, 1.7 it was said that the faces of crystals lay in a zone when they were all parallel to a single direction which was called the zone axis. Similarly, different sets of planes through lattice points which have a common direction are said to lie in a *zone*. Thus in order to specify a zone axis in a particular crystal, the co-ordinates of the first point from the origin along the direction in question are enclosed in square brackets, the crystallographic axes being the co-ordinate axes. In general the symbol used is $[UVW]$, or in American usage $[uvw]$. From the nature of the lattice, the zone-axis symbol must consist of integers and usually of small integers. With the hexagonal axes there is risk of confusion which is avoided by using only the x-, y- and z-axes and inserting a dot, or a small asterisk, in the symbol to show the omission; for example $[UV.W]$ or $[UV^*W]$. When reference is made to the several zone axes in a crystal which are related by the symmetry elements of the point group, brackets of the type $\langle UVW\rangle$ may be used; these correspond to the use of brackets of the type $\{hkl\}$ to indicate all the faces of a particular form.

The relation between the zone-axis symbol and the indices of any face in the zone is given by the equation known as the *Zone Law*:

$$hU+kV+lW=0,$$

where (hkl) is a face lying in the zone $[UVW]$.

Since any two non-parallel faces determine the direction of the axis of the zone in which the faces lie, we can find the zone-axis symbol if we know the indices of the two faces. Two simultaneous equations of the above form can be solved, since there are only two unknowns, the ratios $U:V$ and $V:W$. The solution is most simply obtained by the method of determinants. The indices of the two faces $(h_1k_1l_1)$ and $(h_2k_2l_2)$ are arranged and cross-multiplied in the following way.

$$\begin{array}{c|c|c|c|c} h_1 & k_1 & l_1 & h_1 & k_1 \quad l_1 \\ & \searrow\nearrow & \searrow\nearrow & \searrow\nearrow & \\ h_2 & k_2 & l_2 & h_2 & k_2 \quad l_2 \end{array}$$

$$\begin{array}{ccc} (k_1l_2-k_2l_1) & (l_1h_2-l_2h_1) & (h_1k_2-h_2k_1) \\ U & V & W \end{array}$$

It does not matter which set of indices is written first, because if we reverse the order this merely results in a change of all the signs, thus $[\bar{U}\ \bar{V}\ \bar{W}]$, which still defines the same line.

Similarly, if two zone-axis symbols are given, the indices of a face which is common to both zones are obtained by cross-multiplication of the two zone-axis symbols.

$$\begin{array}{c|c|c|c|c} U_1 & V_1 & W_1 & U_1 & V_1 \quad W_1 \\ & \searrow\nearrow & \searrow\nearrow & \searrow\nearrow & \\ U_2 & V_2 & W_2 & U_2 & V_2 \quad W_2 \end{array}$$

$$\begin{array}{ccc} (V_1W_2-V_2W_1) & (W_1U_2-W_2U_1) & (U_1V_2-U_2V_1) \\ h & k & l \end{array}$$

If we reverse the order, we obtain the face $(\bar{h}\,\bar{k}\,\bar{l})$,

which is opposite to the face (*hkl*). A proof of the zone equation by the method of determinants is given by Donnay (1934).

3.9 Equations of the normal. If we imagine the normal *ON* drawn to the plane *hkl* in Fig. 4, it is clear that

$$\frac{a}{h}\cos\widehat{Nx}=\frac{b}{k}\cos\widehat{Ny}=\frac{c}{l}\cos\widehat{Nz},$$

where *Nx*, *Ny* and *Nz* are the angles between the normal and the crystallographic axes. These are known as the *equations of the normal*, and examples of their use in crystallography are given by Phillips (1946). They are most used in the orthogonal systems because in these the angles *Nx*, *Ny* and *Nz* are respectively the angles *hkl* : 100, *hkl* : 010 and *hkl* : 001 which are often easily obtainable.

From direction cosines we can derive an equation for the angle ω between any two known face normals. But this equation is very cumbersome and is not much used except in the simplified form applicable only to the cubic system :

$$\cos\omega=\frac{h_1h_2+k_1k_2+l_1l_2}{\sqrt{h_1^2+k_1^2+l_1^2}\,.\,\sqrt{h_2^2+k_2^2+l_2^2}}.$$

4. Twin Crystals

4.1 Crystal aggregates. Crystals of the same substance occur frequently in aggregates, and in these there are four main types of relation between the individual crystals :

i. The individuals have a completely random orientation relative to each other : *polycrystalline aggregate*.

ii. The individuals are arranged with one crystallographic direction in common : *fibrous aggregate*.

iii. The individuals have more or less the same orientation : *parallel growth*.

iv. Two or more individuals are joined together in a definite geometric relation to each other ; such crystals are said to be *twinned*. The term ' twin crystal ' is often loosely used to include also crystal aggregates in which more than two individuals are related in this way.

Twinning is a common phenomenon, and some substances are rarely found untwinned. It is, therefore, necessary to understand the crystallographic relations of the parts of a twin crystal.

4.2 Classification of twins. Twins are classified on the basis of the symmetry operation which brings one part of the twin into coincidence with the other, and the statement of this symmetry operation is called the *twin law*.

Rotation twins. In rotation twins, one part has to be rotated through an angle of 180° about the twin axis in order to bring it into coincidence with the other part : the twin axis has the same relation to both parts. There are two sub-divisions of this type.

i. *Normal twins*. In normal rotation twins the twin axis is normal to a face or a possible face of the crystal, and the plane of this face or possible face is called the *twin plane*. The twin plane coincides with the composition plane along which the two parts of the twin are usually joined. In crystals with a centre of symmetry, the composition plane is a plane of symmetry of the twinned individual if there are only two parts.

ii. *Parallel twins*. In parallel rotation twins, the twin axis is a zone axis lying in the composition plane which is nearly always parallel to a face or to a possible face of the crystal. In parallel twinning the composition plane is never a plane of symmetry of the twinned individual.

Symmetric twins. In symmetric twinning one part has to be reflected across the composition plane in order to bring it into coincidence with the other part, and the two parts cannot be related by any rotational operation. The composition plane is parallel to a face or possible face of the crystal and is a plane of symmetry of the twinned individual if there are only two parts.

4.3 Examples of twinning. Crystalline substances provide examples of twinning on many different laws, but only a few of these are common. These can be best explained by examples.

Example 1. Diamond (cubic). *Spinel law* : normal rotation twin. The twin plane is a face of the form {111} : the twin axis is the normal to this plane and in the cubic system is a triad axis. In Fig. 17 (*a*) is shown a simple twin of this type in a crystal of octahedral habit. This law of twinning is by far the commonest in the cubic system.

Example 2. Gypsum (monoclinic). Normal rotation twin with a plane of the form {100} as twin plane. In Fig. 17 (*b*) is shown a simple twin of this type in a crystal with a habit common in gypsum. This twin-law, with (100) as twin plane, is by far the commonest in crystals of the monoclinic system.

Example 3. Plagioclase felspar (triclinic). *Albite law* : normal rotation twin, always multiple and lamellar. As this mineral is triclinic, the normal to the plane (010) is not a diad axis, and in this twin the plane (010) is both the twin plane and the composition plane.

Example 4. Quartz (trigonal). *Japan law* : symmetric twin on plane of form $\{11\bar{2}2\}$. Quartz is enantiomorphous as it occurs in both right- and left-

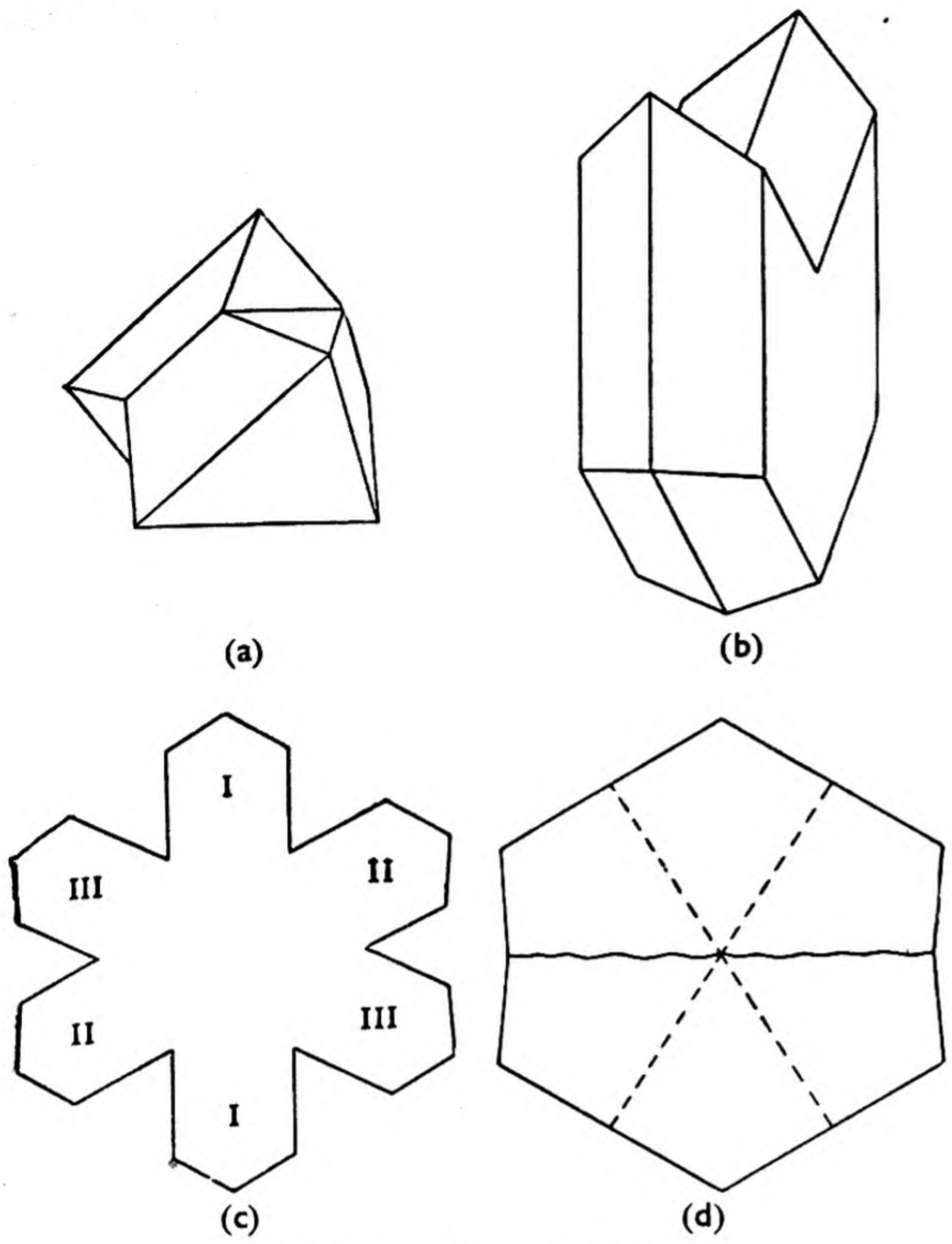

FIG. 17. Twin crystals
(*a*) Octahedron twinned on $(11\bar{1})$
(*b*) Gypsum twinned on (100)
(*c*) Interpenetrant twin of aragonite on {110}
(*d*) Pseudo-hexagonal twin of aragonite

handed types. In this twin a right- and a left-hand part are joined along a plane of the form $\{11\bar{2}2\}$ which is a plane of symmetry in the twinned individual.

Example 5. Quartz. *Brazil law* : symmetric twin on plane of form $\{11\bar{2}0\}$. This is another example of a symmetric twin, but in this kind the two parts often interpenetrate completely and produce an individual which is still trigonal, but which has more symmetry than a single crystal of quartz has. This type of twin possesses a centre of symmetry and three vertical planes of symmetry, in addition to the vertical triad axis and the three horizontal diad axes possessed by quartz. Thus it mimics the symmetry of the highest symmetry class in the trigonal system.

Example 6. Quartz. *Dauphiné law* : parallel rotation twins. In this law the triad axis is the twin axis. The theoretical composition plane is parallel to a face of the prismatic form $\{10\bar{1}0\}$, but this is seldom visible in specimens owing to the typically interpenetrant nature of this twinning. The two parts of this twin are both either right-handed or left-handed and are usually interpenetrant. Sometimes interpenetration is complete, and then, when the twin axis is both a zone axis and the normal to a possible face, as it is here, a pseudosymmetrical twin results. This twin mimics the symmetry of the hexagonal system, and has, in fact, the same symmetry as the high-temperature modification of quartz.

Example 7. Aragonite (orthorhombic). Normal rotation twin with a plane of the form {110} as twin plane. This mineral is orthorhombic but is pseudohexagonal with the z-axis as the pseudohexagonal axis and the angle $110 \wedge 1\bar{1}0$ nearly 60°. The twin crystal often consists of six parts, and a section perpendicular to the z-axis shows 'sector twinning' under the microscope (Fig. 17, *c*, *d*). When interpenetration is complete the re-entrant angles disappear, and the twin crystal becomes apparently hexagonal.

4.4 Glide-twinning. When some crystalline substances are subjected to external pressure, either natural or artificial, they yield by gliding along certain lattice planes. When the deformation is homogeneous, each lattice plane parallel to the glide plane is moved in the glide direction by the same amount relative to the two planes on either side of it. The amount of glide may be variable, but in certain substances showing the special type of homogeneous deformation called *glide twinning* the amount of relative displacement is absolutely fixed for a particular glide in a given substance. It therefore follows that the relation of the glided to the unglided part of the crystal corresponds to a definite crystallographic orientation, and the term 'twin' can be properly applied. In order to define a glide twin completely, it is necessary to specify (i) the glide plane, (ii) the glide direction, and (iii) the amount of glide (Wooster, 1938). The mineral calcite provides an easily studied example of glide twinning. The phenomenon is also of great importance in metals.

5. Crystallographic Projections

5.1 Introduction. In the study of crystals it is necessary to represent on paper the three-dimensional relations of the crystal. Such representations are called *projections* of the crystal, and two main kinds of projection are used. The first kind is required for the representation of the actual appearance of the crystal, so as to bring out the spatial relations of the various faces and zones ; also for the representation of models showing the spatial relations between the atoms, or between the symmetry elements, in the structure of the crystal. For such purposes either the clinographic or the orthographic projection is used, and these are similar to the plans and perspective drawings of architects. The second kind of projection is required for the representation of directions in the crystal and

of the angles between these directions. For this purpose a projection of the surface of a sphere of reference is used, as in the various projections employed by map-makers. In crystallography, the surface of this sphere of reference is represented on paper most commonly by means of either the stereographic or the gnomonic projection. For only one particular purpose is it desirable to employ a projection which preserves equality of areas, although such projections are common in maps. In the sections which follow, the main features of these five projections are discussed in relation to their crystallographic applications. For detailed study of the constructions and for geometrical proofs, the works mentioned in the references should be consulted.

5.2 Clinographic and orthographic projections. The clinographic and orthographic projections are of the perspective type, which means that they could be produced by casting a shadow of a body from a point source of light on to the plane of the projection. In both of them the point of projection is at infinity, and so they are called *parallel perspective projections*. In the orthographic projection the projection lines are perpendicular to the plane of the paper. If the faces of a crystal are being drawn in orthographic projection, the choice of the orientation of the plane of projection is important. In order to make side-faces appear in the drawing, it is necessary to turn the crystal through a small angle, generally about 18°, about the vertical axis. The projection lines remain perpendicular to the plane of the paper, but the orientation of the crystal relative to that plane is changed. Now in order to make the top face also appear as an area on the drawing, *either* of two steps must be taken :

(*a*) The crystal is tilted forward through a small angle, generally about 10°, about a horizontal line parallel to the plane of projection as in Fig. 18.1 ; this is still an orthographic projection because the projection lines are perpendicular to the plane of the paper,

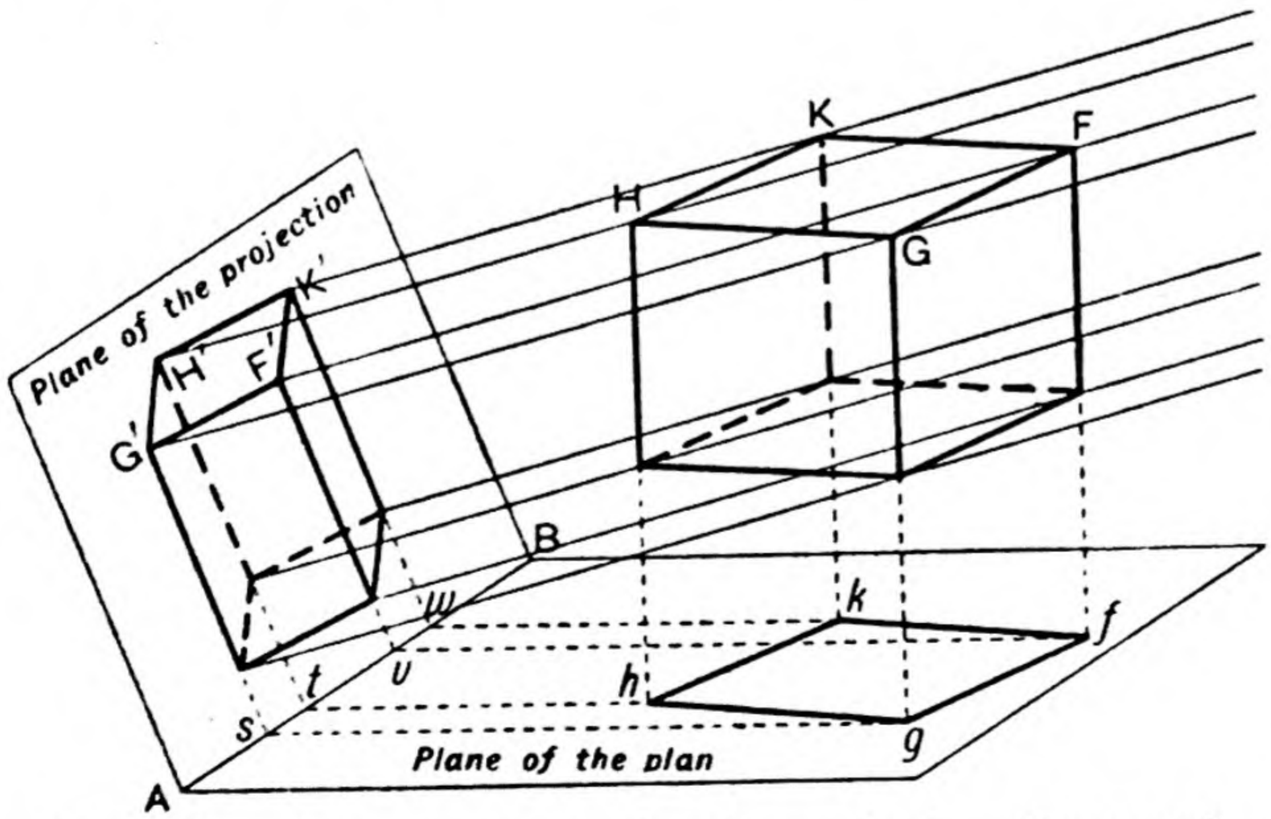

FIG. 18.1. Diagram illustrating the projection of a crystal

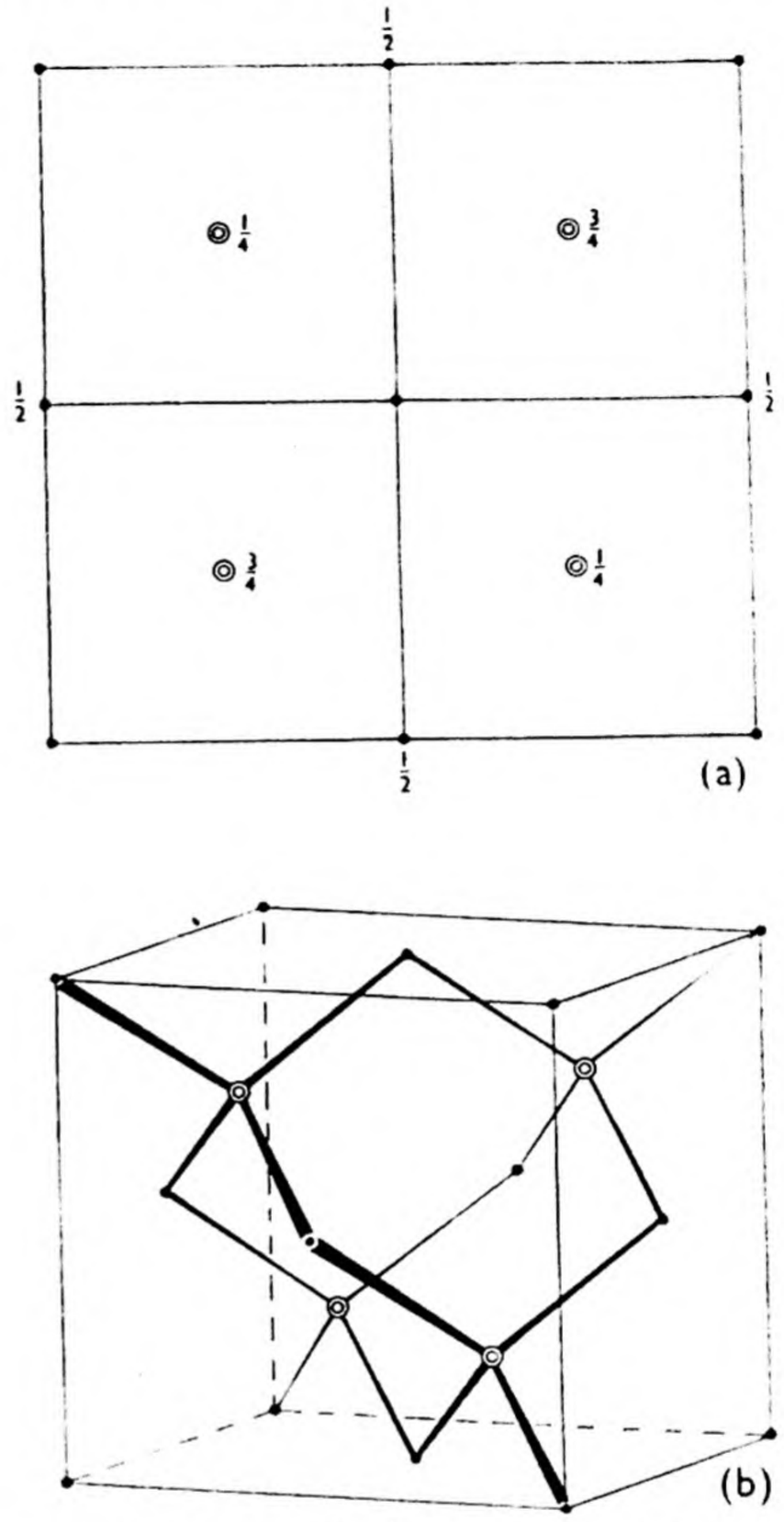

FIG. 18.2. Structure of sphalerite
One kind of atom is shown by dots and the other by rings
(*a*) Plan projected on (100) (*b*) Clinographic drawing

but the orientation of the crystal relative to that plane is further altered.

(*b*) The parallel projection lines are tilted up through the same angle of about 10° in the vertical plane ; this is equivalent to moving the infinitely distant point of projection, and the projection is a clinographic one because the projection lines are no longer perpendicular to the plane of the paper.

There is only a very slight difference in the appearance of crystal drawings of the same crystal projected by these two methods. A full description of the methods of drawing crystals by means of these projections, and also from the stereographic and gnomonic projections, is given by Phillips (1946).

The orthographic projection could be used in the plotting of poles of faces, but for reasons given in the table at the end of this chapter, it is not really suitable for this purpose. Both these projections are, however, widely used in the representation of the structures of crystals (Fig. 18.2). The orthographic plan on the plane of an important crystal

face is very easy to draw and is often used, but it needs practice to interpret these plans, except in simple cases. The vertical heights of atoms or molecules with reference to a specified base are usually stated as fractions of the perpendicular distance between the bases of successive unit cells, as in Fig. 18.2 (*a*). The use of a positive sign, which is sometimes omitted, indicates that the fraction is to be measured upwards from the base stated; the use of a negative sign indicates that the fraction is to be measured downwards from the base stated.

5·3 Stereographic projection. In the stereographic projection, which is a non-parallel, perspective one, a sphere is imagined surrounding the crystal, and from the centre of the sphere normals are drawn to the planes in the crystal. Each of these radii meets the surface of the sphere in the spherical pole of the corresponding face. From each spherical pole in the northern hemisphere a line is drawn to the south pole of the sphere (Fig. 19.1). The points where these lines cut the equatorial plane are the *stereographic poles* of

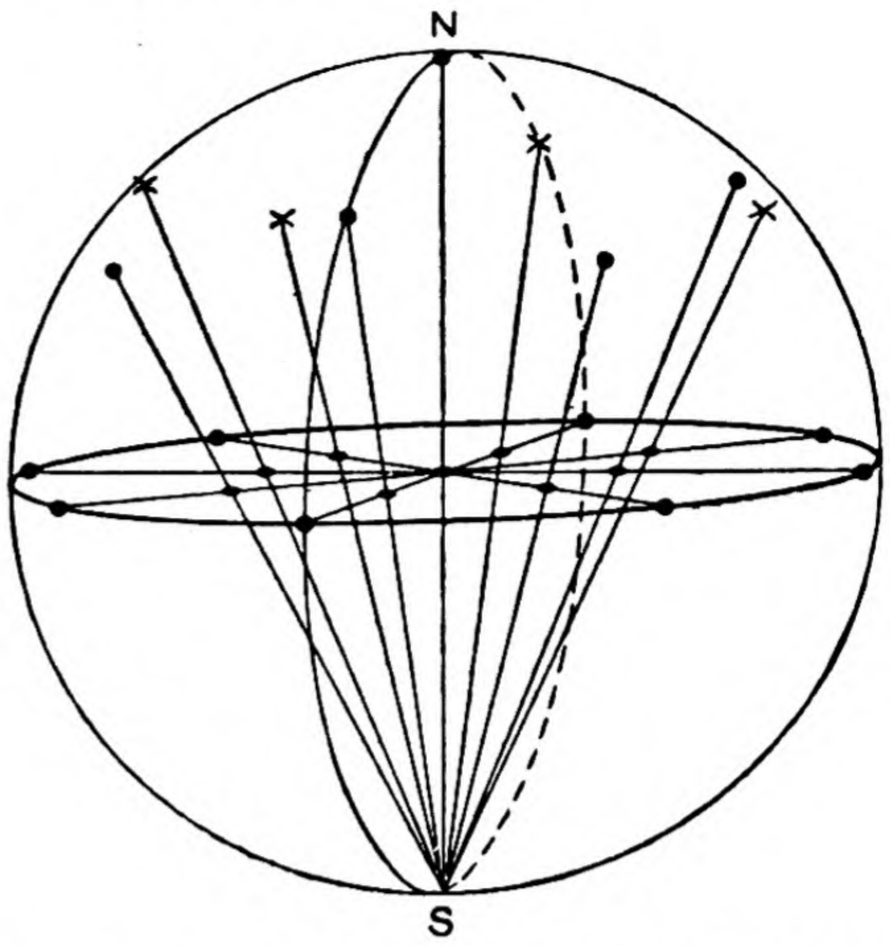

FIG. 19.1. Stereographic projection of poles on the sphere. Poles at the back of the sphere are shown by crosses

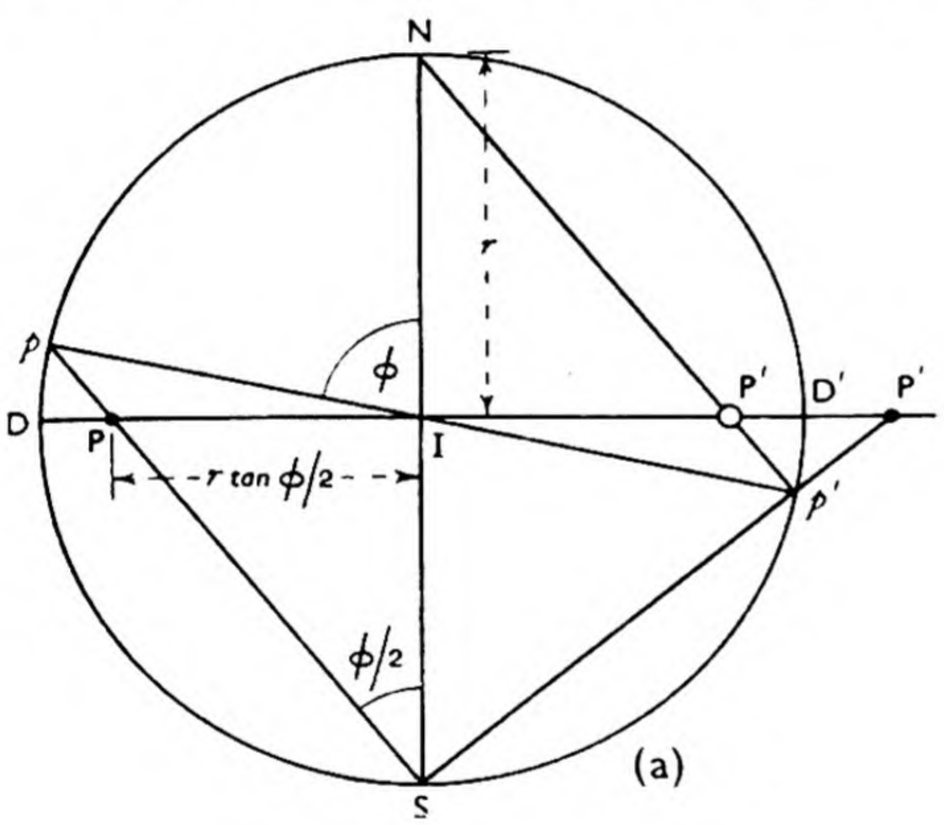

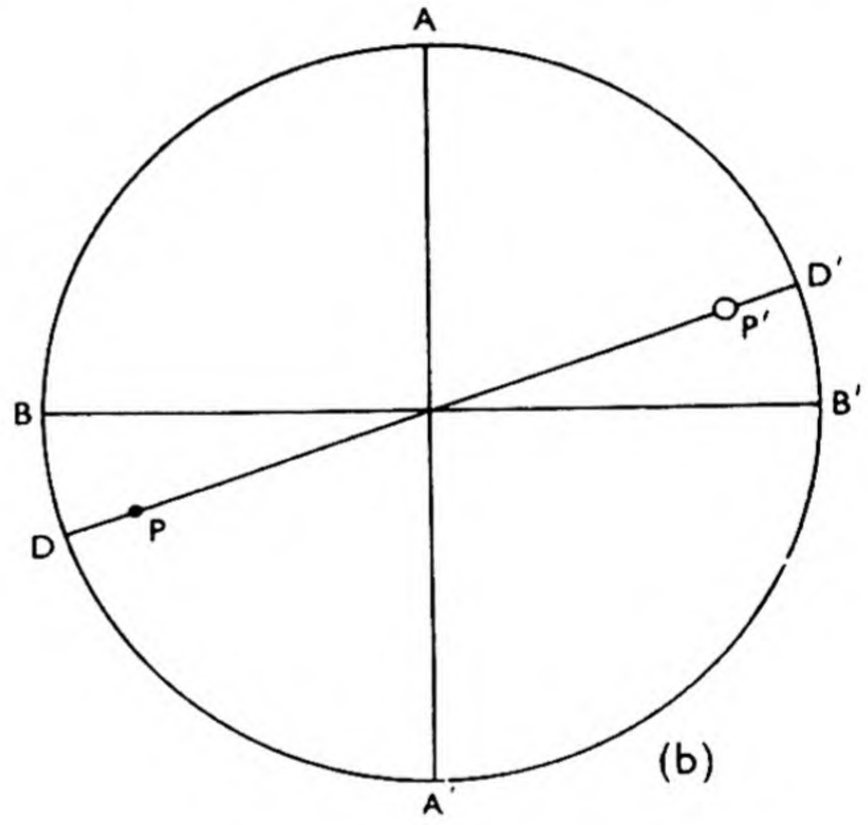

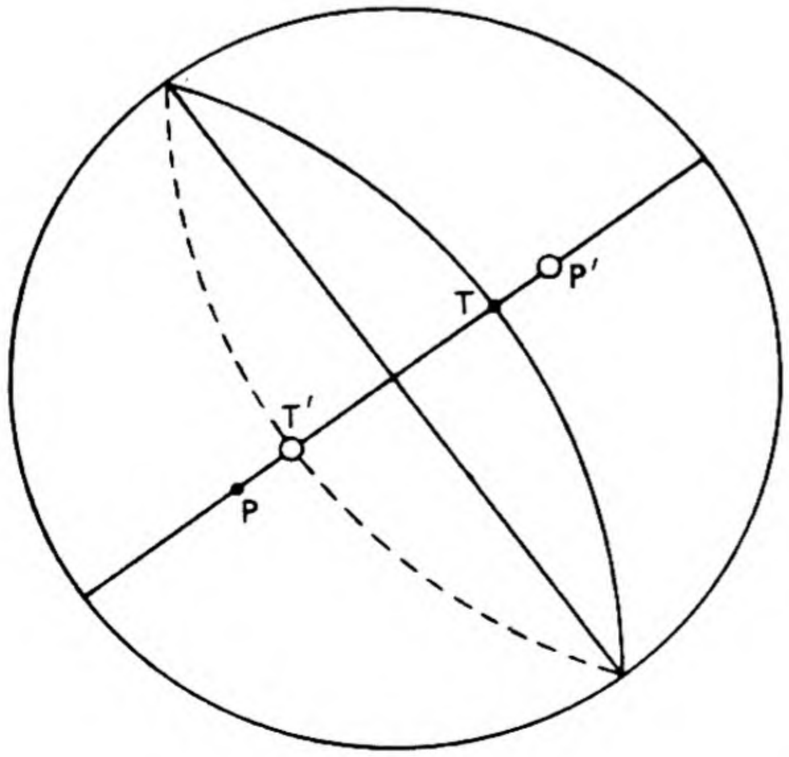

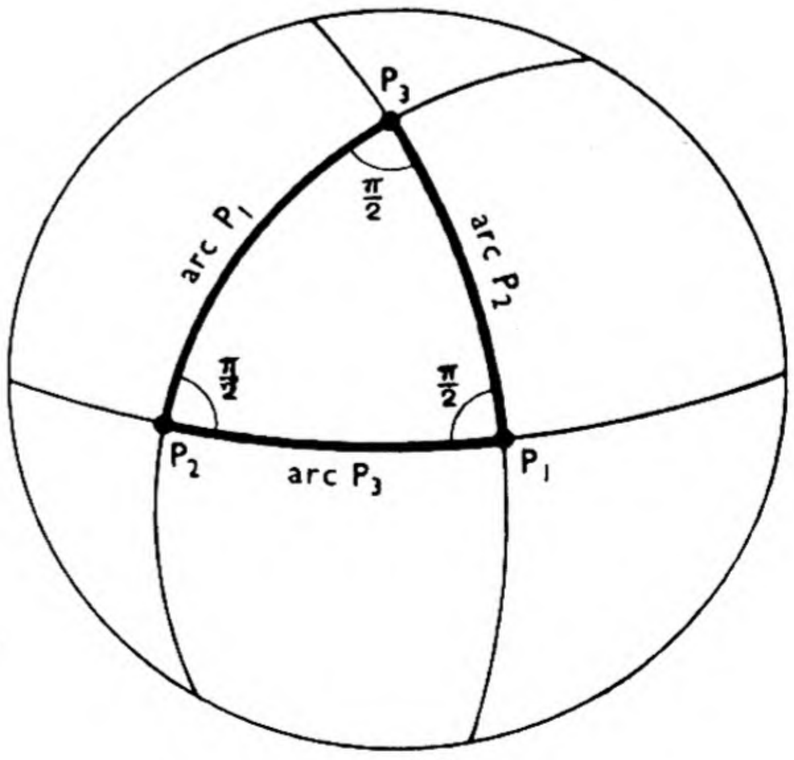

FIG. 19.2. Diagrams illustrating the stereographic projection
(*a*) Vertical section through sphere (*b*) Projection of a point and its opposite (*c*) Projection of a plane and its two poles (*d*) Projection of three mutually-perpendicular great circles and their poles

the corresponding faces. Any plane perpendicular to the diameter through the point of projection can be used, but the geometry is simplified if the equatorial plane is chosen. A plane in the crystal can be stereographically represented by its pole, as just described, or by the projection of the great circle in which the surface of the sphere is cut by a plane through the centre of the crystal, parallel to the crystal face (Fig. 19.2*c*). Spherical poles on the southern hemisphere will, if the above construction is used, project outside the projection of the equator (or primitive circle); but they can also be projected inside the circle by drawing lines from them to the north pole. In the latter case the stereographic poles are shown by small open circles, to distinguish them from poles projected from the northern hemisphere, which are shown by dots.

Great circles, which are the intersections with the spherical surface of planes passing through the centre of the sphere, project as circles on the stereogram. If these pass through the centre of the projection, they will project as straight lines through this point. Great circles pass through pairs of diametrically opposite points on the sphere and consequently through the corresponding points on the stereogram (Fig. 19.2). If two great circles are at right angles to each other, so

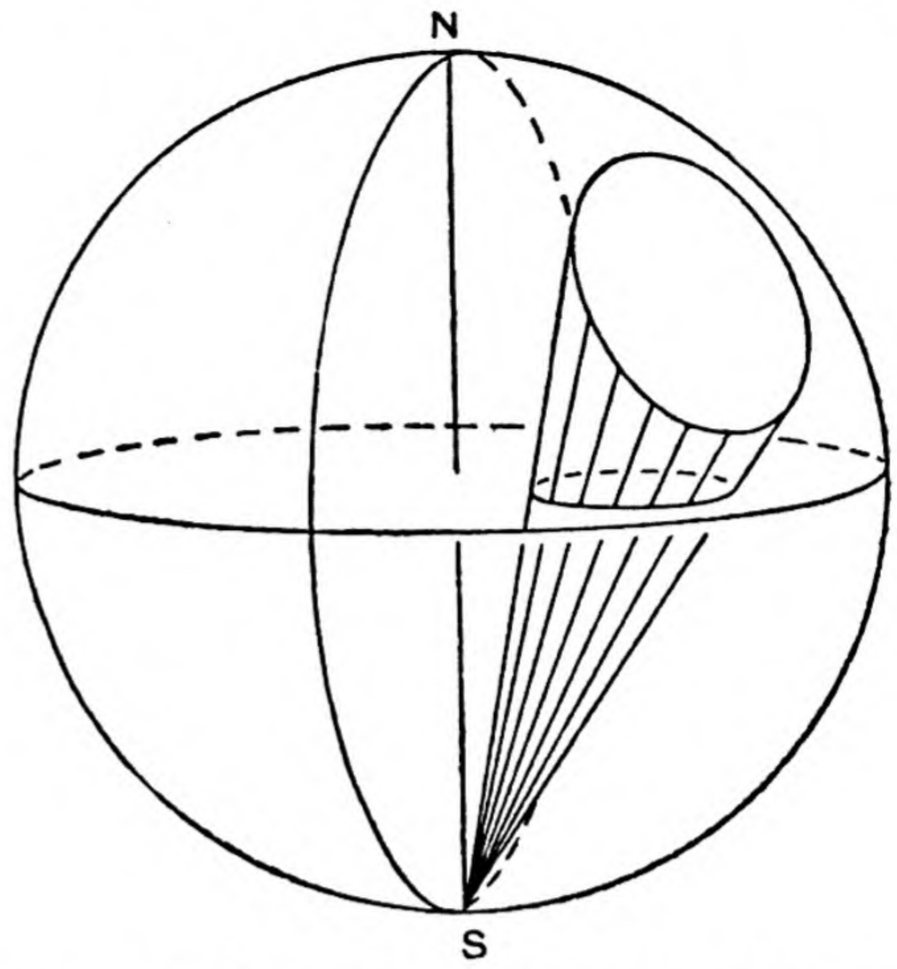

FIG. 20.1. Projection of a circle on the sphere on to a stereogram

are their normals, with the result that each of the two great circles passes through the projection of the normal to the plane of the other. All the planes lying in a given zone will project into poles lying on a single great circle which is known as the *zone circle*.

A *small circle* on the projection sphere is the intersection with the spherical surface of a cone of directions making a constant angle with the direction which forms its axis, and having its apex at the centre of the projection sphere. A small circle is the locus of points which are at equal angular distances from a point on the surface. Small circles on the sphere, like great circles, project as circles on the stereogram (Fig. 20.1). A small circle of radius 90° is a great circle.

One very useful chart is the stereographic net (Fig. 20.2), either on white or on transparent paper. On the stereographic net a series of great circles, at a suitable angular interval, is drawn between two diametrically opposite points on the primitive circle; superposed on this is a series of small circles, at the same angular interval, drawn about these two diametrically opposite points. Such stereographic nets with an angular interval of 2° for a projection sphere of $2\frac{1}{2}$ inches radius are published on transparent

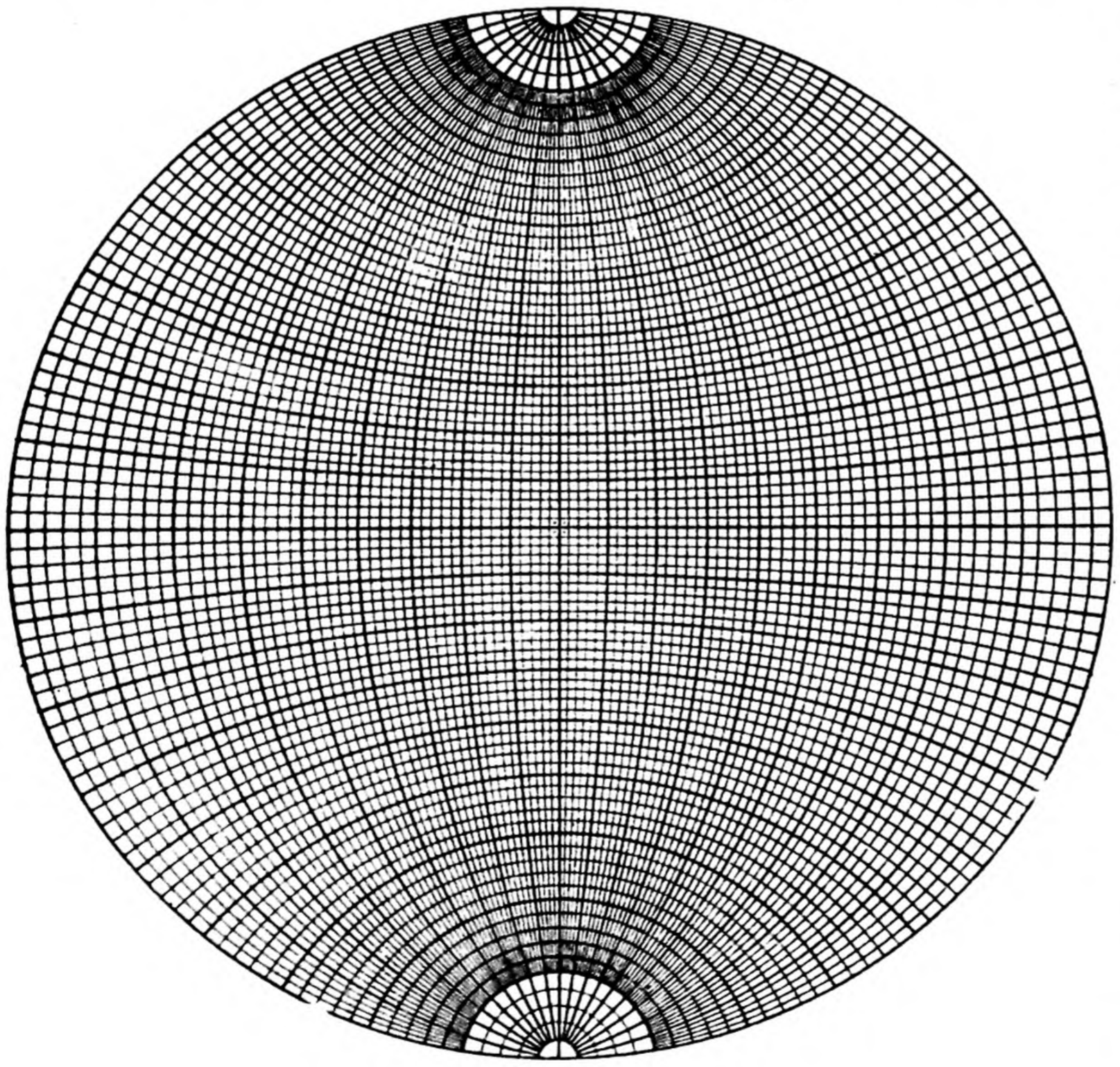

FIG. 20.2. Stereographic net

paper, but larger ones are available for more accurate work. By rotation of the net about its centre all possible great circles can be obtained and, also, all possible small circles about all points on the primitive circle.

5.4 Gnomonic projection. In this projection, which is also a non-parallel, perspective one, the poles on the surface of the sphere are projected from the centre of the sphere on to any plane, except, of course, a plane passing through the centre; the plane is commonly taken tangent to the projection sphere at some important pole, as this simplifies the geometric relations. In this case the distance of any pole from the centre of the projection is

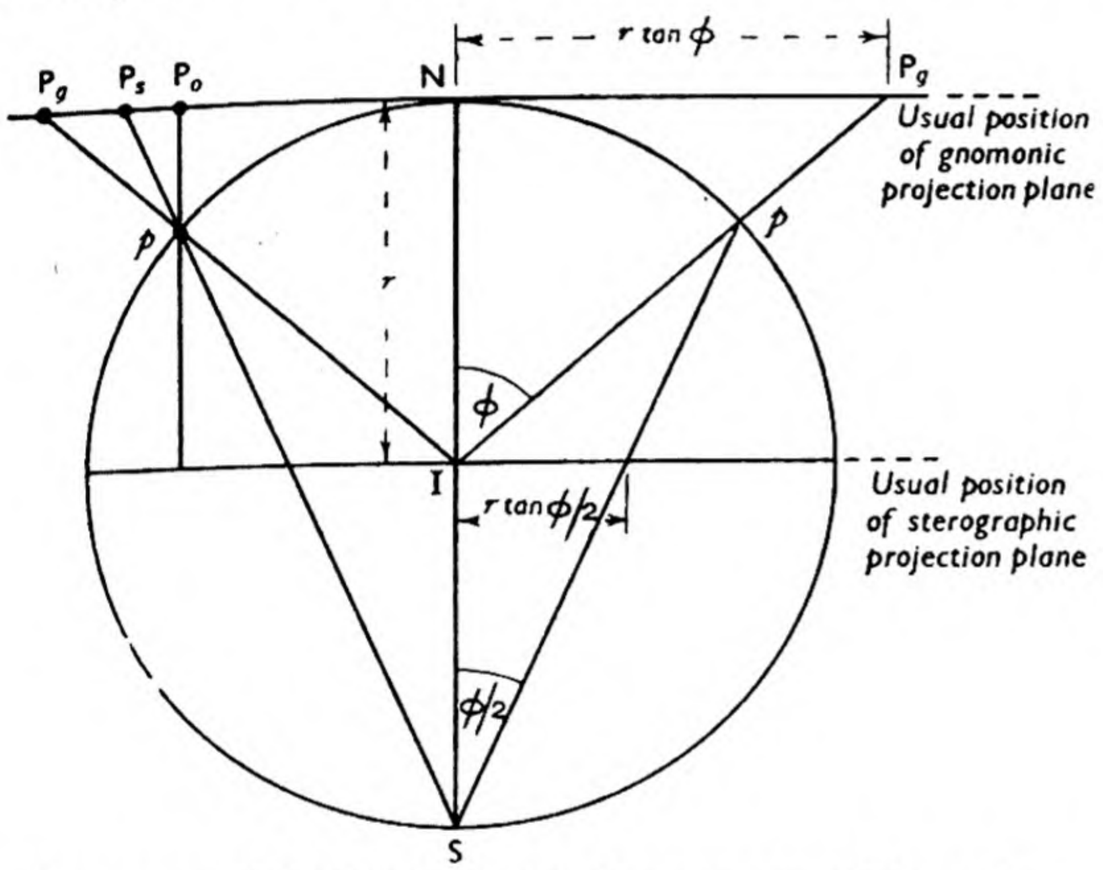

FIG. 21.1. Relations between the stereographic, orthographic and gnomonic projections.
The subscripts distinguish the poles of the three projections

$r \tan \phi$, where ϕ is the angle between the pole and the point of tangency. One obvious limitation of this projection is that all directions parallel to the plane of projection project at infinity, and only a limited angular range can be represented. The general relation between the gnomonic, the stereographic and the orthographic projections is shown in Fig. 21.1.

All great circles project as straight lines which are the intersections of the projection plane with the planes of the great circles (Fig. 21.2); it is thus very easy to draw a zone between any two poles. As we saw, a small circle on the sphere is the intersection of the surface of the sphere with a cone; this cone has its apex at the centre of the sphere and its axis is the normal to the face about which the small circle is drawn, while its semi-angle is the radius of the small circle. It is clear, therefore, that on the gnomonic projection the projected small circles will be conic sections, and will be circles only

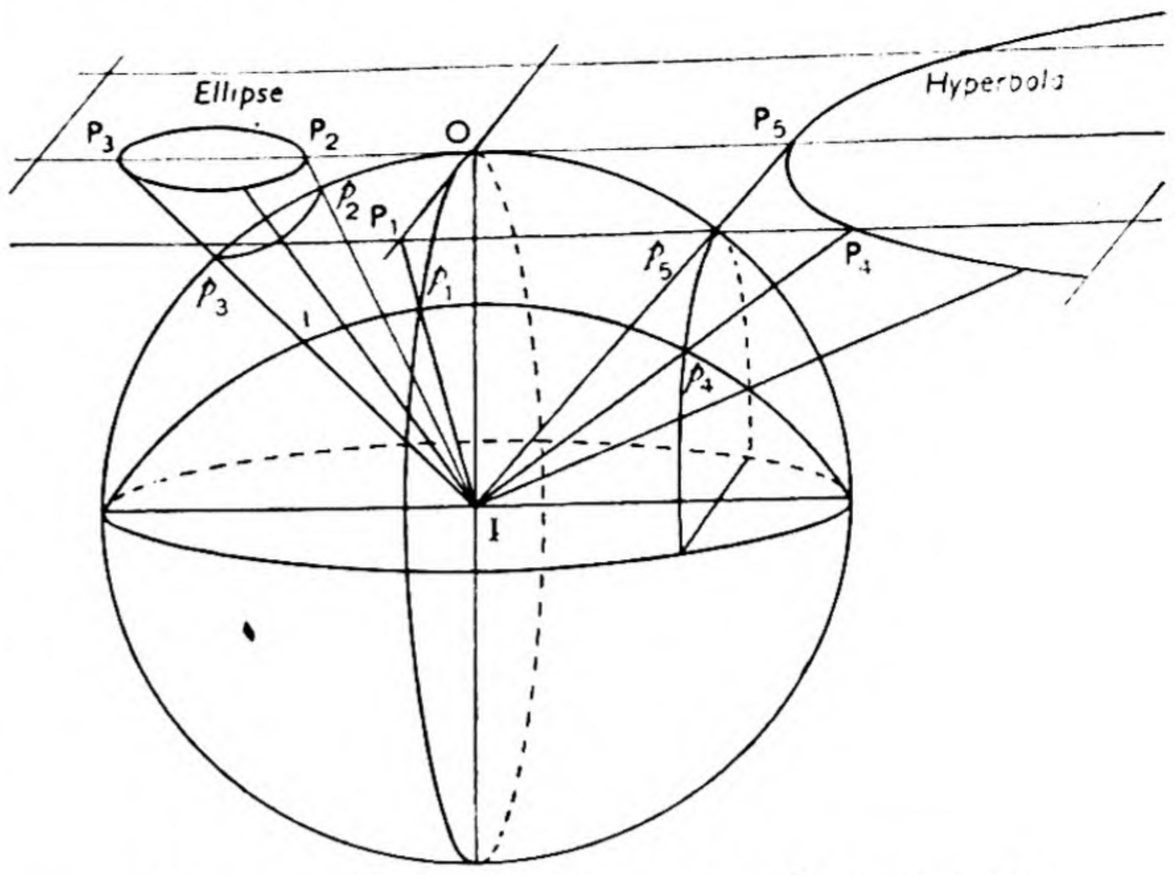

FIG. 21.2. Diagram illustrating the gnomonic projection

when drawn about the centre of the projection (Fig. 21.2).

The gnomonic net corresponding to the stereographic net may be prepared for any given radius of projection sphere (Fig. 21.3). The great circles are represented by straight lines and the small circles by hyperbolae because they are drawn about directions parallel to the plane of projection. The net can be used for the same sort of operations as the stereographic net, within the limits of the gnomonic projection, for example in finding the angle between two poles.

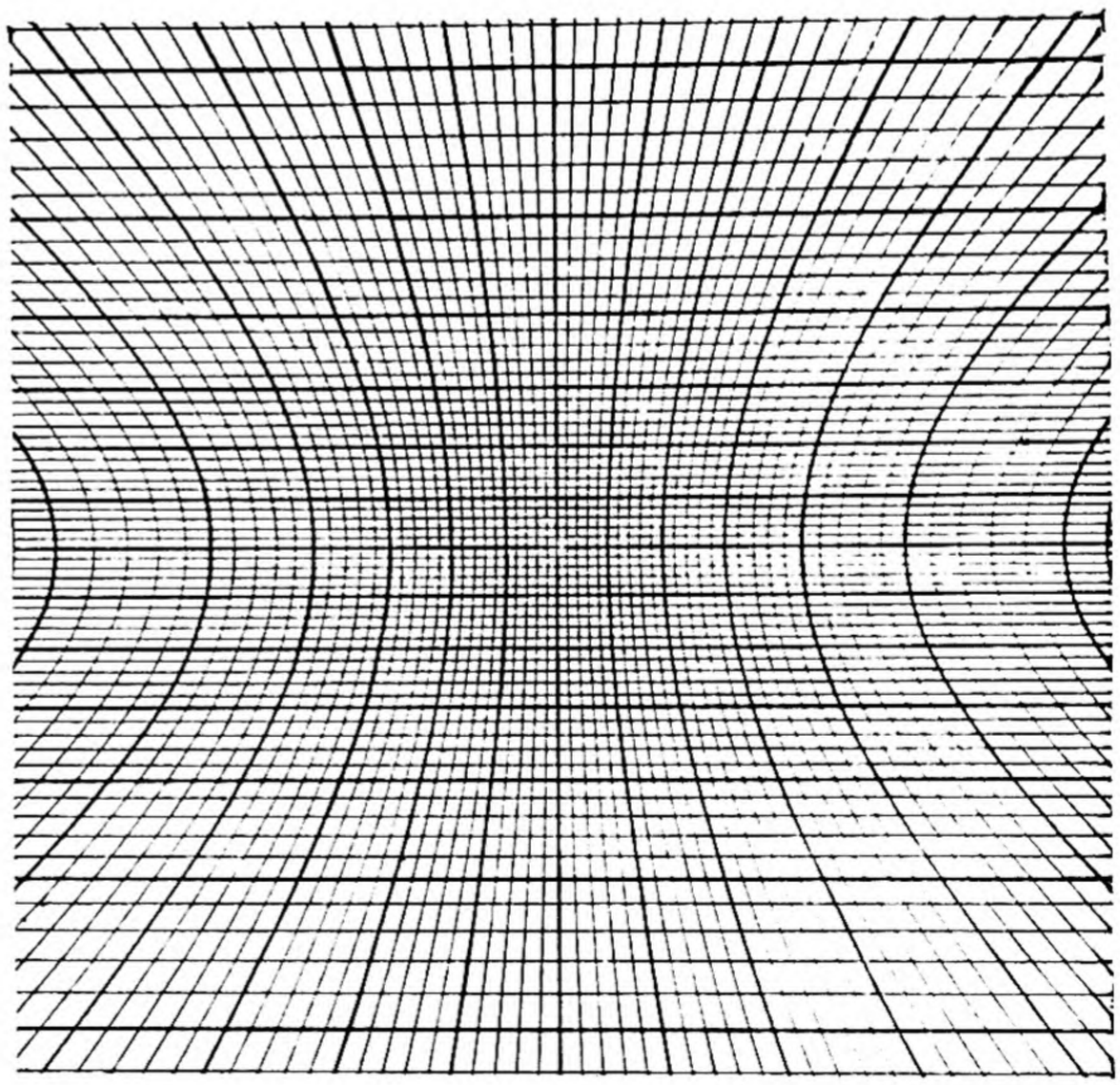

FIG. 21.3. Gnomonic net with lines at 2° intervals and a 2 cm. radius of projection sphere

5.5 Equal-area projection. None of the perspective projections preserves the proper ratio of any two areas on the sphere, and to achieve this property the projection has to be modified. From Fig. 22.1 it is clear that the two equal areas on the sphere are represented by two unequal areas on the stereographic projection. By the modification described below, the stereographic projection can be turned into an equal-area projection which is called *Lambert's Equal-area*

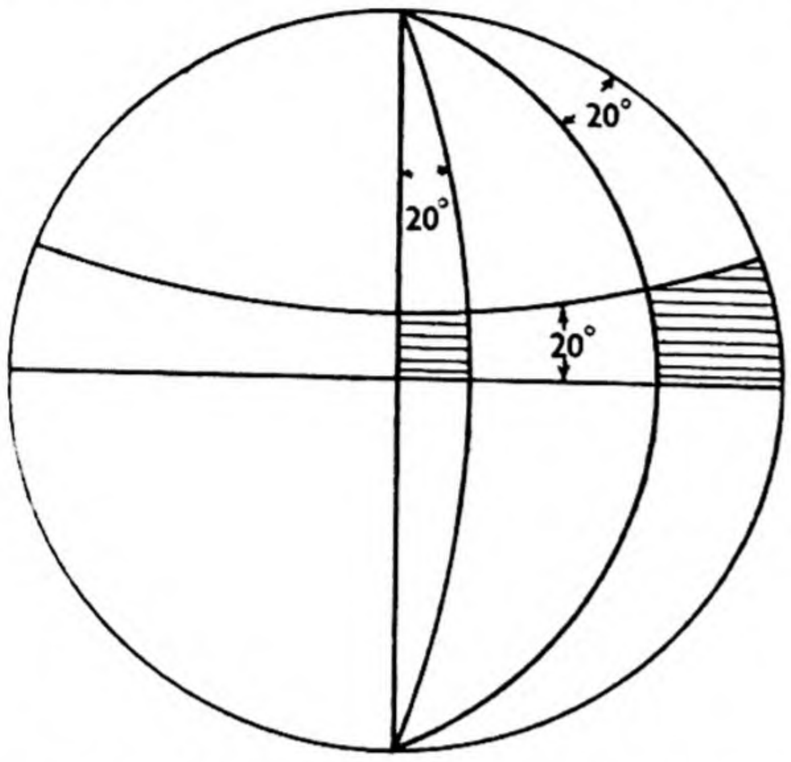

FIG. 22.1. Diagram showing that the stereographic is not an equal-area projection

Zenithal (or Azimuthal) Projection. In this, great circles passing through the point of projection are straight lines, as in the stereogram, and small circles described about the centre of the projection are circles, but all other great circles and all other small circles consist of curves of higher order than the second. Because of this it is difficult to carry out constructions on the equal area projection; but for certain purposes the use of a previously prepared equal-area net is convenient.

The polar net is easily constructed, as can be seen from Fig. 22.2. To obtain the radius of a small circle of angular radius ϕ about the centre of the projection, the chord Np is first drawn; the required radius is the length Np if the plane of projection is tangential to the sphere at N, and is half the length Np if the plane of projection passes through the centre of the sphere. It is clear that $\frac{1}{2}Np = r \,.\, \sin \phi/2$, while the corresponding circle in the stereogram has a radius given by $IP_s = r \,.\, \tan \phi/2$. As a consequence of this, if the same radius of sphere is taken, the diameter of the primitive circle of the equal-area projection will be in the ratio $1/\sqrt{2}$ to the corresponding radius in the stereogram. If it is desired to construct the equal-area projection so that the linear distance from the north pole to the equator is the same as on the stereogram, the radius of the sphere must be taken as $\sqrt{2}$ times that taken for the stereogram.

The construction of great circles which do not pass through the centre, and of small circles about points

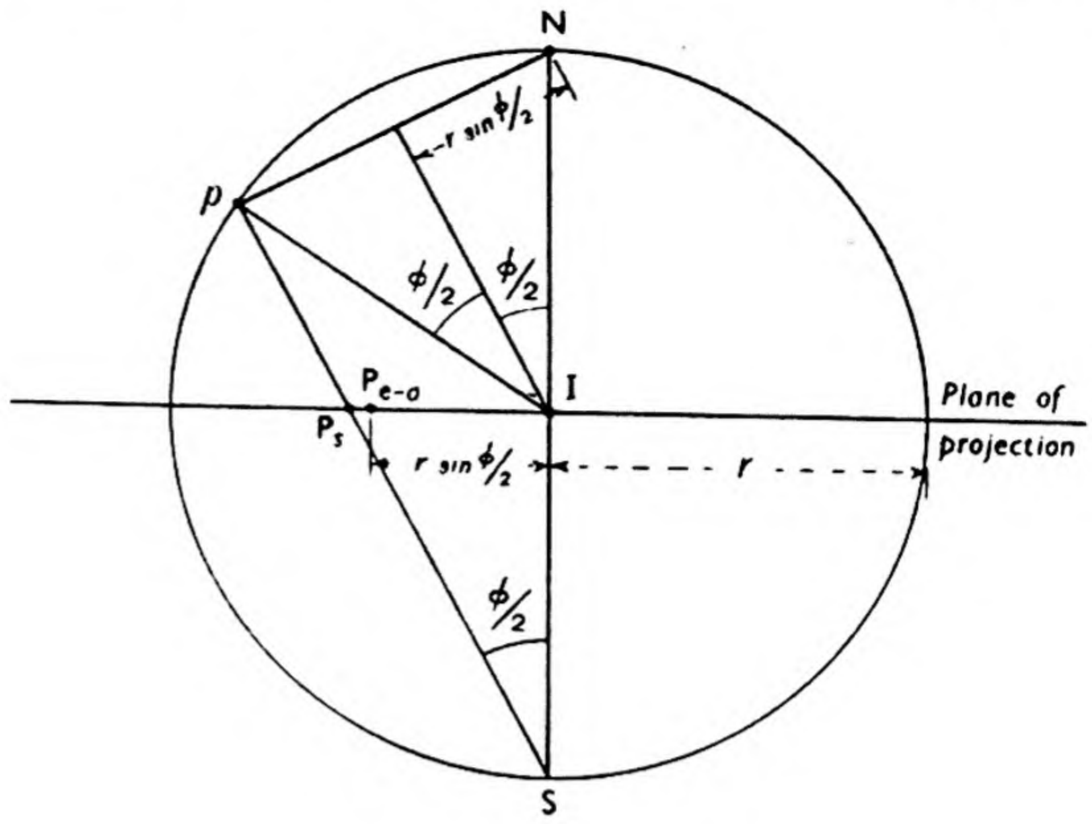

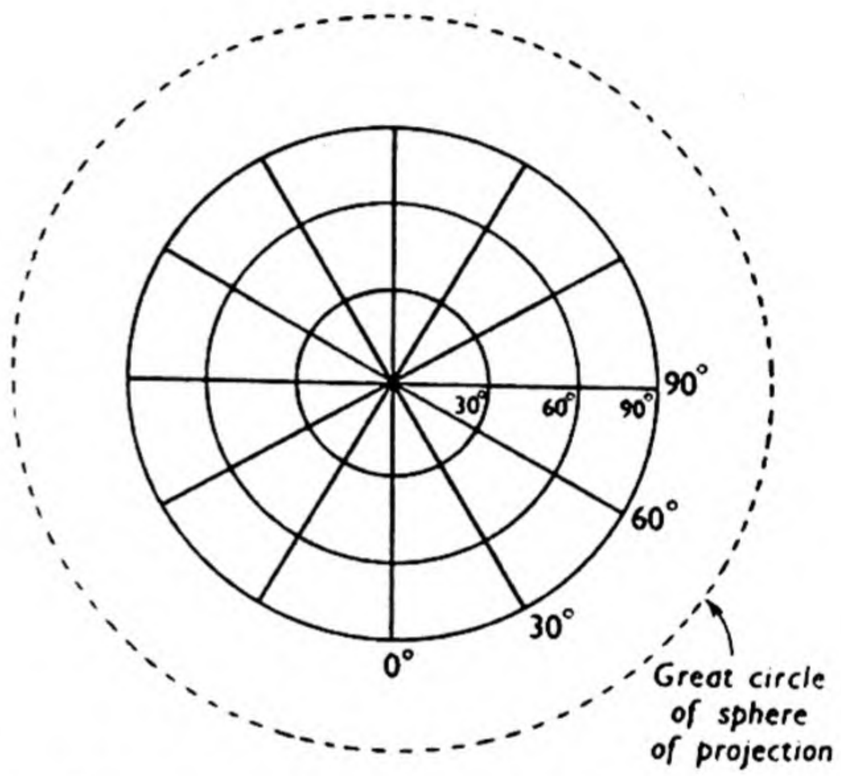

FIG. 22.2. Diagrams illustrating the equal-area projection

on the bounding circle, is tedious, but a graphical method of drawing these is given by Steers (1942), who also gives a proof of the method described above for finding the radii of small circles about the centre of the projection. In Fig. 23 is shown an equal-area net corresponding to the stereographic net of Fig. 20.2.

5.6 Use of projections in crystallography. In **1,** 5.1 mention was made of the use of the orthographic and clinographic projections for showing both the morphological development and the atomic and molecular structure of crystals. The other important use of projections in crystallography lies in the study of the angular relations of crystal directions.

The stereographic projection is the most generally useful in this field for the following reasons:

(*a*) The angle between any two great circles on the sphere is correctly projected on the stereogram (that is, the stereographic projection is angle-true); the whole sphere can be represented on one stereogram.

(*b*) The geometry of the projection is simple, and both great and small circles project as arcs of circles.

This projection is very useful for the representation of faces and zones in morphology, of point groups of symmetry, and of optic axes, vibration directions, etc., in optical work; it is quite indispensable in optical work with the universal stage. In crystal physics it is used in the representation of gliding processes in crystals, and in crystal chemistry for the representation of bond directions linking atoms. In X-ray crystallography the main use of the stereographic projection is to represent the normals to reflecting planes in the study of the orientation of single crystals; it is particularly useful for this when a cylindrical camera is used, because of the wide range of angles required to represent all the spots. An important extension of this use is in the representation of the limits of variation of crystal directions in polycrystalline aggregates such as fibres and foils (Chapter 9). Although any projection of poles is a *pole figure*, this name has come to refer to a stereogram (or an equal-area projection) of a polycrystalline aggregate. A stereogram can also be used for the determination of the orientation of surface markings on crystalline substances, such as Widmanstätten figures on meteorites. The stereographic projection is also used in the drawing of crystals, and this method has advantages over the others mentioned in **1**, 5.2. Perhaps the only disadvantage of the stereographic projection in general is that poles may become crowded together near the centre, but this can be obviated by use of a larger scale.

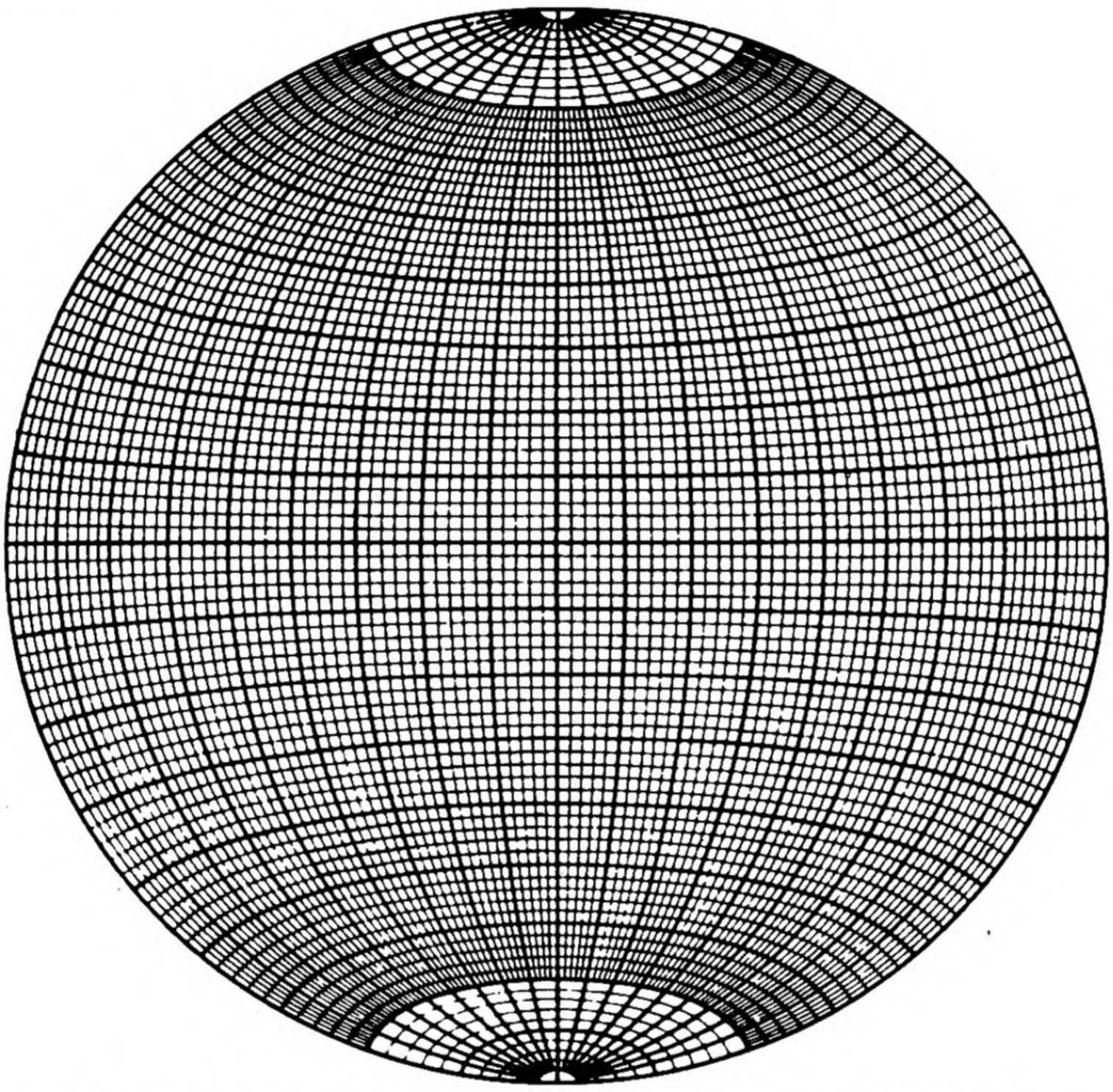

FIG. 23. Equal-area net (Lambert's equal-area azimuthal projection)

The gnomonic projection has been widely used in morphological work and in the interpretation of symmetrical Laue photographs taken on flat plates (Chapter 6). It is used also in the study of Laue photographs for determining the orientation of single crystals (Chapter 8). The orientation of surface markings on crystalline substances is sometimes studied more conveniently on the gnomonic than on the stereographic projection. In morphological work a large-scale gnomonogram is useful in the study of complex zones where, owing to the crowding together of poles, the stereographic projection is at a disadvantage. Another use which the crystal morphologist makes of this projection is in the drawing of crystals from the gnomonogram.

The equal-area projection is used in crystallography for the construction of pole-figures showing the

proportion of crystallites having orientations within a given range in a polycrystalline aggregate. Although the stereographic projection is often used for this purpose, misleading results can be obtained owing to its failure to preserve the ratios of areas existing on the sphere. As standard nets for the equal-area projection can be obtained, the greater difficulty of its construction should not prevent its use for this purpose.

The principal features of the various projections described and their chief uses in crystallography are summarised in the table below.

CRYSTALLOGRAPHIC PROJECTIONS

	PROJECTION	TYPE OF PROJECTION	ADVANTAGES	DISADVANTAGES	MAIN USES
For projecting crystal shapes and structures	ORTHOGRAPHIC	Perspective, of parallel type (projection point at infinity) with projection lines perpendicular to plane of projection: azimuthal (surface of projection is a plane which is normal to the projection line at the centre of the projection, from which point azimuths are correct in the projection)	Parallel lines remain parallel on the projection	Not angle-true; small circles are ellipses in general and are circles only about the centre of projection	Drawing of crystal forms and habits; drawing of crystal structures and of plans of crystal structures
	CLINOGRAPHIC	Perspective, of parallel type but all projection lines are oblique to the plane of projection, hence it is non-azimuthal	Parallel lines remain parallel on the projection	Not angle-true	Drawing of crystal forms and habits; drawing of crystal structures
For projecting crystal directions and angles	GNOMONIC	Perspective, of non-parallel type, azimuthal; point of projection at centre of sphere and the plane of projection can be anywhere except through the centre of the sphere, but is usually taken as tangential to it	Great circles project as straight lines; poles are usually well spaced	Not angle-true; small circles are conic sections and are circles only about the centre of the projection; limited angular range	Indexing of symmetrical Laue photographs; determination of orientation of surface markings on crystals. Morphological work
	STEREOGRAPHIC	Perspective, of non-parallel type, azimuthal; point of projection on the surface of the sphere, and plane of projection perpendicular to the diameter through this point; the plane may be in any such position but is usually taken to pass through the centre of the sphere	Preserves angular truth; all great and all small circles project as true circles, and the projection is therefore easily constructed; complete angular range	Unless scale is large, poles may be crowded together near the centre of the projection	Morphological work; optical work, especially useful with Universal stage; study of deformation in crystals; plotting of normals from X-ray data in the study of orientation; representation of bond-directions in crystal structures
	EQUAL-AREA (LAMBERT'S)	Non-perspective, azimuthal; can be considered as a modified type of stereographic projection *Note*: In all 'azimuthal' projections, bearings are true from the central point of the projection	Preserves true ratio of spherical areas in projection	Is difficult to construct, except the polar net; great circles are complicated curves, except when they pass through the centre of the projection; small circles are also complicated curves, except when they are described about the centre of the projection	Construction of pole figures in the determination of orientation in polycrystalline aggregates such as metals and rocks

CHAPTER 2

X-RAYS

1. Nature of X-rays

1.1 Introduction. X-rays are an electromagnetic radiation and thus fall into the same class of phenomena as visible light. The production of such radiations is associated with the loss of energy of electrons, but far greater energy is needed for the production of one quantum of X-rays than is needed for the production of one quantum of visible light. For example, potential differences of a few hundred volts will produce a visible discharge in a gas, but tens of thousands of volts may be needed to produce X-rays.

The wave-lengths of X-rays are about a thousand times shorter than those of visible light, and this results in great differences between the properties of the two radiations. The transparency of aluminium to X-rays and its opacity to light are a striking example. The two radiations have, however, many features in common, and one of the most important of these is that similar types of diffraction spectra can be produced under certain conditions.

1.2 White radiation. It is common knowledge that white light can be analysed into a spectrum of colours, and that each colour has a different wave-length. In other words, the spectrum of white light consists of a set of wave-lengths varying continuously from one end of the spectrum to the other. Most of the radiation emitted from an X-ray tube is of a similar type and so, by analogy, it is called ' white radiation '.

White radiation is produced in the following way. A high potential, V, of the order of 50,000 volts, is maintained between two electrodes; electrons are introduced into the field, and by virtue of their negative charge, e, they are attracted to the positive electrode. An electron starting from the negative electrode will have an energy eV when it reaches the positive electrode; here it suffers an abrupt stoppage, which gives rise to the radiation of X-rays.

If the energy eV is converted into one quantum of energy, the wave-length λ of the resultant radiation is given by the relation

$$eV = hc/\lambda,$$

where h is Planck's constant and c is the velocity of light. Thus

$$\lambda = hc/eV.$$

By substituting numerical values, we arrive at the relation

$$\lambda = 12{\cdot}4/V,$$

where V is in kilovolts and λ is in Angstrom units 1 A. being equal to 10^{-8} cm.

This relation gives the minimum wave-length that is produced. For example, if an X-ray tube is run at 50 kV., the shortest wave-length of the white radiation is 0·25 A. The white radiation will, however, contain many longer wave-lengths also, for it is only rarely that all the energy of an electron is converted into X-rays. In most cases the electron will lose its energy in several collisions with atoms in the positive electrode before it is brought to rest. It is found that the intensity of X-rays of wave-length greater than the minimum rises sharply, but decreases again for very long wave-lengths. The general forms of the curves relating intensity to wave-length for several different voltages have been obtained experimentally by Ulrey (1918) and are shown in Fig. 25. The curves show the sharp cut-off at the minimum wave-length, the

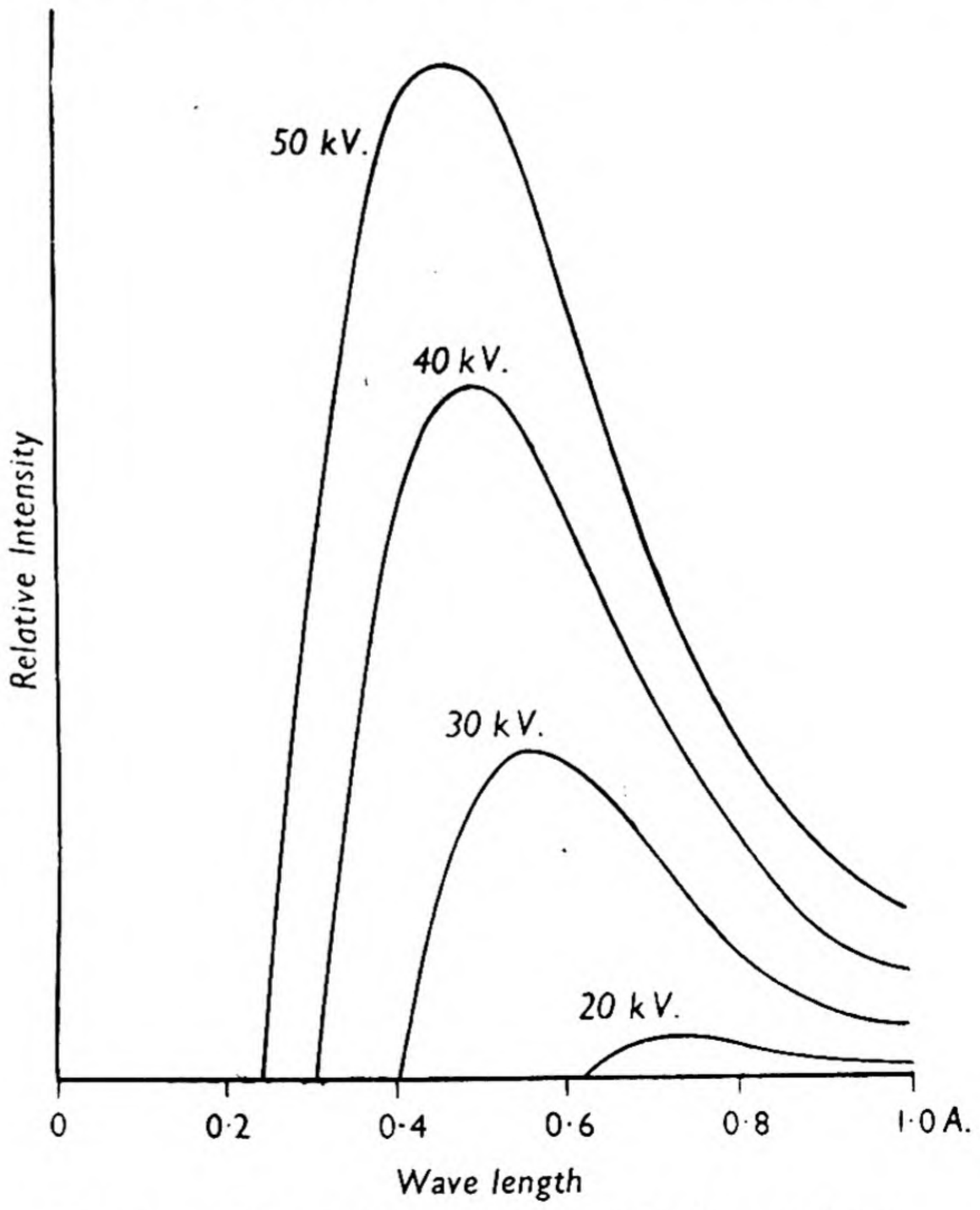

FIG. 25. Distribution of intensity in the continuous spectrum from a tungsten target (after Ulrey)

rise to a maximum, and the more gradual decrease with longer wave-lengths.

1.3 Characteristic radiation. Under certain conditions an optical spectrum consists of a set of lines; that is, it is composed of a set of discrete wave-lengths. For example, the spectrum of light from a simple mercury discharge tube is of this type. The wave-lengths of the lines can be measured extremely accurately and are characteristic of the element producing them; it is often possible to recognize even by eye the nature of the gas producing a certain colour of discharge. In the same way, a radiation that is characteristic of the element forming the positive electrode of an X-ray tube can also be produced. This is called the *characteristic radiation*.

Characteristic X-rays are, of course, also produced by the loss of energy of electrons. This loss of energy is not directly that of the impinging electrons, but of the electrons in the atoms that compose the positive electrode. If the impinging electrons have energy which is great enough, they can dislodge even the most securely-held electrons in these atoms. When such an electron is dislodged, there is a place into which an electron with higher energies can fall. It is the energy released in this process that is converted into characteristic radiation.

The curves shown in Fig. 25 have to be modified in order to represent the state of affairs that exists when characteristic radiation is being emitted. In Fig. 26.1 are shown curves relating intensity and wave-length when X-rays are produced from a molybdenum and from a copper target under a potential difference of 35 kV.; the former curve is due to Ulrey; the latter is hypothetical. Despite the height of the characteristic peaks, the amount of energy they represent is much smaller than that of the white radiation.

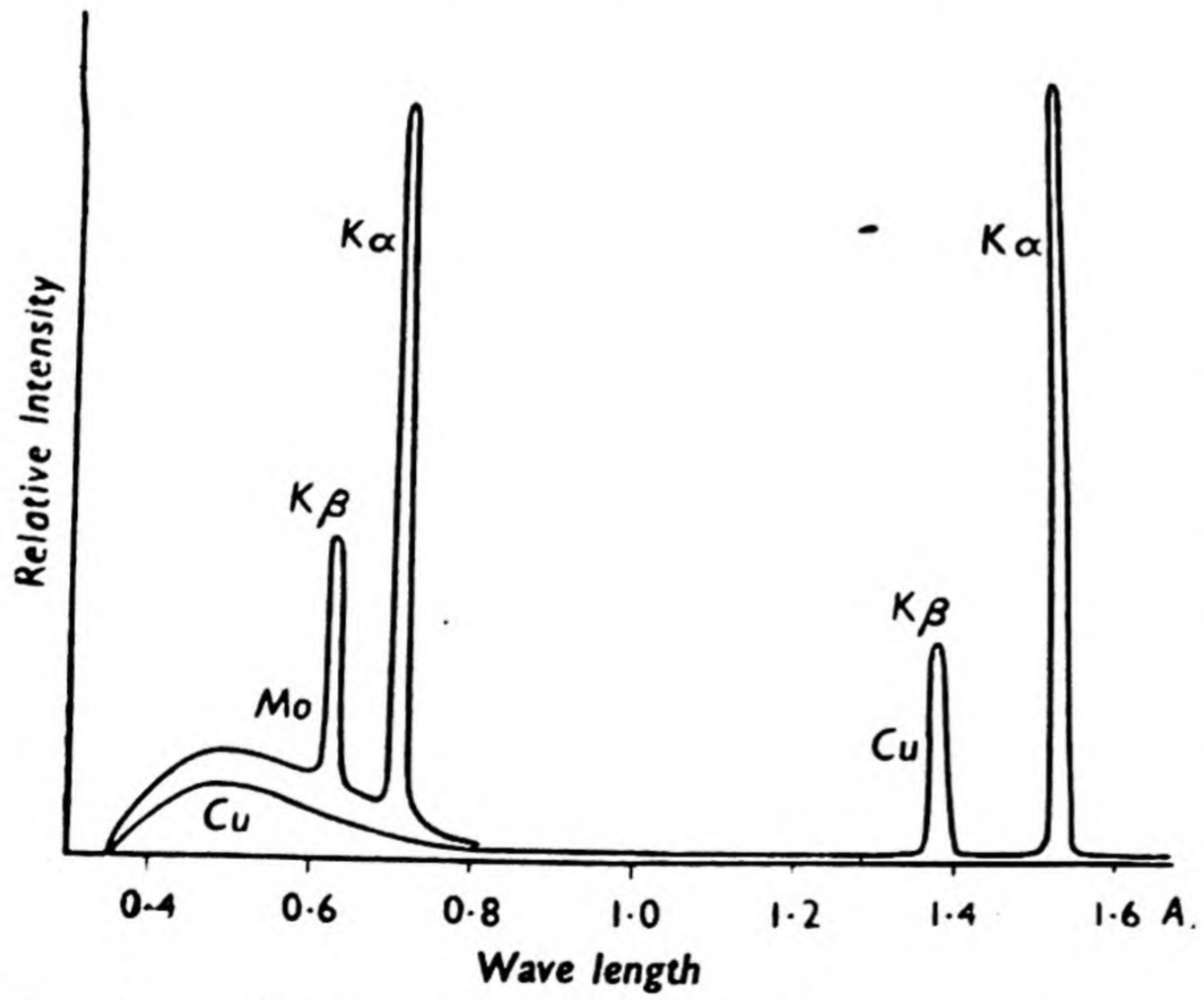

FIG. 26.1. Distribution of intensity in the spectra from targets of molybdenum and copper, with a voltage of 35 kV.

The reason for the relatively small wave-length spread of the characteristic radiations can be seen from a consideration of atomic structures. A particular atom can be considered as a nucleus surrounded by a number of shells or orbits $K, L, M \ldots$ (Fig. 26.2). These shells represent possible energy-levels of electrons, but the number in each shell is limited: K can have 2, L can have 8, M can have 18, and so on. To a first approximation the energies of all electrons in the same shell are equal.

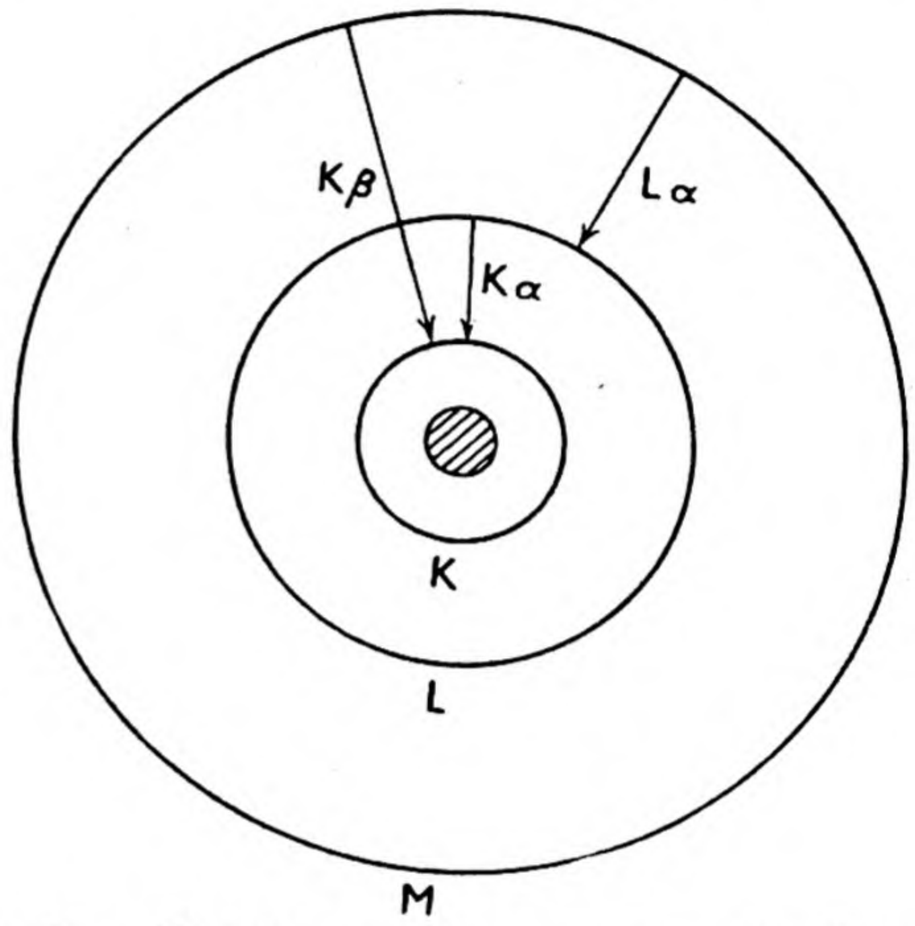

FIG. 26.2. Electronic orbits in an atom, showing transitions associated with the production of characteristic radiation

The K electrons are the most tightly held. When one of these is dislodged another electron must take its place, and it is most likely that one of the L electrons will do so. This electron will lose an amount of energy which is precisely determined by the difference between the energies of the K and L shells; and since this energy will be radiated as one quantum of X-rays, the wave-length will be completely fixed.

The $L - K$ transition is only one possibility, and the existence of other transitions explains why X-ray spectra contain several lines. These lines can be grouped together in series. The K series is that emitted when electrons drop into the K shell; $L - K$ gives $K\alpha$; $M - K$ gives $K\beta$, as shown in Fig. 26.2. In the next series, the transition $M - L$ gives $L\alpha$.

This description of the origin of the characteristic spectra is inaccurate in that the energies of the electrons in one shell are not necessarily exactly equal. The two K electrons have the same energy, but three values are possible in the L shell, and more still in the higher shells. Thus three different energy differences are possible for the $L - K$ transition, but one of these

is associated with forbidden transitions and so only two occur. This explains why the $K\alpha$ line is a doublet.

There are also some faint lines the existence of which does not fit in with the theory (Cauchois and Hulubei, 1947). Since they account for only about one per cent of the total intensity of the K spectrum and since their origin is still uncertain, it is not proposed to discuss them here.

The magnitudes of the voltages V necessary to excite the characteristic radiations of an element are also simply explained in terms of the atomic model. It is obvious that in order to produce K radiation the impinging electrons must have an energy great enough to dislodge the K electrons from the atoms. The voltage necessary to give the electrons the required energy is called the *excitation voltage*. All the lines of a given series will be emitted as soon as the excitation voltage is reached; it is impossible to excite, for example, the $K\alpha$ lines without the $K\beta$ lines. This follows directly from the theory, for the production of the lines of the K series depends only upon the dislodgement of the K electrons.

Excitation potentials of several different K radiations are given in Table 1. It is customary to use much higher voltages than those required for excitation, to ensure a reasonable intensity of characteristic radiation. On the other hand, if too high a voltage is used a great deal of white radiation is produced. The voltages recommended in Table 1 form a reasonable compromise between these two conditions but they are not very critical; for example, 35 kV. is often used for copper $K\alpha$ radiation instead of the recommended 50 kV., and a deviation of about this magnitude will not produce any great difference in the quality of the photographs taken, although it will increase the time of exposure.

2. Production of X-rays

2.1 The two types of tubes. An X-ray tube must consist of at least two electrodes across which a high potential can be maintained, and some arrangement for producing electrons. There are two main ways in which such a supply of electrons can be produced, and the corresponding X-ray tubes are called the *gas tube* and the *hot-cathode tube*.

2.2 The gas tube. In the gas tube the space between the electrodes is evacuated to a pressure of about 0·01 mm. of mercury; this pressure is maintained by allowing air to enter through a regulated leak. Under the conditions of operation there are enough gaseous ions to start a discharge, which consists of negatively-charged electrons and positively-charged ions moving under the action of the field; the electrons strike the anode and so produce X-rays. Such a tube provides a simple and effective source of X-rays.

The main features of a gas tube are shown in Fig. 27. The cathode is made of a light metal such as

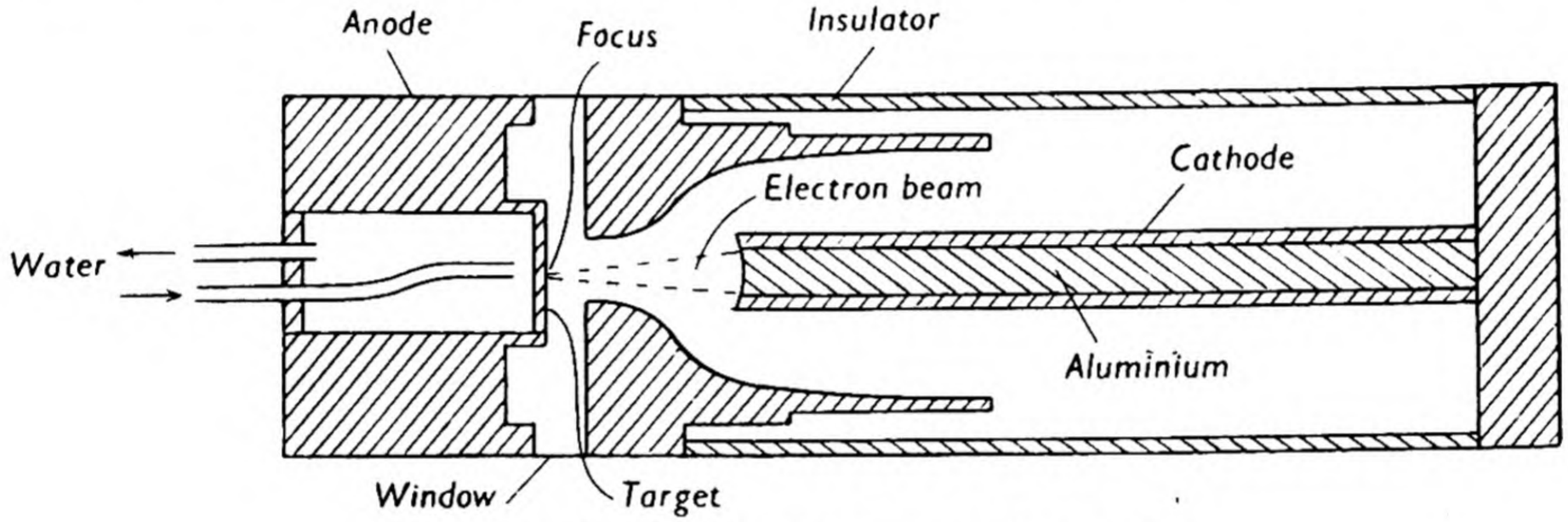

FIG. 27. The main features of a gas X-ray tube

aluminium, which has been found by experience to produce electrons easily under positive-ion bombardment. The part of the anode on which the electrons fall is called the *target* or the *anticathode*; the part of the target from which the X-rays are produced is called the *focus*.

Much heat is produced in the target, which must be kept cool by a continuous stream of water. Some heat may also be produced in the cathode by the positive-ion bombardment, but the natural cooling by radiation is usually sufficient to dissipate this without too great a rise in temperature.

2.3 The hot-cathode tube. In the hot-cathode tube the vacuum is sufficiently good to prevent any appreciable discharge in the residual gas; the pressure should be less than about 0·0001 mm. of mercury. The electrons required to produce X-rays are supplied by emission from a hot tungsten filament. The main features of a hot-cathode tube are shown in Fig. 28.1.

One of the advantages of the hot-cathode type of tube is that it can be permanently evacuated, and so no pumping equipment is necessary. A permanently

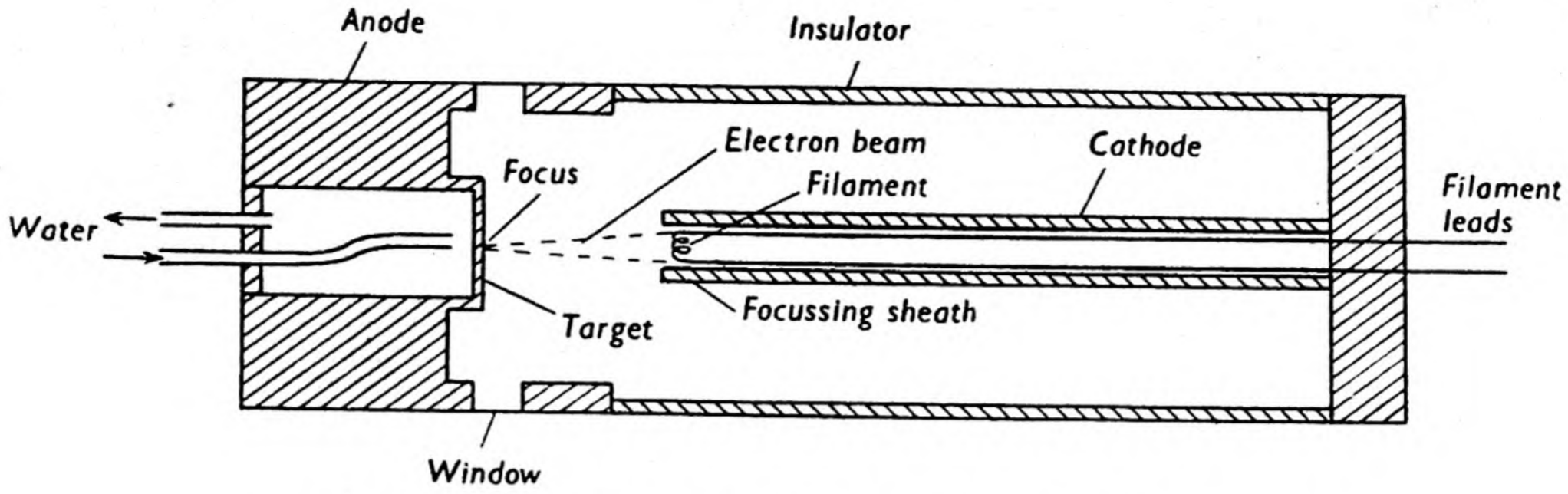

FIG. 28.1. The main features of a hot-cathode X-ray tube

evacuated hot-cathode tube forms the most trouble-free source of X-rays, and there are several varieties of commercial tubes on the market.

On the other hand, there are advantages in making even hot-cathode tubes continuously evacuated, and so demountable. They can be made in an ordinary workshop, if necessary, and mishaps such as the puncturing of a target or the burning-out of a filament can be easily remedied. Most important of all, targets of different metals can be used in the same tube. In the study of the structures of metals and alloys it is almost a necessity to have many different radiations available, as described in **13**, 3.3.

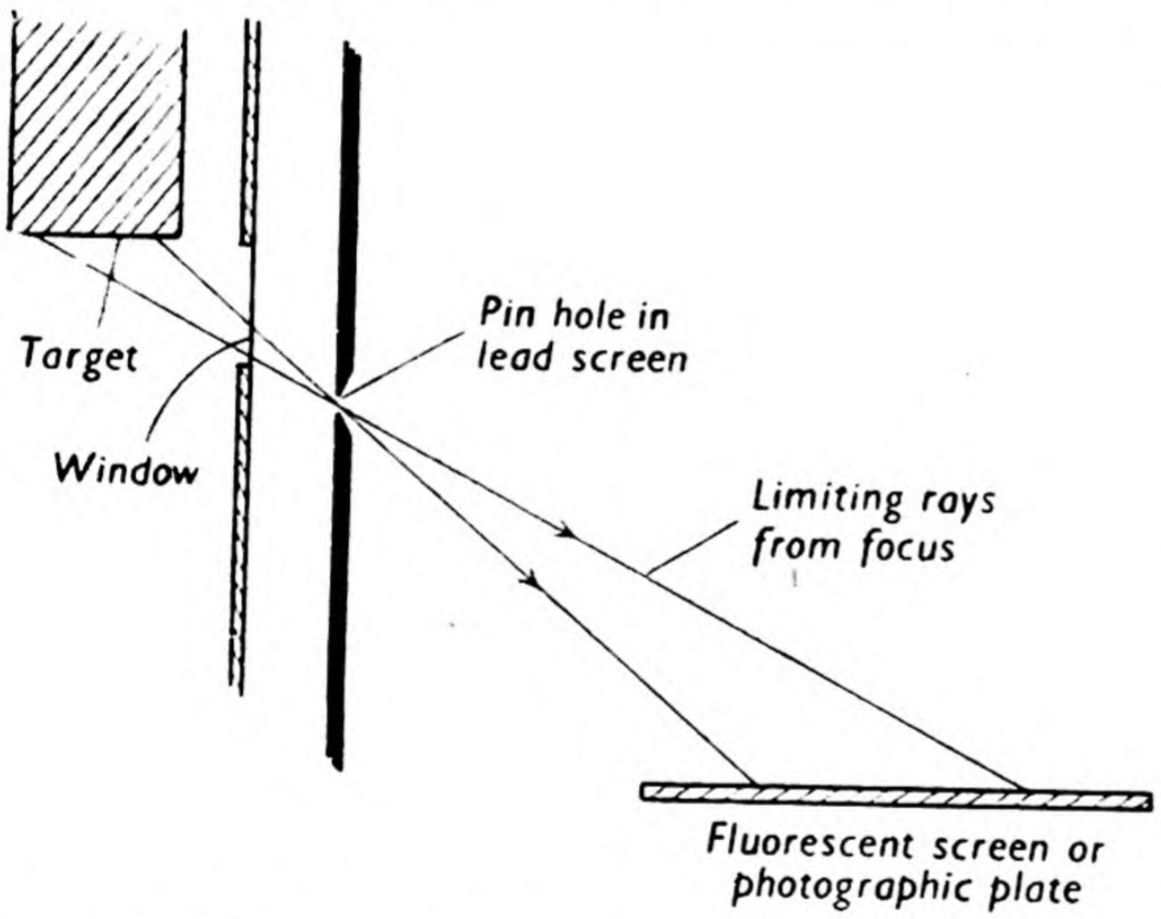

FIG. 28.2. Pin-hole method of examining the focus in an X-ray tube

The main disadvantage of the hot-cathode tube is that tungsten from the filament is gradually deposited upon the internal surfaces. Its deposition upon the target causes the radiation to be contaminated by tungsten L radiation (**2**, 1.3) and its deposition on the windows reduces the intensity of the beam. In a demountable tube this can be remedied by cleaning or replacing the target and windows; but in a sealed-off tube there is no real remedy. The filters used for several of the β-radiations (**2**, 5.5) will remove the tungsten L radiation also, so the presence of this is not a grave problem, but the user of a sealed-off tube must be prepared for a gradually decreasing efficiency during its life.

It is desirable to have some simple and quick method of viewing the focus in an X-ray tube, particularly in a demountable tube. A pin-hole camera, the principle of which is illustrated in Fig. 28.2, will be found useful for this purpose.

3. X-ray Wave-lengths

3.1 Accuracy of measurement. Great use is made of the ease of production of the characteristic radiations and the constancy of their wave-lengths; there are very few physical quantities that can be so relied upon to be independent of the conditions under which they are produced.

The wave-lengths of the important lines in the X-ray spectra of the elements have been measured on a relative scale to within about $\pm 0{\cdot}001$ per cent, chiefly by Siegbahn's school (1925) and by Bearden and Shaw (1935); but when measurements of this order of accuracy are required, it is essential that certain properties of the spectra should be taken into account. In the first place the lines are by no means strictly monochromatic. Fig. 28.3, drawn from data given by Spencer (1931), shows the distribution of

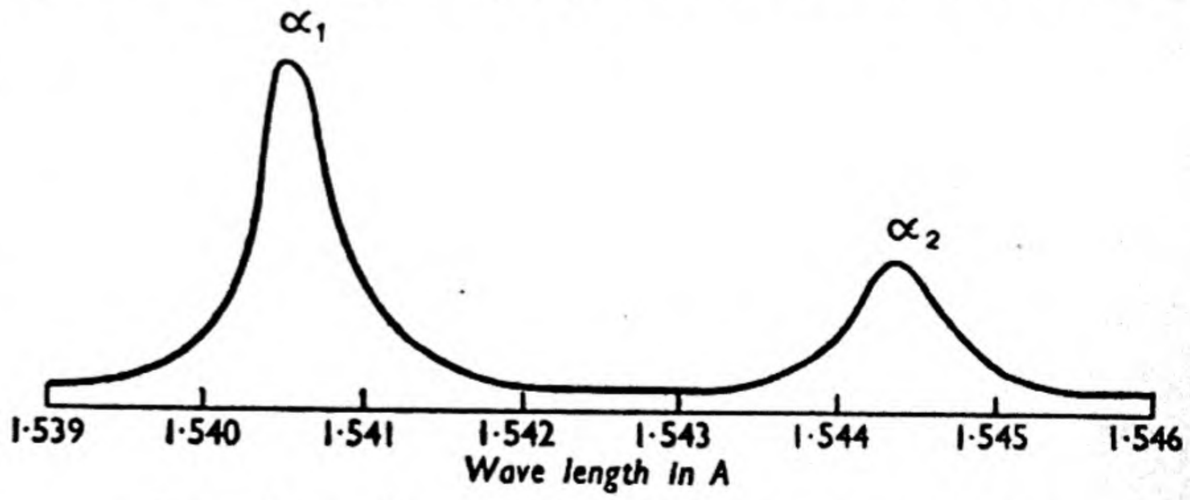

FIG. 28.3. The distribution of intensity in the doublet Cu$K\alpha_1\alpha_2$

wave-lengths in the copper $K\alpha$ doublet, and it will be seen that the spread is quite considerable. Secondly, the lines are not quite symmetrical and so the wave-lengths corresponding to the peaks do not coincide with the wave-lengths corresponding to the centres of gravity. The methods of measurement of the wave-lengths given in the literature are such that the values probably correspond to the peaks, but for most ordinary work the wave-lengths corresponding to the centres of gravity would be more directly useful. The difference between the two measurements for copper $K\alpha$ is about 0·003 per cent.

3.2 Units. Siegbahn (1925) pointed out that one could not expect as great an accuracy in absolute measurements since they were based on less-accurately determinable constants such as e, the electronic charge. He therefore adopted a unit for wave-length descriptions and made it as near to 10^{-11} cm. as the current values of the physical constants allowed. This he called the *X-unit* ; it is defined as 1/3029·45 of the {200} spacing of calcite at 18° C.† This unit has been universally adopted, but it has been largely forgotten that the X-unit is not an absolute one ; the common practice has been to express results in 'Angstrom units' (1 A. = 10^{-8} cm.), although they are really in thousands of X-units. (Wilson (1943, *a*) has suggested that this unit be called the 'kilo X-unit,' kX.) This practice, however, has not led to any confusion, because in calculating, for example, the number of atoms in a unit cell, any error in e would be eliminated (Lipson and Riley, 1943).

It is now possible, however, to measure X-ray wave-lengths absolutely to an accuracy of about 0·003%, by diffraction from ruled gratings (Bearden, 1941), and it is found that the X-unit is larger than 10^{-11} cm. by 0·2%. The values of the fundamental constants have been modified in the light of this discrepancy, and therefore the X-scale should not be used in conjunction with the latest values of these constants, such as those given by Birge (1941). For absolute calculations the wave-lengths in X-units should be multiplied by $1{\cdot}00202 \times 10^{-3}$ in order to convert them to Angstrom units.

A table of some of the more useful wave-lengths is given in Table 1.

4. Refraction of X-rays

The wave-lengths of X-rays are altered by refraction when they pass from one medium to another.

† The X-unit is defined in practice as 1/3029·04 of the effective {200} spacing of calcite at 18° C. The phrase 'effective spacing' has to be used because, owing to the refraction of X-rays within the crystal (**2,** 4), it is the quantity used in the equation $\lambda = 2d_{200} \sin\theta$. The use of the effective spacing is a simple way of making the correction for refraction, and is of importance only in the measurement of wave-lengths. For a note on the {200} spacing of calcite see **10,** 3.7.

Since the wave-lengths given in Table 1 are those *in vacuo*, there will be slight differences within the diffracting crystal. The differences are, however, very small since the refractive indices of ordinary materials for X-rays differ from unity by a quantity of the order of 10^{-5}. Values of some typical refractive indices are given below from data by Bragg (1933) ; it will be observed that they are less than unity.

REFRACTIVE INDICES OF SOME SUBSTANCES FOR X-RAYS

λ in A.	Substance	n (observed)
0·52	Glass	0·9999991
0·71	Calcite	0·9999980
0·71	Speculum	0·9999952
1·54	Glass	0·9999919
1·93	Glass	0·9999876

The effect of refraction on the accurate measurement of cell dimensions is considered in **13,** 2.5.

The refractive index, n, of a material can be obtained from the formula :

$$1 - n = \frac{Ne^2\lambda^2\rho\Sigma A}{2\pi mc^2\Sigma W}.$$

N, Avogadro's number
e, electronic charge
m, mass of electron
c, velocity of light
λ, wave-length of X-rays
ρ, density of material
ΣA, sum of atomic numbers of constituent elements per unit cell
ΣW, sum of atomic weights of constituent elements per unit cell

On substituting numerical values, this becomes :

$$1 - n = 2{\cdot}71 \times 10^{-6}\lambda^2\rho\Sigma A/\Sigma W,$$

where λ is in A.

5. Absorption of X-rays

5.1 Absorption coefficients. When a beam of X-rays passes through matter it is partly transmitted, partly scattered and partly transformed into other forms of energy. These processes are summarized below.

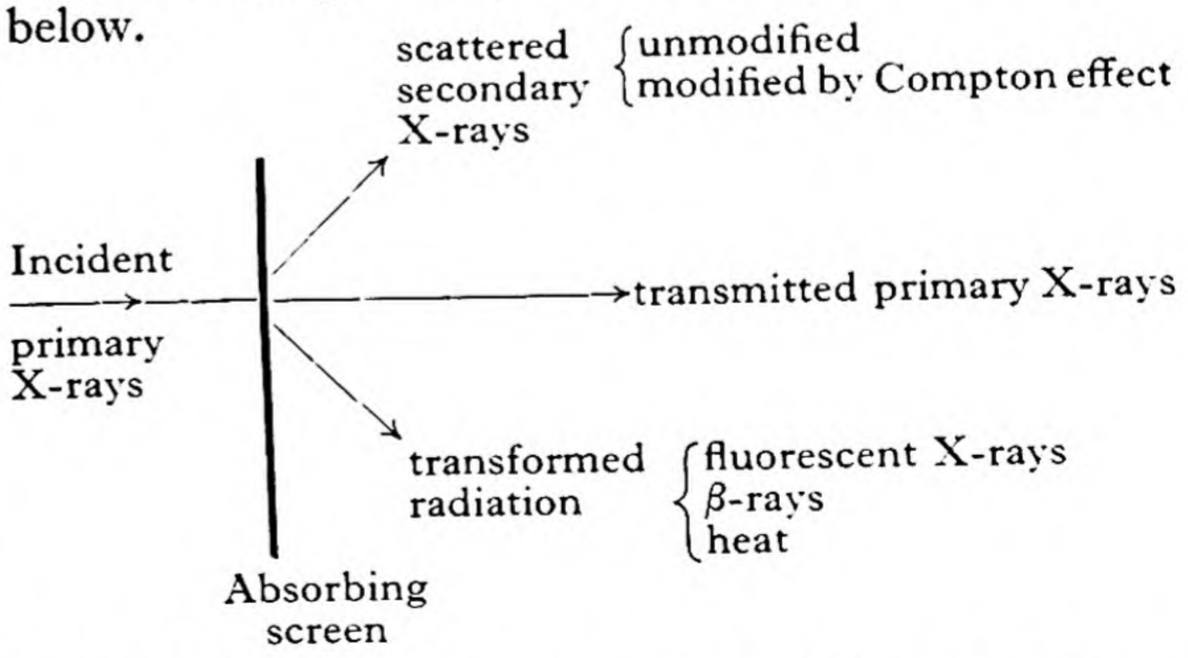

The diffraction of X-rays by crystals is a special case of the scattering of unmodified X-rays.

When a beam of monochromatic X-rays is allowed to pass through an absorbing screen of thickness t, it is found that the intensity, I, of the original wave-length transmitted, is related to the incident intensity I_0 by the relation

$$I = I_0 \exp.(-\mu t),$$

where μ is a constant called the *linear absorption coefficient*. This is merely a statement of the fact that equal thicknesses of a given absorber reduce the intensity by the same ratio.

The constant μ takes into account both the scattered and transformed radiations and is not easily calculated theoretically. The values of μ for most of the elements have, however, been measured, and these provide a basis for calculating the linear absorption coefficient of any compound the composition of which is known. The linear absorption coefficient of an element is not, however, an absolute quantity; it depends on the physical state of the element. For example, it would be much less for the gaseous than for the solid state. Other absorption coefficients which are independent of the state of the element have been devised and values of these for most of the elements are given in Tables 3 and 4.

All absorption coefficients are based on the above equation, but they differ in the method of measuring the quantity t, which should be regarded rather as a measure of a quantity of matter than as a length. For the linear absorption coefficient, μ, t is measured in centimetres. For the *mass absorption coefficient*, μ_m, t is taken as the number of grams per square centimetre; μ_m is therefore equal to μ/ρ, where ρ is the density. For the *gram-atomic absorption coefficient*, μ_g, t is taken as the number of gram atoms per square centimetre; μ_g is therefore equal to $\mu_m W$, where W is the atomic weight. For the *atomic absorption coefficient*, μ_a, t is taken as the number of atoms per square centimetre; μ_a is therefore equal to $\mu_m W/N_0$, where N_0 is Avogadro's number. The coefficients μ_m, μ_g and μ_a of an element are all independent of the physical state of that element.

The mass absorption coefficient (Table 3) is specially useful for calculating the linear absorption coefficients of materials the compositions of which are known in terms of the fractions p, by weight, of the component elements. The expression is

$$\mu = \rho \Sigma p \mu_m,$$

where ρ is the density of the material. For example, suppose we require the linear absorption coefficient for copper $K\alpha$ radiation of an alloy containing 77 per cent silver and 23 per cent zinc. The density of the alloy is 9·57 gm./c.c. and the mass absorption coefficients of silver and zinc for this radiation are 223 and 59 cm.^{2}/gm. respectively.

Thus $\mu = 9{\cdot}57(0{\cdot}77 \times 223 + 0{\cdot}23 \times 59)$ cm.$^{-1}$

$= 1773$ cm.$^{-1}$.

In dealing with compounds, it is more usual to be given the relative numbers, n, of the atoms present. The values of the gram-atomic absorption coefficients are then of most direct use, since the formula for the linear absorption coefficient is

$$\mu = \frac{\rho \Sigma n \mu_g}{\Sigma n W},$$

where ΣnW is the sum of the atomic weights of the elements concerned. For example, suppose we require the linear absorption coefficient for copper $K\alpha$ radiation of $BaCO_3$, of which the density is 4·43 gm./c.c. The values of μ_g for Ba, C and O are 49300, 66 and 203 respectively.

Thus $\mu = \dfrac{4{\cdot}43\,(49300 + 66 + 3 \times 203)}{137{\cdot}4 + 12{\cdot}0 + 3 \times 16{\cdot}0}$ cm.$^{-1}$

$= 1122$ cm.$^{-1}$.

The atomic absorption coefficient μ_a is employed when the volume V of the unit cell and its contents are known. The formula is

$$\mu = \Sigma \mu_a / V,$$

where the summation is taken over all the atoms in the unit cell, and V is in c.c. It is rarely necessary to calculate linear absorption coefficients in this way since the density of a material is usually more readily obtainable than its cell dimensions. Values of μ_a are therefore not given in this book, but they can be obtained, if required, from the *International Tables* (1935, Vol. 2, p. 579).

The mass absorption coefficient of a given element usually increases rapidly as the wave-length of the radiation increases. It is often stated that μ_m is proportional to λ^3, and this is accurate enough for most purposes. Thus to find the mass absorption coefficient for a wave-length not given in Table 3, the value for the nearest wave-length should be taken and multiplied by the ratio of the cubes of the two wave-lengths concerned. This method will be accurate only if the wave-lengths are approximately equal; there is no general law that will apply to all the elements, and μ_m is often more nearly proportional to $\lambda^{2{\cdot}5}$ than to λ^3. There are, however, important exceptions to this rule, produced by the discontinuities known as absorption edges.

5.2 Absorption edges. Suppose we plot the values of μ_m given in Table 3 for a given element, say iron, against wave-length. We find that a smooth curve cannot be drawn through them; the values for Zn$K\alpha$, Cu$K\alpha$ and Ni$K\alpha$ fall well above the curve through the others. Experiment shows that the

change in the curve is not a gradual one but occurs at a definite value of λ, so that the curve relating μ_m and λ has the form shown in Fig. 31. The discontinuity is known as an *absorption edge*.

The existence of absorption edges can be simply explained in terms of the theory of X-ray emission outlined in this chapter. The first process necessary for the production of the K series of spectra is the dislodging of a K electron from its shell. Although this is usually achieved by bombardment with electrons, it can also be achieved by the absorption of X-radiation, the only condition necessary being that the quantum of energy of the exciting radiation shall be greater than the energy required to dislodge the K electron. If λ is larger than a certain value, the

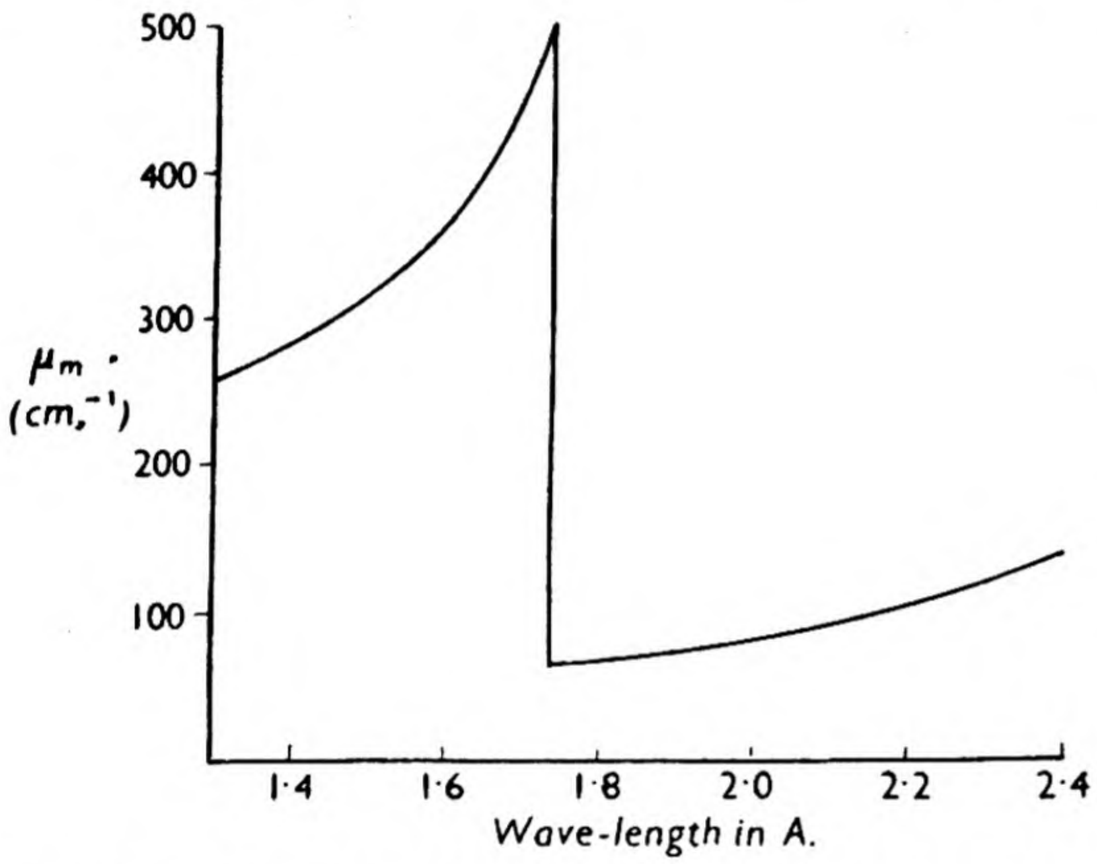

FIG. 31. The mass absorption coefficient of iron as a function of wave-length

quantum hc/λ may be too small to satisfy this condition; but as λ decreases, the quantum will increase and a value will be reached which is sufficient to dislodge the K electron.

Three effects will then occur:

(*a*) The absorption will increase suddenly because the energy of the incident rays is almost all taken up in dislodging the K electrons. This is the absorption-edge effect.

(*b*) Characteristic K-radiation will be emitted from the material irradiated, since another electron must drop into the place of the one dislodged. This is called *fluorescent radiation*, and is always of *longer* wave-length than the exciting radiation.

(*c*) The scattering power of the material will change. This is discussed in more detail in **15,** 3.2.

It will be seen that the wave-length of the absorption edge is necessarily shorter than that of any line in the spectrum excited, since the quantum of energy required to remove the K electron completely from the atom must be greater than that emitted when an electron from another shell drops into the K shell.

5.3 Choice of radiation for a given specimen. The absorption-edge effects make it imperative that careful consideration be given to the choice of radiation for a particular problem. If λ is less than that of the absorption edge, the large absorption will cause the reflections to be weak, as can be seen from **15,** 2.4. Moreover, the fluorescent radiation emitted from the specimen will produce a heavy background. The resulting photograph will not be clear, and in the worst cases may be impossible to interpret. For example, the wave-length of the K absorption-edge of iron is 1·74 A.; that of Cu$K\alpha$ radiation is 1·54 A.: thus Cu$K\alpha$ radiation is quite unsuitable for taking photographs of specimens that contain a large amount of iron.

The photographs will improve in quality as the gap between the absorption edge of the specimen and the wave-length of the incident radiation increases. If the absorption edge is such that the fluorescent radiation is easily absorbed by the air in the camera, there will be no noticeable effect; this is the case when photographs of aluminium are taken with Cu$K\alpha$ radiation, although the wave-length of Cu$K\alpha$ is less than the wave-length of the K absorption edge of aluminium (7·9 A.). On the other hand, if photographs of iron are taken with Mo$K\alpha$ radiation, the wave-length of which is less than that of the absorption edge of iron, the fluorescent radiation from the iron is not appreciably absorbed in the air, and consequently fogs the film.

5.4 Use of screens. It may be possible to eliminate the effect of fluorescent radiation partly or almost completely by interposing a layer of suitable absorbing material between the specimen and the film. Such a layer is called a *screen*, to distinguish it from a *filter*, which is an absorbing layer placed between the X-ray tube and the specimen. The wave-length of the fluorescent radiation is always greater than that of the exciting radiation and is therefore more absorbed by any ordinary screen. For example, a screen of aluminium, 0·2 mm. thick, will reduce the intensity of Mo$K\alpha$ radiation (0·71 A.) by a factor of 0·875, but will reduce that of Fe$K\alpha$ radiation (1·93 A.) by a factor of 0·007. Thus photographs of iron taken with Mo$K\alpha$ radiation are much improved by the interposition of such a screen between the specimen and film.

Although this method is a general one, it becomes difficult to apply when the difference between the wave-lengths of the exciting and excited radiations is small.

5.5 Filters for β-radiation. The interpretation of X-ray photographs is often simplified by the removal of the β-radiation. This can be achieved

by passing the radiation through a filter that has an absorption edge between the wave-lengths of the α- and β-radiations. The thickness of material necessary to reduce the intensity of the transmitted β-radiation to any desired fraction of the intensity of the incident β-radiation can be calculated by the methods described in **2,** 5.1. Such filters should reduce the intensity of $K\alpha$ by about one half.

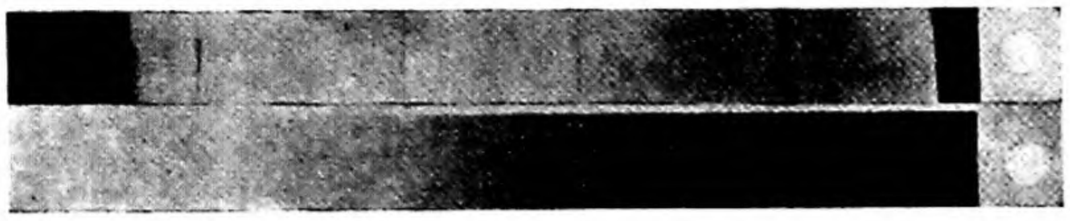

FIG. 32. Two powder photographs of iron using zinc $K\alpha$ radiation. Upper photograph taken with a screen of copper 0·004 cm. thick covering all except the ends of the film, lower photograph taken without any screen, the exposures being adjusted to give equal backgrounds

It is sometimes possible to remove the fluorescent and β-radiations by the same absorber, with a consequent reduction in exposure time. This is achieved by omitting the filter and using the material of the β filter as a screen around the specimen. For example, if Zn$K\alpha$ radiation is used to examine a specimen containing iron, a screen of copper of thickness 0·004 cm. may be used ; the effect of such a screen is shown in Fig. 32.

6. Crystal-reflected Radiation

While a filter can be made to absorb completely the β-radiation from a target and most of the neighbouring wave-lengths, it will not remove all the white radiation ; owing to the greatly reduced absorption of the very short wave-lengths, much of the white radiation will be transmitted. This will produce pronounced streaks on single-crystal photographs and will increase the background on powder photographs ; in both types of photograph important detail may be obscured.

These difficulties can be overcome by using the radiation reflected from a crystal as the incident beam for the specimen. Naturally a crystal that gives a strong reflection should be used, and details of some of those that have been suggested are given below.

SOME CRYSTALS FOR USE AS REFLECTORS, WITH BRAGG ANGLES FOR VARIOUS $K\alpha$ RADIATIONS

CRYSTAL	REFLECTION	RADIATION, $K\alpha$						
		Mo	Cu	Ni	Co	Fe	Mn	Cr
β-alumina	00·2	1·8°	3·9°	4·2°	4·6°	4·9°	5·4°	5·8°
Gypsum	020	2·7	5·8	6·3	6·8	7·3	8·0	8·7
β-alumina	00·4	3·6	7·9	8·5	9·1	9·9	10·8	11·8
Pentaerythritol	002	4·7	10·1	10·9	11·8	12·8	13·9	15·2
Quartz	10·1	6·1	13·3	14·4	15·6	16·9	18·4	20·1
Fluorite	111	6·5	14·1	15·2	16·5	17·9	19·5	21·3
Urea Nitrate	002	6·5	14·2	15·3	16·6	18·0	19·6	21·4
Calcite	200	6·7	14·7	15·8	17·1	18·6	20·3	22·2
Rocksalt	200	7·2	15·9	17·1	18·5	20·1	21·9	24·0
Diamond	111	9·9	22·0	23·8	25·8	28·1	30·8	33·9

From this list a crystal can usually be chosen to fulfil the requirements for a particular investigation. For general work, where an intense and not very narrow beam is required, pentaerythritol and urea nitrate are suitable ; they decompose, however, under the action of X-rays, and have to be replaced when their efficiency is found to have decreased appreciably. If a particularly narrow beam is required, as for the study of small-angle scattering (**16,** 4.2), more perfect crystals, such as quartz, calcite or β-alumina, should be used (Lipson, Nelson and Riley, 1945). For cameras that make use of convergent or divergent radiation (**11,** 4.3) a strong beam of crystal-reflected radiation can be obtained from a bent crystal ; quartz (Johansson 1933) is eminently suitable, as it can be bent elastically, and plastically-bent rock salt has also been employed (Bozorth and Haworth 1938).

With all these crystals, however, a problem arises that may have an important bearing on certain types of work ; the reflected beam contains wave-lengths that are submultiples of that of the reflected characteristic radiation. This arises because when the crystal is set to reflect a beam of wave-length λ, the reflecting planes will also reflect the wave-length $\lambda/2$ in the second order, the wave-length $\lambda/3$ in the third order, and so on. These wave-lengths are called *harmonics*. Under ordinary conditions of operation of a tube with a copper target, some harmonics may be near the peak of the white radiation (**2,** 1.2) and so may be quite intense. For photographic work their presence may not be serious since, for equal intensity, the blackening produced in a photographic emulsion is smaller for shorter wave-lengths ; but for quantitative work with the ionisation spectrometer it is essential that harmonics be eliminated. They can always be eliminated by making the potential on the tube such that the harmonic wave-lengths are not emitted, but since this would mean that a potential less than twice the excitation potential of the characteristic radiation (**2,** 1.3) must be used, this practice is not recommended. The alternative is to use a reflection for which the higher orders are all of negligible intensity. This again is only possible to a limited extent, but by combining the two methods of eliminating harmonics a considerable amount of success can be achieved. If the (111) planes of crystals such as diamond or fluorspar are used, the second order 222 is of inappreciable intensity, and so the first harmonic that can occur is $\lambda/3$. To eliminate this, the X-ray tube must be run at less than three times the excitation potential of the characteristic radiation. For Cu$K\alpha$ radiation this is still only 24 kV., and with this potential the characteristic radiation would constitute only a small fraction of the total radiation emitted by the tube. It will therefore be seen that sacrifices have to be made to achieve a beam of complete purity. Another factor

which must be considered in quantitative work is the partial polarisation of the beam reflected from a crystal used as a monochromator.

7. Precautions against Harmful Effects of X-rays

It is very important that all who work with X-rays should be aware of their harmful effects. The harder X-rays (those of shorter wave-length) are used in medical radiography, but are harmless only when the dosage is strictly controlled. Particularly harmful are the softer X-rays (those of medium or long wave-length), as these are strongly absorbed in the body tissues. It is these X-rays that are commonly used in crystallography, and a brief exposure of any part of the body to the direct beam from an X-ray tube such as is used for diffraction work can produce a serious burn which is very slow in healing. Perhaps more dangerous because unnoticed is the insidious effect of repeated small doses of X-rays, as these are cumulative. Such repeated small doses damage the tissue which produces the white blood corpuscles and later, also, that which produces the red blood corpuscles. These effects can be detected at an early stage by a ' blood count'.

X-ray tubes should be shielded in such a way that neither direct nor scattered radiation reaches a person working with the tube in the usual manner. In this connection it should be remembered that X-rays are produced to some extent in parts of the tube other than the target and that they come off at all angles from the target. Tests can be carried out either by photographic methods or by means of an ion counter. Lead is the most generally useful screening material, and the thickness required increases with the applied voltage because of the more penetrating short-wave X-rays produced at higher voltages.

If vacuum-tube rectifiers are used in connection with an X-ray tube, they should be frequently tested also. Towards the end of the useful life of such a rectifier it is specially liable to emit X-rays.

Ventilation is another important matter. Many X-ray tubes are housed in badly ventilated rooms or cellars. Proper forced ventilation should be installed in every X-ray room, particularly if the apparatus is not as free from brush discharge as it should be, because fumes are then produced to a considerable extent. Precautions of this kind should be observed, especially when young workers are involved.

The chief precautions to be observed are as follows :

1. All parts of the tube should be screened with lead sheet which should be at least 1mm. thick for peak voltages not exceeding 75 kV.
2. Proper ventilation should be installed.
3. Systematic blood counts should be carried out every few months on all workers concerned.

The most convenient sources of information on X-ray protection and on the recommended procedures are, Recommendations of the British X-ray and Radium Protection Committee (1948) and *Handbook of Industrial Radiology* (1949).

CHAPTER 3

GEOMETRY OF X-RAY REFLECTIONS

1. Diffraction of X-rays by Crystalline Matter

1.1 Diffraction from a three-dimensional lattice. A crystal consists, as we have seen, of a three-dimensional array of atoms. X-rays are scattered from these atoms in a manner similar to that in which light waves are scattered from the ruled lines of a diffraction grating. In this chapter we shall consider only diffraction from the gratings occurring in the form of crystals. The conditions for additive interference between the X-rays scattered from corresponding points along any line in the lattice may be seen from Fig. 34. The incident rays travelling

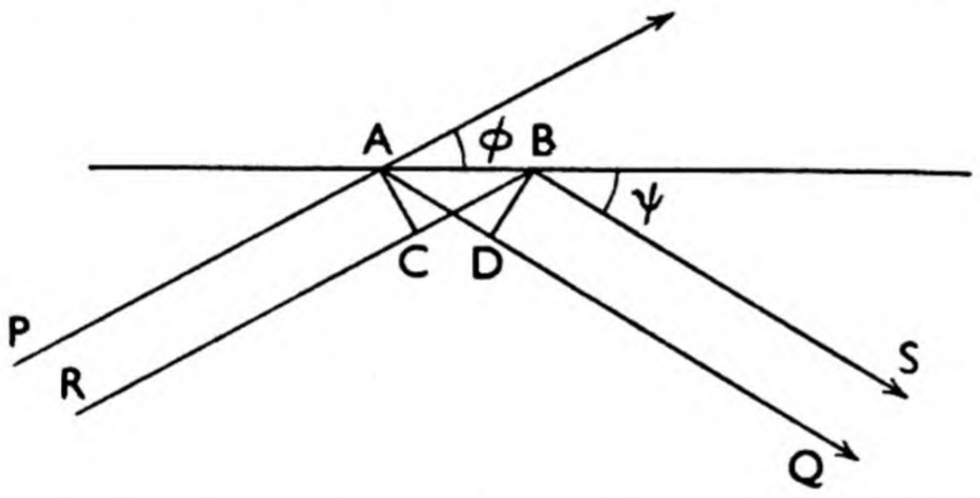

FIG. 34. Geometry of X-ray scattering from two points A, B

in the direction PA make an angle ϕ with the line AB passing through a row of lattice points. The diffracted rays travelling in the direction AQ make a corresponding angle ψ with AB. Contrasting the rays PAQ and RBS, we see that up to the line AC which is perpendicular to PA, there is no difference in the distance they have travelled. Similarly, after passing the line BD, which is perpendicular to AQ, there is no change in the difference in distance they have travelled. This path difference amounts to :

$$BC - AD = AB\,(\cos\phi - \cos\psi). \qquad (1)$$

The condition for additive interference is that the path difference evaluated in equation (1) shall be equal to a whole multiple of λ, hence,

$$n\lambda = AB\,(\cos\phi - \cos\psi). \qquad (2)$$

The row of lattice points AB has been chosen arbitrarily and there are, of course, an infinite number of such lattice rows for each of which an equation such as (2) could be written down to correspond with the occurrence of additive interference. It is enough, to obtain a complete specification of the conditions of interference in three dimensions, to choose three non-coplanar lattice rows and write down the equations corresponding to equation (2) for each of them. If these axes of reference are mutually perpendicular, the equations can be expressed in terms of the direction-cosines of the incident and reflected rays. Thus, if the direction-cosines of the lines drawn from a given lattice point in the *directions of propagation* of the incident and diffracted rays are respectively i_1, i_2, i_3, and f_1, f_2, f_3, and if the repeat distances along the three non-coplanar lattice rows are a, b, c, then the three interference equations are,

$$\begin{aligned} h\lambda &= a\,(i_1 - f_1), \\ k\lambda &= b\,(i_2 - f_2), \\ l\lambda &= c\,(i_3 - f_3). \end{aligned} \qquad (3)$$

The integers h, k, l, represent the number of wave-lengths in the path-difference between the rays diffracted from consecutive lattice points along the three lattice rows defined by a, b, c.

The first of the three equations (3) states that the path-difference between the rays diffracted from the origin and from the lattice point at a distance a from the origin along the x-axis is h wave-lengths. It follows, therefore, that the point along the x-axis from which diffracted rays are just one wave-length out of phase with those diffracted from the origin, is distant a/h from the origin. Similarly, the points along the y- and z-axes which give diffracted rays with the same path difference, are distant b/k and c/l from the origin. These three points define a plane of indices (hkl). Further, if the path-difference between the rays scattered from the origin and from three given points is constant, then the same path-difference must arise when rays are scattered from *any* point in the plane passing through the three points. Thus we may look upon the family of parallel and equidistant planes of indices (hkl) and spacing d_{hkl} as scattering the X-rays additively. The path-difference between the rays scattered from successive planes is one wave-length. The spacing, d_{hkl}, is, of course, equal to the perpendicular distance from the origin to the plane which has intercepts a/h, b/k, c/l on the axes x, y, z respectively.

1.2 The Bragg Law. If the three lattice rows are taken as the axes of reference and if they are also

mutually perpendicular, as we have assumed, the equations are very simple. The direction cosines of the normal to a plane of Miller indices (*hkl*) are respectively,

$$\frac{h/a}{E}, \frac{k/b}{E}, \frac{l/c}{E},$$

where $$E=\sqrt{h^2/a^2+k^2/b^2+l^2/c^2}.$$

The angle between the direction of propagation of the incident X-ray beam and the normal to the plane is therefore,

$$\cos^{-1}\left(i_1\frac{h}{a}+i_2\frac{k}{b}+i_3\frac{l}{c}\right)\Big/E. \qquad (4)$$

Also the angle between the direction of propagation of the diffracted X-ray beam and the normal to the plane (*hkl*) is

$$\cos^{-1}\left(f_1\frac{h}{a}+f_2\frac{k}{b}+f_3\frac{l}{c}\right)\Big/E. \qquad (5)$$

If the cosines of these angles be added, we obtain

$$\left\{(i_1+f_1)\frac{h}{a}+(i_2+f_2)\frac{k}{b}+(i_3+f_3)\frac{l}{c}\right\}\Big/E.$$

Substituting the values of h/a, k/b, l/c from equation (3) we obtain for the sum of the cosines,

$$\{(i_1^2-f_1^2)+(i_2^2-f_2^2)+(i_3^2-f_3^2)\}/\lambda E,$$

which is equal to zero, since,

$$i_1^2+i_2^2+i_3^2=f_1^2+f_2^2+f_3^2=1.$$

Thus the angles between the direction of propagation of the incident beam and the normal to (*hkl*) and between the direction of propagation of the diffracted beam and the normal to (*hkl*) are supplementary. It should be noted that in this analysis account must be taken of the direction of propagation of the incident and diffracted rays. Each angle is measured between a vector drawn from the origin in the direction of propagation and the vector drawn from the origin normal to the plane (*hkl*).

Further, we can show that the incident beam, the normal to the plane (*hkl*), and the diffracted beam, are co-planar. The condition for this is that,

$$\begin{vmatrix} i_1 & i_2 & i_3 \\ h/aE & k/bE & l/cE \\ f_1 & f_2 & f_3 \end{vmatrix}=0.$$

Substituting the values for h, k, l from equation (3), we obtain for the determinant

$$\begin{vmatrix} i_1 & i_2 & i_3 \\ (i_1-f_1)/\lambda E & (i_2-f_2)/\lambda E & (i_3-f_3)/\lambda E \\ f_1 & f_2 & f_3 \end{vmatrix}$$

which is equal to zero.

From these two results it follows that the plane (*hkl*) bisects the angle between the positive directions of the incident and diffracted beams. The lattice planes having the indices *hkl* therefore behave like a reflecting plane to the incident X-rays. It is for this reason that we shall frequently speak of the X-rays as being reflected from lattice planes.

The process is, however, not one of simple reflection, because all three equations (3) must be simultaneously satisfied; so that for a particular size of unit cell and wave-length of X-rays, reflections can occur only for certain incident directions and not, as with visible light and a mirror, for all incident directions. This can be seen more easily by rewriting equations (4) and (5). If the angle between the incident beam and the reflecting plane be put equal to θ, then equation (4) may be written,

$$\sin\theta=\left(i_1\frac{h}{a}+i_2\frac{k}{b}+i_3\frac{l}{c}\right)\Big/E,$$

and equation (5) may be written

$$-\sin\theta=\left(f_1\frac{h}{a}+f_2\frac{k}{b}+f_3\frac{l}{c}\right)\Big/E.$$

Hence

$$2\sin\theta=(i_1-f_1)\frac{h}{a}+(i_2-f_2)\frac{k}{b}+(i_3-f_3)\frac{l}{c}\Big/E.$$

Substituting values from equation (3) we have,

$$2\sin\theta=\left(\frac{h^2}{a^2}+\frac{k^2}{b^2}+\frac{l^2}{c^2}\right)\lambda/E$$

$$=E\lambda.$$

When the axes of reference are mutually perpendicular, the spacing of consecutive lattice planes is given by,

$$d_{hkl}=\frac{1}{\sqrt{h^2/a^2+k^2/b^2+l^2/c^2}}=\frac{1}{E}.$$

Hence, $$2\sin\theta=\lambda/d_{hkl} \quad \text{or} \quad \lambda=2d_{hkl}\sin\theta. \qquad (6)$$

Equation (6) is an expression of the Bragg law, and it will be seen that, only for a particular value of θ and a value of d fixed by the crystal lattice, can there be a reflection of the given wave-length λ.

An elementary proof of the Bragg law can be given as follows. Suppose that we choose parallel equidistant planes of lattice points such as A, B, C . . . so that they bisect internally the angle between the incident and diffracted beams, Fig. 36.1. Such planes must be chosen because for these planes there is no path-difference between the rays scattered from any two points lying in any one of them. In Fig. 36.1 the ray scattered from plane B is drawn from a point where there is no lattice point. This does not matter because the path-difference between the rays QRS and QT is the same as between QT and any ray scattered from a lattice point in plane B. The line RU is drawn perpendicular to QT, QV perpendicular

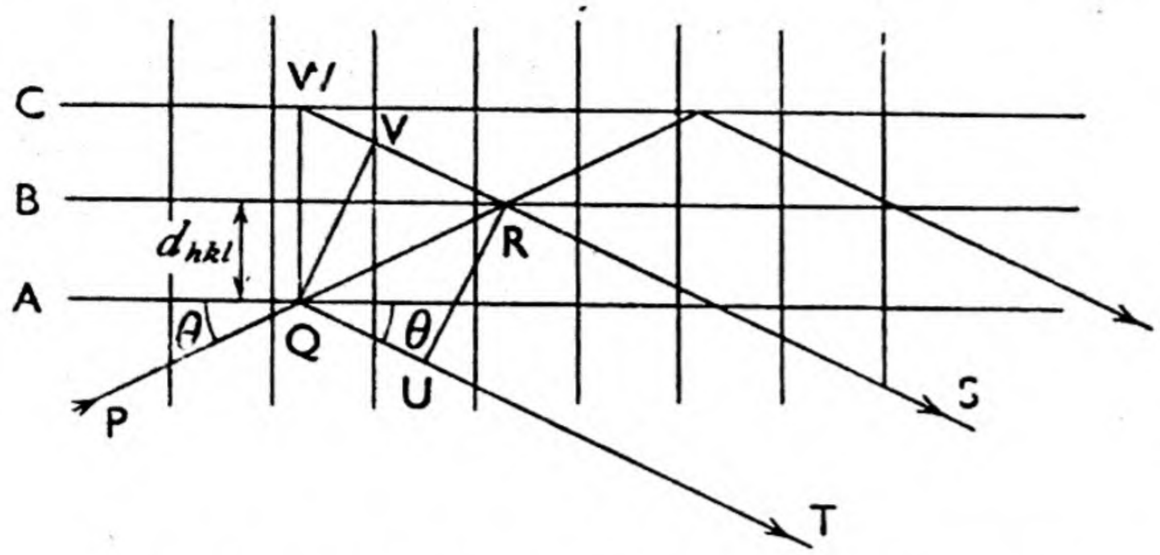

FIG. 36.1. Reflection of X-rays from consecutive lattice planes *A*, *B*, *C*

to *RS*, and *QW* perpendicular to the planes *A*, *B*, *C*. It will be seen that after passing the points *R* and *U* there will be no further change in the path-difference. Hence, if the path-difference is one wave-length, we have

$$\lambda = QR - QU = RW - RV = WV,$$

hence

$$\lambda = 2d_{hkl} \sin \theta.$$

The above analysis has utilised mutually perpendicular axes of reference. The Bragg law is, however, valid for all systems of crystallographic axes. The most elegant treatment of this is a vector one as follows.

The path difference between two rays scattered from consecutive points separated by a vector **a** is equal to $AB - CD$ (Fig. 36.2), that is $\mathbf{a} \cdot \mathbf{i} - \mathbf{a} \cdot \mathbf{f}$, where

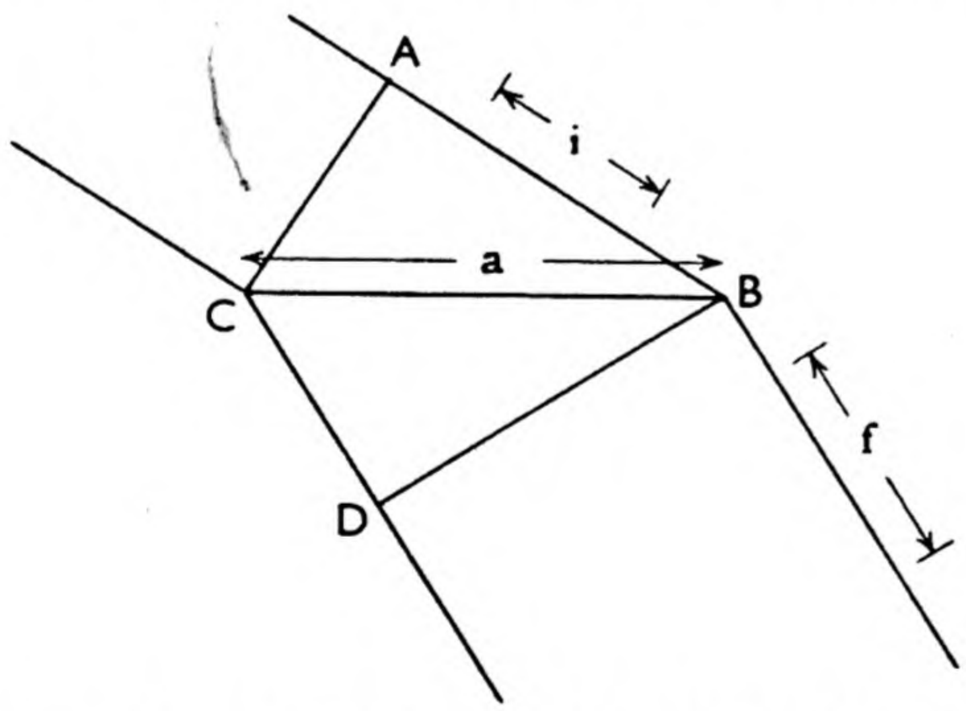

FIG. 36.2. Diagram showing vectors **a**, **i** and **f**

i and **f** are vectors of unit length the positive directions of which are along the directions of the incident and diffracted rays respectively. The interference condition is therefore

$$\mathbf{a} \cdot (\mathbf{i} - \mathbf{f}) = h\lambda.$$

For scattering from the lattice rows having separation of points **b** and **c** respectively, the interference conditions are

$$\mathbf{b} \cdot (\mathbf{i} - \mathbf{f}) = k\lambda,$$
$$\mathbf{c} \cdot (\mathbf{i} - \mathbf{f}) = l\lambda.$$

The only solution of these three equations is

$$\mathbf{i} - \mathbf{f} = \lambda (h\mathbf{a}^* + k\mathbf{b}^* + l\mathbf{c}^*),$$

where $\mathbf{a}^* . \mathbf{a} = 1$; $\mathbf{a}^* . \mathbf{b} = \mathbf{a}^* . \mathbf{c} = 0$; etc.

Now the normal to the plane *hkl* is $\mathbf{d}^*$ and, as shown in **3**, 2.1,

$$\mathbf{d}^* = h\mathbf{a}^* + k\mathbf{b}^* + l\mathbf{c}^*.$$

Hence $\mathbf{i} - \mathbf{f} = \lambda \mathbf{d}^*$ and the three vectors are coplanar. Further since **i** and **f** are both of unit length, the incident and diffracted rays are equally inclined to the normal to the reflecting plane (*hkl*). Finally, if the angle between **i** and **f** is 2θ, $\mathbf{i} - \mathbf{f} = 2 \sin \theta$, and, since $d^* = 1/d$,

$$\lambda = 2d \sin \theta.$$

It is implicit in the above discussion that reflections from opposite sides of a parallel plate of crystal must occur at the same angles. It is usually true, also, that the intensities of reflection of X-rays from the two sides of such a plate under comparable conditions are equal ; this is known as *Friedel's law*. In rare cases only, when the wave-length is close to a resonance level for one kind of atom in the crystal, is there a differential phase change on scattering, which enables *hkl* to be distinguished from $\bar{h}\,\bar{k}\,\bar{l}$ in a crystal lacking a centre of symmetry (Coster, Knol and Prins, 1930). In this book, therefore, we shall work within the operation of *Friedel's law*, and it will be taken that the reflections from the two sides of a set of planes are identical for all crystals.

1.3 Orders of reflection. In the preceding analysis we have shown that when the lattice planes of indices (*hkl*) give rise to an X-ray reflection, the path-difference between the rays reflected from successive planes is one wave-length. It is quite common to find the Bragg law stated in the form,

$$n\lambda = 2d_{hkl} \sin \theta,$$

where n is here the 'order' of the reflection. For example, if the reflection from the (100) planes of the lattice occurs, let us say, at an angle θ_1, then, when the path-difference between the rays reflected from these planes is 2λ instead of λ, reflection will occur at an angle θ_2 and the above equation will be satisfied with $n = 2$. For a certain angle θ_3, a third reflection may occur corresponding to $n = 3$. These reflections from the planes of the lattice containing the directions of the *y*- and *z*-axes are called respectively the *first*, *second* and *third order reflections* of 100.

This terminology is a transfer from the science of spectroscopy, but it has little to recommend it. In spectroscopy it is common to speak of the second-order reflection when the path-difference between consecutive scattering elements of the grating is 2λ ; but in X-ray crystallography it is not necessary to regard the reflection 200 as the second-order of 100 since the (200) planes of the lattice are as uniquely defined as any other (*hkl*) family of planes (**1**, 1.3).

We shall therefore understand throughout this book that the planes (*hkl*) have a spacing determined by the size and shape of the unit cell, according to the equations given in Appendix 2. It is important to remember that *hkl*, written without brackets, refers to the X-ray reflection from the planes (*hkl*).

2. The Reciprocal Lattice

2.1 Nature of the reciprocal lattice. Many of the characteristics of a crystal are most simply represented by means of the Bravais lattice. But other characteristics are more easily dealt with in terms of the *reciprocal lattice*, which, like the Bravais lattice, consists of a set of points through which may be drawn a framework of equidistant and parallel lines. Each reciprocal point represents a family of planes in the Bravais lattice. The reciprocal point lies on the normal through the origin to a set of parallel and equidistant planes in the Bravais lattice, and its distance from the origin is inversely proportional to the spacing of the planes. The definition may be expressed formally † as

$$d^*_{hkl} = K/d_{hkl},$$

where d^*_{hkl} is the distance from the origin to the reciprocal point corresponding to the family of planes having the spacing d_{hkl}. The coefficient of proportionality, K, is arbitrary; sometimes it is convenient to make it equal to unity, but sometimes it is better to make it equal to the wave-length of the X-rays used. In this book, unless otherwise stated, K will be taken equal to λ. We shall trace out the development of a monoclinic reciprocal lattice by the continued application of the above definition.

The Bravais lattice is constructed on the unit cell *OABC*, *OA* and *OC* being in the direction of the crystallographic *x*- and *z*-axes respectively (Fig. 37 *a*). The family of parallel equidistant planes of which two consecutive members are *OC* and *AB* has the Miller indices (100). The corresponding reciprocal point, denoted by the square with 100 written beside it, lies on the normal to the (100) planes at a distance from the origin equal to the reciprocal constant divided by the perpendicular distance between the planes (100). Similarly, the point marked 001 is at a distance from *O* equal to the same arbitrary constant divided by the perpendicular distance between the planes *OA* and *CB*, and lies along the normal to *BC* passing through *O*. A reciprocal point 101 is located in the same way along a line through *O* perpendicular to *AC* and at a distance from *O* inversely proportional to the perpendicular distance from *O* to *AC*. When the geometrical construction has been applied throughout, it will be found that the distance between the reciprocal points 001 and 101 is equal to that between the reciprocal points 000 and 100, and further, that the lines joining these pairs of points are parallel. The area bounded by the points, 000, 100, 101, 001 is one face of a unit cell of the reciprocal lattice which is built up by a repeated application of the procedure described above, and its edges are taken as the x^*- and z^*-axes. The points of the reciprocal lattice have indices which are their co-ordinates along the axes x^* and z^* in the reciprocal lattice.

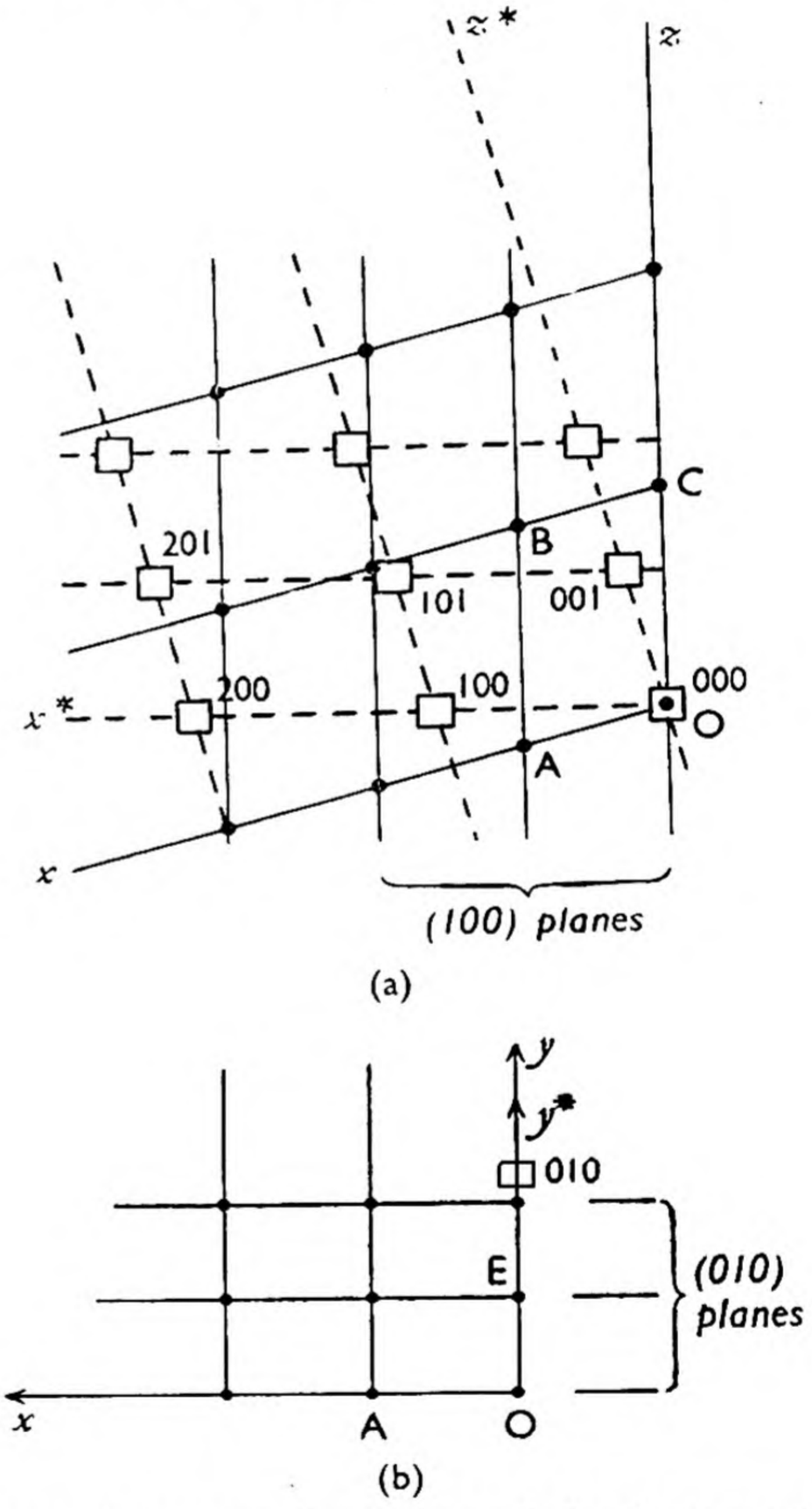

FIG. 37. Diagrams illustrating relation between Bravais lattice and reciprocal lattice for a monoclinic crystal. Dots represent Bravais-lattice points, and squares represent reciprocal points

So far we have only discussed points lying in one plane of the reciprocal lattice. The *y*-axis of the Bravais lattice is perpendicular to the paper in Fig. 37 *a*, and so is the corresponding reciprocal-lattice axis y^*,

† Lengths and angles within the reciprocal lattice will throughout this book be distinguished from the corresponding quantities in the Bravais lattice by an asterisk. This system, although not in conformity with the usage of some mathematical works, is so common in crystallographic literature that its continuance seems justified.

since it is perpendicular to the family of parallel equidistant planes (010). The reciprocal point 010 shown in Fig. 37 (*b*) is, however, along the y^* axis at a distance from O inversely proportional to OE, the spacing of the (010) planes. Proceeding in the same way we can plot 020, 030, etc., as reciprocal points along y^*.

To find the positions of the reciprocal point corresponding to the set of planes of indices (*hkl*), we could carry out the same geometrical construction as that described above. If this were done, the reciprocal points would be found to form a lattice as shown in the vector proof below. Thus each set of parallel planes (*hkl*) in the Bravais lattice is represented by a point in the reciprocal lattice. These points can also be obtained by marking off ha^* along x^*, then from this point marking off a length kb^* along a line parallel to y^*, and from the end of this line marking off a length lc^* along a line parallel to z^*. At the end of the third line is the same lattice point as we arrive at by constructing the normal to the family of planes (*hkl*) through the origin and marking off a length k/d_{hkl} as described.

The vector proof mentioned above is as follows. The intercepts of the first plane out from the origin belonging to the set (*hkl*) in the Bravais lattice can be expressed as the vectors.

$$\mathbf{a}/h,\ \mathbf{b}/k,\ \mathbf{c}/l.$$

If we can show that

$$\mathbf{d}^*_{hkl} = h\mathbf{a}^* + k\mathbf{b}^* + l\mathbf{c}^*,$$

then the reciprocal points form a lattice with unit vectors $\mathbf{a}^*$, $\mathbf{b}^*$ and $\mathbf{c}^*$.

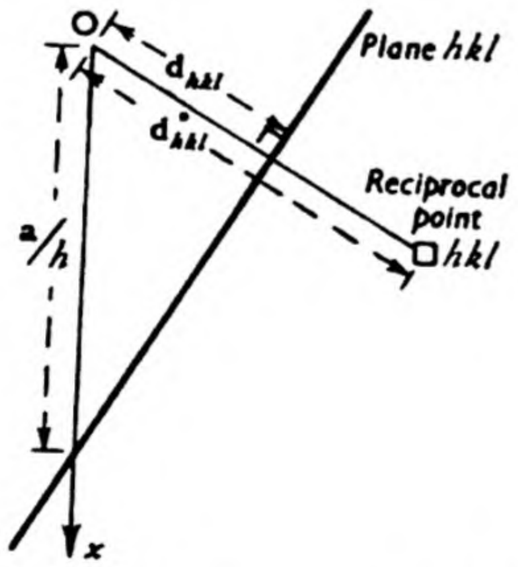

FIG. 38.1. Diagram showing vectorial relation between $\mathbf{d}_{hkl}$ and $\mathbf{d}^*_{hkl}$

If $\mathbf{d}_{hkl}$ is the vector from the origin normal to the plane *hkl* (Fig. 38.1), and $\mathbf{d}^*_{hkl}$ the collinear reciprocal vector, then we shall put $\mathbf{d}_{hkl} \cdot \mathbf{d}^*_{hkl} = 1$.

Hence $\mathbf{d}_{hkl} \cdot \mathbf{a}/h = (d_{hkl})^2 = \dfrac{1}{(d^*_{hkl})^2}$, where d_{hkl} corresponds to the numerical value of the distance between consecutive planes of the set (*hkl*).

Then by the substitution,

$$\mathbf{d}_{hkl} = \mathbf{d}^*_{hkl}/(d^*_{hkl})^2,$$

we have $$\frac{\mathbf{d}^*_{hkl} \cdot \mathbf{a}/h}{(d^*_{hkl})^2} = \frac{1}{(d^*_{hkl})^2},$$

and therefore, and similarly,

$$\left.\begin{aligned} \mathbf{d}^*_{hkl} \cdot \mathbf{a} &= h \\ \mathbf{d}^*_{hkl} \cdot \mathbf{b} &= k \\ \mathbf{d}^*_{hkl} \cdot \mathbf{c} &= l \end{aligned}\right\}.$$

Now, since $\mathbf{a} \cdot \mathbf{a}^* = 1$ and $\mathbf{a} \cdot \mathbf{b}^* = 0$, etc., these three equations can only be satisfied simultaneously by the value,

$$\mathbf{d}^*_{hkl} = (h\mathbf{a}^* + k\mathbf{b}^* + l\mathbf{c}^*).$$

It therefore follows that the reciprocal points form a lattice with unit vectors $\mathbf{a}^*$, $\mathbf{b}^*$, $\mathbf{c}^*$ and that any point having co-ordinates $h\mathbf{a}^*$, $k\mathbf{b}^*$, $l\mathbf{c}^*$ is the reciprocal point of the family of planes (*hkl*) in the Bravais lattice.

2.2 Reciprocal lattices corresponding to the seven systems of crystal symmetry. In the preceding section the method of deriving the reciprocal lattice corresponding to a monoclinic Bravais lattice

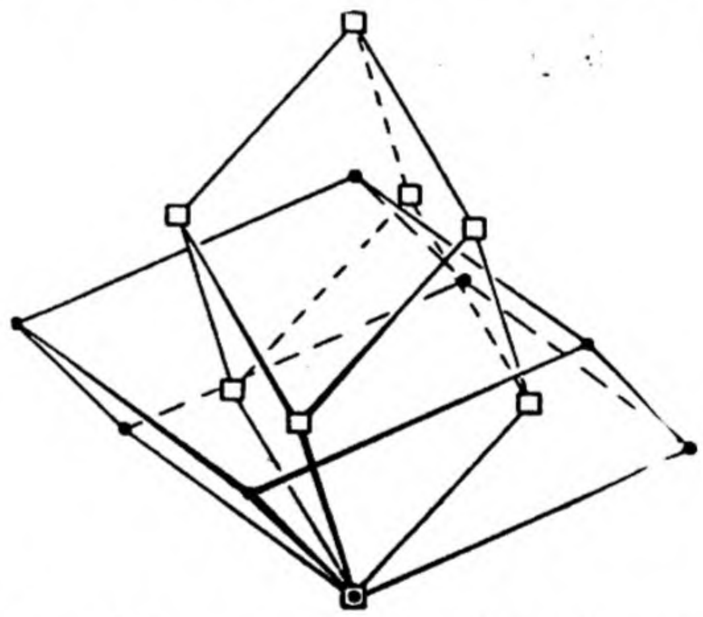

FIG. 38.2. Diagram showing the relation between Bravais lattice and reciprocal lattice for rhombohedral axes. Dots represent Bravais-lattice points and squares reciprocal-lattice points.

has been described. By carrying out the same geometrical process on each of the other lattices in turn, we obtain the corresponding reciprocal lattices. The reciprocal lattice of any cubic crystal is itself cubic, and, of course, its cell-side is inversely proportional to the cell-side of the Bravais lattice. A tetragonal reciprocal lattice has the same symmetry elements as the Bravais lattice from which it is derived ; but if the *c*-axis is longer than the *a*-axis in the Bravais lattice, the converse is true in the reciprocal lattice. Similarly, an orthorhombic reciprocal lattice is like the Bravais lattice, but the corresponding cell dimensions are inversely proportional to one another. A monoclinic reciprocal lattice, as we have seen, has its y^*-axis in common with the y-axis of the Bravais lattice and the angle β^* is equal to $180° - \beta$. The unit cell of a triclinic reciprocal lattice has its edges perpendicular to

the faces of the unit cell of the Bravais lattice and the lengths of the edges of the reciprocal unit cell are inversely proportional to the perpendicular distances

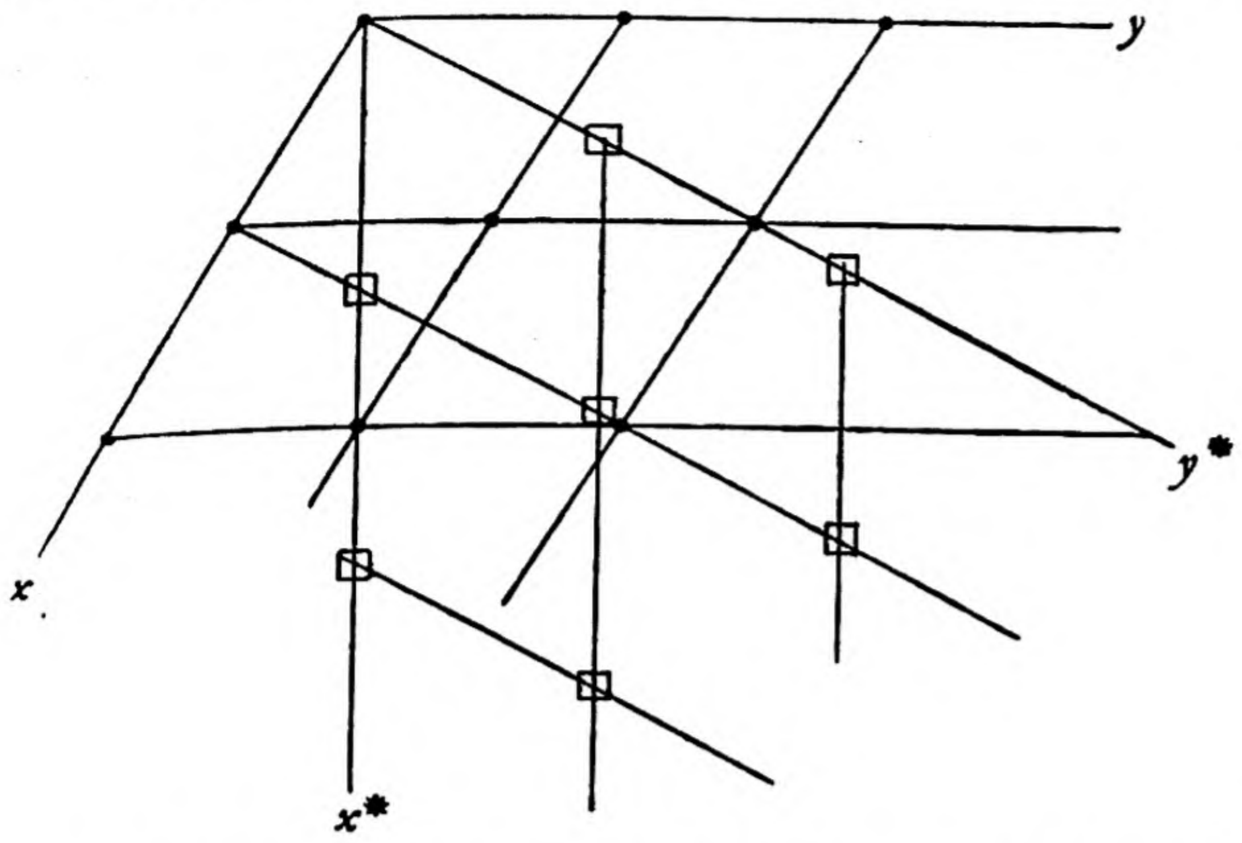

FIG. 39.1. Diagram showing relation between Bravais lattice and reciprocal lattice for hexagonal axes. Dots represent Bravais-lattice points and squares reciprocal-lattice points

between the opposite faces of the unit cell of the Bravais lattice. The rhombohedral Bravais lattice has a unit cell which can be regarded as derived from a cube either by compression or extension along a body diagonal which becomes the unique triad axis of the rhombohedron. The reciprocal lattice also has a rhombohedral unit cell, but this is compressed along the triad axis when the corresponding Bravais lattice is elongated in the same direction and vice versa (Fig. 38.2). A hexagonal reciprocal lattice has a unit cell which has the hexad axis in common with the Bravais lattice, but the angle between $+x^*$ and $+y^*$ is 60°, while in the Bravais lattice the angle between the $+x$- and $+y$-axis is 120° (Fig. 39.1).

2.3 Co-ordinates used in reciprocal space. The reciprocal lattice is normally employed in the interpretation of various types of X-ray photographs. There are several ways of specifying the position of a point in three-dimensional space. The axes of reference are normally chosen as follows :

(1) OX (Fig. 39.2), parallel to the incident beam of X-rays, the positive direction being that from the origin towards the source of X-rays.

(2) OV, the axis of oscillation or rotation, or, if the crystal is stationary, any selected direction passing through the origin and perpendicular to the direction of the incident beam. The positive direction is usually taken to be upwards from the origin.

(3) OS, a direction perpendicular to OX and OV. The positive direction of OS will be taken as forming with the directions OX and OV a right-handed set of axes when read in the order OX, OS, OV. The position of the reciprocal point N (Fig. 39.2) may be defined in terms of cylindrical co-ordinates ξ, ζ and ϕ, such that ξ is the radius of a cylinder having OV as axis and passing through N, ζ is the distance from the origin of a plane perpendicular to OV and passing through N, and ϕ is the angle between two planes intersecting in OV and passing through N and OS respectively. The position of N may also be defined by the indices hkl of the corresponding lattice planes. The co-ordinates of N are ha^*, kb^* and lc^* and these lengths are measured parallel to the edges of the reciprocal unit cell (Fig. 39.3).

When it is necessary to define only the direction of the normal to the reflecting planes ON, as distinct from the position of the point N, this may be done by polar co-ordinates ρ and ϕ (Fig. 39.2). The polar co-ordinate ρ is the angle NOV, and ϕ is the angle already defined. A further pair of polar co-ordinates which may be used is $(\pi/2-\theta)$ and ψ. Since the reflecting planes make an angle θ with the incident beam, the angle NOX is $(\pi/2-\theta)$.

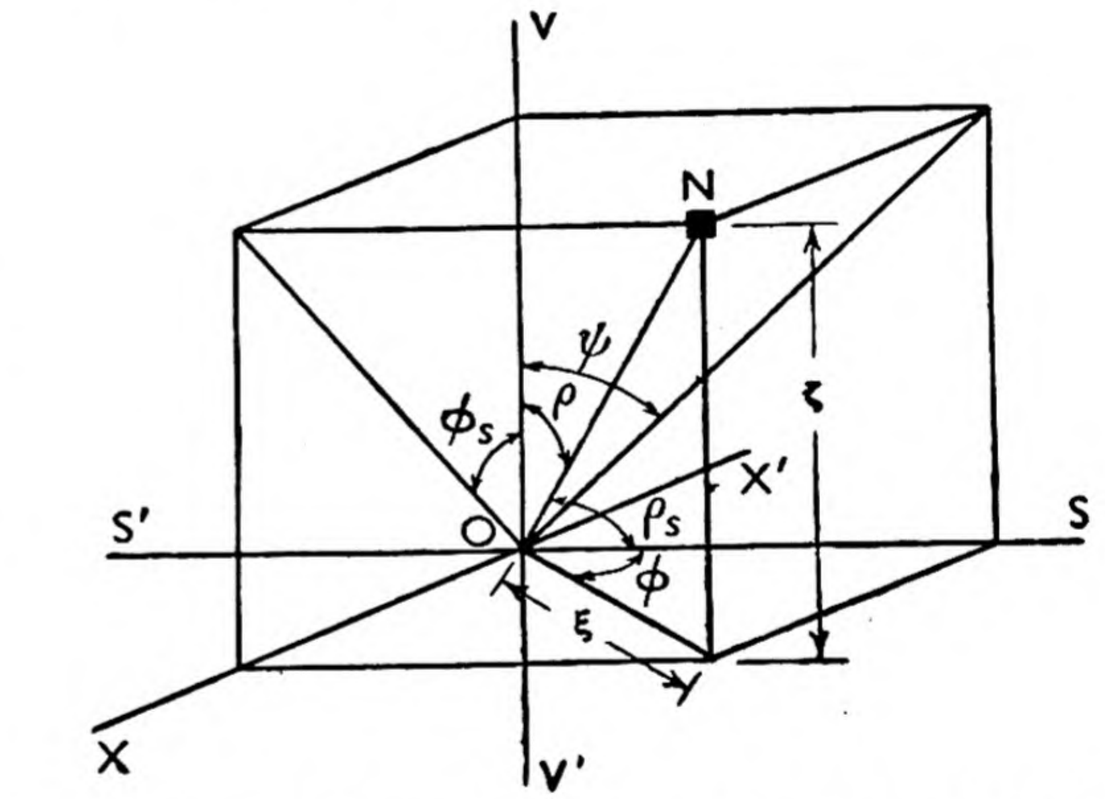

FIG. 39.2. Diagram showing the relation of the cylindrical co-ordinates and the pairs of polar co-ordinates. Angle $NOX=(\pi/2-\theta)$

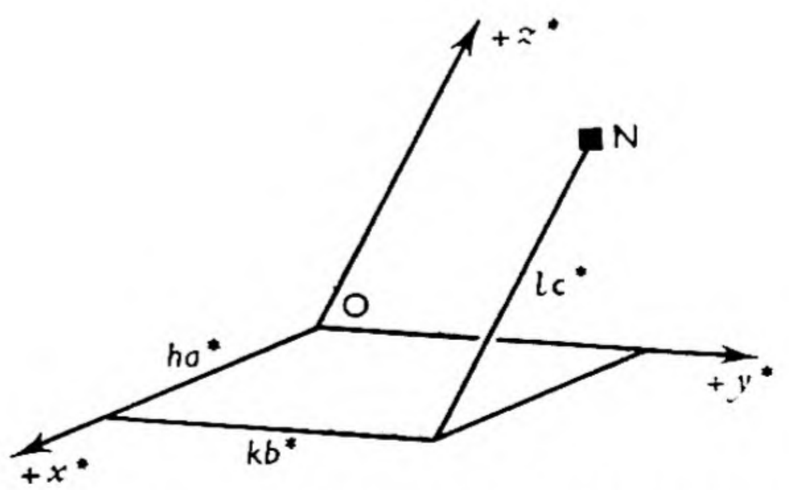

FIG. 39.3. Co-ordinates of reciprocal point N

3. Interpretation of the Bragg Law in terms of the Reciprocal Lattice

There is a very important relation between the reciprocal lattice and a sphere known as the *reflecting sphere* which is constructed in the following way.

On the line OP, which passes through the origin parallel to the incident X-ray beam (Fig. 40), the point P is chosen at a distance of two units of length from the origin. On OP as diameter a sphere known as the reflecting sphere is constructed. If a reciprocal point lies on the surface of this sphere, then we can show that the corresponding lattice planes are in the correct setting relative to the incident beam and have the correct spacing to reflect the X-rays. In Fig. 40 the circle on OP as diameter is a central section of the sphere, that is, a great circle, which passes through the reciprocal point N. The angle ONP is therefore a right-angle and

$$\frac{ON}{OP} = \frac{\lambda}{d}\Big/ 2.$$

Further, PN is parallel to the planes corresponding to N and hence angle $NPO = \theta$. Since $\sin\theta = ON/OP = \lambda/2d$, the Bragg law is thus obeyed and these planes corresponding to N can reflect the X-rays. It will be noted that the direction of the reflected beam is given by the line CN.

The simple relations of the construction described above are of great use in the interpretation of X-ray photographs of all kinds, as will be seen in subsequent chapters. There is only one variant of this construction. In this the radius of the reflecting sphere is put equal to $1/\lambda$ and any reciprocal point is distant $1/d$, instead of λ/d from the origin. Since the ratio of these distances is the same as that given above for ON/OP, the Bragg law is still obeyed when the reciprocal point lies on the surface of the reflecting sphere. This is the variant commonly used in Laue photographs for reasons which will be explained later. In all other

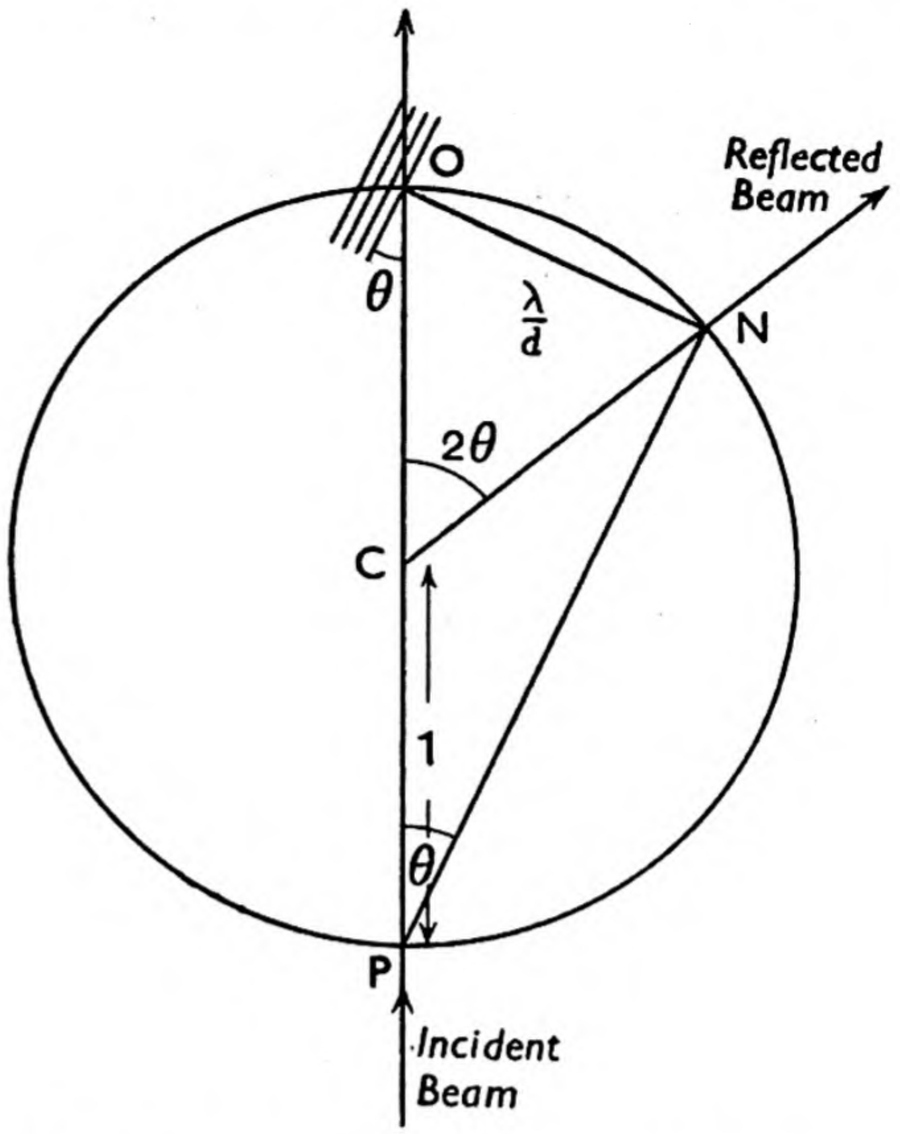

FIG. 40. Great circle through O and N on reflecting sphere

photographs the reciprocal distances are all defined as λ/d, and the radius of the reflecting sphere is a dimensionless quantity of numerical value unity.

A general definition of the radius of the reflecting sphere, which includes the two special cases given above, is that it is equal to K/λ where K is the constant used in the equation

$$d^* = K/d.$$

By giving K the values λ and unity respectively, the two special radii of the reflecting sphere quoted above will be seen to result.

CHAPTER 4

SINGLE-CRYSTAL AND FIBRE PHOTOGRAPHS

1. Introduction

FROM the Bragg equation it can be seen that, for a given set of lattice planes, reflection can occur in general only if there is variation either in wave-length of X-rays (λ) or in the orientation of the planes (θ). If white radiation is used with a single crystal, a Laue photograph is obtained, and this type of photograph is studied in Chapter 6. Laue photographs can also be taken of simple twin crystals. If a characteristic radiation is used, there must be variation of the angle θ, and this can be brought about in different ways. If the material occurs only in powder form or as a completely-disorientated aggregate, then the powder photograph alone can be obtained. For some purposes single crystals are crushed and used for taking powder photographs, and such photographs are studied in Chapters 11–17. When the specimen is in the form of a fibre, either natural or artificial, the specimen can be kept stationary during the exposure, and a fibre photograph results (Chapter 9). When there is a high degree of common orientation of the crystallites so that the specimen approximates to a 'single-crystal mosaic', a number of such photographs is required to give the necessary information about the orientation. In such cases it is advantageous to use a special type of moving-film method which is described later (**9**, 3.3). If the specimen is a single crystal, variation of the angle θ can be obtained either by turning the crystal, or by means of a convergent X-ray beam. In the first case the crystal is either rotated or oscillated about the axis of the X-ray goniometer; when the film (flat or cylindrical) is stationary, the rotation or oscillation photograph results (see Chapter 5). For some purposes, however, information can be more easily obtained when the film is moved during the exposure. A screen with an aperture is arranged so that only certain reflections can be recorded. There are various types of moving-film methods (**4**, 2.5; Figs. 43, 44), of which the most important is studied in Chapter 7. Divergent-beam methods have considerable disadvantages in practice and are little used except for special purposes.

There are two main features of a single-crystal photograph, namely the positions of the spots and the intensities of the spots. From the positions of the spots we can derive the shape and size of the unit cell of the lattice; after indexing the various reflections we can obtain information required in the determination of the space group. These procedures are geometric, but the determination of the intensities of the various reflections and the use of such data in finding the structures of crystals are physical procedures.

In general it can be said that, the more complex the apparatus, the simpler is the derivation of the required information from the photographs. For many purposes, however, it is sufficient to use quite simple apparatus. In this chapter a general account is given of the chief methods of taking single-crystal and fibre photographs, and in subsequent chapters the more fundamental methods are studied in detail. A summary of these methods is given on p. 42.

2. Types of Photograph

2.1 The Laue photograph. In the earliest type of X-ray diffraction photograph to be taken, a narrow beam of 'white' X-rays impinged on a stationary single crystal and the diffracted beams were registered on a flat film. This type of photograph is called the Laue photograph and the essentials of it are the stationary single crystal, the stationary film and the white X-rays. Since the crystal is stationary, the angle θ is fixed for any given set of lattice planes, and when characteristic radiation alone is used no diffracted beams would, in general, occur. The film may be cylindrical, with its axis normal to the incident beam, or flat, usually with its plane normal to the incident beam. When the flat plate intercepts only diffracted beams with low angles of deviation, it is called a front-plate and the photograph a *transmission Laue photograph*. When the incident beam passes through a hole in the film before impinging on the crystal, the film is called a back-plate and the photograph a *back-reflection Laue photograph*.

Although the experimental technique is very simple, the interpretation of Laue photographs is generally more difficult than the interpretation of other types of X-ray photograph. It is very difficult to determine cell dimensions by using this method. Laue photographs are at present used in the study of the symmetry of crystals and in the determination of the orientation of crystals. When a crystal is suitably orientated, the pattern of the Laue photograph may show symmetry which can provide evidence as to the

Radiation		White	Characteristic				
		Narrow beam	Divergent beam	Narrow beam			
Specimen		Single crystal			Partially-orientated aggregates	Powder, natural or crushed	
Types of X-ray photograph		Stationary		Rotating or oscillating		Stationary	
	Film stationary	Laue	Divergent beam	Rotation, Oscillation, Tilted-crystal		Fibre†	Powder‡
	Film moving	—	—	Weissenberg, etc.	Moving-film fibre	—	—

† Foil specimens are sometimes oscillated through small angles during the exposure, but this is not essential.
‡ Powder specimens are usually rotated during the exposure, but this is not essential.

Laue group of the specimen. Laue photographs are useful in the determination of the orientation of a single crystal because the specimen is stationary during the exposure.

2.2 The divergent-beam photograph. In addition to the Laue method, the only other method in which a single-crystal specimen is stationary during the exposure is that which uses a widely-diverging beam. In the most suitable apparatus for this kind of photograph the anode consists of a thin metal foil of the target material. From the focal spot a diverging beam emerges within a wide cone of which the semi-angle approaches 90°. The crystal is mounted on the outside of the foil and must not be too thick to transmit the characteristic radiation. The transmitted reflected rays form a number of conic sections on the flat plate placed in front of the crystal (Fig. 42). Each conic section is produced by the reflection of the characteristic radiation at the same angle by a given set of parallel lattice planes in the crystal. The patterns produced by this method give the same kind of information about the symmetry of the specimen as is given by the Laue method. Back-reflection photographs can also be taken, but these require a special arrangement of the X-ray tube. The divergent-beam method has also been used (Lonsdale, 1944, 1947 *a*, 1947 *b*) for the accurate determination of cell size.

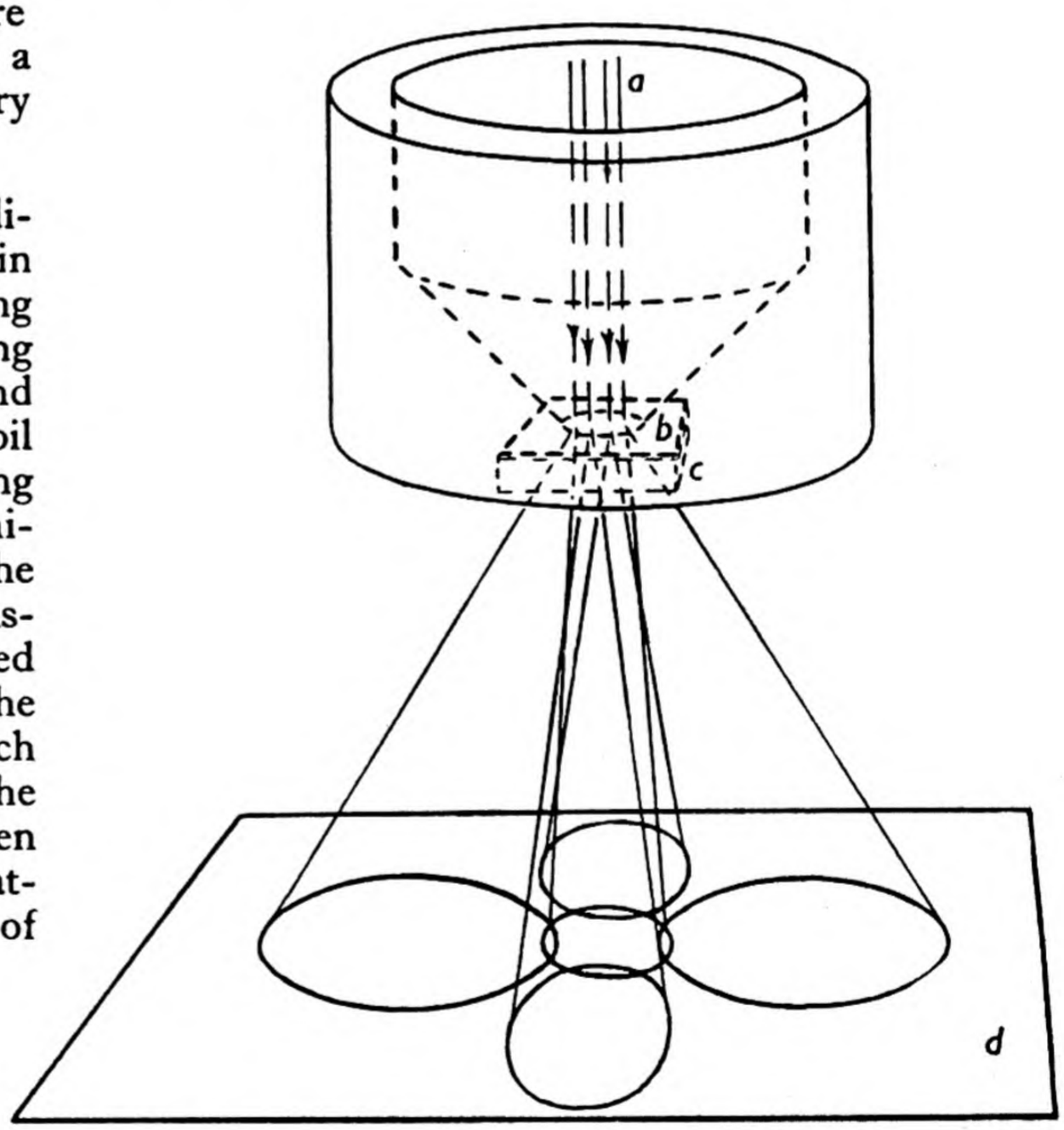

FIG. 42. Formation of divergent-beam photograph.
a, electron beam generated in X-ray tube;
b, metal foil forming anticathode;
c, crystal plate attached to metal foil *b*;
d, photographic plate

2.3 The rotation photograph. If a narrow beam of characteristic radiation is used with a

single-crystal specimen, the specimen has to be turned during the exposure in order to provide variation in the angle θ. In the rotation goniometer there is a spindle mounted perpendicular to the collimator. The specimen is set with a zone axis parallel to the axis of the instrument and is rotated continuously about this axis during the exposure. The film may be cylindrical with its axis coincident with the rotation axis of the crystal, or else a flat plate for transmission or for back-reflection photographs. From such rotation photographs the lengths of the sides of the unit cell can be quickly determined with an accuracy of about 1 per cent. But in most rotation photographs there is considerable overlapping of spots, and this limits the possibility of indexing the reflections unambiguously.

In order to overcome the difficulty due to the overlapping of spots, the ' tilted-crystal ' modification of the rotation photograph method has been introduced (Bunn, Peiser and Turner-Jones, 1944). In this method the zone axis of the crystal is inclined at a small angle to the axis of rotation in the instrument. Spots which would overlap in the ordinary rotation photograph are separated by this means.

2.4 The oscillation photograph. For many years, however, the oscillation photograph has been the one most used to overcome the difficulty of overlapping spots. In this method the crystal is oscillated through an angle, usually not exceeding 15°, instead of being completely rotated. In other respects the experimental technique is the same as for the rotation photograph. Although the angle of oscillation can be reduced in order to exclude ambiguities in indexing, this increases the number of oscillation photographs required to record all the different reflections which occur, especially in crystals of low symmetry. In such cases moving-film methods are superior, but the oscillation photograph, with its simple technique, remains the standard method for preliminary examination of crystals and is often needed as an auxiliary to moving-film methods.

2.5 Moving-film photographs. All moving-film goniometers have certain features in common. The movement of the film is mechanically or electrically coupled to the rotation of the crystal, and between the crystal and the film a screen with an aperture is inserted so that only certain reflections can be recorded on the film. The most widely used method is that due to Weissenberg (1924). In this the X-rays are incident at right angles † to the axis of rotation of the crystal, and the cylindrical camera is coaxial with the rotation axis of the crystal. The screen is also coaxial with the camera and has an annular aperture on the circumference. This arrangement allows the recording of reflections only from planes of a given type of indices, for example *hk*o if the crystal is rotating about the z-axis. Provided that the sides of the unit cell are known approximately there is no ambiguity whatever in the assignment of the indices, because each spot corresponding to planes of given indices can only occur at a particular point on the film. The advantage of this goniometer over other moving-film goniometers is that all angles of reflection up to a value close to 90° can be recorded. The only disadvantage is that an undistorted representation of a section of the reciprocal lattice is not obtained.

The Schiebold-Sauter method largely overcomes the disadvantage of the Weissenberg method mentioned above, but has other disadvantages of its own.

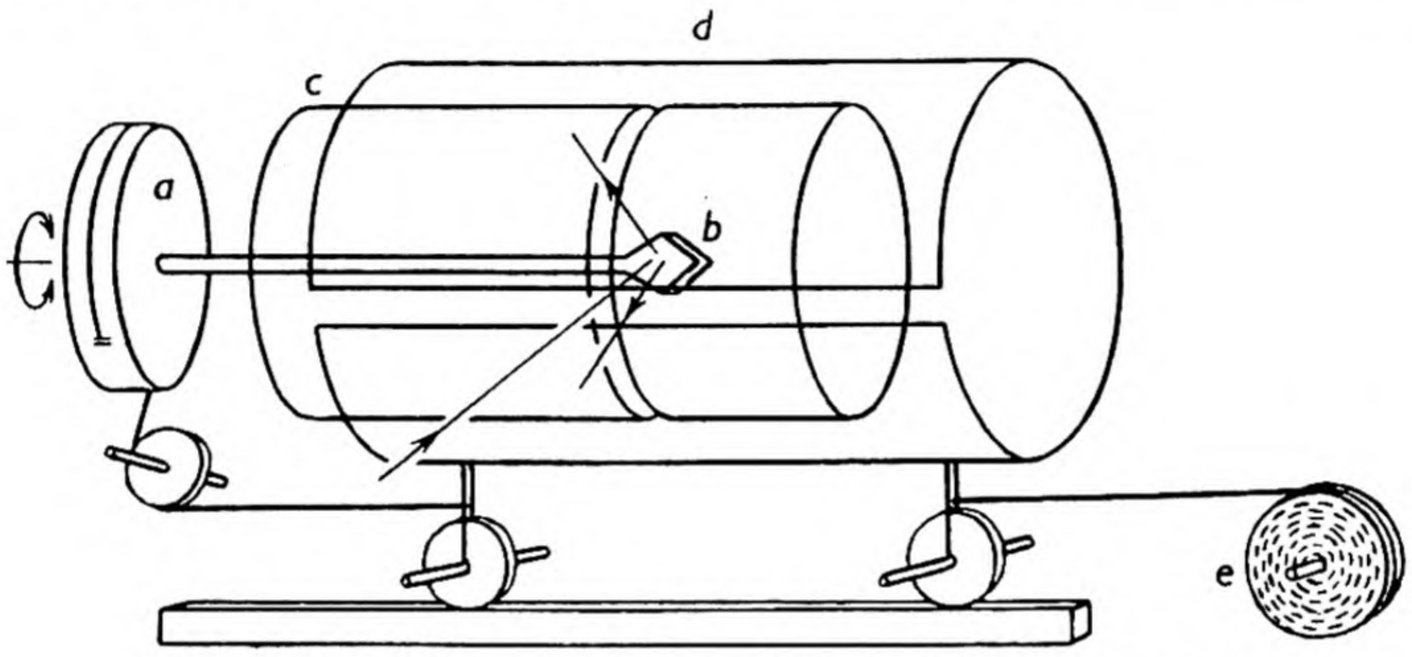

FIG. 43. Component parts of Weissenberg goniometer
a, drum carrying steel tape by which camera is drawn backwards and forwards ;
b, crystal mounted on axis of *a* ;
c, screen having circumferential slot permitting only one layer line of reflections to reach film in camera ;
d, camera ;
e, spring box keeping steel tape taut

† This is true in the *normal-beam* Weissenberg method but *inclined-beam* photographs are also used (**7**, 3.2 and 4.5).

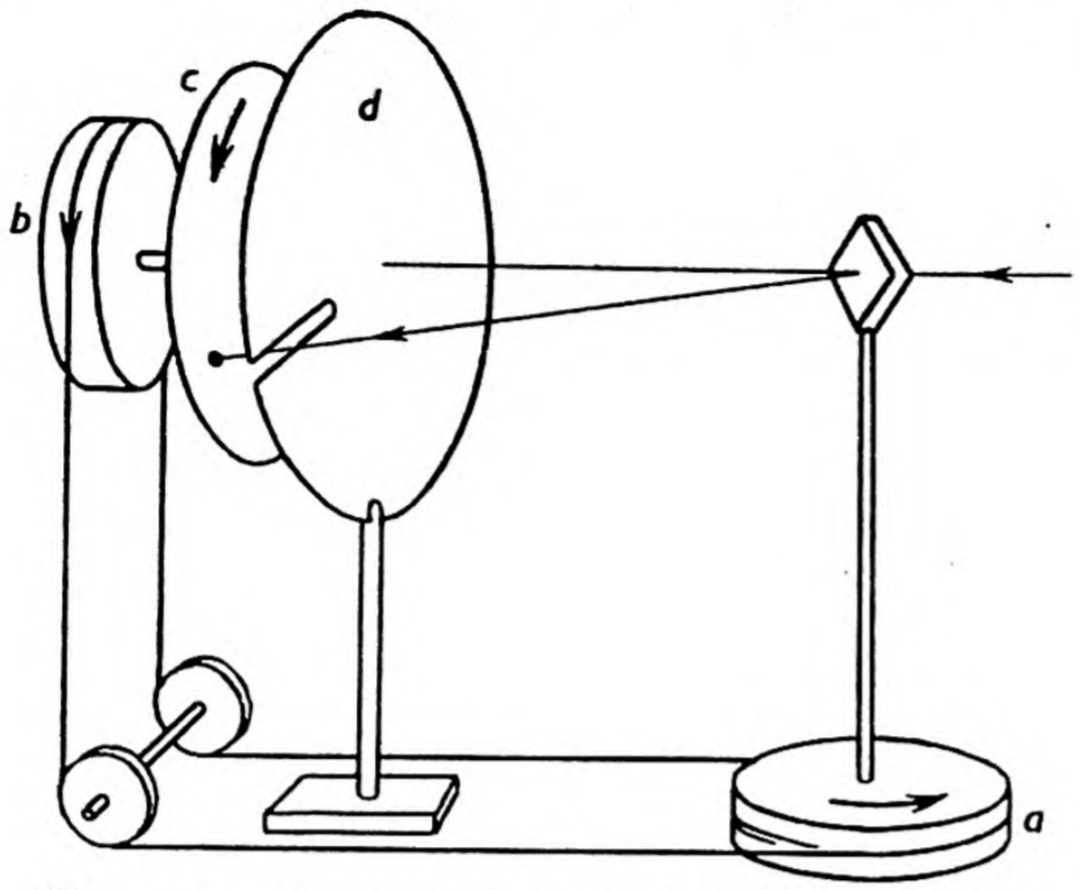

FIG. 44.1. Component parts of Schiebold-Sauter goniometer

a, drum rotating crystal about a vertical axis ;
b, drum of same size as *a* rotating camera *c* ;
c, flat film camera ;
d, fixed screen with horizontal radial slot

The X-ray beam is perpendicular to the axis of rotation of the crystal and to the flat disc-shaped film. The film rotates about an axis coincident with the incident beam of X-rays. The pattern obtained can be readily indexed but it is restricted to relatively small values of the glancing angle of reflection. Further, the angle at which the X-rays strike the film varies markedly from the centre to the periphery. When the substance is such that no reflections occur at large angles of reflection, this limitation may not matter and then the advantage of the simple interpretation may be utilised.

The de Jong and Bouman (1938) method provides a photograph which is geometrically similar to a corresponding section of the reciprocal lattice. In the normal-beam application of this method, the X-rays are incident perpendicular to the axis of rotation of the crystal. The screen and disc-shaped film are parallel to the direction of the incident beam of X-rays and only one cone of reflected X-rays is allowed to be recorded on the film in any one photograph. The film rotates about an axis parallel to that about which the crystal rotates. The advantage of this type of goniometer is that the photograph is an undistorted representation of one plane of the reciprocal lattice. The disadvantages are that the X-rays are incident on the flat film at varying angles and that the geometry of the instrument makes it less convenient to handle than the other types. Also, in normal-beam photographs there is no record of reflections corresponding to the zero layer of the reciprocal lattice.

It is probably true to say that the most generally useful moving-film goniometer is that due to Weissenberg, though for particular purposes one of the other types may be preferable. For the determination of space groups and the intensities of reflection of sets of planes having a given type of indices, for example *hk*o, moving-film methods are invaluable. Whereas with oscillation photographs it might be necessary to take

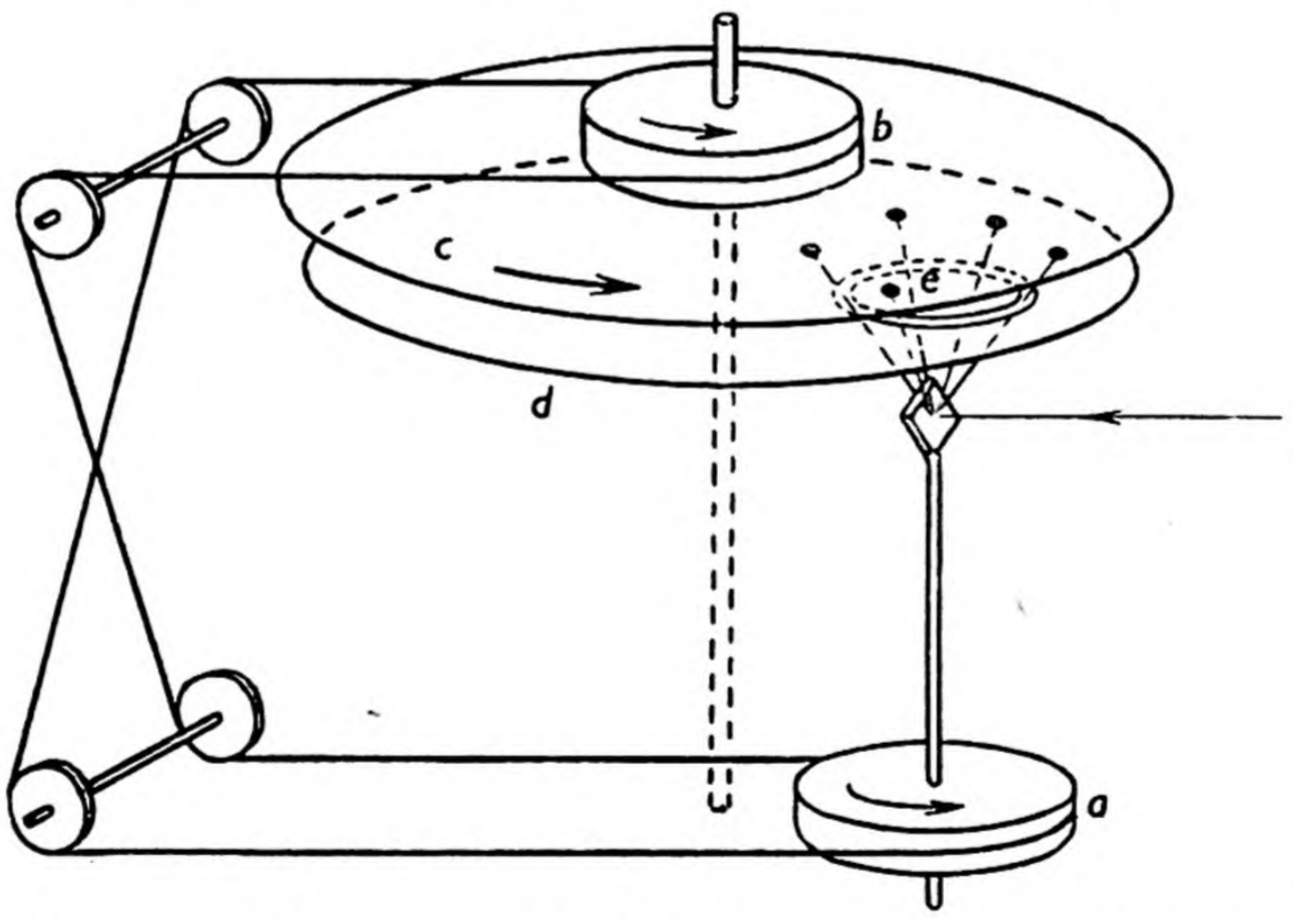

FIG. 44.2. Component parts of de Jong and Bouman goniometer

a, drum rotating crystal about a vertical axis ;
b, drum of same size as *a* rotating flat camera *c* in synchronism with *a* ;
c, disc-shaped camera rotating about a vertical axis displaced sideways relative to axis of *a* ;
d, stationary screen with circular slot *e* ;
e, slot in screen *d* transmitting one layer line

Name of method	Shape of film	Direction of incident beam in normal-beam photographs	Movement of crystal	Movement of film
Weissenberg (Fig. 43)	Cylindrical, with axis normal to the incident beam.	Normal to the film-axis.	Rotation about the film-axis.	Translation parallel to the film-axis.
Schiebold-Sauter † (Fig. 44.1)	Disc, with its plane normal to the incident beam which passes through its centre.	Normal to the film at its centre and to the rotation axis of the crystal.	Rotation about an axis parallel to the plane of the film.	Rotation in its own plane about its centre.
De Jong and Bouman (Fig. 44.2)	Disc, with its plane parallel to the incident beam.	Normal to the rotation axis of the crystal and parallel to the plane of the film.	Rotation about an axis normal to the incident beam and to the plane of the film.	Rotation about an axis parallel to, but not coincident with, the rotation axis of the crystal.
Buerger (precession)	Flat, with the film-normal set parallel to a selected zone axis of the crystal.	Inclined at a constant angle μ to the film normal and the zone axis.	The zone axis generates a cone of semi-angle μ with the incident beam as axis, but there is no continuous rotation about this axis.	The film normal is kept parallel to the zone axis and so describes a similar cone, but there is no continuous rotation of the film about the film normal.

† This method was first mentioned by Schiebold in 1931 but was more fully described by Sauter in 1932 ; a modification of it which employs a cylindrical film is sometimes referred to as the " Schiebold method ".

ten or twenty separate photographs in order to obtain unambiguous indices for all the spots corresponding to a given type *hk*o, only one Weissenberg photograph is necessary. From Weissenberg photographs also, the angles between co-planar directions in the crystal can be easily obtained. The essential features of the various moving-film goniometers are shown in the table.

In the above table and in Figs. 43 and 44, the descriptions refer to the normal-beam methods ; in these the incident beam is normal to the rotation axis of the crystal. In all the different types of moving-film methods, however, several ' inclined-beam ' variants have been described, and some of these have special uses. A full description of the various moving-film methods is given by Buerger (1942) and of the precession method in particular by Buerger (1944).

2.6 The fibre photograph. When the specimen consists of a large number of very small crystals having one direction in common it is called a ' fibre ', this word being used to cover organic fibres, drawn metal wires, mineral fibres, etc. Owing to the range of orientation in the constituent crystals, such a specimen can reflect characteristic radiation without being moved during the exposure. The resultant ' fibre photograph ' is intermediate between a rotation photograph and a powder photograph with rather spotty lines (**11**, 1). In rolled sheets of material the constituent crystals may develop parallel orientations to a varying extent, depending on the substance and on the treatment. Fibre photographs can also be taken of such specimens, but it is usually necessary to take several photographs in order to obtain the information required.

3. Experimental Details

3.1 Size and shape of specimen. The chief factor which limits the desirable size of crystal specimens for X-ray photography is the absorption. Back-reflections can, of course, be obtained from any crystal, no matter how large, but transmission photographs require the use of small crystals. If the absorption is large, the density of the spots in transmission photographs is low, unless very small crystals are used. Crystals as small as 0·1 mm. in length can be mounted and photographed, but

special techniques are needed to handle such small specimens.

When estimation of intensity of reflection is to be made, it is desirable to use a crystal of thickness such that the absorption factor, which is discussed in **2**, 5·1, is nearly unity. But when the linear absorption coefficient is high, the thickness for which the absorption factor is almost unity is so small that it is impossible to handle a specimen of such a thickness. Larger crystals have to be used, but the problem of correcting for absorption is simplified if these can be made cylindrical, either by grinding or by solution. If this cannot be done, a crystal of the least awkward shape should be chosen ; but the irregularity of shape may result in serious errors in the intensities of reflections calculated from the experimental data.

3.2 Collimation of the incident X-ray beam. The size of the spot on the film produced by a diffracted beam is controlled by several factors, but the chief of these are the cross-section and the divergence of the incident beam. Even when a very small crystal specimen is used, the size of spot is increased by use of a larger collimator owing to increased divergence of the incident beam. General scattering, both from the specimen and from the air in the camera, can be reduced by use of a small collimator, and this is very desirable with certain types of specimen. In practice, a central aperture of 0·5 mm. diameter is as small as it is normally convenient to employ.

Care must be taken in the construction of the collimator in order that it should give no diffraction effects of its own on the film. The general principles of collimator design are illustrated in Fig. 46. The

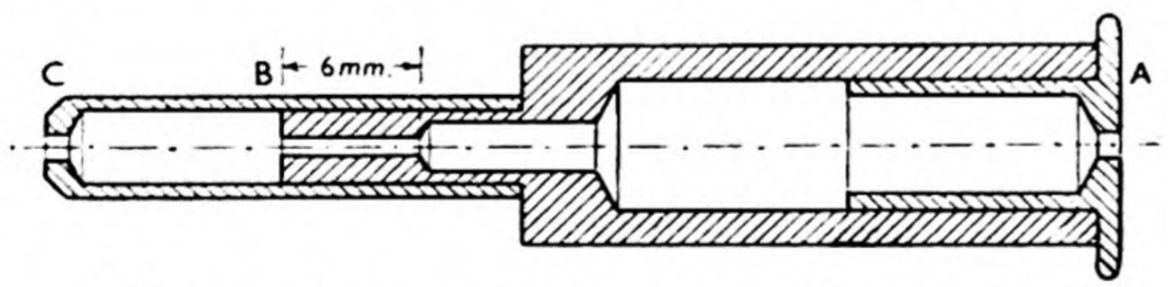

FIG. 46. The construction of a collimator ; *A*, *B* are defining apertures, *C* is a shield to catch stray radiation scattered from the end of *B*

beam is limited by two apertures, *A* and *B* ; a slightly larger aperture *C* serves to stop practically all the rays scattered by the edge of aperture *B*.

Collimators are usually made of brass, but since the linear absorption coefficient of brass is not high, attention must be paid to the length of the limiting aperture. An X-ray beam contains a great deal of white radiation which, if the applied voltage is 50 kV., will contain wave-lengths with a minimum of 0·25 A. The linear absorption factor of brass for this wave-length is about 25 cm.$^{-1}$ (Compton and Allison 1935) ; a thickness of 5 mm. is therefore needed to reduce the intensity to about 10^{-6}. In other words, if a collimator as described in the previous paragraph is used made entirely of brass, the aperture *B* should be at least 5 mm. long. This length can be much reduced by the use of lead.

Precautions should also be taken to see that the film does not receive any X-rays scattered from the point where the X-rays leave the camera. If the X-rays leave through a hole in the film, or in a piece of metal, care should be taken that neither the film nor the metal lies in the path of the beam, otherwise diffraction lines of the type shown in Fig. 124 will be observed. Such lines can easily be recognized because of their shape.

3.3 Methods of oscillating the specimen. There are two main methods of producing the oscillatory motion of the crystal required for oscillation photographs and in moving-film photographs The first method is by means of an arm attached to the axis of the instrument at one end while the other end is kept pressed against a cam which is rotated by a motor. This method is commonly used for small angles of oscillation, but a separate cam is required for each different angle used in the taking of oscillation photographs. In the second method, the axis of the instrument is driven by an electric motor which is constructed so that it reverses each time its motion is impeded by stops. This method is the most suitable for moving-film photographs as the large angles of oscillation required make the use of cams very difficult. For purposes which do not require estimated intensities of reflection, the achievement of a high degree of uniformity of angular motion is not essential. Even if there is an appreciable period of rest at the two extremities of the motion, the usefulness of an oscillation photograph for certain purposes is unimpaired. A photograph taken on such an apparatus with unfiltered radiation would in general show a Laue spot at each end of each streak, while there would be enhancement of the density of a characteristic spot which happened to be produced when the crystal was at either end of its oscillation.

When information is required on intensities of reflection, however, the degree of uniformity of angular motion is very important. Complete uniformity can never be achieved in practice, and some limit has to be set to the non-uniformity of motion which is allowable. The divergence of the incident beam causes any reflecting plane to continue reflecting for a finite time, during its rotation through the reflecting position. Such divergence is usually less than 1° and greater than 15′. If we require the times of reflection of corresponding planes as they pass through the reflecting position to be equal within 5 per cent, we must have an instrument in which the time of rotation through each successive 15′ interval does not vary by more than 5 per cent. If the

crystal is imperfect, so that any one plane reflects over an angle of about 1°, then the requirement stated above need not be so stringent.

If a heart-shaped cam is used, it must not possess a plane of symmetry as otherwise the velocity of rotation would not be uniform as the arm rotates. The precise form for cams of various sizes in relation to the length of the arm riding on them has been worked out (Yu, 1937). Such cams must be accurately cut to achieve the accuracy stated above. If the last wheel of the gear train in the synchronous motor has any defect, this will at once diminish the uniformity of rotation of the cam. However, this system gives good results with the synchronous motors used in electric clocks and cams cut by precision methods.

The second method of oscillating the crystal by means of a gear train requires very careful attention to the gears if it is to be successful. In the first place the speed of rotation of the crystal must not exceed a certain value which is set by the frequency of the electric mains supply. This is so for the following reason. When an X-ray tube is operated directly from a high-tension transformer there are, depending on the frequency of the supply, about fifty pulses of X-rays emitted from the tube per second. In between two consecutive pulses there is an interval of about 1/100 sec. when practically no X-rays are emitted. If during this interval the crystal comes into a reflecting position and then passes beyond it, no reflection at all is recorded on the film for that passage through the reflecting position. When a crystal is driven by a synchronous motor, as used for a clock, there is a danger that every time the same reflecting plane comes into the reflecting position it will pass through it just when no X-rays are being produced by the tube. One remedy for this is to ensure that the speed of rotation of the crystal is so slow that during a rotation through an angle of about 15′, the X-ray tube has emitted at least ten pulses. This corresponds to a speed of rotation of the crystal not exceeding one revolution in five minutes. Another solution is to arrange by special gearing that if the crystal rotates at such a speed that in between two X-ray pulses it turns through an angle θ, then $2\pi/\theta$ is not a whole number, but, for example, an integer plus a tenth. In this case the crystal makes ten complete rotations in completing one cycle of reflections from a given plane. At the beginning of the cycle let us suppose that the crystal is passing through the reflecting position when the X-ray intensity is zero. After one complete rotation of the crystal the phase of the X-ray beam is $2\pi/10$ removed from its previous value ; after two complete rotations the phase of the X-ray beam is $4\pi/10$ and so on. Thus after ten complete rotations every reflecting plane of the crystal has experienced ten phases of the cycle of X-ray intensities. In this way all planes receive the same exposure to the X-rays.

CHAPTER 5

INTERPRETATION OF OSCILLATION PHOTOGRAPHS

1. Geometry of X-ray Reflection

1.1 Introduction. The oscillation photograph can be regarded as the fundamental type of single-crystal photograph; consequently a clear understanding of this method is essential. In this method the crystal is oscillated (or rotated) about an axis perpendicular to the incident X-ray beam. This allows many lattice planes to come into the appropriate positions for reflecting the characteristic radiation. If white radiation is present in the beam, a streak is produced on the film by the reflection of the white radiation by each of these sets of lattice planes. Although useful information can often be obtained from such streaks, it is the spots produced by the characteristic radiation with which we are most concerned in this chapter. The first task is to assign indices to each reflection. This is most conveniently done if a crystallographic axis is selected as the axis of oscillation. The process of indexing is quite straightforward, provided that all the lattice parameters are approximately known and that the orientation of the lattice relative to the specimen is known. If only some of this information is available, less direct procedures have to be adopted. For very large unit cells, such as occur in many crystals of biological importance, special methods of indexing are employed (Carlisle and Dornberger, 1948).

1.2 The oscillation goniometer. The crystal is set on two mutually-perpendicular adjusting arcs fitted with centring slides and mounted on a spindle as on an ordinary spectrometer; and, except on the simplest instruments, the positions of the arcs may be read to tenths or to sixths of a degree. The X-ray beam enters through a collimating slit system at right angles to the oscillation axis and passes out through a hole in the camera or else is absorbed by a lead stop. A low-power microscope is fitted for adjusting the crystal visually and for centring it. In more elaborate instruments the removal of a lens turns this into a telescope for viewing signals reflected by crystal faces from an optical collimator which can be attached to the instrument.

The most suitable camera for general use is a cylindrical one with a radius of about 3 cm., the axis of the camera being coincident with the oscillation axis of the crystal. For special purposes plate cameras are used—a front-plate for low-θ spots and a back-plate for high-θ spots. Although both these can record only a limited range of spots, they have one advantage over the cylindrical camera in that the crystal-to-film distance can be easily varied.

1.3 Use of the reciprocal lattice. In order to understand the formation of the spots on an oscillation photograph it is helpful to think in terms of the reciprocal-lattice concept developed in **3**, 2.1. The crystal is represented by its reciprocal lattice in the correct orientation and the condition of reflection given by the Bragg equation is expressed by the geometrical construction shown in Fig. 40. The reflecting sphere of this construction has a radius of K/λ, where K is the reciprocal constant. For our present purpose it is convenient to take $K=\lambda$, so that the radius of the reflecting sphere is one dimensionless unit. As shown in **3**, 3, if this is done, the Bragg law is obeyed for a set of lattice planes when the reciprocal point corresponding to them lies on the surface of the reflecting sphere. The direction of the reflected beam is given by the line joining the centre of the

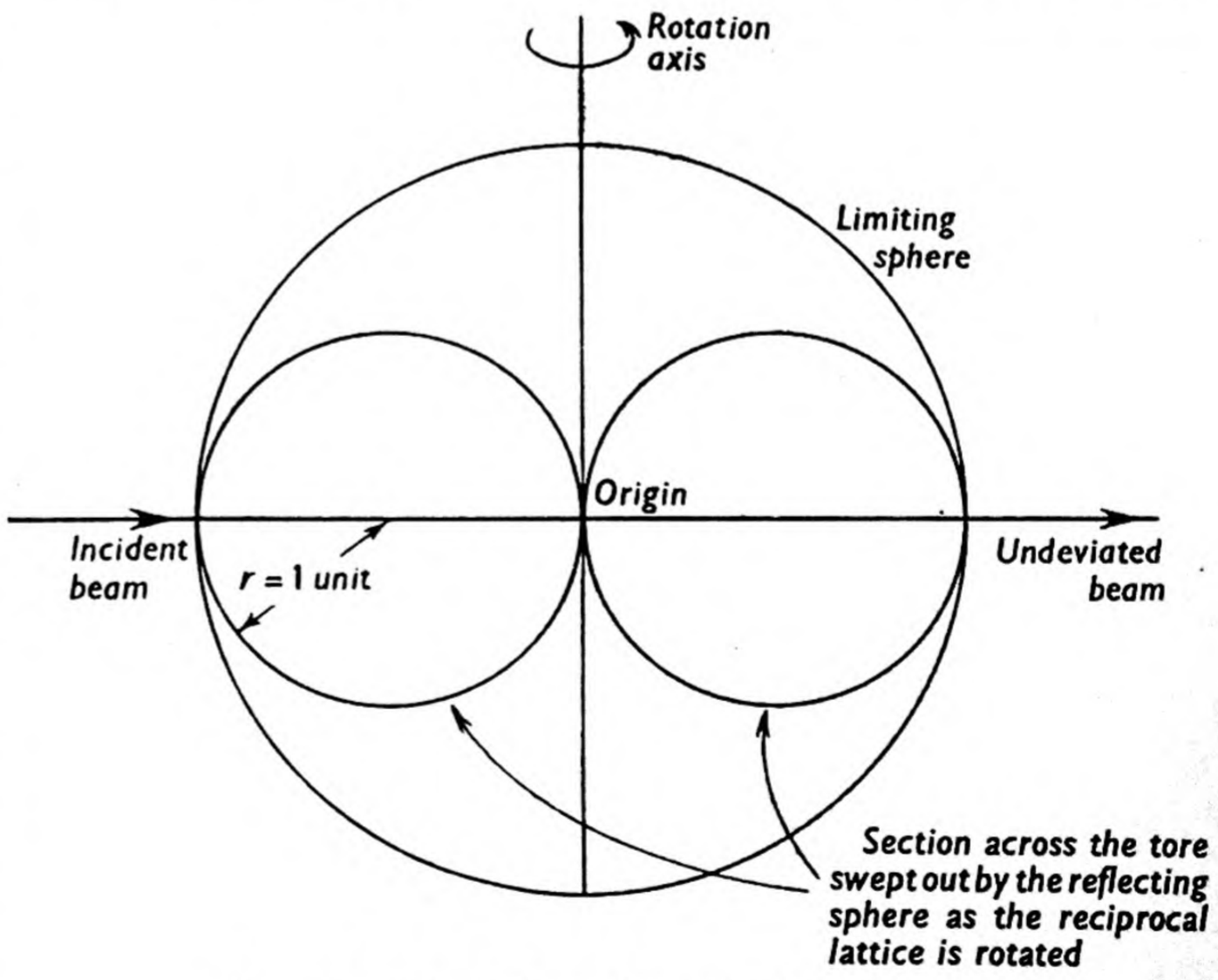
Rotation axis
Limiting sphere
Origin
Incident beam
r = 1 unit
Undeviated beam
Section across the tore swept out by the reflecting sphere as the reciprocal lattice is rotated

FIG. 48. Vertical section of limiting sphere

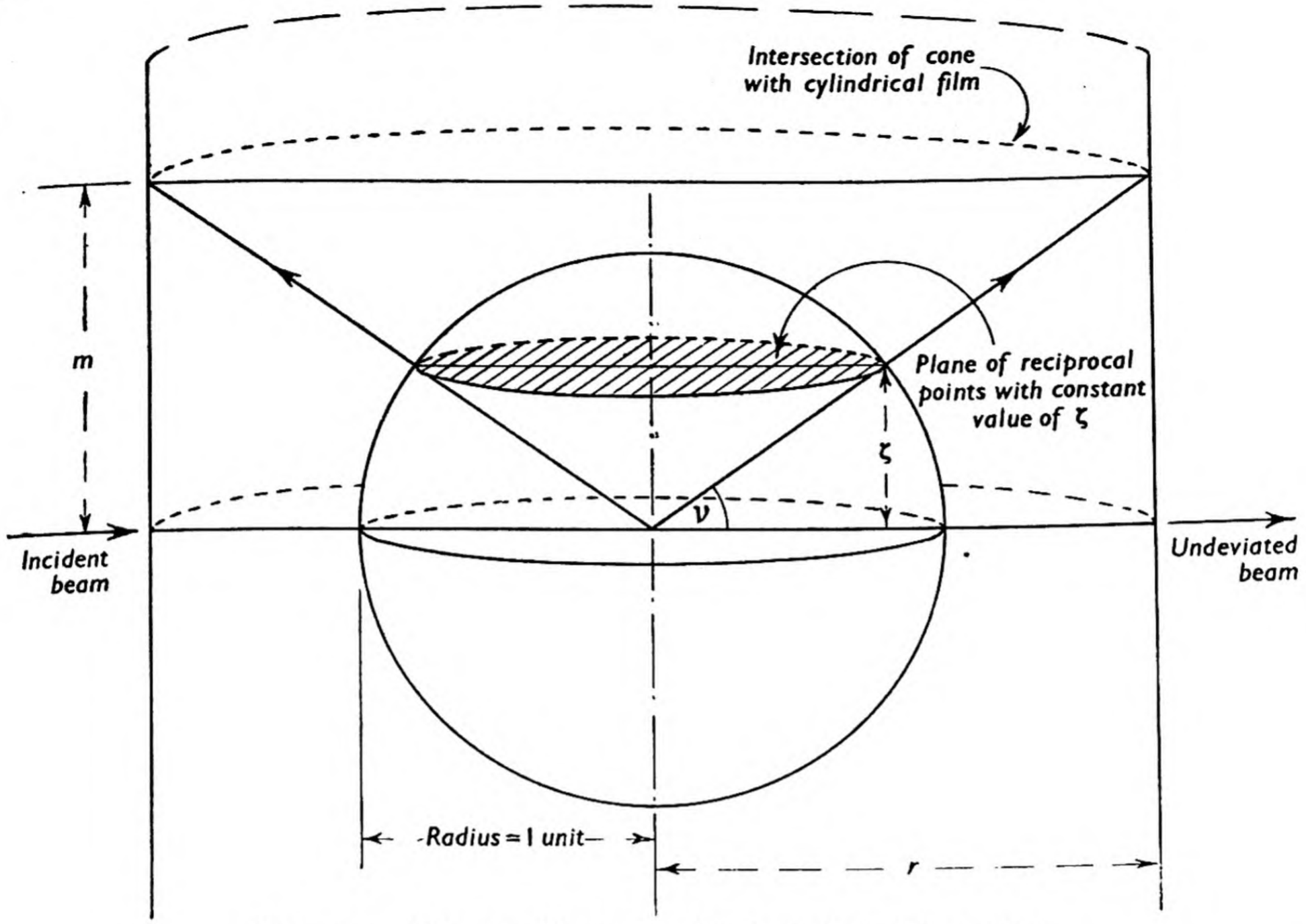

FIG. 49.1. Diagram illustrating the formation of layer lines

reflecting sphere to the reciprocal point lying on the surface. When the crystal is oscillated or rotated, a number of reciprocal points pass through the surface of the reflecting sphere and so can be imagined as giving rise to the reflections which are recorded on the film. In Fig. 48 is shown the nature of the volume swept out of the reciprocal lattice by the reflecting sphere during the rotation of the crystal. When the crystal is oscillated, only a part of this volume will be swept by the sphere. This reciprocal-lattice method of dealing with the problem is geometrically elegant and is easily visualised.

1.4 Layer lines, row lines and the Bernal Chart. The most obvious feature of an oscillation (or rotation) photograph on a cylindrical film is the set of parallel straight lines of spots. A photograph such as this can be produced only when a zone axis of the crystal is chosen as the oscillation axis, and it is easy to see why this is so. A zone axis is a direction in the Bravais lattice to which a group of lattice planes is parallel: the normals to all these planes lie in the plane perpendicular to the zone axis. Correspondingly there is a plane of reciprocal points perpendicular to the zone axis direction and passing through the origin. From the nature of the reciprocal lattice there are exactly similar planes of points parallel to the first one. These planes of reciprocal points intersect the

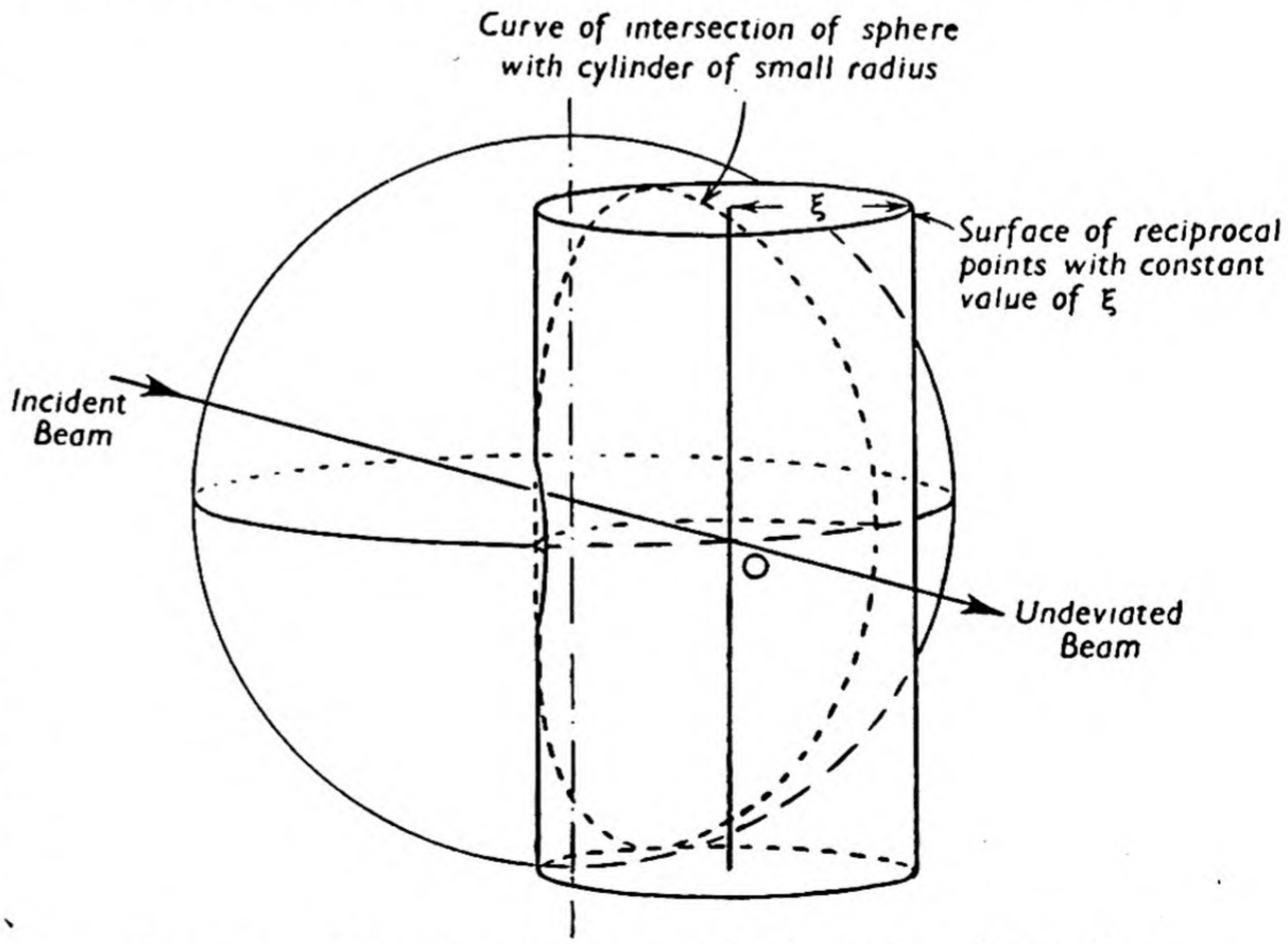
Curve of intersection of sphere with cylinder of small radius
ξ
Surface of reciprocal points with constant value of ξ
Incident Beam
O
Undeviated Beam

FIG. 49.2. Diagram illustrating the formation of row lines

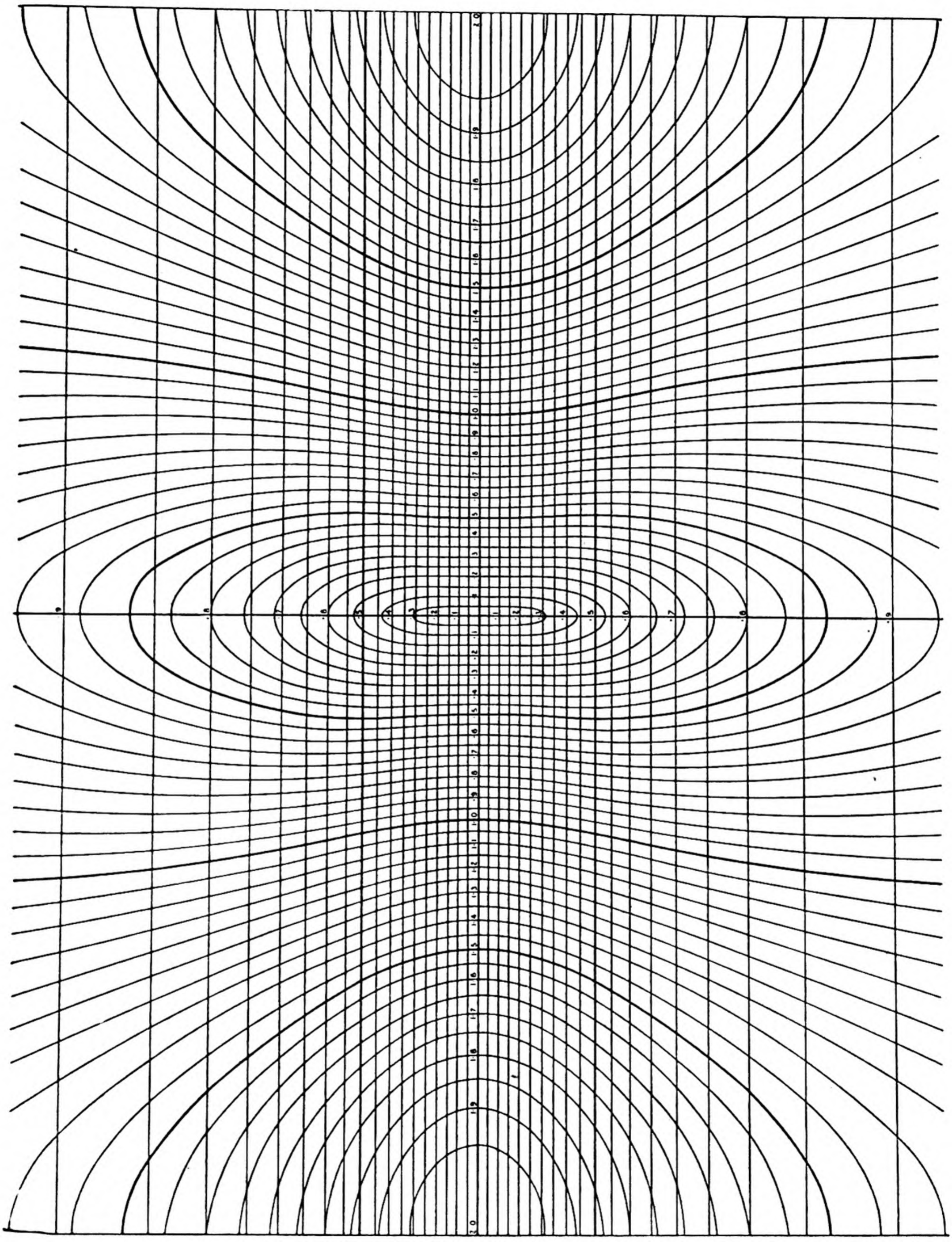

FIG. 50. Bernal chart (ξ and ζ) for cylindrical camera of radius 3 cm.

sphere of reflection in small circles (Fig. 49.1); (the equator can be considered as a small circle of radius 90° about either the north or the south pole). If we join the centre of the reflecting sphere to these intersections, we obtain a series of cones co-axial with the north-south axis of the sphere and with a semi-angle $(90° - \nu)$ where $\nu = \sin^{-1}\zeta$. Each of these cones is the locus of reflections which correspond to the points lying in the appropriate plane of the reciprocal lattice. The cones of reflected rays intersect the circumscribing cylindrical film in a series of circles which form straight lines when the film is laid flat. The zero *layer line*, for which $\nu = 0°$, always passes through the point of exit of the incident beam, but the positions of the non-zero layer lines vary with the angle ν. If a flat plate is used (either front or back) the cones intersect it in a series of hyperbolae of different eccentricities (Fig. 51). Thus all spots on the nth layer line correspond to reciprocal points on the nth plane of reciprocal points perpendicular to the oscillation axis. Such a plane is specified by the axial co-ordinate ζ of the set of cylindrical co-ordinates (**3**, 2.3). All reciprocal points on this plane and the corresponding spots on the nth layer line have the same value of ζ.

If we now consider the surface in reciprocal space defined by a single value of the radial cylindrical co-ordinate ξ, it can be seen from Fig. 49.2 that this is a cylinder with its axis through the origin of the reciprocal lattice. A set of such cylinders, with ξ varying in steps of 0·05 from zero up to two units, intersects the sphere in a set of curves. If ξ were greater than 2·00 the cylinder would not intersect the sphere. If we join the centre of the sphere to these intersections, the surfaces of reflected rays are produced which intersect the film in the sets of curves shown in Fig. 50. These are curves of constant ξ, and the photograph (Fig. 63.2) shows marked rows of spots lying on these curves which are called *row lines*.

For our present purpose we shall not deal with the curves of constant ϕ, the third cylindrical co-ordinate, because we do not need these until Chapter 8. It is clear that a chart of curves of constant ζ and ξ is extremely useful in the study of oscillation photographs. These charts—generally called *Bernal Charts*—can be constructed for any given crystal-to-film distance (Figs. 50 and 51). One chart suffices for all cylindrical cameras of the same radius; another for all front-plate cameras of the same crystal-to-plate distance; and a third for all back-plate cameras of the same crystal-to-plate distance. Each kind can be increased or reduced in scale photographically for other cameras of the same type, but if the change in scale is considerable a new chart should be constructed to obtain a suitable thickness of line.

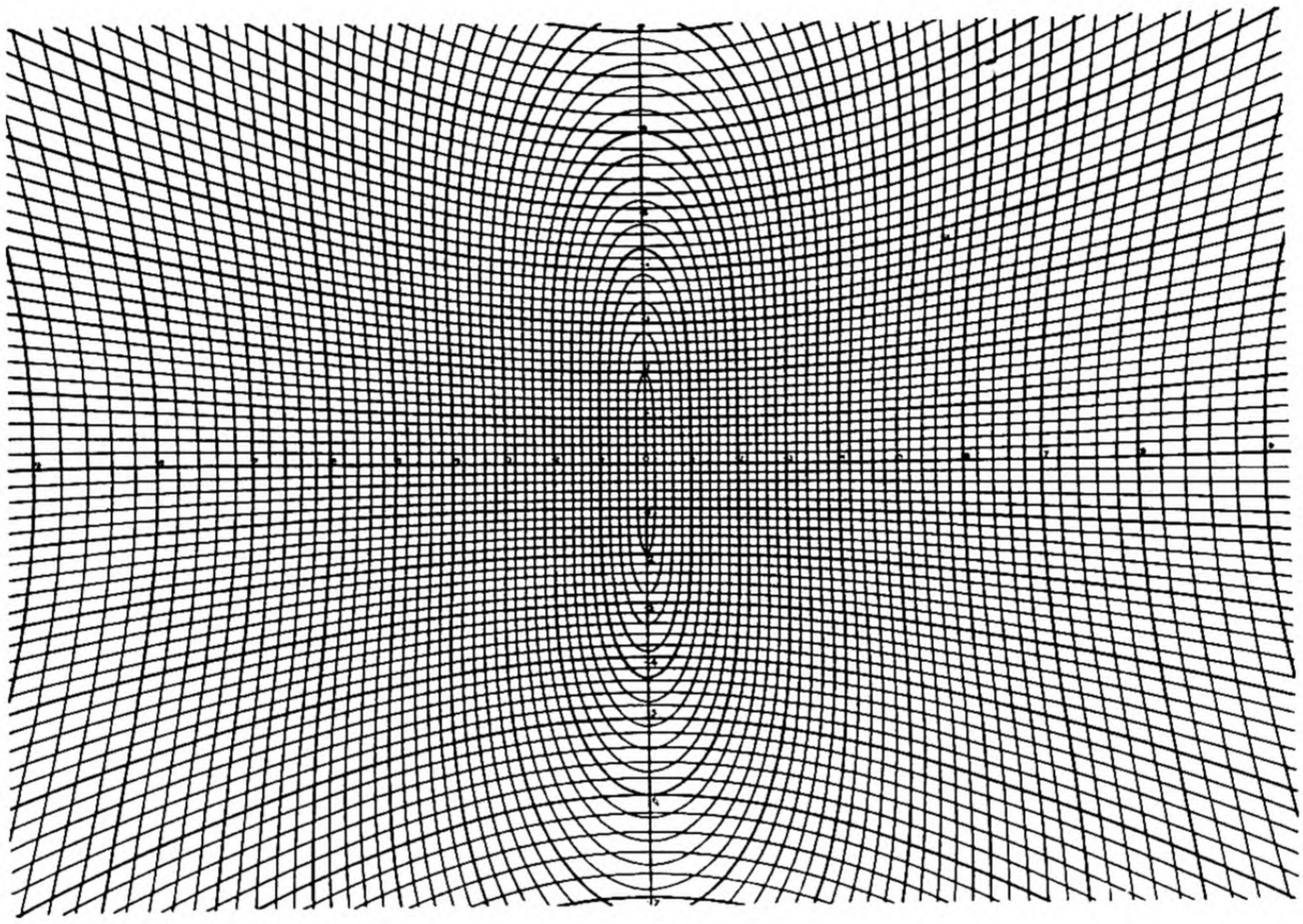

FIG. 51. Bernal chart (ξ and ζ) for a flat-plate (front) camera at a distance of 4 cm.

1.5 Measurement of unit-cell dimensions. We have seen that straight layer lines are produced only when a zone axis of the crystal is taken as the oscillation axis. From the ζ values of the layer lines on the

photographs we can obtain directly the *repeat distance* (*identity period*) of the Bravais lattice along the direction of the zone axis which is taken as oscillation axis.

In Fig. 52 is shown the unit cell of a triclinic Bravais lattice with the three reciprocal axes inserted. By definition the directions of x^*, y^* and z^* are normal to the planes yz, zx and xy respectively. Hence the set of planes of reciprocal points parallel to x^* and y^* is perpendicular to the zone axis [001].

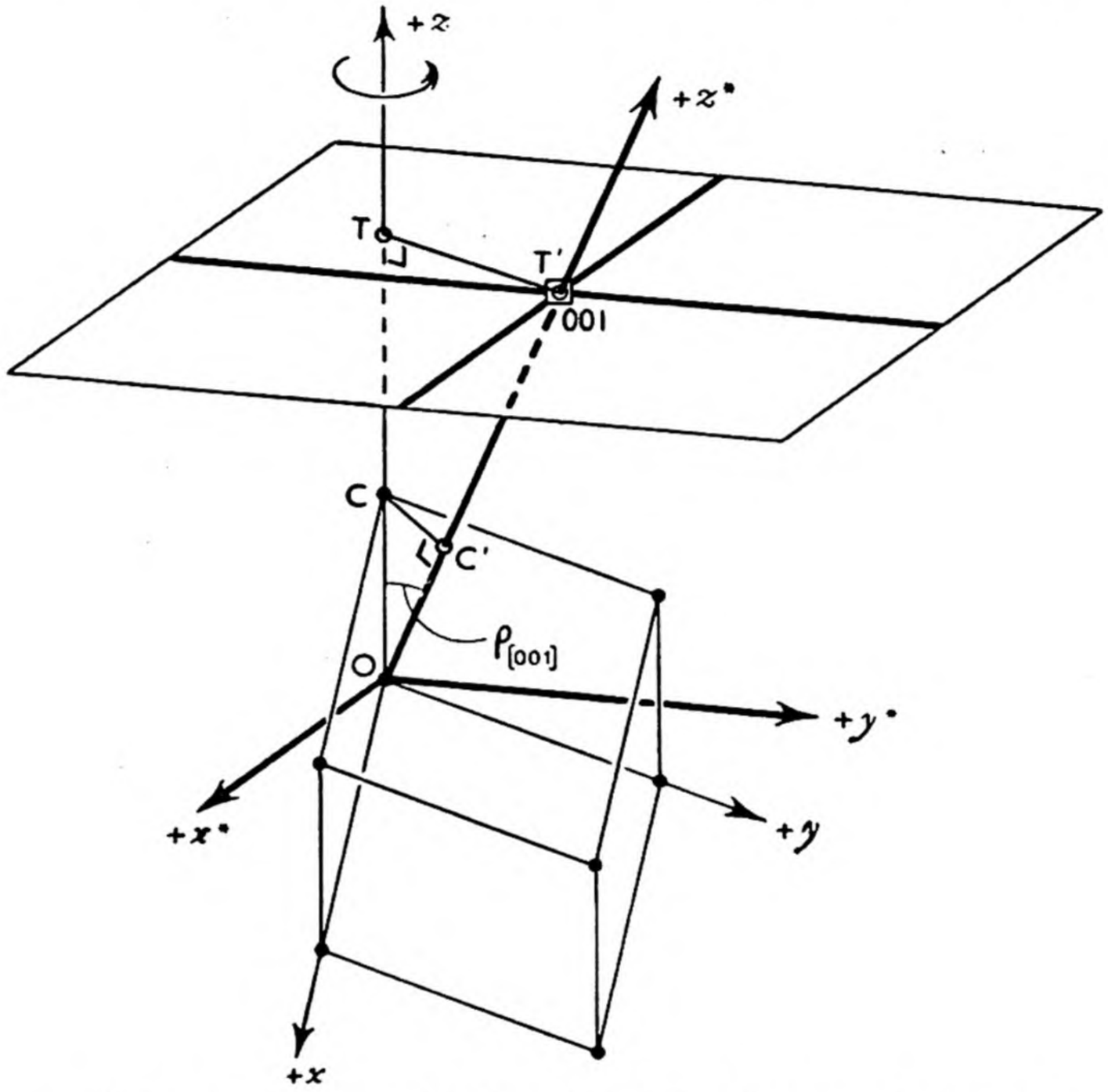

FIG. 52. Diagram showing the relation between the z axes of the Bravais lattice and of the reciprocal lattice.

$$OC = c \quad , \quad OT = \zeta_{[001]}$$
$$OC' = d_{001}, \quad OT' = c^*$$

The perpendicular distance between these planes of reciprocal points is denoted by $\zeta_{[001]}$ and, where $\rho_{[001]}$ is the angle between the z-axis and the direction of z^*,

$$\zeta_{[001]} = c^* \cos \rho_{[001]}.$$

By definition, $c^* = \lambda/d_{001}$,

but it is clear that $d_{001} = c \cos \rho_{[001]}$.

Hence $\zeta_{[001]} = \lambda/c$.

Since a set of parallel planes through reciprocal points exists perpendicular to each zone axis in the Bravais lattice, this result is general and we can write

$$d_{[uvw]} = n\lambda/\zeta_n,$$

where $d_{[uvw]}$ is the repeat distance along a zone axis in the Bravais lattice and ζ_n is the value of ζ for the nth layer line in a photograph taken with the zone axis as the axis of rotation or oscillation.

If a Bernal chart is not available, the value of ζ can be easily obtained from a measurement of the distance of any layer line from the zero layer line. In Fig. 49.1 it is clear that $\zeta/1 = \sin \nu$, and for a cylindrical camera of radius r, $m/r = \tan \nu$, where m is the height of the layer line above the zero layer line; while for a flat camera at a distance p from the crystal, $m/p = \tan \nu$, m being measured to the vertex of the hyperbola.

Thus, by taking oscillation photographs with each of the three crystallographic axes as oscillation axis in turn, we can determine from the heights of the layer lines the dimensions a, b and c of the unit cell of the Bravais lattice of any crystal. One method of determination of the angle β of a monoclinic unit cell is given in **5**, 2.7.

As the linear separation on the photograph between successive layer lines increases with increase of ζ, a more accurate value of the repeat distance along the zone axis of oscillation can be obtained by measuring ζ from a high layer line. The resultant gain in accuracy

is diminished to some extent by the greater vertical elongation of the spots in the higher layer lines which is partly due to the divergence of the X-ray beam. Accordingly, even with a good, small crystal, the accuracy with which repeat distances can be measured from layer line separations is only of the order of one per cent.

1.6 Comparison of rotation and oscillation photographs. If, in a rotation photograph showing regular layer lines, we take the ζ- and ξ-values of any spot, we have located the reciprocal point as lying on a circle in reciprocal space which has its plane perpendicular to the zone axis of rotation. In fact a given value of ζ and a given value of ξ define two circles, unless we state whether the spot occurs on the upper or on the lower part of the film. Spots on the lower part can be indicated by negative values of ζ. If the zone axis of rotation is an axis of symmetry, more than one reciprocal point will lie on such a circle. If the mesh of the reciprocal lattice is small, several points may lie on or nearly on the circle, whether the zone axis of rotation is a symmetry axis or not. If the crystal is turned through a complete rotation, all such reciprocal points will pass through the same two points on the surface of the reflecting sphere (Fig. 53). All corresponding reflections will fall on the same two points on the film. Because of the superposition of such reflections, ordinary rotation photographs are seldom used. But if the spots on a layer line happened to be few, no trace of the layer line might appear on a particular oscillation photograph. In such a case, the rotation photograph provides the most certain method of determining the repeat distance along an axis of the crystal.

If the crystal, instead of being rotated, is oscillated through a small angle (usually not more than 15°) the superposition of reflections can be largely avoided. If we know the orientations of the crystal at the two extremities of oscillation, the values of ϕ for the reciprocal points are known, at least within limits which are usually sufficiently narrow. This knowledge can be applied graphically as described below, and when the indices of the reflecting plane are in doubt, we can reduce the angle of oscillation until the ambiguity disappears.

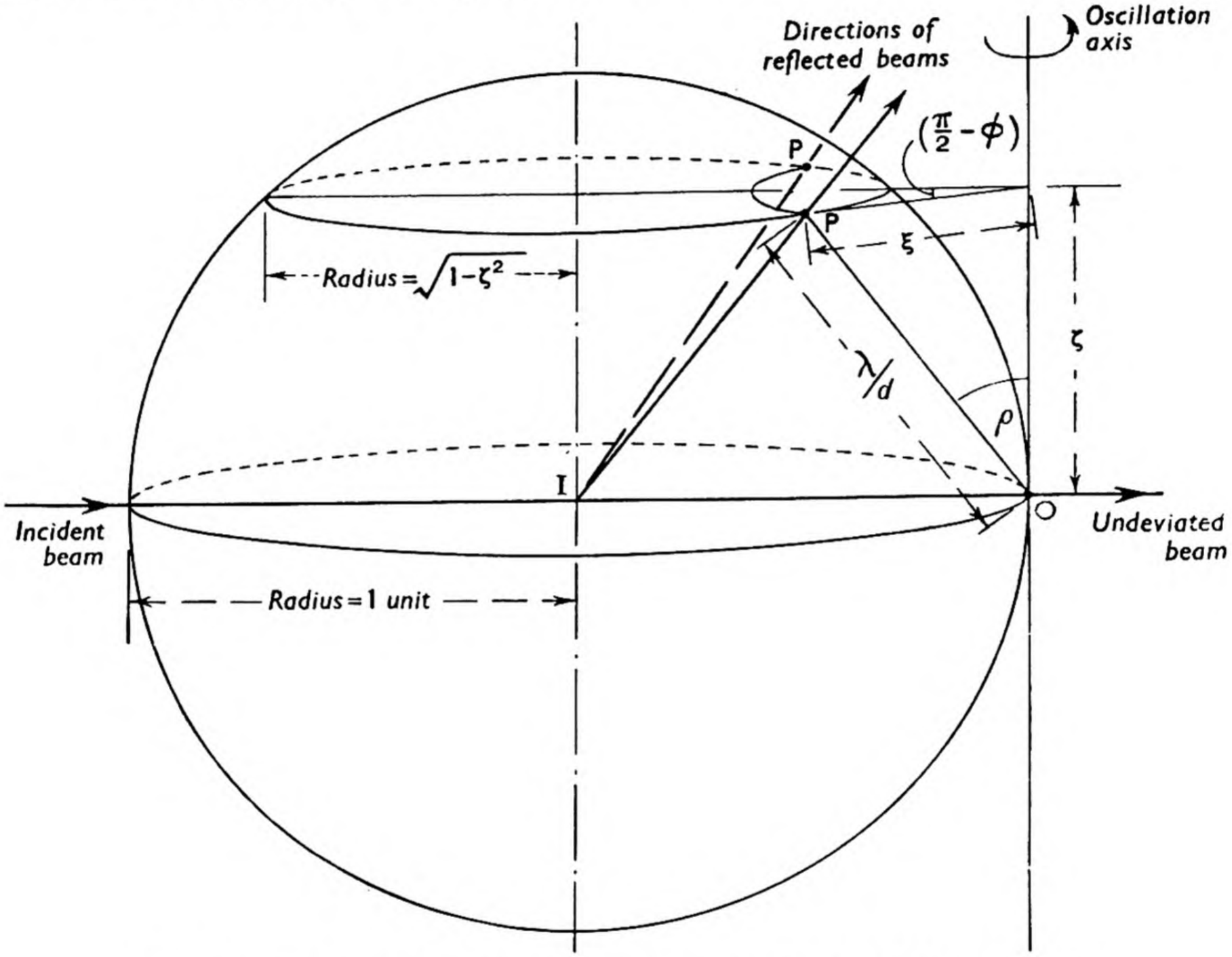

FIG. 53. Diagram showing the geometry of reflection of X-ray beams

1.7 Geometrical constructions. After the requisite number of photographs has been taken with different zone axes as oscillation axes, the shape and size of the unit cell of the Bravais lattice can be determined. The calculations are done below for the mineral topaz as an example. With this information we can go on to construct the reciprocal lattice, for

which a convenient scale, such as 10 cm. to one unit, is chosen, the wave-length being taken as the reciprocal constant. Three projections of the reciprocal lattice are drawn, one perpendicular to each crystallographic axis taken as oscillation axis. In all reciprocal lattices every layer perpendicular to a given zone axis has exactly the same arrangement of points within it, and in orthogonal crystals these layers are laid exactly on top of each other.

When layers of the reciprocal lattice have been drawn, the appropriate reflecting circles are inserted. correspond to the actual movement of the crystal. It is, however, easier to move the reflecting circle, carrying with it the incident X-ray beam. A clockwise movement of the crystal from its initial position (looking down) corresponds to an anti-clockwise movement of the reflecting circle, and vice versa.

When the two reflecting circles corresponding to the two limits of the oscillation have been drawn, they define two lune-shaped areas. These areas are sections through the volume swept out by the oscillating sphere of reflection and they are perpendicular

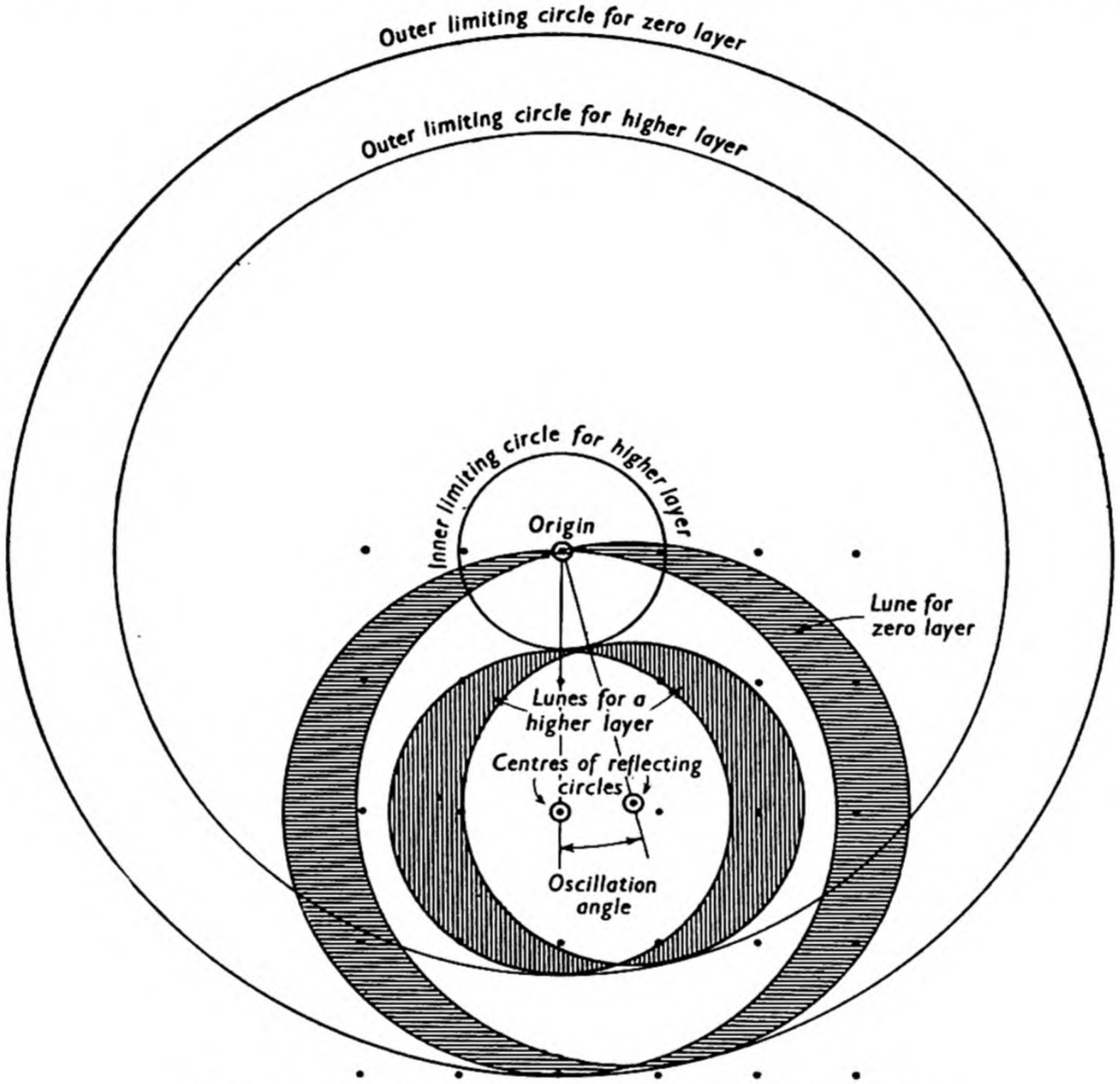
Outer limiting circle for zero layer
Outer limiting circle for higher layer
Inner limiting circle for higher layer
Origin
Lune for zero layer
Lunes for a higher layer
Centres of reflecting circles
Oscillation angle

FIG. 54. Horizontal sections of the limiting sphere
Scale: 1 unit = 2·5 cm.

Each layer of the reciprocal lattice cuts the reflecting sphere in a circle, the radius of which is given by $r' = \sqrt{1 - \zeta^2}$. This radius can be easily determined graphically from an accurate scale drawing. Each reflecting circle inserted on the reciprocal lattice has its centre on a vertical line which intersects the horizontal incident X-ray beam at a distance of one unit from the origin, as shown in Fig. 54. It should be noted that only the equatorial reflecting circle on the zero layer of the reciprocal lattice passes through the origin of the layer. The appropriate oscillation of the reciprocal lattice relative to the stationary reflecting circle and incident X-ray beam would to the axis of oscillation (Fig. 54). Only those reciprocal points which lie within these lunes represent lattice planes which could reflect, because only these points have passed through the surface of the reflecting sphere during the oscillation. Since the movement of the reflecting circle is made to correspond to that of the crystal, the points on the right side of the reciprocal lattice give rise to spots on the right side of the film, and similarly for the left side. When the direction of the movement of the crystal from its initial position is not known, it can be found by trial indexing of the spots as shown below.

1.8 Effects of different wave-lengths. When an oscillation photograph is taken with unfiltered radiation, the reflections consist of streaks with stronger spots superposed on some of them (Fig. 55). Reference may be made to **2,** 1.2 and **2,** 1.3 for the general nature of the radiation emitted from an X-ray tube. Each streak is produced by the reflection of various wave-lengths by one set of lattice planes. In terms of the reciprocal lattice, the relation $d^* = \lambda/d$ implies that a given set of lattice planes is represented by a different reciprocal point for each wave-length involved. These reciprocal points all lie on the same straight line from the origin perpendicular to the set of lattice planes. When the crystal is rotated, this line describes a cone of which the axis is the rotation axis and the semi-angle is ρ (Fig. 53). This cone intersects the reflecting sphere in a curve. The projection of this curve from the centre of the sphere produces the corresponding curved trace on the photographic film. Each streak, therefore, lies on a curve of constant ρ which is the locus of all spots reflected from a given set of lattice planes. On a photograph a streak is brought to an end either by the limit of the oscillation or by the decrease to zero intensity of the radiation needed to satisfy the Bragg equation for the angle θ which has been reached. Which of these factors operates in any particular experimental arrangement depends on the orientation and spacing of the particular set of lattice planes. Of the two ends of the streak, that which is nearer to the centre of the film is produced by the shorter wave-length, since d^* is directly proportional to λ. These streaks provide information which is useful for certain purposes as is shown in **8,** 3.3.

When a streak shows a stronger spot superposed on it, this is due to the greater intensity of the characteristic radiation, usually either $K\alpha$ or $K\beta$; but one or both of these reflections will be absent unless the corresponding reciprocal point passed through the surface of the reflecting sphere. When a filter is used to cut out the $K\beta$ radiation (**2,** 5.5) a gap occurs in those streaks which cover reflections from this part of the radiation. This effect can be seen in Fig. 56.1, although the filter used for this photograph was thinner than usual and sufficient $K\beta$ radiation has penetrated it to record the strongest reflections. This figure also shows that beyond the gap the short radiation penetrates the filter. Short-wave effects are most prominent near the centre of the film, because in general the intensity of reflection from planes decreases with increase of angle θ (**15,** 2.2). When the incident radiation is first reflected from another

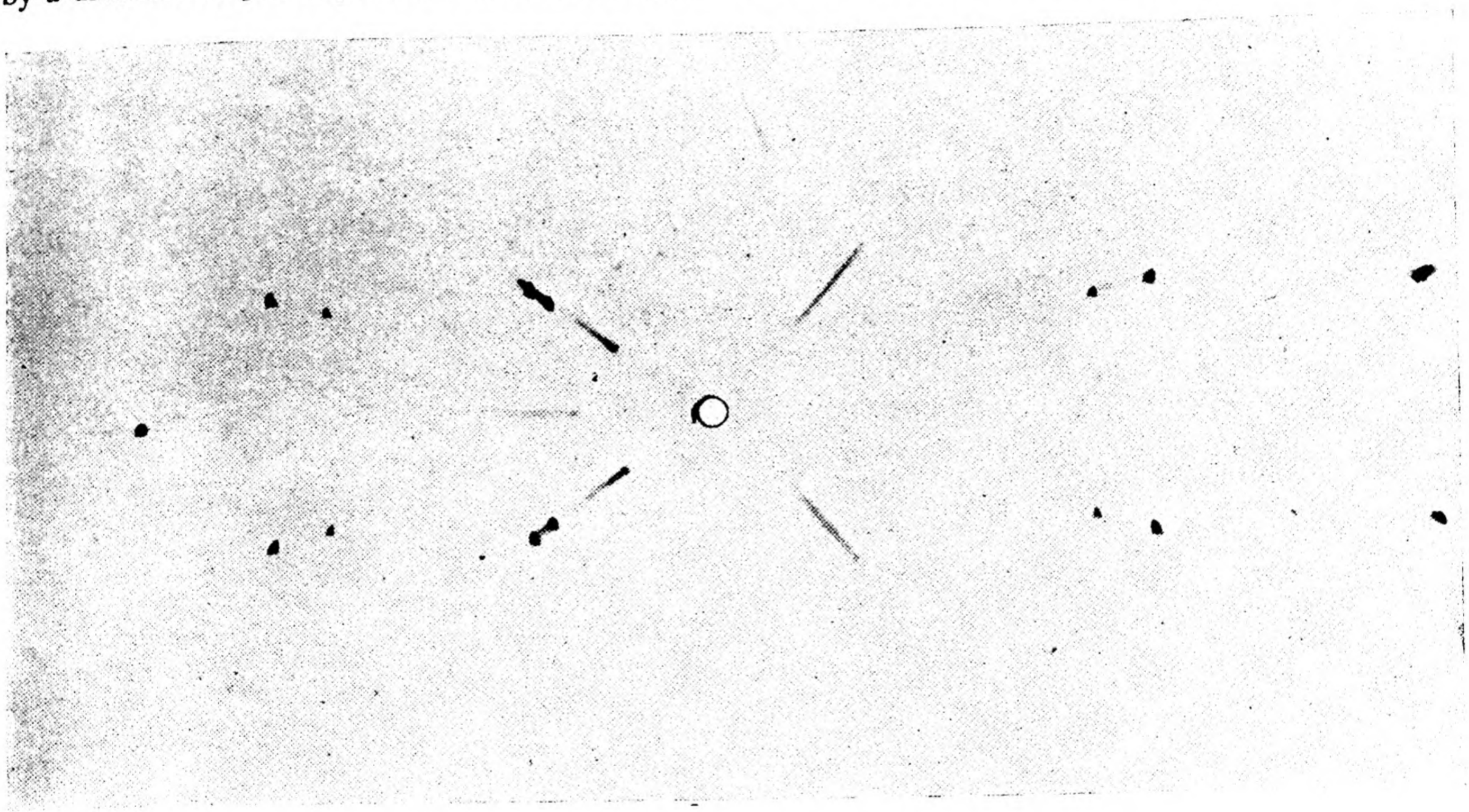

FIG. 55. Oscillation photograph.
Specimen: diamond oscillated through 15° about [100] as axis.
Camera: cylindrical, $r = 3$ cm. Radiation: CuK (unfiltered)

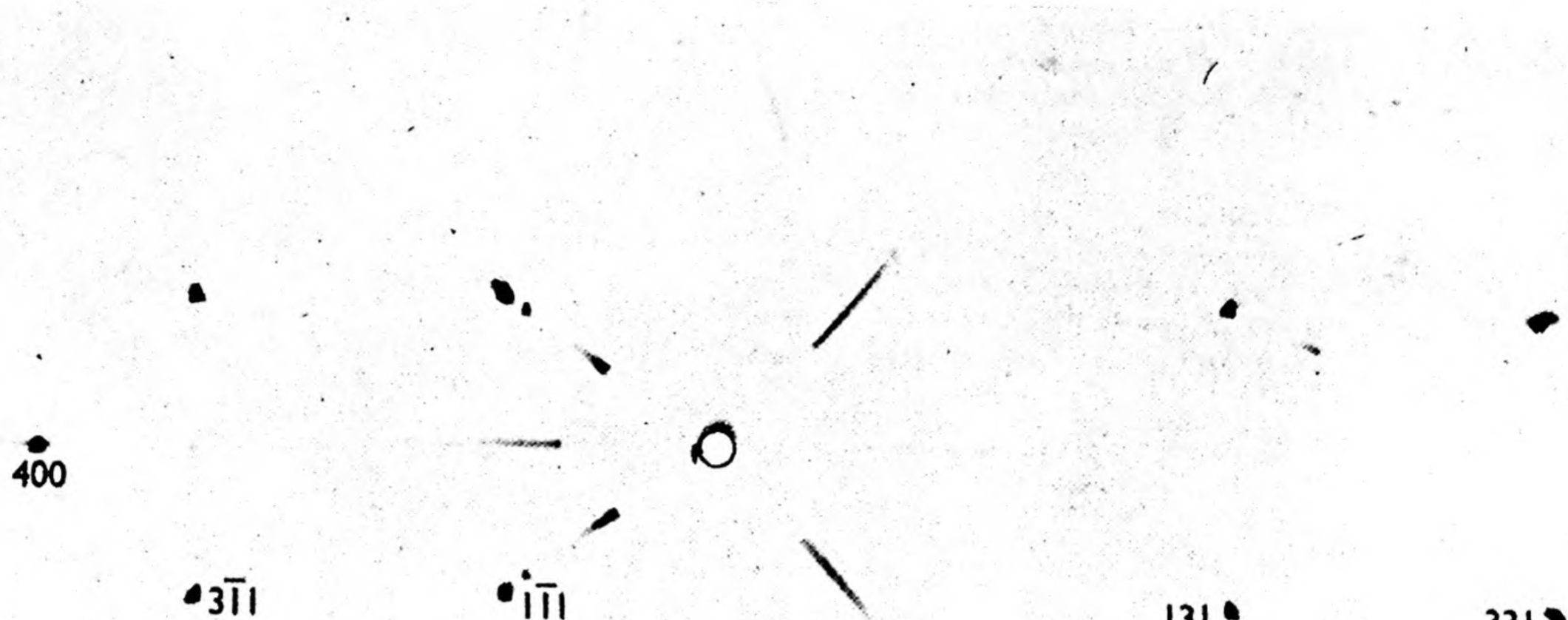

FIG. 56.1. Oscillation photograph (indexed).
Same as for Fig. 55 but a nickel filter has been used which is too thin

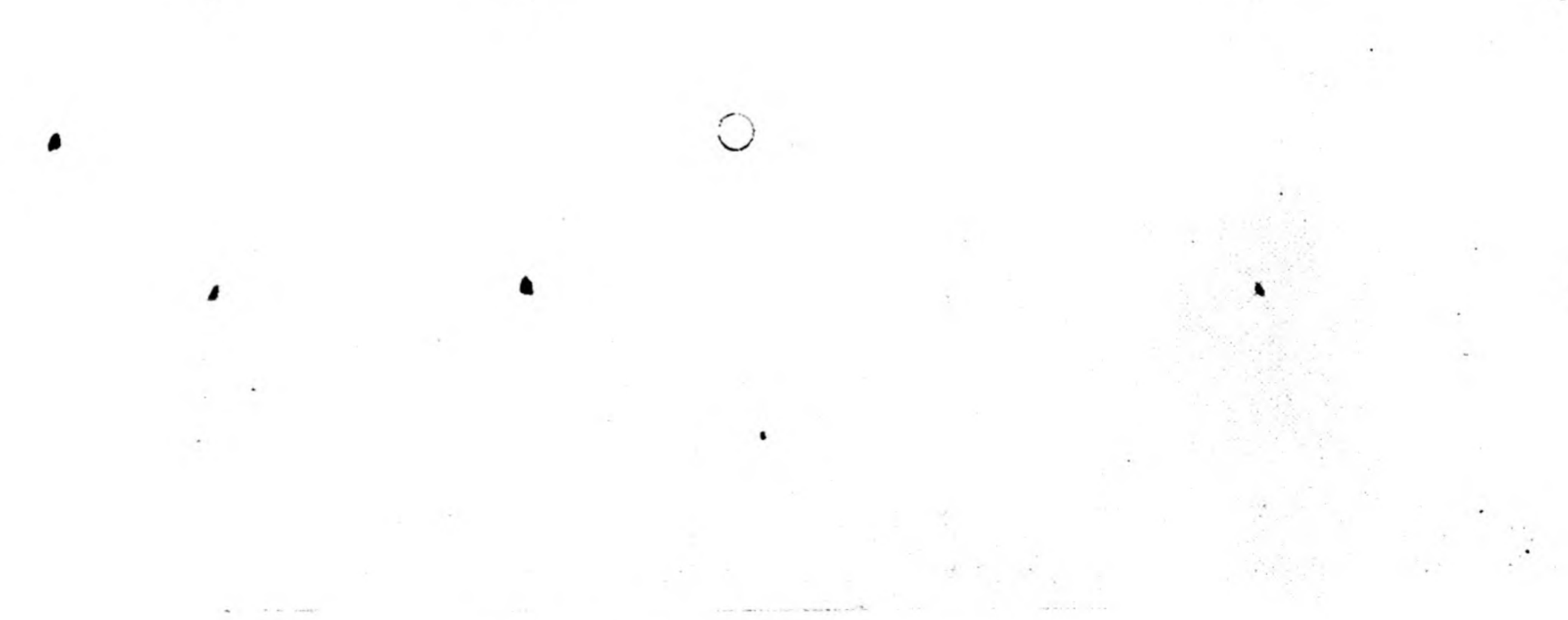

FIG. 56.2. Oscillation photograph.
Same as for Fig. 55 but with monochromatised Cu$K\alpha$ radiation

crystal before it falls on the specimen (**2,** 6), all the streaks on the photograph disappear and only the characteristic spots remain, as in Fig. 56.2.

Even when the incident beam is crystal-reflected, the characteristic radiation $K\alpha$ still consists of two main wave-lengths $K\alpha_1$, and $K\alpha_2$, which are resolved only at high values of θ in ordinary cameras. The spots produced by these two wave-lengths are not separated in Fig. 56.2 because the width of each spot is greater than the distance between their centres.

Continuous radiation

(1) A streak is produced along the corresponding curve of constant angle ρ.

(2) The streak is terminated either by the limits of the oscillation or by the fading out of the radiation before one of these limits is reached.

(3) The end of the streak nearest the centre of the film is produced by the shortest wave-length reflected, and the other end by the longest.

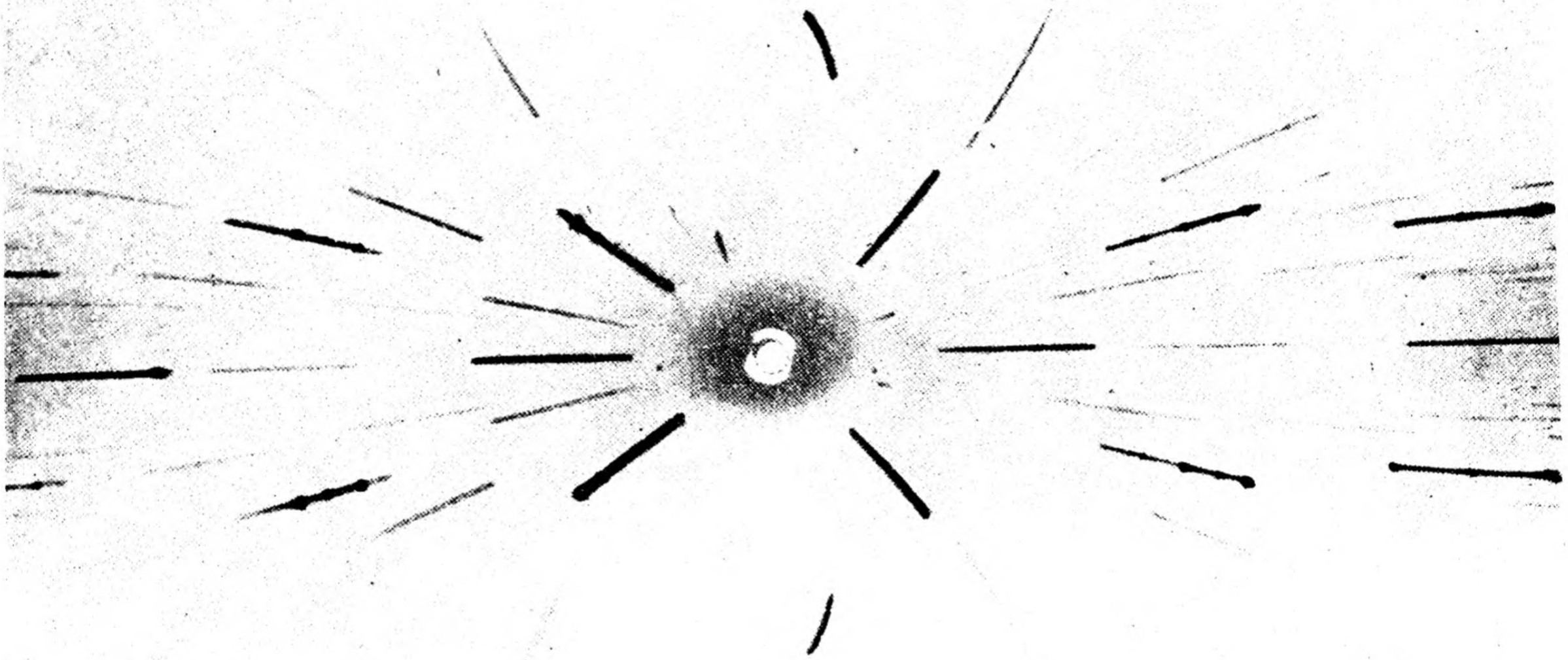

FIG. 57. Oscillation photograph.
Same as for Fig. 55 but taken with unfiltered radiation from an old Cu target containing some tungsten

Fig. 59.1, however, shows these doublets because a smaller part of the crystal was irradiated and because the separation of the two spots is greater for Mo$K\alpha$ than for Cu$K\alpha$. The appearance of these $K\alpha$ doublets always distinguishes the high-θ from the low-θ end of a cylindrical film, and when different types of film mounting are employed this may be useful. The photograph of Fig. 57, taken with unfiltered radiation from an old, sealed-off tube with a copper target, shows the ' dirtiness ' of the radiation : the extra spots between Cu$K\alpha$ and Cu$K\beta$ are due to tungsten L radiation from material sputtered on to the target from the filament.

We may summarise the effects of reflection of X-rays by one set of lattice planes of given spacing as follows :

Characteristic radiation

(4) One or more spots are produced on the corresponding curve of constant ρ by reflection of the characteristic radiations, usually $K\alpha$ and $K\beta$, but L radiations from some targets are used. The K radiation consists of a doublet α_1 and α_2, of which the α_2 has the longer wave-length. This doublet can in general be resolved only by reflection at high values of the angle θ.

(5) A spot due to a shorter wave-length occurs nearer the centre of the film than one due to a longer wave-length.

(6) If continuous radiation is also present then the characteristic spots will be superposed on the streak ; but part or all of the radiations other than

the characteristic required can be removed from the incident beam.

(7) By means of a β-filter a range of wave-lengths from immediately below the $K\alpha$ line can be removed, but the still shorter wave-lengths will be transmitted.

(8) All radiation other than one characteristic ($K\alpha$ or $K\beta$ usually) can be removed by means of crystal reflection of the incident beam. Unless special precautions are taken, weak harmonics of the characteristic radiation may be present (**2**, 6).

1.9 Symmetry of oscillation photographs. Owing to the nature of the oscillatory motion, the oscillation photograph cannot provide full information about the Laue symmetry of the specimen, except in an indirect way. We can, however, derive some useful information about the Laue symmetry of the specimen from oscillation photographs. The only requirement is that the crystal should be carefully set with a zone axis parallel to the axis of oscillation.

If the two parts of the photograph which are separated by the zero-layer line are mirror images of each other, then the Laue group of the specimen possesses a symmetry plane perpendicular to the oscillation axis. It should be emphasised that if this is observed, it implies a symmetry plane in the Laue group and not necessarily in the point group to which the specimen belongs. Also, by careful comparison of oscillation photographs taken at regular angular intervals around the oscillation axis, we can determine the nature of the symmetry of this axis in the Laue group. If we suppose that a photograph has been taken with the oscillation-angle reading 0°–15°, we can proceed to take other photographs for comparison with it. If the photograph with reading 180°–195° is identical with the first one, then the axis is a diad, a tetrad, or a hexad; this can be decided from photographs with readings 90°–105° and 60°–75°. If the photograph 180°–195° is different from the first one, we next take a photograph with the reading 120°–135°; if this is identical with the first, then the axis is a triad. If no two photographs taken about the same oscillation axis are identical, then the direction of the oscillation axis is a direction of no symmetry in the Laue group to which the specimen belongs.

2. Indexing the Reflections

2.1 Indexing photographs of diamond. We shall first index the spots on two photographs of diamond, as the process is easier for a cubic crystal of small cell-size than for any other crystal. By means of the Bernal chart we obtain the following values from the photographs of Figs. 59.1 and 56.2.

$$\text{Cu}K\alpha\ (\lambda = 1{\cdot}54\ \text{A.})$$

$$\zeta_{[100]} = a^* = 0{\cdot}43,$$

hence $$a = 1{\cdot}54/0{\cdot}43 = 3{\cdot}58\ \text{A. (approx.)}.$$

$$\text{Mo}K\alpha\ (\lambda = 0{\cdot}71\ \text{A.})$$

$$\zeta_{[100]} = a^* = 0{\cdot}20,$$

hence $$a = 0{\cdot}71/0{\cdot}20 = 3{\cdot}56\ \text{A. (approx.)}.$$

From these values of a^* we draw the appropriate reciprocal nets as in Figs. 59.2, 60, the axes being interchangeable since the specimen is cubic. On these are inserted the reflecting circles corresponding to the limits of the oscillation in each example. By means of the Bernal chart the values of ξ and ζ for each spot on the photograph are read and tabulated, the indices being added subsequently.

A pair of compasses is now set to each value of ξ in turn and, with centre at the point where the oscillation axis cuts the plane of the reciprocal lattice, arcs are drawn through the lunes. Each of these passes through or close to a reciprocal point which is the one corresponding to the reflection in question; the indices of this point are

Diamond (Fig. 59.1)

ζ \ ξ	*Left side*							*Right side*									
	0·55	0·84	1·15	1·40	1·51	1·63	1·79	0·40	0·55	0·62	0·80	1·02	1·25	1·43	1·51	1·70	1·72
0	$2\bar{2}0$										040		260				
·20		$3\bar{3}1$	$5\bar{3}1$		$7\bar{3}1$		$9\bar{1}1$					151			371	571	
·40						$8\bar{2}2$		022						462			
·60				$7\bar{1}3$						133		153					753
·80									224								

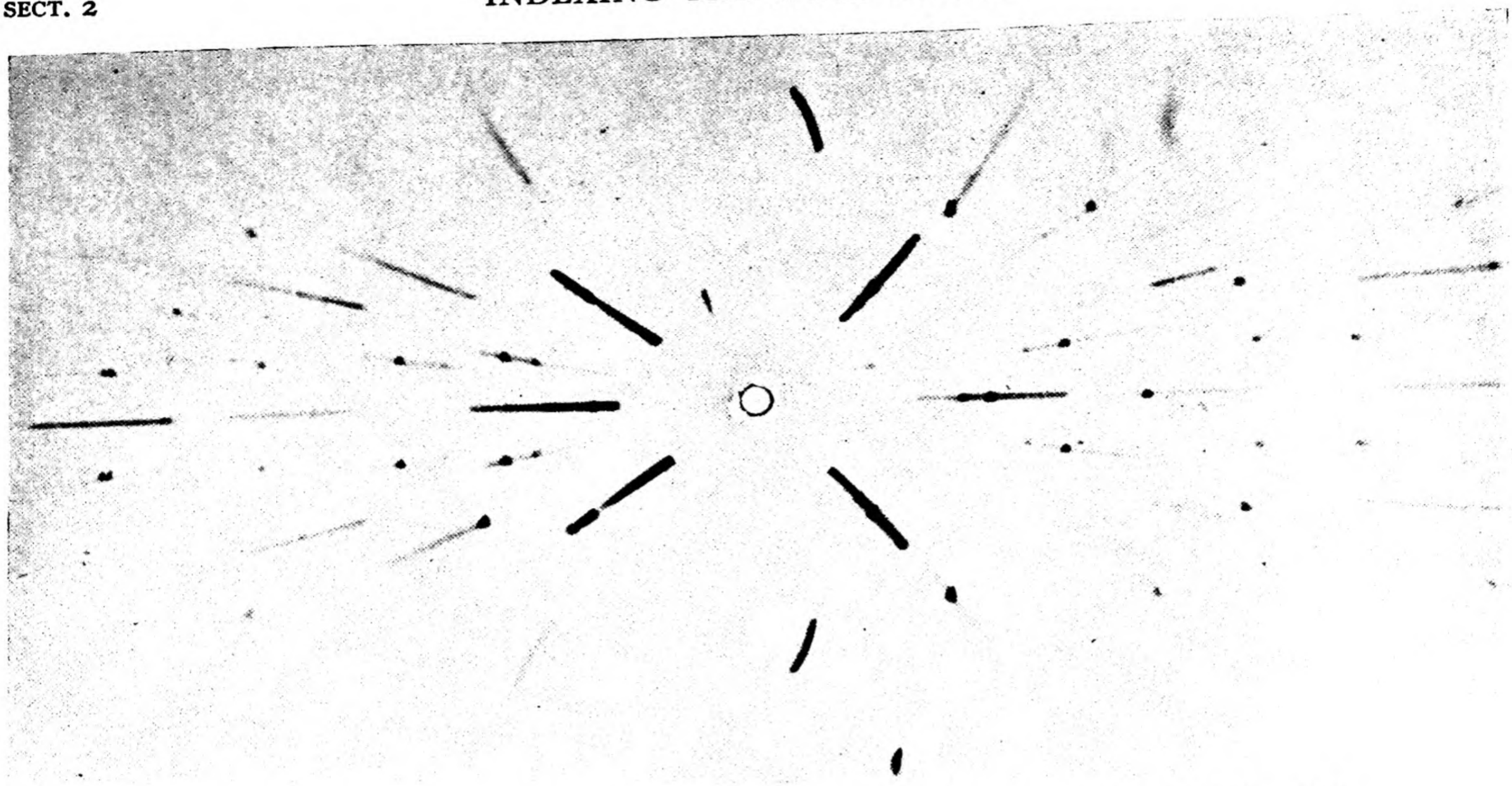

FIG. 59.1. Oscillation photograph. Same as for Fig. 55 but taken with unfiltered MoK radiation

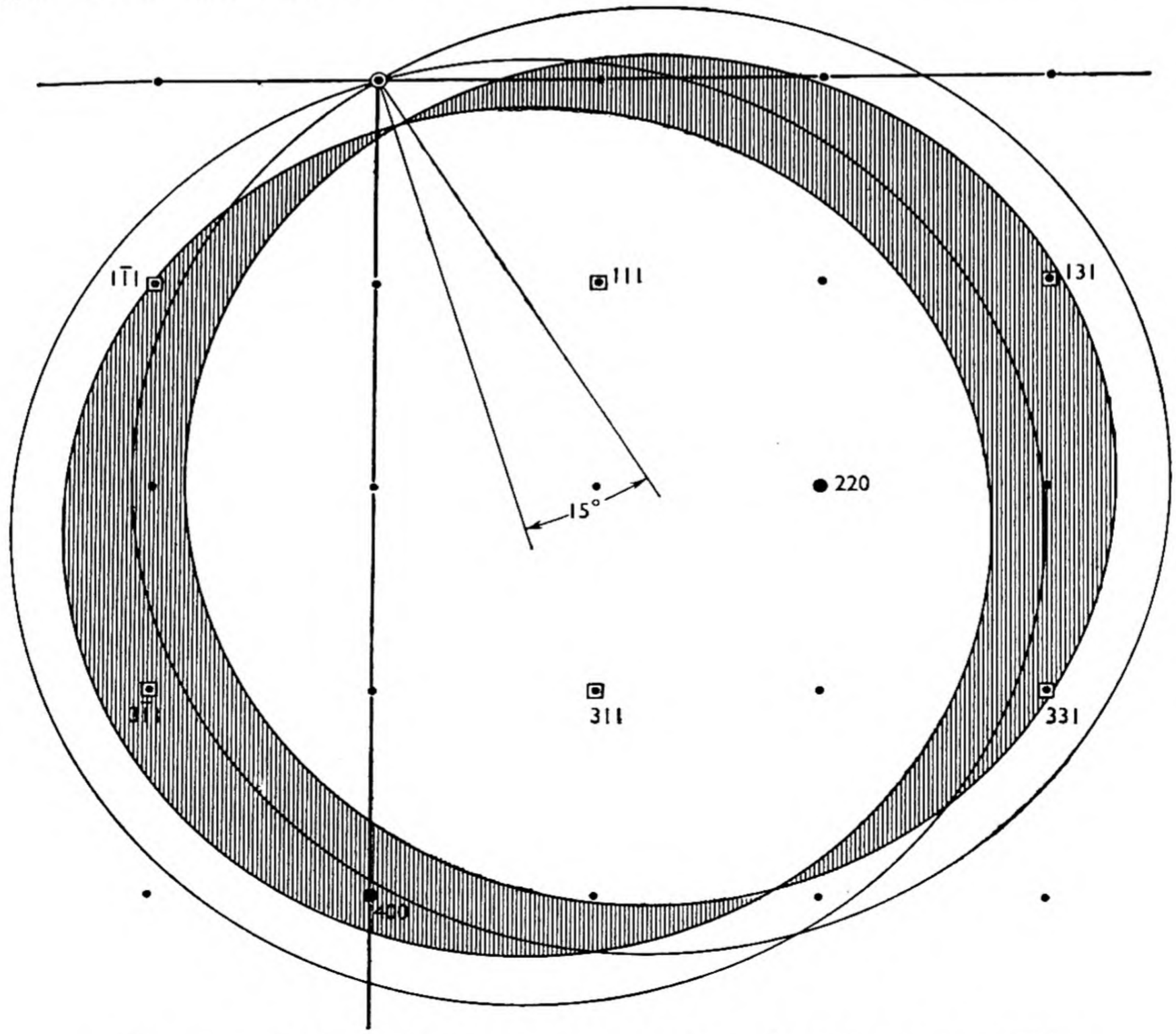

FIG. 59.2. Reciprocal lattice for indexing Fig. 56.2 (Diamond, Cu$K\alpha$).
Possible reflections are shown by large dots (zero layer) or squares (first layer). Scale: 1 unit = 5 cm.

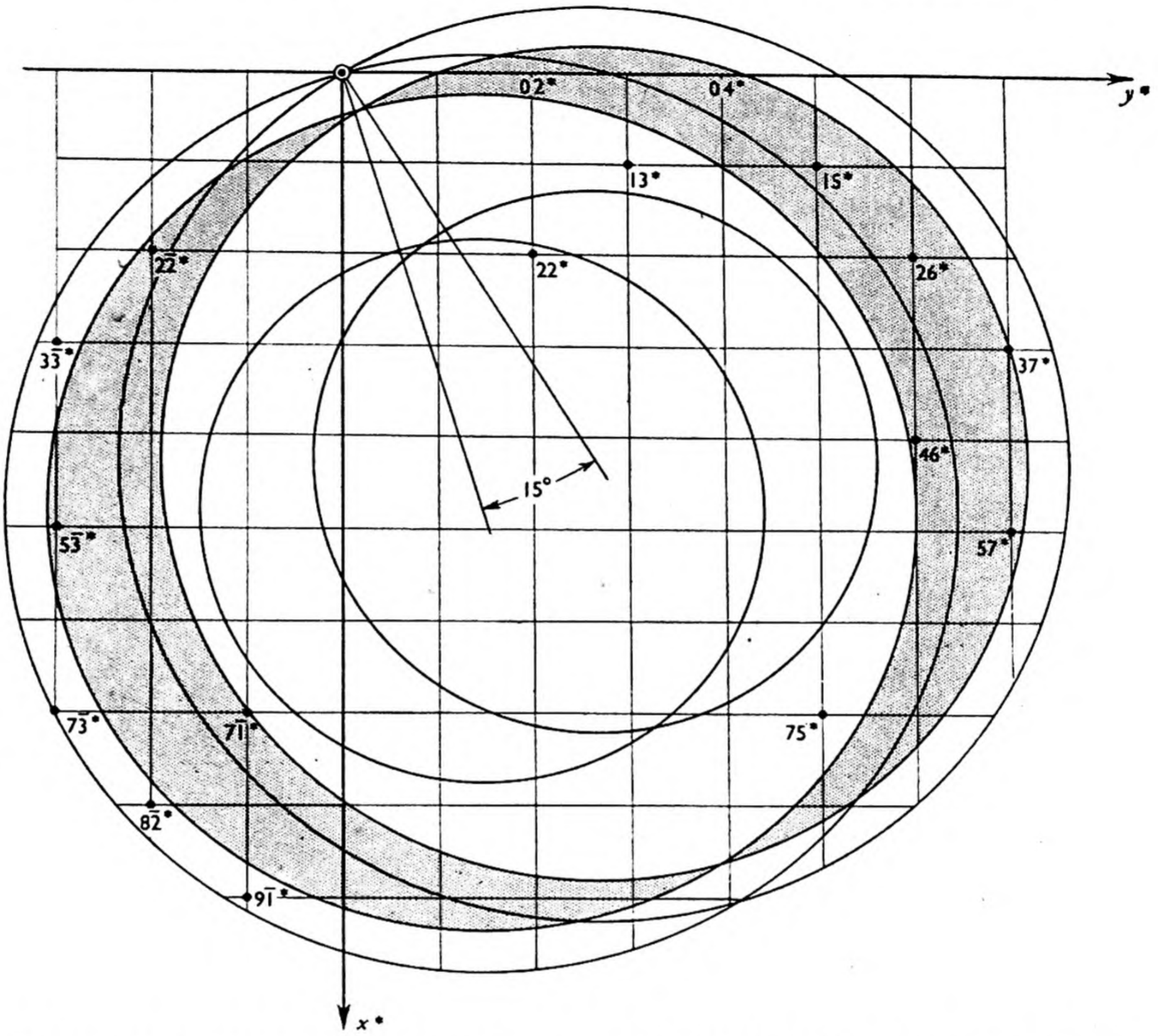

FIG. 60. Reciprocal lattice for indexing Fig. 59.1 (Diamond, Mo$K\alpha$). Scale : 1 unit = 5 cm.

added to the table. For the non-zero layer lines the same drawing of the reciprocal lattice will serve because successive layers are identical and are superposed directly above each other along the crystal axis of oscillation. It is necessary, however, to draw the reflecting circles again for each layer, because the radii of these are equal to $\sqrt{1-\zeta^2}$ (Fig. 53). It should be noted that the centres of these reflecting circles lie on a line parallel to the oscillation axis at a distance of one unit from it. Although the same drawing of the reciprocal lattice can be used for the two layer lines of the photograph taken with Cu radiation, it is better to use a separate copy for odd layer lines for the photograph taken with Mo radiation on account of the closeness of the layer lines. The indices obtained can be inserted in the photographs as in Figs. 56.1 and 61.1.

The 15°-oscillation photograph of diamond taken with Cu$K\alpha$ radiation (Fig. 61.2) is remarkable in that it shows only two spots on the zero layer line and none on any other layer line. The main reason for the appearance of so few reflections in this photograph is the very small size of the unit cell of diamond, which is one of the smallest known. As a consequence of this, the reciprocal lattice has a large mesh and so only a small number of reciprocal points lie within the volume swept out by the reflecting sphere. If the appropriate lunes were added to Fig. 59.2, they would be seen to enclose six lattice points on each side; yet, of these points, only one gives rise to a reflection. The other reciprocal points within the lunes represent reflections which cannot occur for structural reasons. Thus, owing to the combination in diamond of a very small unit cell with a structure which results in the absence of several types of reflections, oscillation photographs of diamond show very few spots. It would, in fact, be easy to take a 15°-oscillation photograph of diamond with Cu$K\alpha$ radiation which would show no characteristic reflections whatever.

When the crystal is turned on a tetrad axis to a more favourable position, spots appear which mark out the first layer line, as in Fig. 55. When a shorter wavelength is employed, as in Fig. 59.1, more spots appear, because the mesh of the reciprocal lattice is now

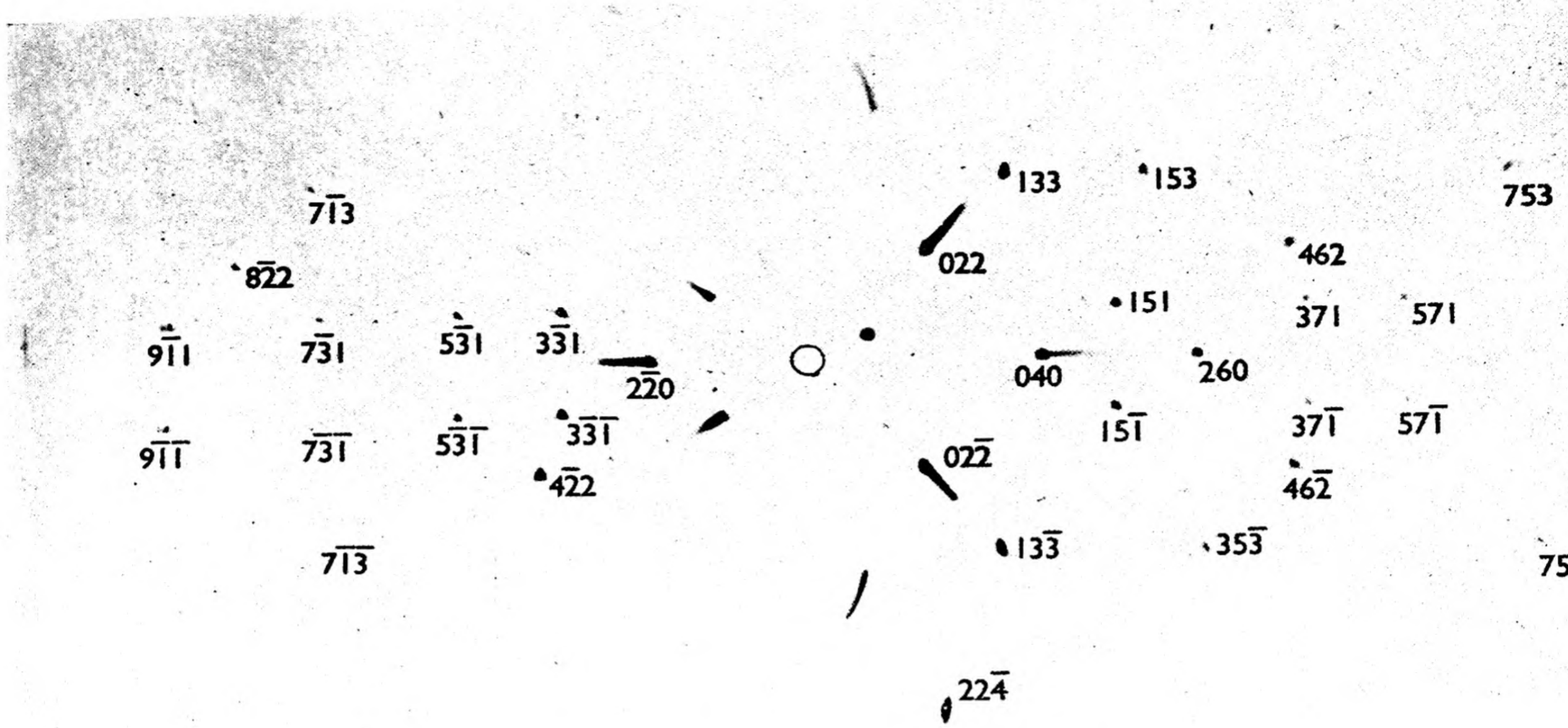

FIG. 61.1. Oscillation photograph (indexed).
Same as for Fig. 55 but taken with filtered Mo$K\alpha$ radiation

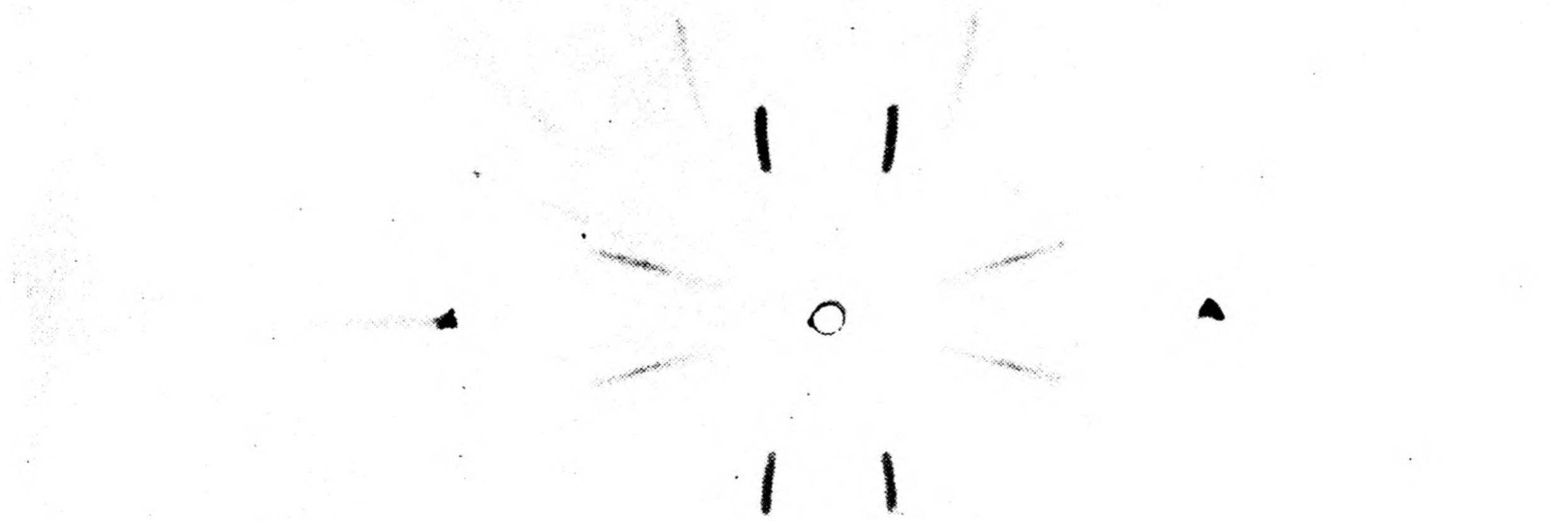

FIG. 61.2. Oscillation photograph showing only {220} reflections.
Specimen : diamond oscillated about one crystallographic axis through $7\frac{1}{2}°$ on each side of another crystallographic axis.
Camera : cylindrical, $r = 3$ cm. Radiation : CuK (unfiltered)

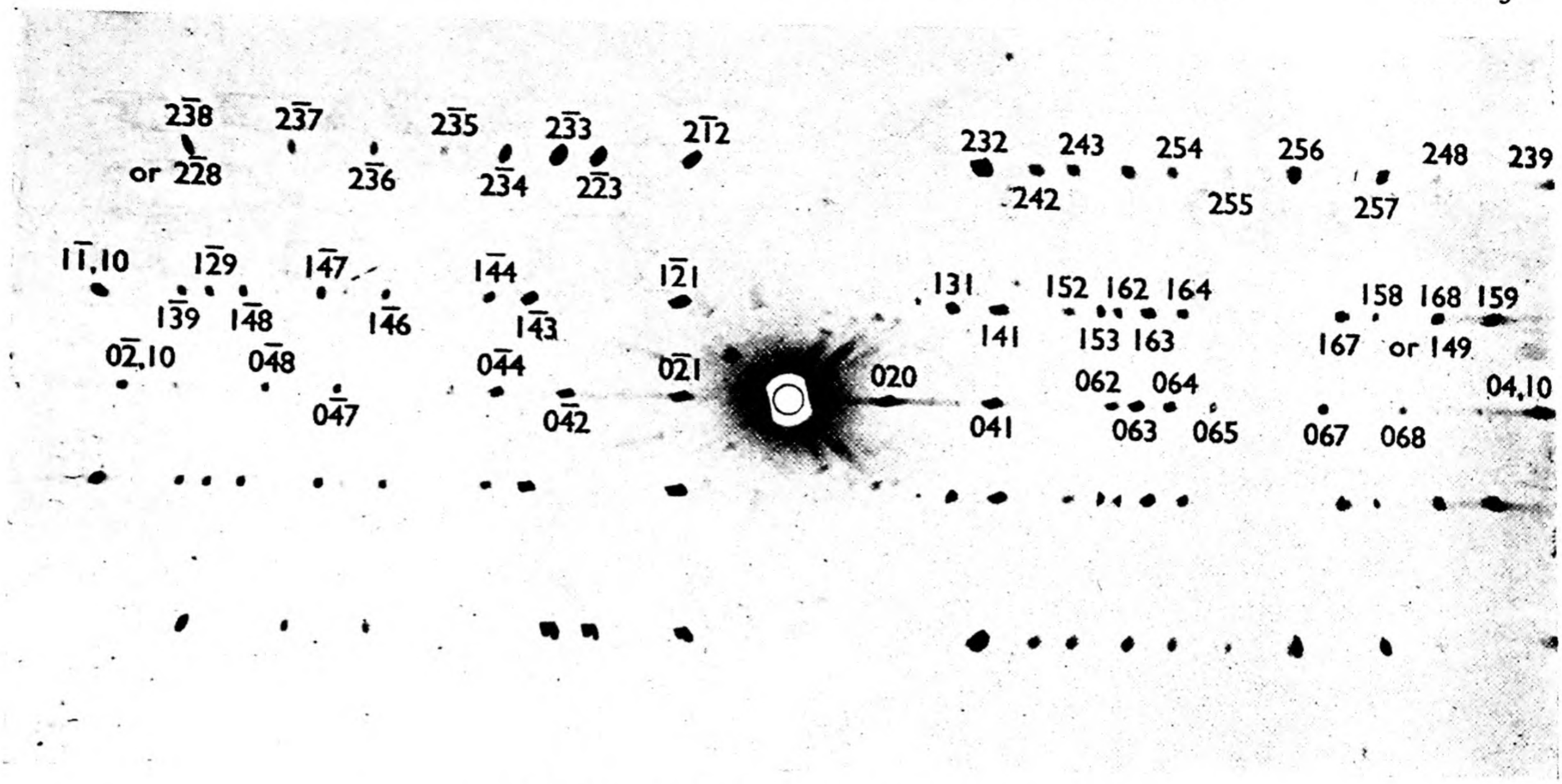

FIG. 62. Oscillation photograph (indexed).
Specimen : topaz oscillated 15° clockwise from position where beam is parallel to z-axis, with [100] as oscillation axis.
Camera : cylindrical, $r = 3$ cm. Radiation : Cu$K\alpha$ (filtered)

smaller, owing to the decrease in the reciprocal constant λ. Comparison of these photographs shows that for the shorter wave-length each spot has moved to a new position along the appropriate curve of constant ρ towards lower values of θ (**8,** 2.2).

2.2 Determination of the unit cell of an orthorhombic crystal. We shall take a specimen of the mineral topaz, which is orthorhombic, as an example. The three crystallographic axes are fixed in direction by the symmetry. Three oscillation photographs are taken with each of the axes x, y and z in turn as the axis of oscillation (Figs. 62, 63). By means of the Bernal chart, we measure ζ on each film from the highest suitable layer line, and hence we obtain approximate values of the lengths a, b and c, the sides of the unit cell of the Bravais lattice.

OSCILLATION AXIS	AVERAGE VALUE OF ζ FOR nTH LAYER LINE	RECIPROCAL LATTICE UNIT-CELL DIMENSIONS	BRAVAIS LATTICE UNIT-CELL DIMENSIONS
x	0·670 (second)	$a^* = 0{\cdot}335$	$a = 4{\cdot}61$ A.
y	0·710 (fourth)	$b^* = 0{\cdot}177$	$b = 8{\cdot}75$
z	0·745 (fourth)	$c^* = 0{\cdot}186$	$c = 8{\cdot}33$

These photographs were taken without much care in order to show the difficulties which often arise in practice. In the second photograph the zone axis [010] does not quite coincide with the axis of oscillation and consequently the layer lines are not quite straight. (A discussion on the setting of crystals is given in Chapter 8.) If ζ is measured along the vertical median line of the film a reasonably good value can be obtained, and in order to get an approximate value of ζ it is generally not worth while spending the time necessary to set the zone axis accurately parallel to the oscillation axis. In the third photograph, unfiltered radiation was used, so that the layer lines produced by the $K\alpha$ radiation must be distinguished from those produced by the $K\beta$ radiation. This is easy in the present example since the cell side of the crystal along the oscillation axis is not large and the wave-length is a medium one. When the layer lines are very close, it is better to filter out the $K\beta$ radiation, and also to use the approximate value of ζ from the first layer line as a check on the number of the higher layer line used.

Even if the measurement of ζ is done with care on a good photograph, the value of the repeat distance along the zone axis in the Bravais lattice can be determined with an accuracy of only one per cent. Measurements of unit-cell dimensions should be refined before being stated, and methods of doing this are discussed later (**13,** 4.1 to **13,** 4.4). Even in the process of indexing, however, a small inaccuracy in ζ may lead to difficulties in assigning indices to the

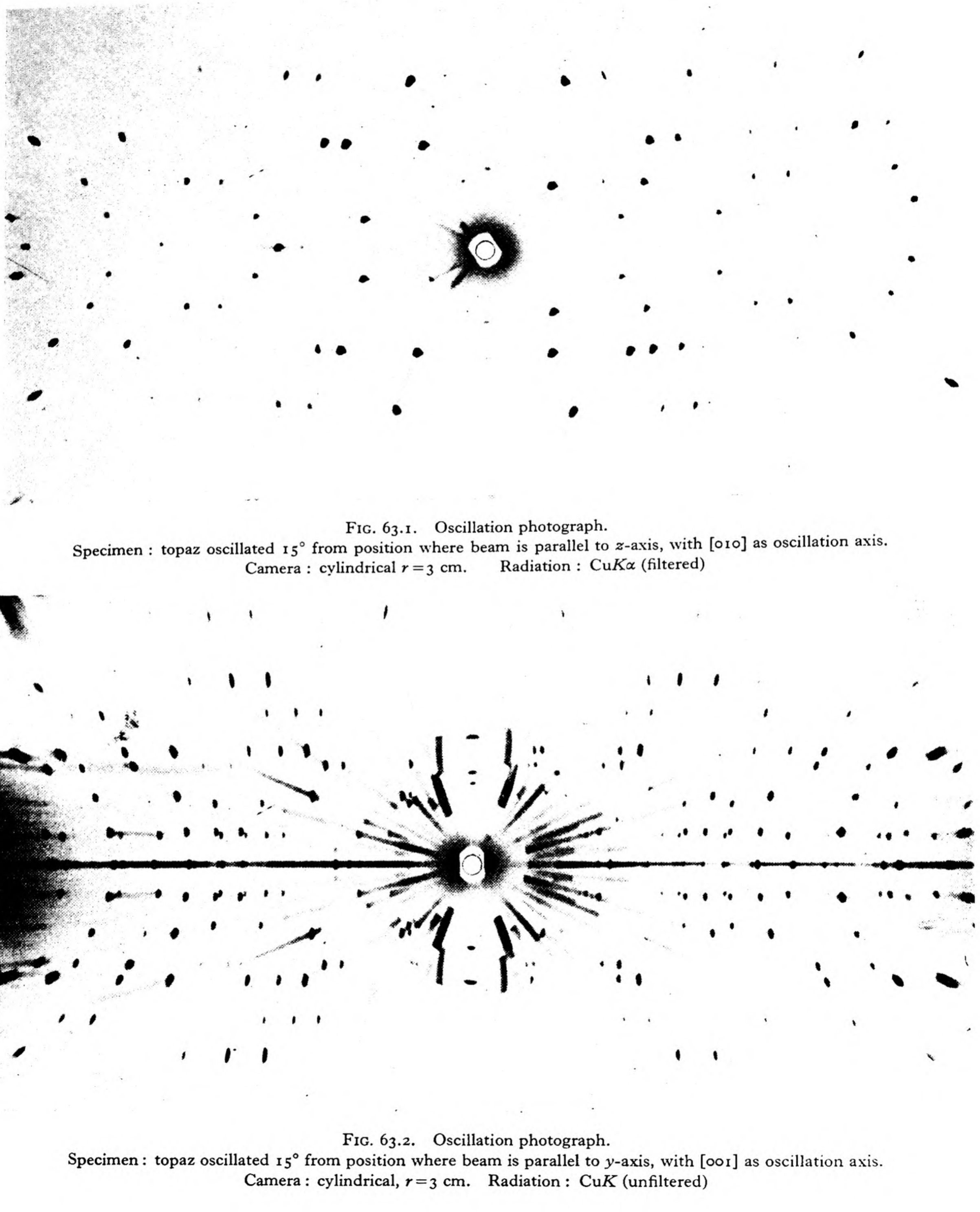

FIG. 63.1. Oscillation photograph.
Specimen : topaz oscillated 15° from position where beam is parallel to z-axis, with [010] as oscillation axis.
Camera : cylindrical $r = 3$ cm. Radiation : Cu$K\alpha$ (filtered)

FIG. 63.2. Oscillation photograph.
Specimen : topaz oscillated 15° from position where beam is parallel to y-axis, with [001] as oscillation axis.
Camera : cylindrical, $r = 3$ cm. Radiation : CuK (unfiltered)

spots of large ξ-values, owing to the cumulative effect of the error. It is generally best to use the first values of a^* b^* and c^* to start the process of indexing; but if difficulties are encountered, these values should be refined before the final indexing is carried out. In dealing with the photograph of topaz we shall use the values,

$$a^*=0{\cdot}332,\ b^*=0{\cdot}175,\ c^*=0{\cdot}184,$$

which correspond to the lengths of the sides of the unit cell given by Bragg (1937),

$$a=4{\cdot}64\text{ A.},\ b=8{\cdot}78\text{ A.},\ c=8{\cdot}37\text{ A.}$$

2.3 Tabulation of ζ and ξ for each spot. The ζ and ξ values for each spot are read by means of the Bernal chart and are tabulated as shown below, the k, l indices being inserted subsequently.

RIGHT-SIDE OF PHOTOGRAPH (FIG. 62)

ξ	k, l	$h=0$	$h=1$	$h=2$	ξ	k, l	$h=0$	$h=1$	$h=2$
0·35	2 0	vs			0·96	5 2		w	
0·57	3 1		s		1·04	5 3		s	m
0·65	3 2			vs	1·12	6 2	m	m	
0·73	4 1	s	s		1·15	5 4			m
0·79	4 2			m	1·19	6 3	s	s	
0·89	4 3			m	1·27	5 5			vw

vw—very weak: w—weak: m—medium: s—strong: vs—very strong

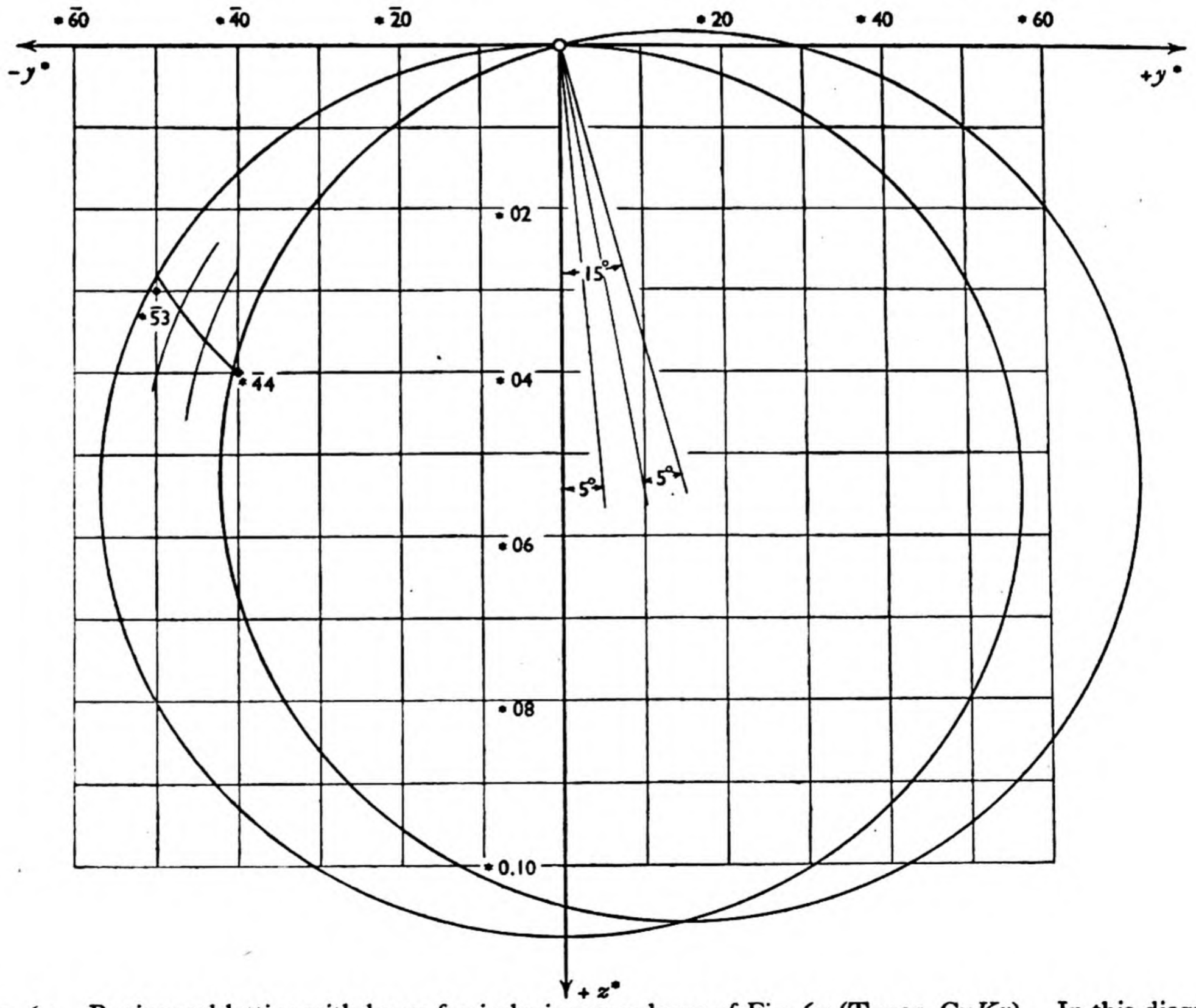

FIG. 64. Reciprocal lattice with lunes for indexing zero layer of Fig. 62 (Topaz, Cu$K\alpha$). In this diagram the positive direction of the x-axis is downwards. Scale: 1 unit = 5 cm.

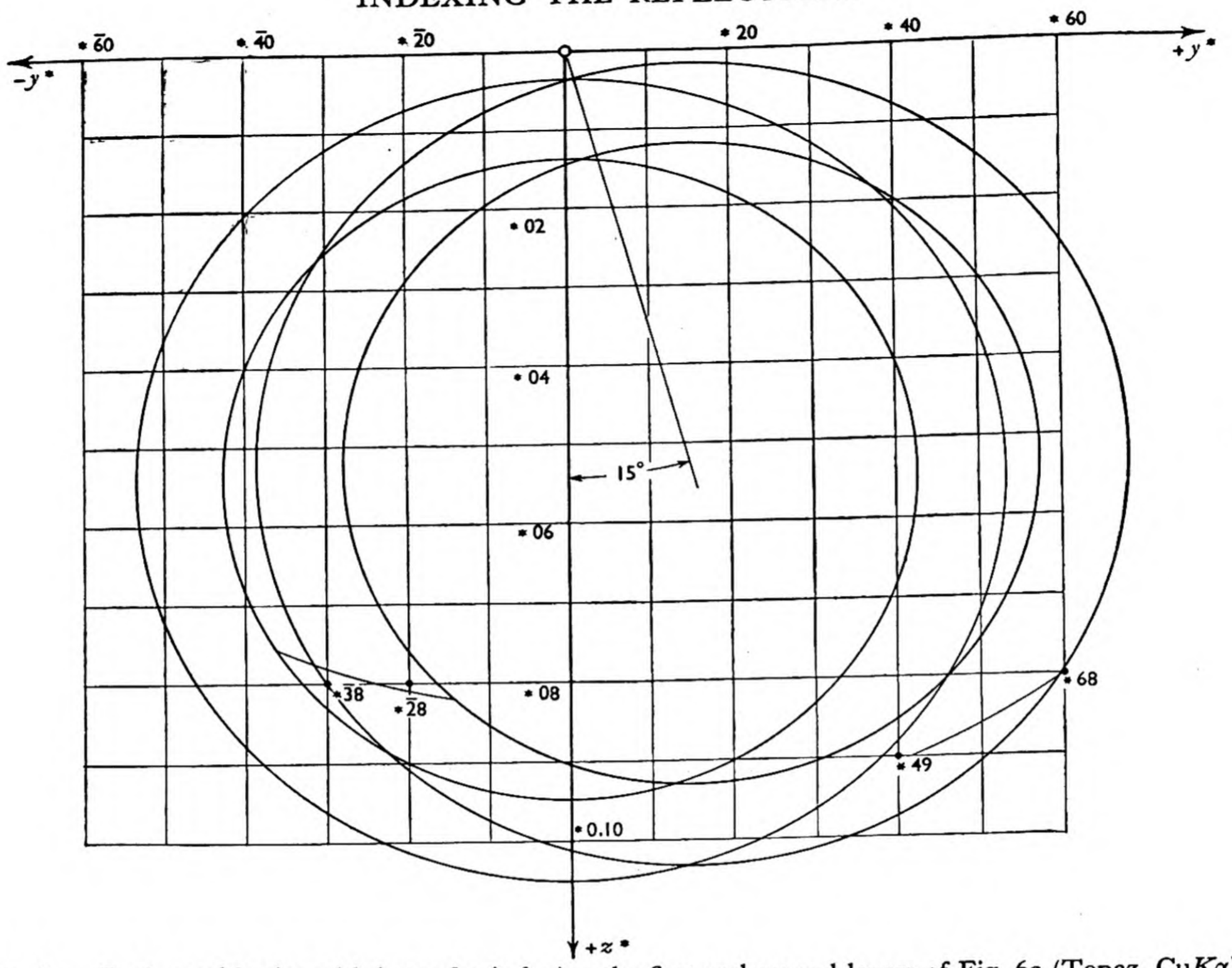

FIG. 65. Reciprocal lattice with lunes for indexing the first and second layers of Fig. 62 (Topaz, Cu$K\alpha$). In this diagram the positive direction of the x-axis is downwards. Scale: 1 unit = 5 cm.

When the x-axis is the oscillation axis, all spots on the zero layer line correspond to reflections of the type $0kl$: similarly all spots on the first layer line are of the type $1kl$. In general, all spots on the nth layer line of a photograph with a crystallographic axis as oscillation axis have n as the index corresponding to that axis. Also it can be stated that there is a relation between the indices of reflections which produce spots on exactly the same row line. When the x-axis is the oscillation axis, all spots on the same row line have the same values of k and l because these correspond to reciprocal points on the same point row parallel to the oscillation axis; and similarly for the other two axes of oscillation. In practice, however, there is usually some overlapping of reflections from point rows with the same, or closely similar, values of ξ; so that the constancy of two indices for spots apparently on the same row line should never be presumed. Overlapping of this kind tends to decrease with decrease of the cell-size of the crystal and with increase of the wave-length of the radiation.

2.4 Construction of reciprocal lattice and reflecting circles. For the photograph with the x-axis as oscillation axis we construct the b^* and c^* plane of the reciprocal lattice. When the crystal is orthorhombic, like topaz, one or two quadrants are sufficient. The reflecting circles corresponding to the two limits of the oscillation are most conveniently drawn on tracing paper or on thin celluloid. This is especially useful for zero layer lines because it is the same for all photographs with the same angle of oscillation. I. Fankuchen has described a form of this which can be used for oscillations of 5°, 10° and 15° and which has arcs corresponding to the values of ξ marked on it. This transparency is placed over the reciprocal lattice in the correct position as shown in Fig. 64. Since it is known that the crystal was moved clockwise, looking downwards, from its original position, we must move the reflecting circle in the anti-clockwise direction. Where the movement of the crystal is not known, trial will soon show which way the reflecting circle has to be moved, because in the wrong position it will be impossible to assign indices to all the spots.

For the higher layer lines the same drawing of the reciprocal lattice can be employed, but reflecting

circles of radius appropriate to the particular value of ζ must be used. It should be noted that Fig. 62 has been indexed as if $+x^*$ pointed upwards in the reciprocal lattices of Figs. 64 and 65. This makes the axes a left-handed set, which is unconventional; although this does not matter in a photograph of an orthorhombic crystal, it might lead to serious error with a specimen of lower symmetry.

2.5 Assignment of indices. If the crystal has been carefully orientated, we can be sure that we are concerned only with reciprocal points lying within the lunes. But in practice we must allow a margin of error in setting. This margin can usually be determined as indexing proceeds; in Fig. 64 the reflecting circles have been drawn in the positions corresponding to the approximate experimental data printed below the photograph, but we shall see that this is not quite accurate.

The indexing process is carried out as in **5**, 2.1. Where the arc does not pass near a reciprocal point, or where it is equidistant from two such points within or near the lunes, the data should be checked. If the difficulty remains, the procedure described in the next section should be adopted. The indexing of the first photograph of topaz is given on Fig. 62. The other two photographs can be indexed for practice; the results are given in Appendix 4.

The occurrence of the spot 162 (Fig. 65) shows that the setting of the crystal does not conform exactly to the information given below the photograph. The crystal is fairly accurately set with the x-axis parallel to the oscillation axis, but the incident beam cannot have been parallel to the c-axis at one end of the oscillation. There is no ambiguity about the indexing of the spot 162, so we should redraw the reflecting circles to include the corresponding reciprocal point. When this is done, the new lunes include all the indexed reciprocal points if we allow $\frac{1}{2}°$ margin at each side for the divergence of the incident beam. This shows that during the oscillation the angle between the c-axis and the beam changed from 2° to 17° instead of 0°–15°. This type of mis-setting in an oscillation photograph is undetectable in general, except by the process of indexing, but it is serious only if the cell dimensions of the crystal are large in the directions other than the oscillation axis. If this is true of a particular specimen, it should be carefully set by the methods mentioned in Chapter 8.

2.6 Indexing in ambiguous cases. It sometimes happens that two reciprocal points of the same or very similar values of ξ both lie within the same lune. If both give rise to reflections, these will fall on the same spot on the film: consequently we cannot at first tell whether one or both of the reflections are present. It is necessary to take one or two additional photographs to decide this matter. The oscillation angle is reduced usually to about 5° and it is arranged to include only one of the two reciprocal points within the lune. If no reflection occurs with the appropriate value of ξ, we can assume that the spot on the first film corresponded to the other reciprocal point; but if a reflection is obtained, another 5° oscillation should be taken, arranged this time to include the other reciprocal point and to exclude the one previously covered. If a reflection is obtained on this photograph also, we can be sure that both reflections contributed to the spot on the first film. In Fig. 64 it can be seen that the reciprocal points $0\bar{5}3$ and $0\bar{4}4$ have almost the same values of ξ. Two additional photographs were taken with 5° oscillations from the two limits of the original oscillation of 15° respectively. One of these showed no spot with the proper value of ξ, but the other showed the reflection $0\bar{4}4$.

The other main difficulty occurs when no reciprocal point in or near the lunes lies on a particular arc of given value of ξ. An example of this can be seen in Fig. 65, and the alternative indices $2\bar{3}8$ and $2\bar{2}8$ have both been inserted in the photograph of Fig. 62. The value of ξ and the drawing of the reciprocal lattice should be checked. If the difficulty remains, it is probably due, in the case of a large value of ξ, to inaccuracy in the measurement of the cell-sides, and the values of these should be refined. If, however, the specimen is large, and particularly if it is strongly absorbing, the difficulty may be due to displacement of the reflected beam (**13**, 2.2). But this difficulty is marked only at low values of θ, and hence of ξ, while a small error in the cell-side causes trouble only at higher values of θ or ξ.

2.7 Indexing for a monoclinic crystal. As an example of a monoclinic crystal we shall study here the mineral gypsum. (The indexing of oscillation photographs of trigonal crystals is given in **10**, 3.) In monoclinic crystals the x- and z-axes are not perpendicular to each other, but the y-axis is perpendicular to the plane of the other two. In gypsum (Fig. 66) we shall select as the x- and z-axes the two obvious crystal edges perpendicular to the diad symmetry axis. It should be noted that this choice of the x-axis is not the same as that given in text-books.

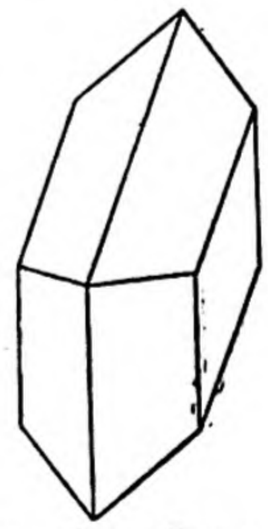

FIG. 66. Gypsum.
A common habit showing {010}, {110} and {111} (morphological indexing)

Three oscillation photographs were taken with the x-, y- and z-axes in turn as oscillation axis, and from these the following data were obtained.

$\lambda = 1{\cdot}54$ A.

Oscillation axis	Values of ζ_1	Values of λ/ζ_1 (in A.)
[100]	0·236	$6{\cdot}51 = a$
[010]	0·102	$15{\cdot}15 = b$
[001]	0·247	$6{\cdot}24 = c$

The approximate value of the angle $\beta = 127\frac{1}{2}°$ was obtained by measuring the angle between the zone edges [100] and [001] with a microscope. From these data we obtain

$$a^* = \frac{\lambda}{a \sin\beta} = 0{\cdot}298, \qquad b^* = \frac{\lambda}{b} = 0{\cdot}102,$$

$$c^* = \frac{\lambda}{c \sin\beta} = 0{\cdot}311.$$

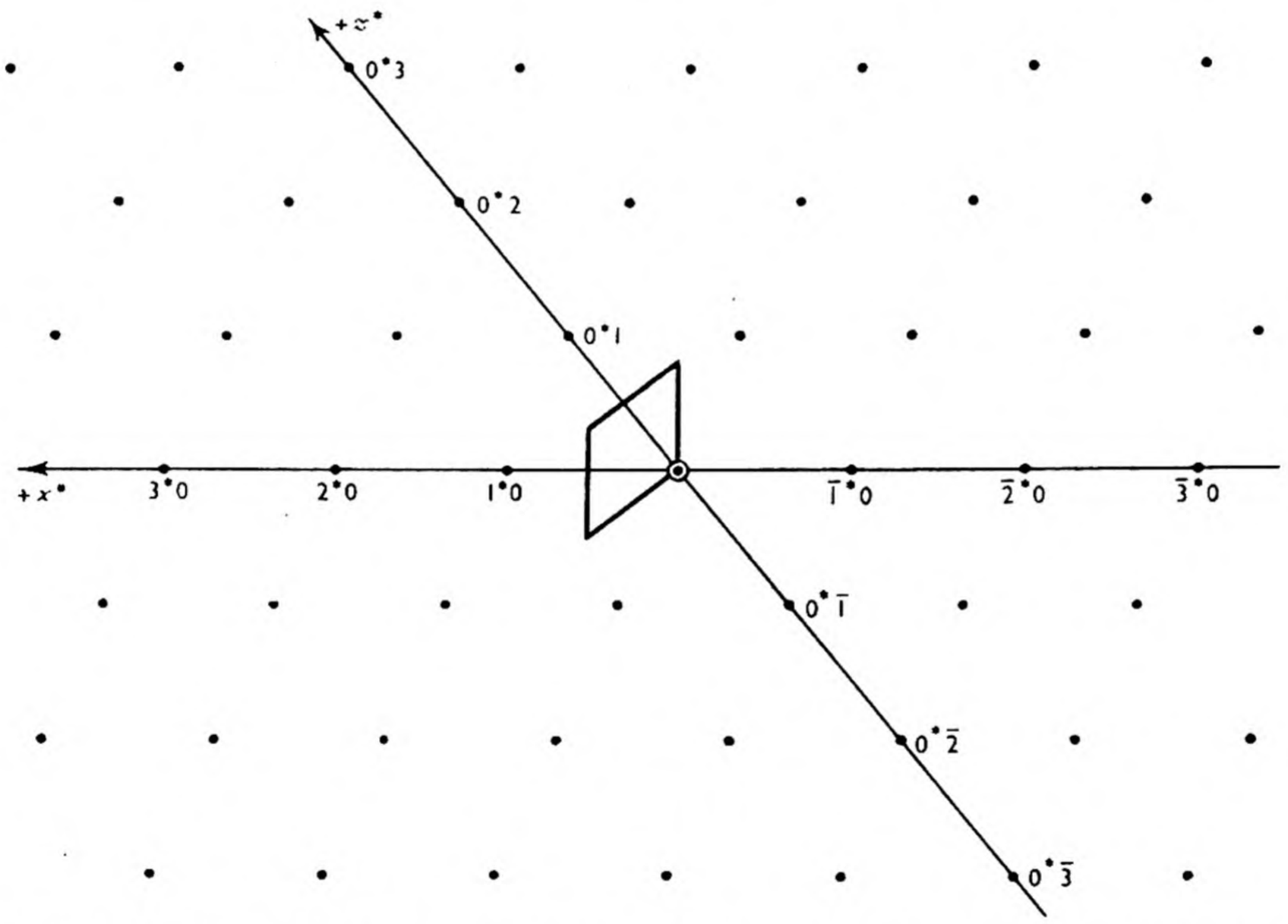

FIG. 67. Reciprocal lattice for gypsum, (Cu$K\alpha$) with prominent zone axis taken as the x-axis, the y- and z-axes being the same as in morphological indexing.
Scale : 1 unit = 5 cm.

For the study of the photograph taken with the y-axis as axis of oscillation we require a projection of the reciprocal lattice on the plane of x^* and z^* ; this is shown in Fig. 67. Since the directions y and y^* coincide, the non-zero layers of the reciprocal lattice are superposed ' in register ' with the zero layer as in the orthorhombic system ; that is, 010 is placed directly above 000, and 110 and 011 over 100 and 001 respectively. For all the layer lines of this photograph, therefore, the indexing procedure is exactly the same as for the orthorhombic example studied earlier in this chapter.

For the study of the other two photographs with x and z as the oscillation axes, we require the reciprocal lattice projected on to the z^*y^* and x^*y^* planes respectively as in Figs. 68. In these cases the third reciprocal axis is oblique to the plane of the projection of the lattice, with the result that the non-zero layer lines do not superpose in register with the zero layer, as can be seen in Fig. 69.1. When these non-zero layers are being indexed, care must be taken to measure the ξ-values from the zero point of the ξ co-ordinate, which no longer coincides with the zero point of the reciprocal co-ordinates. The required zero point for the ξ co-ordinate is the point at which the oscillation axis, either x or z, intersects the particular plane of the reciprocal lattice. The oscillation axis is, of course, perpendicular to these planes of the reciprocal lattice. The relations are shown in Fig. 69.1, from which it can be seen that the required zero point for the ξ co-ordinates, which we shall call T, lies in the plane perpendicular to the y (and y^*) axis at a distance t_n from 00n or n00, the origin of the reciprocal co-ordinates, which is given by

$$t_n = -\zeta_n \,.\, \cot\beta.$$

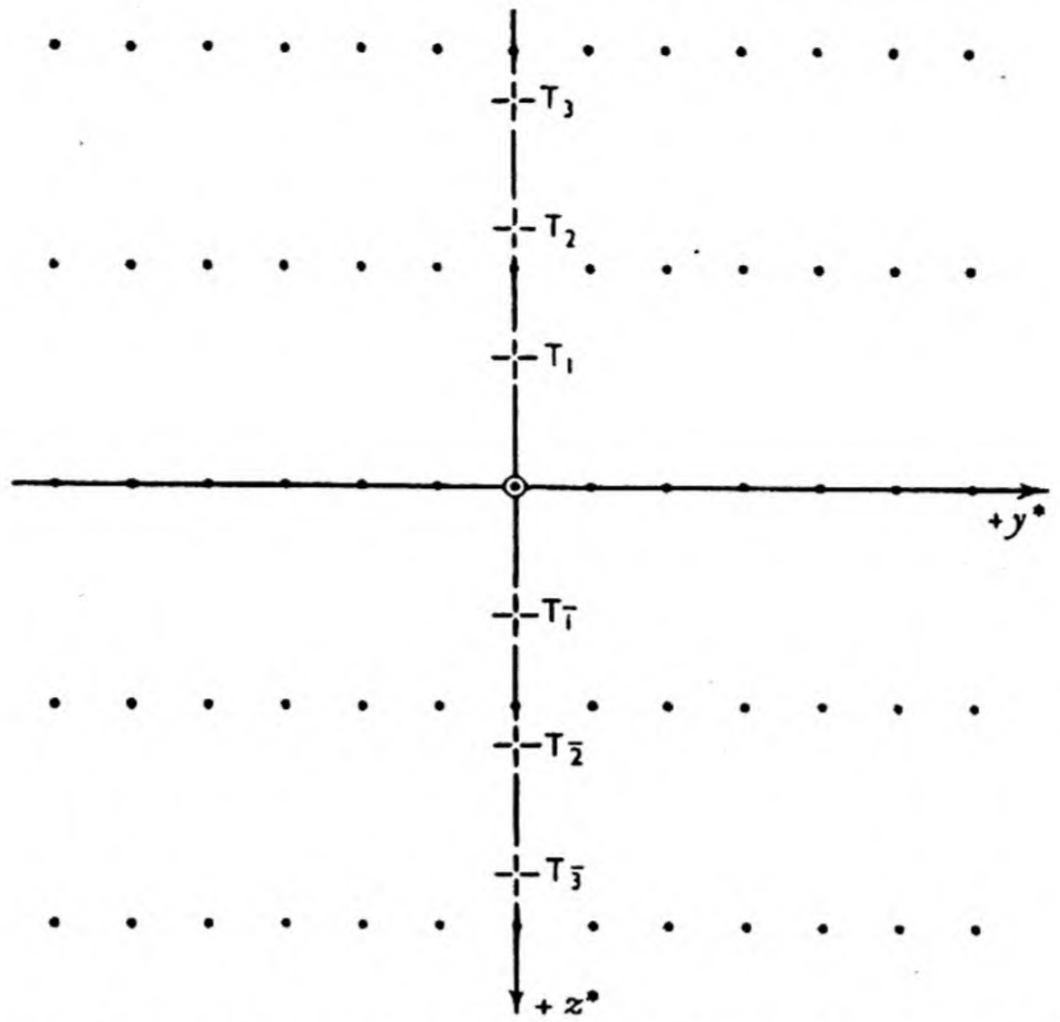

FIG. 68.1. Reciprocal lattice for gypsum (Cu$K\alpha$). Same unit cell as in Fig. 67, but showing the positions of T (zero point for ξ co-ordinates) for three layers (positive) and three layers (negative). Note that $+x^*$ points downward in this drawing.

Scale : 1 unit = 5 cm.

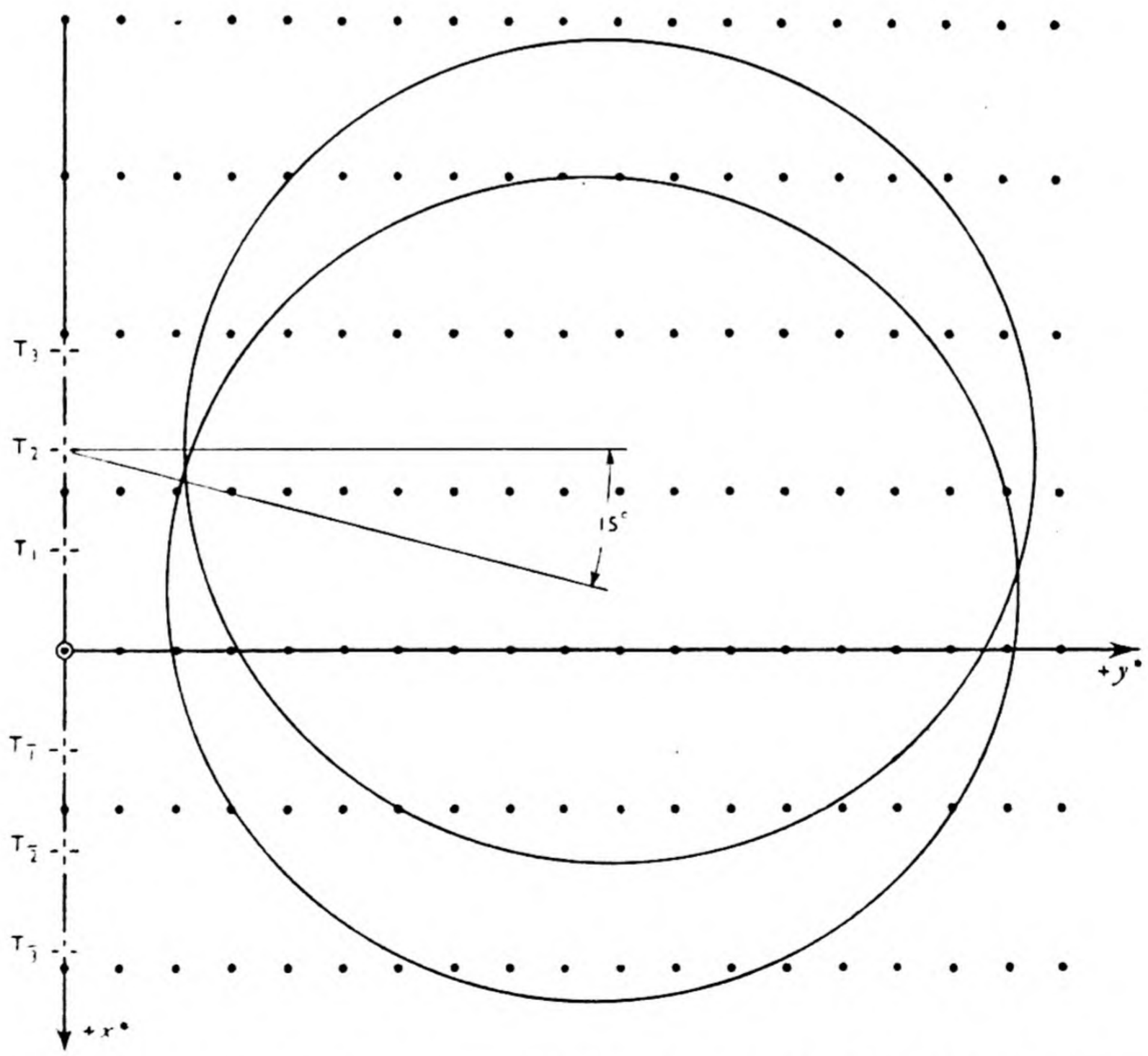

FIG. 68.2. Reciprocal lattice for gypsum (Cu$K\alpha$). Same unit cell as in Fig. 67, but showing the lunes for the second layer (positive). Note that $+z^*$ points upward in this drawing.

Scale : 1 unit = 5 cm.

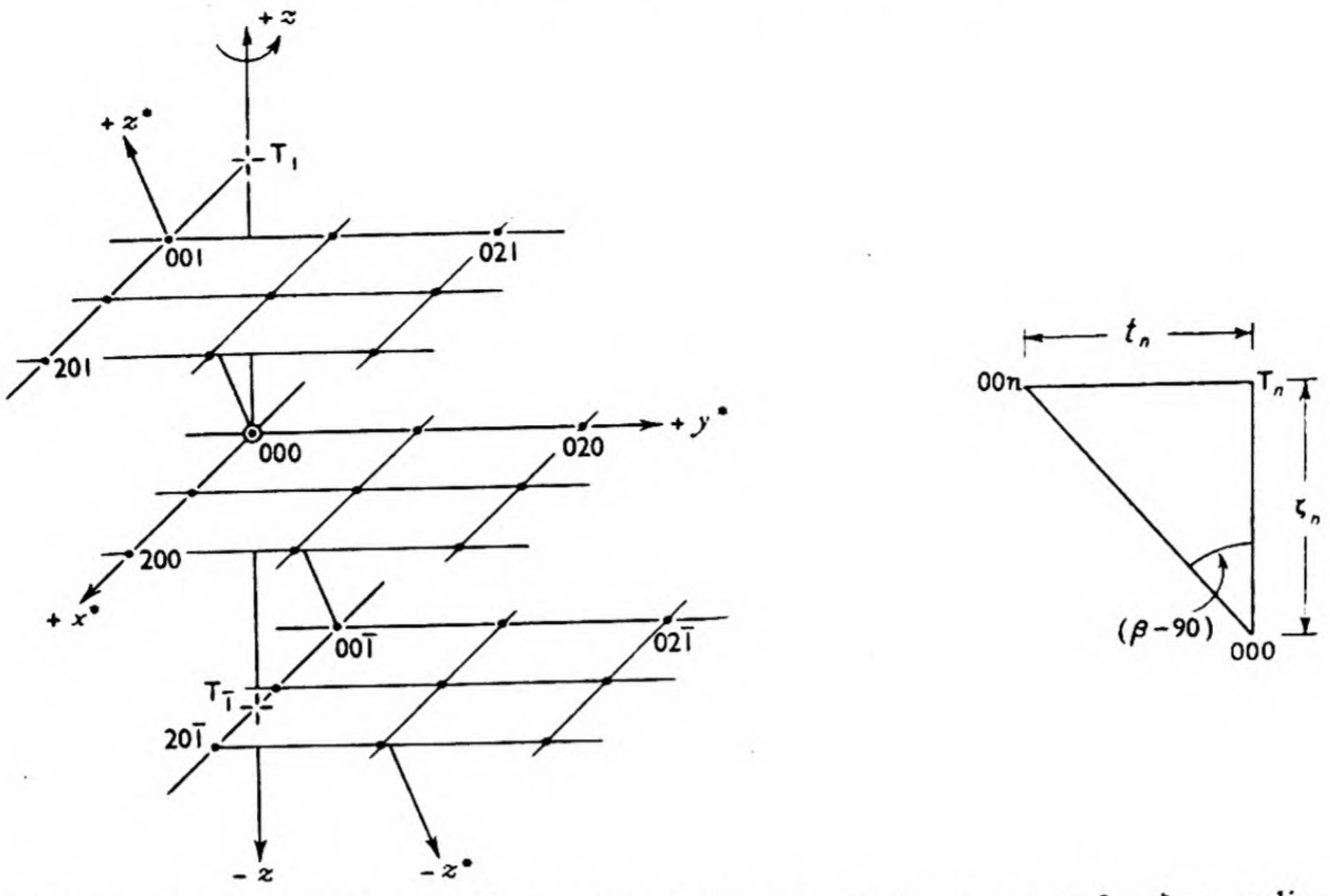

FIG. 69.1. Diagrams showing the positions of points T_n (zero points for ξ co-ordinates) in a monoclinic lattice

Alternatively this could be written

oscillation axis	
x	$t_n = n \,.\, a^* \,.\, \cos\beta,$
z	$t_n = n \,.\, c^* \,.\, \cos\beta.$

When n is positive, the point T_n lies on the negative side of the x^*- or the z^*-axis, whichever is not the axis of oscillation, and vice versa. The values of t_n can be obtained graphically (Fig. 69.1) or calculated from the above equations.

In Fig. 69.2 are shown the positions of T_n for an example of a hexagonal lattice. The hexagonal lattice can be regarded as a special case of the monoclinic and the relative positions of T_n are fixed for all lattices of this symmetry.

The most convenient procedure is to use the same drawing of the reciprocal lattice for each layer line. On this should be inserted the points T_n for the appropriate number of layer lines. The negative positions of T_n should also be inserted to permit

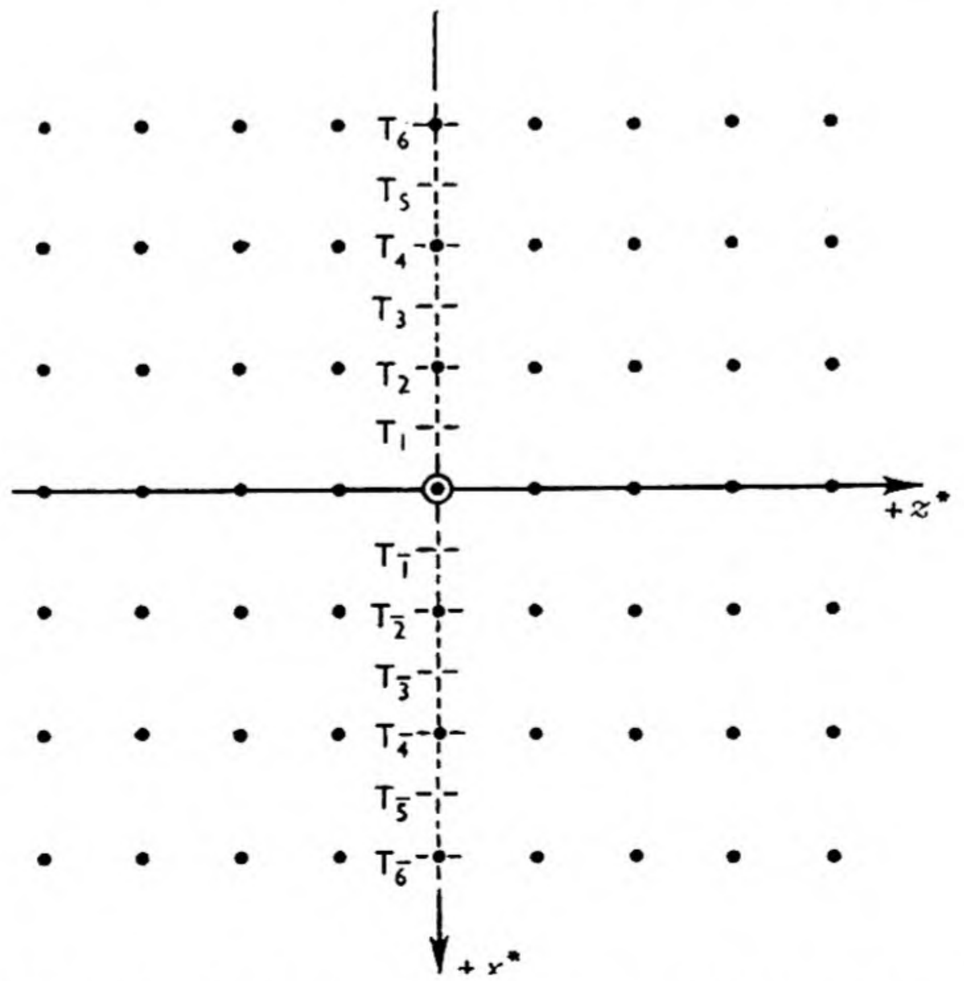

FIG. 69.2. Reciprocal lattice for a hexagonal crystal with $a^* = 0{\cdot}16_8$ and $c^* = 0{\cdot}13_3$, showing the positions of the points T_n. Note that $+y^*$ points downward in this drawing.
Scale : 1 unit = 5 cm.

indexing of the spots on the lower part of the photograph. Next a separate drawing on tracing paper for each layer line is prepared showing the limits of oscillation of the reflecting circle. Now, to index the nth layer line on the upper part of the photograph we proceed as follows (Fig. 68.2):

(1) Place the appropriate tracing with its zero point at T_n. (2) Set its angular position relative to the lattice to correspond to the oscillation of the crystal. (3) Measure values of ξ from the point T_n. (4) Index the points by using co-ordinates from the lattice zero point oo$n$.

For spots below the zero layer line the procedure is exactly the same, only the point $T_{\bar{n}}$ must be used and the index $\bar{n}$ will occur corresponding to the oscillation axis.

For gypsum the values of t_n are given below for $\lambda = 1{\cdot}54$ A.

Values of $n\rightarrow$		1	2	3
oscillation axis	[100]	0·182	0·363	0·545
	[001]	0·189	0·379	0·568

Gypsum is used also as the specimen in an example of a Weissenberg photograph (**7**, 3.2) which provides, in combination with oscillation photographs, a very convenient way of studying a monoclinic crystal by means of X-ray diffraction. As was noted, the orientation of the axes which we have used for gypsum is not a usual one, and alternatives are discussed in **10**, 1.2. A Laue photograph of gypsum is indexed in section **6**, 2.4, and twinning in gypsum is studied in **8**, 5.2.

CHAPTER 6

INTERPRETATION OF LAUE PHOTOGRAPHS

1. Geometry of X-ray Reflection

1.1 The Laue goniometer. The chief feature of a Laue goniometer is that no part of it moves during the taking of the photograph. It is the simplest and also the oldest of all types of X-ray goniometer. In fact the classical photograph of 1912 which demonstrated both the wave nature of X-rays and the lattice foundation of crystal structures was a Laue photograph. In this type of photograph a flat film is most commonly used. In the transmission photograph the incident beam strikes the crystal and then falls normally on the photographic film. In the back-reflection photograph the X-rays pass through an aperture in the film before reaching the crystal; the beams which are reflected backwards are recorded on the film. A side position of the film may also be used for certain purposes (Fig. 71). When the specimen is too thick to transmit X-rays, only back- or side-reflection photographs can be taken, and there are several technical applications of these photographs necessitated by the thickness of the specimen to be examined. For certain purposes it is convenient to use a cylindrical camera in taking a Laue photograph, because in this way the greatest range of angles of reflection can be recorded on one film.

1.2 Formation of Laue spots. We have seen in Chapter 3 that the reflection of X-rays occurs according to the equation $\lambda = 2d_{hkl} \sin\theta$. For a given set of planes (hkl) the spacing d is constant and, since the crystal is stationary in the Laue method, the angle θ is fixed by the setting of the specimen. Hence the wave-length for which the given set of planes can reflect is also fixed. The reflections corresponding to the various planes are each produced by their appropriate wave-length, and hence a Laue photograph requires a range of wave-lengths in the incident beam.

If a set of planes of indices (hkl) reflects a wave-length λ with a particular setting of the crystal, then the set of planes of indices $(2h, 2k, 2l)$ will reflect *in the same direction* a wave-length $\lambda/2$, and so on for the other multiples of (hkl). The reflection must occur in the same direction from all orders of (hkl), because the planes (hkl), $(2h2k2l)$, etc., are all parallel. Any one Laue spot will therefore generally be produced by several wave-lengths in the spectrum which are harmonics of the longest wave-length contributing to the spot.

1.3 Characteristic features of Laue photographs. One of the most characteristic features of transmission or back-reflection Laue photographs is the arrangement of the spots on a series of conic sections, mostly ellipses, all of which pass through the point where the incident beam strikes the film. Each

FIG. 71. Arrangement of incident X-ray beam, crystal and photographic plate for three types of Laue photograph.
(*a*) transmission; (*b*) back reflection; (*c*) side reflection

of these is the locus of reflections from lattice planes which intersect in a common axis, that is, lie in the same zone (**1,** 1.7), as can be illustrated by the following model (Fig. 72). A narrow beam of light is allowed to fall on a glass mirror mounted so as to be capable of rotation about an axis inclined at any suitable angle to the direct beam. The reflected light is received on a screen perpendicular to the direct beam. As the mirror is rotated, the reflected spot of light describes an ellipse passing through the point where the direct beam strikes the screen. The shape of the ellipse depends on the inclination of the axis of rotation of the mirror to the direct beam. The

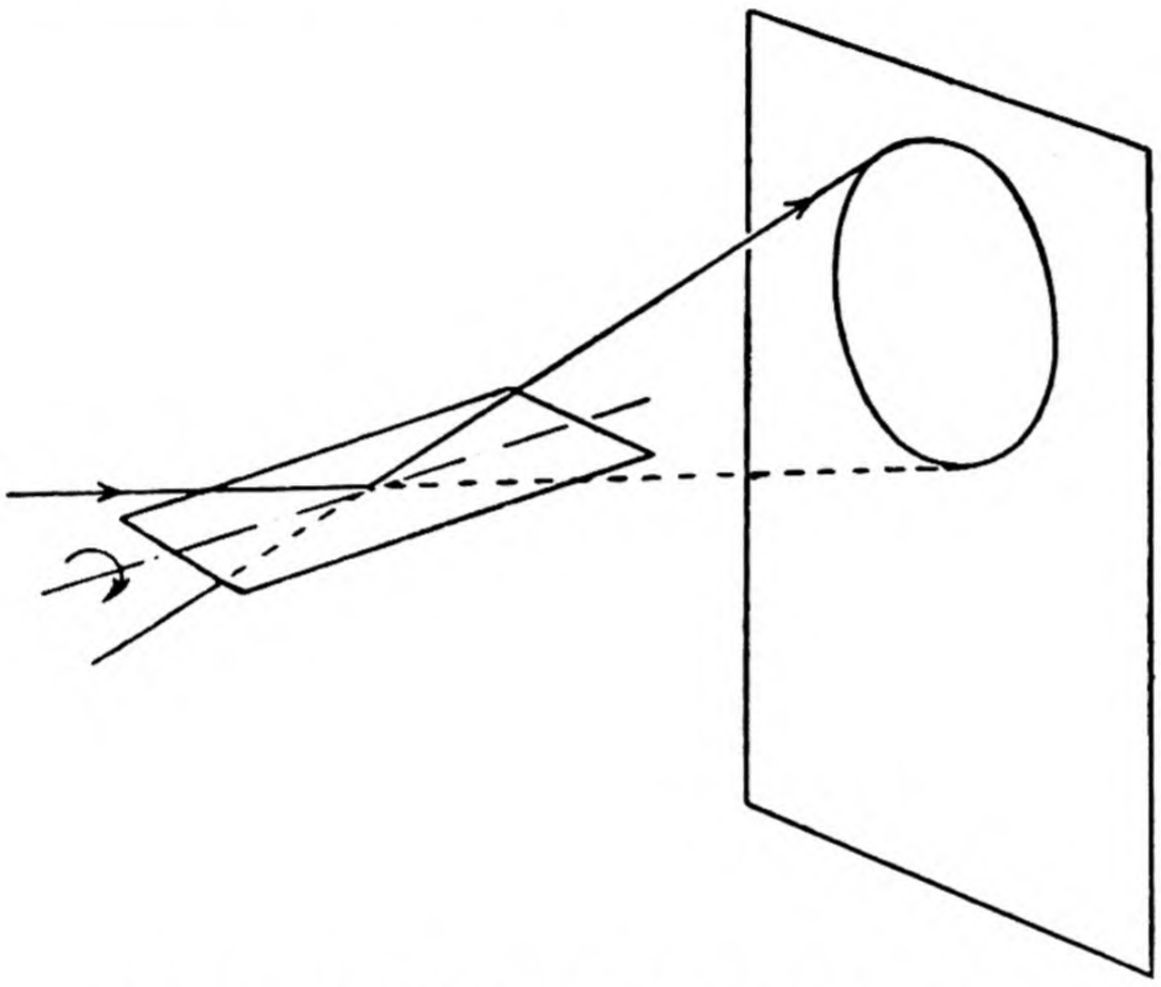

FIG. 72. Optical model illustrating formation of Laue spots

analogy with X-ray reflection is incomplete because the X-ray reflections do not occur except in those directions for which there are lattice planes of appropriate spacing for the available X-ray spectrum. This occurs only for certain directions about the axis of rotation, and hence we have a series of discrete spots along the ellipse and not a continuous ellipse. A consideration of the model will show that the more nearly parallel to the incident beam is the zone axis, the smaller is the angle of the corresponding cone and the smaller is the diameter and eccentricity of the resulting ellipse. The scale of the pattern increases linearly with the distance of the crystal from the film, but the eccentricity of any ellipse is dependent only on the inclination of the corresponding zone axis to the direct beam. When the zone axis is inclined at 45° to the incident beam, the ellipse becomes a parabola. When this angle of inclination of the zone axis exceeds 45°, the intersection of the cone with the film becomes a hyperbola. When this angle is 90° the intersection becomes a straight line.

A feature of many transmission Laue photographs is a region near the centre which is devoid of spots. This is best seen in what are known as *symmetrical photographs*, that is, those in which the direct X-ray beam travels along a symmetry axis (Fig. 162). The effect is due both to the finite size of the unit cell of the crystal and also to the existence of a minimum wave-length in the X-ray spectrum (**2,** 1.2).

As we traverse a Laue photograph from the outside towards the centre, the corresponding value of θ decreases. At the same time the indices (hkl) increase in general. Though this cannot be shown at this stage, it will be proved later (**6,** 1.4). We can, however, illustrate this increase in the indices by a simple example. Suppose that the X-rays are incident along a tetrad axis [100] of a cubic crystal. Then the indices of a reflecting plane making an angle θ with the incident beam are given (**3,** 1.2) by

$$\sin\theta = h/\sqrt{h^2+k^2+l^2}.$$

Thus as θ decreases, the indices k and l must increase, while h falls to unity. Now we have seen (**3,** 1.2) that, for a cubic crystal,

$$d_{hkl} = a/\sqrt{h^2+k^2+l^2}.$$

Consequently as we move towards the centre of the Laue photograph the corresponding value of d_{hkl} must decrease. According to the Bragg equation we have

$$\lambda = 2d_{hkl}\sin\theta,$$

and both terms on the right-hand side of the equation decrease as we approach the centre of the photograph. A limit is set by the minimum value of the wave-length in the X-ray spectrum, and consequently spots cannot occur within a certain distance from the centre of the photograph. In this particular example we can combine the above equations,

$$\lambda = \frac{2a}{\sqrt{h^2+k^2+l^2}} \cdot \frac{h}{\sqrt{h^2+k^2+l^2}} = \frac{2ah}{(h^2+k^2+l^2)}.$$

Near the centre of the photograph h in every spot is equal to unity, because all values of $h/(h^2+k^2+l^2)$ for which h is unity are less than the corresponding values for which h is 2, 3, etc. This is an example of a general rule which will be explained in **6,** 1.4, namely, that *the spots nearest the centre are the most likely to contain first-order reflections.*

1.4 The reciprocal–lattice concept applied to Laue photographs. The reciprocal lattice is derived from the Bravais lattice by constructing normals to the planes of the Bravais lattice and marking off points on these normals at a distance from the origin inversely proportional to the spacing of the planes (**3,** 2.1). In the interpretation of single-crystal photo-

graphs taken with monochromatic radiation, the constant of proportionality K in the equation

$$d^* = K/d$$

is put equal to λ. In taking a Laue photograph we employ a range of X-ray wave-lengths; hence this convention is inappropriate, because each reciprocal point would be drawn out into a line directed towards the origin. Instead we put K equal to unity and, to correspond with this, we make the radius of the reflecting circle $1/\lambda$. We have seen in Chapter 2 that there is a well-defined minimum wave-length in the X-ray spectrum. But at the long-wave end of the spectrum absorption of the beam gradually reduces it to zero intensity. In spite of the ill-defined value of the maximum wave-length we may, for the purpose of our geometrical study, draw two extreme reflecting circles of radius $1/\lambda_{min}$, and $1/\lambda_{max}$ respectively. In Fig. 73 is shown a number of reciprocal points lying in the shaded area between these extreme circles. *Thus all reciprocal points lying within the shaded area represent possible reflecting planes.*

The direction of any reflected ray can be obtained by finding the centre of the reflecting circle which passes through the given reciprocal point and joining this to the point as shown. Thus if P is the reciprocal point and O the origin, we bisect OP normally by QC_m; the centre of the reflecting circle is the intersection of QC_m and the incident X-ray beam. The direction of the reflected X-rays is thus C_mP. Now this direction is independent of the distance of P from O since the length OC_m increases in the same proportion as OP. The angle OC_mP is equal to $2(\pi/2 - \angle POC_m)$. Thus in order to find the direction of reflected rays in a Laue photograph, we can join the corresponding reciprocal point to the origin and find the intersection of this line with an arbitrary reflecting circle, for example, of radius unity. This procedure is equivalent to defining the position of the reciprocal point as for oscillation photographs, the reciprocal constant being equal to λ. We shall revert to this procedure in order to explain the formation of the ellipses of Laue spots. Lattice planes intersecting one another in a common line have reciprocal points which lie in a plane normal to that line. If, therefore, the zone axis is OZ (Fig. 74.1) and OP is the trace of the plane containing the reciprocal points corresponding to the lattice planes intersecting in OZ, then the reflections are in the directions joining C to the circle in which the vertical plane through plane OP cuts the reflecting sphere. The conic section which is obtained on a film perpendicular to OC is in this case an ellipse.

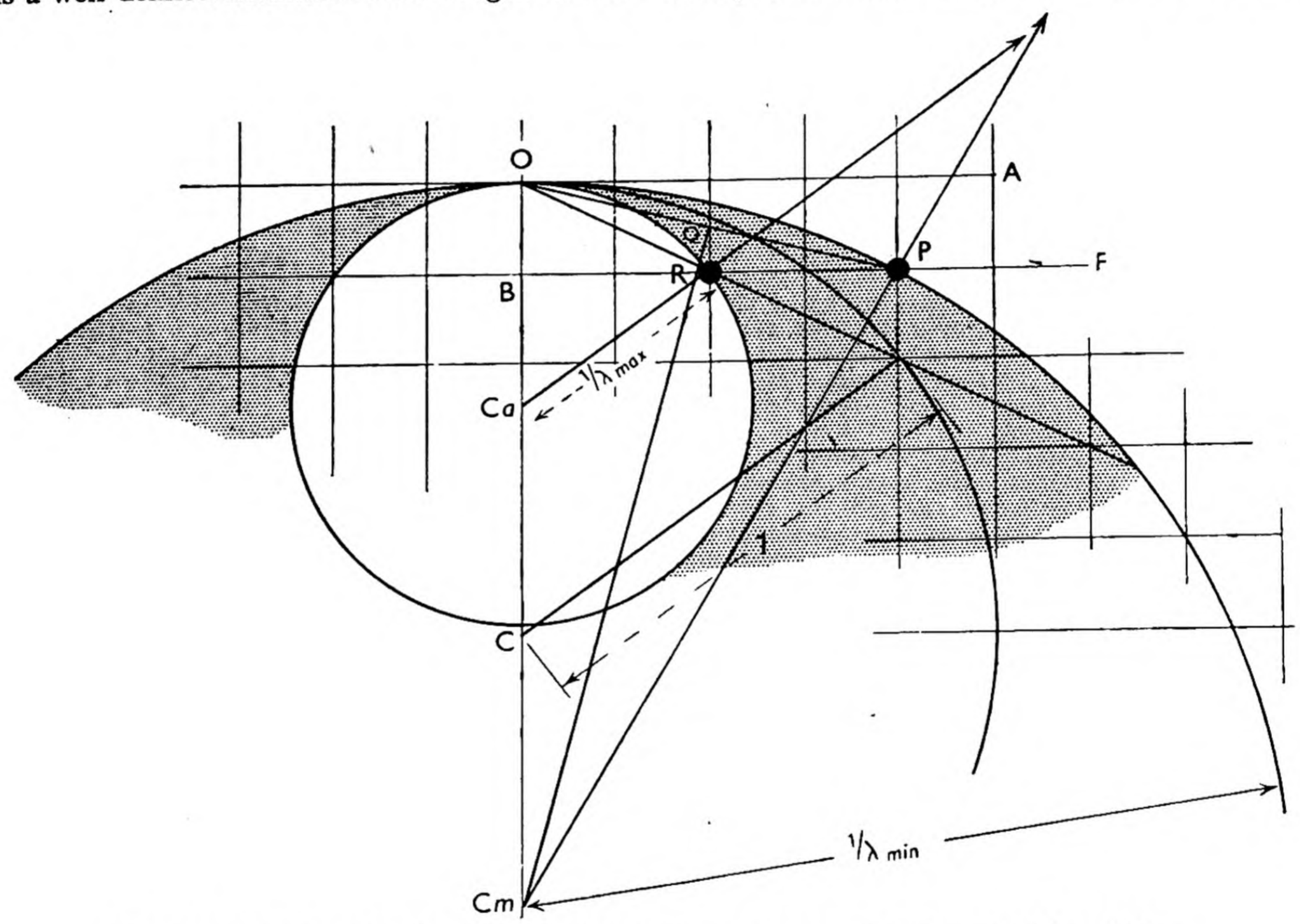

FIG. 73. Portion of reciprocal lattice (shaded), between two limiting reflecting circles

To account for the central region in which no Laue spots occur, we shall take our reciprocal constant equal to unity. In Fig. 73 the lines OA, BF, etc. represent planes of reciprocal points perpendicular to the incident X-rays. The points C_m and C_a are the centres of the reflecting circles for minimum and maximum wave-lengths respectively. It is clear that the angles of deviation of the reflected rays for the

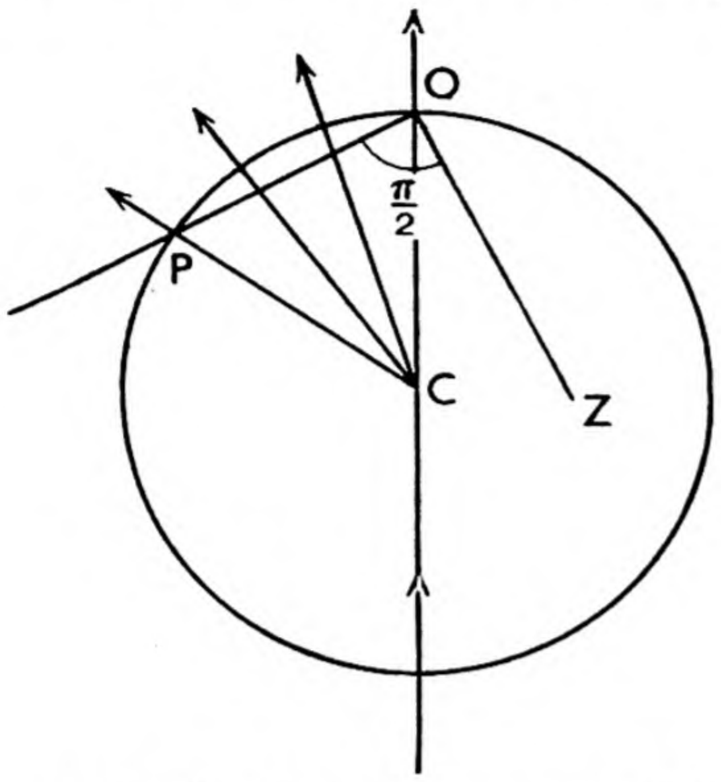

FIG. 74.1. Small circle on diameter OP, having its plane perpendicular to diagram, produces cone of reflected rays OCP

first plane of reciprocal points outwards from the origin are smaller than the corresponding angles for the second and higher planes of reciprocal points. Further, the least deviated rays correspond to the minimum wave-length, as may be seen from the fact that $\angle OC_mP < \angle OC_aR$. We can thus draw the following conclusions: (*a*) the spots nearest to the centre of the photograph will correspond to reflections from points on the first plane of reciprocal points from the origin normal to the incident beam; (*b*) no spots will occur nearer the centre than corresponds to an angle of deviation of $\angle OC_mP$ determined by the intersection of the first reciprocal plane BF and the reflecting sphere for $\lambda_{\min}$. This is a more general statement of the proposition which was illustrated earlier by reference to a cubic crystal (**6,** 1.3); (*c*) the indices for λ_{min} are the highest.

1.5 Relation between the gnomonic projection and the reciprocal lattice. The gnomonic projection (**1,** 5.4) is constructed by drawing normals to the crystal faces or to the lattice planes from an arbitrary origin to cut a plane situated at an arbitrary distance from the origin. The points in which these normals intersect the plane of projection are the *gnomonic poles*. A reciprocal lattice (**3,** 2.1) is likewise constructed by drawing normals to the planes of the Bravais lattice. A gnomonic pole and the corresponding reciprocal point must therefore always lie on the same line drawn through the origin. It is important to remember that the *gnomonic projection represents the intersection of the plane of projection by lines joining reciprocal points to the origin* (Fig. 74.2).

In the interpretation of a gnomonic projection, use can be made of a gnomonic net which, for a symmetrical Laue photograph, is the same as a plane net of the reciprocal lattice. If the z-axis is perpendicular to the plane of the projection, the l index of every point of the gnomonic net is unity (Fig. 74.2). Similarly, if the projection is made perpendicular to y or x, the second and first indices respectively of the points of the gnomonic net are unity. The indices of points at the corners of the unit meshes of the gnomonic projection are therefore the same as those of the corresponding points of the first plane of reciprocal points outwards from the origin.

The gnomonic points which are not situated at the points of the gnomonic net have indices which are higher than those of the surrounding net points. If the co-ordinates of a point relative to the unit mesh of the gnomonic net are, for example, $2\frac{1}{2}$, $3\frac{1}{3}$, the indices of the corresponding planes are 15, 20, 6, while the surrounding four points of the gnomonic net have indices 231, 241, 331, 341 respectively (Fig. 75). The reciprocal point of indices 15, 20, 6 is situated on a reciprocal lattice plane parallel to, but six times farther from, the origin than the plane containing the points

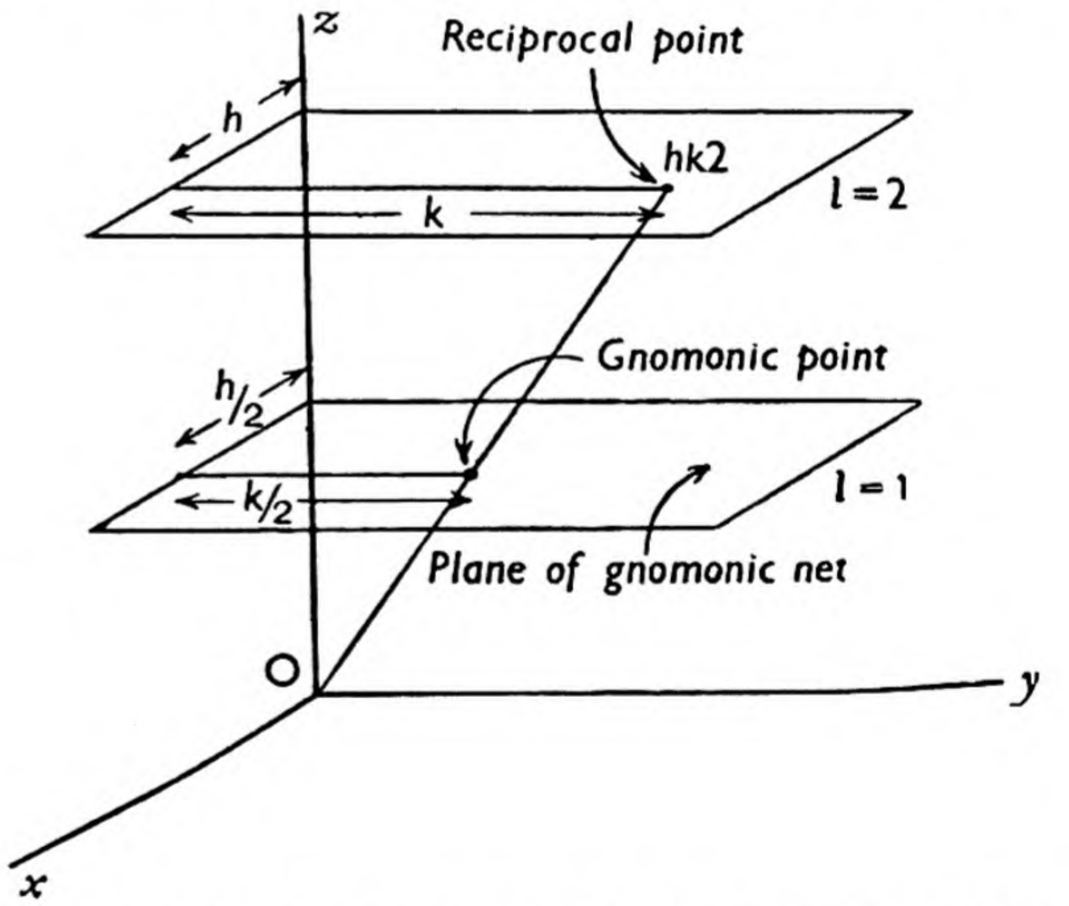

FIG. 74.2. Diagram illustrating relation between reciprocal lattice and gnomonic projection

231, 241, 331. When, however, point 15, 20, 6 is joined to the origin, the line cuts the plane of the gnomonic projection in the point having co-ordinates $2\frac{1}{2}$, $3\frac{1}{3}$.

The gnomonic projection is usually employed in the interpretation of Laue photographs taken on a flat film. It is common usage to make the dots on the gnomonic projection large when they correspond to strong reflections and small when they correspond to weak reflections. It is frequently found that the large

dots representing strong reflections tend to occur at the points of the gnomonic net (Fig. 76). This is because more portions of the X-ray spectrum contribute to these reflections than to the others. From our previous example it will be seen that each index of the plane (15, 20, 6) is approximately six times greater than the corresponding index of each of the surrounding gnomonic net points. Hence the spacing $d_{15,20,6}$ is approximately six times smaller than the spacings of the planes corresponding to the four

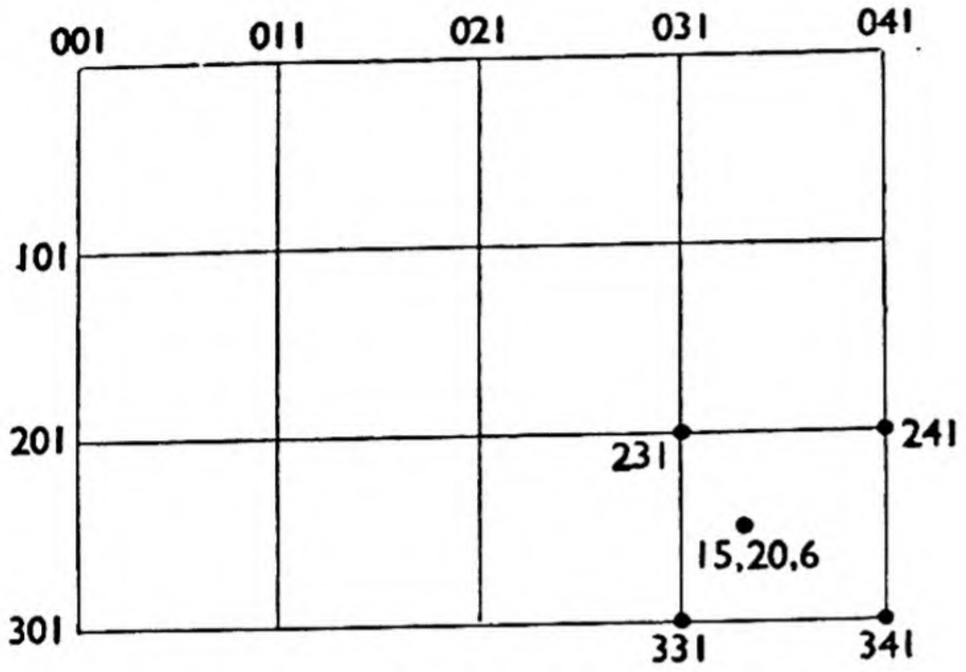

FIG. 75.1. Gnomonic projection

surrounding net points. Thus if the reflection 15, 20, 6 is produced by a single wave-length very near the minimum, the reflections corresponding to the surrounding gnomonic net-points will be produced by wave-lengths approximately six times as great. This makes it possible for the second and other harmonics of the long wave-lengths to contribute to the reflections corresponding to the net-points 231, 241, 331, 341. These net-points will therefore correspond to Laue spots in which up to six orders might be superimposed. As might be expected, such reflections are strong compared with that from the plane of indices (15, 20, 6).

1.6 Effect of alteration of wave-length range. The appearance of a Laue photograph of a given crystal set up in any manner is considerably affected by a change of potential on the X-ray tube. If a low potential is used, the minimum wave-length is relatively large and the clear space near the centre of the photograph is correspondingly large (**6,** 1.4). The pattern is also much less rich in spots than when a high potential is applied. This is due to the fact that when λ_{min} is large the spectral range from which wave-lengths are available for reflection is more restricted than when λ_{min} is small. Thus we summarise these changes by saying that the Laue photograph as a whole becomes richer in spots and these appear closer and closer to the centre as λ_{min} is progressively reduced.

2. Symmetrical Laue Photographs

2.1 Indexing for a cubic crystal. The Laue photograph shown in Fig. 76 is that of iron pyrites orientated so that the X-rays travel along one of the crystallographic axes which we take to be the z-axis. Since the photograph is a transmission one, the relation between the reflected X-ray beam and the gnomonic pole, P, of the reflecting planes is as shown in Fig. 75.2.

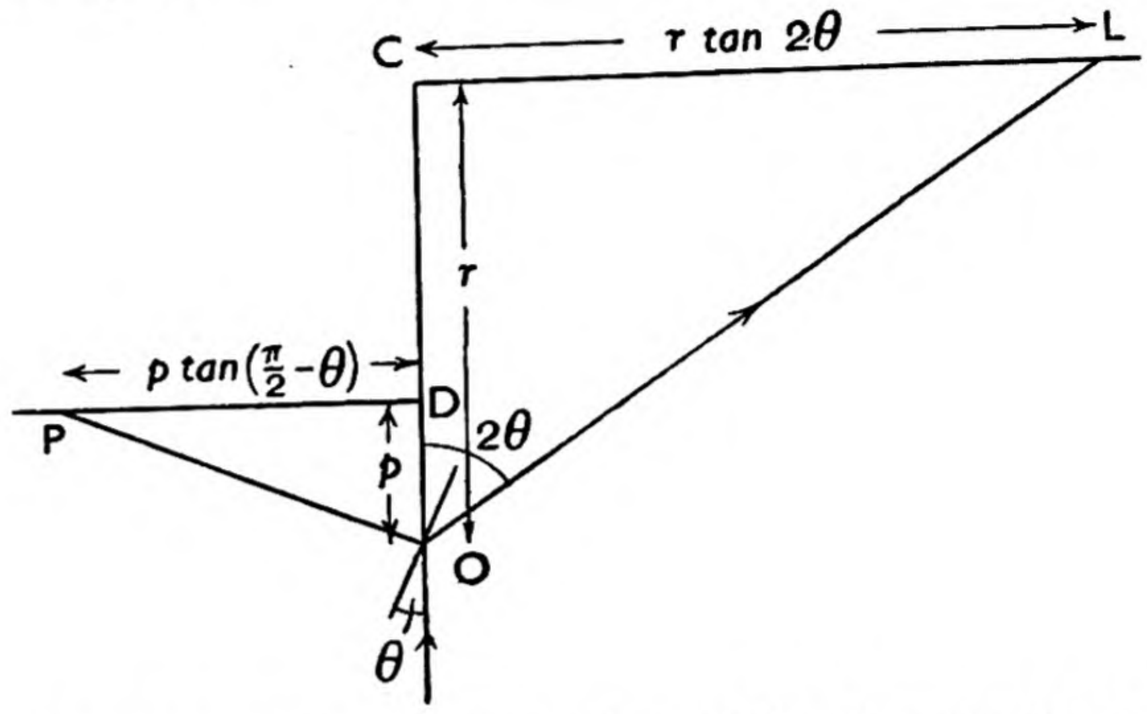

FIG. 75.2. Diagram illustrating relation between Laue spot and gnomonic pole.

O is centre of sphere of projection with radius p
P is gnomonic pole
L is Laue spot

The distance from the centre of the photograph to the Laue spot is $r \tan 2\theta$, where r is the crystal-to-plate distance. If the radius of the projection sphere of the gnomonic projection (**1,** 5.4) is p, the corresponding distance of the gnomonic point P from the centre of the gnomonic projection, D, is $p \cot \theta$. This relation between the lengths of the lines CL and PD is the basis of the method of interpreting the Laue photograph of iron pyrites which is adopted here. In order to avoid the necessity of carrying out a large number of calculations of the lengths PD corresponding to the distances CL of the Laue spots, a table (p. 77) is made of corresponding values of $r \tan 2\theta$ and $p \cot \theta$ for $r = 5$ cm. and $p = 2$ cm. The distance 5 cm. is fixed by the experimental conditions, whereas p is chosen to give a convenient size of gnomonogram. From this table a graph is drawn to assist in interpolation (Fig. 77), and the following procedure may be adopted. The Laue photograph is transferred to a sheet of paper, and the centre of the photograph is carefully determined from the intersections of lines which join corresponding spots on either side of the photograph. A ruler is placed so that a line can be drawn through the Laue spot to the centre and then be produced beyond the centre. One leg of a pair of dividers is set on the Laue spot and the other

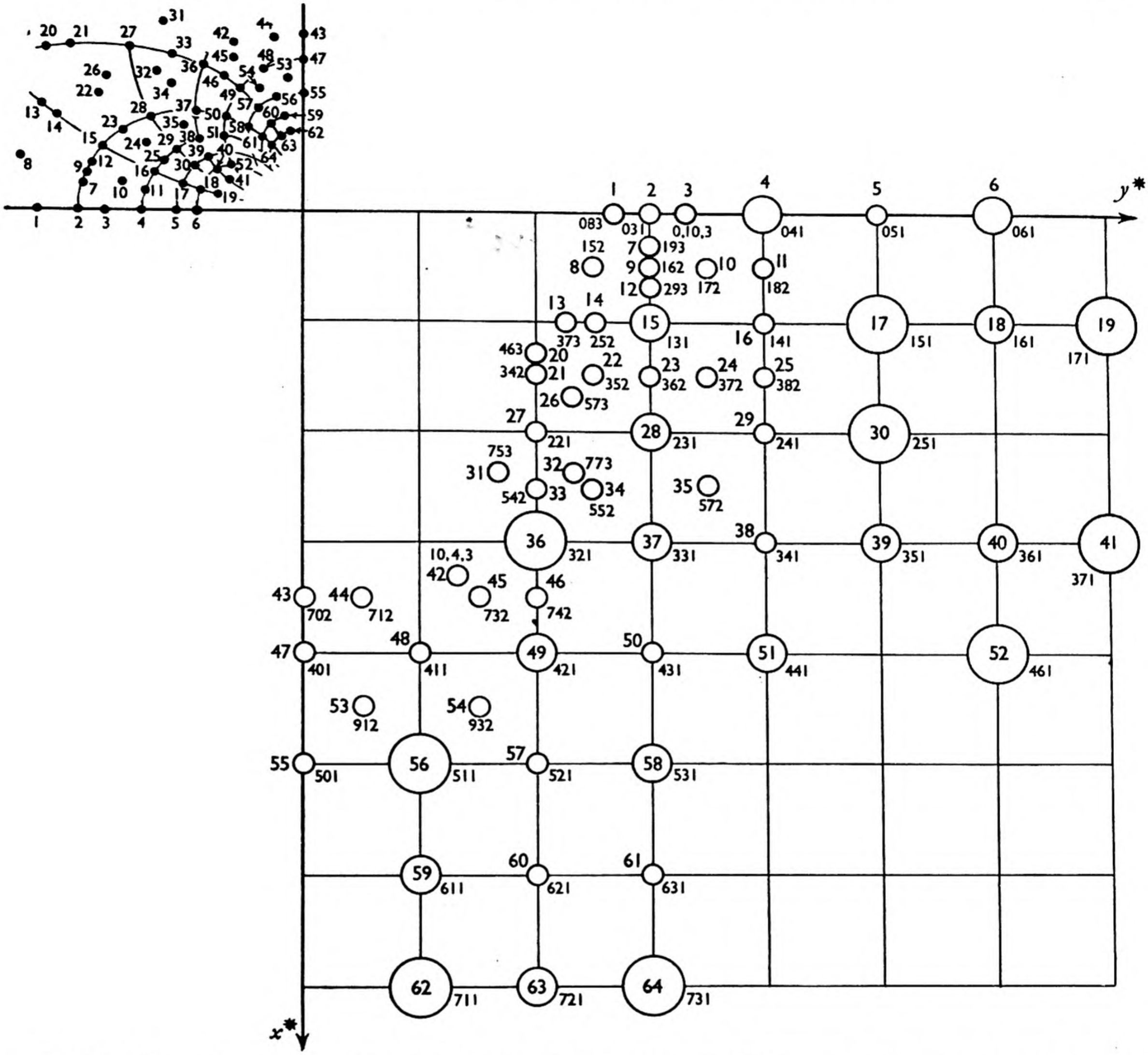

FIG. 76. Gnomonic projection of Laue photograph of iron pyrites. The X-rays are incident along the axis [001]; $r = 5{\cdot}0$ cm., $p = 2{\cdot}0$ cm. In the diagram, the dimensions are all 80 per cent. of the true measurements

on the centre. The distance $r \tan 2\theta$ is in this way transferred to the graph. The points of the dividers are now re-set to the corresponding gnomonic distance, $p \cot \theta$, as given by the graph. This distance is marked off from the centre along the produced line joining this to the Laue spot.

This process is repeated for all the Laue spots. The gnomonogram which is built up in this way consists of the points indicated by circles in Fig. 76. Large circles have been drawn to correspond to the dark spots on the photograph. It will be seen by inspection of the gnomonogram that the points lie on a square net of lines. The separation of the lines is 2 cm. and this is a consequence of chosing, in the cubic system, the radius of the projection sphere, p, to be 2 cm. Since the angle (001) : (101) is 45°, the normal to the plane (101) must strike the plane of projection at a distance from the centre equal to the radius of the projection sphere. It will often be found in plotting gnomonic points corresponding to the Laue spots close to the centre of the photograph that they do not fall exactly on the points of the gnomonic net based

on a square of 2 cm. side. This is due to the difficulty in measuring accurately the small distance between the Laue spot and the centre and also to mis-setting of the crystal. From the graph of Fig. 77 it will be seen that for small values of $r \tan 2\theta$ a change of 0·25 cm. results in a change of 3·9 cm. in $p \cot \theta$; but for large values of $r \tan 2\theta$ a change of 1 cm. results in a change of only 0·58 cm. in $p \cot \theta$.

We have seen in **6,** 1.4 and **6,** 1.5 that the innermost Laue spots correspond to the reciprocal points on the first plane perpendicular to the X-ray beam from the origin, and that the corresponding gnomonic points lie actually on the points of the gnomonic net. It is therefore permissible to move the outermost gnomonic points which have been plotted by the method described above on to the nearest net points constructed on a mesh of 2 cm. This has been done in drawing the net of Fig. 76, although the shifts required were never more than a few millimetres. Some of the points nearer the centre of the gnomonogram correspond to the second plane of the reciprocal lattice and may therefore lie mid-way between the lines of the net. These points can therefore be given small adjustments to bring them on to the correct positions. Still nearer the centre are the gnomonic points which occur at points having co-ordinates expressed in thirds. There are no points which have co-ordinates equal to a whole number plus an odd number of quarters.

By taking the above considerations into account the gnomonic projection can be accurately drawn, and it only remains to assign indices to the points. As explained in **6,** 1.4, the net-points correspond to points lying on the first plane of reciprocal points from the origin perpendicular to the z-axis. The indices of gnomonic points corresponding to such reciprocal points are therefore of the type $hk1$, where h and k are the co-ordinates of the points on the lattice. A glance at Fig. 76 will reveal many examples of such gnomonic points. Points other than those belong to the second and third reciprocal planes from the origin perpendicular to the z-axis, and these have indices of the type $hk2$ and $hk3$.

In Fig. 74.2 is shown a reciprocal point having co-ordinates $hk2$ joined to the origin and cutting the first reciprocal plane in a point having co-ordinates $h/2$, $k/2$. Thus if a gnomonic point has co-ordinates such as $1\frac{1}{2}$, $2\frac{1}{2}$ we know that it corresponds to a plane the last index of which is 2 and the first two indices are 3 and 5 respectively. Hence we arrive at the rule:

Read the two co-ordinates of the point in the gnomonic projection and insert the numeral 1 in the position corresponding to the third axis. Express these numbers as integers with no common denominator and thus obtain the indices of the plane.

$r \tan 2\theta$ ($r = 5$ cm.)	$p \cot \theta$ ($p = 2$ cm.)
1·0	20·14
1·25	16·25
1·50	13·63
1·60	12·81
1·70	12·09
1·80	11·45
1·90	10·89
2·0	10·39
2·1	9·90
2·2	9·56
2·5	8·47
2·7	7·92
3·0	7·22
3·5	6·36
4·0	5·70
4·5	5·22
5·0	4·83
6·0	4·25

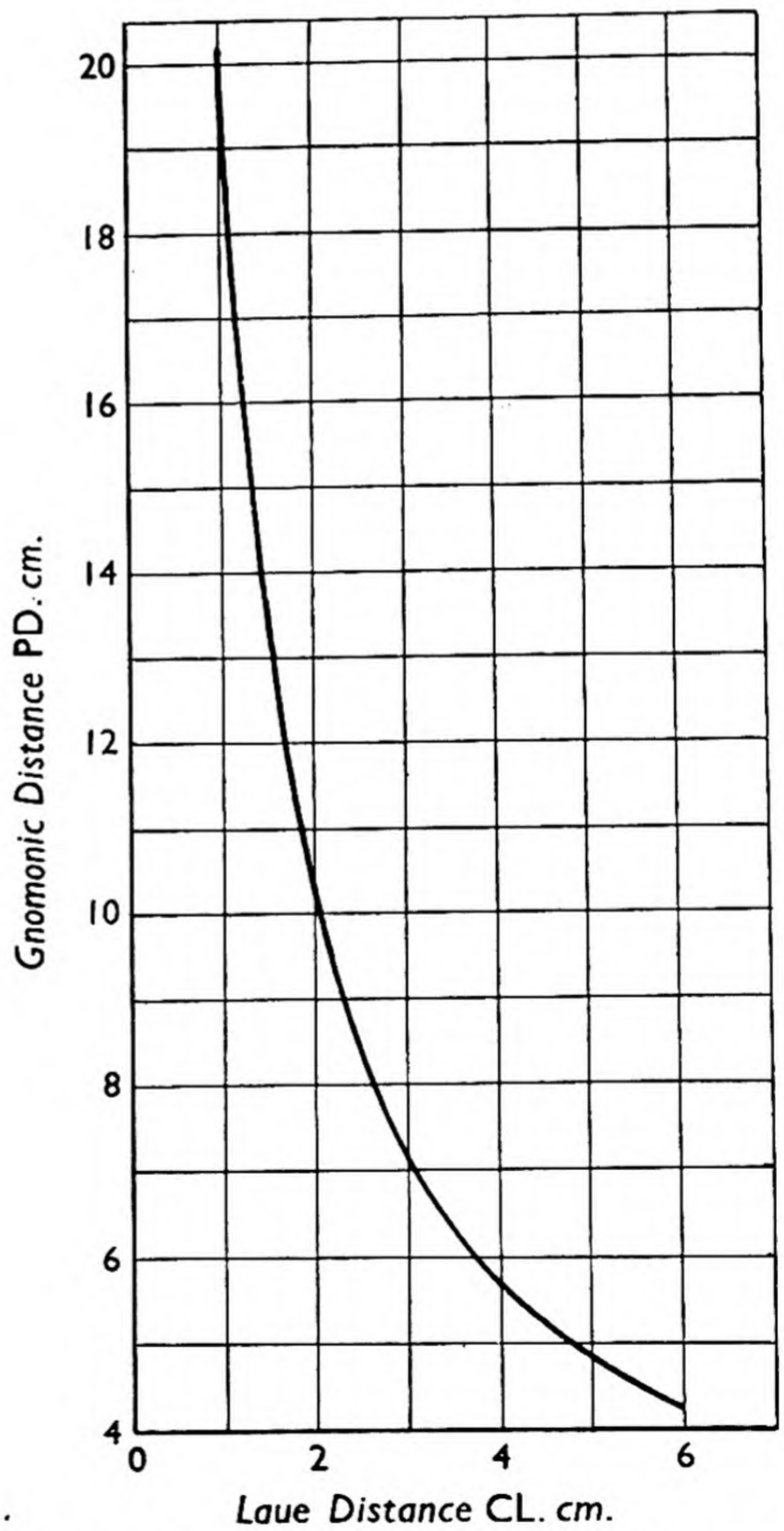

FIG. 77. Graph giving relation between distances of Laue spot and corresponding gnomonic point from centre of photograph. $CL = r \tan 2\theta$ and $PD = p \cot \theta$ where $r = 5$ cm., $p = 2$ cm.

2.2 Determination of unit-cell size. The Laue photograph is not usually employed in order to find the dimensions of unit cells. It may, however, be used to obtain a rough estimate of the dimensions if the indices of the reflections and the minimum value of λ are known. It has been shown (**6,** 1.5) that the outermost gnomonic points are associated with reciprocal points in the first plane from the origin which is normal to the direction of the incident beam. Further, the radiation utilized in the reflections from such points is close to the short wave-length limit of the spectrum. As an illustration of the application of this method we shall consider certain reflections in the photograph of iron pyrites (Fig. 76).

The indices of the gnomonic points which correspond to the spots nearest the centre of the photograph are of the type $hk1$ (**6,** 2.1) and the angle ϕ between the normal to these planes and the z-axis [001] is given (**1,** 3.9) by

$$\cos\phi = \frac{1}{\sqrt{h^2+k^2+1}}.$$

Since the angle θ is the complement of ϕ,

$$\sin\theta = \frac{1}{\sqrt{h^2+k^2+1}}.$$

The expression for $\sin^2\theta$ (Appendix 2) gives

$$d_{hk1} = \frac{a}{\sqrt{h^2+k^2+1}}.$$

By substituting for d in the Bragg equation we obtain

$$\lambda = \frac{2a}{(h^2+k^2+1)},$$

and

$$a = \frac{\lambda}{2}(h^2+k^2+1).$$

Although it is impossible in general to discover the actual wave-length which has produced a given spot, we can fix this between certain limits and hence obtain an approximate value for the cell-side. If the minimum wave-length emitted by the tube is denoted by the symbol $\lambda_{\min}$, then (**2,** 1.2),

$$\lambda_{\min}\ (\text{in A.}) = 12{\cdot}4/V$$

where V is the peak voltage in kilovolts applied to the tube. We can now write

$$a > \frac{\lambda_{\min}}{2}(h^2+k^2+1),$$

$$> \frac{12{\cdot}4}{2V}(h^2+k^2+1).$$

In the example of **6,** 2.1 the highest value of h^2+k^2+1 among the spots near the centre of the photograph is 59, which corresponds to the indices 731. By inserting the value of $V=75$ kV. we obtain

$$a > 4{\cdot}9 \text{ A.}$$

For planes of indices $(hk2)$ the corresponding equation is

$$a > \frac{\lambda_{\min}}{2}\frac{(h^2+k^2+4)}{2}.$$

The greatest value of h^2+k^2+4 in Fig. 76 is 94, which corresponds to the indices 932; this gives,

$$a > 3{\cdot}9 \text{ A.}$$

Similarly from the plane 10, 4, 3 we obtain

$$a > \frac{12{\cdot}4}{2\times 75}\times\frac{125}{3} > 3{\cdot}5 \text{ A.}$$

Thus the value nearest to the true cell-size, namely 5·40 A., is obtained from the spots nearest to the centre of the photograph. The method may be refined by starting with a symmetrical photograph, which can be indexed, and taking successive Laue photographs with the crystal rotated about an axis perpendicular to the X-ray beam through angles of 1°, 2°, 3°, etc. In this way the lowest value of the angle θ at which a particular set of planes such as (731) only just reflects can be determined. It is possible in such a case to be sure that the reflected wave-length was very close to $\lambda_{\min}$ and hence a more accurate value of a can be obtained.

If characteristic radiation is present in the beam it sometimes happens that a Laue spot is produced by one or other of the characteristic wave-lengths. Such a spot is usually much stronger than the others and is often of a different shape from that of neighbouring spots. The photograph can be retaken with the insertion of the appropriate β-filter in order to decide whether the reflected wave-length is α or β. From such a spot it is, of course, possible to obtain a more definite value for the cell-side than by the general procedure described above.

2.3 Indexing for tetragonal and orthorhombic crystals. A Laue photograph of a tetragonal crystal taken with the incident X-ray beam travelling along the z-axis can be interpreted by means of a gnomonic net with a square unit mesh. If the incident beam is parallel to the x- or the y-axis of a tetragonal crystal, the unit mesh of the corresponding gnomonic projection is rectangular. The indexing of such photographs is similar to that of the orthorhombic crystal described below.

The transmission Laue diagram shown in Fig. 79 is of molybdenum trioxide, MoO_3 (orthorhombic), taken with the incident beam parallel to the y-axis. The plotting of the gnomonic points is carried out as described for cubic crystals, and the resulting projection is shown in the figure. The horizontal and

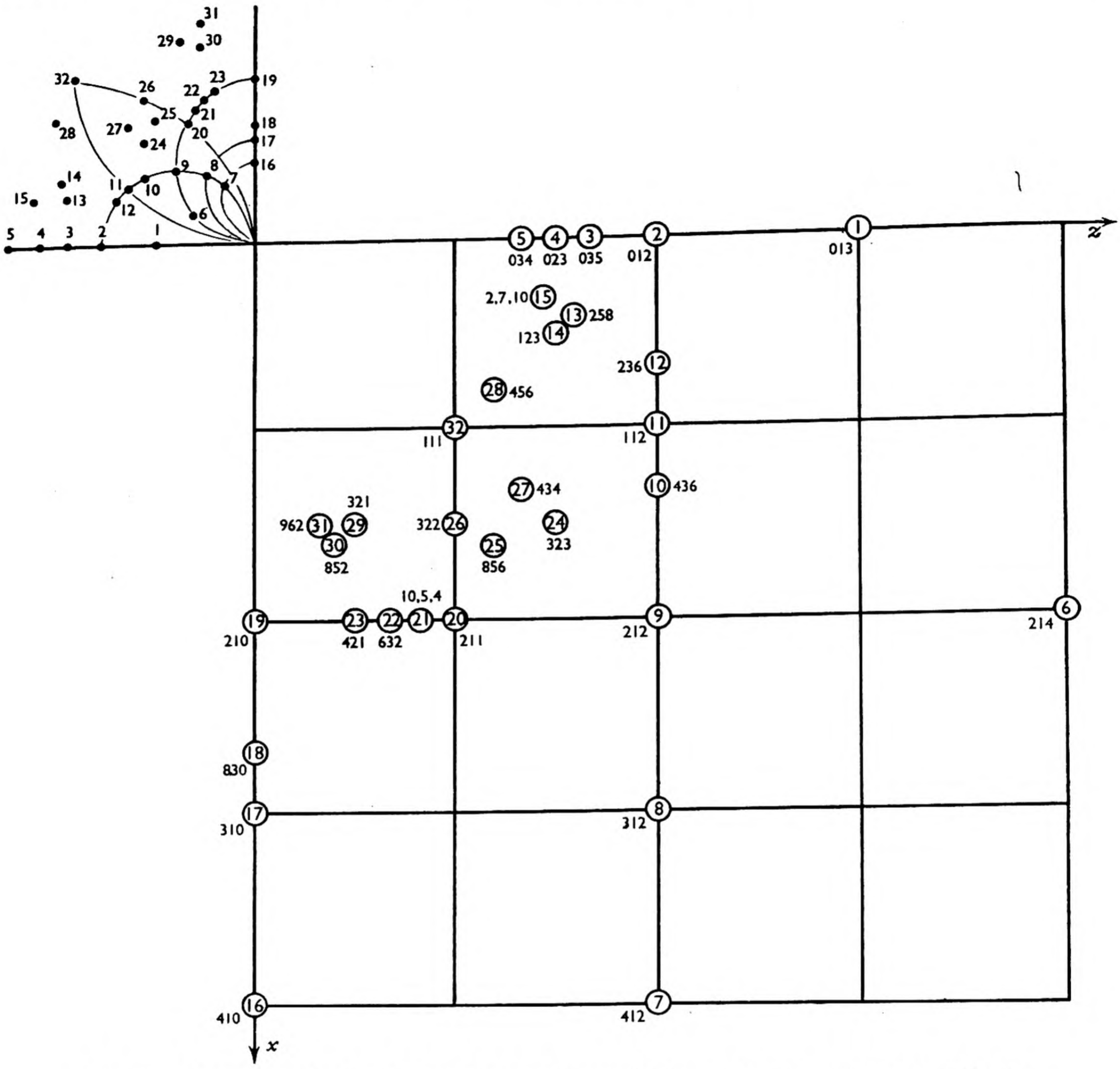

FIG. 79. Gnomonic projection of Laue photograph of molybdenum trioxide. The incident X-ray beam is parallel to the axis [010]; $r = 3{\cdot}76$ cm., $p = 1{\cdot}51$ cm.

vertical lines have been drawn parallel to the lines of symmetry in the photograph. The distance apart of the lines in the gnomonic net is determined by the positions of the outermost points; thus the separation of the horizontal lines is given by the distance apart of the lines passing through points 17, 8 and 16, 7 respectively. Similarly, the points 1 and 6 determine the separation of the vertical lines. The justification for this method of fixing the dimensions of the unit mesh of the gnomonic projection has been given in **6,** 1.4 and **6,** 1.5, where it was shown that the spots on the outside of the gnomonic projection correspond exclusively to reciprocal points on the first plane from the origin along the direction of the incident beam. Every such gnomonic point must therefore lie at the corner of a unit mesh of the gnomonic projection.

When the unit mesh of the gnomonic projection has been decided, the axial ratios, a/b and c/b may be determined. The distance from the centre of the

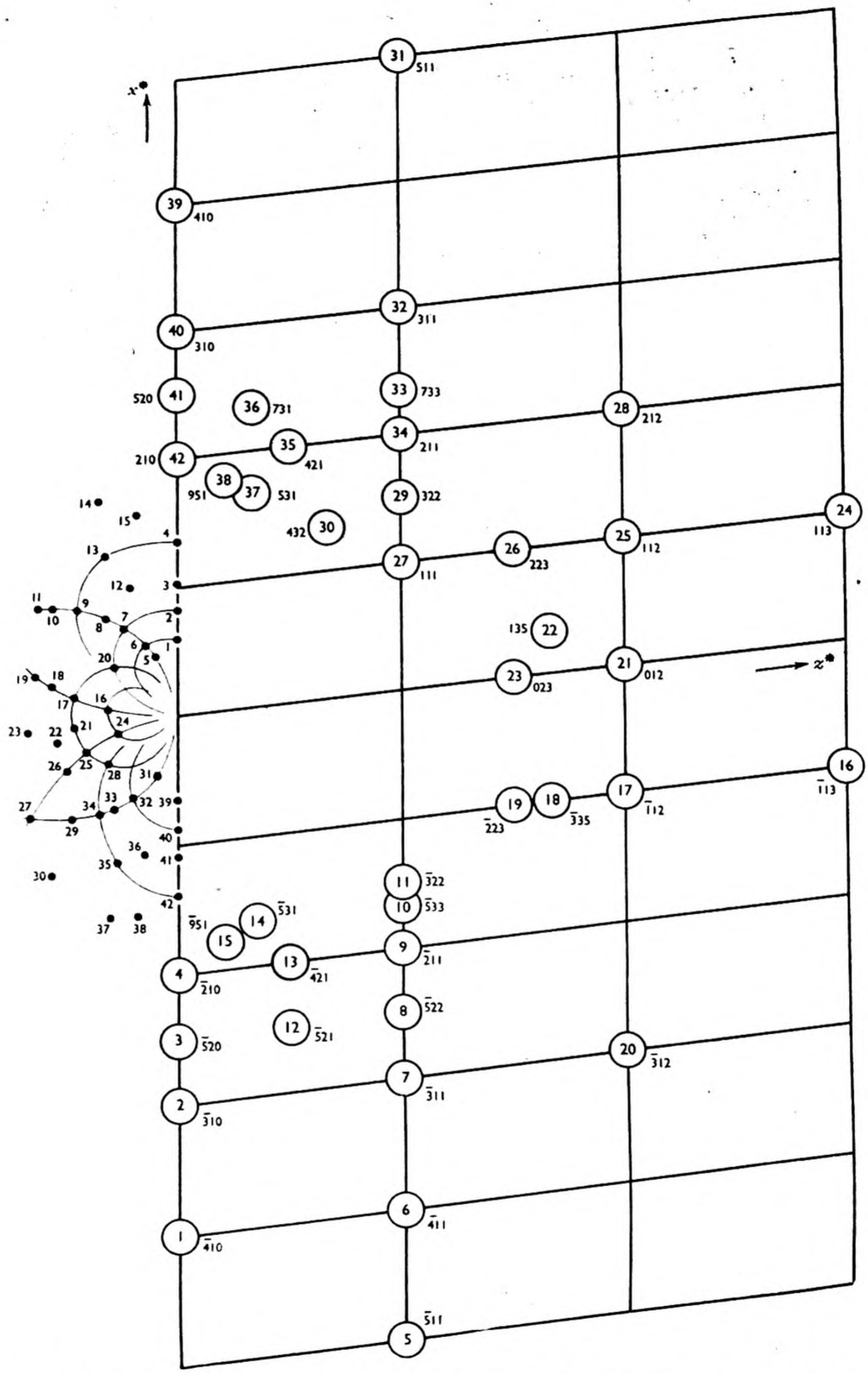

FIG. 80. Gnomonic projection of Laue photograph of gypsum, with indexing on the 'morphological' unit cell (Fig. 138). The incident X-ray beam is parallel to the axis [010], and the actual photograph is given in Fig. 120.2 (*a*). $r = 3{\cdot}05$ cm., $p = 1{\cdot}22$ cm.

projection to the point 110, which may be denoted by e, is related to p, the radius of the sphere of projection, by the equation

$$p/e = \cot 110 \wedge 010 = a/b.$$

Similarly, if the distance from the centre of the projection to the point 011 be denoted by g, then

$$p/g = \cot 011 \wedge 010 = c/b.$$

The values of a/b and c/b for MoO_3 determined in the manner described above are 0·58 and 0·53 respectively. The true axial ratios determined from oscillation photographs are 0·28 : 1 : 0·26, from which it will be seen that, within the accuracy of measurement, the values of a/b and c/b determined from the Laue photograph are just twice the true values. This is due to the nature of the crystal structure, which has a pseudo-repeat distance along the y-axis of one half of the true repeat distance. Consequently all reflections of the type hkl in which k is odd are very weak in comparison with those for which k is even. Thus the projection which has been produced by the application of the usual rules is really the projection of the second layer (above the origin) in the reciprocal lattice and not of the first layer as we have so far assumed. The correct indices of the planes therefore have the k index double that which has been assigned. This rather unusual difficulty in interpreting Laue photographs is included here as a warning against drawing conclusions about cell dimensions without making use of data from oscillation photographs.

2.4 Indexing for a monoclinic crystal. In Fig. 80 is shown a Laue photograph of gypsum (monoclinic). The X-rays were incident on the crystal in a direction perpendicular to the cleavage plane (010), that is, parallel to the y-axis. The plotting of the gnomonogram corresponding to the Laue spots proceeds as in the examples discussed above. It is evident on inspection that the outermost points fall on an oblique-mesh net as shown in the figure. As has already been emphasized, there is a large choice of the x- and z-axes in a monoclinic lattice, and the selection of one particular unit cell is arbitrary. The present choice corresponds to the usual morphological axes. When the directions and the spacings of the lines of the net have been chosen so that the lines go through the plotted points as nearly as possible, the whole set of lines is drawn in as shown in the figure. The previously plotted points are moved, if necessary, through a small distance so as to lie at the correct positions on the gnomonogram. The indices are now inserted as in **6,** 2.1, k being put equal to unity for every intersection of net lines, since the y-axis is normal to the projection. If the co-ordinates are, for example, $1\frac{1}{3}$ along the x^*-axis and $\frac{2}{3}$ along the z^*-axis, the indices are $1\frac{1}{3}$, 1, $\frac{2}{3}$ or 432. It should be noted that the two co-ordinate axes of the projection are the same as for the corresponding reciprocal net and do not coincide with the x- and z-axes of the Bravais lattice. This is obvious when it is realised that the x^*-axis is the projection of the plane containing the y-axis and the normal to (100). Similarly, the z^*-axis is the projection of the plane through the y-axis and the normal to (001).

The axial ratios a/b, c/b and the angle β can be obtained from the gnomonogram. By direct measurement it is found that $\beta = 97\frac{1}{2}°$. The distance apart of the points $\bar{4}10$ and 410 is 22·7 cm. and hence the distance on the gnomonogram between the points 010 and 110 is 22·7/8 = 2·84 cm. Since the distance p of the plane of the gnomonogram from the point of projection is 2·0 cm.,

$$\cot 010 \wedge 110 = 2{\cdot}0/2{\cdot}84 = 0{\cdot}704.$$

Now we have

$$a/b = \tan 100 \wedge 110/\sin\beta = \cot 010 \wedge 110/\sin\beta = 0{\cdot}71.$$

Similarly, the distance apart of the points 010 and 012 is 9·65 cm. Hence, the distance apart of the points 010 and 011 is 9·65/2 = 4·83 cm. It follows, therefore, that

$$\cot 010 \wedge 011 = 0{\cdot}414.$$

Now $$c/b = \cot 010 \wedge 011/\sin\beta = 0{\cdot}42.$$

Thus we have,

$$a : b : c = 0{\cdot}71 : 1 : 0{\cdot}42,\ \beta = 97\tfrac{1}{2}°;$$

which may be compared with those of Dana (1898),

$$a : b : c = 0{\cdot}69 : 1 : 0{\cdot}41,\ \beta = 99\tfrac{1}{2}°.$$

The inaccuracy of our values is due to the errors which occur in setting the film at a given distance from the specimen, and in adjusting the crystal accurately; and also to the alterations which occur in the scale during the processing of the film and print.

It should be noted that the choice of the x- and z-axes used here is the usual morphological one. This is different from the choice of the most prominent zone edges, made in **5,** 2.7, and from that made in X-ray work. The different choices of axes are shown in Figs. 120.1 and 138.

2.5 Example of a back-reflection Laue photograph. In Fig. 82 is shown a back-reflection Laue photograph from a plate of low-temperature quartz cut perpendicular to a diad axis with the optic axis horizontal. In the photograph it can be seen that pairs of spots correspond in position as if the vertical line and the horizontal line were each lines of symmetry. The different intensities of such pairs of spots show that these lines are not lines of symmetry. This point is discussed further in **10,** 2.2. The actual symmetry of this Laue photograph is digonal (**6,** 2.6), but because of the correspondence in position between pairs of spots we can proceed as if it were di-digonal. We shall therefore index the photograph as though it

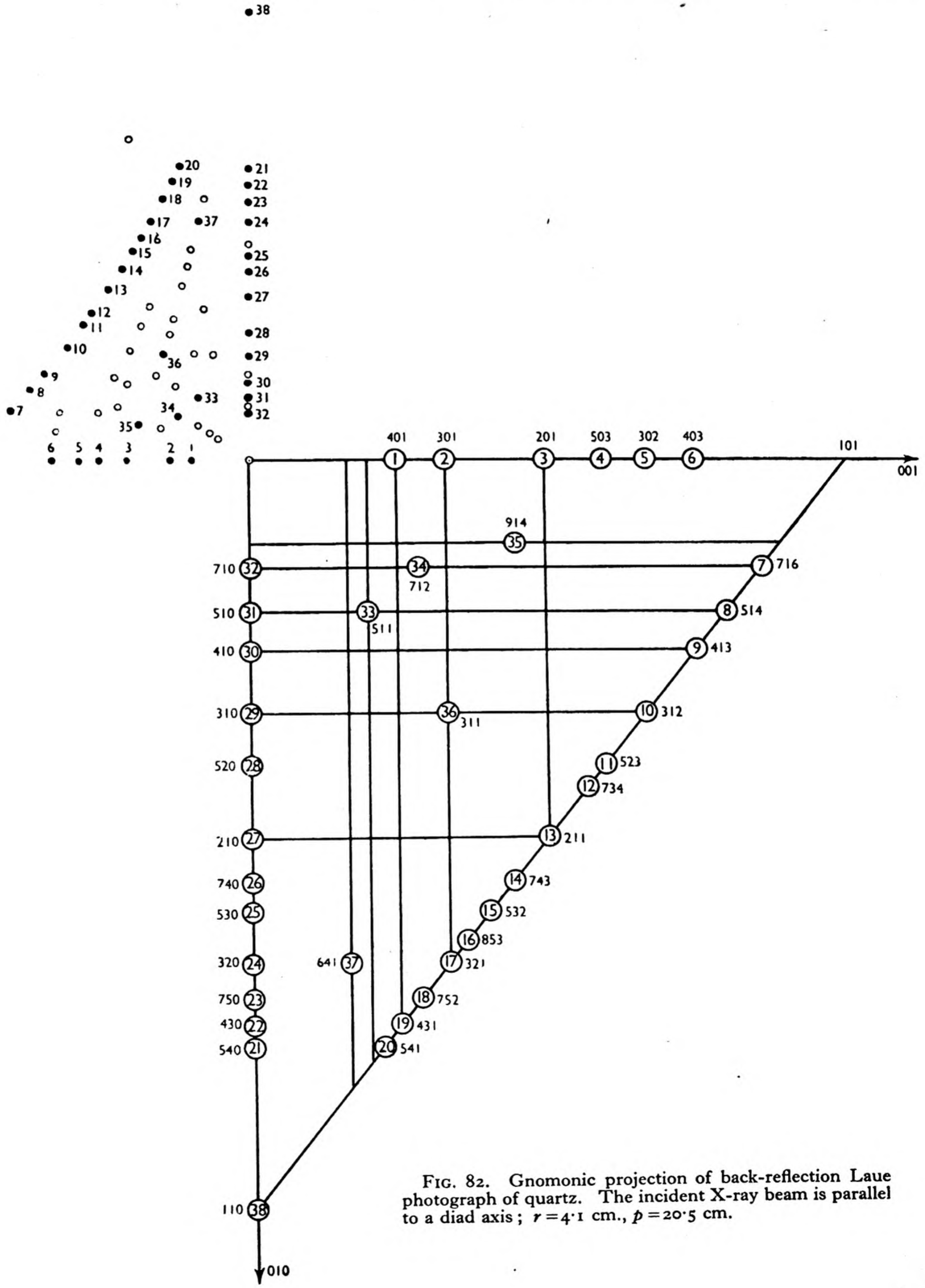

FIG. 82. Gnomonic projection of back-reflection Laue photograph of quartz. The incident X-ray beam is parallel to a diad axis; $r = 4{\cdot}1$ cm., $p = 20{\cdot}5$ cm.

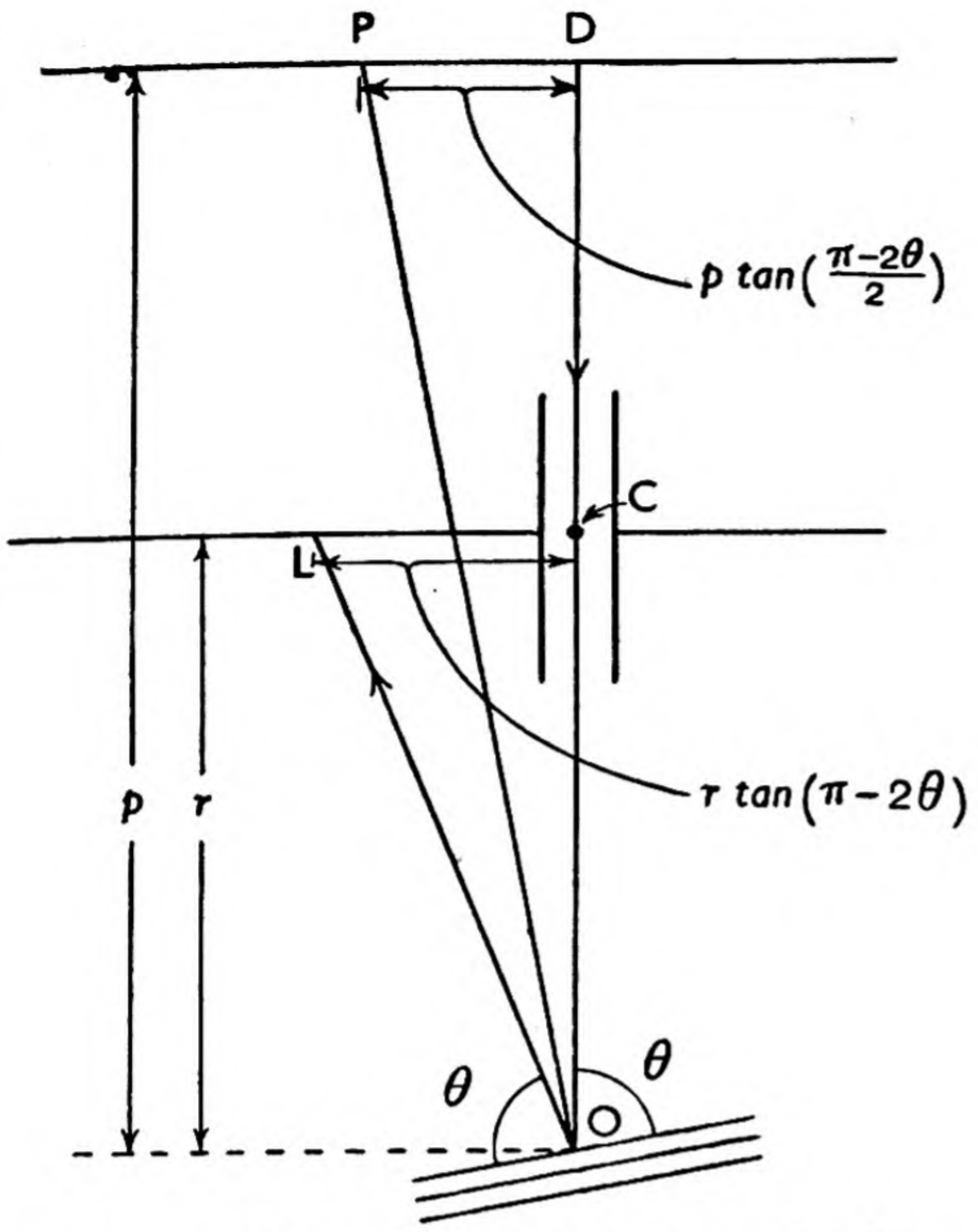

FIG. 83.1. Diagram illustrating back-reflection.
L is Laue spot
P is gnomonic pole
r is crystal-to-film distance
p is radius of sphere of projection

were obtained from an orthorhombic crystal; these indices can then be transferred to the Miller-Bravais hexagonal indices appropriate to quartz.

The directions of the face normals [010] and [001] have been chosen as in Fig. 82, [100] being normal (upwards) to the paper. The procedure for plotting the gnomonic points corresponding to the Laue spots is the same as before, but we must notice that for a back-reflection photograph the distance of the Laue spot from the centre is $r \tan(\pi - 2\theta)$, and that of the corresponding gnomonic point is $p \tan(\pi/2 - \theta)$ (Fig. 83.1). The appropriate table is given below and the graph drawn from it is given in Fig. 83.2.

$r \tan(\pi - 2\theta)$ ($r = 5{\cdot}0$ cm.)	$p \tan(\pi/2 - \theta)$ ($p = 25$ cm.)
0·83	2·07
1·67	4·07
2·50	5·90
3·33	7·57
5·00	10·37
6·67	12·50
8·33	14·15

In Fig. 82 not all the gnomonic points have been plotted but only those corresponding to the three well-marked zones represented by spots 1 – 6, 7 – 20, 21 – 32, and a few strong spots within the region bounded by these conic sections. The corners of the triangle in the gnomonic projection formed by the three plotted zones are assigned the indices 100, 110 and 101. We may denote the distance between the gnomonic points 100 and 110 as f, and that between the gnomonic points 100 and 101 as g. Then, if the co-ordinates of any gnomonic point are y, z, we have seen (**6**, 2.3) that the indices are

$$h = 1,\ k = y/f,\ l = z/g.$$

To obtain integral indices from the fractions y/f and z/g, we multiply all the indices by the same factor. To assist in the indexing it is convenient to draw a series of horizontal and vertical lines at distances $f/2, f/3 \ldots$, and $g/2, g/3 \ldots$ from the horizontal and vertical lines passing through the centre. Thus, the gnomonic point 36 has co-ordinates $f/3$, $g/3$, and its indices are therefore 1, $\frac{1}{3}$, $\frac{1}{3}$, or 311. In this way all the indices can be readily assigned without ambiguity.

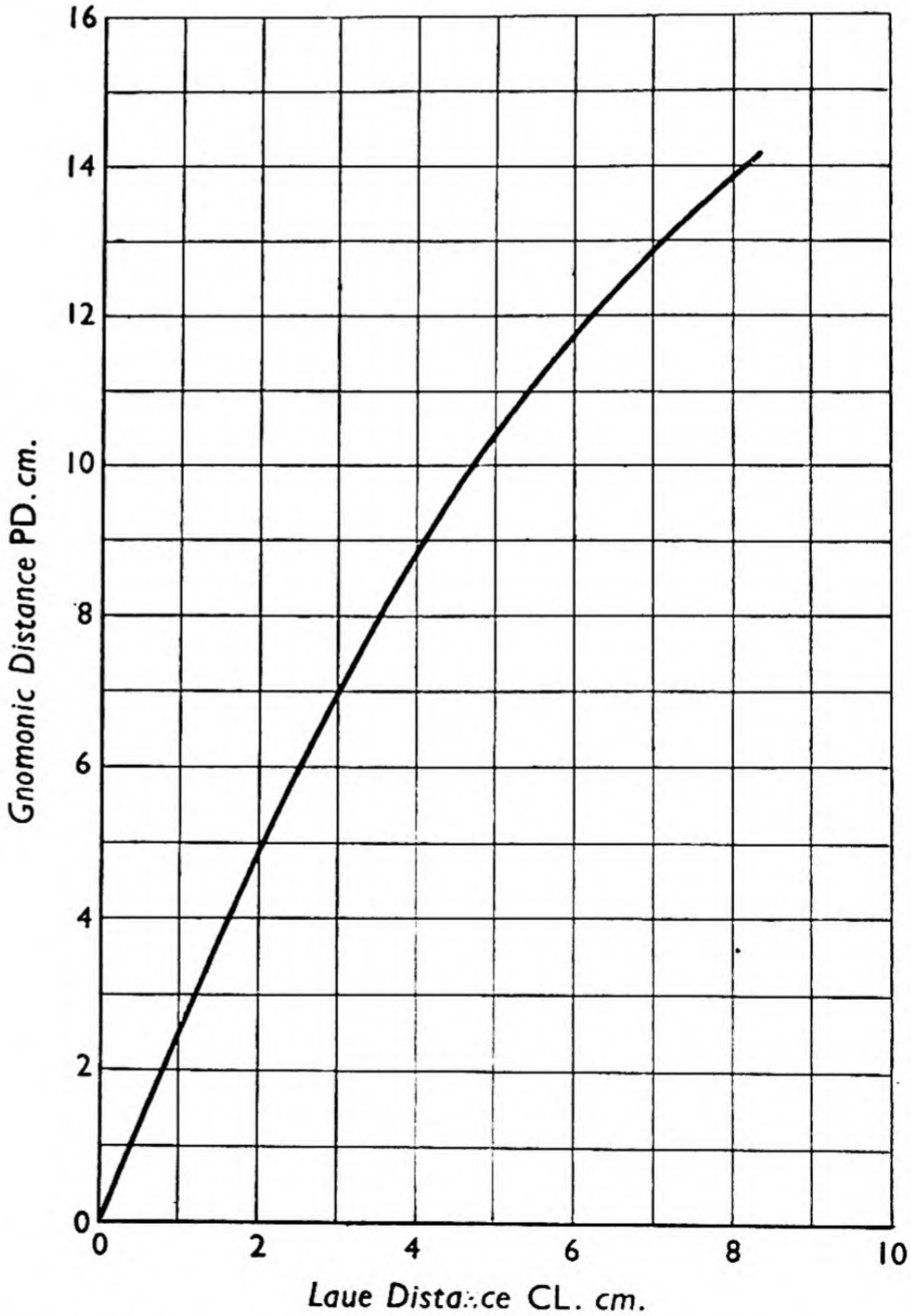

FIG. 83.2. Graph giving relation between distances of Laue spot and corresponding gnomonic point from centre of back-reflection Laue photograph. $CL = r \tan(\pi - 2\theta)$ and $PD = p \tan \cot \theta$. $r = 5{\cdot}0$ cm., $p = 25$ cm.

To convert the orthogonal indices used in Fig. 82 to the usual hexagonal indices of quartz, we notice the following relationships. The x-axis emerges in the centre of the gnomonogram and therefore the orthorhombic pole 100 corresponds to $2\bar{1}^*0$ in hexagonal indexing. Further, the angle 100^110, measured on the gnomonogram, is very close to 30° and we may assume that the plane 110 is 10^*0 in hexagonal indices.

Finally, we have to select a point on the zone containing the optic axis and the point 100 for the point $2\bar{1}^*1$ in hexagonal indexing. The most important point of this type is clearly 101. The distance between the points 100 and 101 on Fig. 82 is 11·5 cm. Therefore the angle

$$2\bar{1}^*0 \wedge 2\bar{1}^*1 = \tan^{-1} 11{\cdot}5/25.$$

Now we have

$$c/a = \cot 2\bar{1}^*0 \wedge 2\bar{1}^*1/2;$$

hence $$c/a = 25/2 \times 11{\cdot}5 = 1{\cdot}09,$$

which is close to the correct value of 1·10 for quartz.

We can now write the corresponding indices.

Orthogonal	*Hexagonal*
100	$2\bar{1}^*0$
110	10^*0
101	$2\bar{1}^*1$

From these indices we can easily derive the transformation matrix as described in **10,** 1.2, which will enable us to transform quickly any of the orthogonal indices to the corresponding hexagonal indices.

2.6 Symmetry of Laue photographs. When a Laue photograph (transmission or back-reflection) is taken on a flat plate with the incident beam parallel to an axis of n-fold symmetry in the crystal, the arrangement of spots shows the nature of the symmetry of the axis. Also, if the incident beam is parallel to a symmetry plane in the Laue group, this plane projects as a line of symmetry on the photograph which can be recognised because the pattern of spots on one side of the line is the mirror image of the pattern on the other side. The following ten types of symmetry therefore, can be observed on Laue photographs, the number of lines of symmetry always being equal to n.

$n=$	Symmetry of axis				
	1	2	3	4	6
Without lines of symmetry	no symmetry	digonal	trigonal	tetragonal	hexagonal
With n lines of symmetry	linear	didigonal	ditrigonal	ditetragonal	dihexagonal

The use of the symmetry observed on Laue photographs in determining the Laue group of the specimen is discussed in **10,** 2.5. If such use is to be made of the photograph, it is essential that the crystal should be very carefully set, and discussion of setting procedures and of the degree of accuracy required will be found in **8,** 2.1 and **8,** 2.3.

The same information concerning the symmetry of the Laue group of the specimen is, of course, also contained in a Laue photograph taken on a cylindrical film with its axis perpendicular to the incident beam; but this information cannot usually be obtained by simple inspection. The shape of the film presents the directly-observable symmetry of the photograph in the following manner:

all axes with n even which are parallel to the incident beam appear as diads;

only those symmetry planes will appear which are either perpendicular to the cylinder axis or which contain both this axis and the incident beam.

If a projection is made of the poles of the reflecting planes, this will show any additional symmetry which may be masked by the cylindrical shape of the film. An example of the construction of a stereographic projection from a cylindrical Laue photograph is given in **8,** 3.2.

3. Non-symmetrical Laue Photographs

3.1 Rotation of the gnomonic projection to a symmetrical position. Unless the setting of a crystal is carried out with great care, it is difficult to obtain a Laue photograph which exhibits the symmetry of the crystal. A slight deviation of an axis of symmetry from parallelism with the incident beam is revealed on the photograph by corresponding spots being at markedly different distances from the centre of the projection. When a gnomonic projection is constructed according to the method described in **6,** 2.1, it will be found that lines which would have been parallel had the specimen been accurately set converge to a point on one side of the photograph.

In Fig. 85 is shown a cubic gnomonogram in which the displacement of the direction corresponding to 001 is 5° to the left of the centre of the projection. The lines of this gnomonogram are drawn heavily whereas the corresponding gnomonogram in which the point 001 coincides with the centre of the projection is shown in lighter lines. To rotate the displaced gnomonogram through the angle, ϕ, required to bring it into the symmetrical position, use is made of the standard gnomonic net (Fig. 21.3). The transparent gnomonic net is placed on the projection so that the vertical lines of the net are parallel to the vertical lines of the gnomonogram. Each gnomonic point is then made to move to the right along the

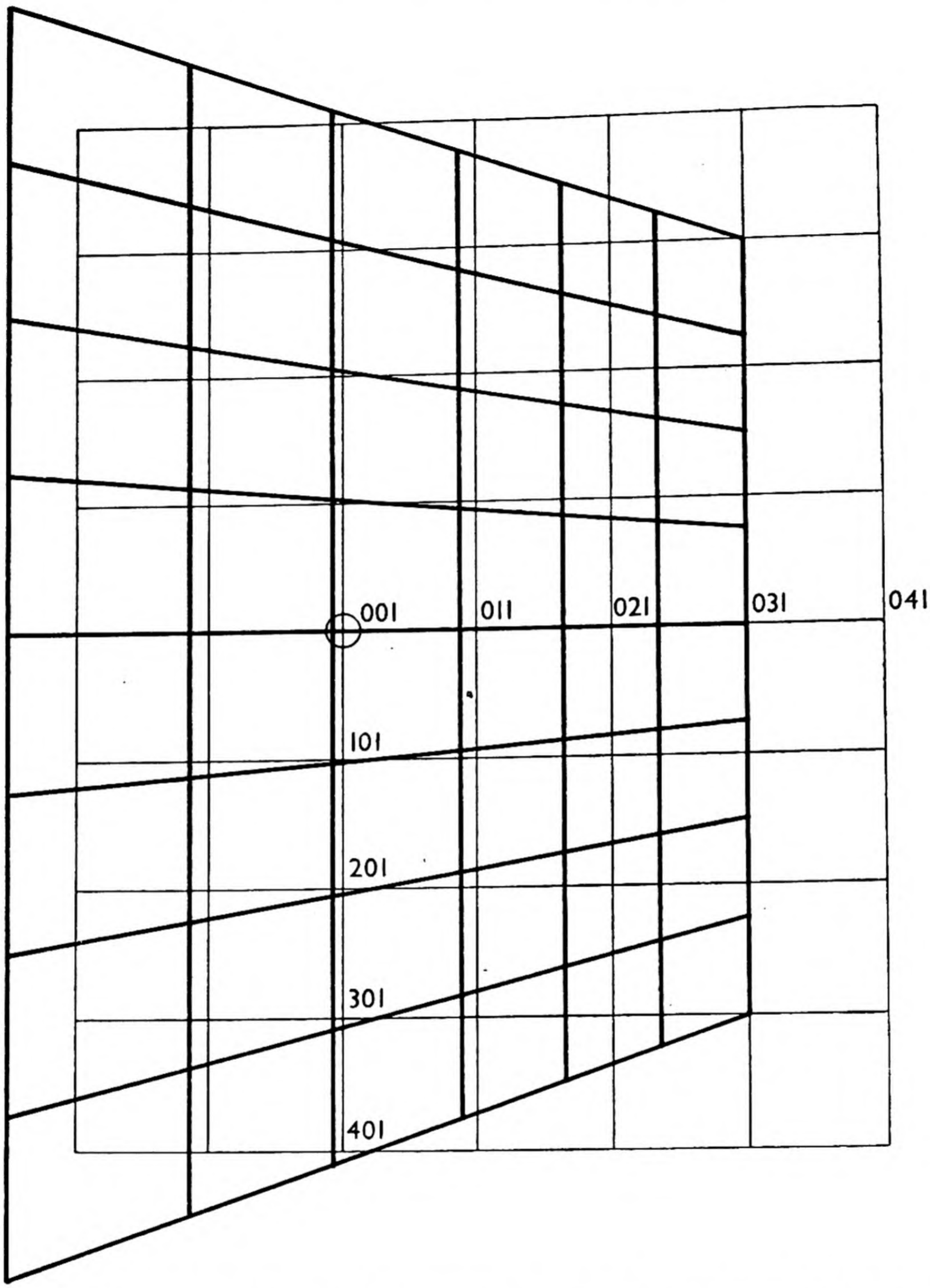

FIG. 85. Gnomonic projection of a cubic crystal. The axis [001] is inclined at an angle of 5° to the normal to plane of the projection

appropriate hyperbola through an angle $\phi = 5°$. After carrying out this process it will be found that the gnomonic points fall on the square-mesh net.

It may happen that the gnomonic net obtained from the Laue photograph has no parallel lines, but instead, the rows of points converge towards two points on the sides of the projection. In such a case the gnomonic net must be placed on the projection with its parallel lines perpendicular to the line joining the point 001 to the centre of the projection. The angle, ϕ, through which each point must be moved along the corresponding hyperbola is equal to the distance of 001 from the centre as read off from the net. This procedure is known as a rotation of the projection, and is required to bring the axis of symmetry into coincidence with the direction of the incident beam.

The axis of rotation lies in the plane of projection and is chosen so that it is normal to the axis of symmetry. Each point on the projection sphere is moved along the corresponding small circle about the pole of the axis of rotation through the angle ϕ. Such small circles project as hyperbolae on the gnomonic projection, and each is divided into a constant angular interval by the straight lines corresponding to the great circles (**1**, 5.4).

3.2 Use of standard sets of photographs. It may be desired to assign indices to the spots on a Laue photograph which is taken with the direction of the incident beam not parallel to a symmetry axis of the Laue group of the specimen. Although a gnomonic net can be drawn no matter how the crystal is orientated during the taking of the photograph, it is very difficult to assign the correct indices to the gnomonic points unless the orientation is approximately known. One method of overcoming this difficulty is to take a standard set of Laue photographs of the same crystalline substance. The angular interval between consecutive settings of the crystal is made small enough, usually 5° or less, to allow any photograph taken with the crystal set in an arbitrary orientation to be identified by simple inspection. With the corresponding standard photograph as a guide, indices may be directly assigned to the spots in the non-standard photograph, and hence the orientation of the crystal can be determined. This method is usually applied only to cubic crystals, but it can be applied to non-cubic crystals if the orientation of one zone axis is known.

Such sets of standard photographs have been made for iron and aluminium (Majima and Togino, 1927). The angle between consecutive settings is 5°, and 55 photographs were required to cover the necessary range of orientations, even though the symmetry of the crystals was the highest possible.

Sometimes a particular physical character of the crystal makes it unnecessary to include all possible orientations in the standard set of photographs. This is true for quartz, for example, since the direction of the optic axis can be found by optical methods. A plate of quartz can therefore be set up on an X-ray goniometer so that the plane containing the optic axis and the direction of the incident X-rays is horizontal. The standard set of photographs is prepared with the optic axis lying in a horizontal plane, so that the likelihood of confusion arising in comparing the Laue photograph of the plate of arbitrary orientation with those of the standard set is much reduced.

The same procedure could be adopted for any transparent uniaxial crystal. The successful use of such methods requires knowledge of the movement of Laue spots corresponding to alterations in the orientation of the specimen; this is discussed in **8**, 2.3.

CHAPTER 7

INTERPRETATION OF WEISSENBERG PHOTOGRAPHS

1. Introduction

THE oscillation and Laue methods described in previous chapters have certain special advantages; the oscillation method is particularly suitable for preliminary determination of cell size, and the Laue method is convenient for the study of the orientation and symmetry of crystals. Both methods suffer from the fundamental limitation that reflections corresponding to reciprocal points distributed in three dimensions of space are recorded on the two dimensions of the photographic film. In a moving-film method only a particular set of reflections, such as *hk*o, or *hk*1, is allowed to fall on the film, and these are spread out over the film in such a way that to each point on the photograph there corresponds a single value of h and a single value of k. In the following sections only the Weissenberg method is described, as this is by far the most commonly employed moving-film method.

The most usual arrangement of the Weissenberg goniometer is that in which the X-ray beam is perpendicular to the axis of rotation and in which only the equatorial reflections are allowed to reach the film. Other arrangements of the goniometer permit the recording of any one layer line, either with the incident beam normal to the axis of oscillation of the crystal (normal-beam arrangement) or with the incident beam inclined to that axis. When it is necessary to incline the incident beam to the axis of oscillation at an angle less than 90°, the following arrangement is usually made. The collimator is mounted on the fixed base of the instrument and the crystal and camera are mounted on an arm which may be turned through an angle usually not greater than 30°. The axis about which this arm turns forms, with the direction of the incident X-rays and the axis of oscillation of the crystal, three intersecting lines similar to monoclinic crystallographic axes. The incident X-ray beam may be called x, the axis of oscillation of the crystal z, and the axis about which the arm turns y. This arrangement ensures that the crystal remains in the X-ray beam when the axis of its rotation is inclined at an angle less than 90° to the beam.

2. Geometry of X-ray Reflection

2.1 The Weissenberg Goniometer. The Weissenberg goniometer consists essentially of a goniometer head mounted on a spindle which is coaxial with a cylindrical camera (Fig. 87*a*). The camera can travel parallel to its axis during the rotation of the crystal, the rotation of the crystal and the translation

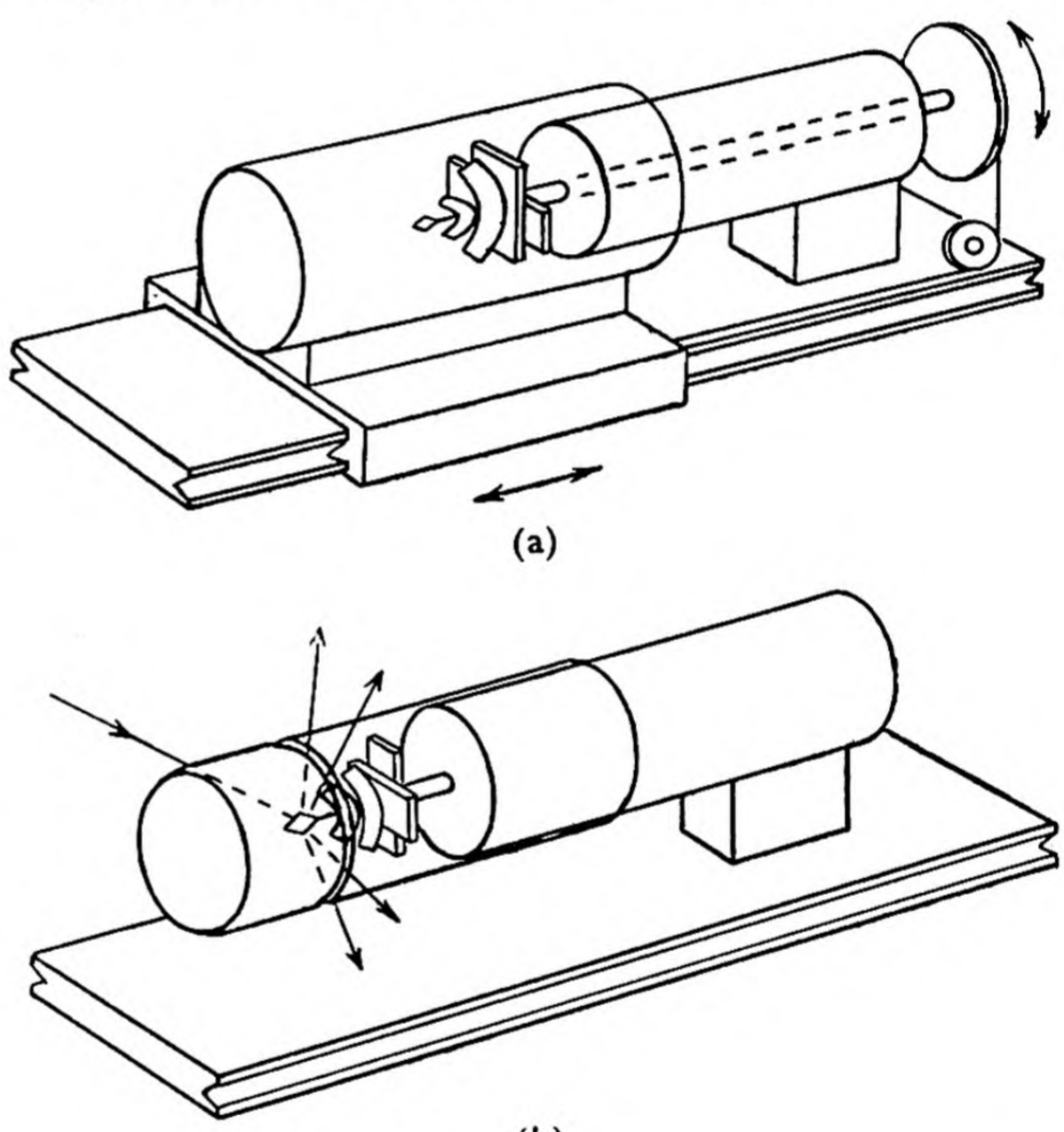

(a)

(b)

FIG. 87. Component parts of Weissenberg goniometer.
(*a*) the coupling between the goniometer head and the camera; (*b*) the mounting of the circumferential slot on the stationary base

of the camera being synchronised. The link is provided either by gears or by a steel tape which passes over a drum on the crystal spindle as shown in the diagram. The drum which winds up the tape (Fig. 87*a*) is spring-loaded so that there is no backlash in the system. The X-ray beam is limited by a narrow cylindrical aperture, usually of a special construction to minimize fogging due to scattering from the slit (**4**, 3.2). The angle at which the

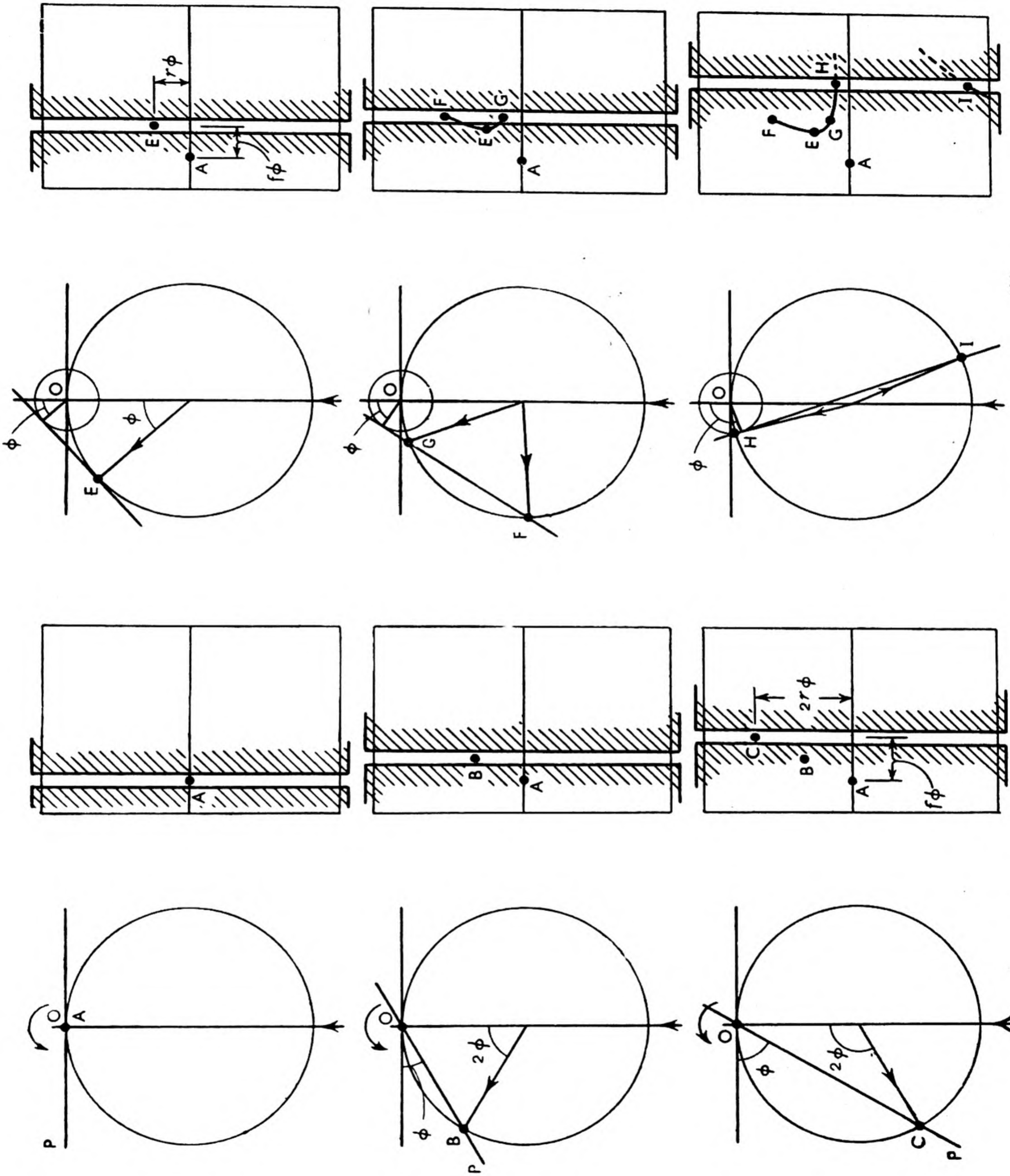

(a)

(b)

FIG. 88. Diagrams showing relation between reciprocal point rows and corresponding lines of spots on Weissenberg photographs

collimator is set, relative to the spindle axis, may sometimes be varied as explained below, or it may be permanently fixed perpendicular to the axis. The X-ray beam falls upon the crystal which has been set on the axis of the spindle by means of the usual adjusting arcs and slides.

When the crystal is oscillated about a zone axis, cones of diffracted rays are produced (**5**, 1.4). In the Weissenberg method a single cone is selected and allowed to fall on the film, while the others are absorbed. This is achieved by making use of a cylindrical screen in the circumference of which is cut a narrow aperture (Fig. 87*b*). The screen is fixed during any one exposure so that all the reflected beams except those giving rise to the selected layer line are prevented from reaching the film.

2.2 Characteristic features of the photograph There are certain striking features of Weissenberg photographs of which use is made in the interpretation. In Fig. 90 is shown a Weissenberg photograph in which some of the spots appear on two straight lines running diagonally across the photograph and others are on a family of curves. The reason for these diagonal lines of spots may be understood from Fig. 88*a*. The row of reciprocal points such as *OP* is called a *central point row* because it passes through the origin of the lattice. We can suppose that *OP* is rotated about the vertical axis through the origin. Now for each position of the point row *OP*, relative to the incident beam of X-rays, there is a corresponding position of the film relative to the screen. In the rectangular diagrams of Fig. 88 the film is supposed to be laid flat and the screen unrolled and laid in its appropriate position on top of the film. In the succeeding diagrams the point row *OP* is rotated and the screen is moved to the right by a distance proportional to the angle of rotation. The coefficient of proportionality is determined by the radius of the drum on which is wound the steel tape which connects the camera to the goniometer spindle ; in modern instruments this is commonly 1 mm. to 2°.

From the geometry of the diagrams in Fig. 88*a* it is clear that if the point row rotates from the initial position through an angle ϕ, the reflected beam is deviated with respect to the incident beam by an angle 2ϕ. The central horizontal band of the film when laid flat corresponds to the trace of the direct beam, and hence the distance of the spot produced by the reflected X-rays from this line is $2r\phi$, where r is the radius of the camera. The translation of the camera during a rotation of the crystal through an angle ϕ is $f\phi$, where f is the appropriate coefficient mentioned above. Since $2r\phi$ is proportional to $f\phi$, the reflected spots must lie on a diagonal straight line sloping at an angle of $\tan^{-1}2r/f$. As the crystal rotates through 180° the points along *OP* will produce two collinear lines of spots, one above the central band on the film and the other below this band. It should be noted that all beams represented by arrows directed to the *left* in the reflecting sphere diagrams (Fig. 88) correspond to spots *above* the central band on the diagrams of the film, and those represented by arrows directed to the *right* correspond to spots *below* the central band. In Fig. 90 there appear to be only two obvious straight lines of spots. This is, however, only apparent, for parallel to these prominent point rows through the origin there are a great number passing through two, three or four spots only. The prominence of the two lines mentioned is due to the closeness of the reciprocal points to one another along these particular central point rows, which are perpendicular to the planes of largest spacing in the Bravais lattice.

The prominent curved lines in Fig. 90 are due to point rows which are parallel to those we have just discussed, but which do not pass through the origin. In Fig. 88*b* three significant instants during the rotation of the crystal are illustrated. In the uppermost diagram the point row is tangent to the reflecting circle. The angle through which the crystal has been rotated is ϕ, and the reflected beam has been deviated through the same angle. The slope of the line joining *E*, the corresponding X-ray spot, to *A*, the point where the aperture in the screen crosses the central line of the film when $\phi=0$, is therefore $\tan^{-1}r/f$, which is half the slope of the straight line through *A* discussed above. The second diagram shows the row of points cutting the reflecting circle in two points and in the right-hand diagram the portion of the curve traced up to this juncture can be seen. It consists of an ascending and a descending portion. In the third diagram the point row has rotated so that one reflecting point lies on the right-hand half of the reflecting circle and the corresponding spot lies in the lower half of the film. The dotted lines on the third right-hand diagram show the rest of the curve on which the spots corresponding to this point row lie.

2.3 The Weissenberg Chart. A set of parallel point rows gives rise to a family of curves on the photographic film, as has been seen in the previous paragraph. A standard family of such curves corresponds to point rows at a distance of 0·1 or 0·05 reciprocal units apart. If such a set is superimposed on the photograph of Fig. 90, it is easy to read off directly the distance apart of the point rows which give the prominent family of curves on that photograph. If we superimpose on the first standard set of reciprocal point rows another set rotated through 90° about the axis, we obtain the curves of Fig. 91. The second set of curves is displaced relative to the first set so that its straight diagonal lines are midway

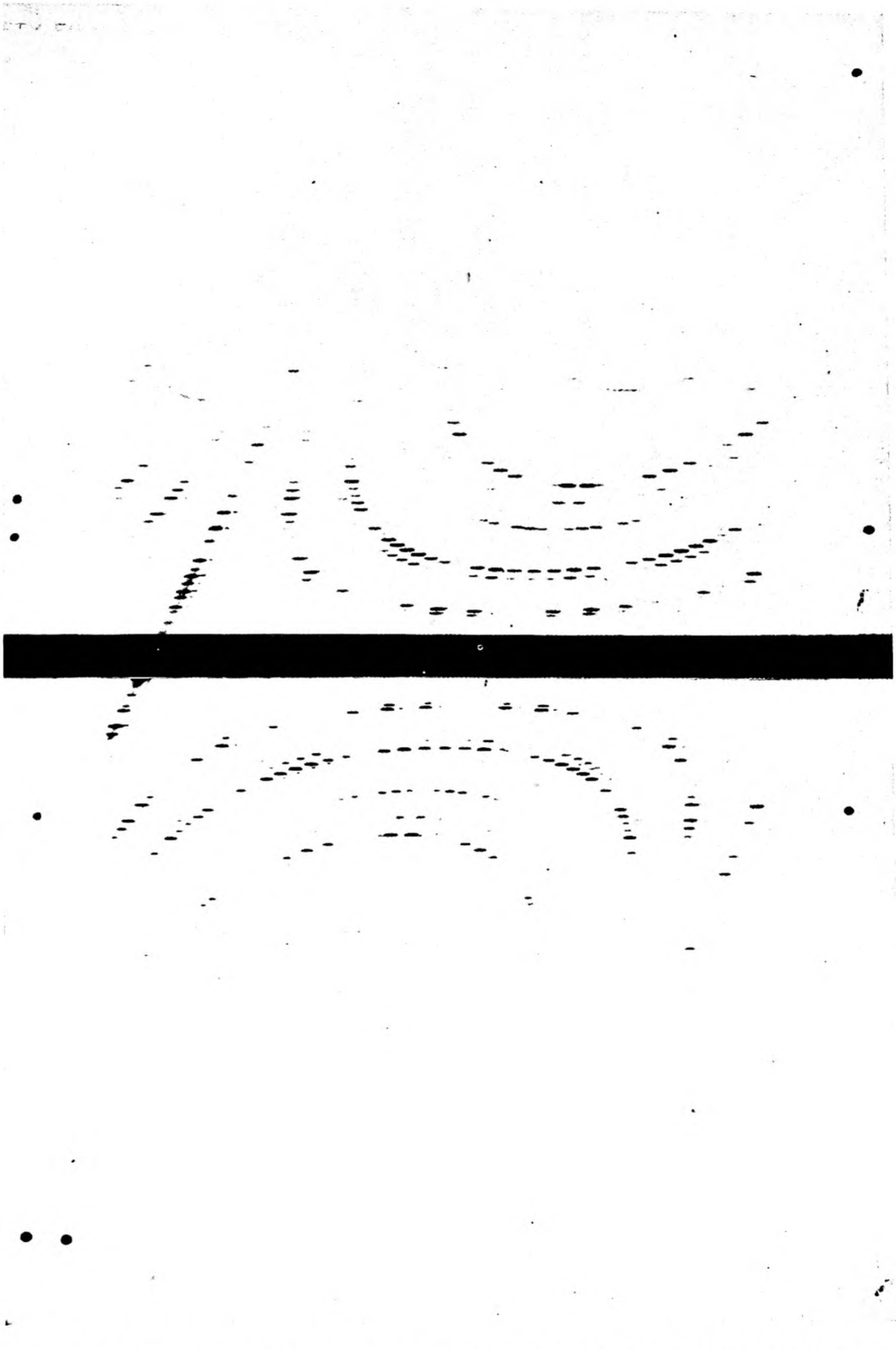

FIG. 90. Weissenberg photograph of di-bromo-cholesteryl chloride. Unfiltered radiation from a copper target was used and the crystal was oscillated about the [001] axis, only spots of indices *hk*o being recorded

between those of the first set. The combination of two sets of standard curves is known as an *equatorial Weissenberg chart* (Fig. 91).

By placing the base line of such a chart on the line of the photograph for which $\theta = 0°$, the rectangular co-ordinates of the reciprocal point corresponding to any spot on the film can be read. This is true whatever the system of symmetry to which the crystal belongs. In general, it does not matter where along

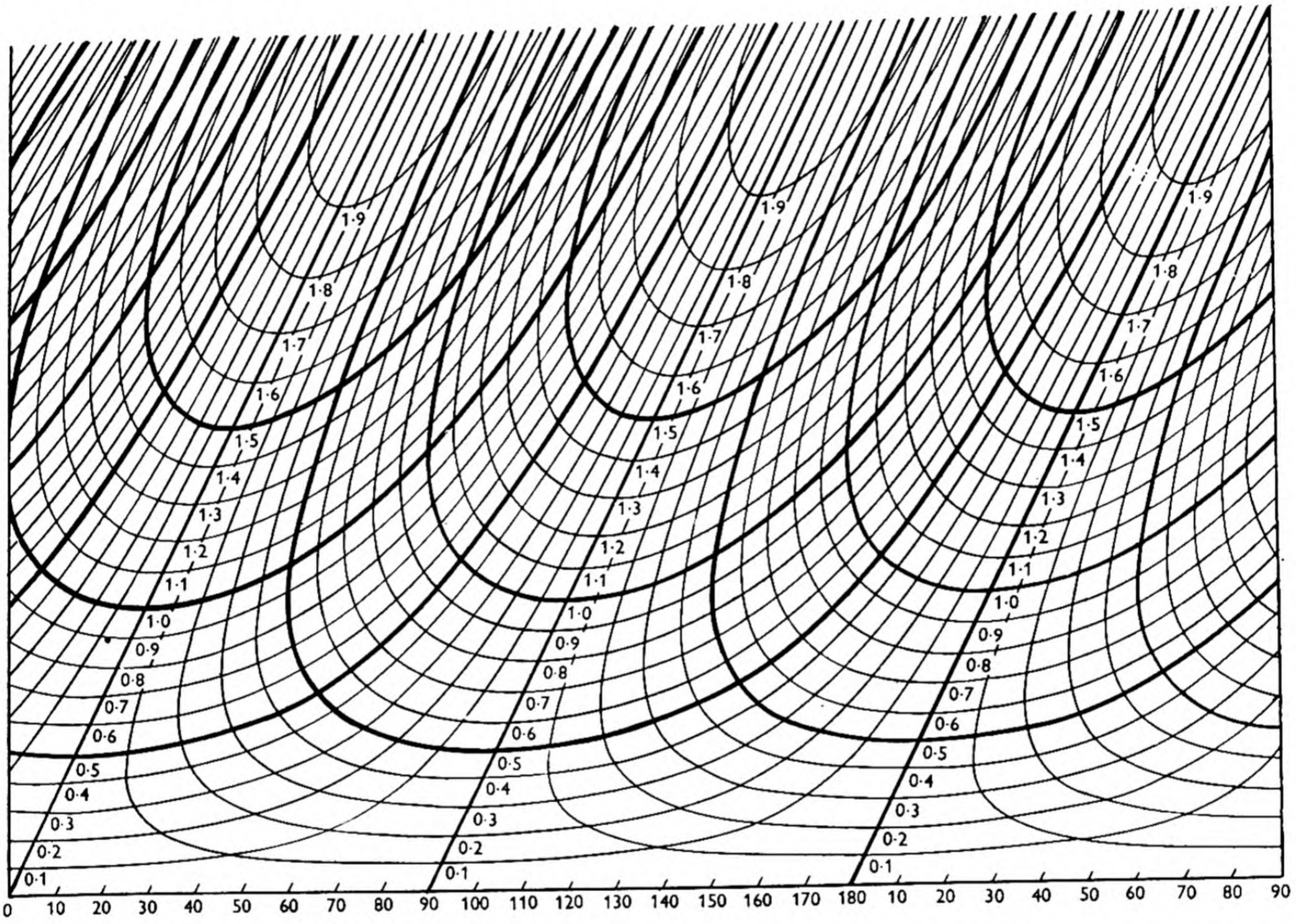

FIG. 91. Equatorial Weissenberg chart for a camera radius of 3 cm. and a camera translation of 1 mm. per 2° rotation of the crystal

the central line of the film the central line of the chart is placed. The co-ordinates read will, of course, depend on the position of one relative to the other; but when the reciprocal points are plotted on squared paper the result will always be essentially the same. The only effect of moving the chart relative to the film is to rotate the reciprocal lattice of the crystal relative to the axes of the graph paper on which the plot of reciprocal points is made. In practice, however, one diagonal line of the chart is made to coincide with a prominent diagonal line on the photograph, for convenience in reading the co-ordinates. With this setting, spots will in general fall consecutively on only one set of curves of the chart.

It may be unnecessary to expose more than one half-cylinder of the camera, in which case use must be made of the fiducial spots shown in Figs. 90, 93. These spots have been produced by allowing X-rays to fall on the back of the camera and so to cast a shadow of the small holes drilled in the camera. A new Weissenberg chart must have ink-spots put on it so that it can be superposed on the film in the correct position. There are two ways of putting these ink-spots on to the chart. The correct positions may be found by measurement of the position of the fiducial holes in the camera. Alternatively, a Weissenberg photograph showing a number of orders of reflection of the same plane lying on a straight diagonal line may be used. When the chart has been placed over the film so that (*a*) these successive orders have ξ-values which are whole multiples of the smallest value and (*b*) the edge of the film is parallel to the base line of the chart, then the chart is correctly placed and the fiducial ink dots can be marked on to the chart.

Whenever the reciprocal net is orthogonal, spots will fall simultaneously on both sets of curves of the chart. In the interpretation of the spots corresponding to an oblique reciprocal net, the co-ordinates are

read and plotted on squared paper as before; in addition, the choice of the unit mesh of the reciprocal net has to be made.

3. The Indexing of Equatorial Photographs

3.1 Normal beam photographs: monoclinic crystal oscillated about the z-axis. In Fig. 90 is shown an equatorial Weissenberg photograph of an organic crystal which was oscillated about the direction of elongation, this being taken as the z-axis. To interpret this photograph, the Weissenberg chart is superimposed on the photograph so that the base line of the chart lies on the middle of the black band running the length of the photograph. This is equivalent to making the base of the chart coincide with the line which would be traced on the film by the undeviated X-ray beam. This relation between the chart and the photograph is preserved and the chart is moved along until its left-hand sloping line lies on the straight row of spots on the left-hand side of the photograph. The co-ordinates of each spot are now read by tracing back to the sloping straight lines (through 0° and 90° on the base line) the curves which go through the spot. These co-ordinates are tabulated and plotted as in Fig. 92.

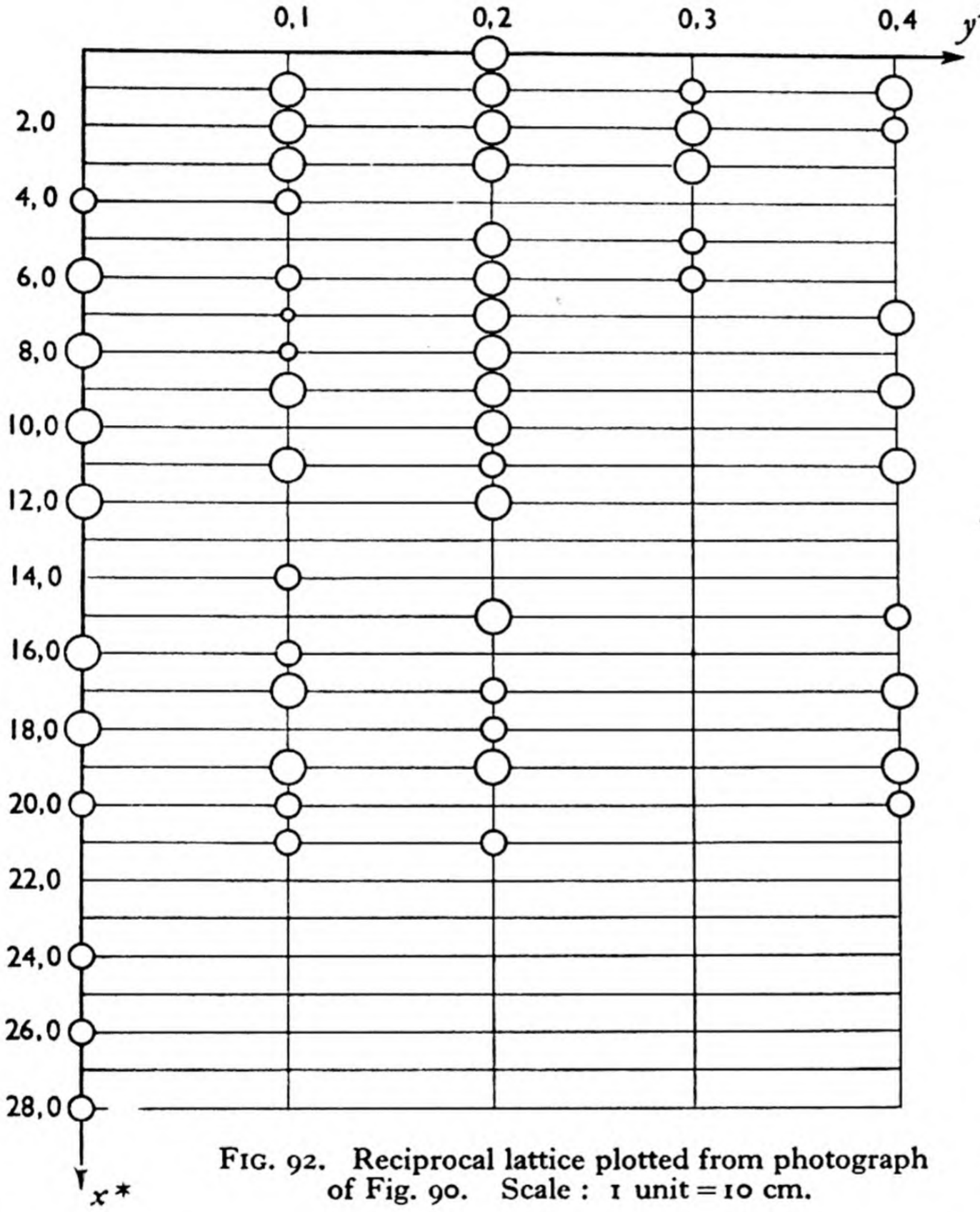

FIG. 92. Reciprocal lattice plotted from photograph of Fig. 90. Scale: 1 unit = 10 cm.

It will be seen that the points lie on a net, the unit mesh of which is a rectangle. If unit length in reciprocal space is represented by 10 cm. in the drawing, then the sides of this mesh will be found to be 0·36 cm. and 1·93 cm. respectively. A more exact value of the side of the unit mesh is obtained by reading the value on the chart for points as far removed from the base line as possible and dividing this by the appropriate factor. Thus in the photograph of Fig. 90 there is a spot on the left-hand sloping straight line of spots with co-ordinates 0·72 and 0·00. This point is found on referring to the plot of the reciprocal lattice (Fig. 92) to be the 20th point along the vertical side. Thus the corresponding side of the unit mesh is 0·036. Similarly, although there is no actual point with co-ordinates 0·00 and 0·77 on the sloping line of spots passing through the middle of the base line of the chart, these are the co-ordinates of the point where the fourth curved row of spots crosses this sloping line. Hence the value of the corresponding side of the unit mesh can be taken as $0{\cdot}77/4 = 0{\cdot}193$.

The indexing of the spots can now be done when it is decided which is the x^* axis and which is the y^* axis. Other data are used to decide the diad (y) direction. The spots on the right-hand side of the diagonal line passing through the point (0, 2) have not been indexed. It will be seen that these spots are of the same intensity and have the same numerical values of co-ordinates on the chart as the corresponding spots on the left-hand side of this diagonal line. The indices of corresponding spots are, therefore, numerically the same, but one of them is negative in sign. Thus, on the first curved row of spots the sequence of indices near the central diagonal line is 2,1; 1,1; $\bar{1}$,1; $\bar{2}$,1; etc. Each spot on the lower half of the photograph corresponds to one on the upper half, and both lie on a diagonal line parallel to those of the chart. Moreover, these corresponding spots are at equal distances from the centre line of the photograph. They arise from the intersection with the reflecting sphere of reciprocal points which are at equal distances from, but on opposite sides of, the origin. The indices of the spots are therefore numerically the same but of opposite sign throughout. For

FIG. 93.1. Inclination Weissenberg photograph of an (010) cleavage flake of gypsum. The axis of oscillation was [010] : the X-rays were incident at an angle of 75° to the axis of oscillation ($\mu = 15°$) and the reflected rays were limited so that only reflections of the type *hol* were recorded. The fibre used to support the crystal intercepted the reflected beams in certain directions and produced gaps in some spots

example, on the diagonal line running down through the spots $3,\bar{3}$; $2,\bar{2}$; $1,\bar{1}$, successive spots have indices $\bar{1},1$; $\bar{2},2$; $\bar{3},3$.

3.2. Inclination photograph: monoclinic crystal oscillated about the y-axis. In Fig. 93.1 is reproduced the Weissenberg photograph of a thin (010) cleavage flake of gypsum, which was oscillated about the *y*-axis (normal to the flake) during the exposure. When a crystal occurs in the form of such a flake, it is better to use an inclination photograph rather than a normal-beam photograph. In taking an inclination equatorial photograph, the X-rays are inclined to the axis of oscillation (Fig. 93.2) at an angle $\pi/2 - \mu$ (here $\mu = 15°$), while the reflected rays leave the specimen inclined at the same angle to the axis, but on the opposite side of the specimen to that on which they entered. The reflected X-rays thus lie on a cone of semi-angle $(\pi/2 - \mu)$ and the thickness of crystal through which the reflected rays have passed is the same whatever their direction of reflection. This can be seen from Fig. 93.2, in which the reflecting circle, of radius unity, has OX as diameter. XO represents the direction of the incident X-rays and is inclined to the axis of oscillation, OV, at an angle of $(\pi/2 - \mu)$. The reflected cone of rays corresponding to the equatorial-layer of reciprocal points is represented by IO and IP. The circle in which the equatorial reciprocal plane cuts the reflecting sphere is represented by OP and is of radius cos μ. When the usual Weissenberg

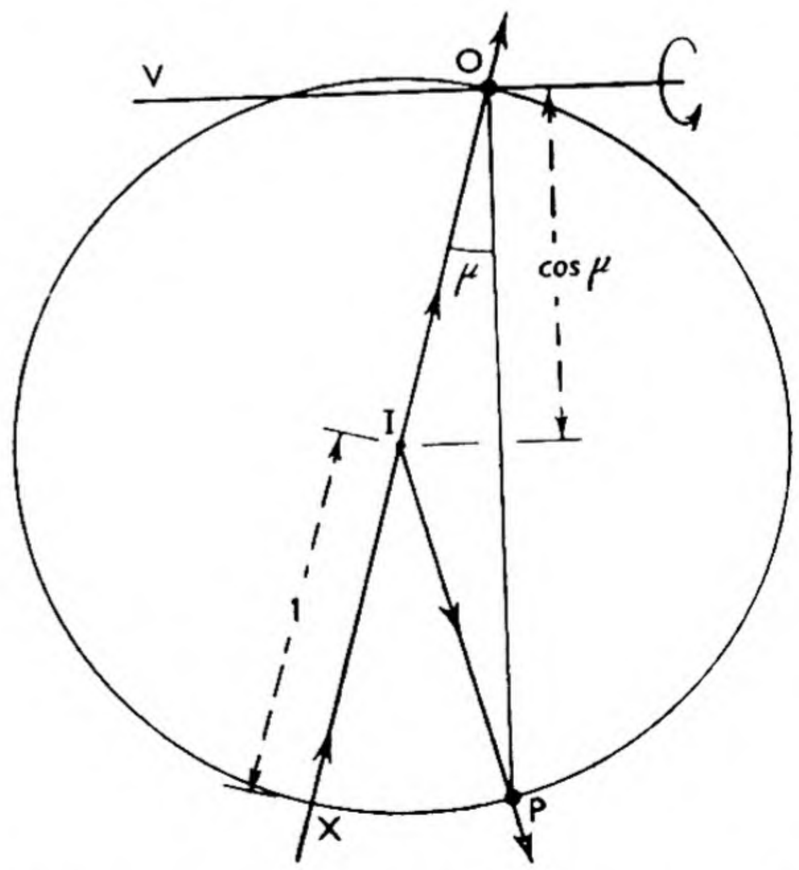

FIG. 93.2. Geometry of a type of inclination Weissenberg photograph. A cone of reflected rays OIP of semi-angle $(\pi/2 - \mu)$ is generated by the reflection of X-rays, incident at the same angle to the axis of oscillation OV, from planes parallel to OV

chart (7, 2.3) is used for the interpretation of a photograph of which the radius of the reflecting circle is cos μ instead of unity, all dimensions of the reciprocal lattice appear larger by a factor sec μ than they really are, since it is assumed in constructing the chart that the radius of the reflecting circle is unity. When a Weissenberg chart is laid on the photograph and the co-ordinates of the spots are read off, a reciprocal net can be plotted. The interpretation of the gypsum Weissenberg photograph is left as an exercise for the reader and the answer is given in Appendix 4.

It is often useful in interpreting normal-beam and inclination photographs of the type discussed above to sketch on the photograph, or a print of it, the curves of the Weissenberg chart which pass through the spots. If one of the straight diagonal lines of the chart be placed so as to pass through several spots, then it will be found that all the other spots lie on equally-spaced curves on either side of the diagonal line. If the indices of the spots on the straight diagonal line are *h*oo, then those on any one of these Weissenberg curves will be *h*o*l*, if the axis of oscillation is *y*, where *l* is fixed. Thus, in the gypsum Weissenberg photograph, Fig. 93.1, the indices *h*o*l* are all even because of symmetry conditions, and hence the first set of spots lying on a Weissenberg curve next to the straight diagonal set is *h*o2. Similarly, if the straight diagonal line be placed on the spots chosen as the oo*l* series, the other spots again lie on the equally-spaced Weissenberg curves, the first of which has spots of indices 2o*l*, the second 4o*l*, etc. Thus, by sketching the Weissenberg curves joining the spots, we trace out the equivalent of the reciprocal net from which the spots may be indexed.

4. Other Types of Weissenberg Photograph

4.1 Normal-beam photographs of non-zero layers. The Weissenberg method of taking photographs always records only the reflections corresponding to a selected plane of reciprocal points normal to the oscillation axis. When the oscillation axis is *z*, *x* or *y*, the indices of the equatorial reflections are therefore of the types *hk*o, o*kl*, or *h*o*l* respectively. Useful as these groups of reflections are, they cannot give all the information which may be required. Some general reflections of the type *hkl* must also be obtained. It would be possible to get such reflections on an equatorial photograph by rotating the crystal about some axis other than *x*, *y* or *z*, but this is seldom done because of the greater complexity of the indexing process. If, however, we oscillate the crystal about the *x*-axis and shift the position of the screen so that reflections of the type 1*kl* are recorded instead of o*kl*, we have obtained some general reflections. Such non-zero-layer Weissenberg photographs are almost as simple to take as the equatorial photographs, and from them we can obtain information essential to the determination of crystal structures.

Before any non-zero layer photographs are taken, the value of ζ should be obtained from the layer lines of an oscillation photograph. To achieve the desired selection of the reflections corresponding to the non-zero layer line, the screen carrying the annular aperture is moved parallel to its axis until the aperture allows the appropriate cone of reflected X-rays to pass through it (Fig. 87*b*). If the semi-angle of the cone of diffraction for the *n*th layer is $(90-\nu_n)$ then the following relation exists (5, 1.4),

$$\zeta_n = \sin \nu_n.$$

Further, if *s* is the radius of the screen, the required lateral displacement from the equatorial position is given by $s \tan \nu$. The Weissenberg goniometer is usually graduated so that the displacement of the screen may be read on a graduated scale.

4.2 The Wooster chart. To interpret normal-beam, non-zero layer photographs a chart, known as the *Wooster chart* (1933), is used. To each value of ζ there corresponds a separate chart and for any arbitrary value of ζ the chart consists (Fig. 95.1) of two sets of lines, one set parallel to the $\theta = 0°$ line of the equatorial photograph, which gives the loci of spots having values of ξ corresponding to 0·05, 0·10, 0·15 etc., and a second set which replaces the straight diagonal line of the Weissenberg chart. Lines of the second set are all similar curves displaced by a fixed distance, for example, 5 mm., relative to one another along the length of the chart. All spots lying on a given line of the second set correspond to reciprocal points which lie on a point row passing through the oscillation axis. The co-ordinates given by the Wooster chart are therefore polar co-ordinates in reciprocal space as compared with the Cartesian co-ordinates of the Weissenberg chart (7, 2.3). In Fig. 95.1 two examples of Wooster charts for $\zeta = 0.0$ and 0.5 respectively are given. The chart for $\zeta = 0$ can be used instead of the Weissenberg chart, though the rectangular co-ordinates corresponding to the latter are usually more convenient than the polar co-ordinates corresponding to the former. However, for normal-beam, non-zero layer-line photographs the standard Weissenberg chart cannot be used.

The theory by which the Wooster chart is constructed is illustrated in Figs. 95 and 96. Fig. 95.2*a* shows a view of the reflecting sphere with the axis of oscillation lying in the plane of the paper. The layer line which is recorded on the film corresponds to a reciprocal plane normal to the oscillation axis

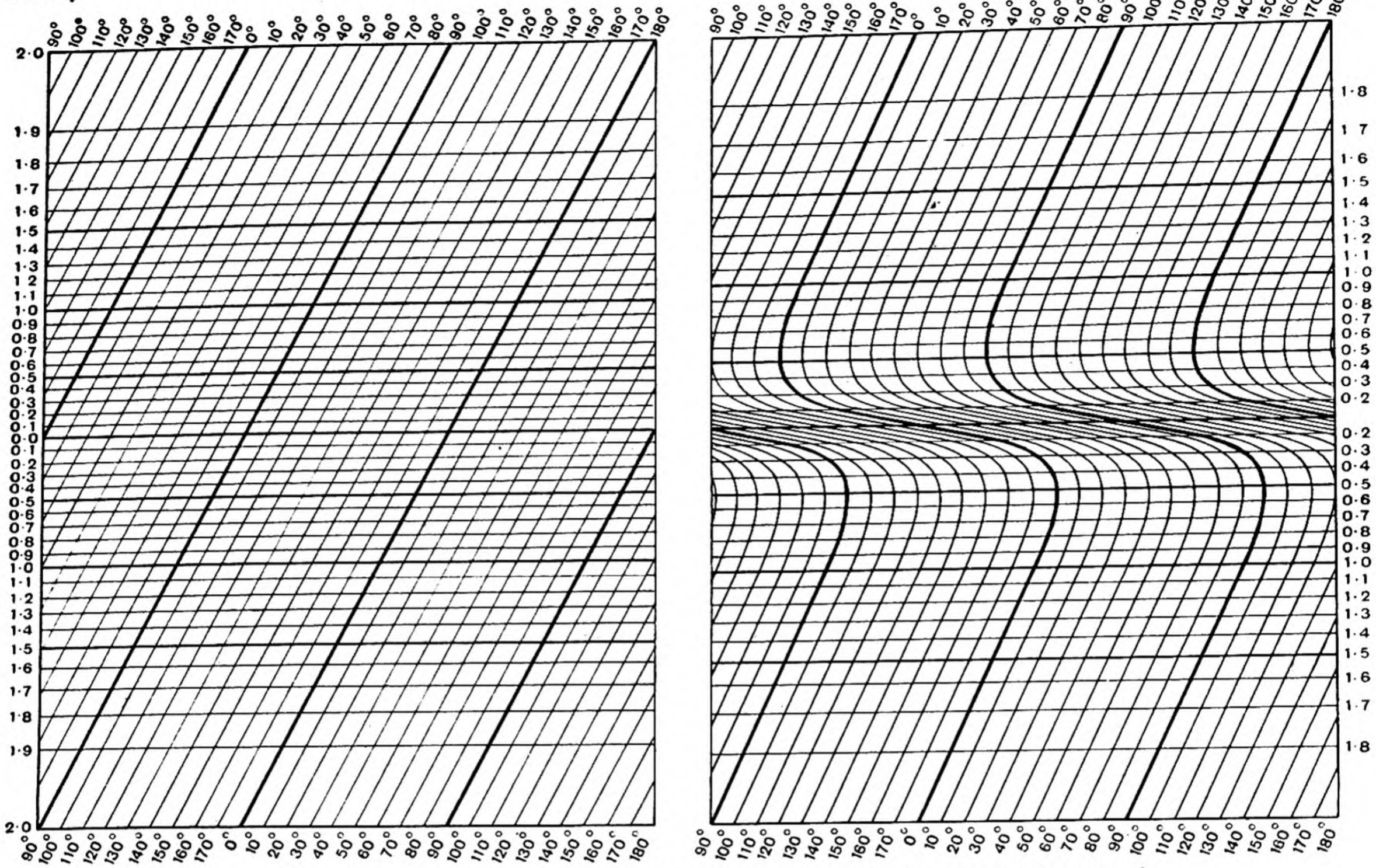

FIG. 95.1. Wooster charts for interpreting normal-beam Weissenberg photographs:
(*a*) for equatorial reflections; (*b*) for a photograph having a ζ value of 0.5.
The charts are drawn for a camera radius of 1·5 cm. and a camera translation of 1 mm. per 4° rotation of the crystal

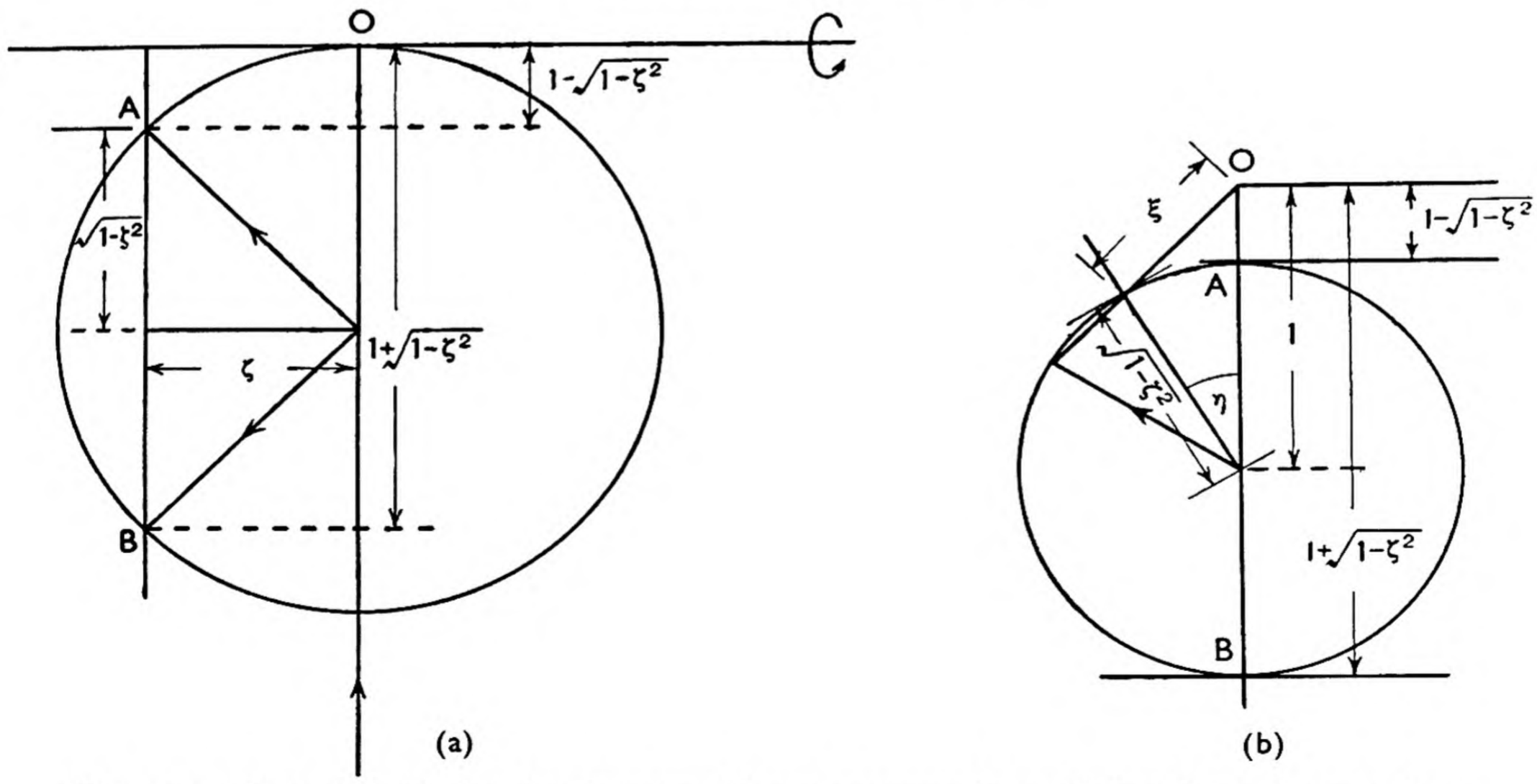

FIG. 95.2. Geometry of reflection for normal beam, non-zero layer Weissenberg photographs:
(*a*) projection of reflecting sphere on to a plane containing the axis of oscillation,
(*b*) projection on to a plane perpendicular to the axis of oscillation.

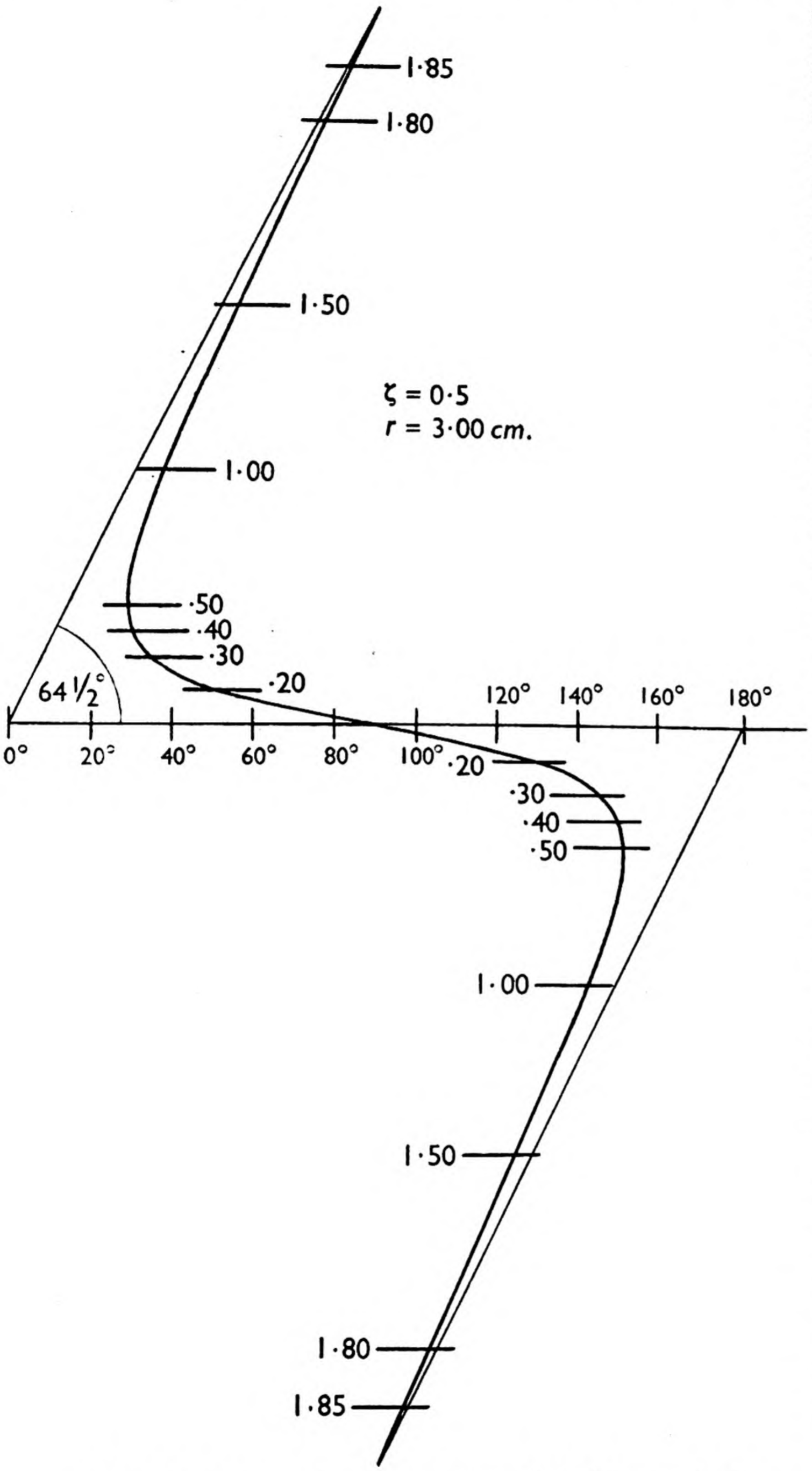

FIG. 96. Diagram showing one curve of the Wooster chart. This is obtained by plotting corresponding values of ξ and η from Fig. 95.2*b*

and at a distance ζ from the origin. In Fig. 95.2*b* is shown a view of the same reflecting circle but with the axis of oscillation normal to the paper. From these figures it will be seen that reciprocal points closer than $(1-\sqrt{1-\zeta^2})$ or further than $(1+\sqrt{1-\zeta^2})$ from the axis of oscillation cannot cut the reflecting circle. If a central reciprocal point-row rotates in the plane of the reflecting circle it becomes tangent to the circle, and after further rotation cuts it in two places.

The same geometrical study may be carried out as in **7**, 2.2, when it will be found that a curved line as shown in Fig. 96 is the locus of spots which correspond to any central reciprocal point row. For the sake of comparison, the straight diagonal lines of Fig. 95.1 are inserted to show the corresponding locus in the equatorial photograph. In the chart constructed for $\zeta=0{\cdot}5$ (Fig. 95.1) a series of such curves is drawn corresponding to central reciprocal point rows inclined to one another at an angle of 10°. According to which of these curves the spot lies on, so one of the cylindrical co-ordinates, the angle ϕ, can be read. The value of ξ can be obtained from the coincidence of the spot with one member of the family of lines in Fig. 95.1 drawn parallel to the central line of the photograph. The positions of these lines can be derived as follows from Fig. 96. For a given value of ξ, the angle η which the reflected beam, projected in a plane perpendicular to the axis of the camera, makes with the incident X-rays, is given by the equation :

$$\xi^2=2-\zeta^2-2\sqrt{1-\zeta^2}\cos\eta,$$

or $$\xi^2=2-\zeta^2+2\sqrt{1-\zeta^2}\cos\eta.$$

The perpendicular distance of a spot from the central line of the photograph is $r\eta$, and hence the line corresponding to a given value of ξ may be drawn in. Usually the range of values of ζ encountered in non-zero layer photographs does not exceed 0·0 to 0·3, and hence four charts for $\zeta=0{\cdot}0$, 0·1, 0·2, 0·3 suffice for all usual requirements.

4.3 The double-crystal photograph. When the intensities of reflection from two separate crystals are

to be compared, we must take into account the fluctuations in the output of the tube and variations in the processing of the photographs. The simplest way of doing this is to expose the crystals alternately for a succession of short periods to the same X-ray beam and to receive both sets of reflections on the same piece of photographic film. Special goniometers

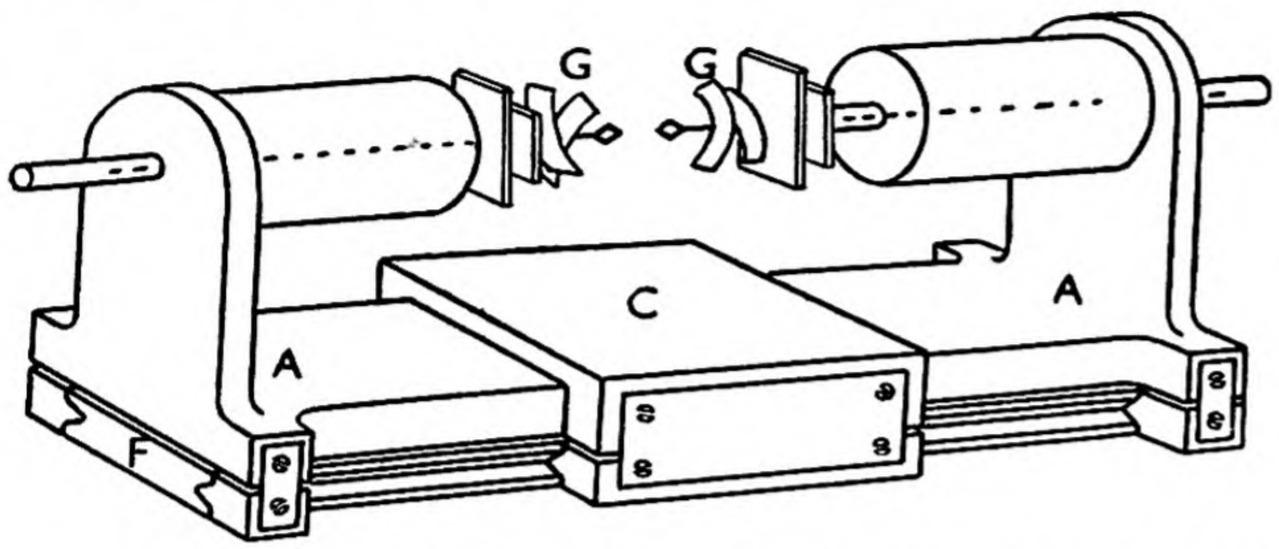

FIG. 97.1. Diagram showing method of mounting specimens on the two-crystal Weissenberg goniometer. The goniometer heads *G* are supported on a frame *AA* which can be translated along the fixed base *F* sufficiently far to remove one crystal from the beam and to bring the second into the beam. The camera is mounted on the base *C*

have been designed for this purpose (Robertson 1934 ; Wooster and Martin 1940).

Though any type of goniometer could be used for such an investigation, one embodying a moving film is best, since there is no ambiguity in the interpretation of the results, and probably the ordinary Weissenberg goniometer is the most convenient of the various types available. In the Wooster-Martin instrument the two crystals are mounted on collinear axes on goniometer heads, so that they are close together (Fig. 97.1). It may be arranged that either one of the heads remains stationary while the other oscillates, or the heads may be linked together and with the camera carriage so that their oscillation about the axis on which the two heads are mounted is synchronised with the motion of the camera. The goniometer heads are mounted on a frame which is set, for an equatorial photograph, perpendicular to the incident beam, which falls on one of the crystals. When the camera carriage reaches the end of its traverse, it operates a mechanism which moves the frame so that the other crystal is irradiated while the camera moves backwards and forwards again.

Because the two crystals are only a few millimetres apart, it is not possible to slip a complete cylindrical camera over them. Therefore, instead of a complete cylinder two hemicylinders are used for the camera. These can be supported in several ways : (1) on the frame supporting the crystals, (2) on the camera carriage moving backwards and forwards along the track, (3) on the fixed base of the instrument. When the camera is carried on the moving carriage, Weissenberg photographs obtained from the two crystals are superimposed on the same film (Fig. 98). One screen is mounted on the frame which supports the crystals, and the other is mounted on the fixed base (Fig. 97.2). The fixed screen is a cylindrical metal tube with a narrow aperture round the circumference, and the moving screen is a tube one half of which is cut away so that during the exposure of one crystal only one of the hemicylinders can receive the reflected X-rays. In this way it can be arranged that one half-cylinder receives reflections from both crystals while the other half receives reflections from one crystal only.

In addition to their use for the comparison of the intensities of reflections from different substances, such photographs can be employed for comparing two crystals of the same substance in different physical states, for example, perfect and mosaic crystals. The same instrument can also be used for comparing the intensities of reflection from two powders to show the ratio of line intensity to the background. For this purpose the powder specimens are mounted on the goniometer heads and the camera is mounted on the frame carrying the crystals. Two powder photographs, each the width of the aperture in the screen, are thus produced side by side under exactly the same conditions. Laue photographs may be compared in a similar manner.

A further use of this instrument is in the measurement of absorption coefficients. For this purpose the specimen is mounted on an arm which is carried on the frame carrying the crystals. This arm extends to

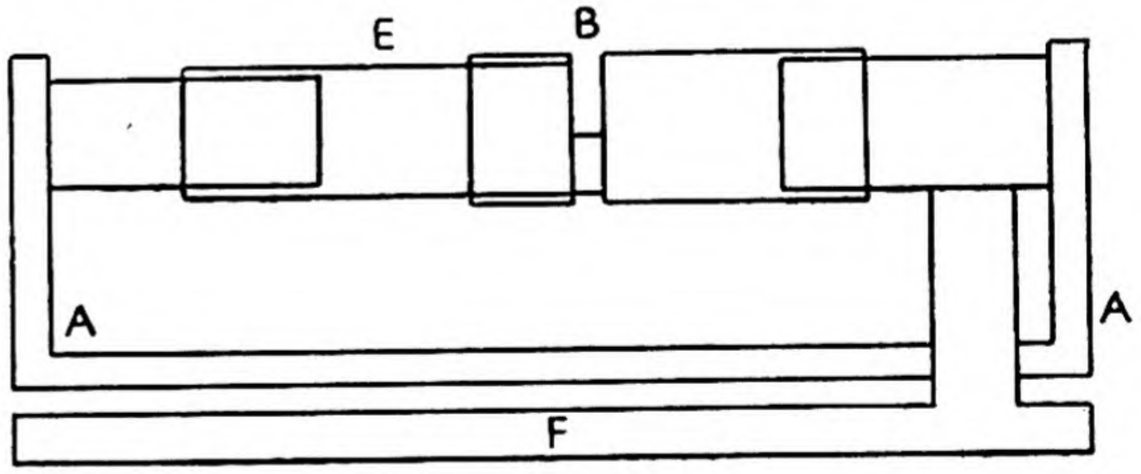

FIG. 97.2. Diagram showing method of mounting screens on the two-crystal Weissenberg goniometer. The screen *B*, which has a circumferential slot, is fixed on the base *F*. The screen *E* moves with the frame *A* and is cut so that only the lower half cuts out the reflected X-rays from the left-hand crystal.

a point just in front of the collimator, and the specimen is mounted there so that, as the frame moves backwards and forwards, the specimen is alternately in and out of the beam. A reflected X-ray beam is obtained from another crystal which does not rotate and is large enough to be in the beam in both positions of the moving frame. This crystal simply acts as a

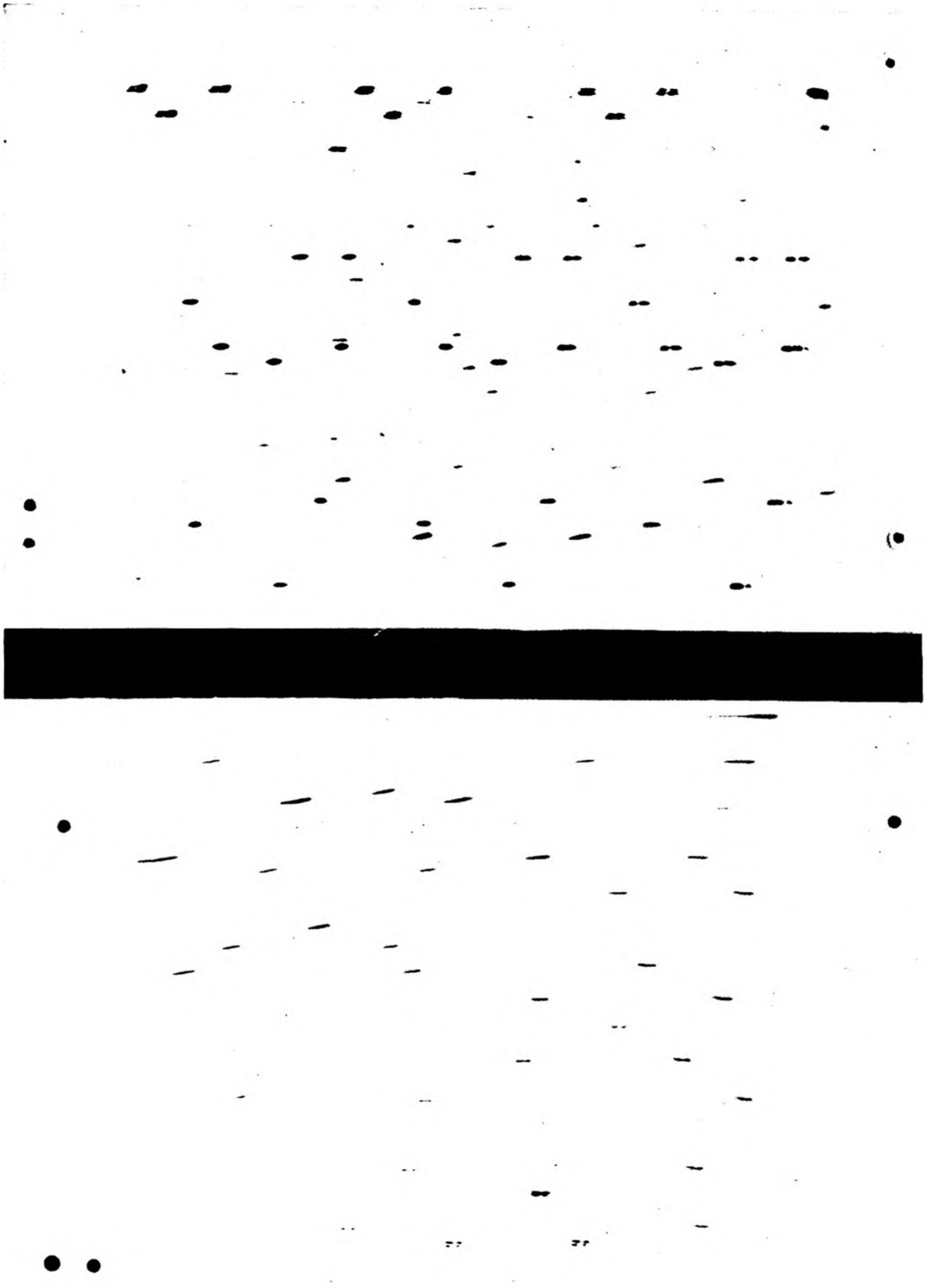

FIG. 98. Two-crystal equatorial Weissenberg photograph. The half-photograph with a horizontal pair of fiducial spots was obtained with a crystal of gypsum set with its morphological [101] axis parallel to the axis of rotation. The half-photograph with a vertical pair of fiducial spots was obtained by superimposing the reflections from a quartz crystal set with its z-axis parallel to the axis of rotation, on the reflections from the gypsum

monochromator. In this way two reflected beams are obtained, the relative intensities of which are determined by the absorption of the specimen. If no time were occupied in moving the absorber into the beam, this ratio could be found merely by comparing the density of the two spots produced in a camera mounted on the moving frame; but in practice an appreciable time is taken up in bringing the absorber into position. In consequence, it is necessary to mount the photographic film so that the record of the reflection from the crystal during the movement of the screen is separated from the reflection while it is in its stationary position. This can be achieved by mounting the film in a camera carried on the goniometer-head axis and rotating in synchronism with the moving camera holder. In this way the record is made to consist of two parallel lines on the film joined by a line at the bottom. The vertical traces are produced by the reflections while the screen is in its two stationary positions, and the horizontal line is produced while it is moving. Usually it is more convenient to make the beam pass through a standard absorber alternately with the substance under test, rather than through nothing at all, as the thickness of the standard can be adjusted until the densities of the two streaks are about equal (Fig. 99.1).

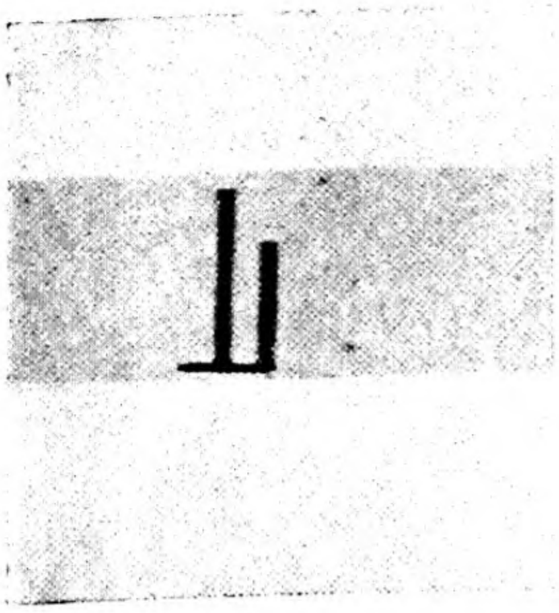

FIG. 99.1.
Absorption photograph taken with two-crystal Weissenberg goniometer

4.4 Goniometers for inclination–Weissenberg photographs. In the most flexible type of Weissenberg goniometer the axis of oscillation of the crystal can be moved about an axis perpendicular both to the oscillation axis of the crystal and to the direction of the incident X-ray beam. This axis of movement passes through the point of intersection of the oscillation axis of the crystal and the incident beam. The annular aperture in the screen is displaced sideways so that the incident beam passes through the aperture when this is set in the manner described in the next section.

4.5 Equi-inclination photographs. We have seen that a plane of reciprocal points normal to the oscillation axis gives rise to a cone of diffracted X-rays with semi-angle $\cos^{-1}\zeta$ (**5,** 1.4). If the incident X-rays, instead of being normal to the axis of rotation, are inclined to it at an angle $\cos^{-1}\zeta/2$, the incident X-rays will form one of the generators of the cone of diffracted rays. In Fig. 99.2, Q is the foot of the perpendicular from O on to the reciprocal plane. If there is a lattice point at Q, the reflecting circle, which has PQ as its diameter, will stand in almost the same relation to the reciprocal points as the equatorial reflecting circle stood to the points of Fig. 88. The only difference is that the radius of the circle PQ is $\sqrt{1-\zeta^2/4}$ instead of unity, and consequently if the co-ordinates are read off on the equatorial Weissenberg chart, the values must all be multiplied by the factor $\sqrt{1-\zeta^2/4}$ to bring them to the correct value. Thus for equi-inclination photographs the same Weissenberg chart can be used as for normal-beam equatorial photographs. It does not matter whether there is actually a lattice point at Q or not. When a plot in

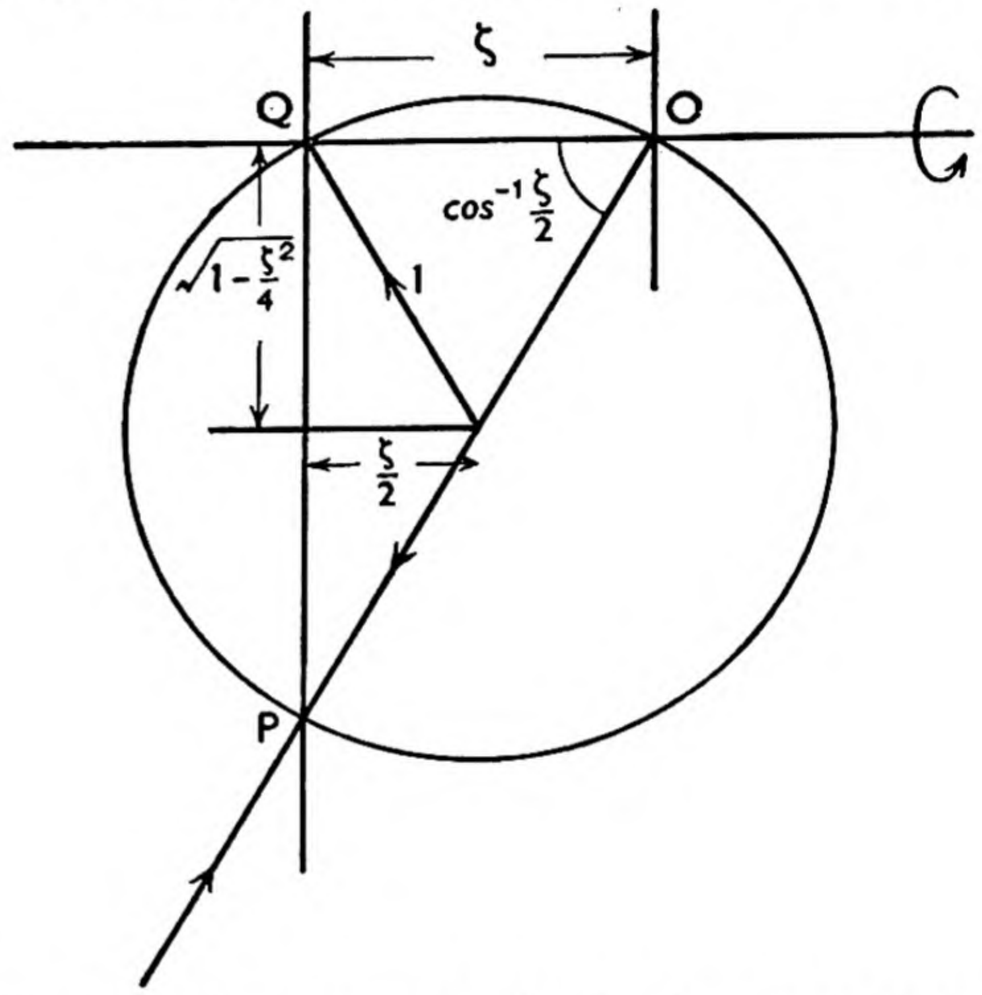

FIG. 99.2. Geometry of reflection in equi-inclination Weissenberg photograph of non-zero-layer

rectangular co-ordinates of the values read from the Weissenberg chart is made, the correct position will be obtained for all spots, but on the non-zero-layer photographs, unlike equatorial photographs, there is no necessity for a reciprocal lattice point to occur at the origin of the layer. A reciprocal-lattice point will not occur at the origin of a non-zero layer when the oscillation axis does not coincide with a point row in the reciprocal lattice. Examples of this are found when triclinic, monoclinic and trigonal crystals are set up about certain axes.

When an equi-inclination photograph of a non-zero-layer is taken, the circumferential slot has to be moved along by an amount $s \,.\, \tan\mu$, where s is the radius of the screen and the angle $\mu = \sin^{-1}(\zeta/2)$. Consequently, for the same orientation of the crystal, and camera radius, r, spots will be displaced by this amount $(r \,.\, \tan\mu)$ along the horizontal line, relative to the corresponding spots in the zero-layer photograph. This translation of the spots corresponds to a rotation of the layer of the reciprocal lattice relative

to the zero-layer; the angle of rotation is given by $(2r \cdot \tan \mu)^\circ$ where r is in mm. and where the crystal turns 2° for 1 mm. of camera traverse. When the reciprocal points of the spots on the second photograph are being plotted on the same diagram as those of the zero layer, it is desirable to avoid this relative rotation. This can be done by moving the chart along the horizontal line on the photograph by the amount $r \cdot \tan \mu$ from its original position fixed by the fiducial marks.

5. Principal Uses of Weissenberg Photographs

5.1 Determination of the unit cell. One of the most important uses of equatorial Weissenberg photographs is in the selection of the simplest unit cell of monoclinic and triclinic crystals. In the orthogonal systems, it is seldom necessary to use Weissenberg photographs for determining the unit cell. In the trigonal and hexagonal systems, however, there are certain problems which are most easily solved by Weissenberg methods. It may happen that a trigonal specimen belongs to the Laue group $\bar{3}$, or a hexagonal specimen to the Laue group $6/m$. Even if faces are present, there may be some doubt about the directions of the shortest repeat distance at right angles to the unique axis. This can be determined by inspection of the reciprocal-lattice plot from an equatorial Weissenberg photograph with the crystal oscillated about the unique axis.

In the example of **7**, 3.2 it was seen that the values obtained from a single equatorial photograph for a^* and c^* were each twice the true values. This would give values for a and c which were half of the true values. This was due to the absence of spots of the type hko with odd values for h and k. This matter is discussed in the following section, but it should be noted that it is always necessary to check repeat distances by means of oscillation photographs or non-zero-layer Weissenberg photographs.

5.2 Study of systematically-absent reflections. The study of systematically-absent reflections is essential in the determination of space groups and is in general most quickly done by means of Weissenberg photographs. The determination of the lattice type requires study of a considerable number of reflections with general indices. This can be done on the non-zero layer lines of oscillation photographs, or on non-zero layer Weissenberg photographs. It would be unwise to rely on the indices from only one of such Weissenberg photographs, because certain peculiarities of the crystal structure might cause, for example, hkl reflections to be very weak when k is odd (**6**, 2.3).

It is, however, in the determination of systematically-absent reflections of special types that the Weissenberg method has a great advantage. In the monoclinic system we require to know if there are any systematic absences of the reflections of the types hol and oko. The first of these can be studied on an equatorial photograph with the crystal oscillated about the y-axis, and the second on a similar photograph with the crystal oscillated about the x- or the z-axis. In the orthorhombic system we require to study reflections of the types hoo, oko, ool, hko, hol, and okl, and for this it is sufficient to take three equatorial photographs with the crystal oscillated about each of the three crystallographic axes. In the tetragonal system we require to study reflections of the types, hoo, ool, okl, hko, hhl. Two equatorial photographs, with the tetrad axis and one of the horizontal axes as oscillation axes respectively, will provide all the information except that concerning reflections of the type hhl; these can be studied on non-zero layer photographs or on oscillation photographs. In the trigonal and hexagonal systems we require to study reflections of the types, $hh\bar{2}hl$, $h\bar{h}ol$, ool. Two equatorial photographs are sufficient, the oscillation axis being one of the horizontal axes and a horizontal direction normal to this axis and to the unique axis. In the cubic system we require to study reflections of the types hoo, okl, hhl; except for hhl, these can be studied on one equatorial photograph with one of the crystallographic axes as oscillation axis.

The convenience of Weissenberg photographs for this work is clear from the following calculation. With a monoclinic specimen we could study all the reflections of the type hol on eighteen 10°-oscillation photographs about the y-axis. From these we would also get the value of b and a large number of general reflections. To complete the work we would have to take several oscillation photographs about either the x- or the z-axis in order to study reflections of the type oko, and one about the other axis to get the third repeat distance. The value of the angle β would have to be found by trial. Even if we check each repeat distance from an oscillation photograph, as should always be done, we could obtain all these data by taking the following five photographs:

Photograph	*Oscill. axis*	*Information derived*
Oscillation	x	a
	y	b and general reflections
	z	c
Equatorial Weissenberg	x or z	reflections of type oko
	y	β and reflections of type hol

From the last of these photographs, also, the most convenient unit cell could be quickly selected.

CHAPTER 8

STUDY OF ORIENTATION IN SINGLE CRYSTALS AND TWINS

1. Introduction

THE problem of finding the orientation of a crystal specimen frequently arises. For some purposes it is required to determine the orientation of the crystallographic axes relative to reference directions on the specimen. The problem is presented in this way when it is desired to cut or drill a crystal in a particular crystallographic direction. In the study of single crystals the specimen has frequently to be adjusted on a goniometer in particular orientations relative to reference directions. In setting specimens it is usually necessary to proceed by trial and error, but the time involved can often be shortened by simple calculations. In the case of industrial procedures, such as the production of piezo-electric plates of quartz, the process has been reduced to a routine. But the crystallographer is continually having to deal with different substances in various forms, and the problems of orientation can only be properly tackled through appreciation of the fundamental geometry of reflection.

In all orientation work it is impossible to lay down a general procedure because of the great variation in the nature of the specimens, and it is necessary to use the techniques most suited to the particular specimen. If the specimen develops natural faces or cleavage planes, it may be possible to solve the problem wholly or in part by means of the optical goniometer. It is convenient to have interchangeable heads on an optical goniometer and on X-ray instruments, so that the adjusted specimen can be transferred for the taking of X-ray photographs. Alternatively, the X-ray goniometer can be adapted for use as an optical instrument if the slit system is replaced by an optical collimator, and if the telescope is moved so that its axis is inclined to the incident beam while remaining normal to the oscillation axis.

If the faces give sharp optical reflections, this method is a very accurate one ; and in such cases the crystal is likely to require only a slight re-adjustment after the first X-ray photograph. But even when the optical reflections are not very good, much time is usually saved by preliminary setting in this way. This method is applicable to any crystal, transparent or opaque, as long as it shows two non-parallel natural faces or cleavage planes. If particular faces can be recognised by the investigator, it may be possible to set the crystal completely by this method. To make full use of the method, especially when more than one zone of faces or cleavage planes is present on the crystal, a good understanding of optical goniometry and of crystal morphology is needed ; a full description of this subject, with examples, is given by Phillips (1946).

When the specimen has neither natural faces nor cleavage planes but is transparent, the methods of crystal optics can be tried. If the crystal is cubic, no information about orientation can be obtained by simple optical methods. In uniaxial crystals the direction of the optic axis can be easily determined with varying degrees of accuracy. Among biaxial crystals it is usually possible to orientate an orthorhombic crystal in this way, sometimes possible to obtain some information about a monoclinic crystal, but not, in general, possible to do so for a triclinic crystal. When the specimen is sufficiently thick, it is convenient to examine it between two sheets of ' Polaroid ' and to mark on the specimen the extinction directions so determined ; with small crystals it is necessary to use a polarising microscope. For material which can be cut into thin sections, the use of the universal-stage microscope is the most accurate procedure for the determination of the orientation of the optical indicatrix and of any cleavage directions. In this method a stereogram of the orientation, relative to the plane of the section and a given direction in it, is plotted.

Each specimen has, of course, to be studied in the way most suited to its particular properties, but a knowledge of crystal optics and some experience saves much time and trouble in the study of transparent crystals. Good descriptions of the theory and practice of crystal optics are given by Hartshorne and Stuart (1950), Winchell (1937) and Wahlstrom (1943).

Another property which is useful in the study of symmetry and orientation is the different rate of solution in different directions of the crystal. When the surface of a crystal is etched with a suitable non-optically-active reagent, etch-pits are often developed. These etch pits are in general polygonal because of the different speed of solution in different directions in the crystal. Hence from examination of these etch pits useful information about the face symmetry and the orientation of the specimen can

often be obtained. A discussion on etch figures and face symmetry is given in **10**, 2.4 and information about the techniques are given by Honess (1927).

Pyro-electric tests can also provide useful information in some cases. If a crystal lacks a centre of symmetry, it may develop pyro-electric charges at opposite ends of a uniterminal (polar) axis. A discussion of the use of pyro-electric tests to give information on symmetry and orientation is given in **10**, 2.7, and information about the techniques is given by Martin (1931).

The sections in this chapter are concerned with the various X-ray methods of determining the orientation of specimens. A list of published methods of setting crystals and a method for difficult cases are given by Jeffery (1949). But in many cases the methods mentioned above are very useful, both in solving the problem completely and as auxiliary methods to those described below.

2. Geometry of X-ray Reflection for Various Orientations

2.1 Effects on oscillation photographs of mis-setting the specimen. It was seen in **5**, 1.4 that in an oscillation or rotation photograph, taken on cylindrical film, straight layer lines are obtained only when a zone axis of the crystal is parallel to the axis of oscillation. In this section, we shall discuss the changes which occur in the pattern of spots when the zone axis is tilted out of this orientation. In studying problems of this kind, we consider the plane of points passing through the origin of the reciprocal lattice and normal to the zone axis. This plane intersects the reflecting sphere in a small circle which gives rise to a cone of reflected rays. These reflected rays intersect the film in a line which is the locus of spots for reflections from Bravais lattice planes in the given zone. This line passes through the centre of the film ($\theta = 0°$) and in general is curved. In considering how tilting of the crystal affects the position of this locus on the film, we shall neglect the non-zero-layer lines as these give no additional information.

If the zone axis is tilted sideways, the great circle in which the zero layer cuts the surface of the sphere of reflection is now inclined to the horizontal and the reflected rays would produce a curve on a cylindrical film. In an oscillation photograph of an actual crystal the same curve can be obtained, provided only that the angle of oscillation is kept small. If this is not done, the curve will consist of a number of superposed parts of different curves, because the spots will be produced when the crystal is in different orientations during the oscillation. To obtain the measurement of the angle of tilt from an oscillation photograph it is, therefore, desirable to keep the oscillation small, but the lower limit of this is set by the need to have a sufficient number of spots on the film to mark the curve. If the cell-size and structure of the crystal are such that the number of spots on the zero-layer line is small, it may be necessary to increase the angle of oscillation, or in extreme cases to use the Laue method instead. Unfiltered radiation should be used for the oscillation method as this gives a more strongly-marked zero line.

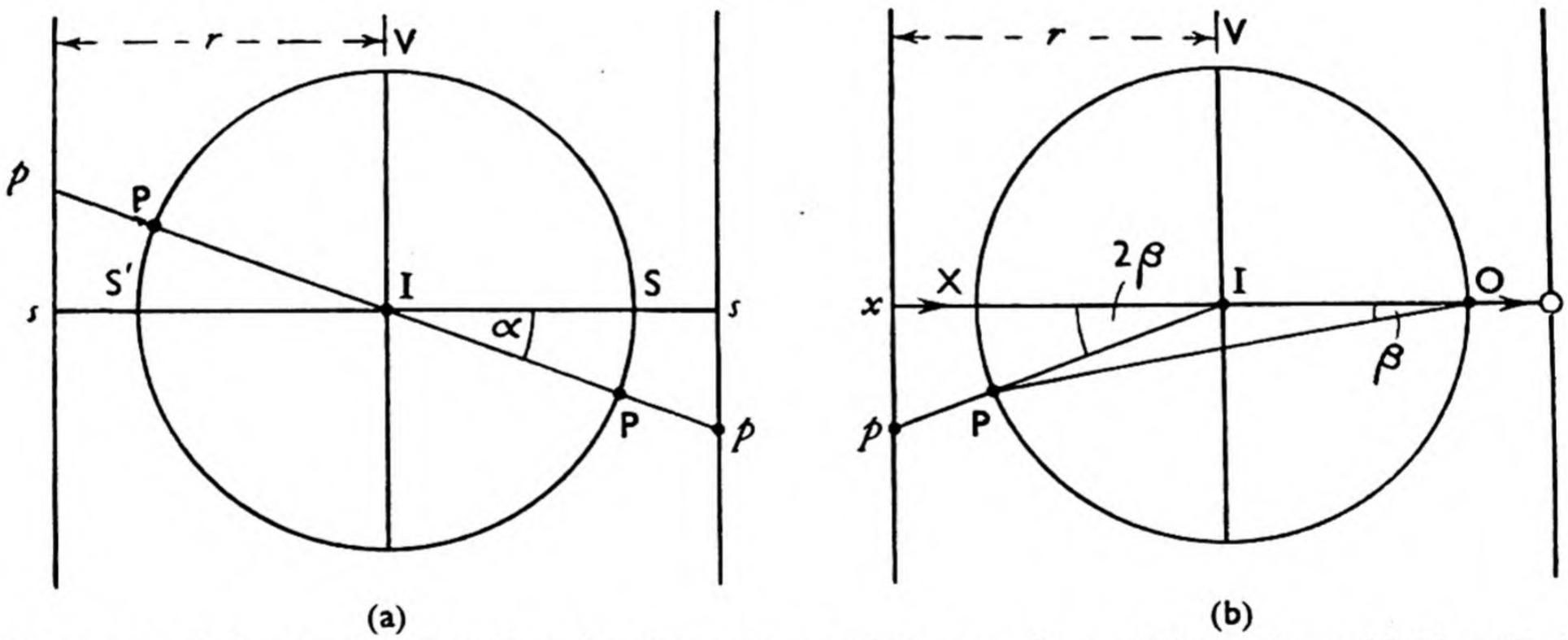

FIG. 102. Diagram showing the reflecting sphere and the zero layer of the reciprocal lattice tilted, (*a*) sideways ; (*b*) back-to-front

In considering how to measure the angle of sideways tilt from a photograph, it can be seen from Fig. 102 (*a*) that

$$\tan \alpha = sp/r,$$

where r is the radius of the cylindrical camera and α is the angle of sideways tilt of the zone axis. In Fig. 103.1 (*a*) these curves are drawn for two values of angle α, and it can be seen that for small values of θ a good approximation can be made by measuring the angle between the horizontal line and the zero-layer-

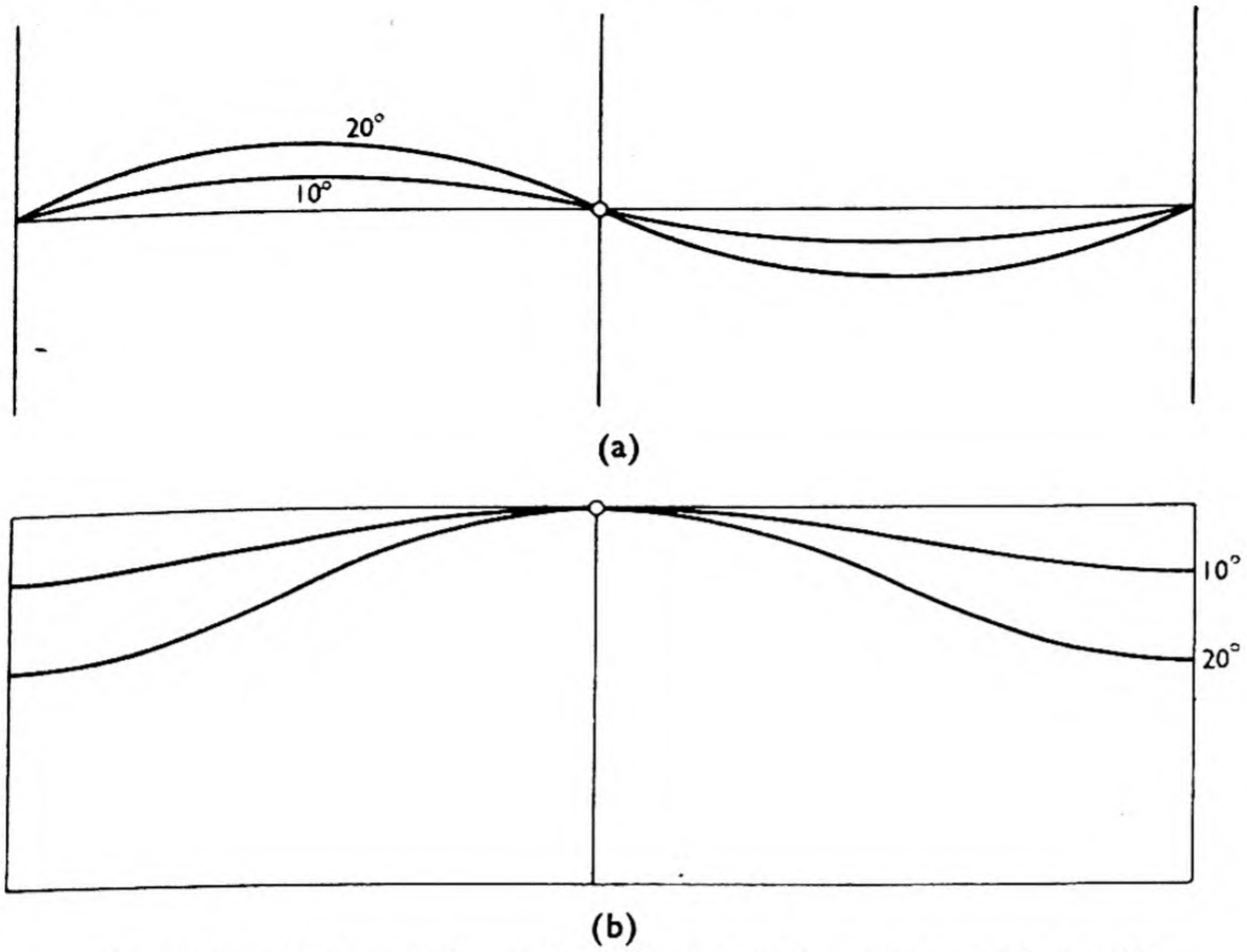

FIG. 103.1. Diagram illustrating tilted zero-layer lines, with a cylindrical camera of radius 1·5 cm.; (*a*) sideways, with values of angle α; (*b*) back-to-front with values of angle β

line curve near the centre (up to a value of θ of about 15°). Although the spots near the centre may be absent for various reasons, including high absorption by the specimen, the streaks caused by the short wave-lengths are usually present in an oscillation photograph. This method of measuring α is the quickest; but if it is not possible to use it, the mean of the two values of sp should be used in the above equation; it should be noted that this latter measurement can be made at any point with θ between 40° and 50°, owing to the flattening out of the curve. The accuracy obtainable in the determination of α depends on the sharpness of the spots and is, of course, greater for a larger radius of camera. The method of measuring α near the centre with a protractor is the only one possible with a flat, front-plate camera, which may have to be used if a long crystal-to-film distance is required.

The corresponding angle for a back-front tilt can be derived (Fig. 102 *b*) from the equation

$$\tan 2\beta = xp/r,$$

where β is the angle of back-front tilt, and r is the radius of the cylindrical camera.

The difference between the two equations should be noted, because the maximum distance from the horizontal to the zero-layer curve is approximately doubled, for equal angles of tilt, in the second case compared with the first.

It can be seen from Fig. 103.1 (*b*) that the flattening of the curve beyond values of θ of about 75° enables accurate measurements to be made with the ordinary mounting of the film with which it is not possible to record a spot in the position p of Fig. 102. For a particular radius of camera and with spots of equal sharpness, it is possible to achieve greater accuracy in determining the angle when the tilt is from back to front than when it is sideways, owing to the division of the result by 2 in the former case. When both tilts are present, the curves become more complicated and the respective angles are more difficult to determine.

2.2 Derivation of curves of various constant angles. Let us suppose that the goniometer head has been set so that the incident X-ray beam lies in the plane of movement of one of the adjusting arcs, and that the reading is zero on both arcs. Then the directions about which the crystal can be rotated are (i) the vertical axis, V, of the goniometer, which is the axis of the cylindrical camera, (ii) the axis, X, of the incident X-ray beam, and (iii) the direction at right angles to these two, S (Fig. 103.2). The lower of the two arcs is anchored to the spindle and its axis of movement is always the same. The upper arc is carried on the first and its axis of movement is altered in direction by change of the setting on the first arc. The axis of movement of the upper arc is always perpendicular to that of the lower, but its inclination to the spindle axis is given by the reading on the lower arc.

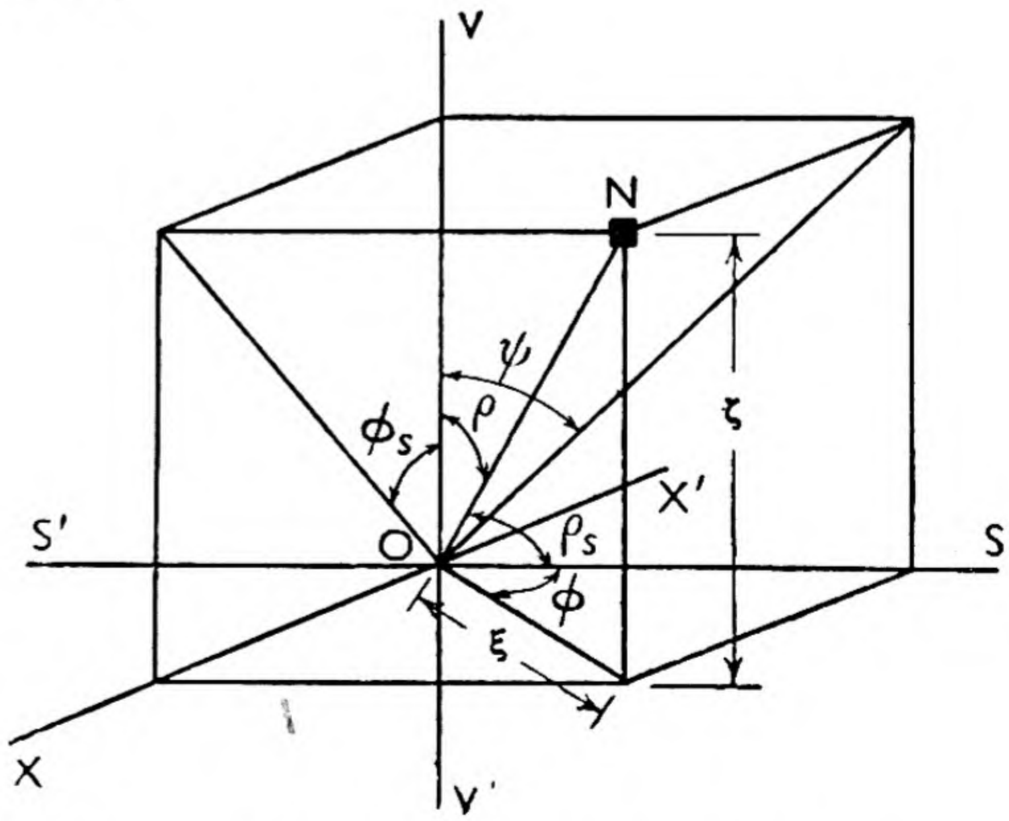

FIG. 103.2. Diagram showing the relation of the cylindrical co-ordinates and the pairs of polar co-ordinates.
Angle $XON = (90° - \theta)$

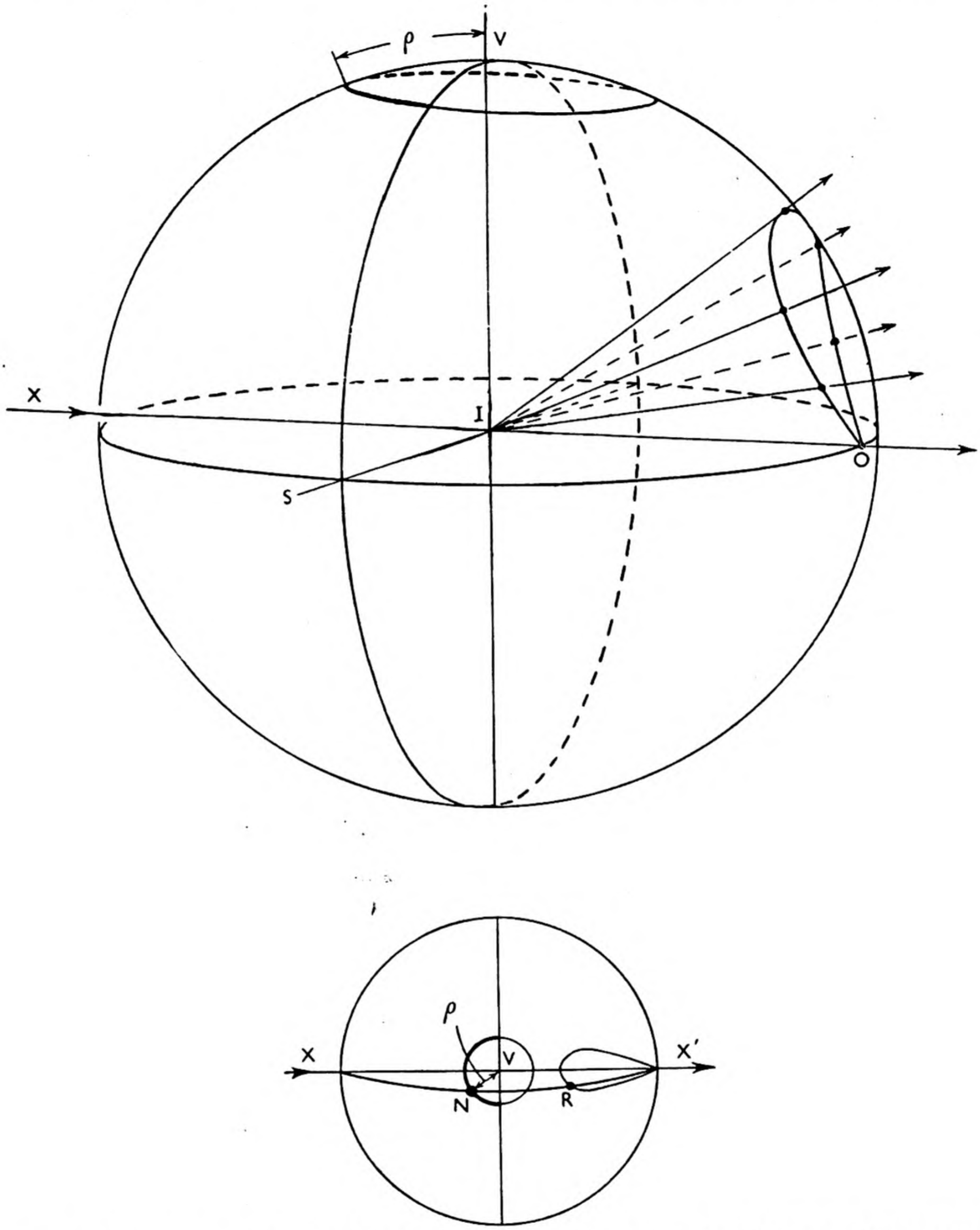

FIG. 104. Diagrams showing the reflecting sphere and the formation of a curve of constant ρ in perspective and in stereographic projection

In Figs. 104, 105, 106 are shown perspective views and stereograms of the reflecting sphere. When the crystal is turned about an axis, the normal to a given reflecting plane will describe a small circle about the pole of the axis. The pole of the direction of the reflected ray will describe a curve, and the projection of this on to the film will give another curve, the shape of which will in general be different on a flat film and on a cylindrical film. Any small circle on the sphere or on the stereogram can be divided regularly by a series of great circles passing through the pole of the small circle. Similarly, any great circle can be divided regularly by a series of small circles described at constant angular intervals, about any point on the

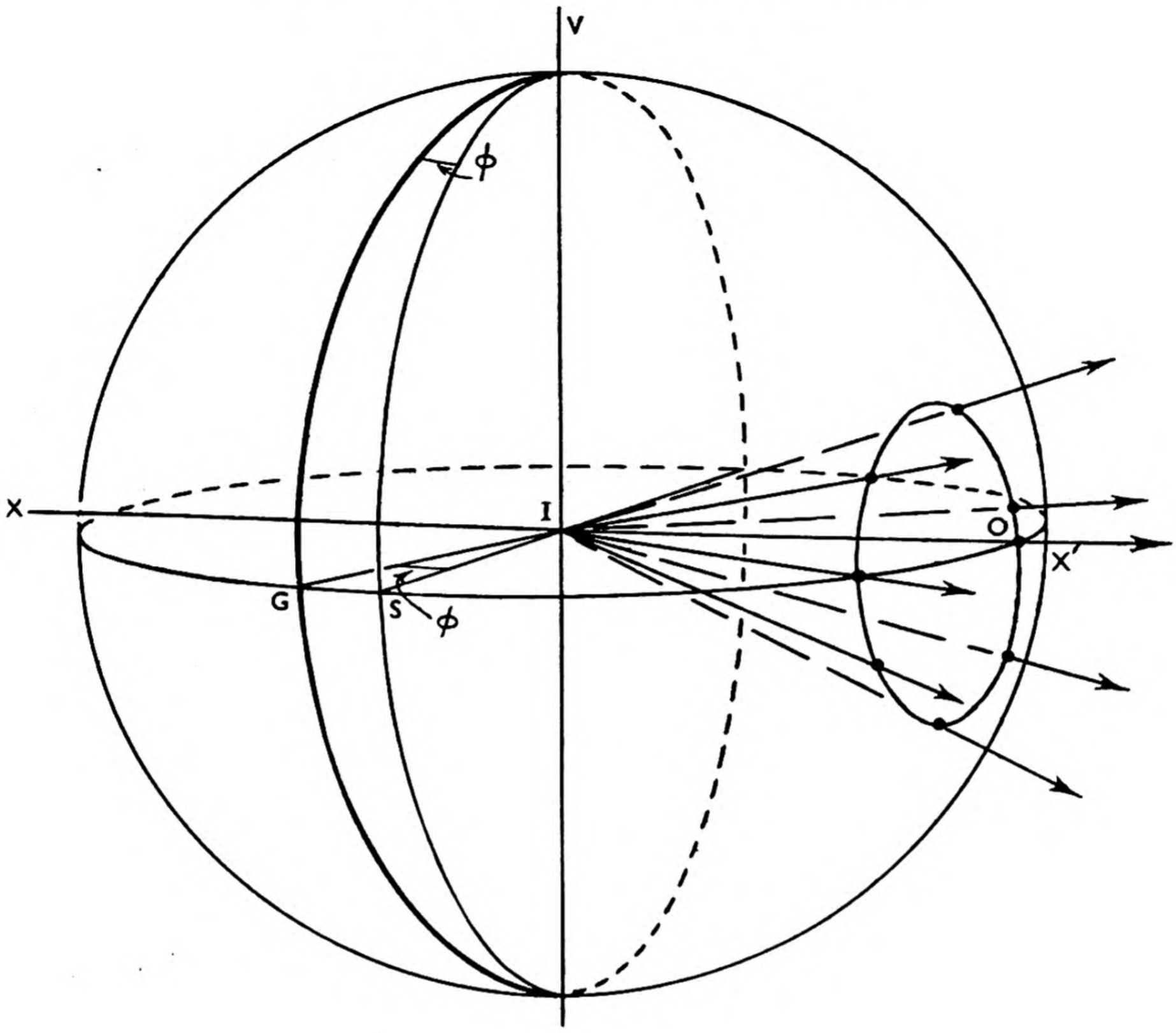

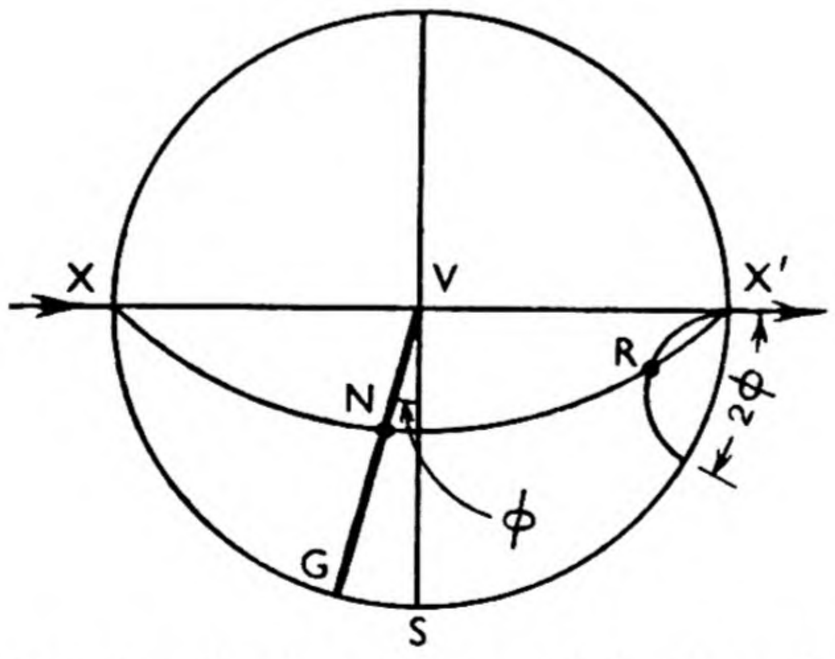

FIG. 105. Diagrams showing the reflecting sphere and the formation of a curve of constant ϕ in perspective and in stereographic projection

great circle. We can imagine the pole of the normal to a given reflecting plane being rotated about the pole of each of the axes V, X and S in turn. For each of these rotations, the reflected beam will trace out a curve on the film, and we need to know the shape of each of these curves, both for a flat and for a cylindrical film. We also require to know the corresponding curves which would be produced by movement of the pole along the series of great circles passing through the poles of the axes V, X and S in turn.

If the pole of the reflecting plane moves along the small circle of radius ρ about the pole V the resulting locus of the pole of the reflected beam is the curve shown in Fig. 104. Alternatively, this curve can be

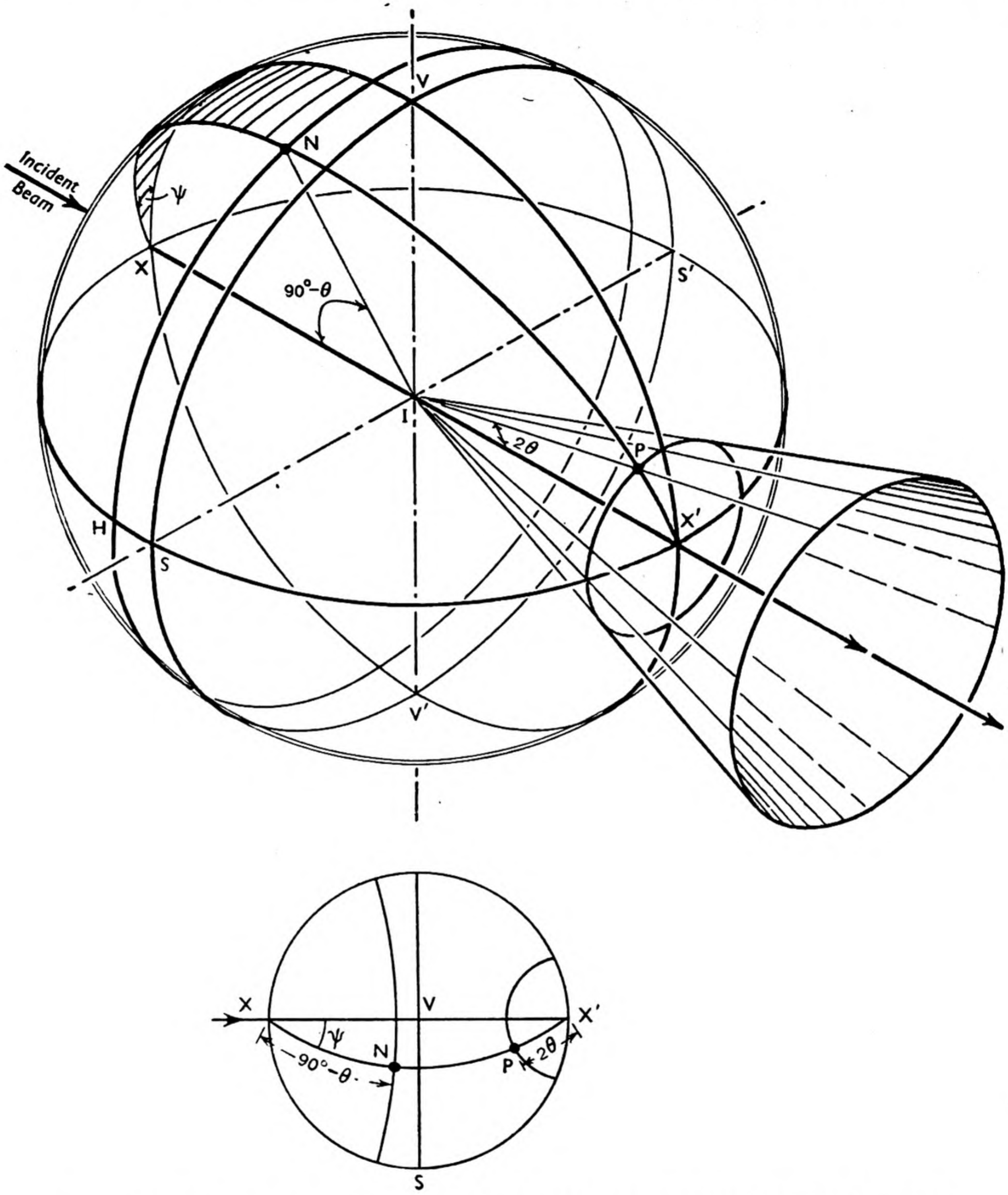

FIG. 106. Diagrams showing the reflecting sphere and the formation of a curve of constant θ in perspective and in stereographic projection

thought of as the intersection of the reflecting sphere with the cone of semi-angle ρ of which the axis is the vertical through the origin, O, of the reciprocal lattice; the curve could then be thought of as the locus of the reciprocal point corresponding to the planes N. The curves for movement of the pole of the reflecting plane along the great circle of constant ϕ are shown in Fig. 105. Here the surface of reflected rays is a cone which would intersect a flat front-plate in an ellipse through the centre of the film. The curves on a cylindrical film corresponding to this pair of polar co-ordinates ρ and ϕ are given in Fig. 108.

Another double set of curves can be drawn for the similar pair of polar co-ordinates ρ_s and ϕ_s, the sub-

script being used to show that these refer to the axis *IS* instead of the commoner axis *IV*. For a flat front-plate these are exactly the same as for the previous pair except that they are turned through a right angle; but for a cylindrical film they are different (International Tables, 1935, p. 639).

The relations for the third pair of polar co-ordinates $(90-\theta)$ and ψ are shown in Fig. 106. For a flat front-plate the curves consist of concentric circles and straight lines through the centre of the film. Curves of θ or of 2θ may be used instead if more convenient. A set of θ, ψ curves for a cylindrical film is given in International Tables, 1935, p. 638. In Fig. 108 are given curves of ρ, $(90-\phi)$ and θ for a cylindrical camera of radius 3 cm.

The curves can be constructed by calculation, but they are more simply made by graphical construction on the stereogram. The nature of the various curves is tabulated below.

Symbol	Locus of pole of normal	Locus of pole of reflected ray
θ	small circle round X of radius $(90-\theta)$	small circle round X' (O) of radius 2θ
ψ	great circle through X, inclined at angle ψ to XVX'	great circle through X, inclined at angle ψ to XVX'
ρ	small circle round V of radius ρ	intersection of sphere with a cone of semi-angle ρ and the vertical through X' (O) as its axis
ϕ	great circle through V, inclined at angle ϕ to SVS'	small circle of radius ϕ about a point in $X'S$ at ϕ from $X'(O)$
ρ_s	small circle round S of radius ρ_s	intersection of sphere with a cone of semi-angle ρ_s, the axis of which is parallel to IS at the point O.
ϕ_s	great circle through S, inclined at angle ϕ_s to SVS'	small circle of radius ϕ_s about a point in $X'V$ at ϕ from $X'(O)$

2.3 Effects on Laue photographs of mis-setting the specimen. In this section we consider the change in position of the Laue spots when the orientation of the specimen is altered in different ways. When a zone axis of the crystal is parallel to the vertical axis of the instrument, a horizontal straight line of spots runs through the centre of the Laue photograph. This is analogous to the zero-layer line of an oscillation photograph in that both consist of reflections from planes in the vertical zone. The other layer lines of the oscillation photograph do not occur in the Laue photograph, in which the prominent features are the conic sections of spots due to reflections from particular zones. When a zone axis lies normal to the X-ray beam, the corresponding spots lie on a straight line through the centre of the flat-plate photograph. We could observe such straight lines of spots in order to pick out zone axes lying in the plane at right angles to the incident beam.

From a flat-film Laue photograph we can derive the angle ψ through which the crystal has to be turned about the X-axis in order to bring a prominent straight line of spots into the horizontal position. This means that a zone axis has been set vertical which is a considerable convenience in work with Laue photographs. It is best to make this first adjustment on the upper arc, which should be set with its plane normal to the X-ray beam. (The reason for this is that movement on this arc does not alter the axis of movement of the lower arc.) Now movement about the lower arc causes the spots to move round the appropriate curve of ρ_s through the angle ϕ_s. Correspondingly, movement about the vertical axis causes the spots to move round the appropriate curve of ρ through the angle ϕ.

Laue photographs are only of use in setting a specimen when it is within a few degrees of some symmetrical position, because of the great change of the appearance of the photograph for a small change in the setting. But this sensitivity is extremely useful for the final setting from an approximate position, a movement of the crystal of 3′ of arc being detectable when the spots are sharp. When there are two mutually-perpendicular lines of symmetry the procedure is straightforward. In other cases several trial photographs may be necessary. It is impossible to lay down rules for setting crystals in detail, as different specimens require somewhat different procedures. In trial settings, the curves described are often useful in showing how a given alteration will affect any particular spot. Also they can be used to determine the first adjustment required to make any given zone axis parallel to the X-ray beam.

3. Determination of Orientation from X-ray Photographs

3.1 Introduction. In the previous sections we discussed procedures for setting the specimen in a known orientation by various methods. Success in setting a specimen involves discovering its approximate orientation at some stage of the adjustment process. This knowledge is usually provisional and some trial is usually needed to make it definite; but it is often acquired before X-ray methods are begun

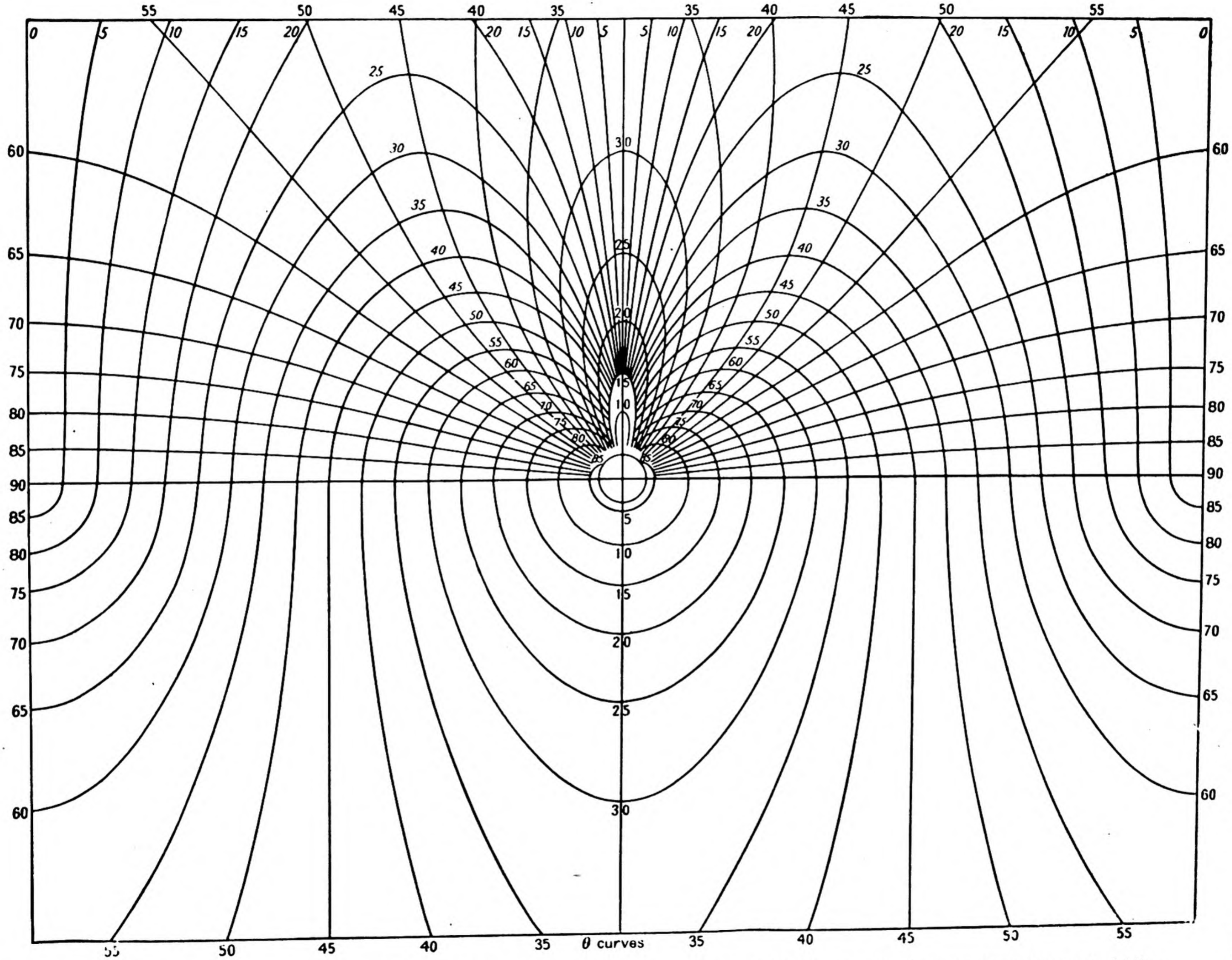

FIG. 108. Chart of curves of constant θ, ρ and $(90-\phi)$. The $(90-\phi)$ curves are those which join on to the θ-curves along the equatorial line.
Camera : cylindrical, $r = 3$ cm.

It is clear that when the orientation is required, without the necessity of setting the specimen for further study, similar procedures will have to be used. In the following sections, however, we study more general X-ray procedures which have to be employed when no preliminary partial information can be obtained by any of the other methods. These procedures are quite direct with simple crystals, but take on the character of trial-and-error methods in less simple cases. Sometimes, however, the practical difficulties are great and the task may be so lengthy that the problem can be considered insoluble by these means alone. References are given below to the various methods which have been used.

Rotation or Oscillation Photographs	Laue Photographs	Moving-film Photographs
Müller (1924)	Gross (1920)	Dawson (1928)
Thewlis (1933)	Schiebold and Sachs (1926)	Davey (1934)
Orowan (1942)	Majima and Togino (1927)	Haworth (1940)
	Schmidt (1929)	Wooster (1946)
	Greninger (1935)	

Combined Oscillation and Laue Photographs

Rinne (1922)
Ekstein and Fahrenhorst (1934)

Rotation or oscillation photographs can be used in the identification of particular zone axes by their characteristic repeat distances. When a crystal is set up with a given zone axis parallel to the axis of rotation or oscillation, the separation of the layer lines at once affords the knowledge of the repeat distance along the zone axis (**5**, 1.5). Unless the symmetry is low, it is usually possible to identify the more important zone axes in a given substance by the repeat distances along them. On an oscillation photograph it may be possible to assign provisional indices to certain reflections, and hence to determine the approximate orientation of other axes. Owing to the fact that any particular reflection may have occurred at any setting of the crystal within the range permitted by the angle of oscillation, there is always some uncertainty in the determination of orientation by means of an oscillation photograph.

Moving-film methods may be used to identify a particular zone axis which is set parallel, or nearly parallel, to the axis of rotation. For this purpose a Weissenberg or other moving-film photograph is taken, using the screen to eliminate all except the spots belonging to one layer line. This use of moving-film methods is the counterpart of the one using rotation or oscillation photographs described above. It is more precise than the rotation or oscillation method since two repeat distances, instead of only one, are provided by these photographs. A method of more general application than that just described is afforded by removing the limiting screens from the Weissenberg goniometer (Wooster, 1946). This method is similar to the combination of Laue and oscillation photographs described in **8**, 3.3. The white radiation is utilised to produce a streak on the photographic film and the shape of this streak determines the ρ-value of the reflecting plane. The indices of the plane are determined by the θ-value of the characteristic spot or spots which occur in the streak. Finally, the displacement of the streak from one end of the centre line of the photograph gives the ϕ-value, and the orientation of the reflecting plane is thereby fixed relative to the specimen. From the orientation of two or three indexed planes the orientation of the crystallographic axes may be determined.

3.2 Laue-photograph methods. The chief merit of the Laue method is that the crystal is stationary during the exposure. The major difficulty is that the lack of knowledge of the wave-length which produced any particular spot makes it impossible in general to identify a spot by direct methods. If any symmetry is visible in the photograph, or if a well-marked ellipse can be seen, that is very helpful; but otherwise, use of the Laue method alone is unlikely to succeed.

For simple cubic crystals, sets of standard Laue photographs have been prepared (Majima and Togino, 1927), but these are just the kind of crystals which are easiest to orientate by more direct methods. A similar procedure could be applied to any given uniaxial crystal which was being studied as a routine process, but it would not in general be practicable for a crystal of lower symmetry than that. Even for a biaxial crystal it is possible for the investigator to learn to identify certain ellipses of spots if he is studying several examples of the same substance, but this would be workable only if the cell size were not too large.

Let us consider the ways in which the problem can be tackled.

(1) It may happen that a Laue spot is produced by reflection of a characteristic radiation, $K\alpha$ or $K\beta$; from the value of θ for this spot it may be possible to index the reflection and hence to get a useful start in plotting the projection; this is particularly true when the identified spot is at the intersections of two or more prominent conic sections.

(2) If the photograph shows some prominent conic sections, the corresponding great circles can be plotted on a projection; on the projection these zones may reveal characteristic angles between them which may enable them to be identified. This of course amounts to the same thing as (1) but is of more general application, and angles of 30°, 45°, 60°, 90° or 120° are of particular use.

(3) If it is thought that a prominent conic section may correspond to a plane of symmetry, the adjustment needed to bring this into a suitable orientation

for checking can be made, and two or more Laue photographs taken before plotting is attempted.

Planes of symmetry containing the incident beam and axes of symmetry parallel to it are more readily displayed on flat-plate photographs than on cylindrical ones. In general, however, a cylindrical film plane of symmetry. Thus the ellipse of spots, 1, 2, 3 . . . 7, which goes upwards from spot 1, has its counterpart in an ellipse which goes downwards through the same spot. The crystal is not set so that the plane of symmetry is exactly normal to the axis of the camera, and therefore allowance must be

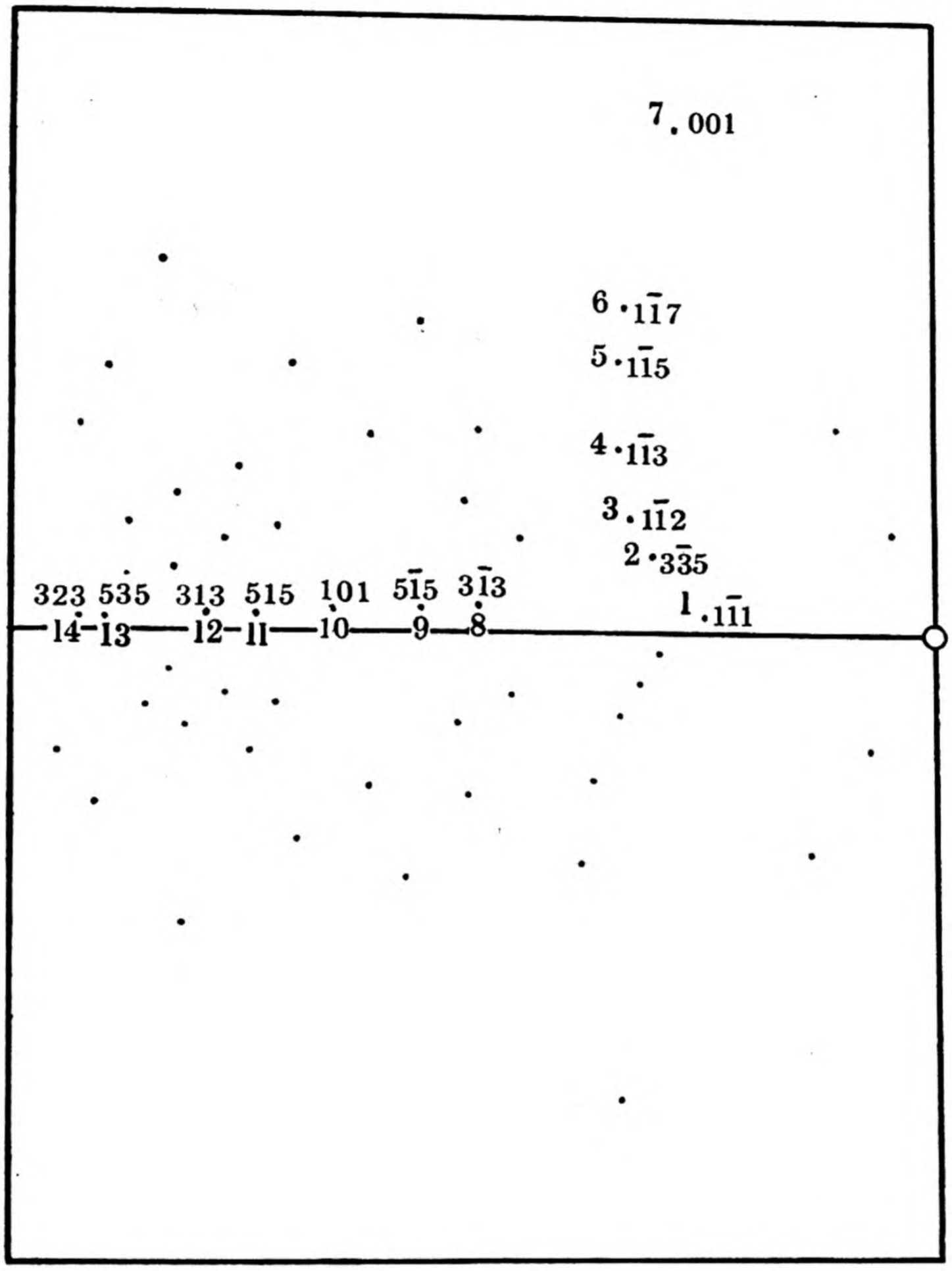

FIG. 110. Indexed diagram of Laue photograph of diamond. Cylindrical (half) film with $r = 3$ cm.

photograph should also be taken, since considerably more reflections are obtained than with flat film.

We shall determine the orientation of the diamond crystal from the Laue diagram of Fig. 110. Since the photograph was taken on a cylindrical film, the stereographic projection is the most convenient method of representation. The ρ and ϕ values of the spots on two of the most prominent ellipses are read by means of the appropriate chart and tabulated. Probably the series of spots, 1, 8, 9 . . . 14 has been produced by planes the normals to which lie in a made for the fact that the portions of the two ellipses passing through spot 1 are not exact mirror images of one another on the photograph. We next proceed to identify the indices of particular spots along the series corresponding to the plane of symmetry. In Fig. 111 great circles have been drawn through both series of poles, and at point 1 it will be seen that they intersect at an angle of 60°. We can therefore be sure that the indices of spot 1 are of the form {111}, since only at poles of this form does a plane of symmetry intersect other important zones at an angle of 60°.

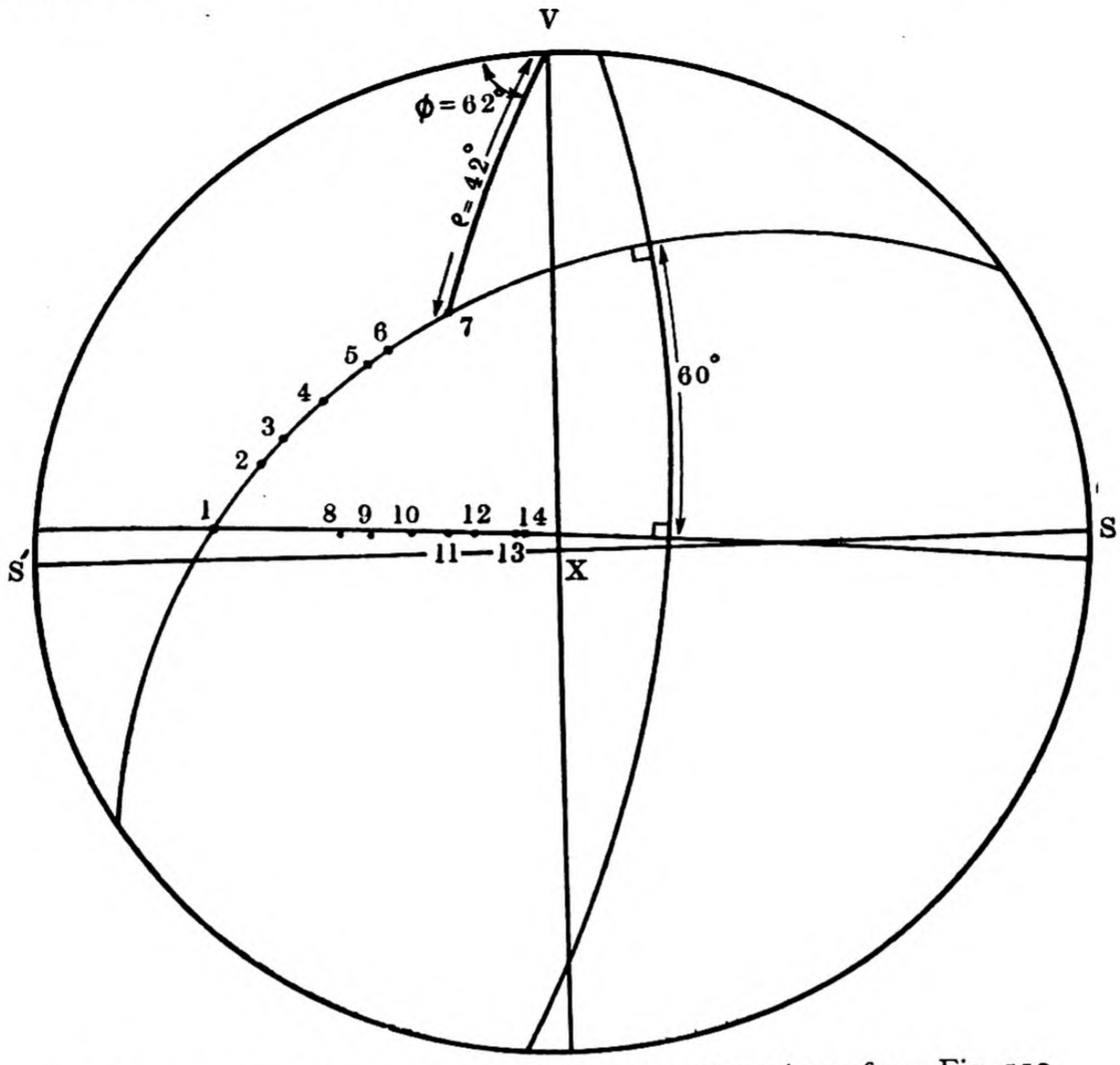

FIG. 111. Stereogram showing orientation of specimen from Fig. 110

Further, by measurement with the stereographic net it can be found that the angle between the poles 1 and 7 in Fig. 111 is 55°, which is the angle between neighbouring poles of the forms {111} and {100}. Thus we can assign indices of the form {100} to spot 7.

NUMBER OF SPOT	ρ	ϕ	INDICES
1	86°	23°	$1\bar{1}1$
2	74°	30°	$3\bar{3}5$
3	69°	33°	$1\bar{1}2$
4	61°	39°	$1\bar{1}3$
5	53°	46°	$1\bar{1}5$
6	50°	50°	$1\bar{1}7$
7	42°	62°	001
8	86°	45°	$3\bar{1}3$
9	87°	51°	$5\bar{1}5$
10	87°	59°	101
11	88°	67°	515
12	88°	72°	313
13	88°	81°	535
14	88°	83°	323

Although it is not necessary to determine the indices of all the other spots in this zone for the purpose of orientating the crystal, this is done here for the sake of completeness. In finding these indices it is best to change the plane of projection so as to bring the poles into their normal positions on a cubic stereogram. From Fig. 112 it can be seen that, in order to bring pole 7 to the centre, the projection must be rotated through an angle of 53° about the direction marked. A subsequent rotation of 18° about the centre will bring the stereogram into the standard orientation. The indices of poles along the zone 1–7 are most easily found by using the ratios of the tangents of the angles which they subtend with the pole (001). For example, tan 6∧7 = (approx.) 1/7 of tan 1∧7 and hence the indices of pole 6 are 117. For the poles along the zone 1–14 a few trials with the equation for the angle between two face normals (1, 3.9) may be used to give the indices. This method is convenient only when the indices are not high, but the equation can be used to calculate all possible angles between poles in a given zone and hence to give the indices of the pole to which the angle is measured.

The treatment given here is expressed in terms of a cubic crystal, but if the crystal had any other symmetry the same principles would be applied. From

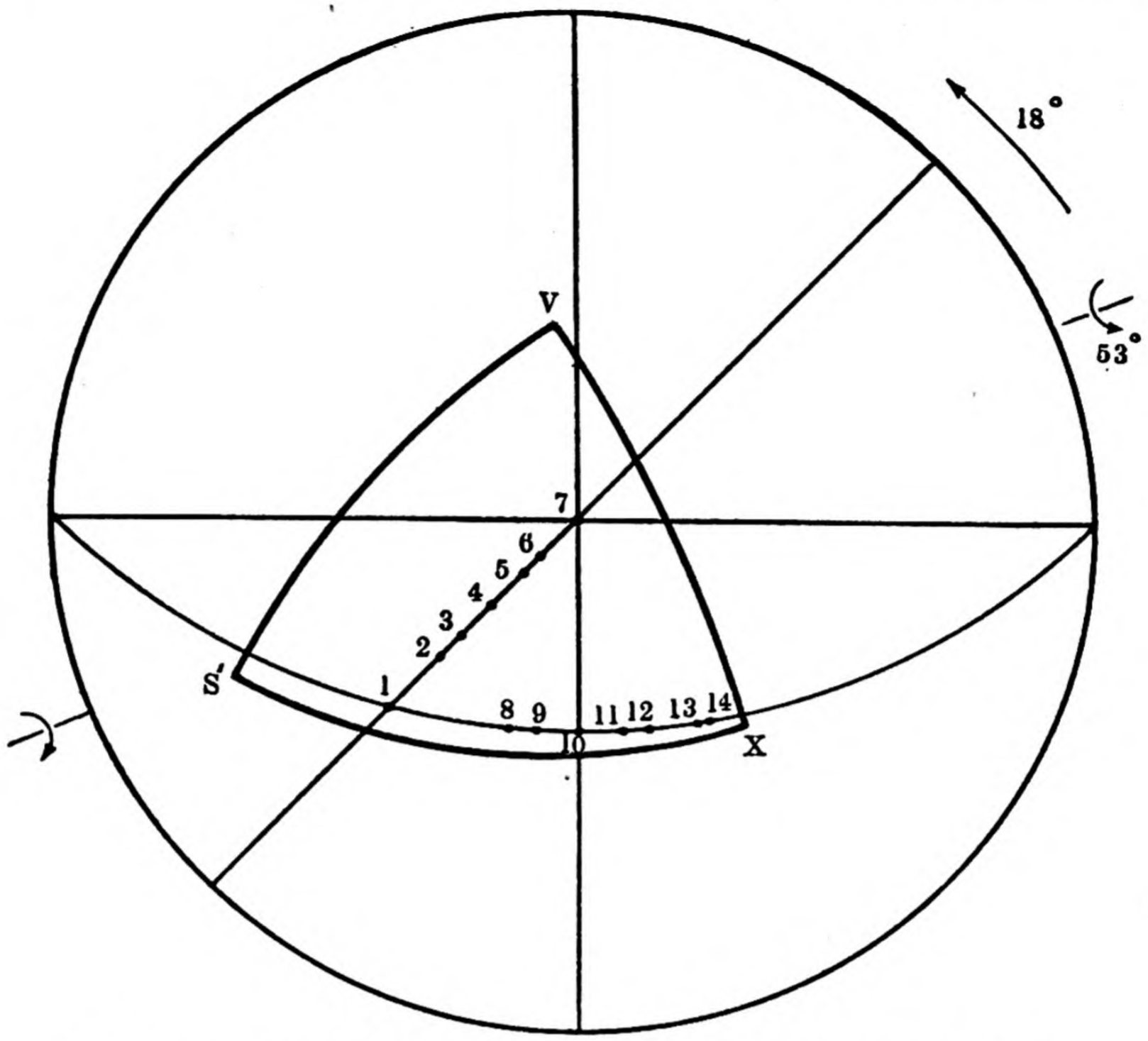

FIG. 112. Stereogram showing the orientation of Fig. 111 re-projected

the ρ-, ϕ-values a stereographic projection would be made and then such rotations as might be necessary to obtain a symmetrical projection would be applied. The indices would then be obtained by comparing the actual stereogram with one drawn on the basis of the known axial ratios and axial angles.

3.3 Combination of Laue and oscillation photographs. The uncertainty of the result of orientating a crystal from an oscillation photograph, owing to the movement of the crystal, can be overcome by combining this photograph with a Laue photograph on the same piece of film. Although this combination method is more elegant and accurate than the simple use of oscillation photographs, it does depend on the identification of at least three spots produced by the characteristic radiation. An oscillation photograph is first taken with unfiltered radiation, and the angle of oscillation, usually 5°, 10° or 15°, is chosen so as to give several characteristic spots. When the crystal has many reflections it is advantageous to reduce the angle of oscillation, as this reduces the likelihood of different streaks running into each other. After the oscillation photograph is finished, the crystal is left stationary at one of the two ends of the oscillation while the exposure is continued long enough to produce Laue spots. Thus a Laue spot is imprinted by reflection from the stationary crystal, and the Laue spot corresponding to a set of planes which gave rise to a characteristic spot will lie at one end of the same streak. According to the extremity at which the crystal was stopped, the Laue spots on one side of the photograph will be at the end of the streak which has either the lower or the higher value of θ; on the other side of the photograph the reverse will occur (Fig. 114.1). There will, of course, be many more Laue spots than characteristic spots, but each streak will carry a Laue spot, except when a streak comes to an end by reason of the fading out of the radiation supplied by the tube before the stationary position of the crystal is reached. This is not troublesome in practice because the streaks which carry characteristic spots will usually carry Laue spots also, unless the potential is unusually low (see **2**, 1.3).

Below are tabulated the possible reflections from diamond ($a = 3{\cdot}56$ A.) for three targets.

From this table it can be seen that copper radiation is the most suitable for diamond, since molybdenum would produce too many spots and iron too few, at

DIAMOND

$h^2+k^2+l^2$	hkl	d in A.	VALUE OF θ IN DEGREES					
			FeKα	FeKβ	CuKα	CuKβ	MoKα	MoKβ
3	111	2·05	28	25	22	20	10	9
8	220	1·26	50	44	$37\frac{1}{2}$	$33\frac{1}{2}$	$16\frac{1}{2}$	$14\frac{1}{2}$
11	311	1·07	$64\frac{1}{2}$	55	46	$40\frac{1}{2}$	$19\frac{1}{2}$	17
16	400	0·89	—	82	60	$51\frac{1}{2}$	$23\frac{1}{2}$	$20\frac{1}{2}$
19	331	0·82	—	—	$70\frac{1}{2}$	$58\frac{1}{2}$	$25\frac{1}{2}$	$22\frac{1}{2}$
24	422	0·726	—	—	—	73	29	$25\frac{1}{2}$
27	511 ; 333	·685					31	$27\frac{1}{2}$
32	440	·629					$34\frac{1}{2}$	30
35	531	·602					36	$31\frac{1}{2}$
40	620	·563					39	34
43	533	·543					41	$35\frac{1}{2}$
48	444	·514					$43\frac{1}{2}$	38
51	711 ; 551	·498					$45\frac{1}{2}$	$39\frac{1}{2}$
56	642	·476					$48\frac{1}{2}$	$41\frac{1}{2}$
59	731 ; 553	·463					50	43
64	800	·445					53	45
67	733	·435					$54\frac{1}{2}$	$46\frac{1}{2}$
72	822	·420					58	49
75	751 ; 555	·411					$59\frac{1}{2}$	50
80	840	·398					63	$52\frac{1}{2}$
83	911 ; 753	·391					$65\frac{1}{2}$	54
88	664	·380					$69\frac{1}{2}$	56
91	931	·373					72	$57\frac{1}{2}$
96	844	·363					$77\frac{1}{2}$	60
99	933 ; 771 ; 755	·358					83	62

Note.—Several other reflections can occur for MoKβ with $\theta > 62°$.

least in certain orientations. From the photograph (Fig. 114.1) the θ values of the characteristic spots are read by means of a chart. This enables us to determine the indices of the streaks, and these can be inserted in the photograph. The Laue spots which belong to the indexed streaks are noted and their ρ- and ϕ-values read by means of the appropriate chart. These values are tabulated below.

INDEXED LAUE SPOTS IN FIG. 114·1

No.	{hkl}	POSITION ON FILM	ρ	$(90-\phi)$
1	311	upper left	68°	27°
2	311	upper right	61°	43°
3	220	upper right	83°	65°
4	331	lower right	72°	20°
5	311	lower right	69°	48°
6	311	lower left	61°	23°
7	400	lower left	86°	25°
8	311	lower left	85°	49°

From these values the poles of the reflecting planes are now plotted on a stereogram (Fig. 114.2), those poles which occur below the plane of the projection being represented by the diametrically opposite pole for convenience. It is clear that the pole (No. 7) of a tetrad axis lies at an equal angular distance of 25° from the poles 1 and 6, and we can index these two latter poles as 113 and $\bar{1}\bar{1}3$ respectively. The great circle of which No. 7 is the pole is now drawn ; the great circle through 113 and $\bar{1}\bar{1}3$ cuts the first great circle at the pole $\bar{1}\bar{1}0$. Along the first great circle the poles $\bar{1}00$ and 010 can be inserted at angles of 45° and 135° respectively from $\bar{1}\bar{1}0$. Now the specimen was set with the reference plane normal to the incident beam and the reference direction vertical during the Laue exposure. Consequently, if we mark the upper end of the reference direction and insert this on the stereogram, the latter is a complete representation of the crystal orientation of the specimen. Alternatively, we can quote the values,

$$X:(\bar{1}00)=73°,\ X:(010)=73°,\ X:(001)=25°.$$

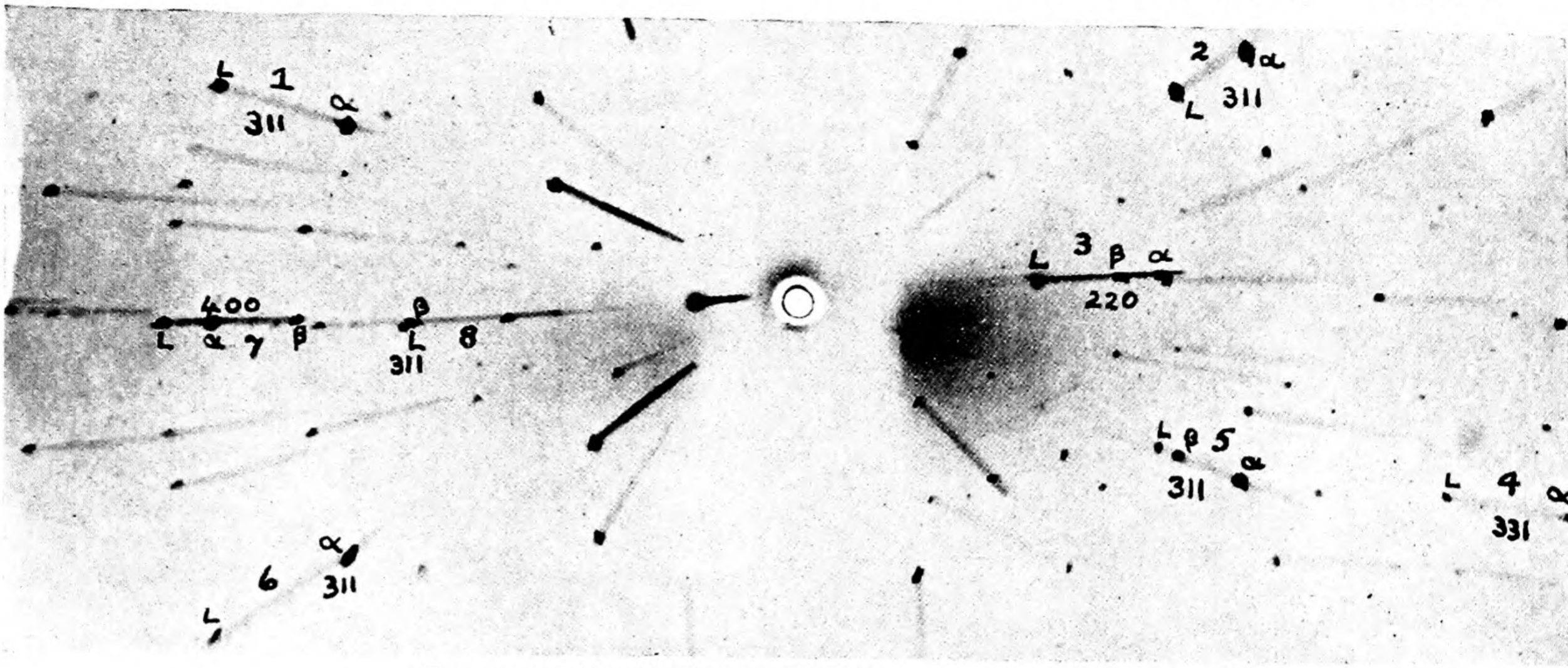

FIG. 114.1. Combined Laue-Oscillation photograph (indexed)
Specimen : diamond, with 15° oscillation. Camera : cylindrical, $r = 3$ cm. Radiation : CuK (unfiltered).
L : Laue spots. α and β : spots produced by characteristic radiations

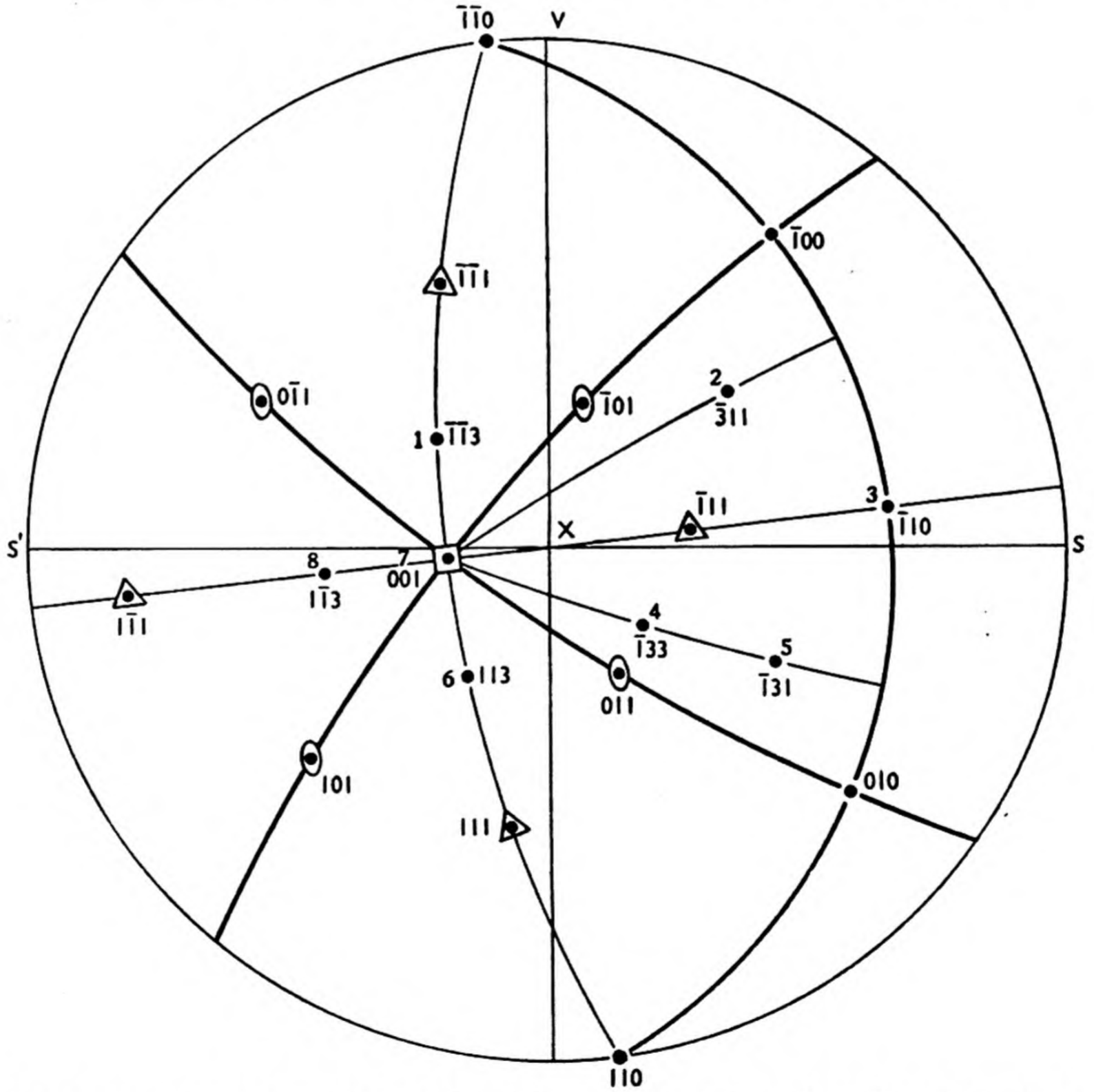

FIG. 114.2. Stereogram derived from Fig. 114·1 showing orientation of specimen.
The numbered poles are those plotted from the photograph

4. Determination of Orientation by the Ionisation Spectrometer

4.1 Introduction. For our present purpose it is only necessary to note that an ionisation spectrometer consists essentially of collimating slits, a crystal holder and an ionisation chamber which is used to record the reflection of X-rays from the crystal. For the orientation of crystals it is an advantage to have a crystal holder of relatively elaborate design, in that all possible orientations of the crystal relative to the incident X-rays and the ionisation chamber can be readily obtained. In contrast with the photographic methods, the recording of the ionisation current is almost instantaneous, and if the investigator is experienced, the orientation can be carried out in a very short time. For routine purposes the ionisation method is generally superior to the photographic and, provided that the crystal gives sharp reflections, the accuracy obtainable is much greater than can be obtained with photographic cameras of normal size. With suitable crystals an accuracy of orientation of a few minutes of arc can be achieved by means of the ionisation spectrometer, whereas with photographic methods the accuracy is usually considerably less.

One of the limitations of the ionisation method which is sometimes serious is that it is not applicable to crystals smaller than a cube of side about one millimetre. However, if Geiger counters are used instead of ionisation chambers, the sensitivity to reflected X-rays is much greater, and crystals as small as can conveniently be handled may be orientated. A further condition which must be satisfied in order that a crystal may be orientated completely is that its unit-cell dimensions must already be known. If a partial orientation is required, such as, for example, the determination of the basal plane, then it is only necessary to know the spacing of that plane.

The procedure in using the ionisation spectrometer is fundamentally the same whatever the purpose in hand. The chamber is set at such an angle (2θ) that it can pick up the reflected beam when the crystal is suitably orientated with respect to the incident beam. The crystal is now turned about one or other of the axes of adjustment until the recording apparatus indicates that reflected X-rays are entering the chamber. A plane of known spacing, and therefore of known orientation with respect to the crystallographic axes, is now arranged at a glancing angle θ to the incident beam, and the normal to the plane bisects the angle between the incident and reflected beams. This procedure may be repeated for two or more planes. Finally, the external faces, whether natural or ground and polished, must be related to the planes reflecting the X-rays. This is usually achieved by using a microscope or telescope mounted on the spectrometer either in line with the incident beam of X-rays or at right angles to it.

4.2 Orientating a flat plate. A problem which often arises is to find at what angle a ground and polished face is inclined to a given crystallographic plane nearly parallel to the face. If the crystal is not too large, it can be mounted on the holder of a vertical graduated circle and the experiment may be carried out in two ways. In one method the polished face is set parallel to the plane of the vertical circle. The vertical circle is now rotated until the X-rays are reflected from a crystallographic plane which is nearly parallel to the polished face. If the inclination of the crystallographic plane to the polished face is ϕ, then if the crystal is rotated to a number of positions about the vertical circle the maximum difference in the glancing angle of incidence would be 2ϕ. Finally, the setting, relative to the vertical circle, for which the glancing angle of incidence is a maximum gives the complete orientation of the normal to the reflecting lattice plane relative to the external form of the crystal. For many purposes this is sufficient, but sometimes the orientation of the crystallographic axes relative to the external form is required, and in that case the process must be repeated for a second lattice plane.

The alternative procedure is to bring the lattice plane into parallelism with the plane of the vertical circle. This is done by adjusting the crystal so that on rotation of the vertical circle there is no change in the intensity of reflection. The direction of the normal to the polished face can then be determined by means of the telescope.

Fundamentally, these two methods are the same, except that the reflecting plane for light is made parallel to the vertical circle in one method, whereas in the other the reflecting plane for X-rays is in this position.

4.3 Orientating a crystal without natural faces. The problem of finding the orientation of the crystal axes with respect to the external form also arises in connection with diamond dies, cutting tools, gramophone pick-ups, and jewel bearings, which usually have no natural crystal faces.

A diamond die is usually prepared with two flat faces perpendicular to the axis of the die channel. One of these faces, together with a straight line drawn on it, defines a set of three reference axes. One of these axes is perpendicular to the flat face, one lies along the line drawn in the flat face, and the third is perpendicular to the other two. Similarly, a diamond cutting tool usually has a flat face on which at least one straight edge has been ground, and this serves to define the axes of reference. On jewel bearings there are usually no optically flat faces, and it is therefore not possible to determine accurately the

orientation of the axes with respect to the external form without further preparation.

We shall suppose that we require to find the orientation of the crystallographic axes of a diamond die relative to one of its flat faces and a line drawn on this face. The die is set up on the vertical circle with any arbitrary orientation; the ionisation chamber is set at an angle of $2\theta_{111}$ (which for Mo$K\alpha$ is 19° 50′) where θ_{111} is the Bragg angle for the 111 reflection. The axis of the inner graduated circle is set vertical and the crystal is slowly rotated about this axis. If no deflection is observed in the indicating meter, the vertical circle is rotated through 5° and the previous rotation about the inner axis is then repeated. As there are eight octahedral planes it does not usually take more than a few minutes to pick up a reflection from one of them in the ionisation chamber. The arcs are now adjusted until the plane of the form {111} which has been found lies exactly in the plane of the vertical circle. It is easy to test when this setting has been achieved, because on rotating the vertical circle the intensity of the reflection remains unchanged. One crystallographic direction, namely the normal to a {111} plane, is now fixed relative to the vertical circle.

To complete the determination of the orientation it only remains to fix another {111} plane. The angle between the normals to pairs of {111} planes is either 70° 32′ or the supplement of this angle. Thus the normal to the second plane we are seeking lies somewhere on a cone of semi-angle 70° 32′ described about the axis of the vertical circle. The plane of the vertical circle is now set to ($\theta_{111} \pm 70°\ 32'$) with respect to the X-ray beam, the chamber being left at the same setting, $2\theta_{111}$, as before. The vertical circle is now rotated about its own axis until a reflection is registered. In this setting another plane of the form {111} has its normal in a horizontal plane. The orientation of the crystallographic axes can be determined from the known orientation of the two {111} planes, the angles between the cubic axes and the normals to these planes being 54° 44′.

We are now at the stage of knowing where the cubic axes are directed relative to the axis of the vertical circle; they are inclined at an angle of 54° 44′ to this axis and lie in three planes intersecting at angles of 120° in the axis of the vertical circle. One of these planes is horizontal, and the tetrad axis lying in that plane is the obtuse bisector of the angle between the two {111} normals, and this makes an angle of 54° 44′ with each of the two normals. We also know how the diamond is orientated with respect to the vertical circle; the exact definition of this relation is simply the usual problem in optical goniometry and is solved by passing a collimated light beam down the X-ray aperture and using a telescope to pick up the reflected light beams. Finally, the crystallographic axes may be referred to the flat face on the die and the line drawn on it.

5. Orientation in Twin Crystals

5.1 Introduction. When there is a chance that the specimen may be twinned, special care is necessary in interpreting X-ray photographs. If the specimen is transparent it should always be examined under the polarising microscope in the first place; twins are often easily recognised in polarised light, except of course in the cubic system. If the incident X-ray beam falls on both parts of the twin, the photographs

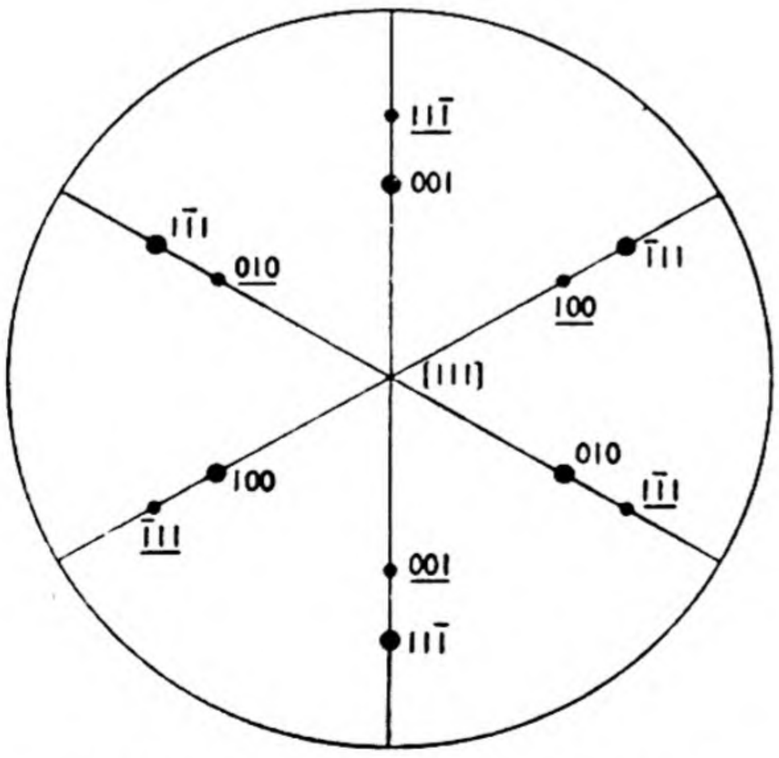

FIG. 116.1. Stereogram of two forms {100} and {111} in a spinel twin of diamond; this shows the pseudo-hexagonal symmetry of the twin. Upper poles only are given and the indices of those in the twinned orientation are underlined

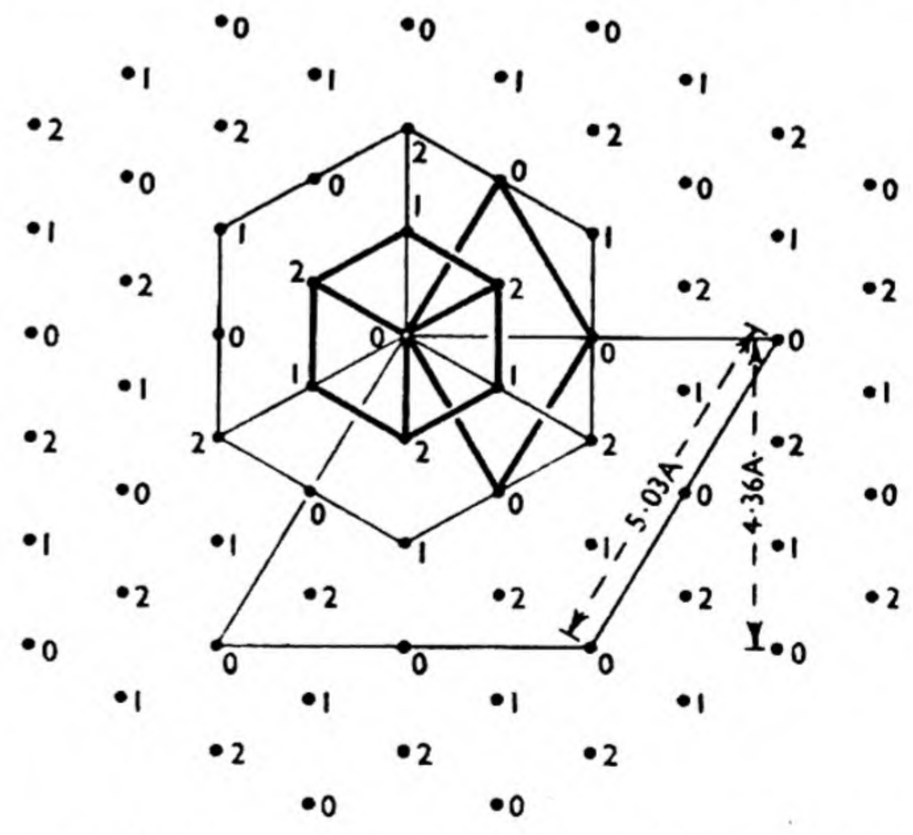

FIG. 116.2. Bravais lattice of diamond projected on (111).

The heavy lines show the smallest unit-cells (rhombohedral and hexagonal) and the light lines the quadruple rhombohedral cell (face-centred cube) and the corresponding hexagonal cell

will contain spots produced by planes belonging to two different crystal orientations. In the following sections, one example of a cubic twin and one of a common type of monoclinic twin are studied briefly in order to illustrate the difficulties which arise in the interpretation of X-ray photographs of twin crystals.

5.2 Study of examples of twins. In the cubic system the commonest type of twinning is that in which the twin axis is ⟨111⟩ and the composition plane. A Laue photograph of a single crystal of diamond, taken with the X-ray beam along the triad axis, shows the symmetry $\bar{3}m$, but the twin operation converts this into $6/mmm$, which is the symmetry observable in such a Laue photograph of a spinel twin. If the specimen were opaque this might present a real difficulty, but with a transparent substance its cubic symmetry could have been detected by optical study.

Let us assume, however, that from the Laue photograph it is deduced that the specimen is a single

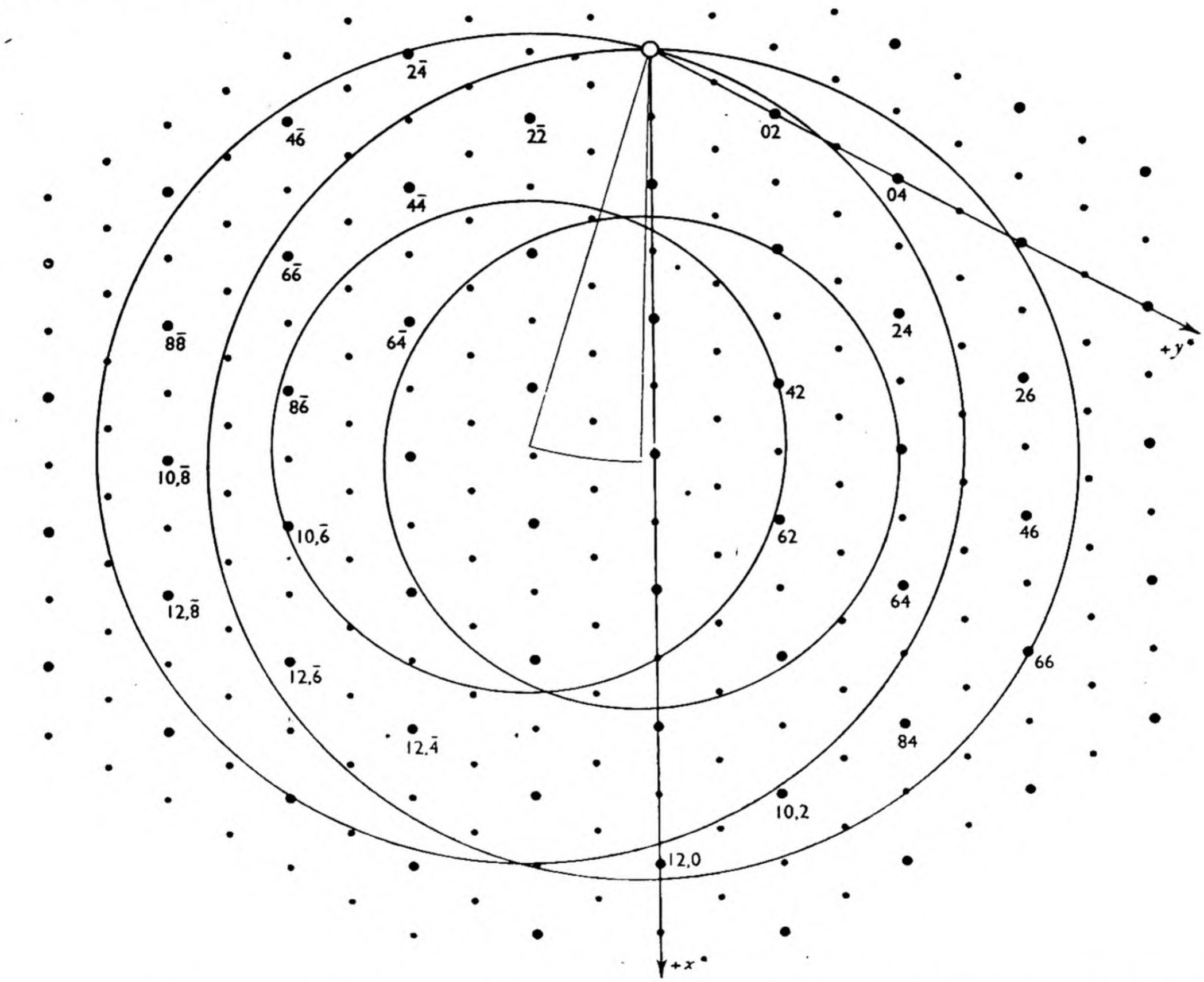

FIG. 117. Reciprocal lattice of diamond, projected on (0001), which is based on the hexagonal unit cell corresponding to the face-centred rhombohedron (cube).

The large dots form the reciprocal lattice based on the smallest hexagonal unit cell. The lunes shown are for the zero and the 7th layers.

Scale : 1 unit = 5 cm. $c^* = 0{\cdot}115$

plane is the plane normal to the twin axis, and these are called *spinel twins* (**1**, 4.2). In diamond such twins are fairly common (Figs. 17 (*a*). 116.1). Since we are concerned only with centro-symmetrical arrangements, a rotation of 180° about the twin axis is equivalent, in a normal twin, to a reflection across the twin crystal of hexagonal symmetry. The cell size can be obtained from oscillation photographs in the usual way and the refined values of these are :

$$c = 6{\cdot}16, \quad a = 2{\cdot}51_7 \text{ A.}$$

But in order to show the relation of the hexagonal

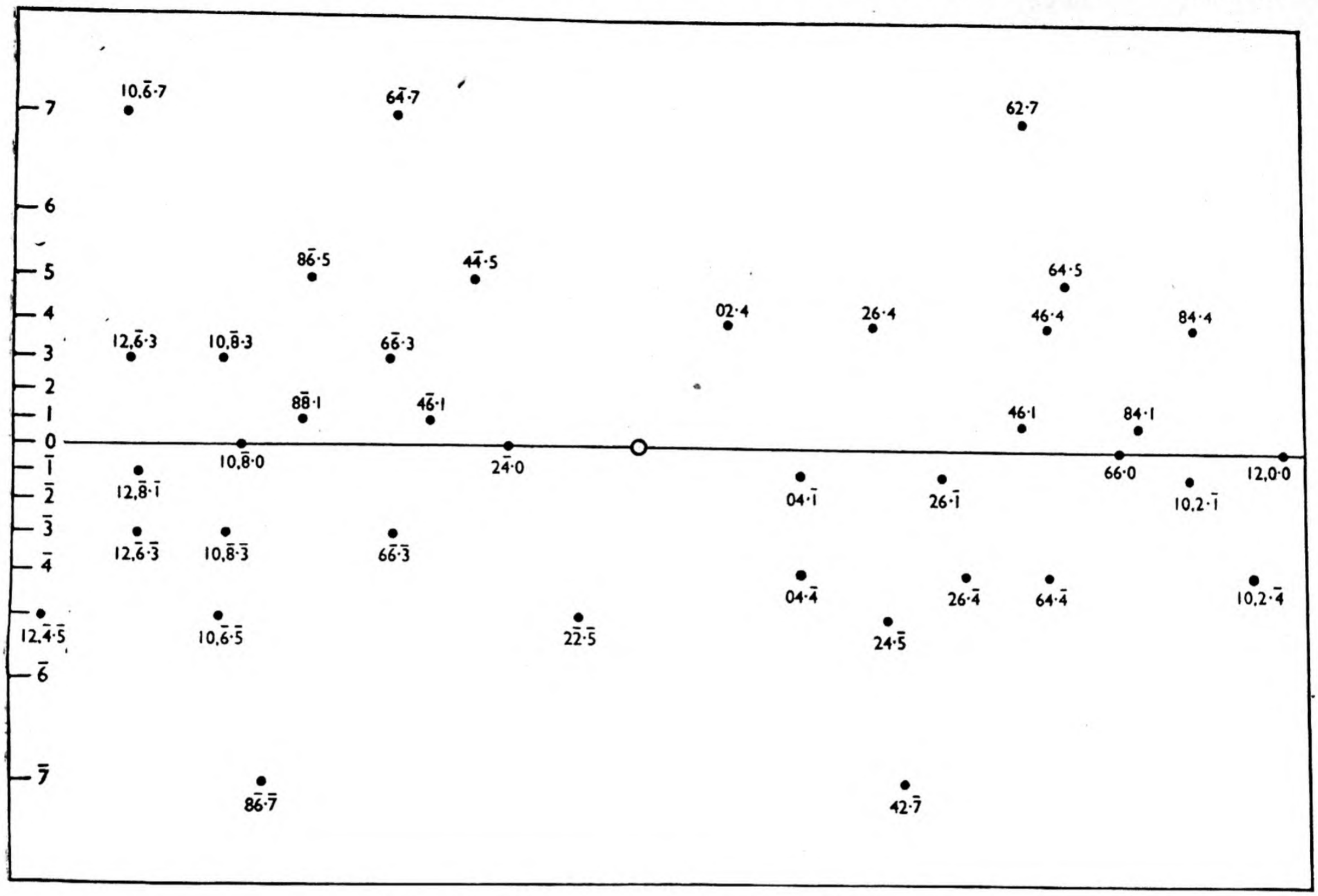

FIG. 118. Indexed diagram of oscillation photograph

Specimen : diamond oscillated through 15° about triad axis (see Fig. 117)

Camera : cylindrical, $r = 3$ cm. Radiation : Mo$K\alpha$, $\lambda = 0{\cdot}71$ A.

The spots shown are those obtained from a single crystal or from one of the two component orientations in a spinel twin

indices to the real cubic ones we shall take a quadruple cell which has

$$c = 6{\cdot}16, \quad a = 5{\cdot}03 \text{ A.}$$

This gives the ratio $c/a = 1{\cdot}224$, which is that for a cube described on hexagonal axes. The projection of the lattice is given in Fig. 116.2, where it can be seen that the rhombohedral cell corresponding to the quadruple cell is face-centred. An oscillation photograph was taken with molybdenum K_α radiation ($\lambda = 0{\cdot}71$ A.) and with the pseudo-hexad axis as oscillation axis. The appropriate reciprocal lattice is given in Fig. 117 and has $c^* = 0{\cdot}115$ and

$$a^* = \lambda/(a \,.\, \cos 30°) = 0{\cdot}163.$$

By means of this, indices can be assigned to all the spots without difficulty. Since the zero-layer line in the photograph is a line of symmetry, to each spot hk^*l there corresponds a spot $hk^*\bar{l}$.

Careful study of these indices, however, reveals certain relations which are not found in hexagonal crystals. If we apply the test for a rhombohedral lattice (**10**, 1.5), we find that half the indices obey the condition for the obverse orientation of the rhombohedron ($-h+k+l = 3n$), whereas the other half obey the condition for the reverse orientation ($h-k+l = 3n$). The positions of the spots produced by the part of the twin in the obverse orientation are given in Fig. 118, and the positions of the spots produced by the other part of the twin can be obtained from these by operating the zero line as a line of symmetry. The indices of both sets of spots are given in the table opposite (columns 2 and 3). The rhombohedral indices of column 1 are derived from those of column 2 by operating the appropriate matrix (obverse) given in **10**, 1.4. The indices of column 1 are the familiar cubic indices of diamond. In this example optical

SECT. 5

INDICES FROM OSCILLATION PHOTOGRAPH OF DIAMOND (SPINEL TWIN)

Left Side			Right Side		
Obverse		Reverse	Obverse		Reverse
1 $p_1q_1r_1$	2 $h_1k_1\cdot l_1$	3 $h_2k_2\cdot l_2$	1 $p_1q_1r_1$	2 $h_1k_1\cdot l_1$	3 $h_2k_2\cdot l_2$
$7\bar{3}3$	10, $\bar{6}\cdot 7$	10, $\bar{6}\cdot\bar{7}$	$71\bar{1}$	$62\cdot 7$	$62\cdot\bar{7}$
$5\bar{1}3$	$6\bar{4}\cdot 7$	$6\bar{4}\cdot\bar{7}$	$71\bar{3}$	$64\cdot 5$	$64\cdot\bar{5}$
$5\bar{3}3$	$8\bar{6}\cdot 5$	$8\bar{6}\cdot\bar{5}$	$80\bar{4}$	$84\cdot 4$	$84\cdot\bar{4}$
$3\bar{1}3$	$4\bar{4}\cdot 5$	$4\bar{4}\cdot\bar{5}$	$62\bar{4}$	$46\cdot 4$	$46\cdot\bar{4}$
$7\bar{5}1$	12, $\bar{6}\cdot 3$	12, $\bar{6}\cdot\bar{3}$	$42\bar{2}$	$24\cdot 4$	$24\cdot\bar{4}$
$5\bar{5}3$	10, $\bar{8}\cdot 3$	10, $\bar{8}\cdot\bar{3}$	$22\bar{0}$	$02\cdot 4$	$02\cdot\bar{4}$
$3\bar{3}3$	$6\bar{6}\cdot 3$	$6\bar{6}\cdot\bar{3}$	$71\bar{5}$	$84\cdot 1$	$84\cdot\bar{1}$
$3\bar{5}3$	$8\bar{8}\cdot 1$	$8\bar{8}\cdot\bar{1}$	$51\bar{5}$	$46\cdot 1$	$46\cdot\bar{1}$
$1\bar{3}3$	$4\bar{6}\cdot 1$	$4\bar{6}\cdot\bar{1}$	$8\bar{4}\bar{4}$	12, $0\cdot 0$	12, $0\cdot 0$
$4\bar{6}2$	10, $\bar{8}\cdot 0$	10, $\bar{8}\cdot 0$	$60\bar{6}$	$66\cdot 0$	$66\cdot 0$
$0\bar{2}2$	$2\bar{4}\cdot 0$	$2\bar{4}\cdot 0$	$11\bar{3}$	$04\cdot\bar{1}$	$04\cdot 1$
$5\bar{7}1$	12, $\bar{8}\cdot\bar{1}$	12, $\bar{8}\cdot 1$	$31\bar{5}$	$26\cdot\bar{1}$	$26\cdot 1$
$1\bar{5}1$	$6\bar{6}\cdot\bar{3}$	$6\bar{6}\cdot 3$	$73\bar{5}$	10, $2\cdot\bar{1}$	10, $2\cdot 1$
$3\bar{7}1$	10, $\bar{8}\cdot\bar{3}$	10, $\bar{8}\cdot 3$	$00\bar{4}$	$04\cdot\bar{4}$	$04\cdot 4$
$5\bar{7}\bar{1}$	12, $\bar{6}\cdot\bar{3}$	12, $\bar{6}\cdot 3$	$20\bar{6}$	$26\cdot\bar{4}$	$26\cdot 4$
$\bar{1}3\bar{1}$	$2\bar{2}\cdot\bar{5}$	$2\bar{2}\cdot 5$	$4\bar{2}\bar{6}$	$64\cdot\bar{4}$	$64\cdot 4$
$3\bar{7}\bar{1}$	10, $\bar{6}\cdot\bar{5}$	10, $\bar{6}\cdot 5$	$6\bar{4}\bar{6}$	10, $2\cdot\bar{4}$	10, $2\cdot 4$
$5\bar{7}\bar{3}$	12, $\bar{4}\cdot\bar{5}$	12, $\bar{4}\cdot 5$	$5\bar{1}\bar{5}$	$24\cdot\bar{5}$	$24\cdot 5$
$17\bar{1}$	$8\bar{6}\cdot\bar{7}$	$8\bar{6}\cdot 7$	$1\bar{3}\bar{5}$	$42\cdot\bar{7}$	$42\cdot 7$

Col. 1. Rhombohedral indices of reflections in column 2.
Col. 2. Hexagonal indices of reflections from part of twin with the *R*-lattice in obverse relation to the hexagonal axes.
Col. 3. Hexagonal indices of reflections related to those of column 2 by the zero line of symmetry ; these are produced by the part of the twin in the reverse relation to the hexagonal axes.

study would show cubic symmetry and consequently the X-ray photographs would reveal the twin. The possibility of twinning should, however, always be kept in mind and tests for this should be made where possible.

As an example of a monoclinic twin, we shall take gypsum, which has been studied in other sections.† In the common twin of gypsum the twin axis is normal to (100) which is the composition plane. It is clear that *y*- and *z*-axes are common to both parts of the twin, but that the *x*-axes are inclined to each other at an angle of $2(\beta - 90°)$ (Figs. 17 (*b*), 120.1). Consequently, oscillation photographs with either the *y*-axis or the *z*-axis as oscillation axis will have straight layer lines, just as with a single crystal, but the spots will be produced by lattice planes of both crystal orientations. If the *x*-axis of one part is taken as oscillation axis, the spots produced by the other part will lie on curved layer lines ; if these are seen the twinned nature of the specimen will be obvious. If the twin axis is taken as oscillation axis, neither part will give rise to straight layer lines, but the combined effect of the two sets of spots will show a horizontal line of pseudosymmetry (Fig. 119).

In Fig. 120.2 are shown a Laue photograph of gypsum and a 'twin photograph' produced by superposition of a second exposure on the first, after a rotation of 180° about the *z*-axis of the crystal. Such an operation is not morphologically equivalent to a rotation of 180° about the normal to {100}, but both operations have the same effect on the projection of the Laue

† Gypsum is studied also as an example in the following sections : oscillation photograph **5,** 2.7 ; Laue photograph **6,** 2.4 ; Weissenberg photograph **7,** 3.2 ; lattice and transformations of axes **10,** 1.2.

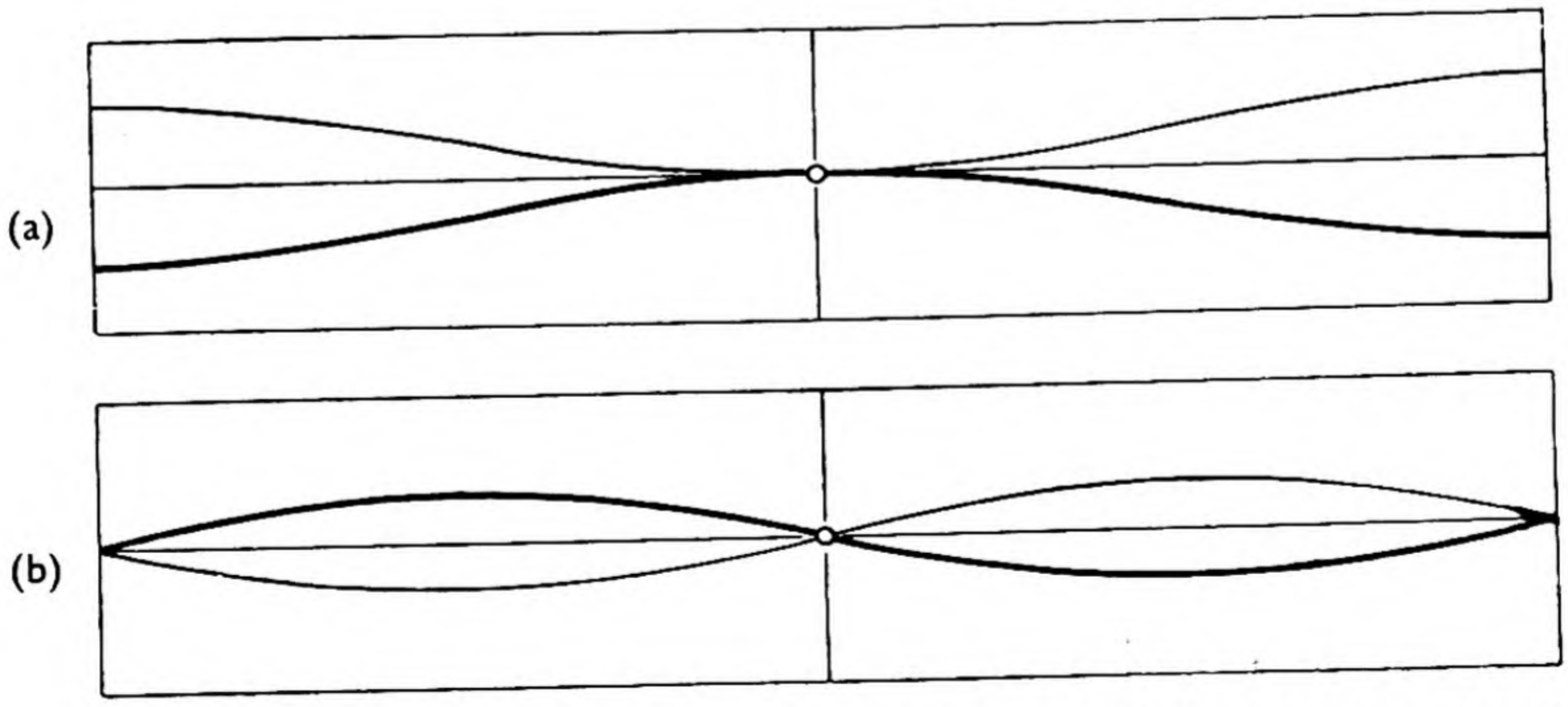

FIG. 119. Diagram of the zero-layer lines in oscillation photographs of a gypsum twin.

Vertical axis : the twin axis, normal to (100) (morph.).
Oscillation : (*a*) symmetrical about *z* (morph.)
(*b*) symmetrical about *y*.

The angle of tilt of the layer line corresponds to $\zeta_{[100]\ \mathrm{M\ \&\ W}}$ in Fig. 120.1.

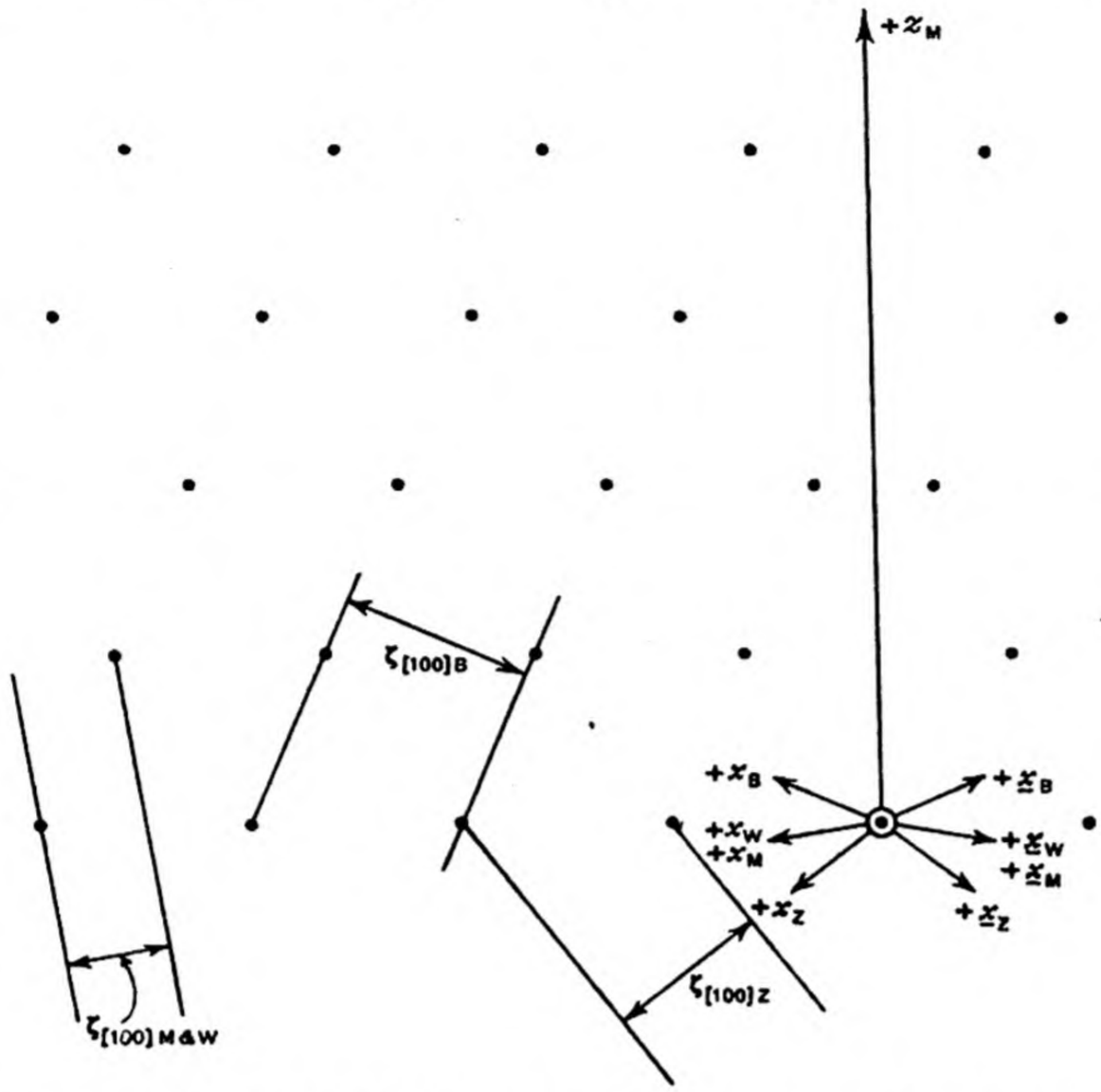

FIG. 120.1. Reciprocal lattice on (010) of gypsum twinned on (100) for $\lambda = 1{\cdot}54$ A. Scale: 1 unit = 5·0 cm. The directions of the crystallographic axes (of the Bravais lattice) are shown, along with $\zeta_{[100]}$ for the various choices of unit cell.

W, Wooster cell
B, Bragg cell
M, morphological cell } (Fig. 138)
Z, ' zone-edge ' cell (**5**, 2.7)

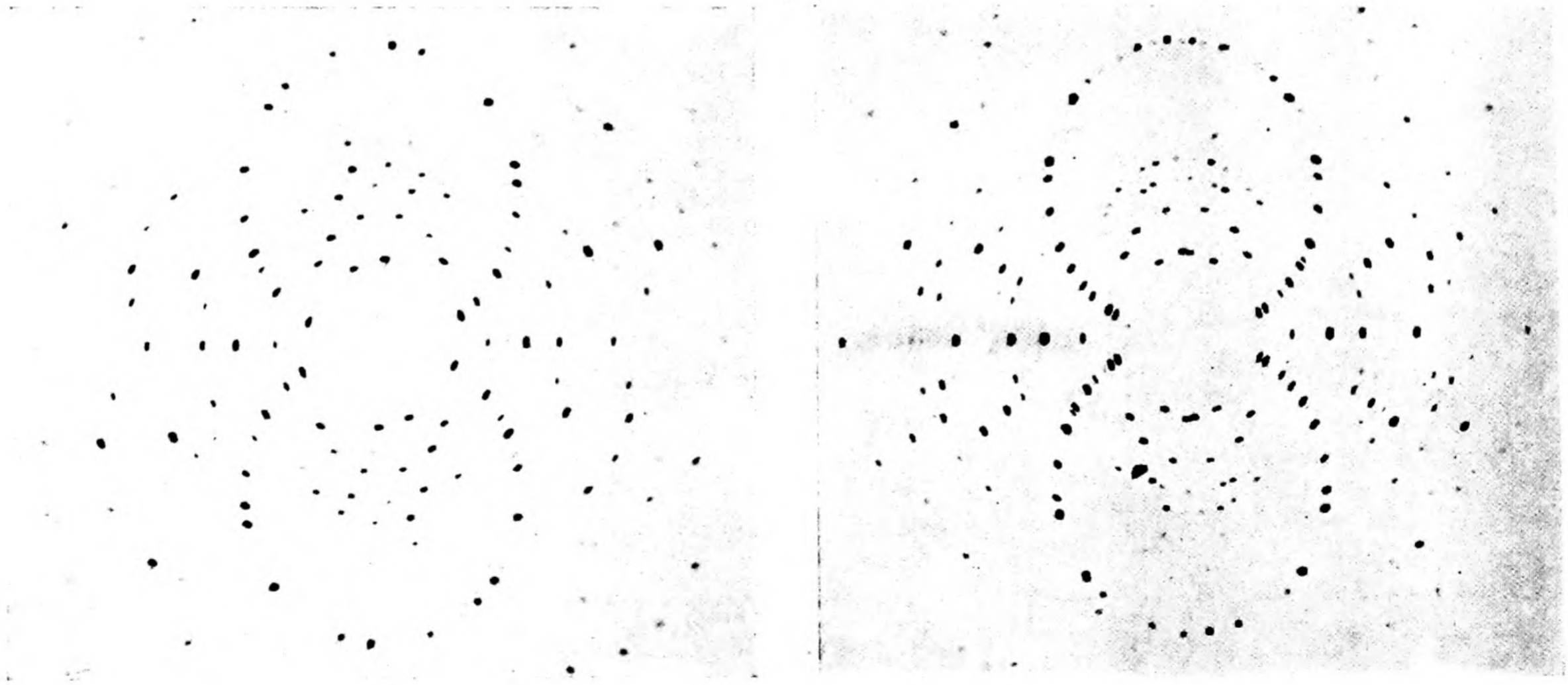

(a) (b)

FIG. 120.2. Laue photographs of gypsum on a flat front-plate camera at 3 cm. distance

(*a*) Single crystal with *z* (morph.) vertical and *y* parallel to the X-ray beam.

(*b*) Same as (*a*), but with a superposed photograph taken with the crystal turned through 180° about the vertical axis.

group which is obtained by taking such a Laue photograph. This second photograph simulates that of a twin on {100}, but owing to the very slight misadjustment of the crystal some of the spots do not quite match. In a photograph of a real twin the two sets of spots might be perfectly matched and the Laue group would then be taken as *mmm*. Preliminary optical study would, however, have revealed the twinned nature of the specimen.

In the examples of diamond and gypsum the twins are simple since there are only two individuals. In the gypsum twin, and along the triad twin axis in diamond, the effect is to raise the diffraction symmetry. In many examples of twinning, however, the effect is only one of pseudo-symmetry, which can be detected by proper technique. Pseudo-symmetric twinning is often repeated, giving rise to several individuals in the twin crystal, or else it is lamellar and consists of many individuals in two different orientations.

The mineral chrysoberyl is a good example of a pseudo-symmetric twin with six individuals. It is orthorhombic with $a = 4{\cdot}24$, $b = 9{\cdot}39$, and $c = 5{\cdot}47$ A. and the ratio $b : c = 1{\cdot}72$. This ratio is close to the value of $\sqrt{3}$ which occurs as the ratio of the two unit lengths of orthohexagonal axes normal to the hexad axis. The x-axis in chrysoberyl is, therefore, a pseudo-hexad axis, and normal twinning on 031 produces a combined twin lattice which is very close to that of a true hexagonal lattice. The angle between faces of the form {031}, twinned and untwinned, is only 28′. If such a specimen were equally developed and so small that all the individuals diffracted the incident beam to the same extent, it would be very difficult to discern that it was a twin and not a simple hexagonal crystal. Such specimens are usually large enough, however, to permit of adjustment so that only two individuals are involved and so that these diffract unequally. A Laue photograph of such a specimen, taken with the X-ray beam along the pseudo-hexad axis, would be hexagonal in the pattern of the spots, but not in their densities; the outer spots, also, would probably show a tendency to split up into two. An oscillation photograph, with the pseudo-hexad as oscillation axis might also show the split spots, but this would be likely only for high values of θ.

When twinning of this pseudo-symmetric type is on a fine scale, it is impossible to adjust the crystal so as to obtain different densities of spots from the two orientations and so use must be made of the splitting of the spots in order to detect the twinning. The technique employed must be adequate to show the splitting of the spots, the difficulty being greater the smaller the angle between the twinned and untwinned planes in the crystal. If the twinning has been observed under the microscope, the task is simply to find the twin law from the X-ray data. But sub-microscopic twinning has been postulated in order to account for some crystalline phenomena, and this could only be detected by X-ray methods. Even where the photographs show splitting of the high-θ spots, care must be exercised in the interpretation of this. A good example of this is given by Ito (1939) in the study of a special kind of felspar. He shows that three hypotheses could be advanced; first, a twinned triclinic crystal with the y-axis common to both orientations, thus simulating monoclinic symmetry; secondly, an intergrowth of a triclinic crystal with a monoclinic one, the y-axes being common; thirdly, an intergrowth of two monoclinic crystals with very similar unit cells. By constructing theoretical oscillation photographs from the three different reciprocal lattices and comparing these with the experimental data, Ito was able to show that the third hypothesis was the correct one. This is undoubtedly the only safe method in dealing with the splitting of spots observed on X-ray photographs.

CHAPTER 9

STUDY OF PREFERRED ORIENTATION IN POLYCRYSTALLINE AGGREGATES

1. Introduction

An unworked lump of metal usually consists of crystals randomly orientated; but any process of working such as rolling, forging, or drawing, tends to bring about a characteristic re-orientation of the crystal grains. When corresponding axes of the crystals tend to lie in certain directions, the crystals are said to exhibit *preferred orientation*. A similar phenomenon is encountered in some rocks and in natural and artificial tissues and fibres. The term *fibre* has acquired a rather wider meaning in crystallography than in ordinary usage. In the widest sense it includes all polycrystalline aggregates in which there is preferred orientation. But it is more properly restricted to those aggregates in which the crystals tend to lie with a particular zone axis parallel to the fibre axis, and in this book we shall restrict the term 'fibre' to polycrystalline aggregates of this type. It should be noted that, in the crystallographic use of the term, it is not necessary for the external shape of the specimen to be 'fibrous', since we are concerned only with the orientation of the constituent crystal grains. For aggregates in which there is no cylindrical symmetry but which tend to approach more closely to the state of a single crystal, we shall use the general term 'preferred orientation'.

Preferred orientation is of great scientific and technical importance. The properties of metal wires and sheets frequently depend very much on the degree of preferred orientation. Drawn wires of most metals exhibit more and more preferred orientation as their diameter is progressively reduced by cold drawing without annealing. The breaking strength of the wires usually increases as the preferred orientation increases. Many sheet metals when rolled develop preferred orientation, which greatly affects the ease with which they can afterwards be pressed to a desired shape.

In the processes associated with the growth of certain minerals in rocks, the crystals sometimes tend to have a common orientation. The mechanical strength of the rock may be different in different directions, depending on the character of this preferred orientation. The stresses in the earth's crust at the time of the formation of a mineral may also be correlated in some cases with the type and extent of its preferred orientation in rocks. The examination of preferred orientation in thin sections of rocks has hitherto been done chiefly by optical means. More recently, however, petrologists have been using X-ray methods with suitable types of rocks (Fairbairn, 1949).

In organic fibres the long molecules may either be arranged with their lengths more or less parallel to the fibre axis, or they may be wound round it like a helix. Synthetic organic fibres, such as rayon and nylon, are made stronger by inducing preferred orientation in the long molecules. This is done at the time when the last trace of the solvent used in the preparation is being driven off. Thus in the field of organic chemistry, as well as in that of metallurgy, the study of preferred orientation is of great technical importance. In this chapter only the fundamentals of the X-ray methods of study are discussed.

2. Fibre Texture in Wires

2.1 Geometry of X-ray reflection by fibres. In a polycrystalline aggregate the component crystals are generally arranged in a random manner. But in natural and artificial fibres and metal wires, the small crystals are arranged with a particular zone axis more or less parallel to the axis of the fibre. If a fibre is irradiated with a fine beam of X-rays, a modified form of powder photograph is produced. In the

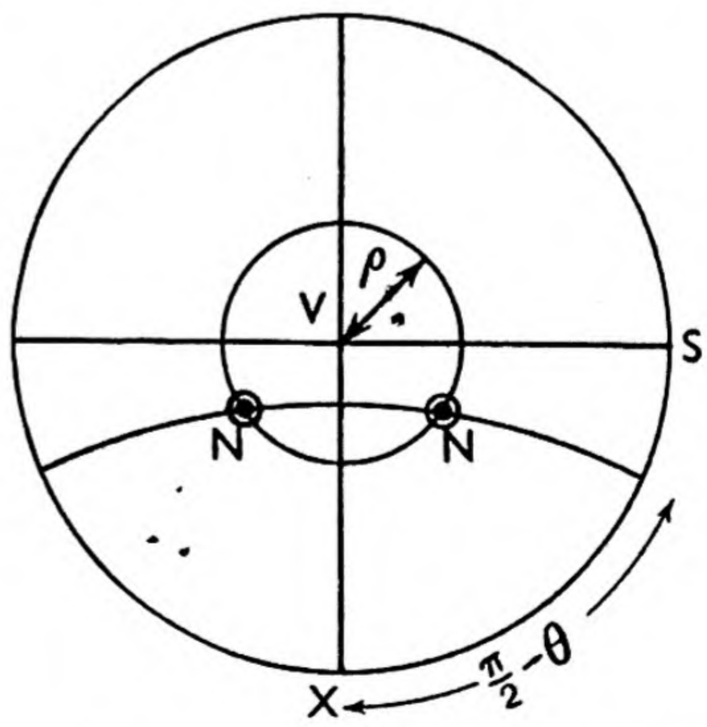

FIG. 122. Stereogram showing plotting of poles from a fibre photograph

ordinary type of powder photograph (**11**, 1), the lines are continuous because the specimen is made up of very small crystals in all possible orientations. In a fibre, only certain orientations of each plane are present because the component crystals have a common zone axis parallel to the length of the fibre. However, all longitudinal sections of the fibre are identical, (that is, the fibre has *cylindrical symmetry*) and hence, if there is a normal to a reflecting plane making an angle ρ with the axis of the fibre, there will be a large number of such normals directed so as to form a cone of semi-angle ρ about the axis of the fibre. If θ is the Bragg angle of reflection for this reflecting plane, the normal to the plane must lie on a cone of semi-angle $(90^\circ - \theta)$ with the direction of the incident X-rays as axis. When the axis of the fibre is set perpendicular to the direction of the incident X-ray beam, the intersections of these two cones define four directions N (Fig. 122), two above the central plane perpendicular to the fibre axis and two corresponding directions below this plane.

To interpret a fibre photograph, we first index the powder lines and determine the corresponding values of θ. Then we read the ρ-values corresponding to the centres of the regions of greatest blackness. The values of ρ and of $(90 - \theta)$ are plotted on a stereogram, and hence the normals to the reflecting planes are determined. An idealised pole figure consisting of circles with radii ρ about the centre (Fig. 124.1) can then be drawn. The main problem is to find the indices of the zone axis coinciding with the fibre axis. Usually the fibre axis in cubic specimens is ⟨100⟩, or ⟨110⟩ or ⟨111⟩, and it is a simple matter to see which of these corresponds to the actual distribution of the small circles about the centre of the pole figure.

A pole figure representing all the information available on the photograph can be constructed only if the variation of density of the powder lines around the darkest points is determined. This requires a careful photometric study. The results when plotted on a pole-figure give a series of circular bands instead of the simple circles of the idealised pole figure. A method of representing this fuller information is to draw a series of circles within each band and to assign to each circle a number indicating the blackness of the band along that circle. Contours, similar to those used on maps, may be used for this type of representation.

2.2 Determination of crystalline orientation in a metal wire. In Fig. 124.2 is shown a photograph of a stationary tungsten wire taken on a cylindrical film. It will be seen that the lines are not uniform in intensity but are broken into regions of greater and lesser blackening. For a powder of tungsten, in which the crystals had a completely random orientation the lines would be smooth and continuous. We shall concern ourselves only with the points of greatest blackening in the powder lines of the fibre photograph. The values of θ and ρ (**9**, 2.1) for these points are determined from the photograph by means of the appropriate chart (Fig. 108) and these values are given in the following table.

FIBRE PHOTOGRAPH OF TUNGSTEN
(Cubic, $a = 3{\cdot}16$ A.).
Values of θ and ρ for the dark arcs on Fig. 124.2
($\lambda = 1{\cdot}54$A.)

θ	hkl	$(90-\theta)$	ρ
$20\frac{1}{2}^\circ$	110	$69\frac{1}{2}$	90°, 62°
29°	200	61	90°
37°	211	53	90°, 73°
43°	220	47	90°, 59°
$50\frac{1}{2}^\circ$	310	$39\frac{1}{2}$	76°
58°	222	32	90°
66°	321	24	continuous

Small circles of radii ρ have been drawn on the stereogram (Fig. 124.1) about the pole of the axis of the fibre (and of the cylindrical film). From this it will be seen that the directions normal to the cube {100}, rhombic dodecahedron {110} and octahedron {111} are all perpendicular to the length of the wire. This result could be deduced by simple inspection of the photograph. It follows from this that an axis ⟨110⟩ must be parallel to the length of the wire. Additional confirmation is obtained from the fact that the ⟨110⟩ and ⟨220⟩ directions are respectively 62° and 59° from the axis of the wire. For an ideal fibre this angle would be 60°. Similarly, two small circles with indices 211 and 310 are at angles of 73° and 76° respectively from the centre, whereas the ideal values are 73° and 77° respectively.

If the fibre were perfect, in the sense that every crystallite had the particular zone axis parallel to the fibre axis, the resulting photograph would consist of spots and would be identical with the corresponding single-crystal rotation photograph. The imperfection of the crystallite orientation causes the spots to 'spread' along the powder lines, and by measuring this we can obtain some information about the degree of the imperfection. It will be seen that, on superposing the ρ-chart on the fibre photograph (Fig. 124.2) the darkest regions of the powder lines extend over a range of ten to fifteen degrees in the angle ρ. Thus in order to produce a pole figure which represents more nearly the preferred orientation in the wire, the small circles labelled 110, 211 and 310 should be replaced by bands of radial width corresponding to about 10°.

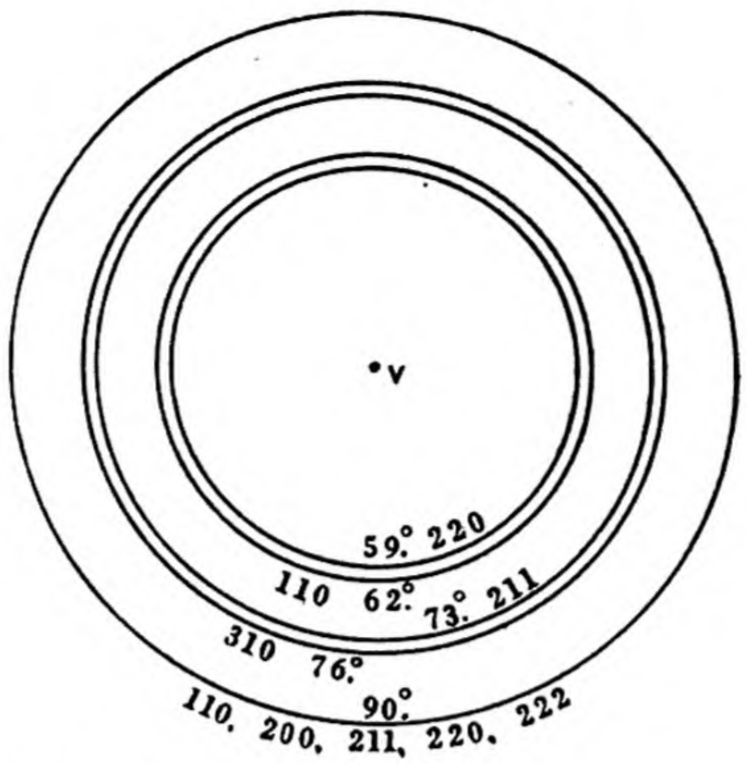

FIG. 124.1. Idealised pole figure for tungsten wire

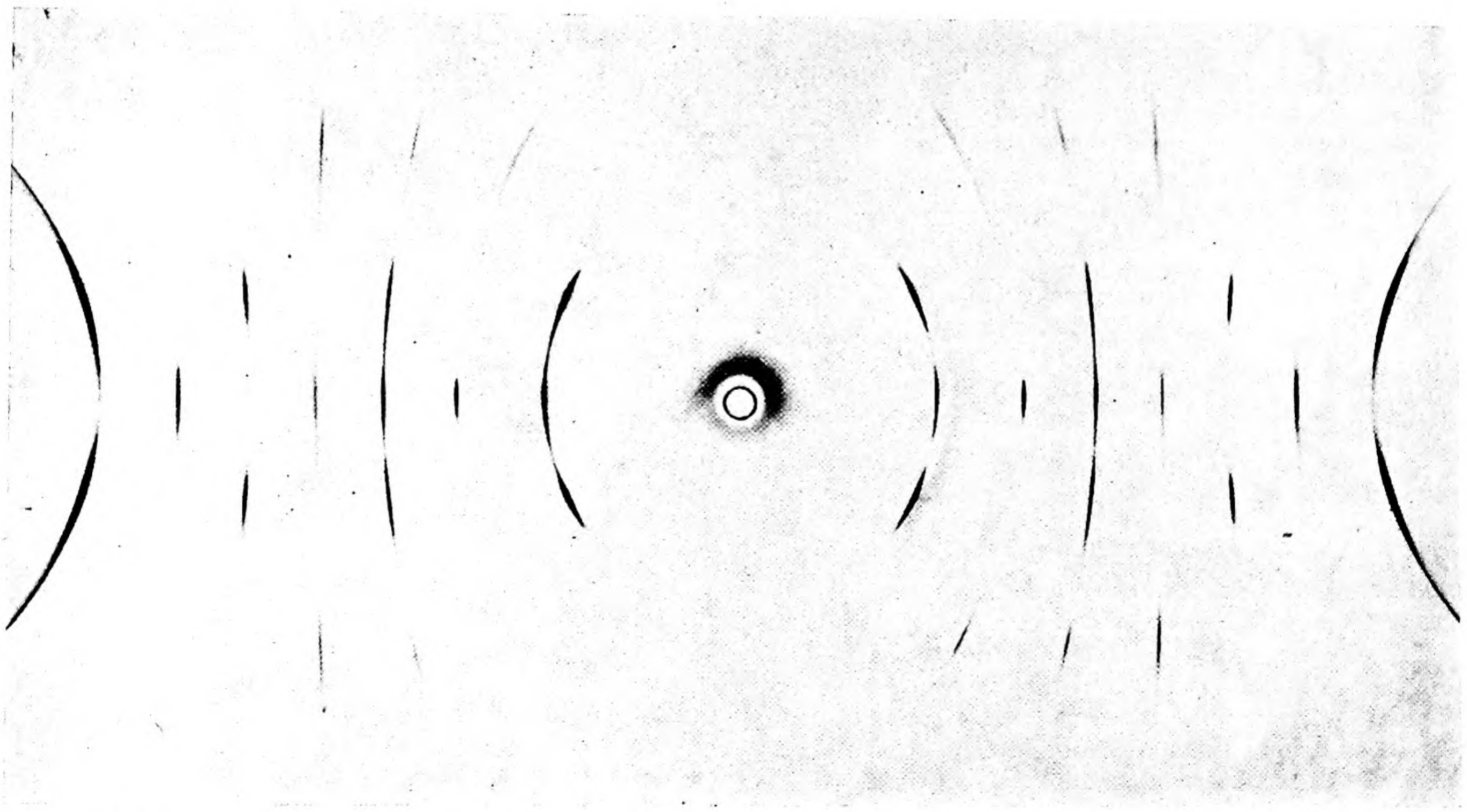

FIG. 124.2. Fibre photograph of tungsten wire. The length of the wire was parallel to the axis of the cylindrical camera of 3·0 cm. radius. The powder lines of small θ are near the centre of the photograph. The characteristic radiation used was Cu$K\alpha$.

3. Preferred Orientation in Metal Sheets

3.1 Geometry of X-ray reflection by rolled metal sheets. The fundamental geometry of the reflection of X-rays from a sheet with a preferred orientation in its constituent crystals is similar to that for fibres discussed above. We shall assume that a stationary film, either cylindrical or flat, is used and that the specimen is also stationary. If the specimen is coarse grained so that the lines become spotty, it is better to move it during the exposure. This can be done by oscillating it through a small angle. Another, and perhaps better, procedure is to translate the specimen in its own plane, so as to allow more crystals to be irradiated. This can be done either by a mechanism on the camera or by superposing several exposures on the same film after moving the crystal

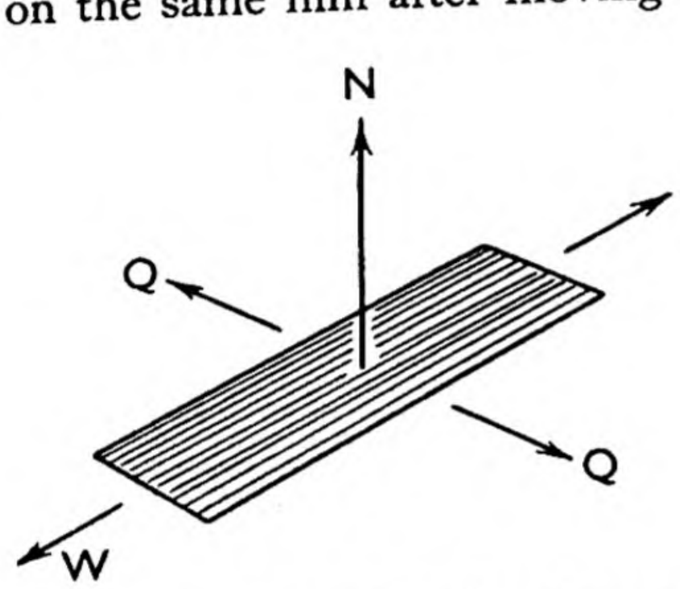

FIG. 125.1. Diagram showing directions on a rolled sheet

between each exposure. The direction of the normal to the plane of the plate is denoted N (*Normalrichtung*), the direction of rolling W (*Waltzrichtung*) and the transverse direction Q (*Querrichtung*) (Fig. 125.1). Along each powder-line there are more or less well-defined regions in which the density is greatest. The centre of each of these regions is defined as before by the angle ρ or by the angle ψ (Fig. 126). For a flat plate the chart of lines of constant ψ is so simple that this angle is commonly used. For a cylindrical film it is commoner to use the angle ρ, though either ψ or ρ serves as a co-ordinate.

From the angles $(90 - \theta)$ and either ρ or ψ a plot is made on a stereogram of the position of the normal corresponding to the centre of each darkened arc (Figs. 125.2). The small circle of radius $(90° - \theta)$ is drawn about the pole of the X-ray beam. The small circle of radius ρ is drawn about the direction in the specimen which is vertical when the photograph is being taken.

The essential difference between the study of a wire and the study of a sheet is that only one photograph is required to obtain all the necessary information about the orientation in a wire, whereas a considerable number are necessary for a sheet. For

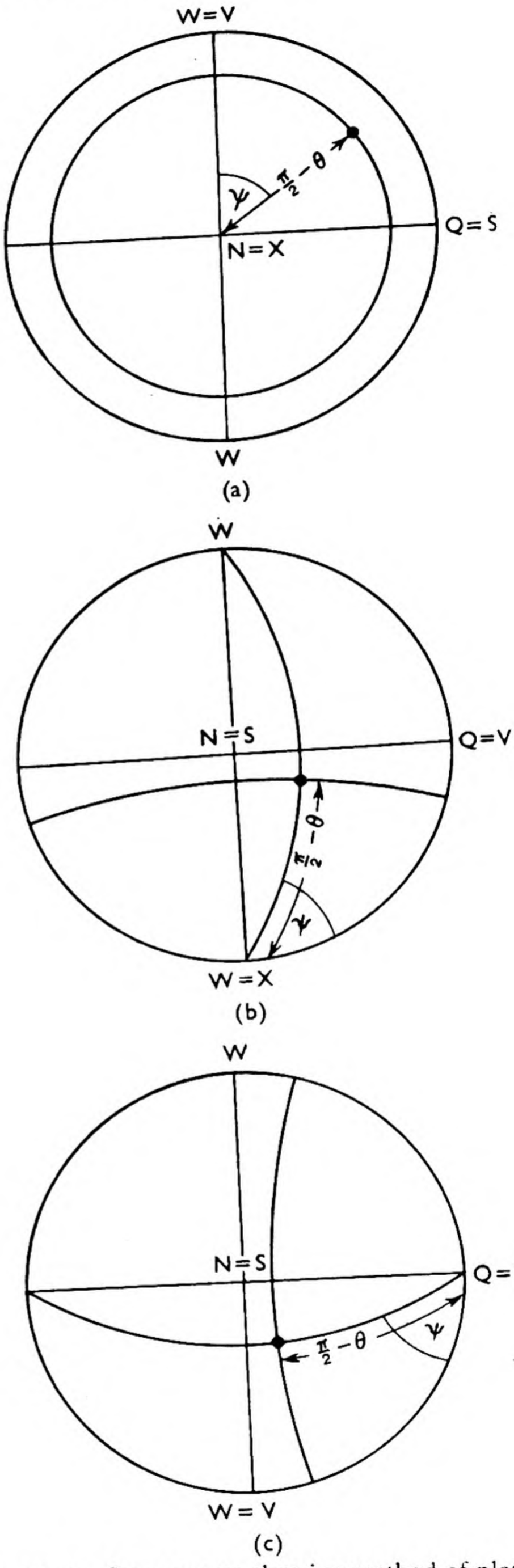

FIG. 125.2. Stereograms showing method of plotting for three orientations of the metal sheet. These three stereograms correspond respectively to the three photographs of Fig. 127

this reason it is probable that moving-film methods, which produce photographs showing a more or less distorted picture of the complete pole-figure for a particular set of reflecting planes, will become more used (**9**, 3.3). When a sufficient number of values of $(90-\theta)$ and either ρ or ψ have been plotted on the stereogram, it can be seen in what regions the normals are concentrated. A separate stereogram is made for each type of reflecting plane. For cubic metals three

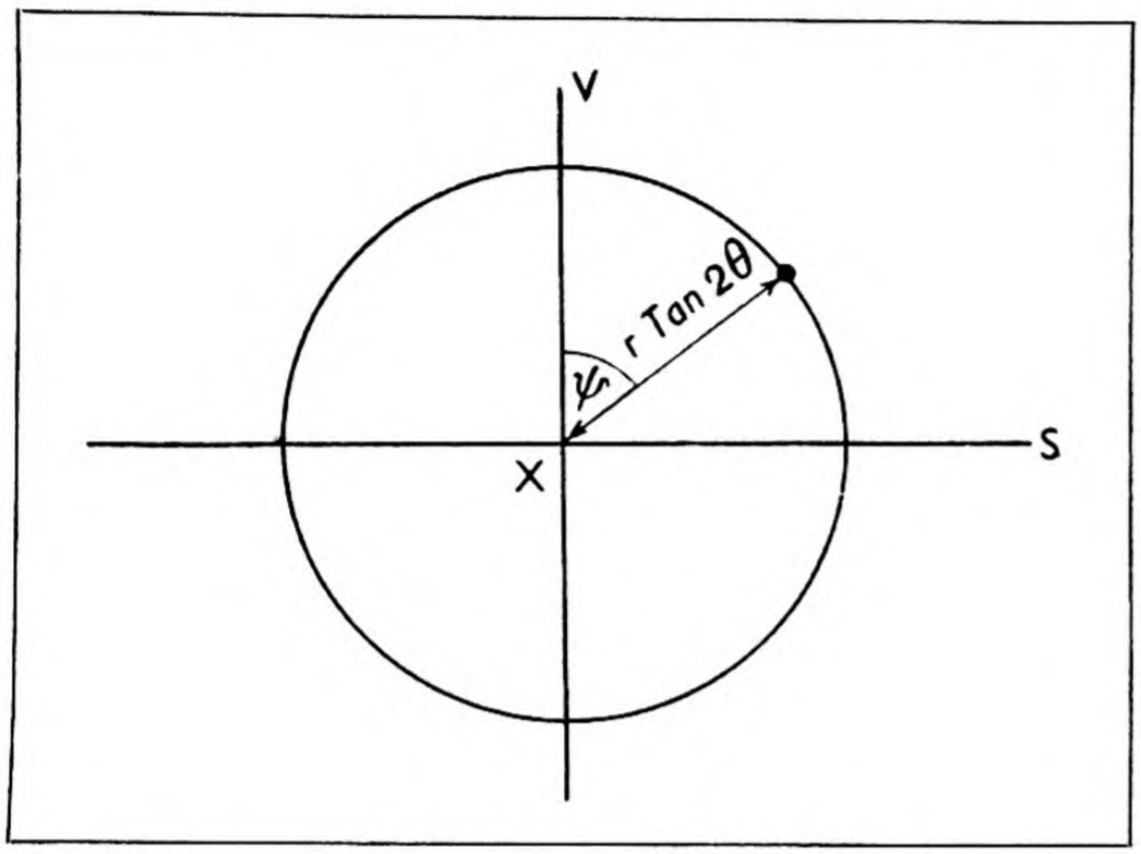

FIG. 126. Diagram giving definition of angle ψ

stereograms, showing the distribution of normals corresponding to the *h*oo, *hh*o and *hhh* reflections respectively, are usually given. For crystals of other systems, stereograms are made showing the distribution of the normals corresponding to reflections of special types, such as ooo*l*, *ho*$\bar{h}$o and *hh*2$\bar{h}$o for hexagonal crystals.

3.2 Determination of preferred orientation in a metal sheet. The principles discussed in the previous section are applied here to the study of the preferred orientation in a piece of rolled molybdenum foil. The three photographs of Fig. 127 were taken in the manner indicated, and the values of θ and ψ are read as described above. Molybdenum has a body-centred cubic lattice, and hence the indices of the successive lines, starting from the centre, are 110, 200, 211, 220, 310 respectively (**12**, 3.1). The table gives the values of θ and ψ for the 110, 200 and 220 reflections. The cell size is 3·14 A. and $\lambda = 0{\cdot}71$ A.

VALUES OF ψ FOR BEGINNING AND END OF EACH DARK ARC.

Indices→	110	200	220
Values of $(90-\theta)$→	81°	77°	71½°
W vertical *N* parallel to X-rays	0°–7°, 54°–65°, 76°–90°	37°–52°	85°–90°
Q vertical *W* parallel to X-rays	0°–34°, 36°–65°	78°–90°	40°–70°
W vertical *Q* parallel to X-rays	0°–2°, 53°–66°	84°–90°	53°–60°

The normals to reflecting planes are plotted on stereograms (Figs. 128.1, 128.2) from these values. It will be seen that the shaded areas do not extend beyond the points on the stereogram which correspond to the darker parts of the arcs on the photographs of Fig. 127, except for the 220 powder line. This is probably due to the fact that the 220 lines are underexposed and hence the arcs are not so long as they would be in a photograph of longer exposure. The shading could be done precisely only if sufficient photographs were taken for each shaded part to be represented on a photograph. With only three photographs the shading is largely conjectural. In Fig. 129.1 is given a stereogram in which the orientation of the normals to the {100} and {110} faces correspond to the centres of the shaded areas in Figs. 128.2 and 128.1. From this it will be seen that the plane of the metal sheet approximates to a cube face, the direction of rolling to a ⟨110⟩ axis and the direction *Q* also to a ⟨110⟩ axis.

When more precise data are required, additional photographs have to be taken. If the specimen is set with *N* vertical, it can be turned about this axis and photographs taken at 10°-intervals. Since the pole (*X*) of the incident beam is normal to *N*, the data from such photographs are easily plotted on the master stereogram, such as those shown in Figs. 128, by means of the ordinary stereographic net. But when the specimen is set up with either *W* or *Q* vertical, the pole *X* lies at different points along the diameters *QN* or *WN*. We could draw the appropriate small circles of radius $(90° - \theta)$ and the great circles which divide them up according to the range of the angle ψ, but this would have to be done again for each additional photograph. This would be a clumsy procedure, and it is simpler to use the following method. The data for each separate photograph are plotted on a transparency, the pole *X* being placed either at the centre or on the circumference, whichever is most convenient. The points obtained are then rotated in the usual way by means of the stereographic net before being pricked through on to the master stereogram on which the final pole figure is obtained. This is a simple operation, but care is needed to preserve the correct orientation during each transfer of data.

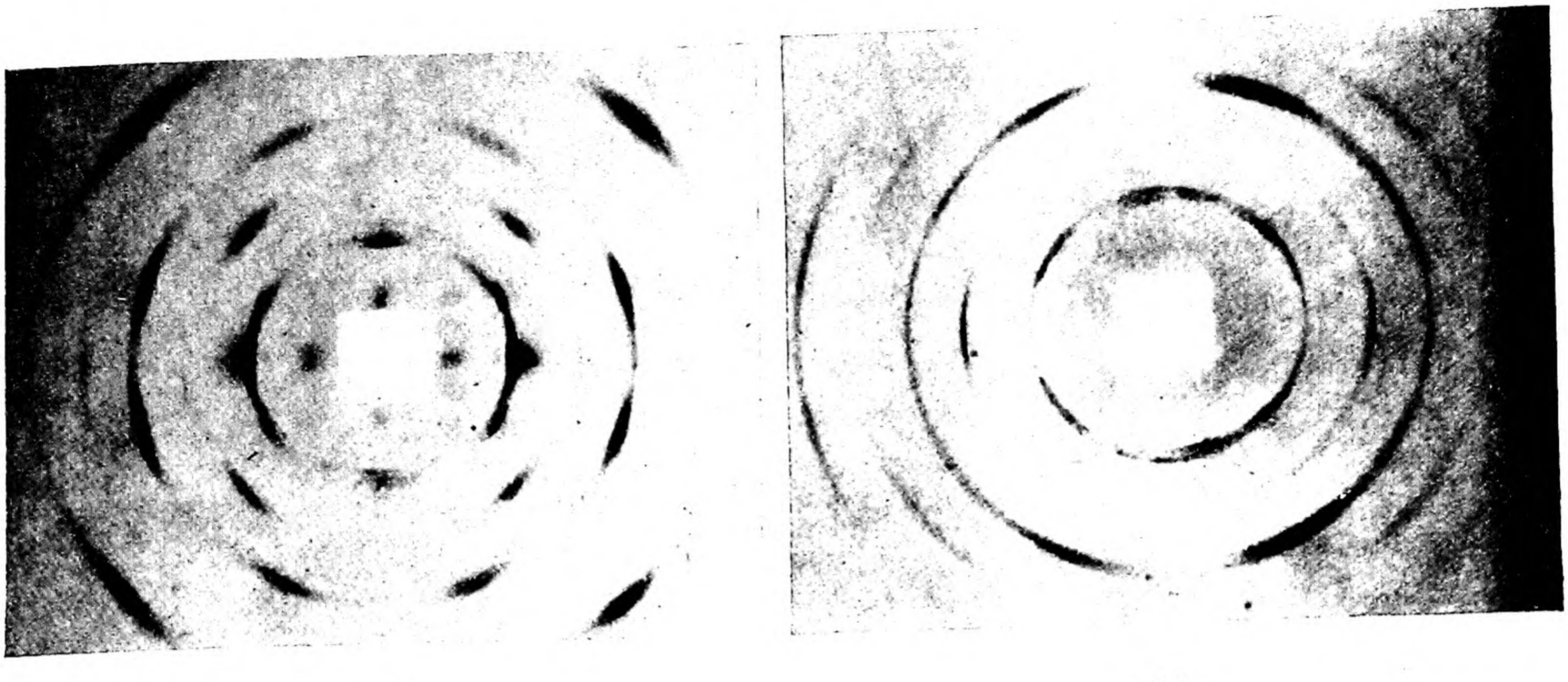

(a) (b)

(c)

FIG. 127. Fibre photographs of molybdenum foil. The radiation was filtered Mo$K\alpha$ and the flat plate was 4 cm. from the specimen. The orientation of the directions N, W, Q relative to the camera was defined as follows :

	Parallel to vertical direction	Parallel to X-rays
(*a*)	*W*	*N*
(*b*)	*Q*	*W*
(*c*)	*W*	*Q*

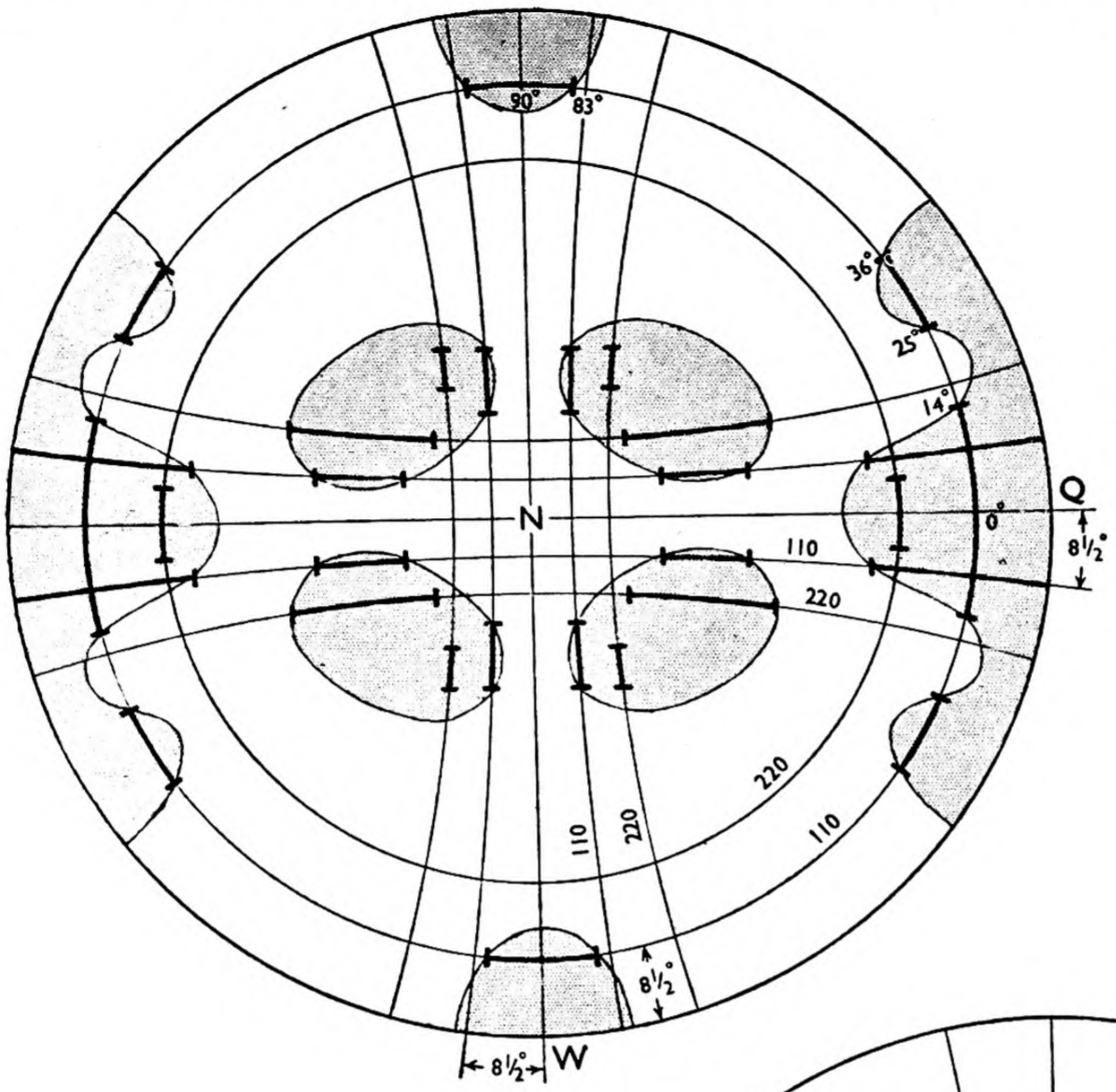

FIG. 128. Two pole figures of rolled molybdenum sheet. The thick arcs on the stereogram correspond to the dark portions on the powder lines of Figs. 127. The shaded areas represent regions within which it is estimated that the thick arcs would be contained if more photographs were available

Fig. 128.1 Pole figure {110}

(see note below)

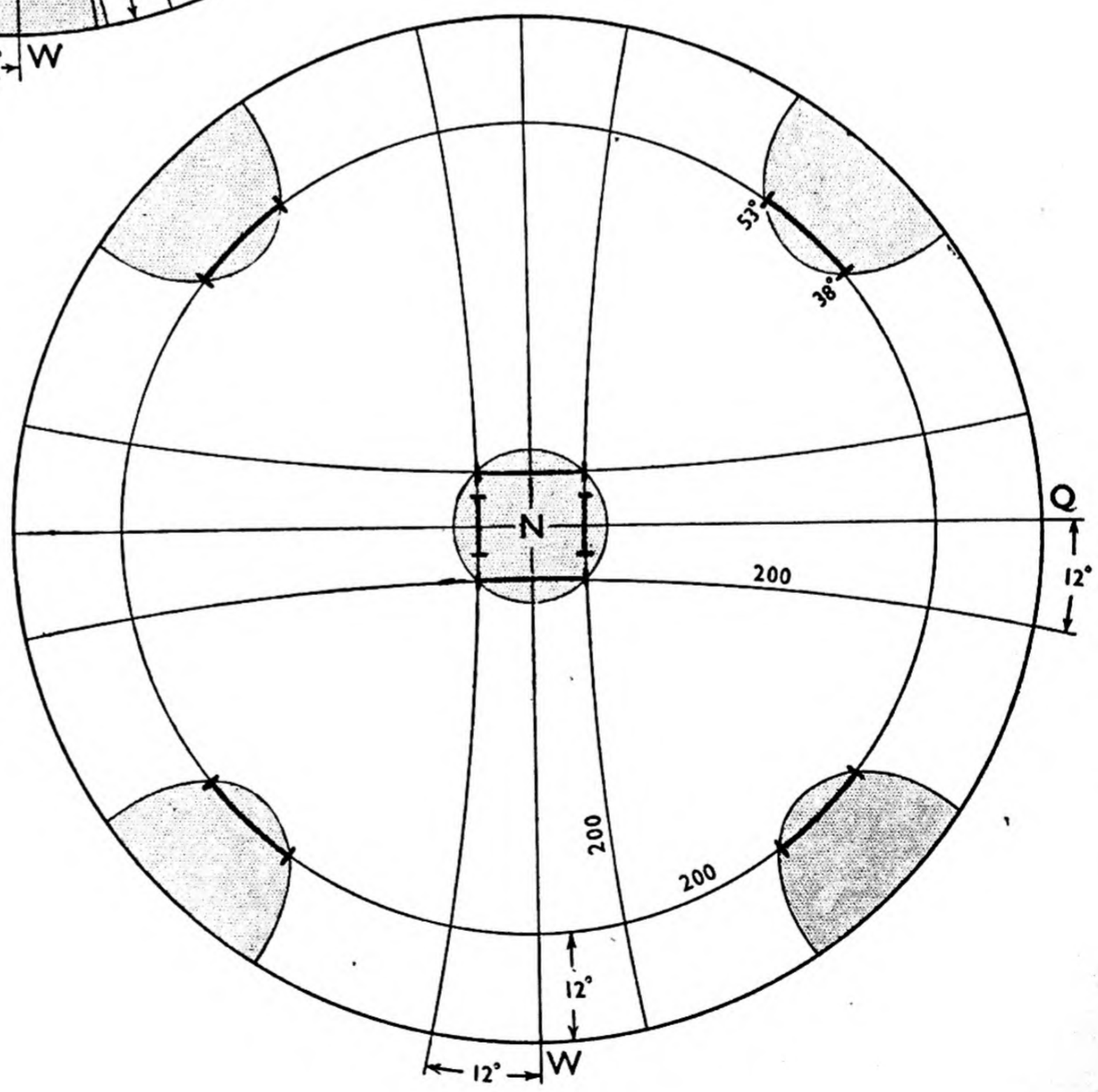

Fig. 128.2 Pole figure {100}

Note: In Figs. 128.1 and 128.2, the readings of angle ψ are the complements of this angle as defined in Fig. 126.

In the values of angle θ,
for $8\frac{1}{2}°$ read 9°,
for 12° read 13°.

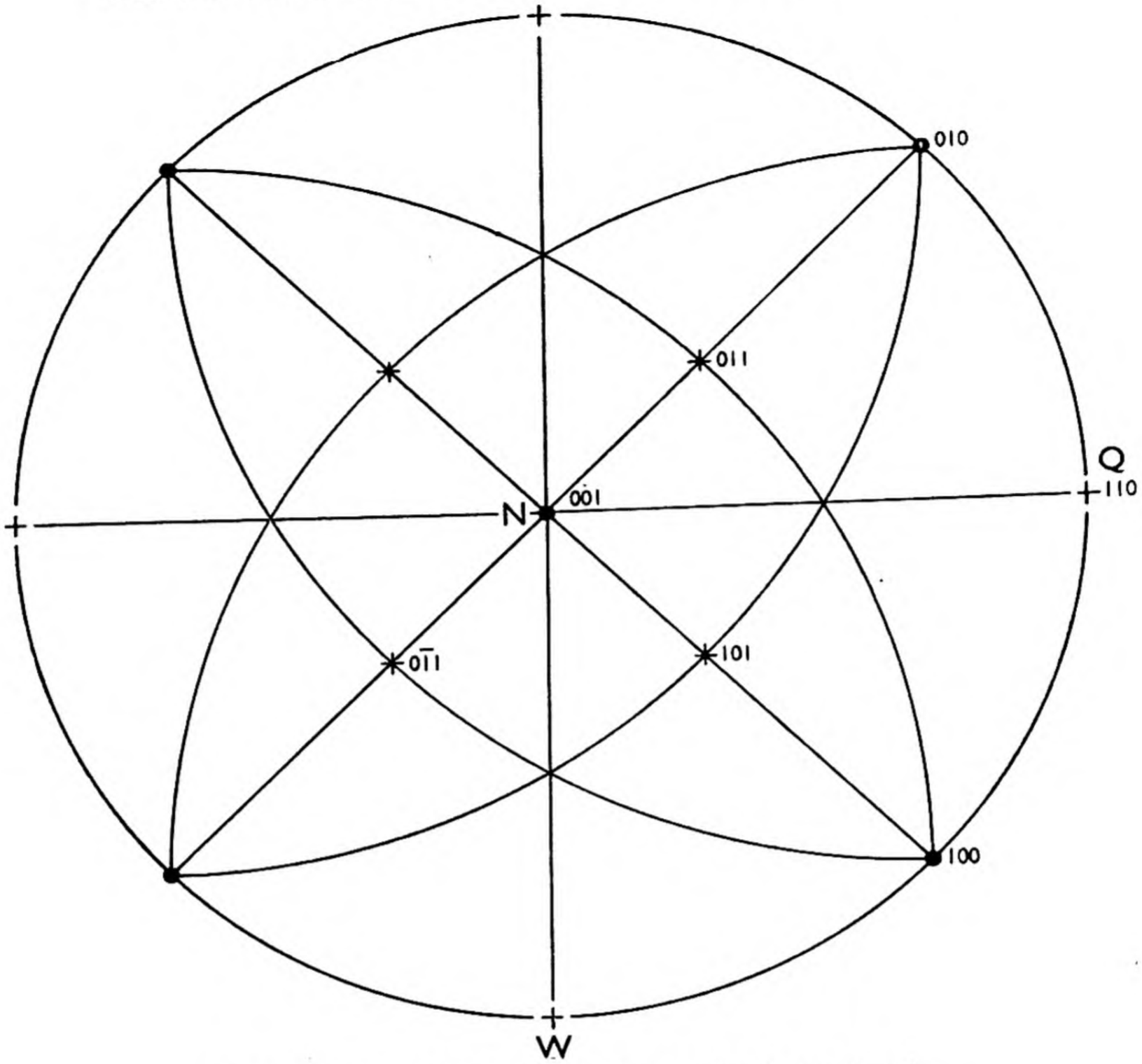

FIG. 129.1. Idealised pole figure, {100} and {110}

3.3 Use of a moving-film method. The disadvantage of the method described in **9,** 3.2 is that a considerable number of oscillation photographs must be taken in order to obtain complete information concerning the preferred orientation of the crystals in a sheet of rolled metal. This disadvantage can be overcome by using a moving-film goniometer. A modification of the type originally proposed by Kratky (1930) has been developed for the study of metal sheets (Wooster, 1948). In this instrument (Fig. 129.2) the direction of the incident beam of X-rays is defined by a collimator *C*. Coaxial with this collimator are the cylindrical screen *S*, with its annular aperture, and the cylindrical film *F*. The film is mounted on a camera which can move along a track parallel to the direction of the incident X-rays. The specimen, *G*, is mounted on a spindle, *R*, about which it can be rotated; at the end of this spindle there is a cylindrical drum *D*. The movement of the camera is synchronised with that of the specimen by means of a steel tape which joins one end of the camera to the drum D.

Each photograph obtained with such an instrument gives all the information required to plot a pole figure covering almost the whole of a normal stereogram. However, the information is not quite enough to fill the stereogram owing to the fact that the Bragg

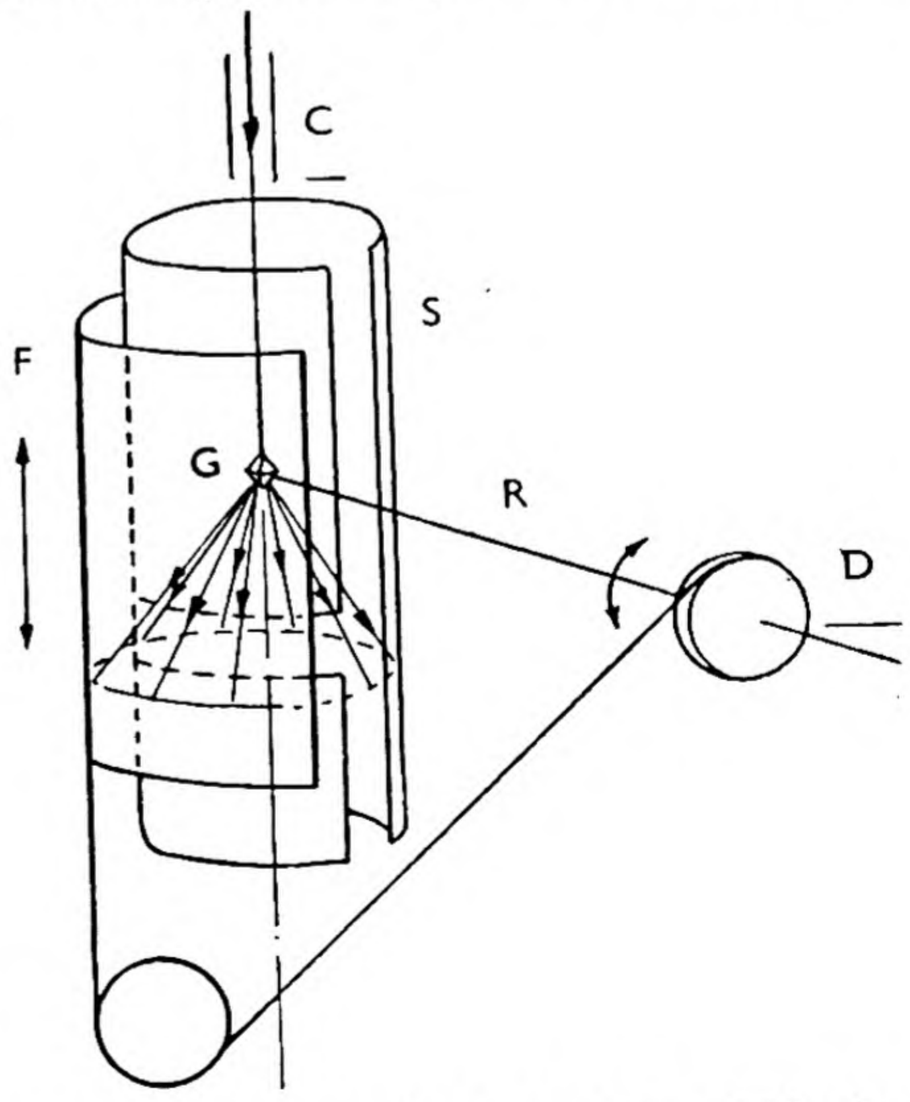

FIG. 129.2. Diagram of components of Kratky-type preferred orientation goniometer

angle is always greater than zero. However, with a little experience all the salient features of the pole figure can be obtained by simple inspection, because of the close relation between the disposition of the darkened parts of the film and the corresponding areas of the stereogram.

4. Study of Fibre Photographs of Organic Materials

The substance of many natural fibres does not occur as single crystals, and so all the X-ray data have to be obtained from fibre photographs. Since these substances often belong to the monoclinic system, the task of determining the unit cell is not always straightforward. Photographs obtained from natural fibres are sometimes very difficult to interpret, either because there are too few spots or because the pattern is too confused. Rubber, for example, gives only a few blurred rings, unless it is stretched, whereupon the molecules are pulled more or less into parallelism, and give the photograph shown in Fig. 130.

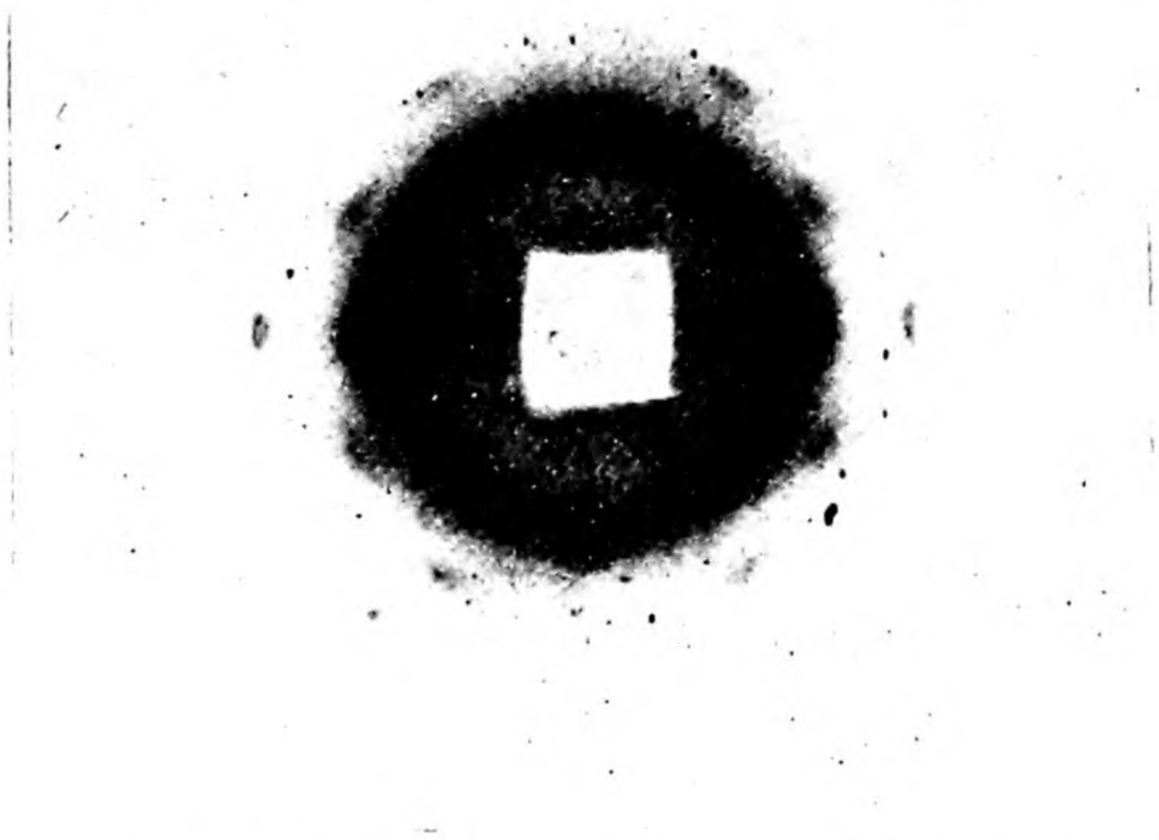

FIG. 130. Fibre photograph of stretched rubber band. The direction of stretching was vertical and the plane of the band was perpendicular to the X-ray beam. Crystal-reflected Cu$K\alpha$ radiation was used and the camera-specimen distance was 4 cm.

An essential pre-requisite for the study of organic fibres is, therefore, the production of a specimen in which the molecules have been forced to adopt a markedly preferred orientation. This is sometimes achieved by stretching a thread, thus bringing its component fibres into parallel alignment, or it may be done by stretching or rolling a sheet of the material. The reason why this last treatment overcomes the irregular orientation of the crystals may be illustrated by the following analogy. Suppose a number of rectangular bodies like dominoes are set at random in a rubber latex which is then allowed to solidify. If the rubber sheet is now stretched in one direction the dominoes will tend to be pulled so that their lengths lie parallel to the direction of stretching. Alternatively, if the sheet is simultaneously stretched in two perpendicular directions, the dominoes will tend to set with their planes parallel to the sheet. Further, if the stretching is greater in one direction than in the other, the lengths of the molecules tend to set parallel to the direction of greatest extension.

This process is employed in obtaining orientated specimens of cellulose in 'Cellophane' sheet. Cellulose is dissolved in a suitable solvent and then squeezed out in the form of a thin sheet. The solvent evaporates leaving a coherent film which is gradually stretched in two mutually perpendicular directions until all the solvent has evaporated. A specimen prepared in this way shows considerable preferred orientation. In X-ray photographs of such a sheet the 'powder' rings are broken up into arcs similar to those discussed in connection with molybdenum foil (**9,** 3.1). It is possible to make a number of pole figures from such photographs.

This technique for producing preferred orientation in a sheet is also used when it is desired to determine the shape and size of the unit cell. It sometimes happens that in these substances two of the cell dimensions are nearly equal, and in the absence of preferred orientation it is not possible to separate overlapping lines. When a preferred orientation can

be induced, this ambiguity is avoided and the true cell dimensions can be determined.

However, even when everything possible has been done to bring about preferred orientation, it is often difficult to obtain unambiguous interpretations of many fibre photographs. The photograph of rubber (Fig. 130) shows the possibilities and limitations of study of this type of photograph. We are not concerned here with the broad halo which is due to the non-crystalline part of rubber, but with the six spots in each of the four quadrants. These spots lie on the equatorial-layer line, on the first-, and on the second-layer line. By using the appropriate Bernal chart (**5**, 1·4), we can read off the values of ζ for the layer lines. For the second-layer line we obtain $\zeta = 0{\cdot}37$ and hence a repeat distance of 8·3 A. The accuracy with which this measurement can be made depends on the sharpness of the spots, and this in turn depends on the extension of the rubber. The specimen used for the photograph of Fig. 130 was an ordinary brown rubber band stretched on a wire frame. Sharper spots can be obtained with specimens stretched further on a stronger frame. But even with this simple method, the repeat distance along the direction of stretching, which is characteristic of the substance, can be measured with sufficient accuracy to distinguish between rubber and other rubber-like substances, such as guttapercha.

If we call the axis parallel to the direction of stretching the z-axis, then the spots on the equator have indices of the type hko. To determine the values of h and k we proceed in the following way. The spot nearest the centre of the photograph is called 100, and the next spot, 010. The ξ-values for these spots are read from the Bernal chart and give $a^* = 0{\cdot}25$ and $b^* = 0{\cdot}38$. A plot of the reciprocal lattice is made and this is made orthogonal in the first place. The value of ξ for the third equatorial spot is found to be 0·50, which is equal to $2a^*$; this reflection is therefore called 200. In this simple case a reciprocal net is not necessary for the indexing, but in a photograph showing a considerable number of spots it would be. The three spots on the photograph which remain to be indexed lie on row lines through 100 and 010 and therefore have the indices 101 and 011 on the first layer line, and 102 on the second. If there were more spots on the photograph we would proceed in the same way to index all of these. If any spot could not be indexed from the reciprocal lattice selected, it would be necessary to try another possible unit cell.

The unit cell which we have chosen is orthorhombic with $a = 6{\cdot}2$, $b = 4{\cdot}1$, $c = 8{\cdot}3$ A. The accepted unit cell is monoclinic (Bunn, 1942) with $a = 12{\cdot}5$, $b = 8{\cdot}9$, $c = 8{\cdot}1$ A. and $\beta = 92°$. It is clear that the reflections which we called 100 and 010 are really 200 and 020 respectively, which could be determined only by a study of more strongly stretched specimens. In photographs of such specimens the weaker reflections would become visible. After making this correction, we obtain $a = 12{\cdot}4$, $b = 8{\cdot}2$, $c = 8{\cdot}3$ A., the inaccuracy being largely due to the lack of sharpness in the spots.

CHAPTER 10

FURTHER STUDY OF THE GEOMETRY AND SYMMETRY OF CRYSTALS

1. Further Study of Crystal Lattices

1.1 Derivation of the 14 Bravais lattices. In **1,** 3.1 and **1,** 3.2 we began the study of crystals as three-dimensional patterns and developed the concept of the crystal lattice. The crystal lattice is an infinite three-dimensional array of regularly-spaced points such that all points have identical environments with similar orientation. Any lattice can be defined by three vectors which fix the translations of the lattice. We noted that these vectors might have particular relationships, as a result of which the lattice would have elements of symmetry additional to the centres of symmetry present in every lattice. In practice, the vectors are made proportional in magnitude to the repeat distances in the corresponding directions within the actual crystal being studied. It is obviously best to select the unit vectors, and hence the unit-cell, so that the symmetry of the lattice is revealed. When this is done, there are seven types of lattice with points only at the corners of the unit-cell parallelepiped, such lattices being called *primitive*. We saw that it is also possible in certain systems to have other types of lattices with additional points, such lattices being called *centred*. There are, in all, fourteen types of crystal lattice which conform to the definition given above. In each of these it is possible to select a unit cell so that it has points only at the corners; but, owing to the great importance of conformity with the symmetry, it is extremely convenient to adopt the conventional choice of unit cell in the fourteen *Bravais lattices*.

THE SEVEN PRIMITIVE LATTICES

ANGULAR RELATIONS	LINEAR RELATIONS	SYMMETRY
$\alpha=\beta=\gamma=90^\circ$	$a=b=c$	Cubic
$\alpha=\beta=\gamma=90^\circ$	$a=b\neq c$	Tetragonal
$\alpha=\beta=\gamma=90^\circ$	$a\neq b\neq c$	Orthorhombic
$\alpha=\gamma=90^\circ\neq\beta$	$a\neq b\neq c$	Monoclinic
$\alpha\neq\beta\neq\gamma\neq90^\circ$	$a\neq b\neq c$	Triclinic
$\alpha=\beta=90^\circ$, $\gamma=120^\circ$	$a=b\neq c$	Hexagonal
$\alpha=\beta=\gamma\neq90^\circ$	$a=b=c$	Rhombohedral

Note. In this table, when the numerical value of an angle or the equality of two lengths is given, this is a consequence of the symmetry.

In this section we shall derive the centred lattices systematically. We shall start with the seven primitive lattices, each of which has the same symmetry as the holo-symmetric class of the corresponding crystal system.

In addition to the primitive cubic lattice, with angles 90° between pairs of the three shortest vectors, there are two other lattices, with angles of 60° 00′ and 109° 28′ respectively, which have also cubic symmetry. In these two lattices, when the unit vectors are selected so as to reveal the symmetry, the unit cells possess centring points, at the centres of all faces in the first and at the intersection of the body-diagonals in the second (Fig. 136). These lattices are called respectively *cubic all-face-centred* (*F*) and *cubic body-centred* (*I*) (from German, *innenzentrierte*). It is clear that they have more lattice points per unit cell than the primitive lattice. The various symbols used for lattices are given in the table.

LATTICE SYMBOL	LATTICE POINTS	NO. OF POINTS PER UNIT CELL
P	points only at corners	1
R	points only at corners	1
A, *B*, *C*	points at corners plus points at middle of *A* (100) or *B* (010) or *C* (001) faces	2
F	points at corners plus points at middle of all faces	4
I	points at corners plus one point inside at centre	2

The symbols *R* and *C* are discussed on pp. 135 and 137.

Unit cells with centring points can be outlined in all systems, and the following discussion is quite general. To a primitive lattice other points can be added in any of the following ways:

(i) at the centres of one pair of opposite faces;
(ii) at the centres of each of the six faces of the unit cell;
(iii) at the intersection of the body-diagonals.

Trial shows that combinations of additional points other than these destroy the lattice condition that all points of a lattice have identical environments in similar orientation. After each of these operations has been tried, it is necessary to ask three questions:

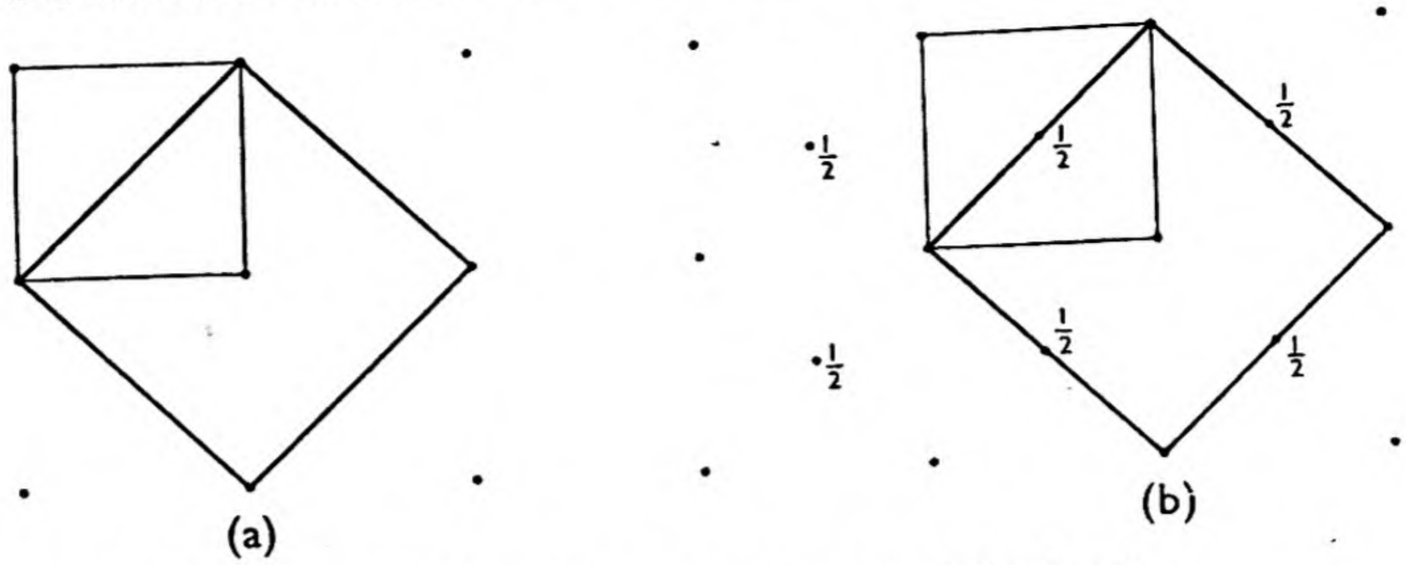

FIG. 133.1. Projections on (001) of tetragonal lattices :
(*a*) $C=P$ (*b*) $F=I$

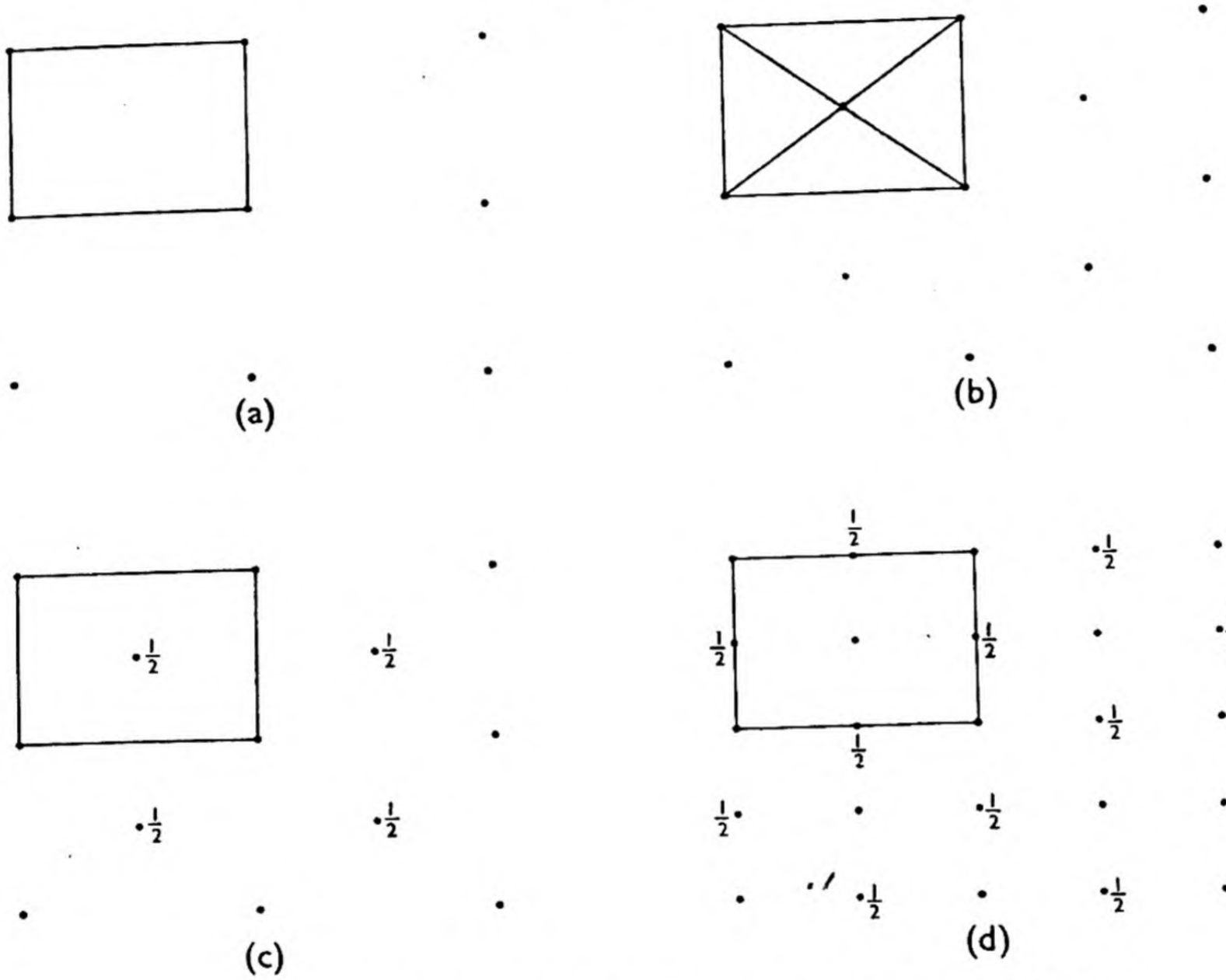

FIG. 133.2. Projections on (001) of orthorhombic lattices :
(*a*) P (*b*) C (*c*) I (*d*) F

(i) Is the resulting arrangement still a lattice?
(ii) If it is, has the symmetry been altered?
(iii) If the symmetry is unaltered, as we are considering one system at a time, is the lattice different from all those previously identified in the same system?

If we start with the cubic system, it can be seen that all three operations produce lattices, but the first operation destroys the cubic symmetry. That leaves three lattices, P, F and I, for this system. In the tetragonal system, operation (i) destroys the symmetry, except when the centred face is the C-face (001), but the lattice which arises from centring on the C-face is simply the primitive lattice with the axes turned through 45° ; this is permitted by the symmetry, though the relative lengths of the sides of the unit cell have been changed. Similarly, the F lattice is simply the body-centred lattice turned through 45°. There are therefore only two different lattices in this system, these being described usually in the orientations which result in the unit cells of smaller volumes, namely, P and I (see Fig. 133.1).

In the orthorhombic system the symmetry is unaltered by any of these operations, and the four lattices, P, I, F and C (or A or B) are all different, the one-face-centred lattice being described by the letter appropriate to the orientation of the unit cell chosen (Fig. 133.2).

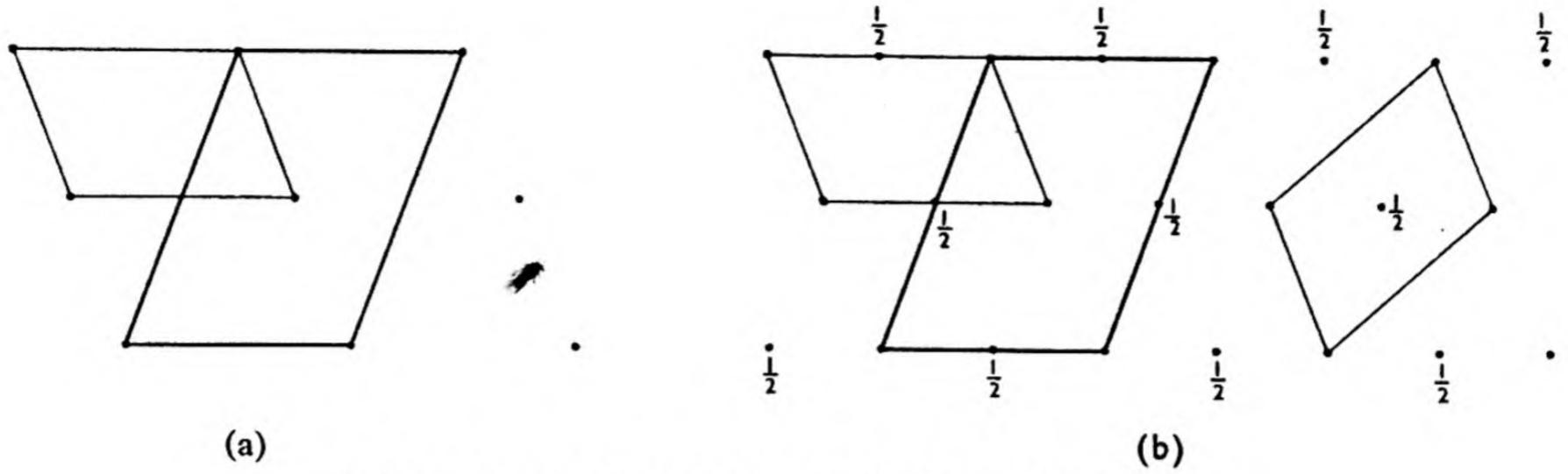

FIG. 134.1. Projections on (010) of monoclinic lattices :
(*a*) $B=P$ (*b*) $F=I=C$

In the monoclinic system, the *C*- (or *A*)- face-centred lattice is different from the primitive, but the *B*-face-centred lattice is the same as the primitive with a different choice of axes (see Fig. 134.1). Similarly, the all-face-centred and the body-centred lattices are the same as the *C*- or *A*-face centred lattice with different axes. In the triclinic system, there is only the primitive lattice, because, owing to the absence of axes and planes of symmetry, a primitive unit cell can always be chosen without breaking any conventions. The smallest unit cell of the hexagonal lattice is primitive, but as explained in **10,** 1.4, it is described by the letter *C*. It can be considered as a special case of the monoclinic with $\beta=120°$ and $a=c$, the hexad axis corresponding to the *y*-axis of the monoclinic. As shown in Fig. 134.2, centring the basal faces (0001) of the smallest hexagonal unit cell destroys the special symmetry and produces a primitive monoclinic unit cell with $c=a\sqrt{3}$ and $\beta=90°$. Centring all faces of the smallest hexagonal unit cell produces another monoclinic unit cell ; if this is taken as body centred, it has $\beta=90°$ and $c=a\sqrt{3}$ as above, but if it is taken as one-face-centred it has $\beta=120°$ and $c=a/2$ (*C*-face centred) or $c=2a$ (*A*-face centred). If the original hexagonal unit cell is body-centred, the lattice becomes monoclinic with $\beta=120°$ and $c=a\sqrt{3}$ (*A*-face centred), or $c=a/\sqrt{3}$ (*C*-face centred). It is clear, therefore, that there is only the primitive hexagonal lattice.

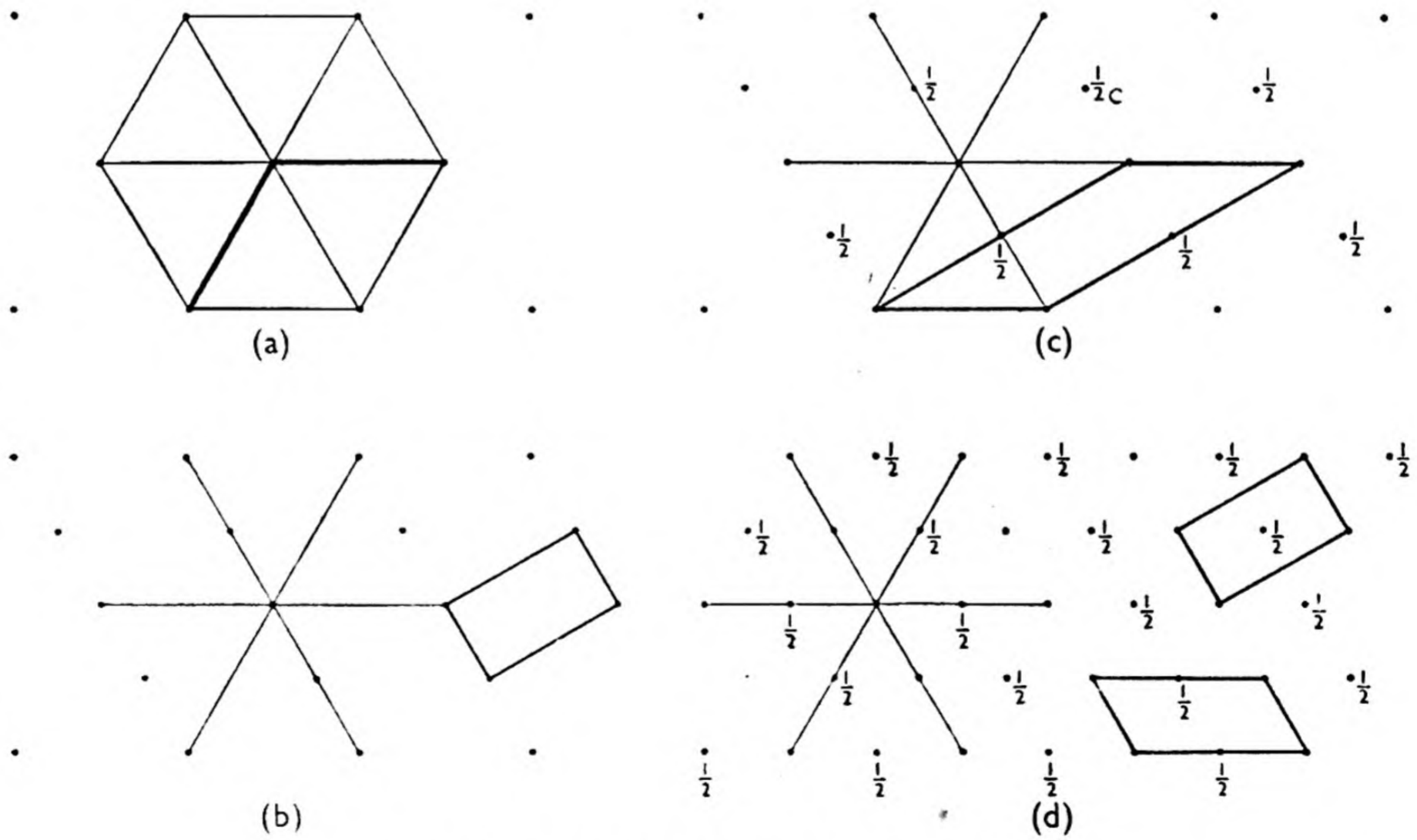

Fig. 134.2. Projection on (0001) of the hexagonal lattice :
(*a*) Primitive (*C*) ; (*b*) effect of *C* face-centring ; (*c*) effect of body-centring ;
(*d*) effect of all face-centring

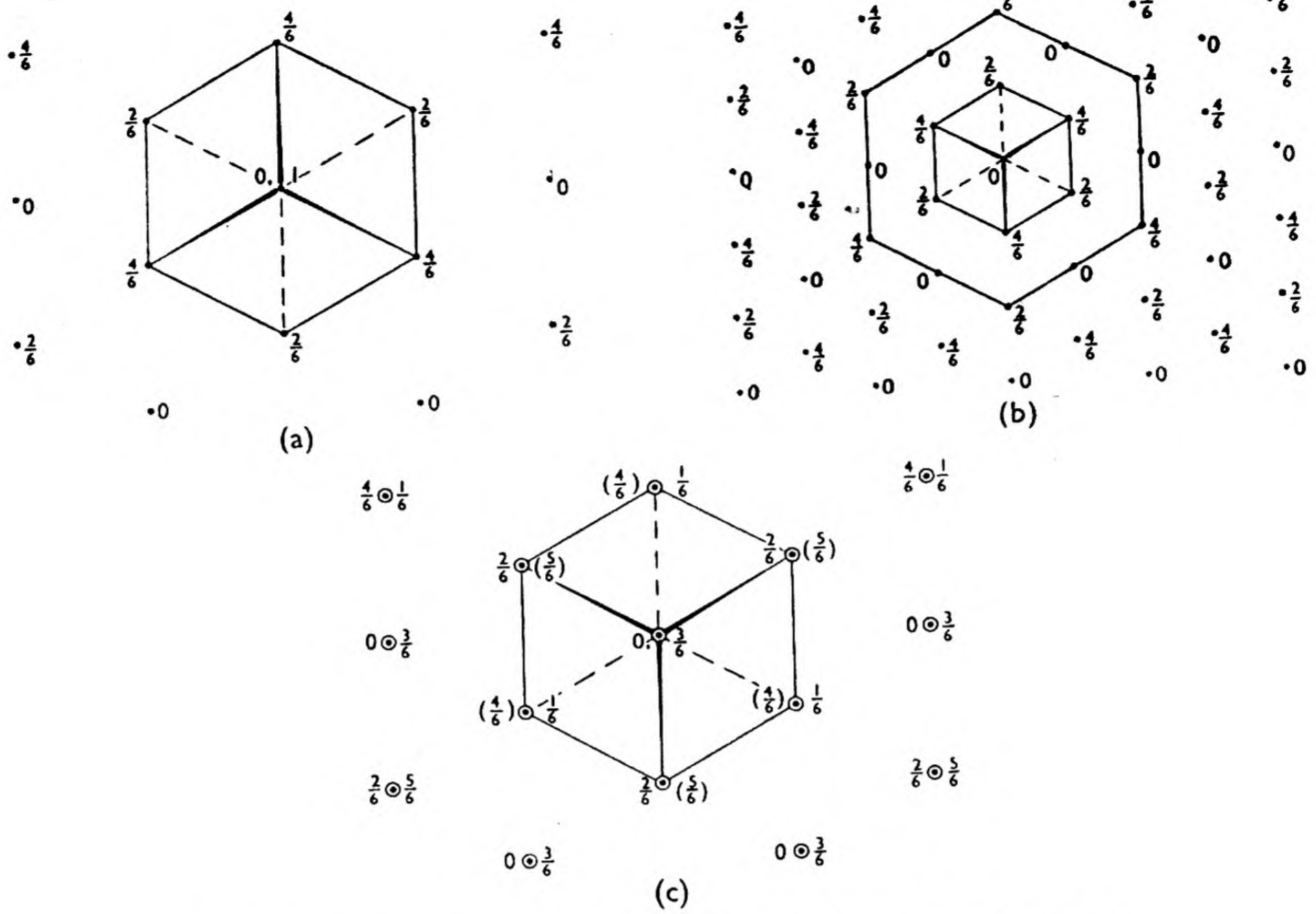

FIG. 135.1. Projection on basal plane of the rhombohedral lattice :
(*a*) primitive (*R*) ; (*b*) effect of all face-centring ; (*c*) effect of body-centring

The primitive rhombohedral lattice (*R*) is shown in Fig. 135.2, and in projection in Fig. 135.1. If a body-centring point is added, a primitive rhombohedron of half the height and half the volume of the original can be outlined without altering the symmetry. Face centring must be done on all faces to preserve the trigonal symmetry, and if this is done, it can be seen from the figure that a primitive rhombohedron of the same height but one-quarter of the volume of the original can be outlined. Thus there is only one rhombohedral lattice. The fourteen space (Bravais) lattices are shown in Fig. 136 and are listed on p. 137.

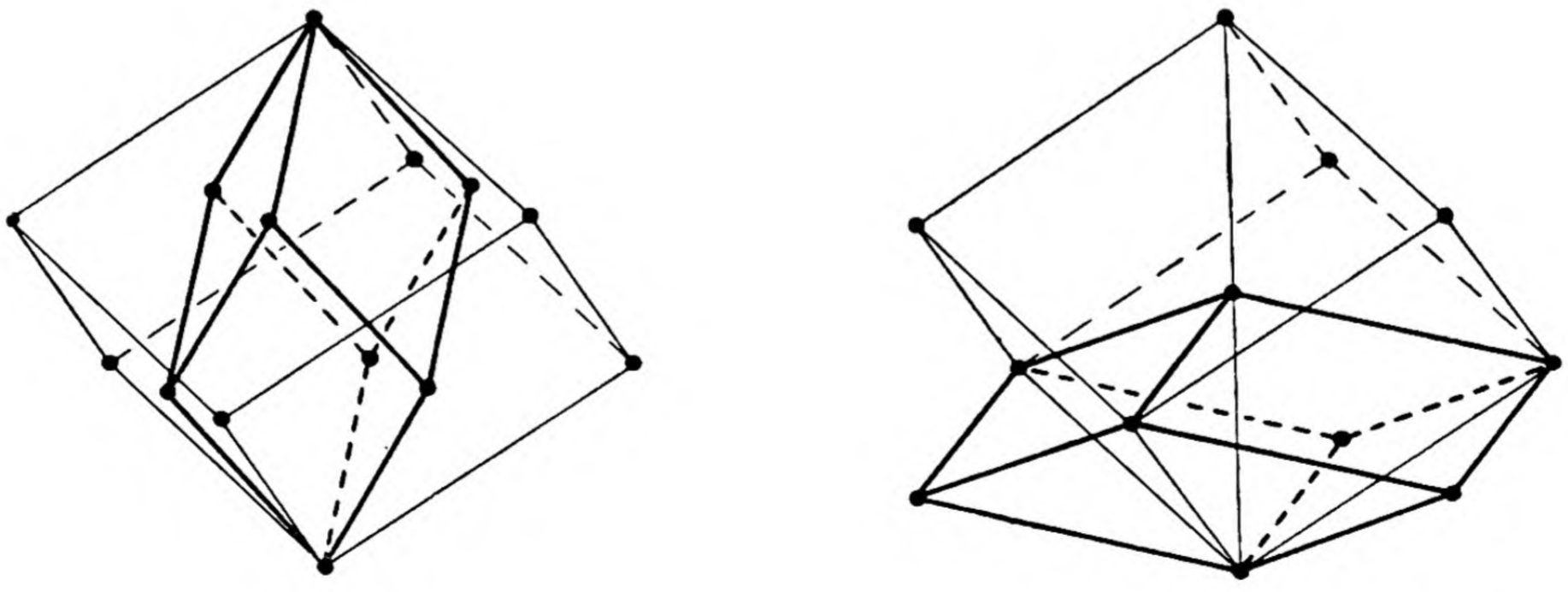

FIG. 135.2. Drawings showing the effect of adding centring points to the rhombohedral lattice :
(*a*) all face-centring ; (*b*) body-centring

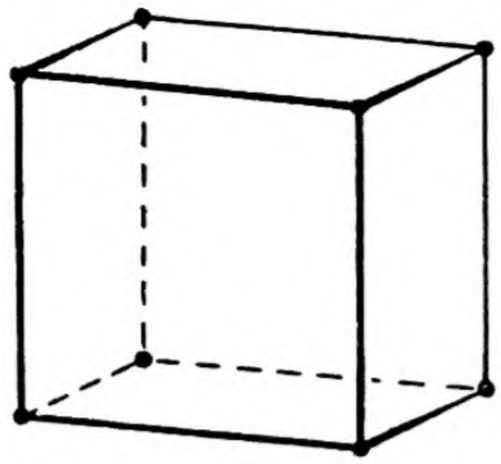

Cubic *P*

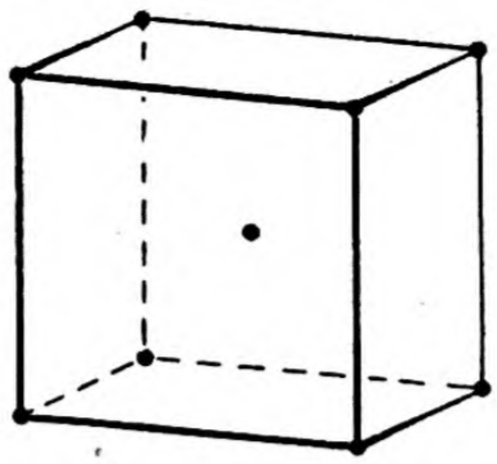

Cubic *I*

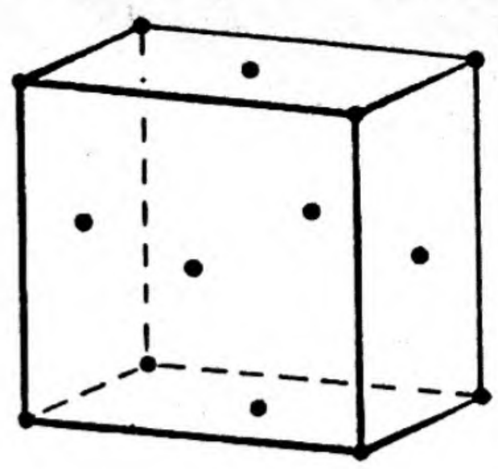

Cubic *F*

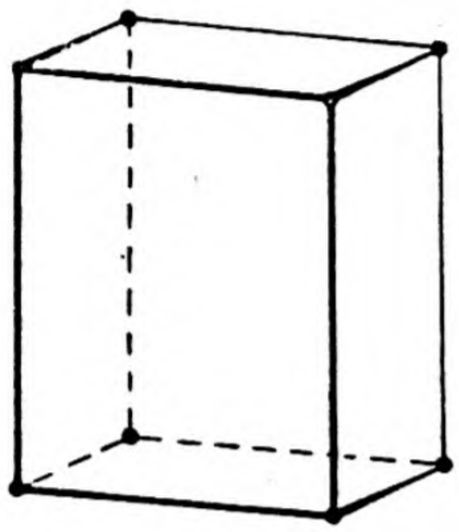

Tetragonal *P*

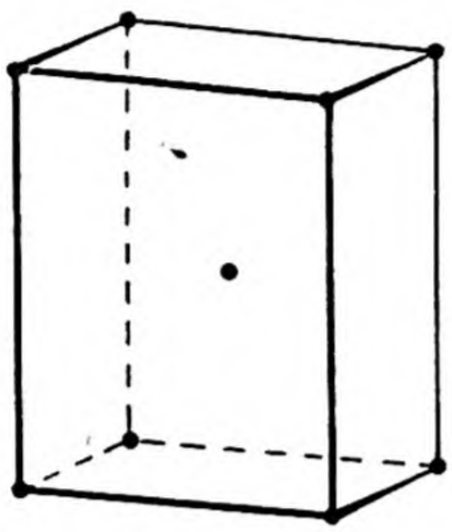

Tetragonal *I*

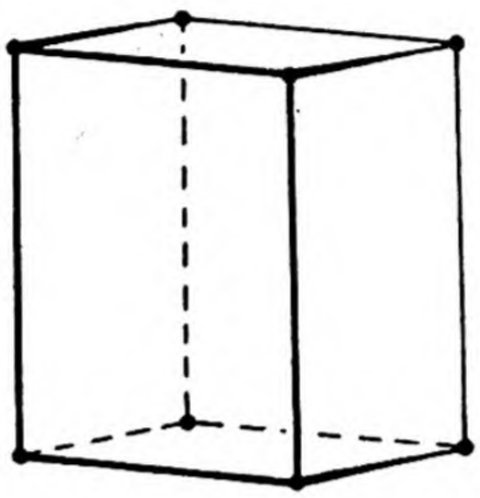

Hexagonal (*C*) or (*P*)

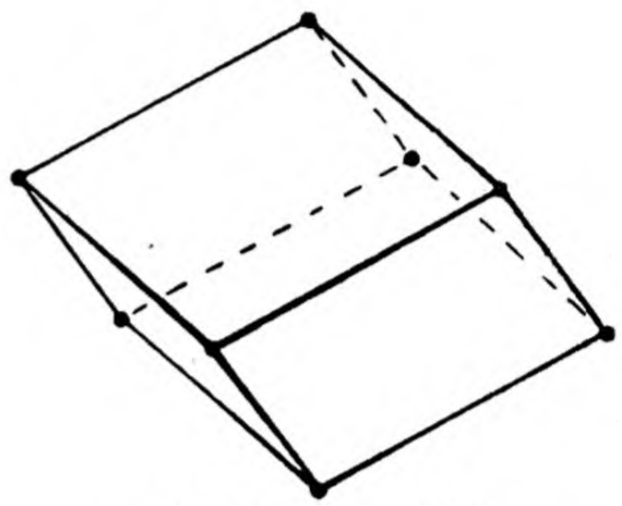

Rhombohedral (*R*)

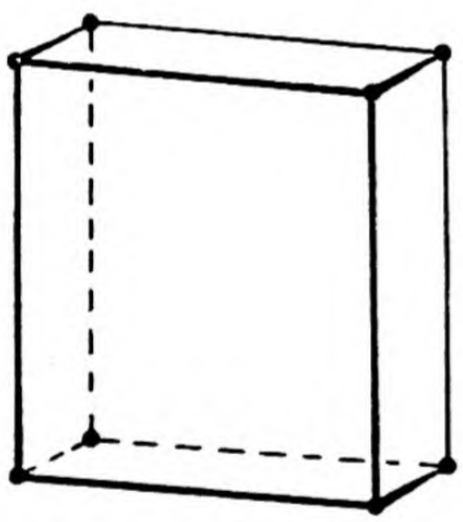

Orthorhombic *P*

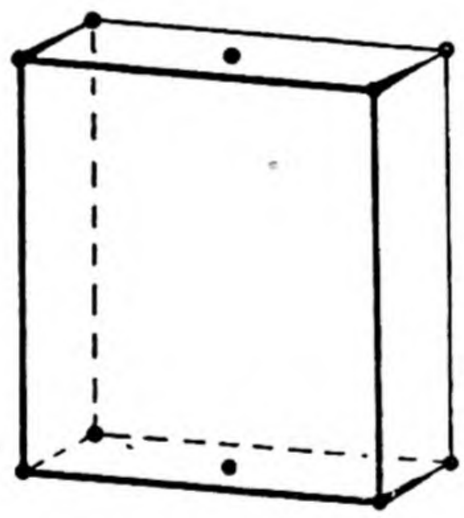

Orthorhombic *C*

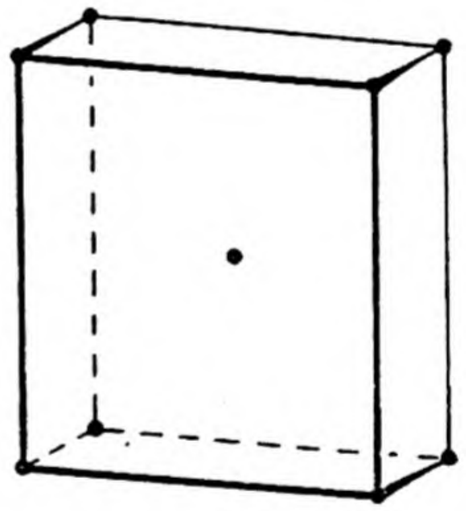

Orthorhombic *I*

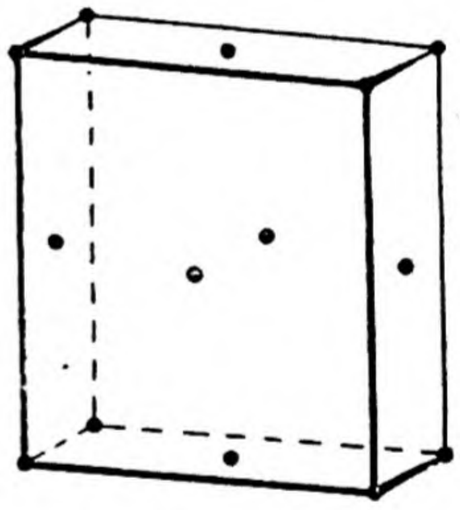

Orthorhombic *F*

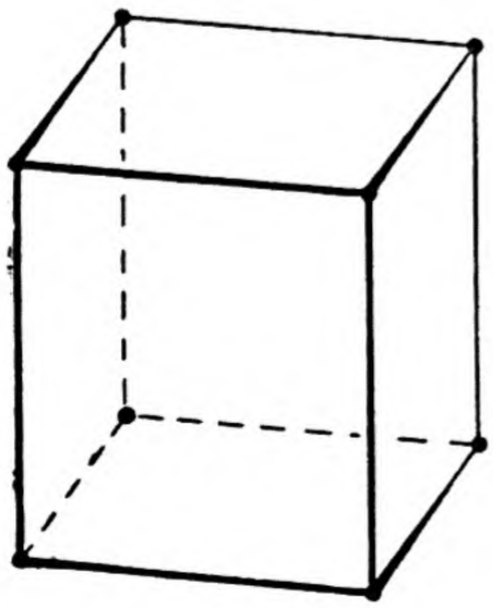

Monoclinic *P*

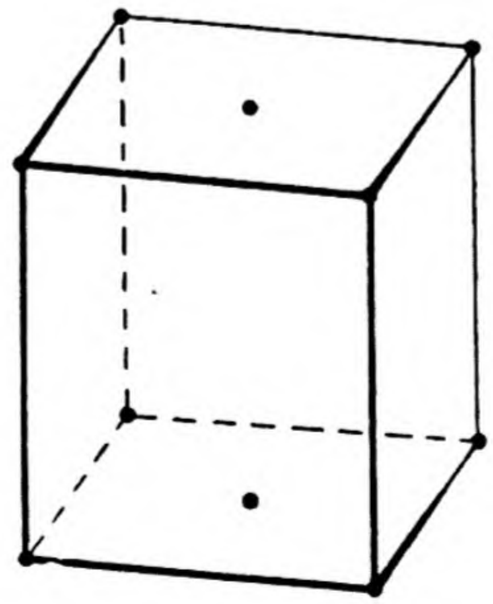

Monoclinic *C*

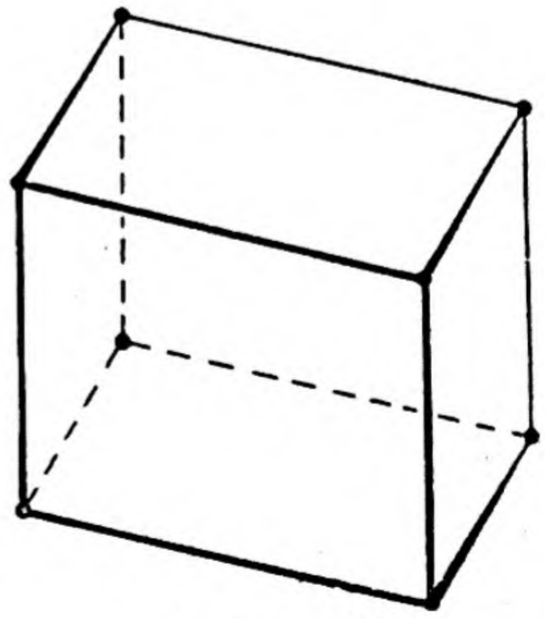

Triclinic (*P*)

FIG. 136. The fourteen Bravais lattices. When the letter symbol is within brackets it is not essential to the unique description of the lattice

THE FOURTEEN BRAVAIS LATTICES

No. in system	System	Usual lattice symbol	Alternative symbols for other orientations
3	Cubic	*P* *F* *I*	
2	Tetragonal	*P* *I*	*C* *F*
4	Orthorhombic	*P* *C* *F* *I*	*A*, *B*
2	Monoclinic	*P* *C*	*B* *A*, *I*, *F*
1	Triclinic	*P*	*A*, *B*, *C*, *I*, *F*
1	Trigonal (rhombohedral lattice)	*R*	
1	Hexagonal and trigonal (hexagonal lattice)	*C*	*H*

Some trigonal structures are based on a rhombohedral lattice and some on a hexagonal lattice. Although the hexagonal lattice has points only at the corners, it has been called *C*; also an alternative symbol *H* has been used. These matters are discussed in **10,** 1.4. In the new edition of the International Tables the *H* symbol is dropped and *P* is used for the old *C* unit cell.

1.2 Transformation of axes and face indices. In the study of crystals it is often necessary to change the axes of reference and the corresponding plane indices to another set; this can be done by fairly simple algebraic methods.

The lattice dimensions of the mineral gypsum were determined by Wooster (1936) who selected the unit cell shown in Fig. 138. Afterwards it was pointed out by Bragg (1937) that another unit cell of the same volume but of more convenient shape could be selected. Neither of these unit cells corresponded to the face-indices assigned by morphologists, and this "morphological unit cell" has been inserted in the figure. Now let us study how to transform from the first set of axes (Wooster) to the second set (Bragg); these have the y-axis in common, as required by convention for monoclinic symmetry; the x-axis is also common to both, which is accidental. We must write the unit vectors $(\mathbf{a}_2\mathbf{b}_2\mathbf{c}_2)$ of the second set of axes in terms of the unit vectors $(\mathbf{a}_1\mathbf{b}_1\mathbf{c}_1)$ of the first set

$$\mathbf{a}_2 = 1.\mathbf{a}_1 + 0.\mathbf{b}_1 + 1.\mathbf{c}_1$$
$$\mathbf{b}_2 = 0.\mathbf{a}_1 + 1.\mathbf{b}_1 + 0.\mathbf{c}_1$$
$$\mathbf{c}_2 = 0.\mathbf{a}_1 + 0.\mathbf{b}_1 + 1.\mathbf{c}_1.$$

Similarly, in transforming from the second set (Bragg) to the third set (morphological) we write the unit vectors $(\mathbf{a}_3\mathbf{b}_3\mathbf{c}_3)$ of the third set of axes in terms of the unit vectors of the second set

$$\mathbf{a}_3 = 1.\mathbf{a}_2 + 0.\mathbf{b}_2 - 1.\mathbf{c}_2$$
$$\mathbf{b}_3 = 0.\mathbf{a}_2 + 1.\mathbf{b}_2 + 0.\mathbf{c}_2$$
$$\mathbf{c}_3 = 1.\mathbf{a}_2 + 0.\mathbf{b}_2 + 1.\mathbf{c}_2.$$

Also we can transform from the first set (Wooster) to the third set (morphological);

$$\mathbf{a}_3 = 1.\mathbf{a}_1 + 0.\mathbf{b}_1 + 0.\mathbf{c}_1$$
$$\mathbf{b}_3 = 0.\mathbf{a}_1 + 1.\mathbf{b}_1 + 0.\mathbf{c}_1$$
$$\mathbf{c}_3 = 1.\mathbf{a}_1 + 0.\mathbf{b}_1 + 2.\mathbf{c}_1.$$

It is clearly unnecessary to go on writing down the **a, b, c** symbols which can be omitted, as in indexing, if we preserve the order. We are concerned only with the nine numbers which form a 'matrix', or, specifically, the matrix of the particular transformation, and which are written out as follows:

Wooster to Bragg	1	0	1
1 to 2	0	1	0
	0	0	1
Bragg to morphological	1	0	$\bar{1}$
2 to 3	0	1	0
	1	0	1
Wooster to morphological	1	0	0
1 to 3	0	1	0
	1	0	2

When there is risk of confusion between such an array of numbers forming the matrix of a transformation and a similar array of another type, the matrix is placed in bars:

$$\begin{vmatrix} u_1 & v_1 & w_1 \\ u_2 & v_2 & w_2 \\ u_3 & v_3 & w_3 \end{vmatrix}$$

An abbreviated form of printing sometimes used is:

$$u_1\ v_1\ w_1/u_2\ v_2\ w_2/u_3\ v_3\ w_3.$$

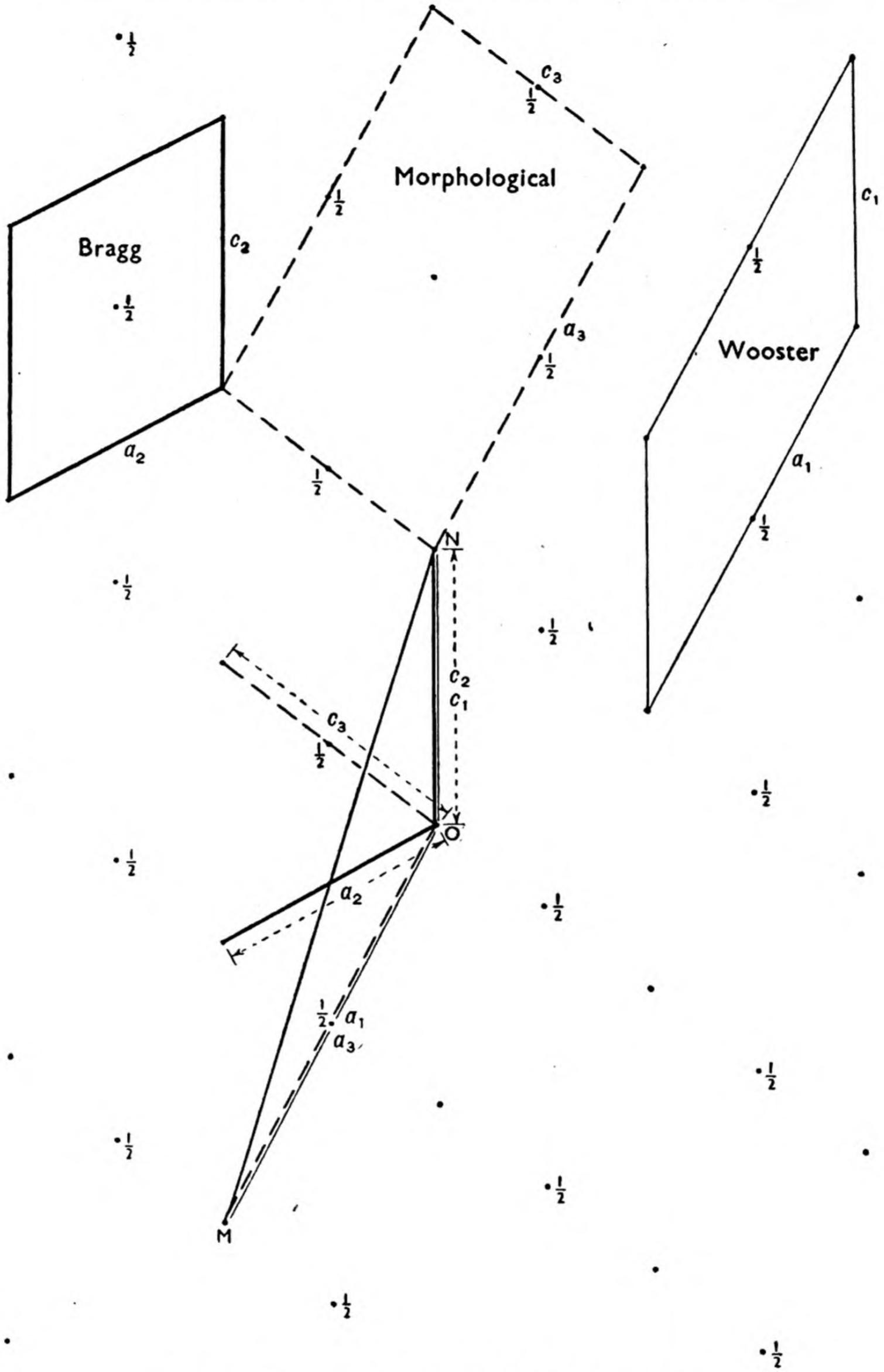

FIG. 138. Projection on (010) of the lattice of gypsum.
Scale : 1 A. = 0·5 cm.

It will be noted that we have used the same letters for the generalised form of the matrix as were used for the symbol of a zone axis in **1**, 3.8. This is because the method used in defining a zone axis by a zone symbol is simply the expression of a vector in terms of the three crystallographic axes of reference, and here we are expressing the three vectors which are to form the new set of crystallographic axes.

Now if we wish to determine the new indices $(h_2k_2l_2)$ of a plane with old indices $(h_1k_1l_1)$, we proceed as follows:

$$h_2 = u_1h_1 + v_1k_1 + w_1l_1$$
$$k_2 = u_2h_1 + v_2k_1 + w_2l_1$$
$$l_2 = u_3h_1 + v_3k_1 + w_3l_1.$$

For example, in fig. 138 the plane *NM* has the indices

$h_1k_1l_1 = (101)$ on Wooster's unit cell ;
$h_2k_2l_2 = (201)$ on Bragg's unit cell ;
$h_3k_3l_3 = (103)$ on the morphological unit cell.

If we apply the appropriate matrices in the manner described, we get :

$W \rightarrow B$	$B \rightarrow$ morph.
(101) $1+0+1=2$	$(201) \rightarrow 2+0+\bar{1}=1$
$0+0+0=0$	$0+0+0=0$
$0+0+1=1$	$2+0+1=3.$

To employ the above method of transforming indices the matrix must be known. It sometimes happens that the only information available consists of the new indices of a few faces. From this the matrix can be derived by the solution of equations, although the process may be tedious. Suppose that in the transformation from 1 (Wooster) to 2 (Bragg) in gypsum we are only given that :

(1)

	Old indices (1)			*New indices* (2)		
	h_1	k_1	l_1	h_2	k_2	l_2
(i)	0	0	1	1	0	1
(ii)	1	0	0	1	0	0
(iii)	0	1	0	0	1	0

We use the general equation :

$$h_2 = u_1h_1 + v_1k_1 + w_1l_1$$
$$k_2 = u_2h_1 + v_2k_1 + w_2l_1$$
$$l_2 = u_3h_1 + v_3k_1 + w_3l_1.$$

Now for the three planes given above, the first equation gives :

(i) $1 = u_1.0 + v_1.0 + w_1.1$
(ii) $1 = u_1.1 + v_1.0 + w_1.0$
(iii) $0 = u_1.0 + v_1.1 + w_1.0$
$\therefore\ u_1 = 1, \quad v_1 = 0, \quad w_1 = 1.$

The second equation gives in the same way :

(i) $0 = u_2.0 + v_2.0 + w_2.1$
(ii) $0 = u_2.1 + v_2.0 + w_2.0$
(iii) $1 = u_2.0 + v_2.1 + w_2.0$
$\therefore\ u_2 = 0, \quad v_2 = 1, \quad w_2 = 0.$

The third equation gives :

(i) $1 = u_3.0 + v_3.0 + w_3.1$
(ii) $0 = u_3.1 + v_3.0 + w_3.0$
(iii) $0 = u_3.0 + v_3.1 + w_3.0$
$\therefore\ u_3 = 0, \quad v_3 = 0, \quad w_3 = 1.$

From this we obtain the same matrix as before :

$$\begin{vmatrix} 1 & 0 & 1 \\ 0 & 1 & 0 \\ 0 & 0 & 1 \end{vmatrix}$$

Planes of simple indices are used in this example ; but the method is a quite general one.

From the matrix we can obtain the ratio of the volumes of the two unit cells involved in the transformation. If the determinant of the matrix is evaluated, the resulting integer or fraction is equal to the ratio, $\frac{\text{vol. of new unit cell}}{\text{vol. of old unit cell}}$, and this is called the *modulus of the transformation*. This is proved by Buerger (1942), but here it will merely be demonstrated by one or two examples. If the transformation is from one unit cell to another of the same volume, the modulus is unity ; if the transformation is to a larger unit cell the modulus will be an integer, while if the new unit cell is smaller than the old one, the modulus will be a fraction. The modulus is also equal to the ratio of the number of lattice points in the new unit cell to the number in the old unit cell, as this is equal to the ratio of the two volumes.

The determinant is evaluated in the following manner :

$$\begin{vmatrix} u_1 & v_1 & w_1 \\ u_2 & v_2 & w_2 \\ u_3 & v_3 & w_3 \end{vmatrix}$$

$$\Delta = u_1 \begin{vmatrix} v_2w_2 \\ v_3w_3 \end{vmatrix} + u_2 \begin{vmatrix} v_3w_3 \\ v_1w_1 \end{vmatrix} + u_3 \begin{vmatrix} v_1w_1 \\ v_2w_2 \end{vmatrix}$$
$$= u_1(v_2.w_3 - v_3.w_2) + u_2(v_3.w_1 - v_1w_3) + u_3(v_1w_2 - v_2w_1).$$

If we apply this to the transformations considered above, we get :

$1 \rightarrow 2$

$$\begin{vmatrix} 1 & 0 & 1 \\ 0 & 1 & 0 \\ 0 & 0 & 1 \end{vmatrix} \quad \Delta = 1 \begin{vmatrix} 1 & 0 \\ 0 & 1 \end{vmatrix} + 0 \begin{vmatrix} 0 & 1 \\ 0 & 1 \end{vmatrix} + 0 \begin{vmatrix} 0 & 1 \\ 1 & 0 \end{vmatrix} = 1$$

$2 \rightarrow 3$

$$\begin{vmatrix} 1 & 0 & \bar{1} \\ 0 & 1 & 0 \\ 1 & 0 & 1 \end{vmatrix} \quad \Delta = 1 \begin{vmatrix} 1 & 0 \\ 0 & 1 \end{vmatrix} + 0 \begin{vmatrix} 0 & 1 \\ 0 & \bar{1} \end{vmatrix} + 1 \begin{vmatrix} 0 & 1 \\ 1 & 0 \end{vmatrix} = 1 + 1 = 2.$$

It can be seen from Fig. 138 that the morphological unit-cell contains twice as many lattice points as either of the two other unit cells.

Now suppose that we have these two matrices and it is required to transform from 1 to 3. We could, of course, transform from 1 to 2 and then from 2 to 3, but if there were many indices, this would be laborious. Alternatively, we could do this for three faces and then derive the matrix (1 to 3) from them as above. In another case we might know the matrix (1 to 2) and require to transform from 2 to 1. We could transform the indices of three faces from 1 to 2 and then derive the matrix (2 to 1) by working backwards from these. The required new matrices

can, however, be obtained by straightforward manipulations.

In order to derive the matrix 1→3, given the matrices 1→2 and 2→3, we proceed in the following way. The two known matrices are written in the order 2→3 then 1→2, and are then multiplied as shown.

$$\begin{vmatrix} U_1 & V_1 & W_1 \\ U_2 & V_2 & W_2 \\ U_3 & V_3 & W_3 \end{vmatrix}_{2\to3} \quad \begin{vmatrix} u_1 & v_1 & w_1 \\ u_2 & v_2 & w_2 \\ u_3 & v_3 & w_3 \end{vmatrix}_{1\to2}$$

$$\begin{vmatrix} (U_1u_1+V_1u_2+W_1u_3) & (U_1v_1+V_1v_2+W_1v_3) & (U_1w_1+V_1w_2+W_1w_3) \\ (U_2u_1+V_2u_2+W_2u_3) & (U_2v_1+V_2v_2+W_2v_3) & (U_2w_1+V_2w_2+W_2w_3) \\ (U_3u_1+V_3u_2+W_3u_3) & (U_3v_1+V_3v_2+W_3v_3) & (U_3w_1+V_3w_2+W_3w_3) \end{vmatrix}_{1\to3}$$

As an example, we shall take the matrices given previously for the transformations 1→2 (Wooster to Bragg) and 2→3 (Bragg to Morphological) in gypsum.

$$\begin{vmatrix} 1 & 0 & \bar{1} \\ 0 & 1 & 0 \\ 1 & 0 & 1 \end{vmatrix}_{2\to3} \quad \begin{vmatrix} 1 & 0 & 1 \\ 0 & 1 & 0 \\ 0 & 0 & 1 \end{vmatrix}_{1\to2}$$

$$\begin{vmatrix} (1+0+0) & (0+0+0) & (1+0+\bar{1}) \\ (0+0+0) & (0+1+0) & (0+0+0) \\ (1+0+0) & (0+0+0) & (1+0+1) \end{vmatrix}_{1\to3} = \begin{vmatrix} 1 & 0 & 0 \\ 0 & 1 & 0 \\ 1 & 0 & 2 \end{vmatrix}$$

The inverse matrix can be derived from the direct matrix in the following manner. The symbol Δ is the determinant of the direct matrix.

Direct matrix.

$$\begin{vmatrix} u_1 & v_1 & w_1 \\ u_2 & v_2 & w_2 \\ u_3 & v_3 & w_3 \end{vmatrix}_{1\to2}$$

Inverse Matrix.

$$\begin{matrix} \begin{vmatrix} v_2w_2 \\ v_3w_3 \end{vmatrix}_{\Delta} & \begin{vmatrix} v_3w_3 \\ v_1w_1 \end{vmatrix}_{\Delta} & \begin{vmatrix} v_1w_1 \\ v_2w_2 \end{vmatrix}_{\Delta} \\ \begin{vmatrix} u_3w_3 \\ u_2w_2 \end{vmatrix}_{\Delta} & \begin{vmatrix} u_1w_1 \\ u_3w_3 \end{vmatrix}_{\Delta} & \begin{vmatrix} u_2w_2 \\ u_1w_1 \end{vmatrix}_{\Delta} \end{matrix}_{2\to1}$$

$$\begin{matrix} \begin{vmatrix} u_2v_2 \\ u_3v_3 \end{vmatrix}_{\Delta} & \begin{vmatrix} u_3v_3 \\ u_1v_1 \end{vmatrix}_{\Delta} & \begin{vmatrix} u_1v_1 \\ u_2v_2 \end{vmatrix}_{\Delta} \end{matrix}$$

Each coefficient consists of a numerator and a denominator. The denominator is the determinant of the direct matrix in each case. The three numerators in any row are the three cofactors of the terms in the corresponding column of the direct matrix. We shall take as an example the transformation 2→3 (Bragg to Morphological) in gypsum.

Direct matrix.

$$\begin{vmatrix} 1 & 0 & \bar{1} \\ 0 & 1 & 0 \\ 1 & 0 & 1 \end{vmatrix} \quad \Delta = 1\begin{vmatrix} 1 & 0 \\ 0 & 1 \end{vmatrix} + 0\begin{vmatrix} 0 & 1 \\ 0 & \bar{1} \end{vmatrix} + 1\begin{vmatrix} 0 & \bar{1} \\ 1 & 0 \end{vmatrix}$$

$$\Delta = 1 - 0 + 0 - 0 + 0 - \bar{1}$$

$$\Delta = 2.$$

Inverse matrix.

$$\begin{matrix} \begin{vmatrix} 1 & 0 \\ 0 & 1 \end{vmatrix}_{2} & \begin{vmatrix} 0 & 1 \\ 0 & \bar{1} \end{vmatrix}_{2} & \begin{vmatrix} 0 & \bar{1} \\ 1 & 0 \end{vmatrix}_{2} \\ \begin{vmatrix} 0 & 0 \\ 1 & 1 \end{vmatrix}_{2} & \begin{vmatrix} 1 & 1 \\ \bar{1} & 1 \end{vmatrix}_{2} & \begin{vmatrix} \bar{1} & 1 \\ 1 & 1 \end{vmatrix}_{2} \\ \begin{vmatrix} 0 & 1 \\ 1 & 0 \end{vmatrix}_{2} & \begin{vmatrix} 1 & 0 \\ 1 & 0 \end{vmatrix}_{2} & \begin{vmatrix} 1 & 0 \\ 0 & 1 \end{vmatrix}_{2} \end{matrix} = \begin{vmatrix} \frac{1}{2} & 0 & \frac{1}{2} \\ 0 & 1 & 0 \\ \bar{\frac{1}{2}} & 0 & \frac{1}{2} \end{vmatrix} \quad \Delta = \tfrac{1}{2}.$$

When a set of axes is unchanged by a transformation, this is called the *identical transformation*. The identical matrix is:

$$\begin{vmatrix} 1 & 0 & 0 \\ 0 & 1 & 0 \\ 0 & 0 & 1 \end{vmatrix} \quad \Delta = 1.$$

If axes are changed in unit length but not in direction, the matrix will be similar to this but with other figures in place of unity. When a matrix consists of the identical matrix with two rows interchanged, the inverse matrix is the same as the direct one. Such a case arises when two axes are interchanged, leaving the third common to both orientations. Then the inverse transformation simply consists in changing these two axes back again.

When the modulus is negative, this indicates a change from a right-handed to a left-handed system of axes or vice versa.

It should be noted that the matrices can be written as follows, where x, y, z are the old axes and x', y', z' the new axes. The shorthand expression 'in terms of' has the following meaning; if we express the vector x' in terms of three co-ordinates along the axes x, y, z,

then 'x' in terms of x' means the first of these co-ordinates.

MATRICES FOR TRANSFORMATION OF FACE INDICES

Old→new

x' in terms of x	x' in terms of y	x' in terms of z
y' ,, ,, x	y' ,, ,, y	y' ,, ,, z
z' ,, ,, x	z' ,, ,, y	z' ,, ,, z

New→old

x in terms of x'	x in terms of y'	x in terms of z'
y ,, ,, x'	y ,, ,, y'	y ,, ,, z'
z ,, ,, x'	z ,, ,, y'	z ,, ,, z'

1.3 Transformation of zone indices. If the face-index matrix is known, we can easily obtain the new index of any given zone axis. This can be done in either of two ways. If only one zone-axis symbol is to be transformed it is simplest to select any two non-opposite faces in the zone, then to transform their indices and finally to cross-multiply the two new indices. But if several zone symbols are to be transformed, it is more convenient to derive the appropriate matrix for the direct transformation of zone symbols. It should be noted that this is not the same matrix as that for the transformation of face indices.

In the example of Fig. 141, the point P is the first lattice point from the origin along the selected zone axis. The point P has the co-ordinates $[3\bar{1}0]$ on the old axes and $[\frac{4}{3}\,\frac{1}{3}\,0]$ on the new axes. It is clear that the simplest two matrices for these transformations are :

ZONE INDICES

Old→new

$$\begin{vmatrix} \frac{1}{3} & \frac{\bar{1}}{3} & 0 \\ \frac{1}{3} & \frac{2}{3} & 0 \\ 0 & 0 & 1 \end{vmatrix}$$

New→old

$$\begin{vmatrix} 2 & 1 & 0 \\ \bar{1} & 1 & 0 \\ 0 & 0 & 1 \end{vmatrix}$$

We can express these in general terms in the following way, the dashed axes being the new set.

ZONE-INDEX MATRICES

Old→new

x in terms of x'	y in terms of x'	z in terms of x'
x ,, ,, y'	y ,, ,, y'	z ,, ,, y'
x ,, ,, z'	y ,, ,, z'	z ,, ,, z'

new→old

x' in terms of x	y' in terms of x	z' in terms of x
x' ,, ,, y	y' ,, ,, y	z' ,, ,, y
x' ,, ,, z	y' ,, ,, z	z' ,, ,, z

The table on this page, where the face-index matrices are given in the same general way, shows that we can obtain the zone-index matrix from the face-index matrices in the following way. To obtain the zone-index matrix (old to new), take the face-index matrix (new to old) and interchange rows and columns. Correspondingly, to obtain the zone-index matrix (new to old), take the face-index matrix (old to new) and interchange rows and columns.

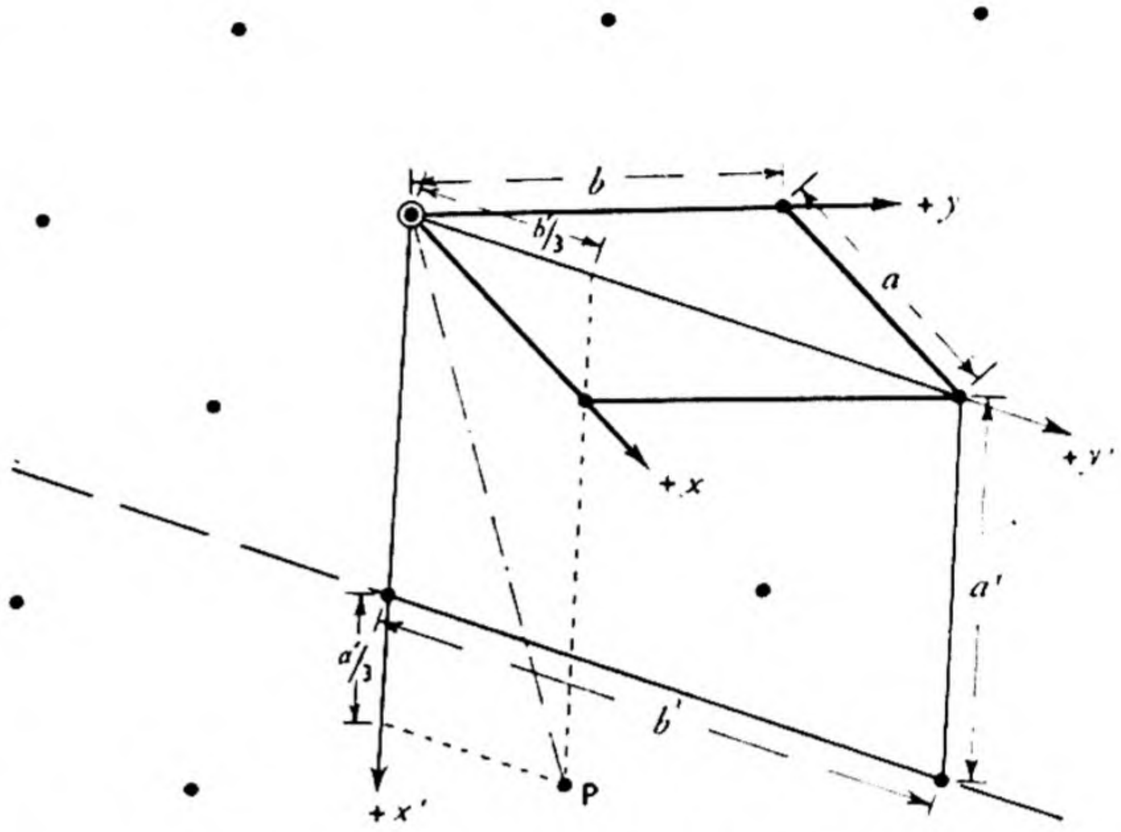

FIG. 141. Diagram to illustrate the transformation of a zone-axis symbol

In the example of Fig. 141 the z-axis is taken as unchanged to simplify the drawing. We can derive the face-index matrices in the manner previously described.

Old→new

$$\begin{vmatrix} 2 & \bar{1} & 0 \\ 1 & 1 & 0 \\ 0 & 0 & 1 \end{vmatrix} \quad \Delta = 3$$

New→old

$$\begin{vmatrix} \frac{1}{3} & \frac{1}{3} & 0 \\ \frac{\bar{1}}{3} & \frac{2}{3} & 0 \\ 0 & 0 & 1 \end{vmatrix} \quad \Delta = \tfrac{1}{3}.$$

It is clear that if we interchange rows and columns in the first of these, we obtain the second of the zone-index matrices given above; while the same treatment of the second of these gives the first of the two zone-index matrices. These zone-index matrices can, of course, be treated algebraically in the same way as the face-index matrices.

1.4 Relation between the hexagonal and the rhombohedral lattices. Even before the days of X-ray crystallography, there were arguments about the number of crystal systems. One point of view was that all crystals possessing either a rotation-or inverse-hexad axis or a single rotation- or inverse-triad axis should be assigned to the hexagonal system; crystals of three-fold symmetry only were allocated to the trigonal (rhombohedral) subdivision of the hexagonal system. The other view was that this subdivision should have the status of a separate system, the trigonal (or rhombohedral).

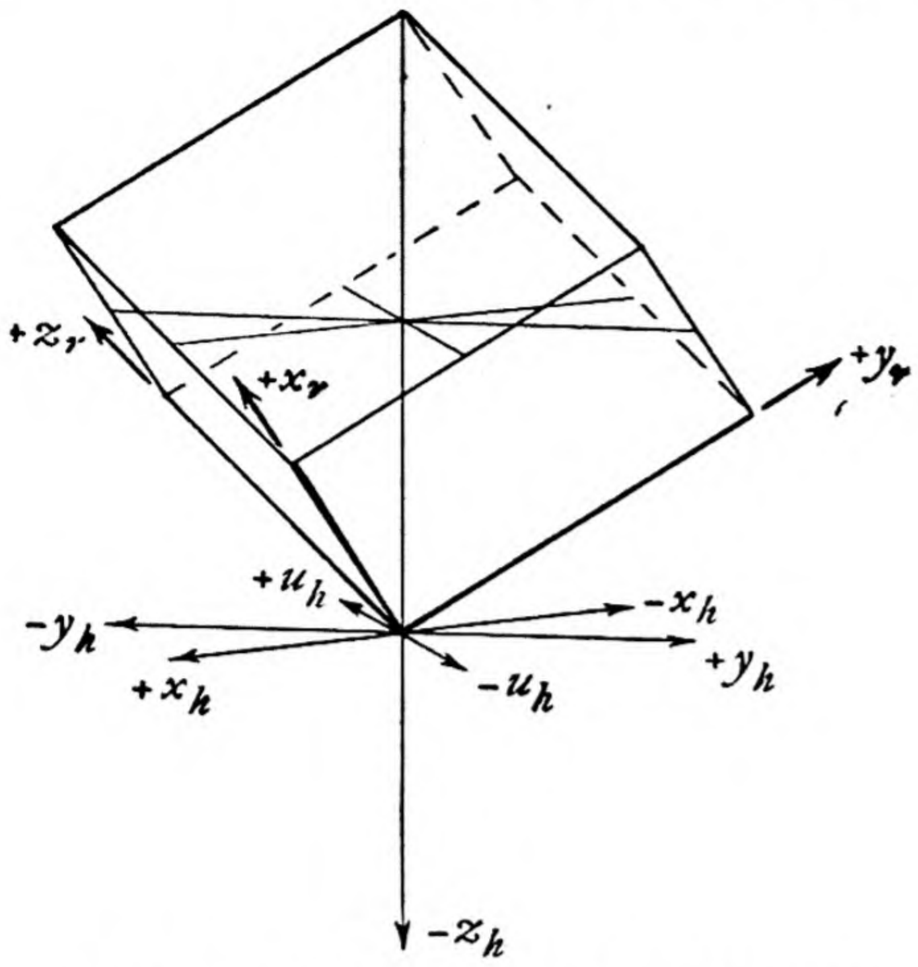

FIG. 142.1. Hexagonal and rhombohedral crystallographic axes

The reason for the difficulty can be seen if the nature of the crystallographic axes of reference is considered. Miller referred the faces of all crystals of six- or three-fold symmetry to three axes of equal unit length which were equally inclined to each other (Fig. 142.1). Such a set of axes has three-fold symmetry but not six-fold symmetry, and so it proved unsuitable for crystals of six-fold symmetry. If the faces of the obverse rhombohedron, a special form of the class $\bar{3}m$, are indexed according to Miller axes, as shown in Fig. 142.2, the indices are {100}. The complementary (reverse)† rhombohedron $\{22\bar{1}\}$ is a quite different form, although it can be brought into morphological coincidence with the first rhombohedron by rotation about the triad axis through an angle of 60°. Now in class $6/m$ the corresponding form is a hexagonal bipyramid (Fig. 142.2) with twelve faces identical in relative position with those of the two rhombohedra taken together. It is clear that the faces of the same form would now be represented by two different groups of indices, if Miller axes were used.

It was to avoid this difficulty that Bravais proposed the addition of a fourth axis in dealing with crystals of six-fold symmetry. As this set of axes has six-fold symmetry, the indexing (Fig. 142.2) is convenient for crystals of six-fold symmetry, but it obscures the difference between the two complementary rhombohedra. It is clear that there is no perfect solution and that convenience must be the deciding factor. But before we pursue this matter further it is necessary to take into account the information provided by X-ray examination.

The hexagonal lattice consists of sheets of points stacked exactly on top of each other (Fig. 143). The unit cell is not taken to be a hexagonal prism, because a smaller unit cell exists which is a right-prism based on a 60°-angle rhombus. This unit cell is primitive and contains only one lattice point, but it has been called *C*. In the figure it is obvious that a *C*-face-centred unit cell is obtained by the choice of ortho-hexagonal axes. Consequently, in the space groups based on this lattice, certain characteristics appear similar to those of space groups based on *C*-face-centred lattices in other systems. Thus the letter *C* was used to designate this lattice even although the smallest unit cell, taking hexagonal (Miller-Bravais) axes, is really primitive. The four-axis (Miller-Bravais) system of axes is clearly the most convenient for such a lattice, although it is common to omit the third of the indices, *u*, and to indicate this by an asterisk. If, however, a rhombohedral unit cell were to be outlined by joining up points in the hexagonal lattice as shown in Fig. 143, it would be a rhombohedron of three times the height of the *C* unit cell and three times the volume. This triple, primitive cell is a true unit cell although not the smallest, as, in addition to the corner points, it contains two other points at $\frac{1}{3}$ and at $\frac{2}{3}$ along the vertical axis.

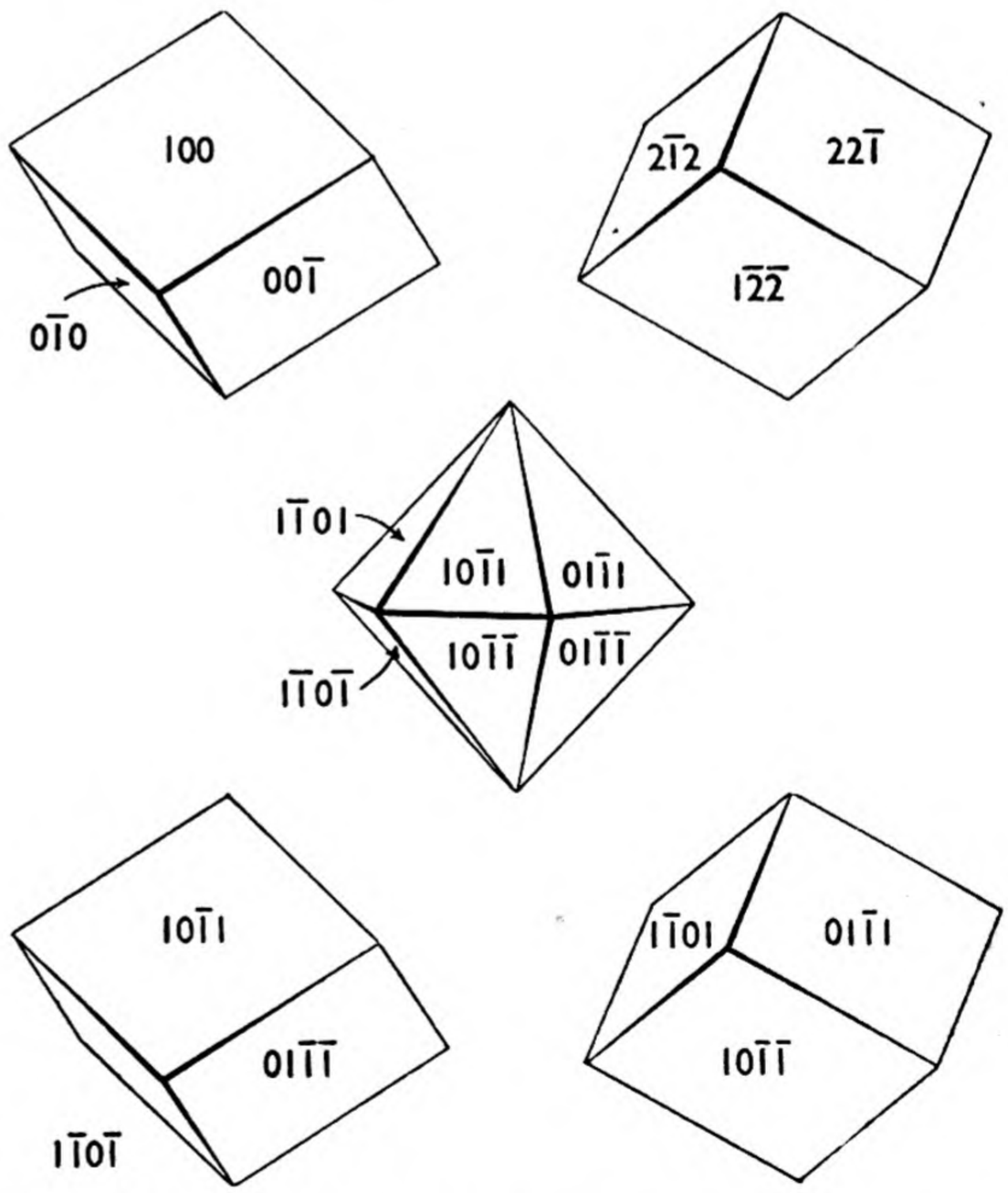

FIG. 142.2. Hexagonal bipyramid with complementary rhombohedra indexed on both sets of axes

† The terms ' obverse and reverse ' are suggested here in place of previously-used terms such as ' positive and negative ', or ' direct and inverse '.

surrounded by a sphere of radius equal to half the smallest distance between lattice points, the first layer can be laid on top of the zero layer (Fig. 144) either in the hollows marked 1 or in those marked 2; it is immaterial, but we will choose those marked 1. Now the second layer can be laid either in the hollows marked 2 or 0; if the latter were chosen, the lattice would be destroyed, because the orientation of the surrounding spheres would not be the same for all the spheres. If the set of hollows marked 2 is used, and the third layer is then placed over the zero layer, a lattice results in which the smallest unit cell is a primitive rhombohedron. In this lattice we can select a triply-primitive unit cell which is a right-prism of the same height as the rhombohedron, with a 60° angle rhombus as a base. The edges of either of these two unit cells could be used as crystallographic axes for indexing the faces either on the three-axes or the four-axes methods respectively. It should be noted that the projections on the basal plane of the rhombohedral axes are inclined at 30° to the hexagonal axes. The triple hexagonal unit cell can be chosen in one or other of two positions relative to the unit rhombohedron. With the hexagonal axes in the standard *C*-orientation (Fig. 144), the unit rhombohedron may be in either the obverse or the reverse positions relative to these axes.

It can be said, therefore, that the hexagonal and the rhombohedral lattices are two quite distinct Bravain lattices because the arrangement of the points is

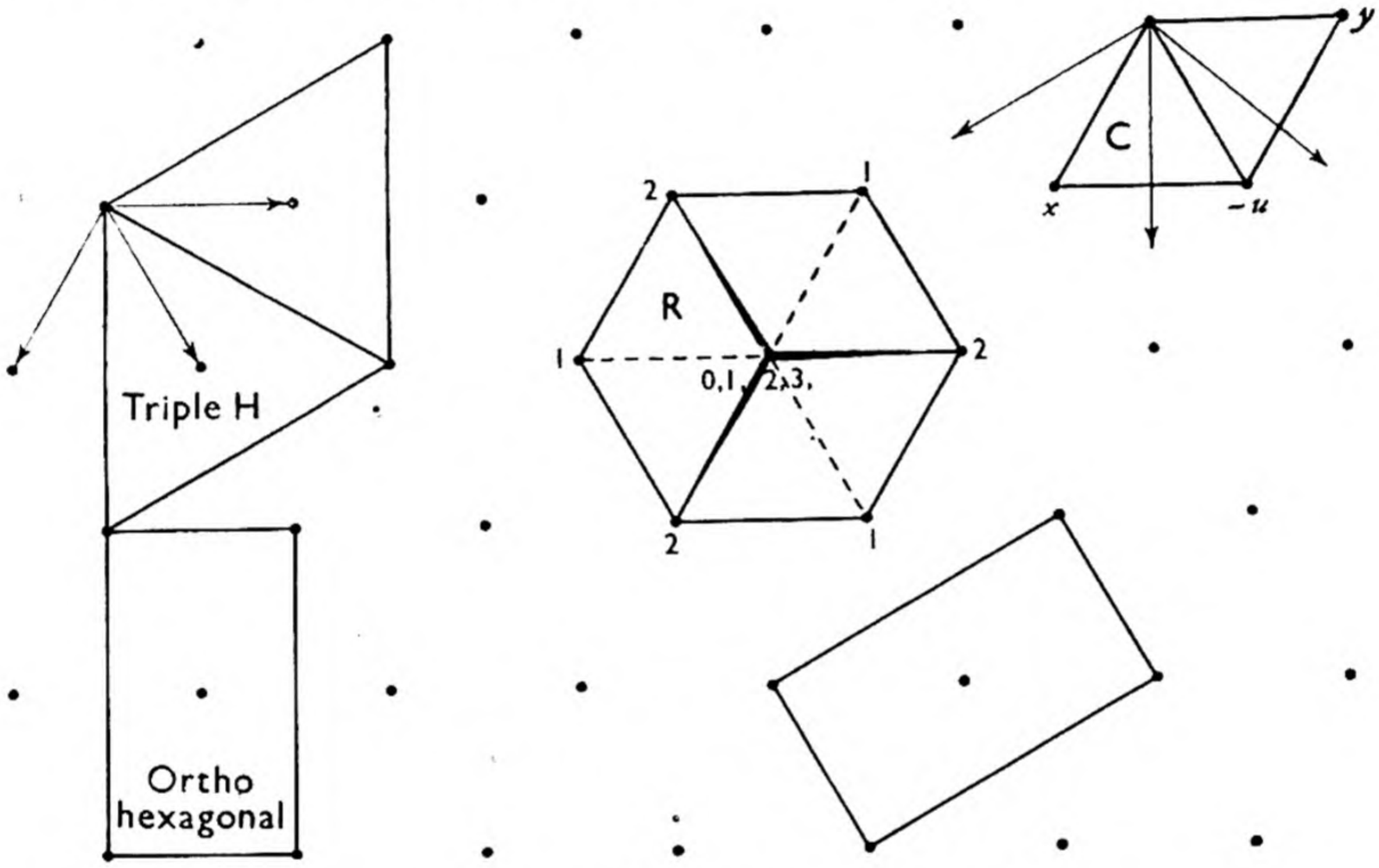

FIG. 143. Hexagonal lattice projected on (0001).
C is the smallest (primitive) unit cell.
H is the triple hexagonal unit cell.
R is the rhombohedral (triple) unit cell.
Two ways of outlining the orthohexagonal unit cell are also shown.
The figures refer to the number of the layer vertically above the zero layer through the origin

space is different. The smallest unit cell in the former is of such a shape that the four-axes (Miller-Bravais) method of indexing is the most convenient, and henceforth we shall refer to this as *hexagonal indexing* and to the axes as *hexagonal axes*. In the rhombohedral lattice the smallest unit is a rhombohedron the edges of which are the axes for the three-axes (Miller) method of indexing, and we shall refer to this as *rhombohedral indexing* and to the axes as *rhombohedral axes*.

It has been seen that a triple rhombohedral cell could be outlined in the hexagonal lattice. In practice, it is seldom necessary to do this, because crystals with a hexagonal lattice are most conveniently indexed on hexagonal axes. But for some purposes it may be useful to employ this transformation in the study

of trigonal crystals based on a hexagonal lattice. The important mineral quartz is one of these, and in older text-books its morphological data were usually in rhombohedral form. For the study of certain physical properties of trigonal crystals also it may be more convenient to use rhombohedral axes even where the lattice is really hexagonal. This is because the symmetry of the crystal is trigonal although the lattice is hexagonal.

study of trigonal crystals, but for X-ray work with trigonal crystals based on a rhombohedral lattice, it is more convenient to use Miller indices. We must, therefore, consider the appropriate matrices for these transformations. In Fig. 144 are shown the relations between the primitive rhombohedron of a rhombohedral lattice and the triple hexagonal cell in two different positions. The second of these corresponds to the choice of hexagonal axes which

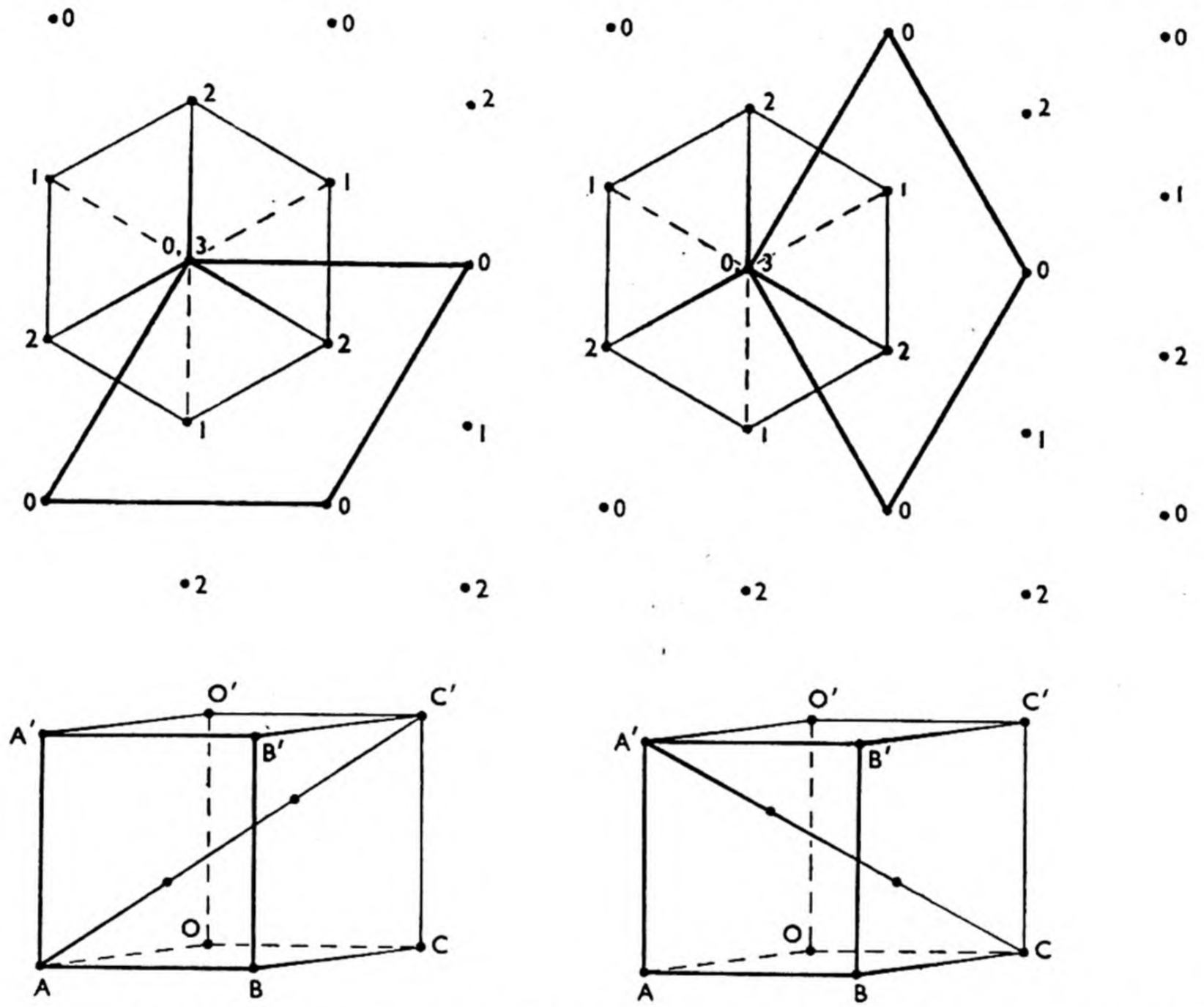

FIG. 144. Rhombohedral lattice showing the obverse (on the left) and the reverse (on the right) rhombohedral unit cells in plan and in clinographic projection

The matrices (face-index) are as follows:

HEXAGONAL LATTICE

C (hexagonal)$\rightarrow R$ (triple) $\quad R$ (triple)$\rightarrow C$ (hexagonal)

$$\begin{vmatrix} 1 & 0 & 1 \\ 0 & 1 & 1 \\ \bar{1} & \bar{1} & 1 \end{vmatrix} \quad \Delta = 3 \qquad \begin{vmatrix} \frac{2}{3} & \frac{\bar{1}}{3} & \frac{\bar{1}}{3} \\ \frac{\bar{1}}{3} & \frac{2}{3} & \frac{\bar{1}}{3} \\ \frac{1}{3} & \frac{1}{3} & \frac{1}{3} \end{vmatrix} \quad \Delta = \tfrac{1}{3}.$$

One of the most important uses of matrices is in the transformation from the hexagonal axes to rhombohedral and vice versa in the rhombohedral lattice. By means of simple morphological study, it is not possible to decide whether the lattice of a particular trigonal crystal is hexagonal or rhombohedral (but see work of Donnay and Harker, an account of which is given by Phillips, 1946). Miller-Bravais indices are much used in the morphological results in the rhombohedron being in the reverse orientation.

RHOMBOHEDRAL LATTICE

STANDARD FACE-INDEX MATRICES

Triple C (hexagonal)$\rightarrow R$ (primitive, obverse) $\quad R$ (primitive)$\rightarrow$ triple C (hexagonal)

$$\begin{vmatrix} \frac{2}{3} & \frac{1}{3} & \frac{1}{3} \\ \frac{\bar{1}}{3} & \frac{1}{3} & \frac{1}{3} \\ \frac{\bar{1}}{3} & \frac{\bar{2}}{3} & \frac{1}{3} \end{vmatrix} \quad \Delta = \tfrac{1}{3} \qquad \begin{vmatrix} 1 & \bar{1} & 0 \\ 0 & 1 & \bar{1} \\ 1 & 1 & 1 \end{vmatrix} \quad \Delta = 3.$$

Triple C (hexagonal)$\rightarrow R$ (primitive, reverse) $\quad R$ (primitive)$\rightarrow$ triple C (hexagonal)

$$\begin{vmatrix} \frac{1}{3} & \frac{\bar{1}}{3} & \frac{1}{3} \\ \frac{1}{3} & \frac{2}{3} & \frac{1}{3} \\ \frac{\bar{2}}{3} & \frac{\bar{1}}{3} & \frac{1}{3} \end{vmatrix} \quad \Delta = \tfrac{1}{3} \qquad \begin{vmatrix} 1 & 0 & \bar{1} \\ \bar{1} & 1 & 0 \\ 1 & 1 & 1 \end{vmatrix} \quad \Delta = 3.$$

There has been confusion about the transformation from hexagonal to rhombohedral axes. In text-books various equations have been given which relate the Miller-Bravais indices $h\ k\ i\ l$ to the Miller indices $p\ q\ r$. This variation arises because the morphologist is concerned only with the directions of the planes and not with their spacing. But for the calculation of spacings, care must be exercised in transforming indices. In Tutton (1922) the equations are given as follows, the symbols i and k having been interchanged to conform to our usage, and the symbol i then omitted.

$$p=2h+k+l \qquad q=-h+k+l \qquad r=-h-2k+l$$

$$h=\frac{p-q}{3} \qquad k=\frac{q-r}{3} \qquad l=\frac{p+q+r}{3}$$

These are equivalent to the following matrices :

Triple C (hexagonal)$\rightarrow R$

$$\begin{vmatrix} 2 & 1 & 1 \\ \bar{1} & 1 & 1 \\ \bar{1} & \bar{2} & 1 \end{vmatrix} \quad \Delta=9$$

$R\rightarrow$triple C (hexagonal)

$$\begin{vmatrix} \frac{1}{3} & \frac{\bar{1}}{3} & 0 \\ 0 & \frac{1}{3} & \frac{\bar{1}}{3} \\ \frac{1}{3} & \frac{1}{3} & \frac{1}{3} \end{vmatrix} \quad \Delta=\frac{1}{3}.$$

It can be seen that these matrices are not in the same ratios as the standard ones above.

From the moduli it is clear that the hexagonal cells involved are *reduced cells* and not true cells of the lattice, because their volumes are only $\frac{1}{3}$ and $\frac{1}{9}$ of that of the primitive rhombohedron. Such cells are quite valid for transformation of data in which only directions are concerned, but are useless in spacing calculations, and nothing is gained by their use in this case. The matrix $C\rightarrow R$ corresponds also to the equations given by Wyckoff (1931).

In the International Tables (1935, p. 471) drawings and equations are given for transformation from hexagonal to rhombohedral axes and vice versa. Unfortunately, these are inconsistent, as several different hexagonal cells are involved without any clear explanation, and use of them should be avoided.

1.5 Systematically-absent reflections due to lattice type. We studied in **10**, 1.1 the different types of Bravais lattice. In practice the lattice type is determined from consideration of the *systematically-absent reflections* from general planes *hkl*. When the vectors of the unit cell have been chosen in such a way that the lattice is centred, then certain kinds of indices *hkl* never appear among the recorded reflections, and from the nature of these the type of centring of the lattice can be deduced. The systematic absence of certain kinds of indices among special reflections (for example, *hol* and *h*oo) is produced by the presence of certain elements of symmetry in the space group, but we shall not concern ourselves with these here. The term *extinctions* is sometimes used for systematic absences, but this is undesirable in view of the various other meanings of this word.

In Fig. 145 the traces of the lattice planes $23l$ are drawn in plan for a C-face-centred lattice. The first plane of this set, out from the origin, has intercepts $\frac{1}{2}$ and $\frac{1}{3}$ on x and y respectively, and no plane of this set passes through the centring points. The path-difference between rays reflected from consecutive planes of the set is, by definition, equal to λ. It can be seen from the figure that the rays

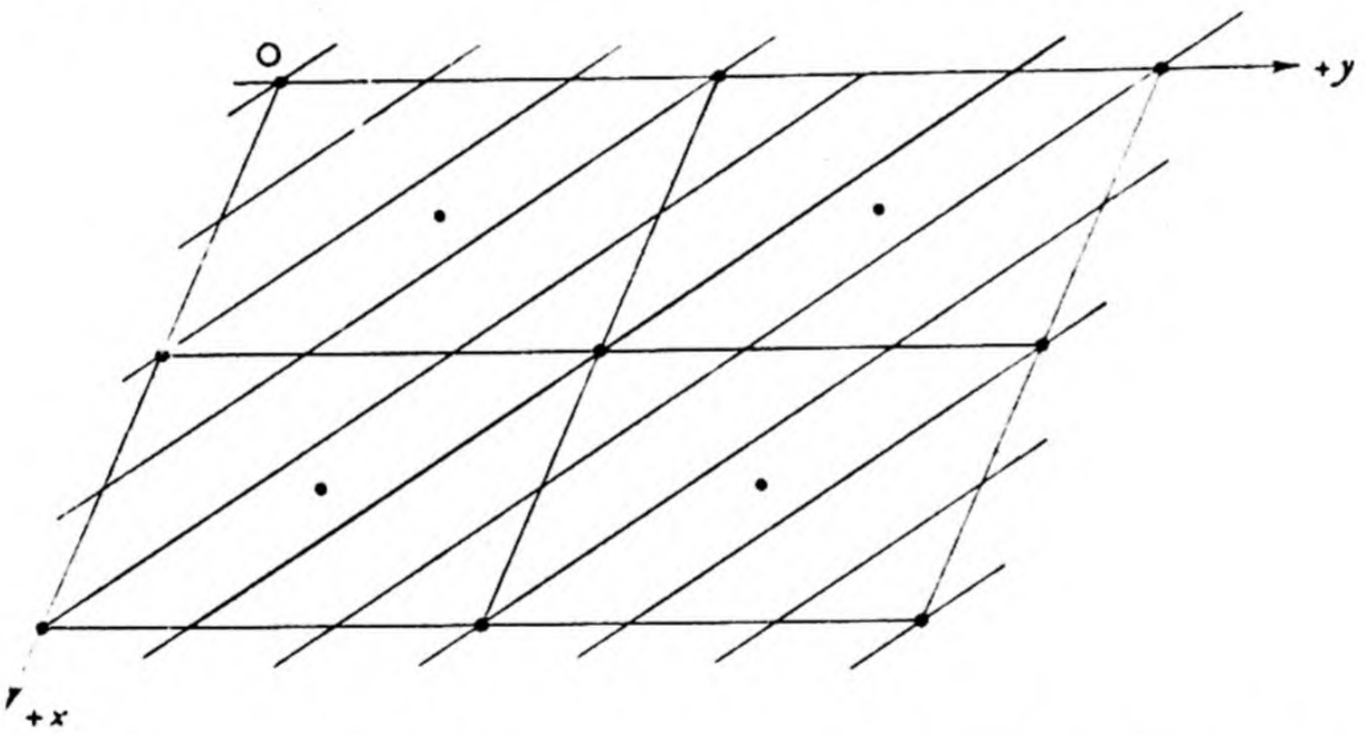

FIG. 145. Projection on (001) of a C-face-centred lattice showing the traces of the planes $23\,l$

scattered from the lattice points on these planes have a path-difference relative to those from the other lattice points of $\lambda/2$. Since the scattering power of the two groups of lattice points is equal, the net scattering is zero. The amplitude will be non-zero only when all the lattice points lie on the set of lattice planes under consideration, the condition for which is that $(h+k)=2n$, where n is any integer. Analogously, we can deduce the condition for reflections to be present for lattices centred on the A or B faces and, by combining the three conditions, we can obtain the condition for the all-face centred lattice (F).

In Fig. 146 is shown a body-centred lattice with the 232 planes inserted. It is clear that the number of planes of this set which interesect the body diagonal

OP is $(2+3+2)=7$. Since this is an odd number, the body-centring points lie half way between adjacent planes of the set. Consequently there will be zero amplitude of reflection, and it can easily be shown that this is so for all planes in which the sum of the indices is odd. When the sum of the indices is even, all the points lie on planes of the set.

We can generalise this argument. The number of planes hkl which intersect the body- (or the face-) diagonal on which the centring points lie in the unit cell is given by $(h+k+l)$, where **a, b, c** are unit vectors on the crystallographic axes and $(\mathbf{a}+\mathbf{b}+\mathbf{c})$ defines the diagonal in question. From the position of the centring points on the diagonal it is easy to

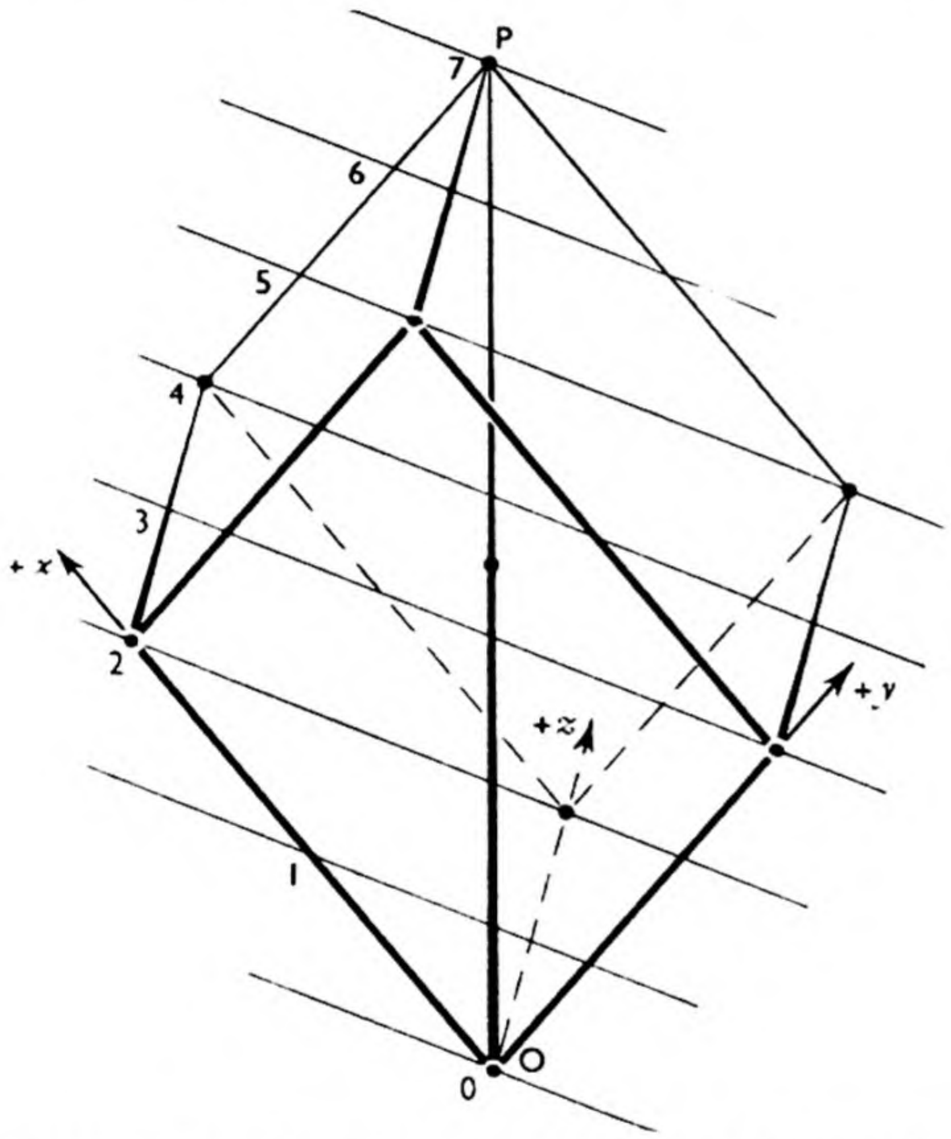

FIG. 146. Drawing of the unit cell of a lattice showing the planes 232

deduce the possible values for $(h+k+l)$ which will correspond to permitted reflections.

In Fig. 144 is shown a rhombohedral lattice on which is outlined the triple hexagonal unit cell within which points lie at $\frac{1}{3}$ and $\frac{2}{3}$ along a body diagonal. Attention must be paid to the particular body diagonal on which the points lie. We can apply the same argument as that used above; we have to find the condition that all the lattice points should lie on planes of the particular set. In the obverse position of the rhombohedron (Fig. 144), the centring points lie on the diagonal AC', which is defined by the vector $(-\mathbf{a}+\mathbf{b}+\mathbf{c})$. It is clear that the centring points will lie on the planes of a set only when $(-h+k+l)=3n$, where n is any integer. Correspondingly, for the reverse position of the rhombohedron, the condition for permitted reflections is, $(h-k+l)=3n$. Although the case of a hexagonal lattice indexed on the axes of the triple rhombohedral unit cell is unlikely to arise in practice, the corresponding condition for reflections to occur might be of interest in a rhombohedral substance with a pseudo-hexagonal structure. In Fig. 143 it is shown that the centring points lie at $\frac{1}{3}$ and $\frac{2}{3}$ along the triad body diagonal. Consequently the condition for reflections to occur is that $(p+q+r)=3n$; the question of the alternative position does not arise in this case.

The conditions for systematically-absent reflections hkl are tabulated below for all lattices. An analytical method of deriving these conditions is given in **15**, 3·5.

CONDITIONS FOR GENERAL REFLECTIONS hkl TO BE PRESENT

LATTICE TYPE	CONDITION
A face-centred	$(k+l)=2n$
B face-centred	$(h+l)=2n$
C face-centred	$(h+k)=2n$
F (all face-centred)	h, k and l homogeneous (that is, all odd or all even)
I (body-centred)	$(h+k+l)=2n$
R (rhombohedral, indexed on hexagonal axes)	$(-h+k+l)=3n$ for obverse orientation of rhombohedron $(h-k+l)=3n$ for reverse orientation of rhombohedron
C (hexagonal indexed on rhombohedral axes)	$(p+q+r)=3n$
P (primitive)	No restriction. But the lattice can be called primitive only after the absence of all of the possible restrictions has been demonstrated

Note. If the C (hexagonal) and R lattices are indexed on hexagonal and on rhombohedral axes respectively, there will be no systematically-absent hkl reflections since in both cases the unit cell is primitive.

2. Symmetry of Crystal Classes

2.1 The 32 point-groups and the international nomenclature. In **1**, 2.1 it was seen that there are thirty-two different combinations of crystallographic elements of external symmetry. These groups of

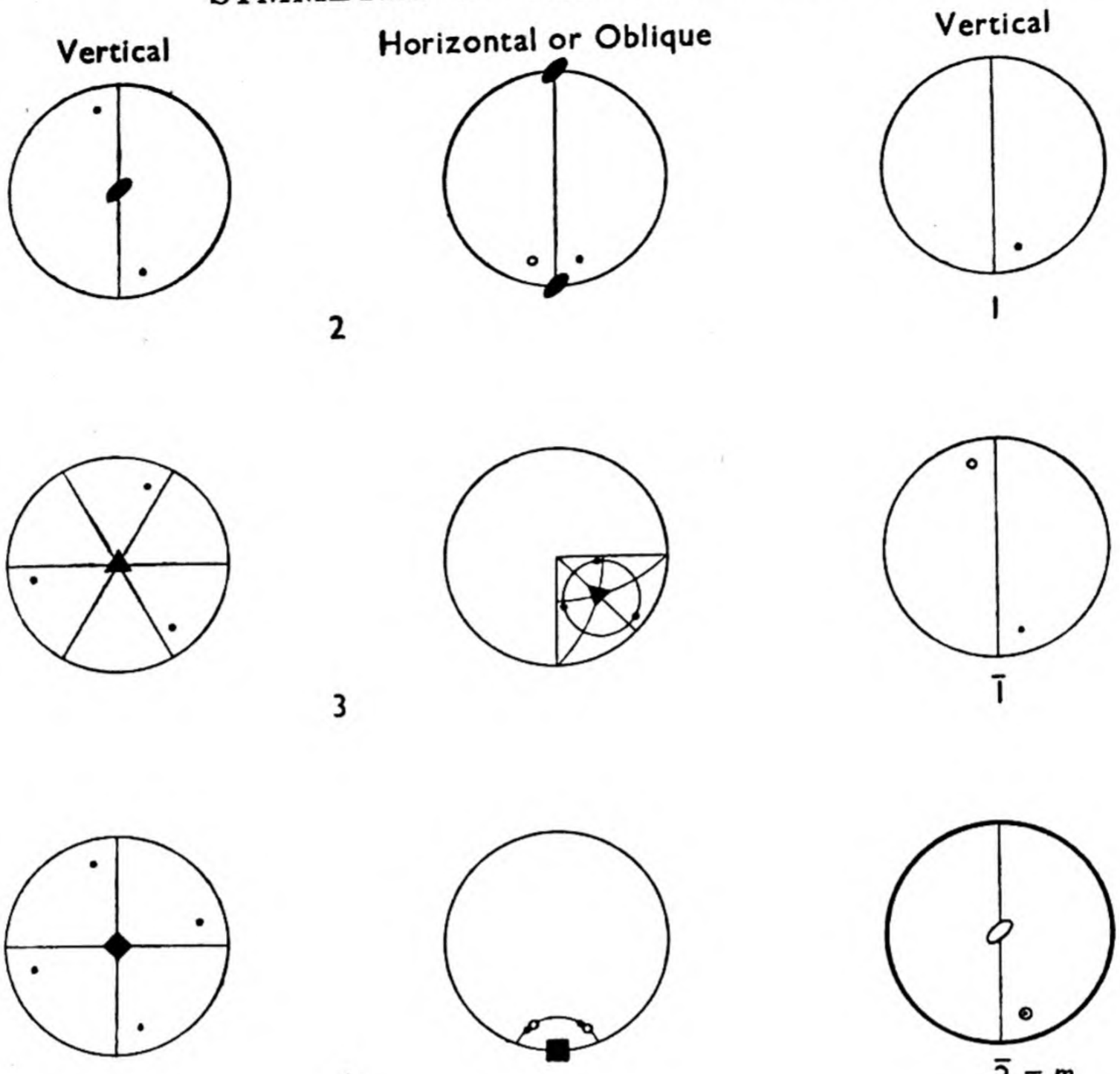

FIG. 147. Stereograms showing the operation of certain symmetry elements

symmetry elements are called *point-groups* because all elements of one group intersect at a single point. The crystal classes are the main sub-divisions of crystalline matter, each being characterised by the presence of the symmetry elements of the corresponding point-group. Formerly, each class was named according to different morphological conventions, but these names have been rendered obsolete by the internationally accepted symbolism for point-groups. In this section we shall study this international nomenclature and also the various ways of representing point-groups on paper.

In studying this nomenclature, it is most convenient to use the stereographic projection for the representation both of symmetry elements and of faces of various forms. In these stereograms a dot represents the pole of a face (or of an axis) directed upwards, while a small open circle represents the pole of a face (or of an axis) directed downwards. In this study it is desirable also to learn how to derive the symbol of the point-group characteristic of a class from the symmetry elements, or from the general form of that class.

The best way to derive all the information about the symmetry of a class from the point-group symbol is as follows. Starting with a face in a general position, that is with no special relation to any symmetry element, operate the symmetry elements given by the symbol, thus producing a complete general form; from this, all the symmetry elements present in the class can be derived. To do this on paper, it is most convenient to use the stereographic projection. The initial pole of a general face is taken, and, after the operation (Fig. 147) in turn of each of the symmetry elements in the symbol, the poles of the new faces produced are added to the projection. The symmetry axes and planes can, of course, be shown on the stereographic projection also, but not the centre of symmetry which lies at the centre of the sphere of projection. But it is always possible to tell at a glance from the stereographic projection of a general form whether the class is centro-symmetrical or not. If a centre of symmetry is present, then every face has a similar face exactly parallel to it on the opposite side of the crystal; on the stereogram this results in each dot having a circle opposite it at an equal distance on the other side of the centre of the stereogram.

The symmetry of a class could be given in five ways, of which the first three are the most convenient: (i) a symbol; (ii) stereogram of the point group of symmetry elements; (iii) stereogram of the general form; (iv) tabulation or drawing of the symmetry elements; (v) a description or drawing of the general form. The example of the full symmetry class of the orthorhombic system *mmm* is given in Fig. 148.

In Fig. 150 are given stereograms of all thirty-two point groups; the first diagram in each case is of the general form produced by the operation of the symmetry elements of the point group on an initial face of a general type; the second diagram is of the complete symmetry elements of the point group. These stereograms of the point groups show the conventional orientation of each class, and reference to them will be found useful. Open symbols are used for inversion axes of even symmetry, that is, for those with lower symmetry than the corresponding rotation axis. Open symbols are not used for inversion axes of odd symmetry as these are equivalent to the corresponding rotation axis plus a centre of symmetry.

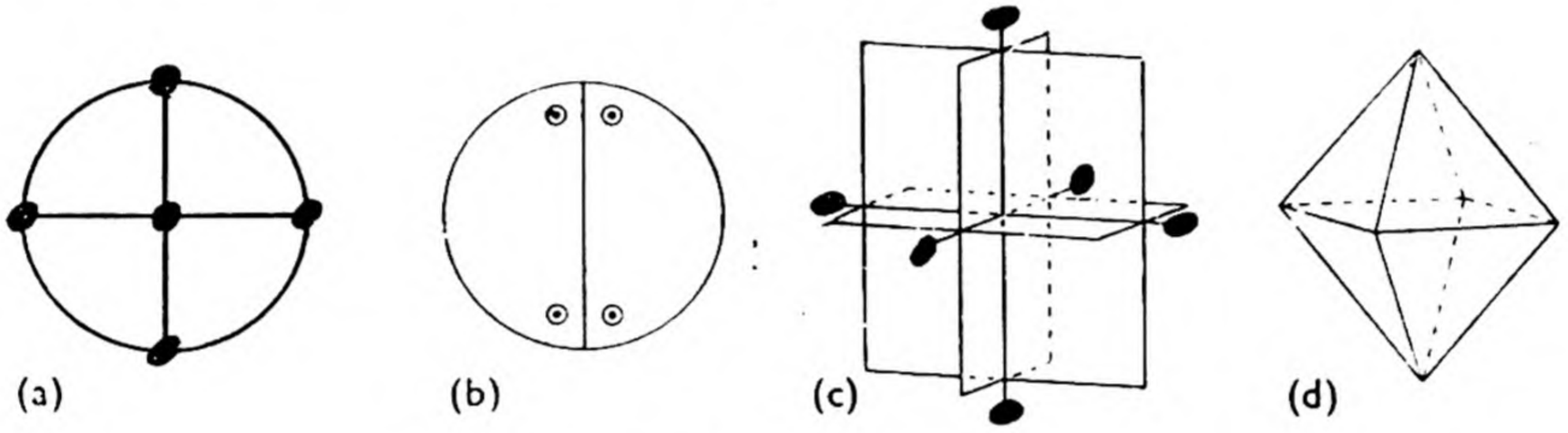

FIG. 148. Diagrams of class *mmm*:
(*a*) stereogram of point group (*b*) stereogram of general form
(*c*) drawing of point group (*d*) drawing of general form

We can put X as the general symbol for a rotation axis, 2, 3, 4, or 6, and $\overline{X}$ for an inverse axis, $\bar{2}$, $\bar{3}$, $\bar{4}$, or $\bar{6}$. The symbol *m* (mirror-plane) is used for a reflection plane or symmetry plane, as it is often called. In symbols of the type $\overline{X}2m$ and $\overline{X}m2$ which occur in the three uniaxial systems, attention must be paid to the order of the subsidiary symbols. The first subsidiary position denotes the direction selected for the *x*- and *y*-crystallographic axes in the tetragonal system and for the *x*-, *y*- and *u*-axes (Miller-Bravais) in the hexagonal and trigonal systems. The second subsidiary position denotes other directions normal to the principal axis but inclined to the first subsidiary direction at an angle of 45° in the tetragonal system and of 90° in the hexagonal and trigonal systems. The conventional orientations require the symbols, $\bar{3}m$, $\bar{4}2m$, and $\bar{6}m2$. The full symbol for the first of these is $\bar{3}2/m$, but this is not required in space-group nomenclature. The shortened symbol $\bar{3}2$ would do for the point group but not for space-group work; the symbol $\bar{3}2/m$ could be used for the point group but not symbols such as $\bar{3}2m$ or $\bar{3}m2$. In class $\bar{4}2m$ the shortened symbols $\bar{4}2$ or $\bar{4}m$ suffice for the point

group, but no other symbol is permissible. The hexagonal class $\bar{6}m2$ differs from the corresponding trigonal class $\bar{3}m$ in that the diads are parallel to and not perpendicular to the symmetry planes. The morphological convention is to make the planes perpendicular to the crystallographic axes so that the latter are not parallel to the diads. The full symbol can, therefore, only be written as $\bar{6}m2$, although the shortened symbols $\bar{6}m$ and $\bar{6}2$ suffice for the point group. In several point groups it is possible to develop the general form from symbols other than those given in the table, but sometimes these other symbols obscure the real symmetry of the classes.

The symbols given in Fig. 150-151 are short forms. For the more symmetrical classes there are complete symbols giving all the symmetry axes and planes present in the point group. These complete symbols are given in the International Tables, but can always be derived from the stereograms constructed in the manner described.

Symbol	Meaning
X or $\overline{X}$	rotation or inverse axis by itself.
$X2$ or $\overline{X}2$	subsidiary rotation diad or diads perpendicular to X or $\overline{X}$.
$X3$ or $\overline{X}3$	the symbol 3 in the second position denotes the four triad axes of the cubic system.
Xm or $\overline{X}m$	symmetry plane or planes containing the axis X or $\overline{X}$.
X/m	symmetry plane perpendicular to axis X.
X/mm	symmetry plane or planes containing the axis X and one plane perpendicular to the axis.
mm	two mutually perpendicular symmetry planes; these intersect in a diad and hence the symbol $=mm2$, ($2mm$ being sometimes used).
$\overline{X}2m$ or $\overline{X}m2$	the symmetry planes contain the axis $\overline{X}$, while the diads are perpendicular to X.
$X/m3m$	the symbol 3 in a subsidiary position denotes the four triad axes of the cubic system; the first m denotes three symmetry planes, each of which is normal to one of the three crystallographic axes the symmetry of which is given by X; the second m denotes the six symmetry planes each containing one of the crystallographic axes and two triad axes.

The symbol 1 can be used in any position to denote the absence of a symmetry plane or symmetry axis. This is unnecessary in point-group symbols but it is used in space-group symbols. In **10,** 1. 4 it was seen that for the hexagonal lattice the symbols C and H are used, one having the two subsidiary directions interchanged with respect to the other. This can be denoted more simply by using the positional symbolism. For example,

$$C\,\bar{3}m(1) = H\,\bar{3}1m$$
$$C\,\bar{3}1m = H\,\bar{3}m(1).$$

2.2 Crystallographic planes. In **1,** 1.5 the crystallographic usage of the word 'form' and the nature of special forms and general forms were studied. The various forms which arise in the thirty-two classes are systematically developed by Phillips (1946). In this section we shall consider general methods of developing them and also certain difficulties which bear on the interpretation of X-ray photographs of crystals.

Each of the thirty-two classes has a general form, and the shape of this, as a general form, is characteristic of the class as it results from the co-operation of all the symmetry elements of the point group. The faces of a special form, on the other hand, have a special relation to one or more of the symmetry elements. When the faces are normal to one or more symmetry elements, the number of faces in the form is less than in the general form. But the term 'special form' is applied also to forms, other than the general form, which have a special shape but which have the same number of faces as the general form. For example, in class 4, the general form of which is the (four-faced) tetragonal pyramid, a form of the type $\{hk0\}$ has also four faces, but, since the faces are all parallel to the tetrad, the shape is the special one called the tetragonal prism. But a special form in one class may be geometrically identical with a general form in a class of lower symmetry. Thus the general form of a class is not necessarily confined to that class, although as a general form it is characteristic of its class. The general form of the following classes occurs as a special form in other classes: 1, $\bar{1}$, 2, m, 3, $\bar{3}$, 4, $\bar{4}$, $4/m$, 6, $\bar{6}$, $6/m$. In all other classes, the general form is confined to its class.

In order to make this point clearer, we shall study the rhombohedron. In Fig. 152.1 it can be seen that as a body, the rhombohedron possesses one triad, three diads, three planes and a centre of symmetry. That group of symmetry elements is characteristic of the point-group called $\bar{3}m$—the calcite class of the trigonal system. The rhombohedron is, accordingly, a form of this class, but it is not the general form. This can be seen because each of the normals to the faces of the form lies in a symmetry plane; and it must, therefore, be possible to produce a rhombo-

Type of Symbol	TRICLINIC	MONOCLINIC	TRIGONAL
X	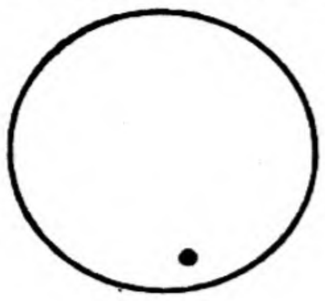 1	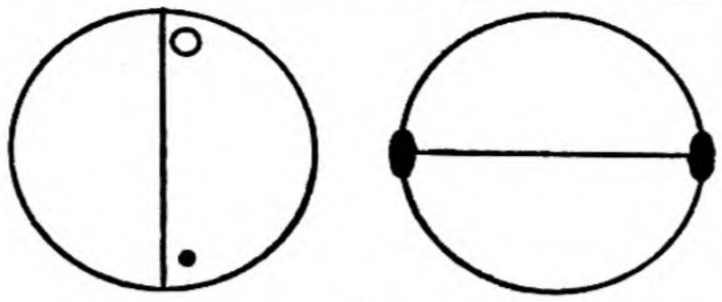 2	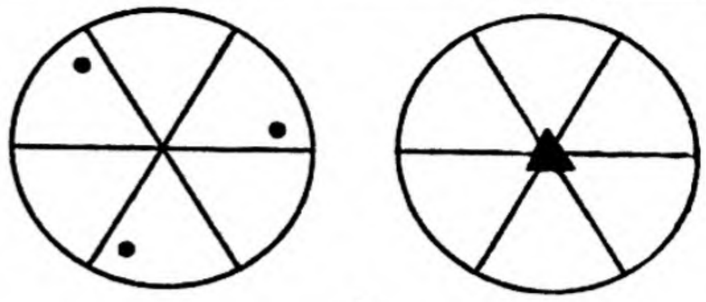 3
$\bar{X}$	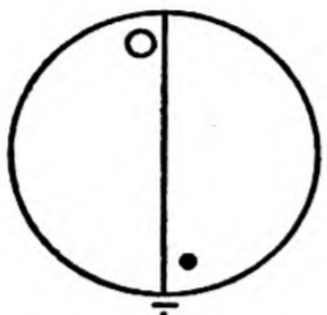 $\bar{1}$	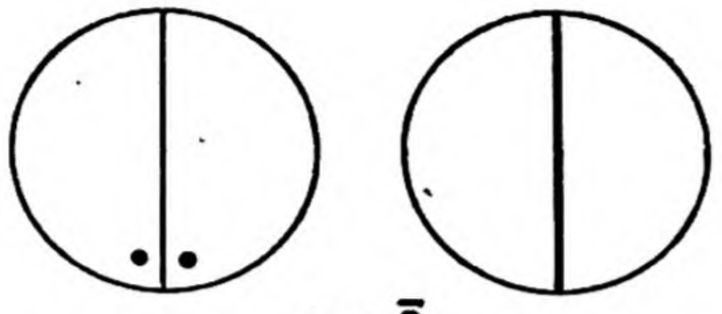 $m = \bar{2}$	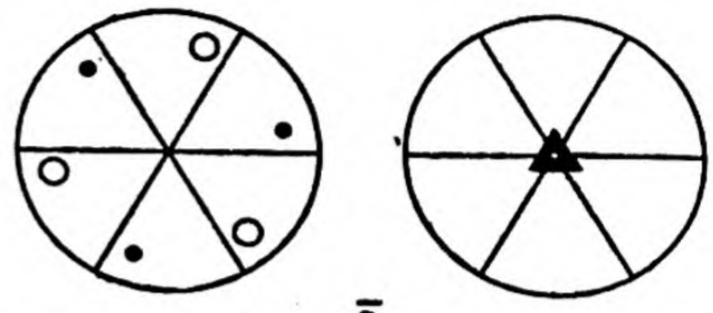 $\bar{3}$
$\frac{X}{m}$	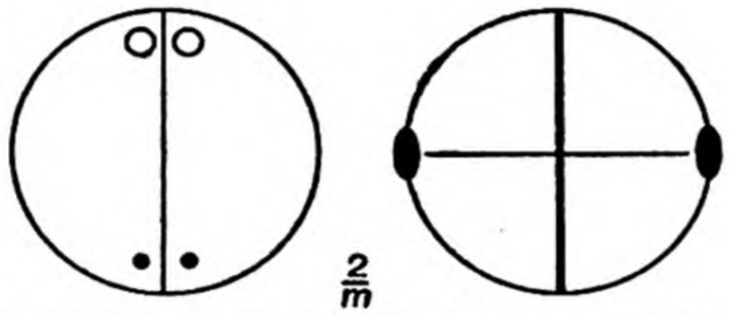 $\frac{1}{m}=m=\bar{2}$	$\frac{2}{m}$	$\frac{3}{m}=\bar{6}$
		ORTHORHOMBIC	
Xm	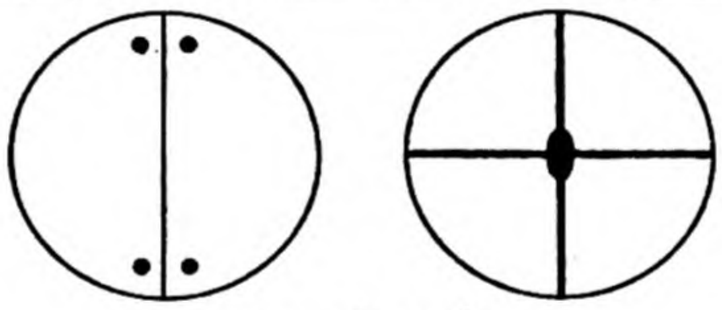 $1m=m=\bar{2}$	$mm=(2mm)$	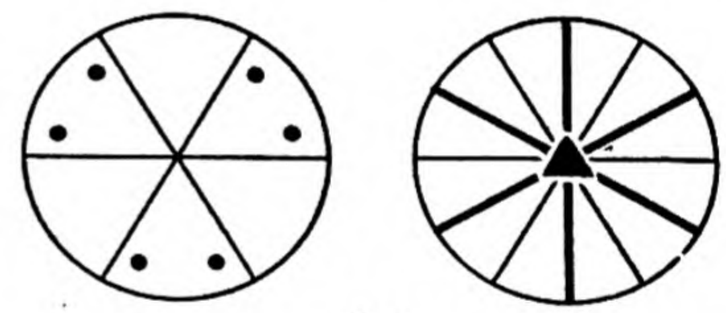 3m
$\bar{X}m$	$\bar{1}m=\frac{2}{m}$	$\bar{2}m=mm$	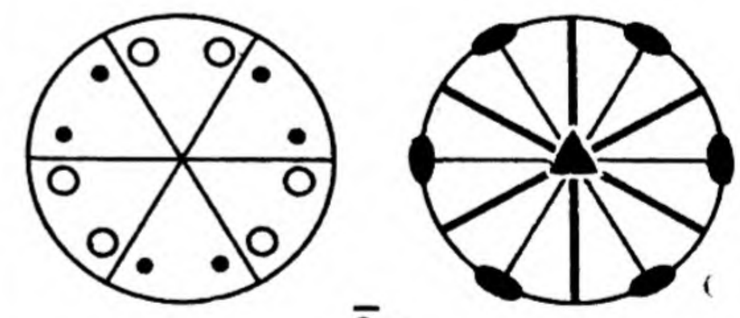 $\bar{3}m$
X2	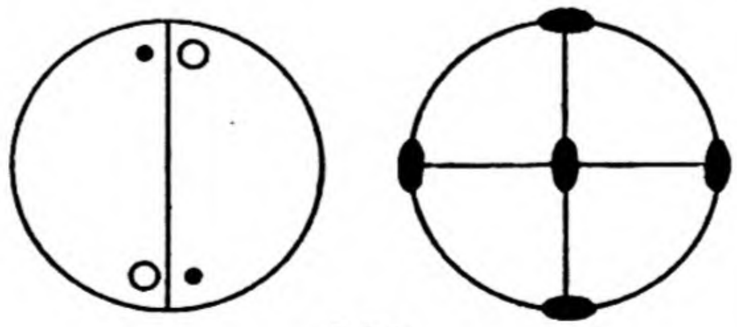 $12=2$	222	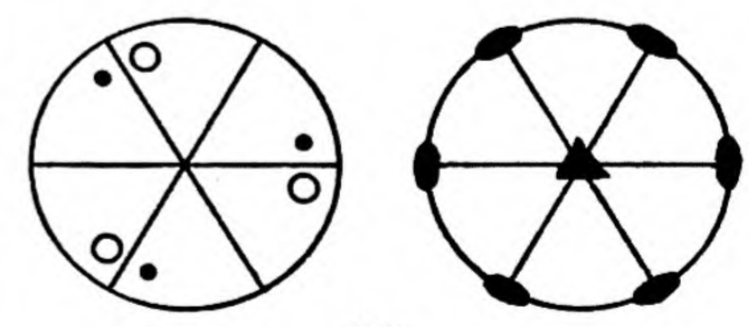 32
$\frac{X}{m}m$	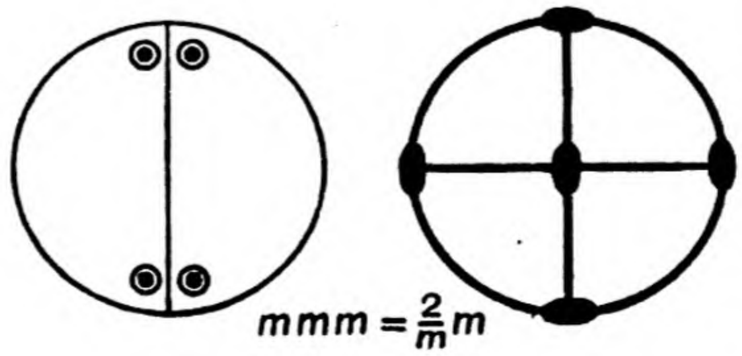 $\frac{1}{m}m=mm$	$mmm=\frac{2}{m}m$	$\frac{3}{m}m=\bar{6}m$

TETRAGONAL	HEXAGONAL	CUBIC
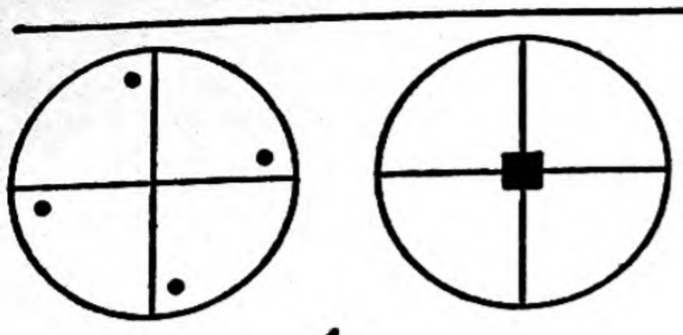 4	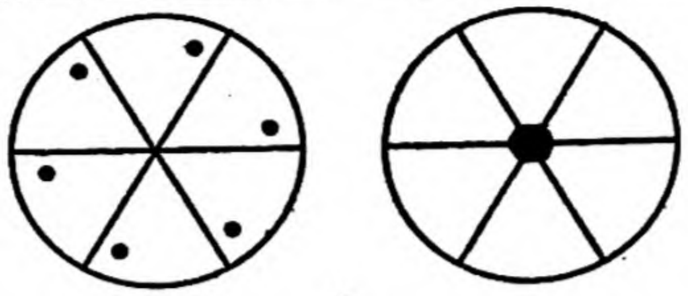 6	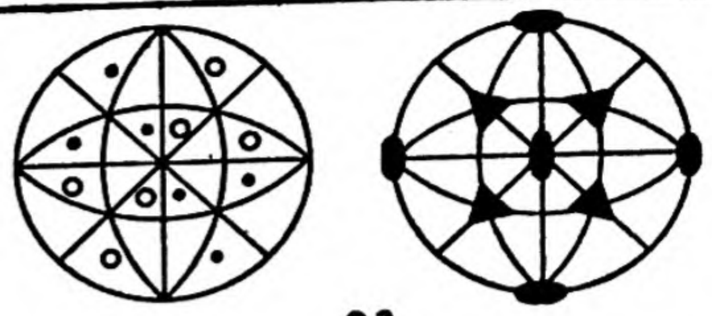 23
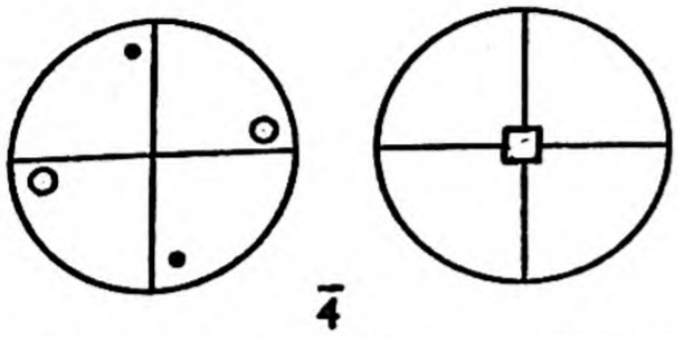 $\bar{4}$	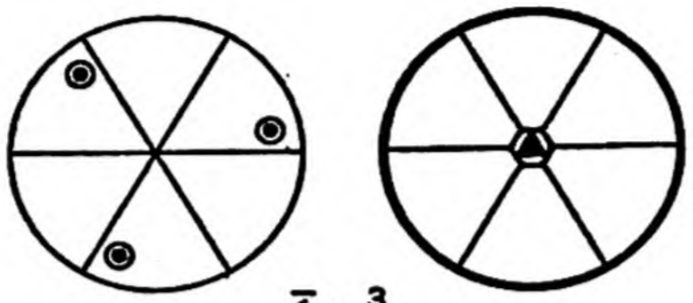 $\bar{6}=\frac{3}{m}$	$\bar{2}3=\frac{2}{m}3$
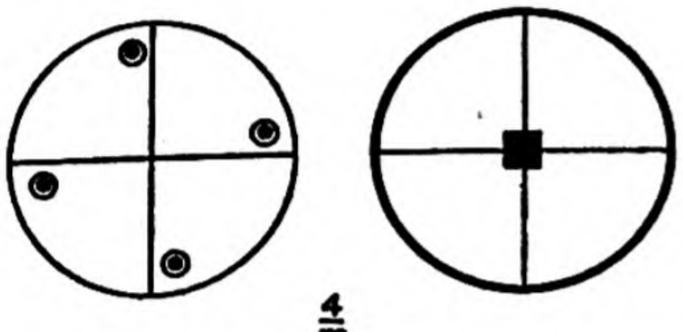 $\frac{4}{m}$	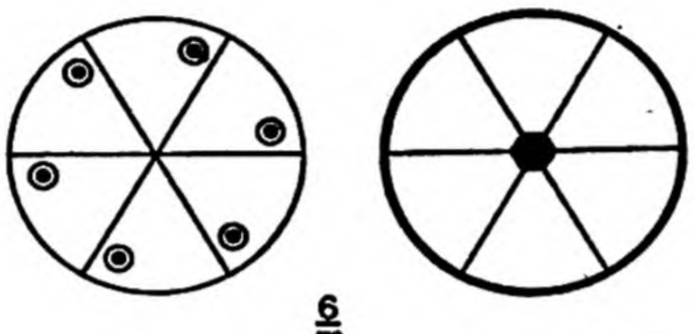 $\frac{6}{m}$	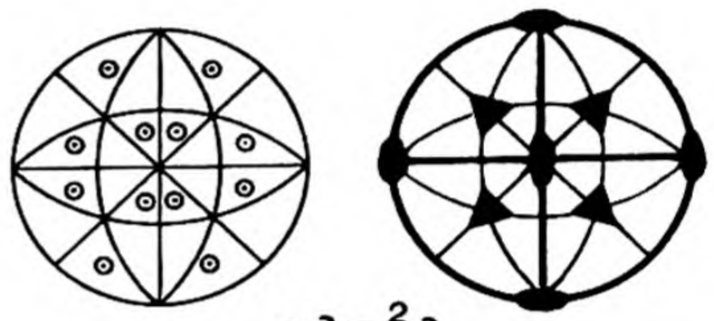 $m3=\frac{2}{m}3$
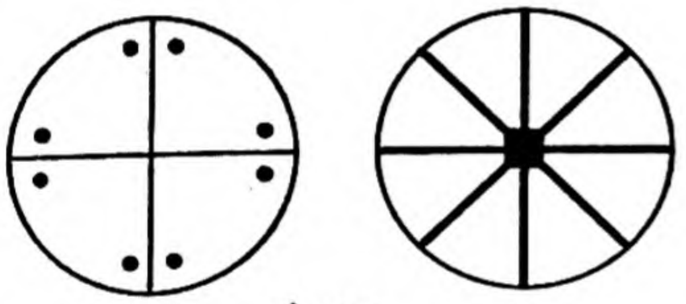 4mm	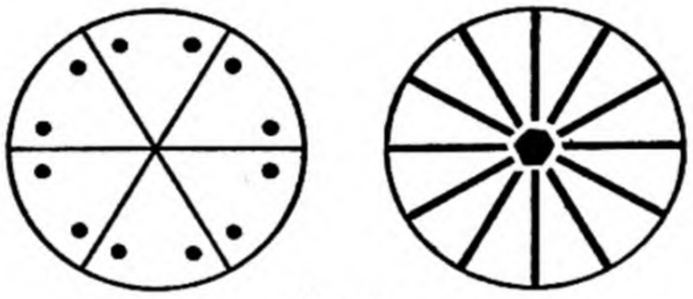 6mm	$2m3=\frac{2}{m}3$
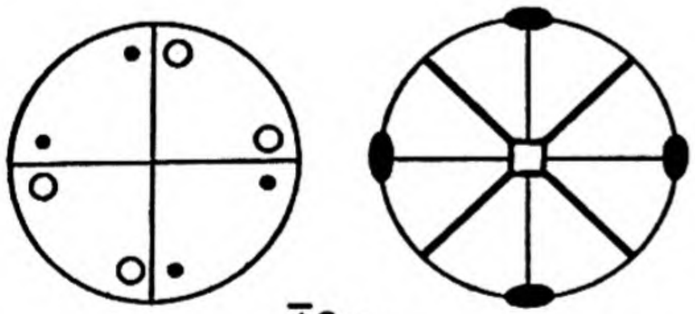 $\bar{4}2m$	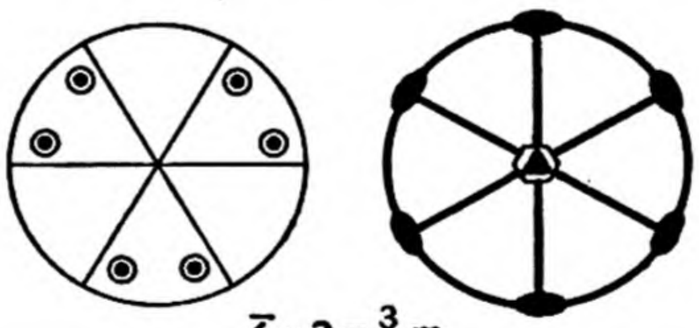 $\bar{6}m2=\frac{3}{m}m$	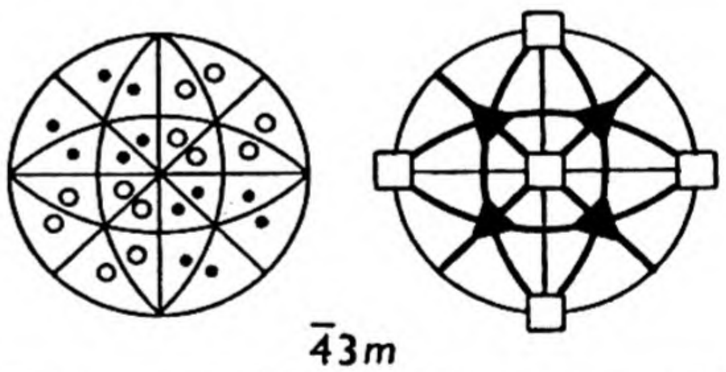 $\bar{4}3m$
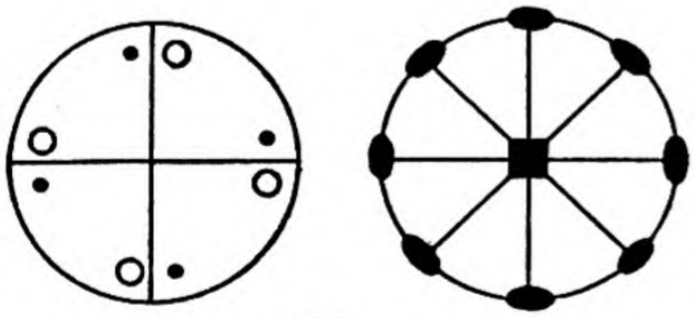 42	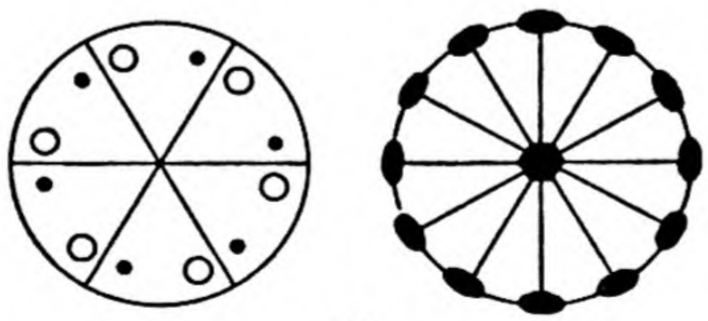 62	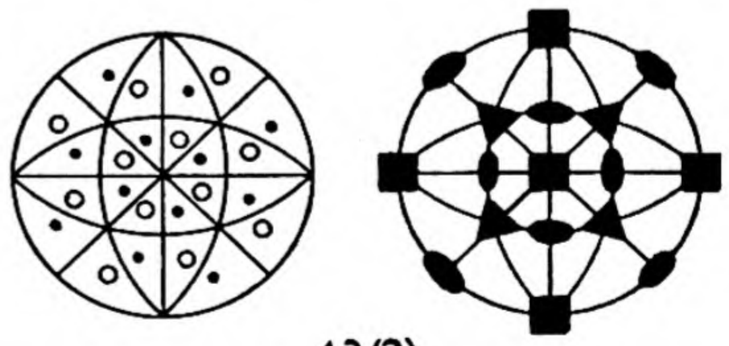 43(2)
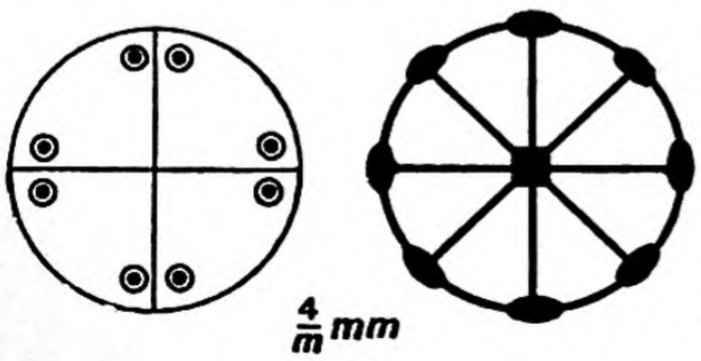 $\frac{4}{m}mm$	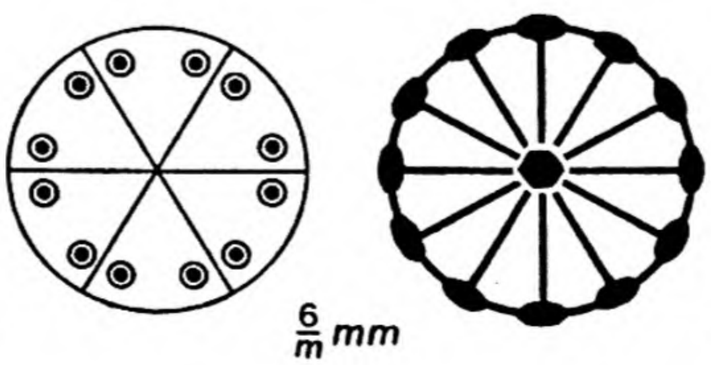 $\frac{6}{m}mm$	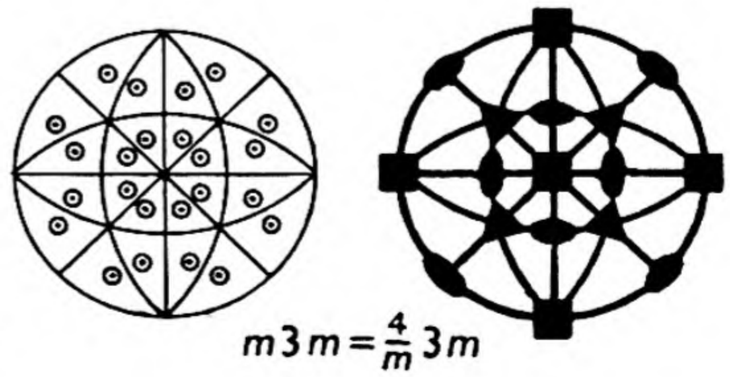 $m3m=\frac{4}{m}3m$

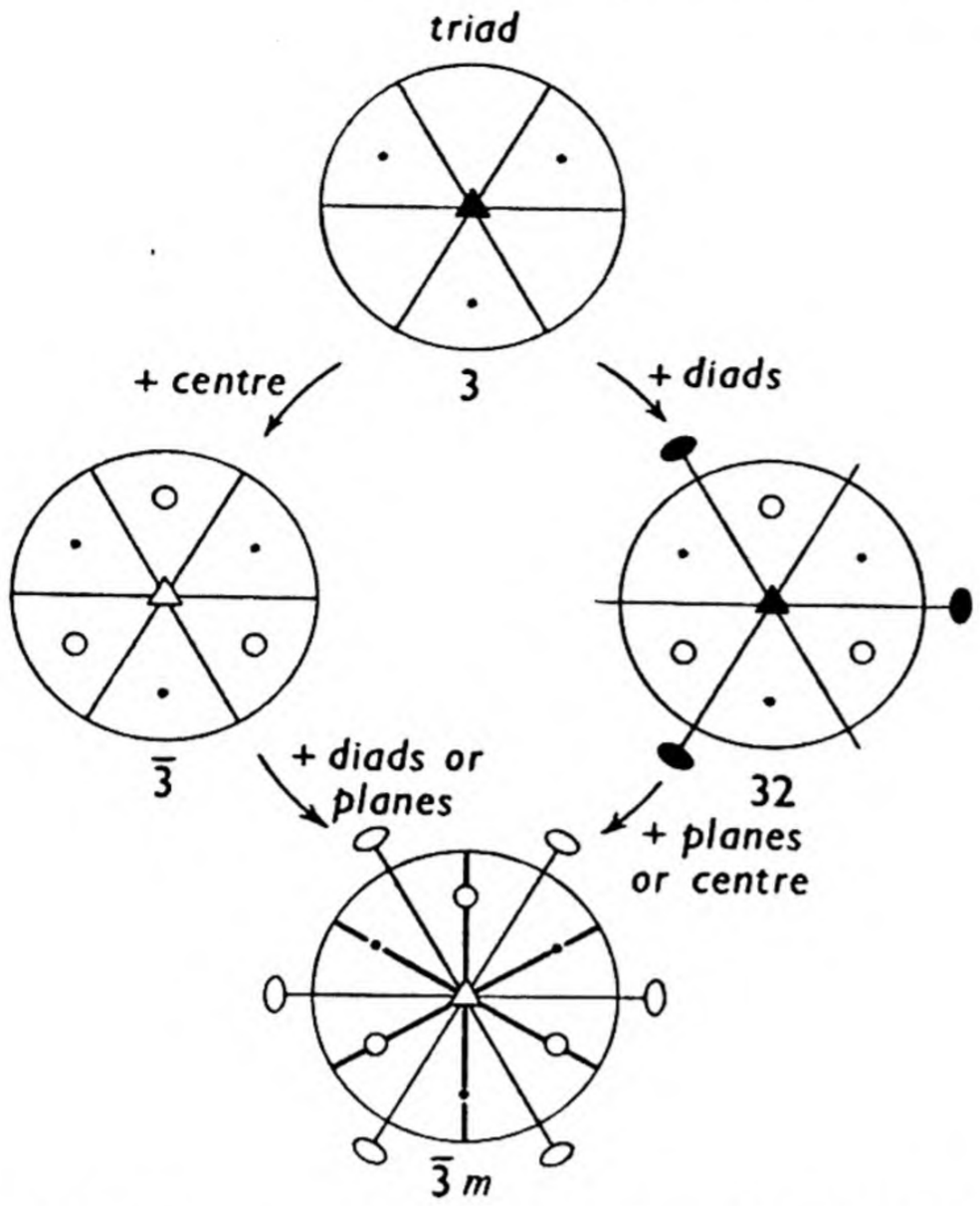

FIG. 152.1. Diagram showing existence of rhombohedron in three classes

hedron by operation on one initial pole of the other symmetry elements alone. Consideration of Fig. 152.1 shows that the rhombohedron can be produced by a combination of the triad and a centre, or by a combination of the triad and the three diads, provided only that in the second case the initial pole is taken so that it subtends an equal angle with the poles of the two adjacent diad axes. From this we can deduce that :

(i) the rhombohedron must be the general form of class $\bar{3}$ which has a triad and a centre;

(ii) the rhombohedron must be a special form both in class $\bar{3}m$ (calcite class) and in class 32 (quartz class), its indices being of the type $\{h\,o\,\bar{h}\,l\}$ or $\{o\,k\,\bar{k}\,l\}$.

The rhombohedron does not occur in either of the other two classes of the trigonal system, 3 and $3m$ (tourmaline class) as in these the triad is polar.

When the angle α between the polar edges is 90°, the rhombohedron becomes a cube. Since a cube can be produced by the operation of the four triads alone on an initial pole at an angle of 54° 44′ from the poles of the four triads, this form is found in all five classes of the cubic system. It is always a special form, as each face is perpendicular to a symmetry axis (diad, tetrad or inverse tetrad); but the actual symmetry elements present will be quite different in each class.

We have spoken of the general form of a class, but there is, of course, a whole family of such general forms in any one class. The family of the general form of the holosymmetric orthorhombic class, *mmm* (Fig. 148) consists of a number of eight-faced bipyramids, the faces of each of which have a different inclination to the axes. These are easily distinguished from any family of special forms. Certain special forms are fixed—the cube for example—and have only one member. In other examples of special form there are whole families with different values of their indices. In the monoclinic and triclinic systems, however, the usual morphological nomenclature cuts across this distinction between general and special forms by assigning special names to certain forms which are geometrically indistinguishable from general forms. This arises because of the special importance of the crystallographic axes. In this nomenclature of forms, which is fully described by Phillips (1946), special names are given to forms with faces bearing a special relationship to a crystallographic axis, whether or not the faces bear a special relationship to a symmetry element.

In obtaining intensity measurements from powder photographs, it is necessary to know the indices of all planes which belong to the same form, and hence the number of possible co-operating planes with exactly the same angle and intensity of reflection. Also, there may be other sets of planes of the same

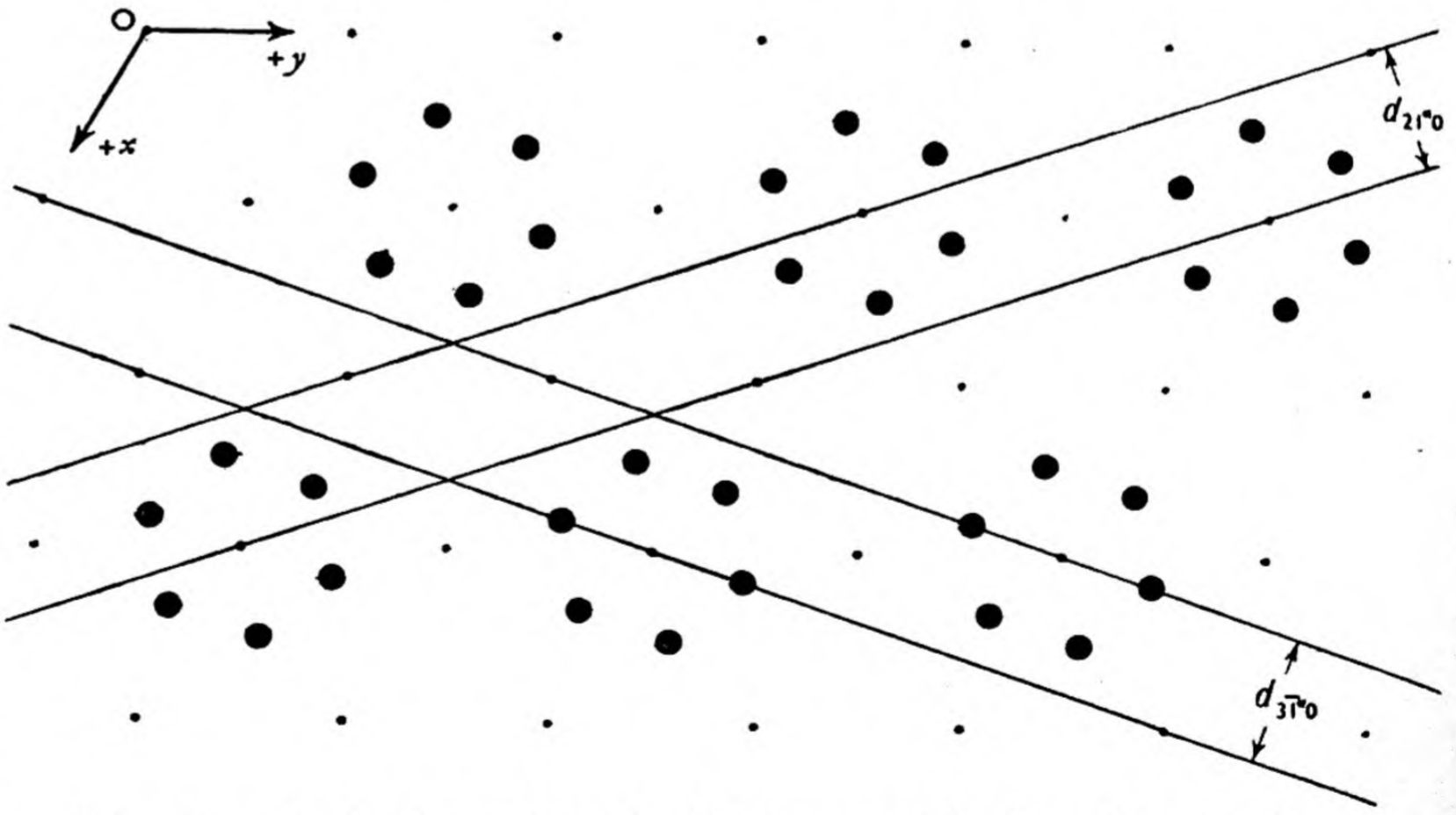

FIG. 152.2. Projection on (0001) of the hexagonal lattice, with scattering centres, having the symmetry 6. The diagram shows that, although the planes $(21\bar{3}0)$ and $(3\bar{1}\bar{2}0)$ have the same spacing, the intensities of the corresponding reflections are unequal

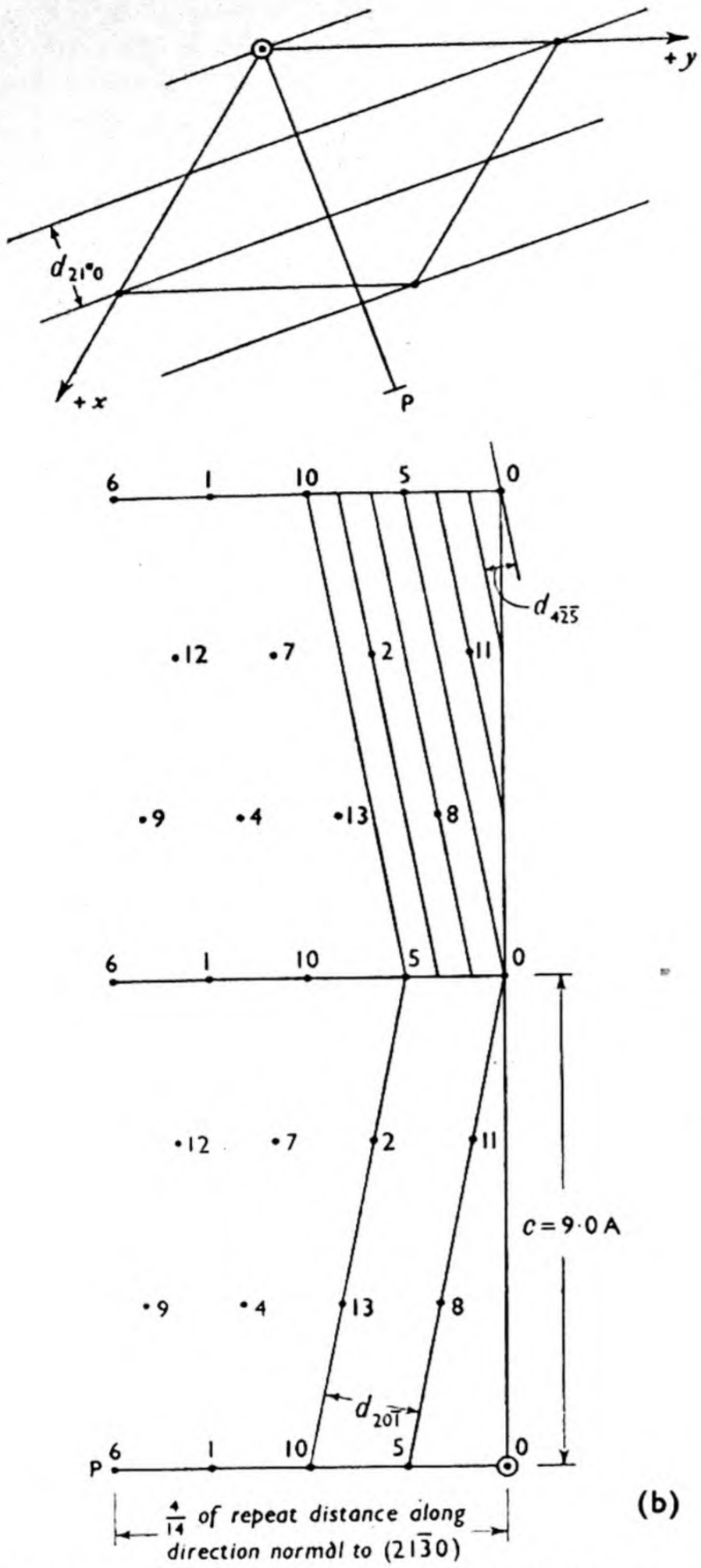

FIG. 153. Diagrams of a rhombohedral lattice :
(*a*) Basal section
(*b*) Projection on the vertical plane normal to $(21\bar{3}l)$
The heights of the points are given in 14ths of the repeat distance along the normal to the plane of projection, which is the direction $[\bar{1}2{*}0]$. Fig. 166 may be found useful in connection with this figure.

spacing as the first, but with different intensities of reflection. One special point arises if a rhombohedral crystal is indexed on hexagonal axes, and in such a case, difference of spacing as well as of intensity can occur between forms with similar indices.

We shall discuss some examples to make these points clear. In the hexagonal Laue symmetry group 6/*mmm*, the general form is a di-hexagonal bipyramid (Fig. 154) and hence has 24 faces, or 12 sets of parallel planes. In the class 6/*m* the reduced symmetry results in a total of 12 faces in the general form—the hexagonal bipyramid. The remaining 12 of the original 24 indices comprise another hexagonal bipyramid, superposable on the first by rotation of 180° about an axis perpendicular to *y* and *z*. These two forms have the same spacing and hence the same Bragg angle, but different intensities. A similar relationship is demonstrated for a prismatic form in Fig. 152.2.

Suppose that we have two trigonal crystals both based on a hexagonal lattice. In class $\bar{3}m$ the general form is a scalenohedron which has twelve faces, but the indices of these are a different set from those of either of the two hexagonal bipyramids of class 6/*m*. Again there is a complementary form superposable on the first by rotation about an axis perpendicular to *y* and *z* (Miller-Bravais). In class $\bar{3}$ the general form is a rhombohedron which has six faces—one quarter of the number of the di-hexagonal bipyramid. The original 24 indices can be divided up in such a way as to give the four complementary rhombohedra of class $\bar{3}$; these are all superposable by rotation, either about the *x*-axis or about the normal to the *y*- and *z*-axes (Miller-Bravais). In class $\bar{3}m$ the two complementary scalenohedra have a similar relation to the hexagonal lattice, and their planes have therefore the same spacing ; but the intensities of reflection are different. In class $\bar{3}$ the four rhombohedra have the same relation to the hexagonal lattice, and hence the four forms have the same spacing, but all have different intensities.

Trigonal crystals may, however, be based on a rhombohedral lattice ; this makes a big difference. The two scalenohedra now have different spacings as well as different intensities, as can be seen from Fig. 153. In class $\bar{3}$ two of the rhombohedra have the same spacing, but this differs from that of the other pair. All four have different intensities.

In the stereogram of Figs. 154 and 155 are given the indices of the various forms with indices $21\bar{3}1$ in the centro-symmetrical classes 6/*mmm*, 6/*m*, $\bar{3}m$ and $\bar{3}$. It can be seen that the four rhombohedra of class $\bar{3}$ have to be combined in different pairs in order to produce the di-trigonal scalenohedra of class $\bar{3}m$ on one hand and the hexagonal bipyramids of class 6/*m* on the other. One important point is that the use of Miller-Bravais symbols masks the difference between the two scalenohedra of class $\bar{3}m$. The use of Miller notation, however, shows up this difference immediately.

The relations which we have been discussing can be summed up in tables which give the number of faces in each form for each Laue symmetry group. When used in the interpretation of powder photographs these numbers are called *multiplicity factors*

for the reason given in **15**, 2.6. It is convenient to group together the three biaxial systems as these have no axis of symmetry greater than two-fold. We can think of *mmm* as being the holosymmetric group of two-fold symmetry while $2/m$ and $\bar{1}$ are of lower symmetry. For each of the possible types of form the table (pp. 156-157) shows the number of faces, and the indications of ± signs show how certain holosymmetric forms are split up in the lower-symmetry groups. In all these tables the absence of any special indication means that all possible combinations of

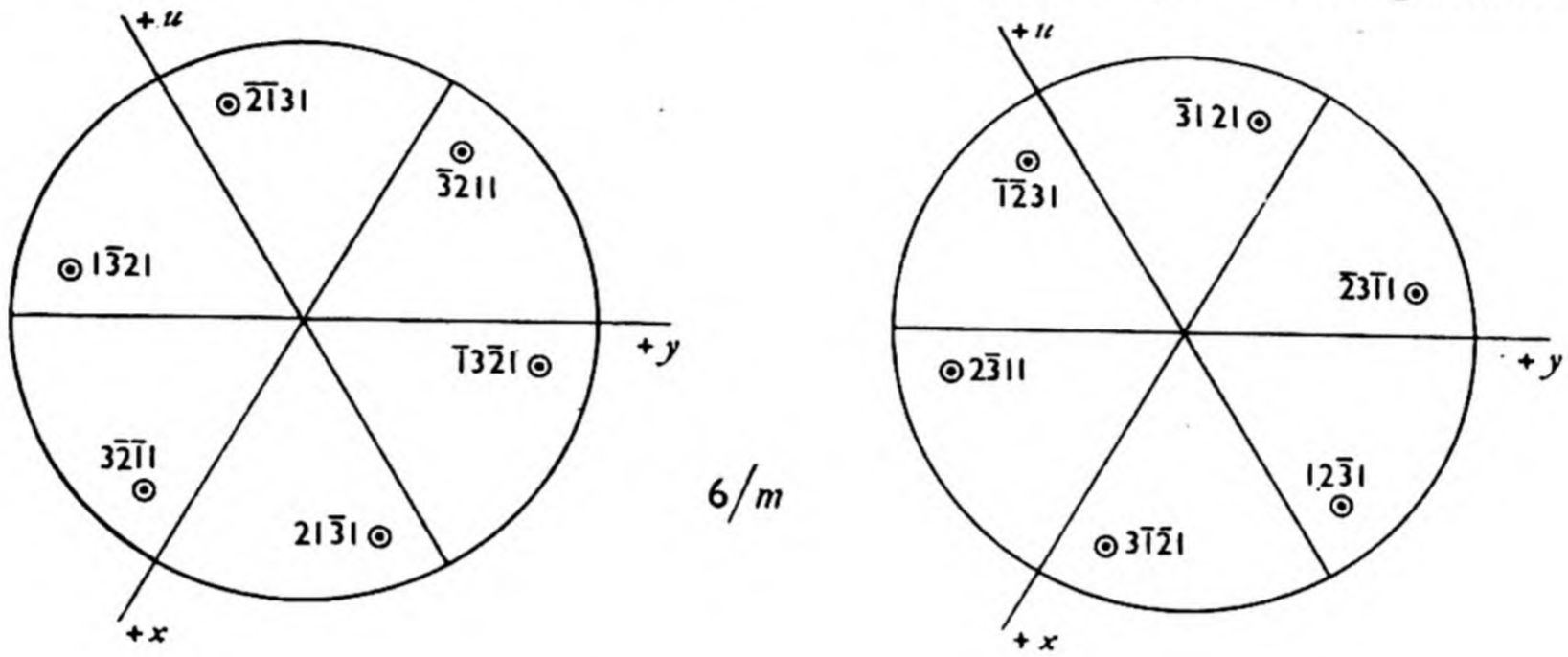

FIG. 154. Stereograms of general forms in two hexagonal classes

sign are permissible. As the first table covers only two-fold symmetry, the possible equality of two, or of all three, of the symbols is without significance. As an example of the method of deriving all the indices of a form from this table, we can take the general form {111}. In $\bar{1}$ this consists of (111) and $(\bar{1}\bar{1}\bar{1})$; if we add the two faces of another quite different form, $(1\bar{1}1)$ and $(\bar{1}1\bar{1})$, we obtain the four faces of the form {111} of class $2/m$. To get the other four faces required to complete the form {111} of *mmm*, we have to add the indices obtained from the last two columns of the table, namely, $(11\bar{1})$, $(\bar{1}\bar{1}1)$ and $(1\bar{1}\bar{1})$, $(\bar{1}11)$.

In the tetragonal system the tetrad axis parallel to z produces interchange of h and k in the same form. We have also to take account of whether h is equal to k or not, the possible equivalence of either with l being without significance. From this point onwards in these tables the use of different symbols implies non-equality except where this possibility is stated. Correspondingly the use of the same symbol in different positions implies necessary equality. In the lower-symmetry groups the enclosing in a rectangle of the numbers corresponding to different forms shows equality of spacing, although the symmetry relations differ.

In the cubic system the operation of the triad axes interchanges h, k and l in a cyclic manner. Since we are concerned here only with centro-symmetric classes, faces of each form will be present in all the eight quadrants of the stereogram; consequently all possible combinations of sign are possible, as is shown by the absence of special sign indications. In $m3$ we have to separate the two forms of type *hk*o and the two of type *hkl* according to whether h is greater or less than k. Since the lattice itself possesses diagonal symmetry planes, the two forms of the same type have the same spacing, as is shown by the enclosing rectangle. This is not so, however, with the two forms of type *hhl* as, for example, {112} and {221}. The poles of the faces of these forms lie on diagonal symmetry planes, and it is a question of whether they

lie between a triad and a tetrad as in {112}, or between a triad and a diad as in {221}, the description being in terms of the symmetry of $m3m$. Consequently, the spacings of these two forms are not the same, as can also be seen from consideration of the spacing equation (Appendix 2).

With hexagonal axes there is cyclic permutation of the first three symbols. The combinations of sign depend on the Laue group and on the particular form. The plus-minus sign implies that a complete change of sign is to be made in the symbol or the part thereof to which it refers, but no other combinations are permissible. Thus, for example, in the last column of the Laue group $\bar{3}$, the six faces in the form $\{3\bar{2}\bar{1}4\}$ are, $(3\bar{2}\bar{1}4)$, $(\bar{1}3\bar{2}4)$, $(\bar{2}\bar{1}34)$, $(\bar{3}21\bar{4})$, $(1\bar{3}2\bar{4})$, $(21\bar{3}\bar{4})$. When hexagonal axes are used we can think of the classes $\bar{3}$, $\bar{3}m$ and $6/m$ as being non-holosymmetric.

For the rhombohedral lattice it is better to use rhombohedral indices if there is any danger of confusion between indices belonging to different forms. The table shows the number of faces in the various forms and the general relations of these. But the safest procedure for deriving the particular indices of faces in a given form is to operate the symmetry elements on the indices of the initial face. The operators are a cyclic permutation, $\circlearrowright \pm(pqr) = \bar{3}$, and an interchange of q and r, $q \longleftrightarrow r = m$ (normal to hexagonal y). The enclosing rectangles have the usual significance of equality of spacing. In the last two columns the symbols $p'q'r'$ are used to show the lack of any numerical relation to the pqr of the two previous columns. This is the difference which is completely obscured by the use of hexagonal axes. Indices of the type ppq occur, in class $\bar{3}m$, in the two kinds of rhombohedra and in the general form; consequently the exact nature of the symbol has to be carefully stated.

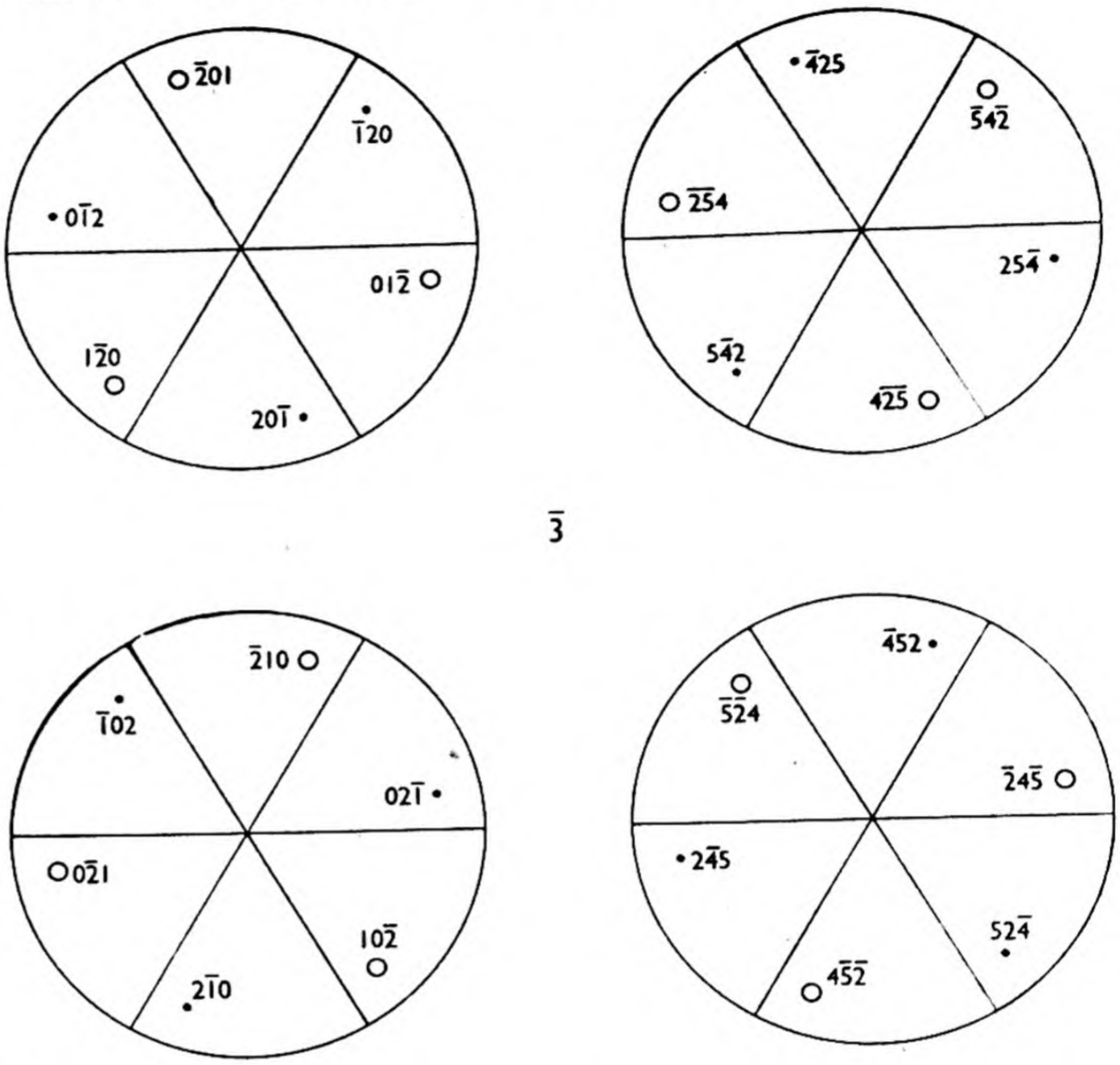

FIG. 155. Stereograms of general forms in two trigonal classes (rhombohedral indexing)

Notes to Tables

1. The use of different symbols indicates non-equality of the corresponding indices, except where the symbol $\overline{\overline{=}}$ shows that the possible equality is without significance. The use of the same symbol in different positions indicates necessary equality.

2. The sign $\pm$ implies a complete change of sign in the symbol or the part thereof to which it refers. Where no indication of sign is given, then all possible combinations have to be made.

3. The symbol $\circlearrowright$ indicates cyclic permutation of the indices within the following bracket. Except where indicated, no interchange of symbols is permissible.

4. Enclosure of two or more numbers in a rectangle indicates that the different forms so enclosed have the same spacing although they are not related by the symmetry of the Laue group.

System	Laue Group	$h00$	$0k0$	$00l$	$0kl\ (k \gtrless l)$		$h0l\ (h \gtrless l)$		$hk0\ (h \gtrless k)$		$hkl\ (h \gtrless k \gtrless l)$			
					0 + + / 0 − −	0 + − / 0 − +	+ 0 + / − 0 −	+ 0 − / − 0 +	+ + 0 / − − 0	+ − 0 / − + 0	+ + + / − − −	+ − + / − + −	+ + − / − − +	+ − − / − + +
Triclinic	$\bar{1}$	2	2	2	2	2	2	2	2	2	2	2	2	2
Monoclinic	$2/m$	2	2	2	4		2	2	4		4		4	
Orthorhombic	mmm	2	2	2	4		4		4		8			

		$\left\{\begin{matrix}h00\\0h0\end{matrix}\right\}$	$00l$	$\left\{\begin{matrix}h0l\\0hl\end{matrix}\right\}$ $(h \gtrless l)$	$hk0$		$hh0$	$hhl\ (h \gtrless l)$	$hkl\ (l \gtrless h \text{ or } k)$	
					$hk0$ / $\bar{h}\bar{k}0$ / $k\bar{h}0$ / $\bar{k}h0$	$h\bar{k}0$ / $\bar{h}k0$ / $kh0$ / $\bar{k}\bar{h}0$			$hk\,l$ / $\bar{h}\bar{k}\,l$ / $k\bar{h}\,l$ / $\bar{k}h\,l$ $\pm l$	$h\bar{k}\,l$ / $\bar{h}k\,l$ / $kh\,l$ / $\bar{k}\bar{h}\,l$ $\pm l$
Tetragonal	$4/m$	4	2	8	4	4	4	8	8	8
	$4/mmm$	4	2	8	8		4	8	16	

		$\bigcirc h00$	$\bigcirc hh0$	$\bigcirc hk0$		hhh	$\bigcirc hhl$	$\bigcirc hhl$	$\bigcirc hkl$	
				$h>k$	$h<k$		$h>l$	$h<l$	$h>k>l$	$h<k<l$
Cubic	$m3$	6	12	12	12	8	24	24	24	24
	$m3m$	6	12	24		8	24	24	48	

			Sum Zero (Prism Zone)				Sum Not Zero							
			$\circlearrowright\pm(pqr)$ (Any one symbol may be zero and any two may be equal)				$\circlearrowright\pm ppq$ $q>p$ same sign $q<p$; $q>2\bar{p}$ opp. sign $q\leqq\bar{p}$ or $\bar{p}<q<2\bar{p}$		$\circlearrowright\pm(pqr)$ (One symbol is mean of other two; any one symbol may be zero) $q\neq\bar{r}$		$\circlearrowright\pm(pqr)$ (Any one symbol may be zero; $q\neq\bar{r}$ but indices are otherwise independent)			
		ppp	$p\bar{q}q$	$po\bar{p}$	*pqr*	*prq*	(*p* may be zero)	(*q* may be zero)	*pqr*	*prq*	*pqr*	*prq*	*p'q'r'*	*p'r'q'*
Trigonal (with rhombohedral lattice)	$\bar{3}$	2	6	6	6	6	6	6	6	6	6	6	6	6
	$\bar{3}m$	2	6	6	12		6	6	12		12		12	

							$l\neq h$ or k or i							
		oool	$ho\bar{h}o$ $\circlearrowright\pm(ho\bar{h})$	$hh\bar{2}ho$ $\circlearrowright\pm(hh\bar{2}h)$	*hkio* $\circlearrowright\pm(hki)$	*ikho* $\circlearrowright\pm(ikh)$	$\pm ho\bar{h}l$ $\circlearrowright(ho\bar{h})$	$\pm\bar{h}ohl$ $\circlearrowright(\bar{h}oh)$	$\pm hh\bar{2}hl$ $\circlearrowright(hh\bar{2}h)$	$\pm\bar{h}h2hl$ $\circlearrowright(\bar{h}h2h)$	$\pm hkil$ $\circlearrowright(hki)$	$\pm ikh\bar{l}$ $\circlearrowright(ikh)$	$\pm khil$ $\circlearrowright(khi)$	$\pm ihk\bar{l}$ $\circlearrowright(ihk)$
Trigonal (with hexagonal lattice)	$\bar{3}$	2	6	6	6	6	6	6	6	6	6	6	6	6
	$\bar{3}m$	2	6	6	12		6	6	12		12		12	

							$l\neq h$ or k or i			
System	Laue Group	*oool*	$ho\bar{h}o$ $\circlearrowright\pm(ho\bar{h})$	$hh\bar{2}ho$ $\circlearrowright\pm(hh\bar{2}h)$	*hkio* $\circlearrowright\pm(hki)$	*ikho* $\circlearrowright\pm(ikh)$	$ho\bar{h}l$ $\circlearrowright\pm(ho\bar{h})\pm l$	$hh\bar{2}hl$ $\circlearrowright\pm(hh\bar{2}h)\pm l$	*hkil* $\circlearrowright\pm(hki)\pm l$	*ikhl* $\circlearrowright\pm(ikh)\pm l$
Hexagonal	$6/m$	2	6	6	6	6	12	12	12	12
	$6/mmm$	2	6	6	12		12	12	24	

2.3 Polar directions in crystals. When the positive and negative senses can be distinguished in a given direction in a crystal structure, this direction is said to be *polar*. In connection with certain

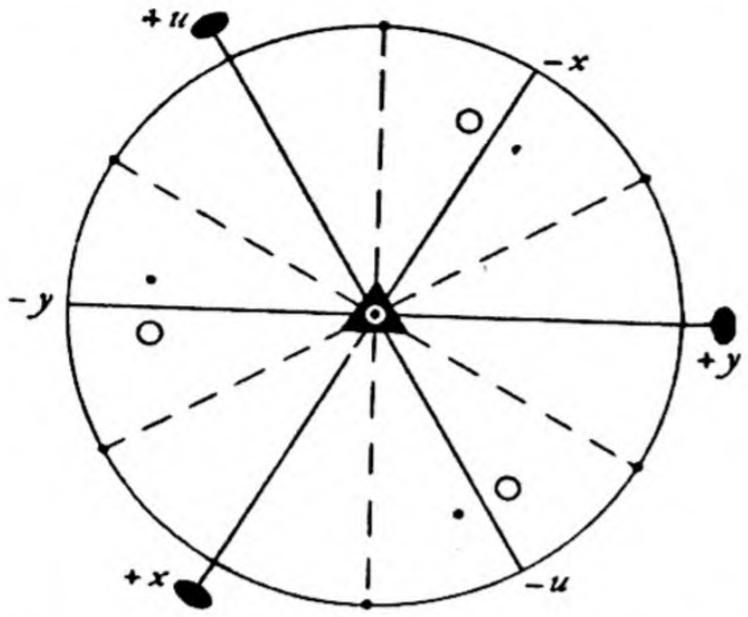

FIG. 158.1. Stereogram showing uniterminal diads in class 32

physical properties of crystals it is important to know which directions are polar and which are *non-polar*. Such a direction is shown morphologically on the crystal as a *uniterminal* axis, the symmetrical arrangement of faces being different at one end of the axis from that at the other end. If an initial face is put perpendicular to one end of a uniterminal axis, then the operation of the symmetry elements of the point group does not repeat this face at the other end of the given axis. It is clear that uniterminal axes can exist only in non-centro-symmetrical classes. In general, the simplest way to decide whether a particular axis in a given crystal class is or is not a uniterminal axis is to consider whether any symmetry element is present which could relate the two ends and hence make the axis a *biterminal* one. These elements are most conveniently listed in the following way :

(i) centre of symmetry ;

(ii) rotation axis of even symmetry perpendicular to the axis ;

(iii) a plane of symmetry perpendicular to the axis ;

(iv) an inversion axis parallel to the axis.

These operations are not all separate because an inversion axis of odd symmetry necessarily involves a centre, while an inversion diad in (iv) is equivalent to (iii). Only if no such element is present in the point group can a particular axis be uniterminal. For example, in the quartz class, 32, the three diads are uniterminal (Fig. 158.1), but the triad is biterminal and so also are the three horizontal zone axes normal to the diads. All possible biterminal axes are given in the table on p. 159 for the thirty-two classes. Hence all other axes are uniterminal ; but of these only the crystallographic and symmetry axes are given in the table.

2.4 Face-symmetry and etch-figures. In **8**, 1, it was seen that etch figures can be used in some cases to give information about the orientation of a crystal specimen. They are used also in determining the symmetry class to which a crystal belongs. The symmetry of an etch figure can be considered as a projection of the symmetry elements of the class on the plane being examined. In this section we study two examples of the use of etch figures in reducing the number of possible classes to which a crystal may be allocated.

Suppose that each of three crystals grows as a simple rhombohedron. This form occurs only in the classes $\bar{3}$, 32 and $\bar{3}m$ of the trigonal system. If we project the symmetry elements of these classes on a rhombohedron plane, we get the result shown in Fig. 158.2. In all etch-figure work, however, it must be remembered that solution may take place with equal facility in two or more directions which are not related by symmetry. It is only possible, therefore, to state the maximum symmetry which the crystal may possess.

If a plane of symmetry appears to exist in the etch figure on the rhombohedron face, then no conclusion can be reached because we cannot assume that such a plane exists in the crystal. Other reagents can be tried and one of these may produce asymmetric etch pits ; this would exclude class $\bar{3}m$. If these asymmetric etch pits appear to be related by diad axes to the pits on certain adjacent faces, then no further conclusion can be reached. If, on the other hand, no such relation was observed, we would be

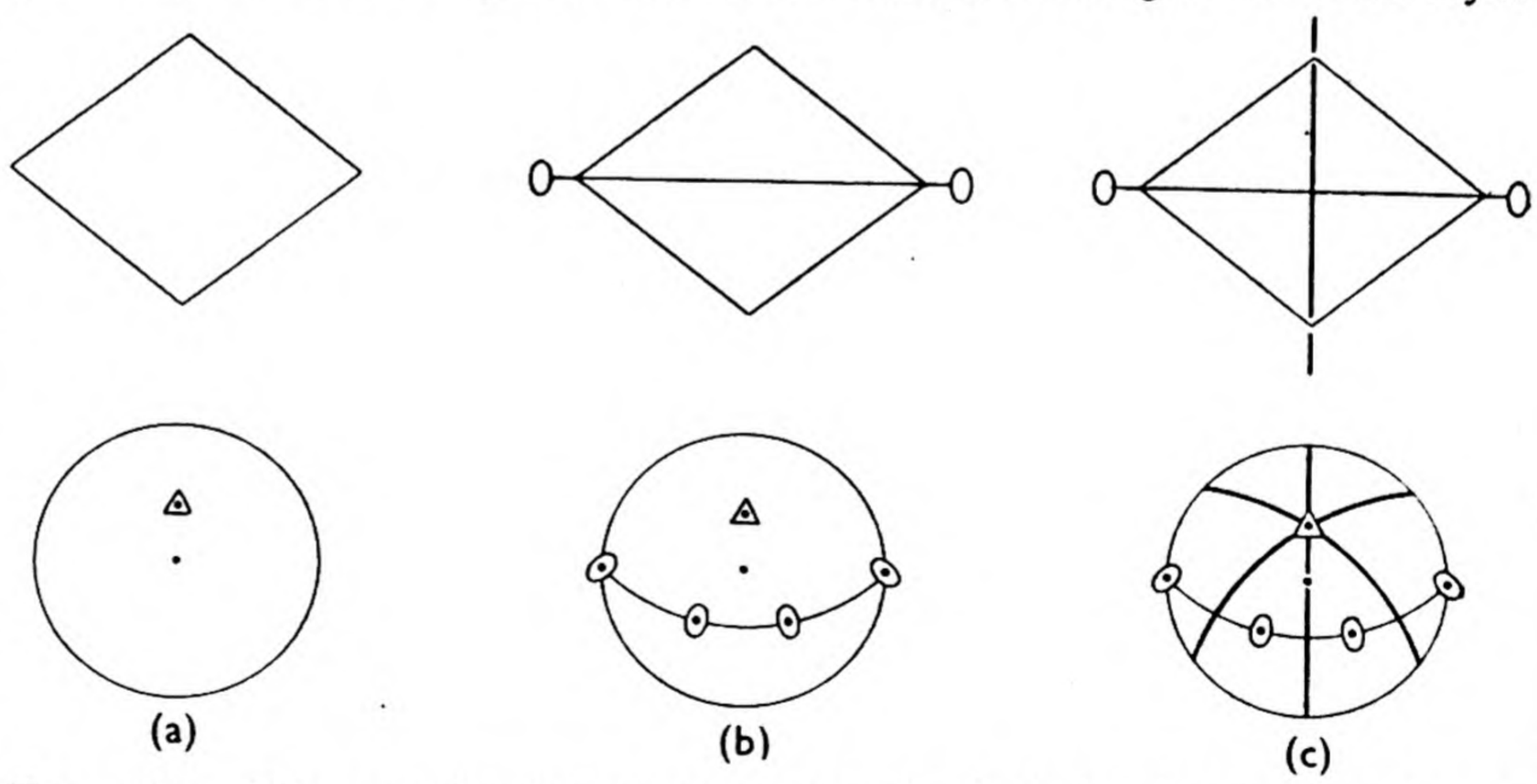

FIG. 158.2. Diagrams showing symmetry on a rhombohedral face in three classes : (*a*) $\bar{3}$ (*b*) 32 (*c*) $\bar{3}m$

Zone-axis Directions in the 21 non-centro-symmetrical Classes

All directions, other than those in the non-polar column, are polar.

System	Class	Polar symmetry and crystallographic axes	Non-polar directions
Triclinic	1	x-, y- and z-axes	none.
Monoclinic	2	y (diad)	all directions normal to y-axis.
	m	x and z (1)	y-axis only.
Orthorhombic	mm	z (diad)	all directions normal to z-axis.
	222	none	all directions normal to x-, y- or z-axis.
Trigonal	3	x, y, u and z (triad)	none.
	$3m$	z (triad)	x-, y- and u-axes only.
	32	x, y, u (diads)	all directions normal to x-, y- or u-axis.
Tetragonal	$\bar{4}$	z (tetrad)	all directions normal to z-axis.
	4	none	z-axis and all directions normal to it.
	$4mm$	z (tetrad)	all directions normal to z-axis.
	$\bar{4}2m$	none	all directions normal to x-, y- or z-axis.
	42	none	all directions normal to x-, y- or z-axis or to [110] or [1$\bar{1}$0].
Hexagonal	$\bar{6}$	z (hexad)	all directions normal to z-axis.
	6	x, y, u(2)	z-axis only.
	$6mm$	z (hexad)	all directions normal to z-axis.
	$\bar{6}m2$	3 horizontal diads	x-, y- and u-axes and all other directions normal to any of the diads which lie between these axes.
	62	none	all directions normal to z-axis, or to the x-, y or u-axes, or to any of the diads which lie between these axes.
Cubic	23	4 triads	all directions normal to any of the x-, y- or z-axes; i.e. directions with only one zero in the zone symbol, } no others.
	$\bar{4}3m$	4 triads	
	432	none	plus all directions normal to any of the six diads ⟨110⟩; i.e. with two figures equal in the zone symbol.

Notes. (1) All zone axes in the (vertical) symmetry plane are polar and no special importance in this connection is attached to those chosen as x and z.

(2) All zone axes in the (horizontal) symmetry plane are polar and no special importance in this connection is attached to the zone axes chosen as x, y and u.

justified in assuming that the specimen belonged to the class $\bar{3}$.

Crystals of apatite often show two hexagonal prisms, and are clearly either hexagonal, or trigonal. Etching on the basal plane shows hexagonal figures, but this does not mean that we can exclude the trigonal system or classes $\bar{6}$ and $\bar{6}$ $m2$ in which the symmetry about the z-axis is three-fold. Those on the first set of prisms show no vertical symmetry plane; this definitely excludes classes $6mm$ and $6/mmm$. A similar result on the second set of prisms also excludes $\bar{6}m2$, $3m$ and $\bar{3}m$. The etch figures on both these prisms also lack two-fold axes, and this excludes classes 62 and 32. The appearance of a horizontal symmetry plane in the etch figures does not help in any definite way. The classes not excluded by the evidence of these etch figures are 3 and $\bar{3}$ in the trigonal system, and 6, $\bar{6}$ and $6/m$ in the hexagonal. This is the only certain conclusion which can be drawn from the evidence of the etch figures.

2.5 Laue symmetry. In studying the symmetry of X-ray diffraction, we are directly concerned only with the eleven Laue symmetry groups and not with the thirty-two actual crystal classes. This results from Friedel's law which states that, in general, every crystal diffracts X-rays as if a centre of symmetry were present. It is important that this should be realised, so that wrong assumptions are not made from X-ray photographs about the symmetry elements which may be present in a crystal. The eleven Laue symmetry groups are shown on p. 161 and their symmetry elements are those of the corresponding centro-symmetrical class in Fig. 150.

As a consequence of Friedel's law it is not possible, in general, to determine by X-ray methods whether a given crystal is or is not centro-symmetrical. But there are two exceptions to this which we must notice here. The first consists of those crystals which belong to any one of the fifty space-groups which can be uniquely determined by the systematically-absent reflections. In these cases the class of the crystal is thus determined from knowledge of the space group. This applies also when the specimen belongs to one of the 11 uniquely-determinable enantiomorphous pairs of space groups. The second exception is the very special case in which Friedel's law breaks down owing to differential absorption in different layers in the crystal (Coster, Knol and Prins, 1930).

2.6 Pyro- and piezo-electricity and symmetry. A crystal which shows a pyro-electric effect cannot possess a centre of symmetry, because the effect involves accumulation of positive and negative charges at opposite ends of an axis. The absence of any detectable effect cannot, however, be considered to prove the presence of a centre of symmetry in the specimen, because the effect might be too small to measure. The presence of a centre in such a case could only be presumed until verified by other methods. When the pyro-electric effect is observed it may provide useful evidence on the assignment of a crystal to its class. A pyro-electric axis must be a uniterminal direction in the crystal, and reference can be made to the table on p. 159, in which the important uniterminal directions are given.

As with pyro-electricity, the property of piezo-electricity can be developed only by crystals belonging to the non-centro-symmetrical classes. Again the effect may be very weak, so that failure to detect it warrants only the provisional assumption that the crystal is centro-symmetrical. The piezo-electric properties of a crystal can be analysed and the moduli can be measured quantitatively. Two types of moduli can be distinguished. One group of moduli connects a compression or extension directed along a reference axis with the electric moment which is directed along the same axis. The symbols for these moduli are q_{ikl}, where $i = k =$ or $\neq l = 1, 2$ or 3. The second group of moduli comprise all except those defined above, and in some cases these moduli connect a torque about one reference axis with the electric moment directed along that axis. For convenience in reference, we shall refer to these two types of moduli as *compression moduli* and *torsion moduli* respectively.

There is a very close relation between the symmetry of crystals and the occurrence of these two types of moduli. Compression moduli occur only in the thirteen classes in which one or more of the crystallographic axes is uniterminal. Torsion moduli unaccompanied by compression moduli occur only in the seven classes in which none of the crystallographic (reference) axes is uniterminal, though other uniterminal axes may be present, for example, in classes 23, $\bar{4}3m$.

In general terms, it is easy to see why this should be so. Compression along a uniterminal axis will produce an electric moment which must be directed along that axis. Similarly, in the absence of a uniterminal axis only a stress component of more general and non-centro-symmetrical character, namely a twist, can develop a directed electric moment. Further comment is required on the three non-centro-symmetrical cubic classes, 23, $\bar{4}3m$ and 432. In 23 and $\bar{4}3m$ the triads are uniterminal, but the application of equal stress components along any one of the triad axes of a cubic crystal only results in a cancellation of charge owing to the symmetry, Only torsion moduli, therefore, occur in these two classes. Class 432, alone of all the non-centro-symmetrical classes, does not show the piezo-electric effect, because the symmetry produces a cancellation of charge for any applied force.

The Thirty-two Crystal Classes:

grouped according to centro-symmetry, Laue symmetry and enantiomorphism

System	Enantiomorphous	Non-enantiomorphous		Enantiomorphous	Non-enantiomorphous	
Cubic	23		$m3$	432	$\bar{4}3m$	$m3m$
Hexagonal	6	$\bar{6}$	$6/m$	62	$6mm$ $\bar{6}m2$	$6/mmm$
Tetragonal	4	$\bar{4}$	$4/m$	42	$4mm$ $\bar{4}2m$	$4/mmm$
Trigonal	3		$\bar{3}$	32	$3m$	$\bar{3}m$
Orthorhombic				222	mm	mmm
Monoclinic	2	$m=\bar{2}$	$2/m$			
Triclinic	1		$\bar{1}$			
	non-centro-symmetrical		centro-symmetrical	non-centro-symmetrical		centro-symmetrical

Note. The classes enclosed within any one rectangle have the same Laue symmetry.

The Twenty-one Non-centro-symmetrical Classes

Optically active	1	2 m	mm	3 32	4	6		Piezo-electric with both compression and torsion moduli
Non-optically active				$3m$	$4mm$	$6mm$ $\bar{6}$ $\bar{6}m2$		
							$\bar{4}3m$	Piezo-electric with torsion moduli only
Optically active			222		$\bar{4}$ 42 $\bar{4}2m$	62	23	
							432	Non-piezo-electric

Note. All these classes may show pyro-electricity. The groups marked ' piezo-electric ' and ' optically active ' are those which, according to theory, may show these effects. The effects have not yet been observed in crystals belonging to several of the classes so grouped.

2.7 Optical activity and symmetry. Optical activity is another property which can exist only in non-centro-symmetrical crystals. It was formerly believed that it could exist only in enantiomorphous crystals. It has been shown theoretically, however, that this is not true and the classes which can display optical activity (Wooster, 1938) are shown on p. 161. In this are included the eleven enantiomorphous classes : 1, 2, 3, 4, 6, 23, 222, 32, 42, 62, 432 ; and also the non-enantiomorphous classes, m, mm, $\bar{4}$, $\bar{4}2m$. The remaining non-centro-symmetrical classes cannot show optical activity : $3m$, $4mm$, $6mm$, $\bar{6}$, $\bar{6}m2$, $\bar{4}3m$.

3. Examples of the Study of Trigonal Crystals

3.1 Introduction. The two crystal specimens, Q and C, are both thin six-sided prisms. Cross-sections were cut and both showed a centred uniaxial interference figure, optically positive with low birefringence for Q, and optically negative with high birefringence for C. A thicker section showed that Q was optically active, but that C was not. The Laue photographs of Figs. 162 *a* and *b* show that both belong to the Laue symmetry group $\bar{3}m$, the direction of the three lines of symmetry in the photographs being perpendicular to the prism faces in both crystals. Tests for pyro-electricity showed regions of charge on the edges but not at the ends of the prism in specimen Q, while the tests were negative in specimen C. These data enable us to decide without doubt that crystal Q belongs to the point group 32. Crystal C belongs to one of the three point groups $3m$, 32 or $\bar{3}m$, and although the evidence is negative, we can proceed on the assumption that the point group is probably $\bar{3}m$.

3.2 Indexing the reflections from specimen Q. Oscillation photographs of specimen Q were taken (with $\lambda = 1{\cdot}934$ kX.) about the triad axis and about two directions normal to it, one perpendicular and one parallel to a prism face, and the results are given below.

Oscillation axis	Value of ζ_n	Value of ζ_1	Value of $d_{[uvw]}$ approx.	Value of $d_{[uvw]}$ refined
z (triad)	$0{\cdot}71$ $n=2$	$0{\cdot}35_5$	$5{\cdot}4_5$	5·393 kX.
⊥ to prism face	$0{\cdot}68$ $n=3$	$0{\cdot}22_6$	$8{\cdot}5_6$	8·492
‖ to prism face and ⊥ to triad	$0{\cdot}78$ $n=2$	$0{\cdot}39$	$4{\cdot}9_6$	4·903

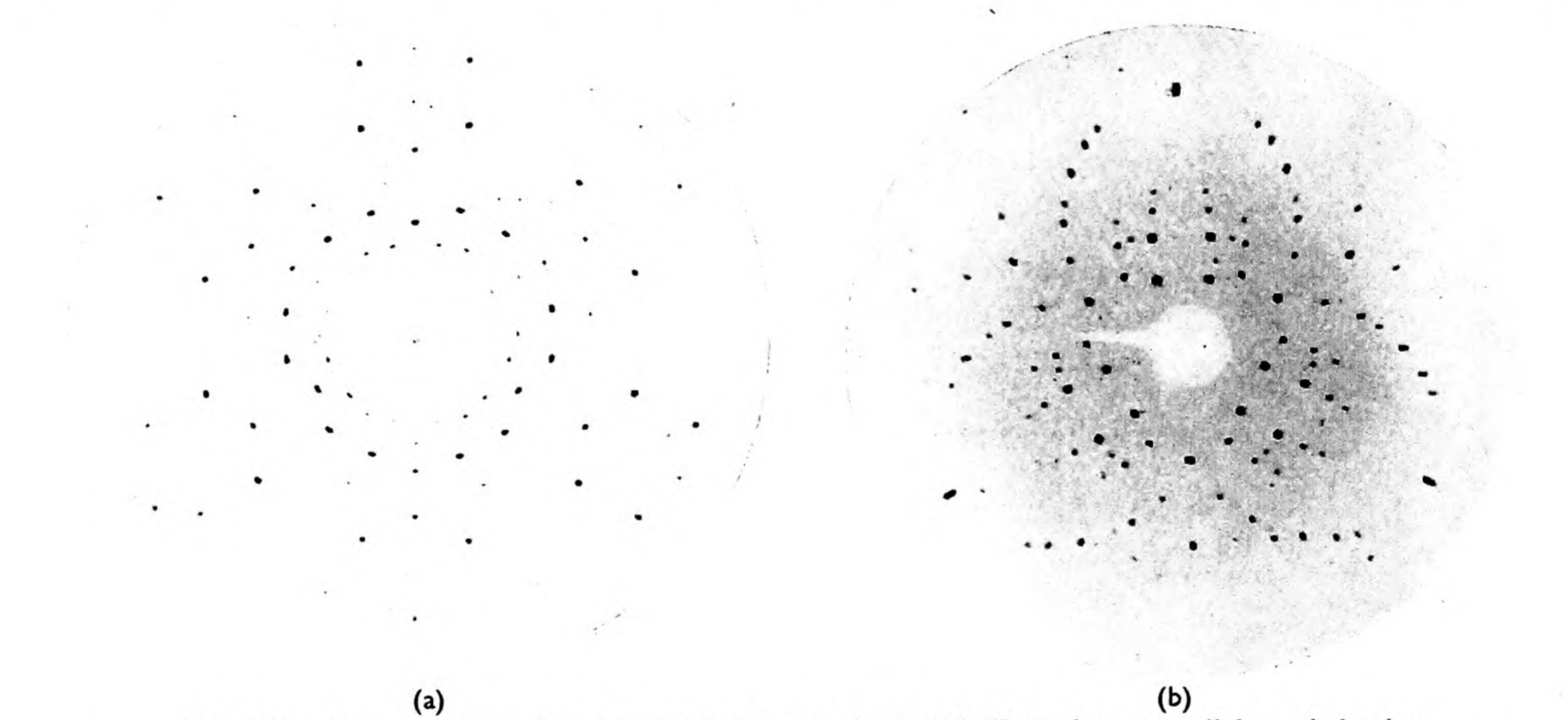

(a) (b)

FIG. 162. Laue photographs taken on flat (front) plates with X-ray beam parallel to triad axis :
(*a*) specimen Q : quartz (crystal to plate = 2·06 cm.). (*b*) specimen C : calcite (crystal to plate = 2·00 cm.)

We will take the x-axis parallel to a prism face and perpendicular to the prism axis, as this has the shortest repeat distance in the plane normal to the z (triad)-axis. In constructing the hexagonal reciprocal lattice we shall use the refined values, although in practice these would not be available at this stage. Thus we have

$$c^* = \frac{1{\cdot}934}{5{\cdot}393} = 0{\cdot}358_7 \; ; \quad a^* = \frac{\lambda}{a.\cos 30^\circ} = \frac{1{\cdot}934}{4.246} = 0{\cdot}455_5.$$

The two projections of the reciprocal lattice are drawn in the usual way and the indices obtained are tabulated below. For the projection on the x^*z^* plane we require to know the projection of the vector a^* in order that the spots on layer lines other than the zero layer may be indexed, and this, as shown in **5**, 2.7, is given by $a^* . \cos 60° = 0.227_7$. It is clear that because of the small value of c^*, very few orders of $ooo l$ can be recorded with iron radiation, which is really unsuitable for a substance such as Q. As these reflections are of great importance in the determination of the space group, other photographs were taken about the x-axis with molybdenum radiation in order to increase the number of $ooo l$ reflections observed.

INDEXED REFLECTIONS FROM SPECIMEN Q

$hk\,i\,l$		$hh\bar{2}hl$	$h\bar{h}ol$		$ooo l$
$\bar{2}1\cdot3$	$\bar{3}2\cdot2$	$\bar{1}\bar{1}\cdot3$	$\bar{2}0\cdot3$	$2\bar{2}\cdot1$	$00\cdot3$
$\bar{2}1\cdot4$	$3\bar{1}\cdot3$	$\bar{1}\bar{1}\cdot4$	$\bar{1}0\cdot5$	$2\bar{2}\cdot2$	$00\cdot6$
$\bar{2}2\cdot3$	$31\cdot0$	$11\cdot2$	$0\bar{2}\cdot3$	$20\cdot4$	$00\cdot9$
$\bar{1}1\cdot5$	$31\cdot1$	$22\cdot0$	$0\bar{2}\cdot4$	$3\bar{3}\cdot0$	$00\cdot12$
$1\bar{2}\cdot0$	$4\bar{3}\cdot0$	$22\cdot1$	$0\bar{1}\cdot5$	$3\bar{3}\cdot1$	
$1\bar{2}\cdot1$	$4\bar{3}\cdot1$		$01\cdot0$	$30\cdot2$	
$1\bar{2}\cdot2$	$4\bar{2}\cdot2$		$01\cdot1$	$40\cdot0$	
$12\cdot0$	$4\bar{1}\cdot2$		$02\cdot0$	$40\cdot1$	
$12\cdot1$					
$2\bar{3}\cdot0$					
$21\cdot1$					
$21\cdot2$					
$21\cdot3$					

Note. Dots have been used in place of asterisks in this table.

3.3 Determination of unit cell and space group of specimen Q. We first decide on the type of lattice. It is clear that general reflections occur for which $(-h+k+l) \neq 3n$ and for which $(h-k+l) \neq 3n$, and so the lattice cannot be R. The smallest repeat distance perpendicular to the triad is also perpendicular to a symmetry line in the Laue photograph of Fig. 162*a*, and therefore it must be parallel to a diad axis in the Laue group $\bar{3}m$. It follows that, if we put the symbol of the twofold axis in the first subsidiary position in the space group symbol (that is, immediately after the triad symbol), the lattice symbol must be C and not H (see **10**, 1.4). The possible space groups † of the point group 32 which remain are: $C\,32$, $C\,3_1 2$, $C\,3_2 2$. But it is clear that orders of $ooo l$ occur only when $l = 3n$, and therefore a screw triad axis must be present. This disposes of $C\,32$; but the remaining two space groups, $C\,3_1 2$ and $C\,3_2 2$, form an enantiomorphous pair, and it is not possible to decide to which of these the structure of our specimen should be assigned. In the table the reflections have been arranged in the usual way for hexagonal axes, but in this case, we need only the general reflections and the $ooo l$ reflections.

† Although in this book space-group theory is not treated because of shortage of space, the study of these two examples is carried to the determination of the space group, as this provides a convenient stopping place.

The crystal Q is a specimen of quartz (low-temperature), SiO_2, which is a trigonal substance with a structure built on the hexagonal lattice. A glance at the photograph taken with the z-axis (triad) as oscillation axis is sufficient to determine that the lattice is hexagonal and not rhombohedral. First, the small repeat distance of 5·4 kX. along the triad precludes the possibility of a rhombohedral structure for this particular substance. Secondly, if we disregard the intensities of the spots, their positions are symmetrical above and below the zero-layer line, and the same values of ξ occur in adjacent layer lines. These features of the photographs taken with the triad axis as oscillation axis are not found with rhombohedral structures (**10**, 1.4).

Finally, we can calculate the volume of the unit cell and the number of formula units of SiO_2 per unit cell,

$$V = a^2 . c . \cos 30° = 112\cdot3 \times 10^{-24} \text{ c.c.}$$

$$N = \frac{D \times V}{\text{Mol. wt.} \times 1\cdot66 \times 10^{-24}} = (2\cdot97) = 3,$$

where V is volume of unit cell in c.c.; D is density (2·65 gm. per c.c.); N is number of units of formula, SiO_2, per unit cell; Mol. wt. is molecular weight of SiO_2 (60·3); and $1\cdot66 \times 10^{-24}$ = weight in gm. of unit of atomic weight.

3.4 Comparison with other descriptions of substance Q. The axial ratio, $c : a$, of the substance Q has the value 1·100, which compares very closely with the figure of 1·09997 given by Dana (1898). The 'unit cell' which corresponds to the morphological indexing is, therefore, the true, smallest unit cell as determined by X-ray methods. Accordingly, there is only one set of valid indices of faces and of reflections in quartz, as nothing is gained by selecting a larger unit cell. In older morphological text-books, three-figure (Miller) indices are used for all trigonal substances, but these should not in general be used for quartz, which has a structure built on a hexagonal lattice.

3.5 Indexing the reflections from specimen C. Oscillation photographs were taken (with $\lambda = 1\cdot539$ kX.) of specimen C about the triad axis and about two directions normal to it, one perpendicular and one parallel to a prism face, and the results are given on p. 164.

Oscillation axis	Values of		Values of $d_{[uvw]}$	
	ζ_n	ζ_1	approx.	refined
z (triad)	0·72 $n=8$	$0{\cdot}09_0$	17·0	$17{\cdot}02_0$ kX.
⊥ to prism face	0·72 $n=4$	$0{\cdot}18_0$	$8{\cdot}5_5$	$8{\cdot}63_0$
‖ to prism face, ⊥ to triad	0·62 $n=2$	$0{\cdot}31_0$	$5{\cdot}0_0$	$4{\cdot}98_3$

We proceed as before to index the reflections on the basis of a hexagonal cell with the x-axis perpendicular to the triad and parallel to a prism face, because this is the smaller of the two repeat distances normal to the triad. Using the refined values we have :

$$c^* = \frac{1{\cdot}539}{17{\cdot}02} = 0{\cdot}090_4\,; \quad a^* = \frac{1{\cdot}539}{a\,.\cos 30^\circ} = 0{\cdot}356_6.$$

The table below includes indices from several photographs :

Indexed Reflections from Specimen C

$hkil$				$hh\bar{o}l$ / $\bar{h}hol$		$hh\bar{2}hl$
$\bar{3}1{\cdot}14$	$\bar{1}\bar{2}{\cdot}13$	$3\bar{2}{\cdot}\bar{1}$	$4\bar{2}{\cdot}0$	$\bar{2}0{\cdot}16$		$\bar{1}\bar{1}{\cdot}6$
$\bar{3}4{\cdot}\bar{4}$	$\bar{1}2{\cdot}18$	$3\bar{2}{\cdot}2$	$4\bar{2}{\cdot}6$			$\bar{1}\bar{1}{\cdot}12$
$\bar{3}4{\cdot}2$	$\bar{1}5{\cdot}\bar{6}$	$3\bar{2}{\cdot}17$	$4\bar{2}{\cdot}12$	$\bar{2}2{\cdot}2$		$\bar{1}\bar{1}{\cdot}15$
	$\bar{1}5{\cdot}6$			$\bar{2}2{\cdot}8$		$\bar{1}\bar{1}{\cdot}18$
$\bar{3}5{\cdot}1$	$1\bar{2}{\cdot}18$	$3\bar{1}{\cdot}\bar{2}$	$4\bar{1}{\cdot}8$	$\bar{2}2{\cdot}14$		
$\bar{3}5{\cdot}\bar{2}$	$12{\cdot}\bar{1}$	$3\bar{1}{\cdot}1$	$4\bar{1}{\cdot}14$			$11{\cdot}\bar{3}$
	$12{\cdot}2$	$3\bar{1}{\cdot}4$		$\bar{1}0{\cdot}20$		$11{\cdot}0$
$\bar{2}\bar{1}{\cdot}14$	$12{\cdot}17$	$3\bar{1}{\cdot}16$	$41{\cdot}6$	$\bar{1}1{\cdot}4$		
$\bar{2}1{\cdot}6$		$3\bar{1}{\cdot}19$	$41{\cdot}12$			$22{\cdot}0$
$\bar{2}1{\cdot}12$	$2\bar{1}{\cdot}0$			$0\bar{1}{\cdot}4$		$22{\cdot}6$
$\bar{2}1{\cdot}15$	$2\bar{1}{\cdot}3$	$31{\cdot}\bar{4}$	$5\bar{2}{\cdot}1$	$0\bar{2}{\cdot}8$		$22{\cdot}12$
$\bar{2}1{\cdot}18$		$31{\cdot}8$	$5\bar{2}{\cdot}4$	$0\bar{2}{\cdot}14$		
	$21{\cdot}\bar{2}$	$31{\cdot}14$	$5\bar{2}{\cdot}7$			$33{\cdot}\bar{3}$
$\bar{2}3{\cdot}\bar{8}$	$21{\cdot}1$		$5\bar{2}{\cdot}10$	$20{\cdot}\bar{4}$		$33{\cdot}0$
$\bar{2}3{\cdot}\bar{5}$	$21{\cdot}4$	$32{\cdot}\bar{5}$		$20{\cdot}20$		$33{\cdot}3$
$\bar{2}3{\cdot}7$	$21{\cdot}16$	$32{\cdot}1$	$5\bar{1}{\cdot}6$			
		$32{\cdot}4$	$5\bar{1}{\cdot}12$	$30{\cdot}\bar{6}$		
$\bar{2}4{\cdot}\bar{6}$	$23{\cdot}8$	$32{\cdot}7$		$30{\cdot}0$		
$\bar{2}4{\cdot}6$		$32{\cdot}10$		$30{\cdot}6$		
	$24{\cdot}\bar{2}$			$30{\cdot}12$		
$\bar{2}5{\cdot}\bar{7}$	$24{\cdot}4$			$30{\cdot}18$		
$\bar{2}5{\cdot}\bar{4}$						
$\bar{2}5{\cdot}\bar{1}$				$50{\cdot}8$		
$\bar{2}5{\cdot}2$						
$\bar{2}5{\cdot}5$						

3.6 Determination of unit cell and space group of specimen C. Inspection of the tabulated indices shows that general reflections occur only when $(-h+k+l)=3n$ and, therefore, the lattice is R. This condition is, of course, imposed also on all special planes, so that the following reflections will occur only under the conditions stated.

$$\begin{cases} hh\bar{2}hl & \text{only when } l=3n \\ h\bar{h}ol & \text{only when } (h+l)=3n \\ \bar{h}hol & \text{only when } (-h+l)=3n \\ ooo l & \text{only when } l=3n. \end{cases}$$

No reflections of the type $ooo l$ have been recorded from these photographs, but it is clearly unnecessary in this case to take photographs specially to record these reflections. Now the space groups with the R lattice within the Laue group $\bar{3}m$ are :

Point group	$3m$	32	$\bar{3}m$	Conditions for spectra to occur
Space-groups	$R3c$		$R\bar{3}c$	in $\begin{Bmatrix} h\bar{h}ol \\ \bar{h}hol \end{Bmatrix}$ $l=2n$,
	$R3m$	$R32$	$R\bar{3}m$	no special absences

In $R3m$, $R32$ and $R\bar{3}m$ there is no condition of systematic absences of reflections other than that imposed by the lattice type. But in $R3c$ and $R\bar{3}c$ the c glide plane causes absences in reflections of the type $h\bar{h}ol$, except when $l=2n$. This additional condition is found in our tabulated reflections, and so we can conclude that the space group of specimen C is either $R3c$ or $R\bar{3}c$. It should be noted that in this case the point group 32 is excluded. Since $R3c$ and $R\bar{3}c$ differ only in the existence of centres of symmetry in the latter, we cannot distinguish between them unless we know whether the substance is or is not centro-symmetrical. In view of the complete absence of any evidence of the presence of a uniterminal triad, we can assume that the space group of specimen C is probably $R\bar{3}c$. From the condition for absences of general reflections, it follows that the true smallest unit-cell is a rhombohedron in the obverse attitude relative to our hexagonal axes.

The crystal C is a specimen of calcite, $CaCO_3$ which is a trigonal substance with a structure built on the rhombohedral lattice. In a substance of this kind the large repeat distance of 17 kX. along the triad and the axial ratio of about $3(c:a=3{\cdot}4)$ both point strongly to the rhombohedral nature of the lattice. Certain features of oscillation photographs of rhombohedral specimens are noted in **8**, 5.2. In calcite there is no matching of the positions of spots above and below the zero-layer line as there is in quartz. Also, in calcite, the same values of ξ tend to repeat every third line but are never found in adjacent layer lines as in quartz. Such features make it easy to see whether a trigonal substance is built on the hexagonal or the rhombohedral lattice from a

glance at an oscillation photograph taken about the triad axis. The check by means of systematic absences among general reflections should, however, always be applied as above. The appearance of the Laue photographs of Fig. 162 also gives strong indications that the lattice of Q is hexagonal and that of C rhombohedral.

We can calculate the elements of the rhombohedron from the refined values for the repeat distances a_h and c along the hexagonal axes. These calculations are given in Appendix 1 and the results are :

$$a_r = 6{\cdot}361 \text{ kX.}, \quad \alpha = 46^\circ\ 07'.$$

The volume of the rhombohedral unit cell is most quickly obtained by calculating the volume of the hexagonal unit cell and dividing the result by 3, as the hexagonal cell is a triple one.

$$V_h = a_h^2 \,.\, \cos 30 \,.\, c = 368{\cdot}5 \times 10^{-24} \text{ c.c.}$$

$$N_h = \frac{D \times V}{\text{Mol. wt.} \times 1{\cdot}66 \times 10^{-24}} = (6{\cdot}012) = 6,$$

$$\therefore\ N_r = 2\ ;$$

where V_h is volume of hexagonal unit cell in c.c. ; D is density (2·71 gm. per c.c.) ; N_h is number of units of formula, $CaCO_3$, per hexagonal unit cell ; N_r is number of units of formula, $CaCO_3$, per rhombohedral unit cell ; Mol. wt. (molecular weight) of $CaCO_3$ (100·1) ; $1{\cdot}66 \times 10^{-24}$ is weight in gm. of unit of atomic weight.

From the elements of the unit rhombohedron which we have calculated, we can derive the elements of the reciprocal lattice on rhombohedral axes. The calculations of Appendix 1 give, for $\lambda = 1{\cdot}539$ kX.,

$$a^* = \lambda / d_{100} = \frac{1{\cdot}539}{4{\cdot}183_6} = 0{\cdot}367_8 \text{ kX.}$$

and for the reciprocal angle :

$$\alpha^* = 114^\circ\ 10'.$$

3·7 Comparison with other descriptions of substance *C*. The axial ratio of the (triple) cell which is the smallest hexagonal unit cell in calcite is $c : a = 3{\cdot}42$, which is very different from the figure of $c : a = 0{\cdot}8543$ given by Dana (1894). It is clear that the unit cell which corresponds to the morphological indexing is not the smallest hexagonal unit cell, and we must discover what it is and study its relation to the unit cell determined by X-ray methods.

We shall work on the basis of hexagonal axes, as this simplifies the calculations. The repeat distance along the x-axis in the 'morphological unit cell' having $c = 17{\cdot}0$ kX. is given by

$$a_h' = 17{\cdot}0 / 0{\cdot}8543 = 19{\cdot}9 \text{ kX.}$$

This is four times the length of a_h, the side of the triple hexagonal cell described above, and the ratio of the volumes of the two hexagonal cells is 48 : 3. The morphological (cleavage) rhombohedral unit is, therefore, sixteen times as large as the true smallest rhombohedral unit cell.

In view of the size of this cell, models of the structure of calcite do not usually show a complete unit cell of this type. If both the a- and the c-axes are halved, the volume of the morphological hexagonal pseudo-cell is reduced to twice that of the triple hexagonal cell, and the morphological rhombohedral pseudo-cell to twice that of the true rhombohedral cell. A structure model of the cleavage rhombohedron can therefore be constructed which contains four $CaCO_3$, but this is not a true unit cell, as can be seen from Fig. 166.

If we calculate the elements of the cleavage rhombohedron (Appendix 1) containing four $CaCO_3$, we obtain : $a_r'' = 6{\cdot}41_2$ kX. ; $\alpha = 101^\circ\ 55'$.

But, as we have seen, this does not give the true repeat distance along the polar edges of this rhombohedron, which is $6{\cdot}41_2 \times 2 = 12{\cdot}82_4$. We can check this by taking an oscillation photograph, which shows a value of $\zeta_1 = 0{\cdot}15$ for $\lambda = 1{\cdot}934$, and hence a repeat distance along the polar edge of about 13 kX.

We can now derive from Fig. 166 the face-index matrices for the transformations between the smallest rhombohedron and the cleavage rhombohedron (true cell), and between the respective triple hexagonal cells.

$R \rightarrow R_{cl}$

$$\begin{vmatrix} 3 & \bar{1} & \bar{1} \\ \bar{1} & 3 & \bar{1} \\ \bar{1} & \bar{1} & 3 \end{vmatrix} \quad \Delta = 16$$

$R_{cl} \rightarrow R$

$$\begin{vmatrix} \frac{1}{2} & \frac{1}{4} & \frac{1}{4} \\ \frac{1}{4} & \frac{1}{2} & \frac{1}{4} \\ \frac{1}{4} & \frac{1}{4} & \frac{1}{2} \end{vmatrix} \quad \Delta = \tfrac{1}{16}$$

Hex.$\rightarrow$Hex.$_{cl}$

$$\begin{vmatrix} 4 & 0 & 0 \\ 0 & 4 & 0 \\ 0 & 0 & 1 \end{vmatrix} \quad \Delta = 16$$

Hex.$_{cl}\rightarrow$Hex.

$$\begin{vmatrix} \frac{1}{4} & 0 & 0 \\ 0 & \frac{1}{4} & 0 \\ 0 & 0 & 1 \end{vmatrix} \quad \Delta = \tfrac{1}{16}$$

The matrices relating a rhombohedral cell to the corresponding hexagonal one are (**10,** 1.4) :

$R \rightarrow$Hex.

$$\begin{vmatrix} 1 & \bar{1} & 0 \\ 0 & 1 & \bar{1} \\ 1 & 1 & 1 \end{vmatrix} \quad \Delta = 3$$

Hex.$\rightarrow R$

$$\begin{vmatrix} \frac{2}{3} & \frac{1}{3} & \frac{1}{3} \\ \frac{\bar{1}}{3} & \frac{1}{3} & \frac{1}{3} \\ \frac{\bar{1}}{3} & \frac{\bar{2}}{3} & \frac{1}{3} \end{vmatrix} \quad \Delta = \tfrac{1}{3}$$

Now the cleavage rhombohedron is indexed as $\{10\bar{1}1\}$ or $\{100\}$ by morphologists ; this becomes $\{10\bar{1}4\}$ with respect to the smallest hexagonal cell and $\{211\}$ with respect to the smallest rhombohedral cell. The angle between two cleavage planes, measured over a polar edge, is 74° 55′. From this we can calculate the rhombohedral angle. The calculation of Appendix 1 gives

$$\alpha' = 101^\circ\ 55',$$

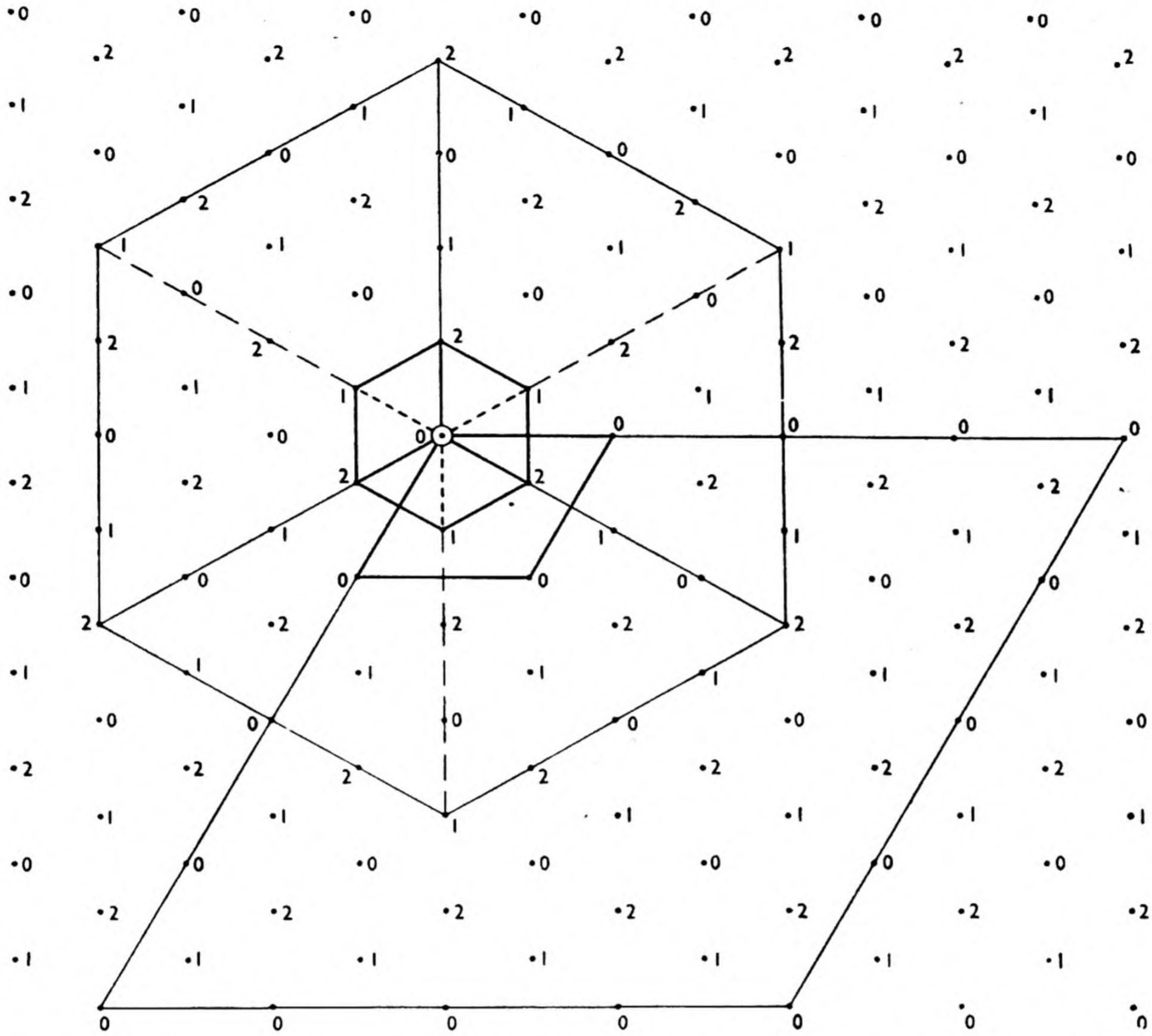

FIG. 166. The rhombohedral lattice of calcite projected on the base. The smallest true unit cells are shown by heavy lines and the unit cells corresponding to the cleavage rhombohedron by light lines. The heights are given in thirds of the repeat distance normal to the base

which agrees with the value previously calculated by another method. We can also calculate the corresponding angle for $\{10\bar{1}1\}$, which has its faces parallel to those of the smallest rhombohedral unit-cell. This gives

$$\alpha = 46^\circ\ 07',$$

which agrees with the previous value.

It is also convenient to calculate the angle between the triad axis and the polar edge of the smallest rhombohedral unit, in order to set the crystal for checking the repeat distance along it. The pole of this direction is plotted on a stereogram, and for setting purposes, it would be sufficiently accurate to determine the angle by measurement with a stereographic net. In Appendix 1, we obtain the angle $\rho = 48^\circ\ 52\frac{1}{2}'$ and the angle $zr = 75^\circ\ 46'$.

Hence $[100] \wedge [111] = 75^\circ\ 46' - 48^\circ\ 52\frac{1}{2}' = 26^\circ\ 53\frac{1}{2}'$.

The crystal was then reset and an oscillation photograph ($\lambda = 1{\cdot}539$) was taken about the polar edge, giving $\zeta_3 = 0{\cdot}72$, $d_{[100]} = \lambda/\zeta_1 = 6{\cdot}4$ kX., where the zone axis subscript to d refers to rhombohedral axes, as shown by the absence of the asterisk. This value agrees with the calculated value previously obtained.

Cleavage flakes of calcite have been used as a standard for spacing measurements (**2**, 3.2) and this is often expressed in the form,

$$d_{200} = 3{\cdot}0290 \text{ kX.}$$

The subscript shows that the cleavage plane is indexed on rhombohedral axes, and is clearly referred to the morphological unit cell.

From Figs. 166 and 167 it can be seen that if we take 3·029 as the second-order spacing of planes parallel to the cleavage, the corresponding unit rhombohedron can be taken with $c = 17/2$ kX and is the pseudo-cell with 4 $CaCO_3$ discussed earlier. With respect to the true morphological unit cell (with 32 $CaCO_3$), this spacing of 3·03 has the indices 400. If we transform from

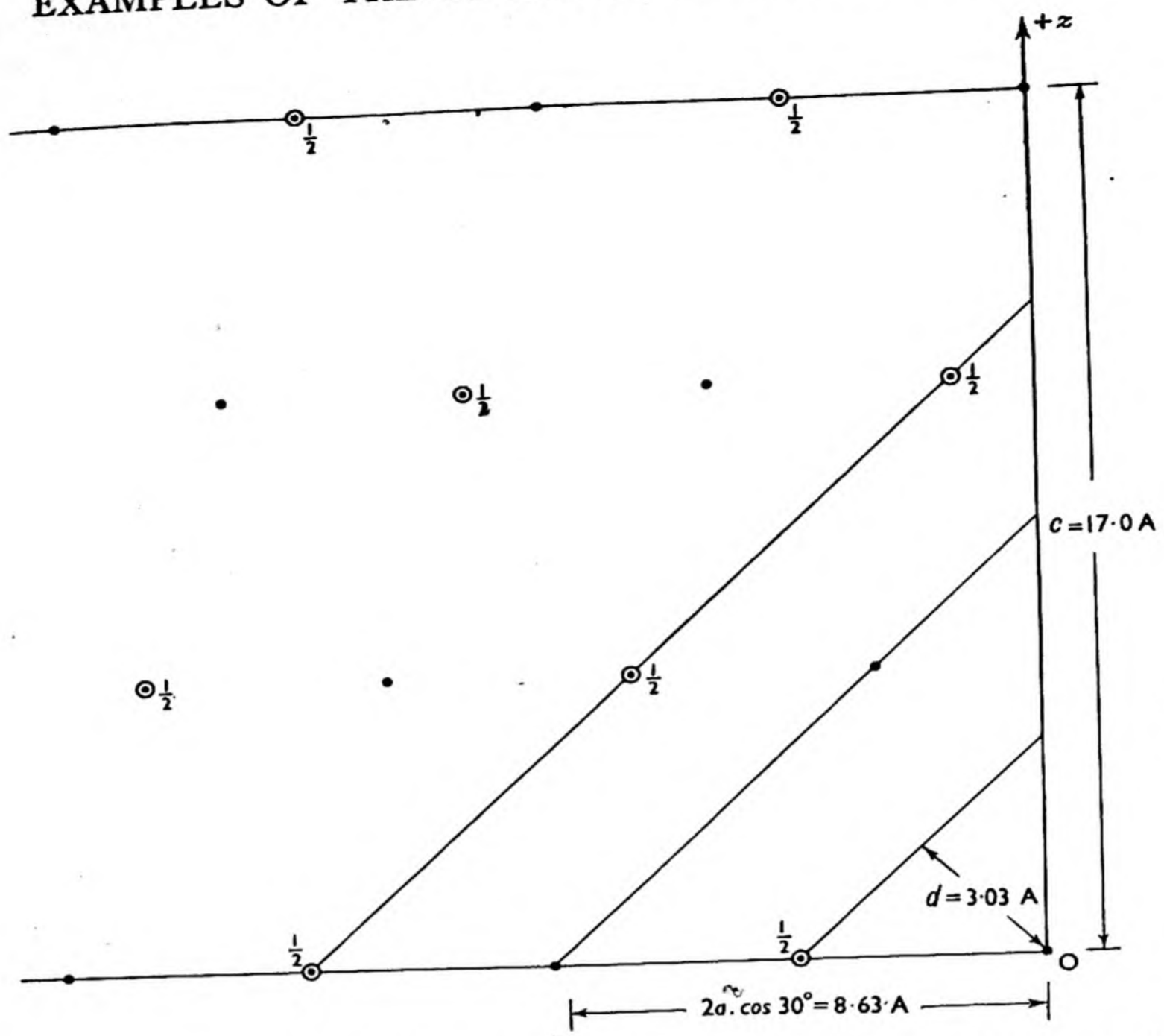

FIG. 167. The rhombohedral lattice of calcite projected on the plane normal to the y-axis (hexagonal). Points at a height of one-half of the repeat distance along the y-axis are marked $\odot\frac{1}{2}$. The planes shown are

211 or 10*4 in the smallest unit cell, and
400 or 40*4 in the true morphological (cleavage) unit cell

this true morphological rhombohedron to the smallest rhombohedral cell, the indices 400 become 211. Thus on the basis of the smallest rhombohedral unit cell, the standard spacing of calcite should be quoted as

$$d_{211} = 3{\cdot}0290 \text{ kX. or } 3{\cdot}0350 \text{ A.}$$

If we transform to the smallest hexagonal cell, the indices 211 become 10*4, which can be seen from Figs. 166 and 167 to represent the same spacing. We can demonstrate the correctness of this by a simple calculation. The distance of the reciprocal point 10*4 from the origin, is given by

$$d^*_{10*4} = \sqrt{a^{*2} + (4c^*)^2} = 0{\cdot}507.$$

Therefore

$$d_{10*4} = 1{\cdot}539/0.5076 = 3{\cdot}03 \text{ kX.},$$

which gives the same spacing.

CHAPTER 11

METHODS OF TAKING POWDER PHOTOGRAPHS

1. Introduction

MANY materials can be obtained only as a mass of randomly-oriented crystals, and consequently the methods described in previous chapters cannot be applied to them. In fact, it might be thought that the diffraction patterns from such materials would be far too complicated for any methods of analysis. While this is often true, there are many substances of which the *powder patterns*, as they are called, are fairly simple, and the powder method has great technical importance because of its wide application.

The photographs previously described have a diffraction pattern of spots ; the powder pattern, on the other hand, is one of lines. The reason for this is that, for a given wave-length, the deviation of a particular reflection is 2θ, and therefore corresponding reflections from all crystals in a specimen must lie on a cone the apex of which is at the specimen, the axis of which is in the direction of the X-ray beam, and the semi-vertical angle of which is 2θ. Such a cone is shown in Fig. 168.1, and its intersection with the film represents a line of the powder pattern. In

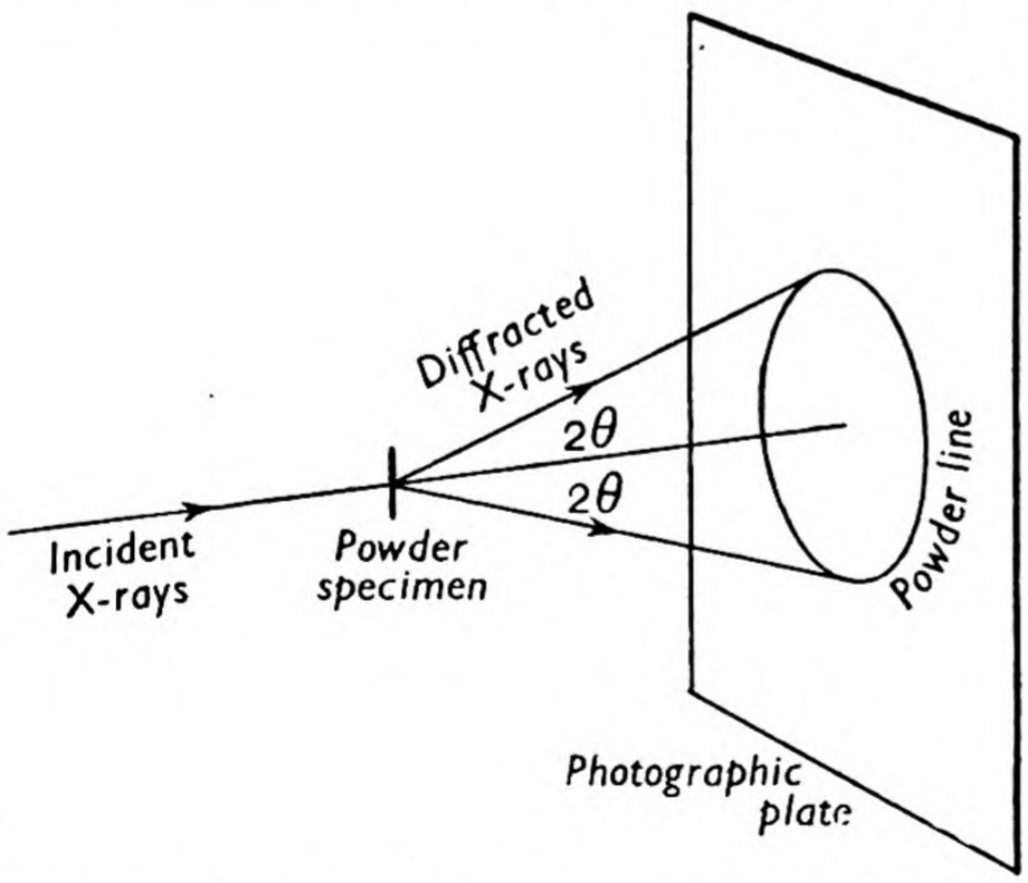

FIG. 168.1. Diagram showing the production of a powder line on a flat plate

general there will be many such lines, each representing a set of reflections with the same value of θ, and therefore the powder pattern of a substance is often extremely complicated. In practice, flat films are rarely used ; it is preferable to surround the specimen by a narrow strip of film, as shown in Fig. 168.2, since this intercepts a greater number of cones of reflection. Only a small part of each cone is recorded,

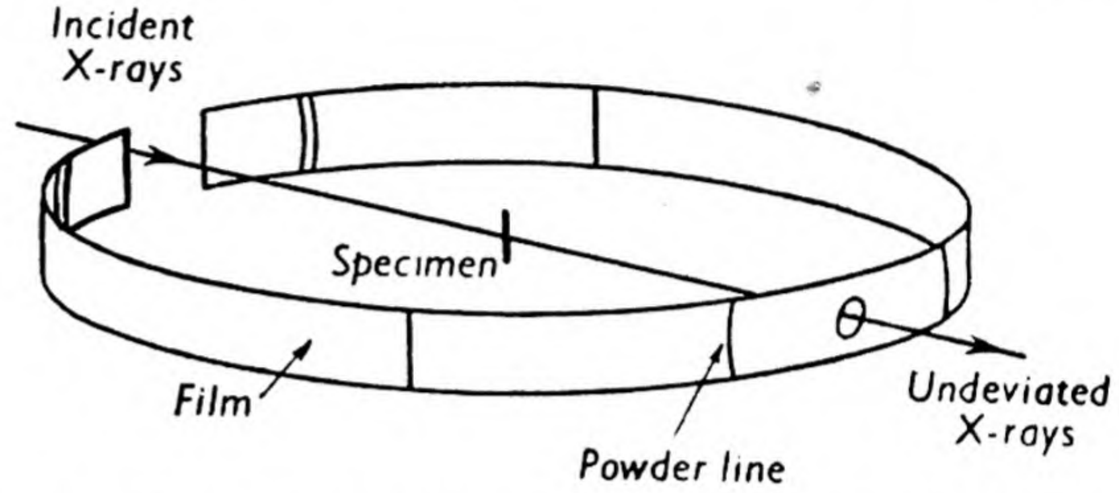

FIG. 168.2. Diagram showing the production of a powder photograph on a cylindrical film

but all reflections except those with θ just greater than 0° or just less than 90° can reach the film.

In this statement of the theory of the production of *powder lines*, it is assumed that in the part of the specimen irradiated there are sufficient crystals in all orientations to give rise to smooth lines. This may be so if the grain-size is less than about 10^{-4} cm., but even in finely ground material the grain-size usually exceeds this. When the grain-size is too coarse, there is not enough room within the volume irradiated for a sufficient number of crystals to lie in all orientations. For a very coarse specimen we can imagine certain crystals to give a Laue reflection of the characteristic radiation from a particular set of lattice planes which lie in the correct orientation. These reflections from several crystals would all lie on a curve of constant θ but would form a line of spots instead of a smooth line. With a less coarse specimen, the 'spottiness' becomes less marked. The spottiness of powder lines can be greatly reduced by rotating the powder specimen during exposure, as this considerably increases the number of crystals which contribute to the formation of each powder line.

Sometimes it is not possible to draw a smooth curve through the spots belonging to a high-angle line on a spotty photograph. This is due to some crystals being in positions to reflect wave-lengths which are a little displaced from the peaks of the characteristic radiations (Bragg and Lipson, 1938). The great resolution at high angles of reflection causes such

spots to be visibly displaced from the true centre of the line. Rotation of the specimen permits these crystals to reflect the whole of the radiation in the α-doublet, and so to produce a powder line of the normal intensity distribution.

So far we have been considering the effects of the characteristic radiation. With ordinary filtered radiation, however, each crystal will also give rise to a Laue pattern by selection of some of the wave-lengths of the white radiation. These patterns from all the crystals will merge to form the 'background' of the film, but with a coarse-grained specimen this background will be uneven. This effect is minimised by the rotation of the specimen, as each Laue spot is then drawn out into a streak which merges into neighbouring streaks.

Only simple apparatus is necessary for taking powder photographs, but the importance of the method is such that a great deal of thought has been given to the construction of powder cameras in order that much more than the general nature of the pattern can be obtained. The first essential is that θ be accurately measurable, since this is the only characteristic by which the line can be identified. The lines must therefore be sharp and their positions must be accurately recorded on the film. Powder lines, however, are weak compared with single-crystal reflections because the diffracted X-rays are no longer concentrated into a spot; if a small pin-hole is used to reduce the divergence of the beam, exposures will be unduly long. This difficulty may be overcome by the use of a slit parallel to the length of the specimen to admit the X-rays. Each line will now be composed of a set of curves displaced along a line parallel to the length of

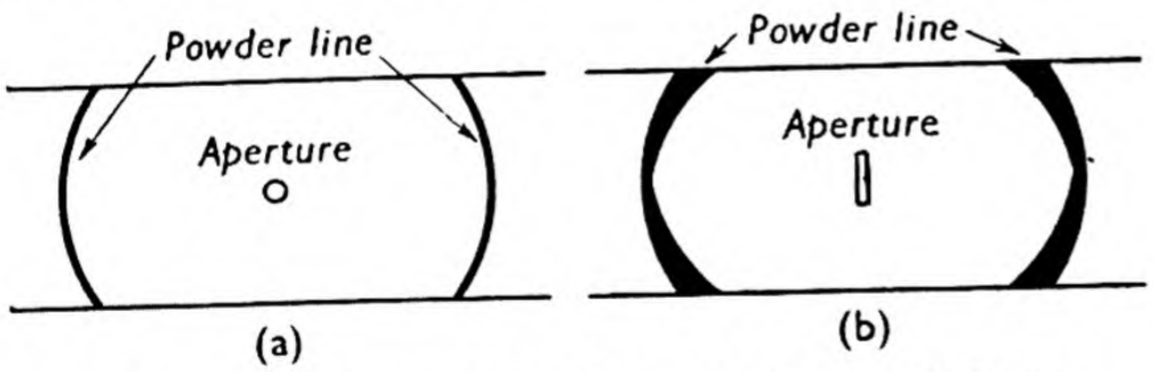

FIG. 169.1. The shapes of powder lines with X-rays admitted through (*a*) a small circular aperture, (*b*) a vertical slit

the slit; as shown in Fig. 169.1, this will not appreciably affect the width of the line at the centre, which is the only part usually measured.

Experience has shown that satisfactory photographs result if the length of the slit is about 1/50 of the diameter of the camera. This dimension has been adopted in the cameras described by Bradley, Lipson and Petch (1941). If, however, this type of collimator is used, it is important that the camera should be carefully adjusted, otherwise broadened lines may result. The camera should be so adjusted that the

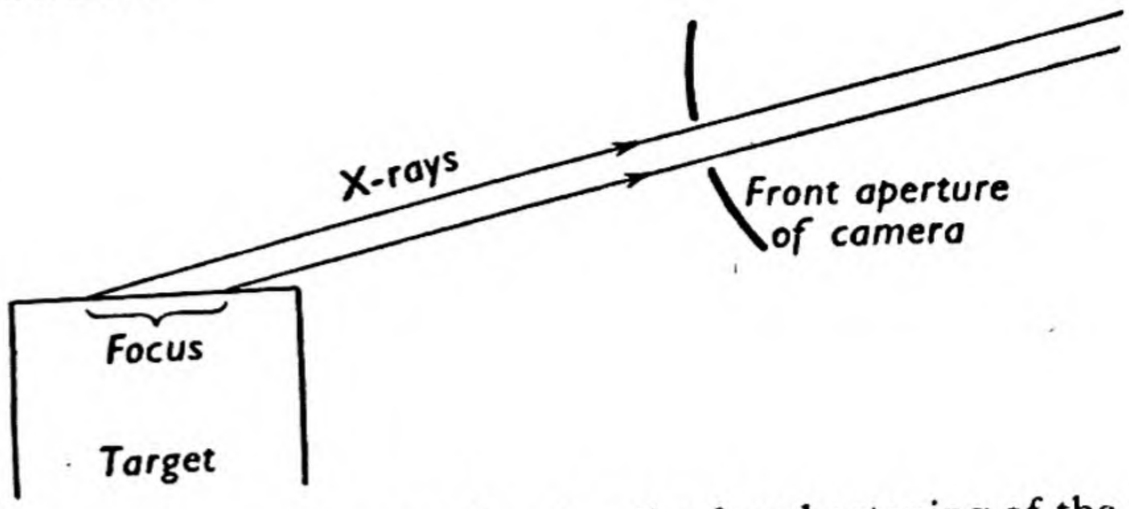

FIG. 169.2. Diagram showing the foreshortening of the focus of an X-ray tube

rays entering it are those that come off the target at a small angle; the focus will then appear foreshortened as shown in Fig. 169.2, and will itself act as a slit, no other slit being needed between the X-ray tube and the camera. If this arrangement is used, it is possible that the X-ray beam will not traverse the camera accurately along the axis of the collimator. The inclination of the beam to this axis may have both a horizontal and vertical component. If the axis of the collimator is horizontal, the horizontal component will not matter greatly, since its effect will be merely to shift the whole pattern by a constant amount; but

FIG. 169.3. The shapes of powder lines when the X-ray beam does not pass along the axis of the collimator

the vertical component will lead to an asymmetric recording of the lines as shown in Fig. 169.3. This fault can be avoided by adjusting the height of the camera with respect to the X-ray tube so that the beam emerges accurately along the axis of the collimator as shown in Fig. 169.4.

These methods can be used only if the focus of the X-ray tube does not vary in position. This will be so in general in a hot-cathode tube, but may not be so in a gas tube. If a gas tube is to be used, therefore, it is necessary to have a fine limiting slit on the camera near the window of the X-ray tube. This will necessitate an increase in exposure, but will give sharper lines.

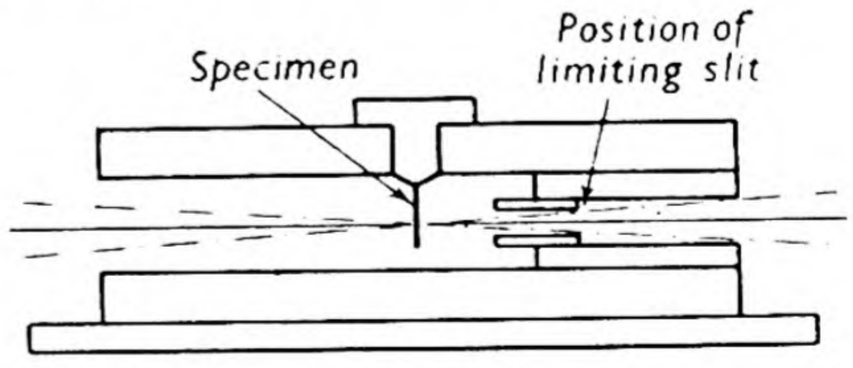

FIG. 169.4. Correct (———) and incorrect (—·—·—) paths for the X-ray beam in a powder camera

2. Preparation of Powder Specimens

The specimens should have the form of a long narrow cylinder of diameter about 0·3–0·5 mm. Many ways of making such specimens, to suit particular requirements, have been described. For ordinary work the powder may be coated on a gummed glass fibre (Buerger, 1936), made into a paste and extruded (Lukesh, 1940), or mixed with Canada balsam and coated on a hair kept taut with a lead weight. Canada balsam, however, gives a strong halo that may obscure some of the low-angle lines. Gum tragacanth does not give such a halo and may be used in the following manner. Mix the powder, which must be fine, with a fifth to a tenth of its volume of powdered gum and make this into a paste with a small amount of water or saliva. After a short time the paste will set sufficiently to be rolled between the fingers into the form of a thin rod which can be made more perfect by rolling between glass plates. It can then be mounted in the camera. It will soon set quite hard, and can be mounted either horizontally or vertically. This method cannot, of course, be used for a substance that is soluble in water.

For special purposes other forms of specimens may be used. If the substance is deliquescent or efflorescent, or otherwise unstable under ordinary atmospheric conditions, it must be enclosed in a tube transparent to X-rays. Such a tube may be made of borosilicate glass (Schleede and Wellmann, 1932; Taylor, 1945) or of collodion (Lonsdale and Smith, 1941). If the specimen is to be raised to high temperatures the enclosing tube may sometimes be made of silica. Silica glass softens at about 1100° C. but even at temperatures below this it may react with the specimen.

3. Measurement of Bragg Angles

3.1 Geometry of cameras. In all forms of powder camera the usual way of deriving θ is to measure the distance S between two opposite parts of the diffraction cone that is recorded on the film. This overcomes any errors due to an uncertainty in the position on the film corresponding to zero θ.

If the photograph is taken on a flat film, the distances S are the diameters of the rings; θ is derived by the relation

$$\tan 2\theta = S/2D, \qquad (1)$$

where D is the distance of the specimen from the film (Fig. 170.1).

Films taken in cylindrical cameras are also usually measured flat and θ is then proportional to S. It can be seen from Fig. 170.2 that

$$\theta = S/4R, \qquad (2)$$

where R is the radius of the camera.

Although this is accurate enough for many purdoses, for precision work the finite thickness of the film and its shrinkage during processing must be taken into account. This is most easily achieved by constructing the camera so that it casts on the film

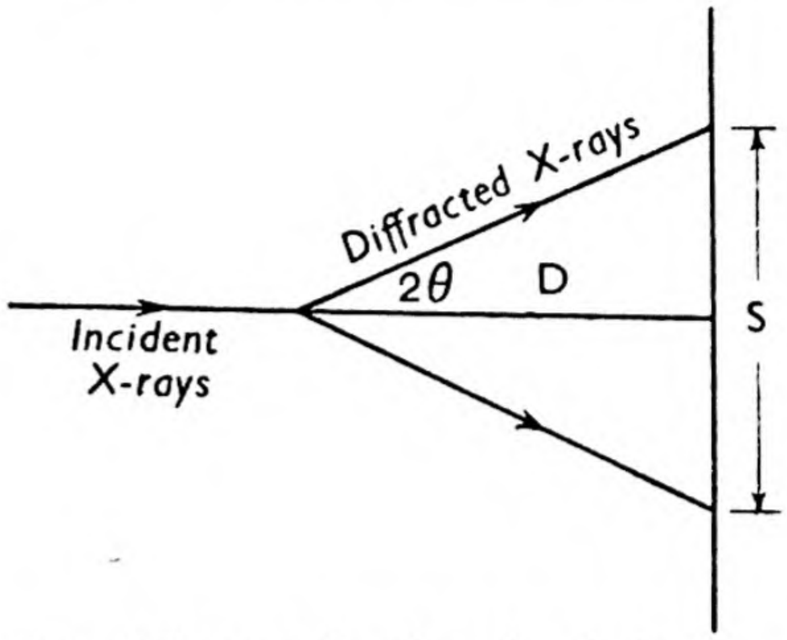

FIG. 170.1. Diagram showing the derivation of θ from D, the distance of the specimen from the film, and S, the diameter of the powder ring

two shadows at a known angular separation; the angular separation of any two lines can then be found by the method of proportional parts. The pieces of metal that cast these shadows should have sharp

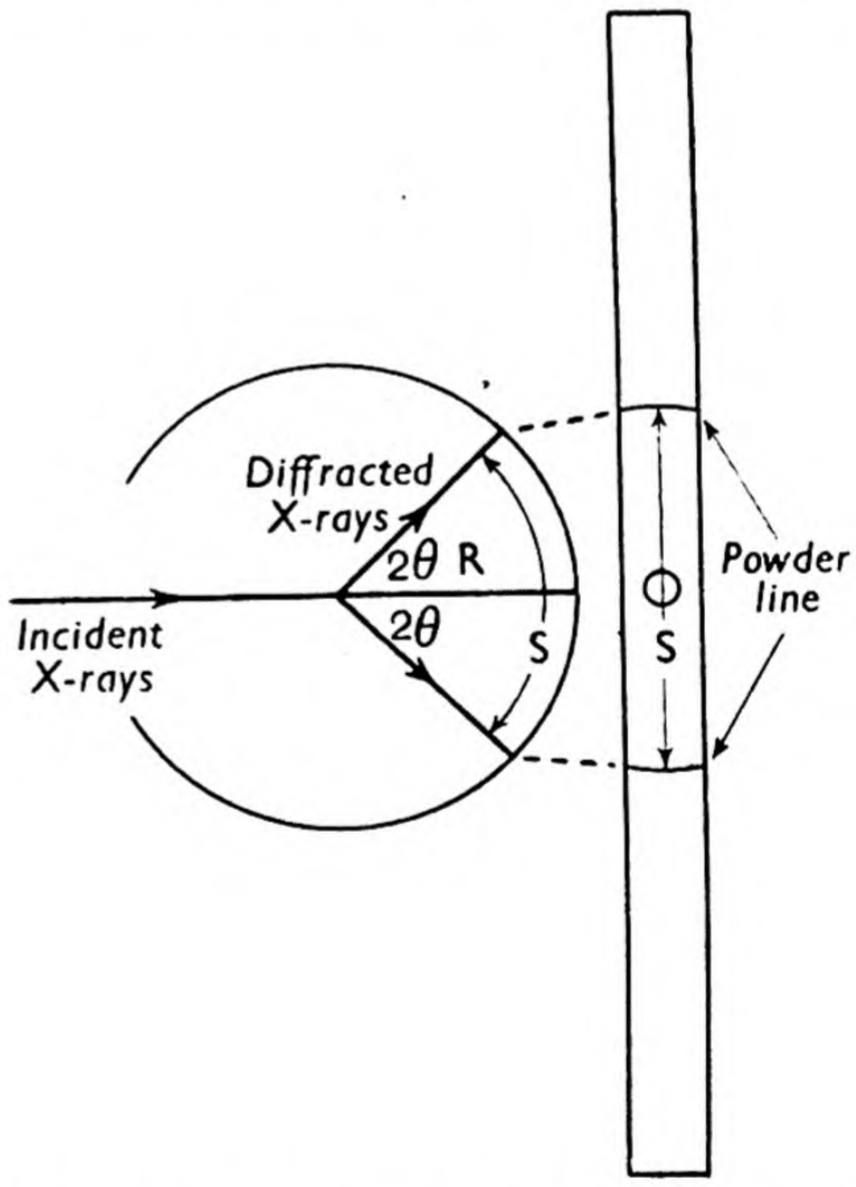

FIG. 170.2. Diagram showing the derivation of θ from R, the radius of the camera, and S, the distance apart of the two powder lines

straight edges, which should be parallel to the axis of the camera and in close contact with the film; they are known as *knife edges*.

Bradley and Jay (1932*b*) first suggested measuring angles in this way. In their camera the X-ray beam enters between the ends of the film and leaves through

a hole in the centre, as shown in Fig. 172 (*a*). When the film is laid flat it looks like that shown. If ϕ_k is one quarter of the angle subtended by the knife edges at the centre of the camera (that is, the value of the Bragg angle for a line which would fall at these positions), θ for any pair of corresponding lines is connected with the distance S between them by the relation

$$\theta = \phi_k \, . \, S/S_k, \qquad (3)$$

where S_k is the distance between the shadows of the knife edges. The assumption is made that the film changes uniformly after processing; this has been found to be true within the accuracy of measurement for one specimen of film measured at intervals over a period of months (Lipson, 1942).

Several precautions are necessary in determining the line positions. If a travelling microscope is used one should first verify, by the absence of parallax, that the images of the cross-wire and the films are in the same plane. The magnification should be not more than four diameters. The film should be adjusted so that its length is parallel to the direction of travel of the microscope. The positions of the lines should be read by placing the cross-wire on the middle of the arc as shown in Fig. 171.1; two or three

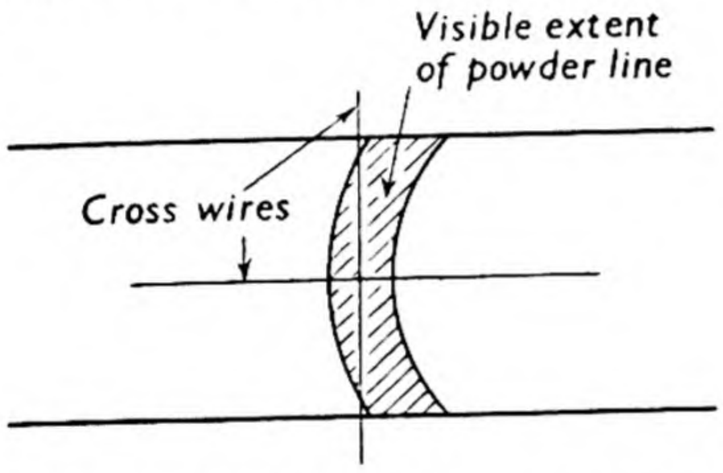

FIG. 171.1. Orientation of cross wires for measurement of a powder photograph containing only strong lines

readings should be taken and the line approached from both sides. If the film contains some rather weak lines, it may be better to have diagonal cross-wires (Fig. 171.2). The visibility of weak lines is also improved by putting opaque screens over that part of the film which has not received any radiation, so that only the exposed part is visible (Fig. 171.2). The eye has then to accommodate itself to only a small range of brightness.

An instrument specially designed for measuring powder photographs has been described by Sears and Turner (1941).

The Bradley-Jay method of mounting films in the camera is useful for obtaining measurements of the low-order spectra. If, however, one wishes to measure the high orders accurately, the error in the angle of the camera can be appreciable. From direct measurement of the diameter of the camera and the distance apart of the knife edges, ϕ_k can be obtained with an accuracy of about $\pm 0{\cdot}01°$. For high values of θ the errors in θ will be almost equal to the error in ϕ_k and, though this is small, it would be better if it

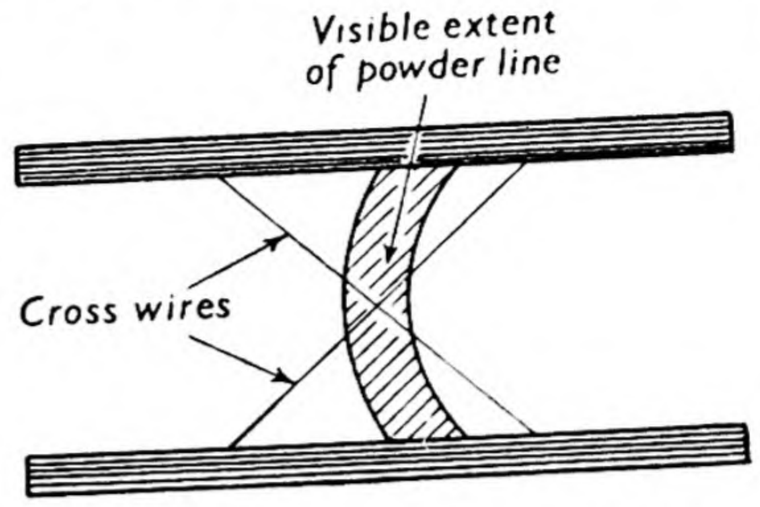

FIG. 171.2. Orientation of cross wires for measurement of a powder photograph containing some weak lines

were eliminated completely. Van Arkel (1926) had previously suggested that this could be achieved by mounting the film in the camera with the X-rays entering through a hole in the film and leaving between the ends (Fig. 172.1 *b*). If shadows of knife edges are cast at these ends, the value of θ for any pair of lines is connected with the distance S between them by the relation

$$\theta = 90° - \psi_k \, S/S_k. \qquad (4)$$

Thus an error in ψ_k will have only a slight effect on θ if S is small, that is, if θ is near 90°. It will be noted that, in equation (4), ψ_k is the complement of the Bragg angle of a reflection that would fall at the positions of the knife-edge shadows.

A third method of mounting the film has been suggested by Ieviņš and Straumanis (1936); they call it the *asymmetric method* and it is illustrated in Fig. 172 (*c*). It involves no calibration of the camera, because on the same film the positions corresponding to $\theta = 0°$ and $\theta = 90°$ can be located. This method might appear to be superior to the other two methods; but in practice the van Arkel mounting gives all the accuracy desired (Cohen, 1936).

These methods can be applied to cameras of any size, but in practice it is inconvenient to have to handle films longer than about 25 cm. For cameras of 19 cm. diameter two pieces of film are used, as shown in Fig. 172.2, and four knife-edge shadows are cast on them. If accurate lattice parameters are required, however, it is better to use the van Arkel mounting of the film, even if it involves recording only the high orders (Lipson and Rogers, 1944).

3.2 Correction for absorption. In the derivation of Bragg angles from powder photographs, systematic errors will result because, owing to absorption in the specimen, the distribution of intensity across a

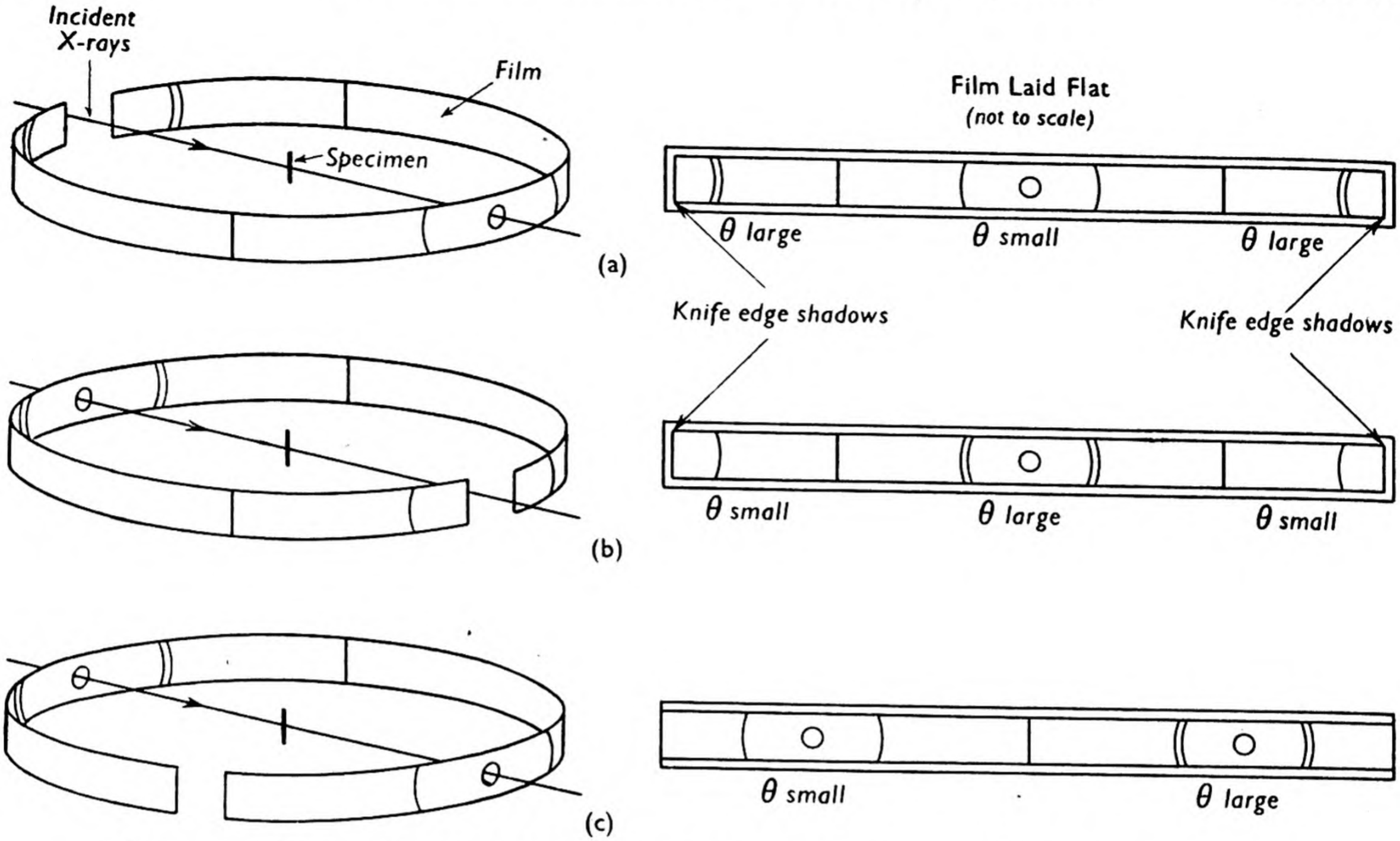

FIG. 172.1. Diagram showing three methods of mounting films in 9-cm. diameter powder cameras:
(*a*) Bradley-Jay (*b*) van Arkel (*c*) Ievinš-Straumanis (asymmetric)

powder line may be irregular and the maximum may not be in the centre. Such errors will decrease as θ increases and as the linear absorption coefficient decreases. This may be seen by considering a low-angle reflection from a specimen of medium absorption.

Suppose that the specimen has a circular section and is irradiated by a parallel beam of X-rays, as shown in Fig. 173. A reflected ray such as B_2C_2, coming from the centre of the specimen, will be greatly weakened by absorption, whereas a ray such as B_3C_3 is weakened less and a ray such as B_1C_1 less

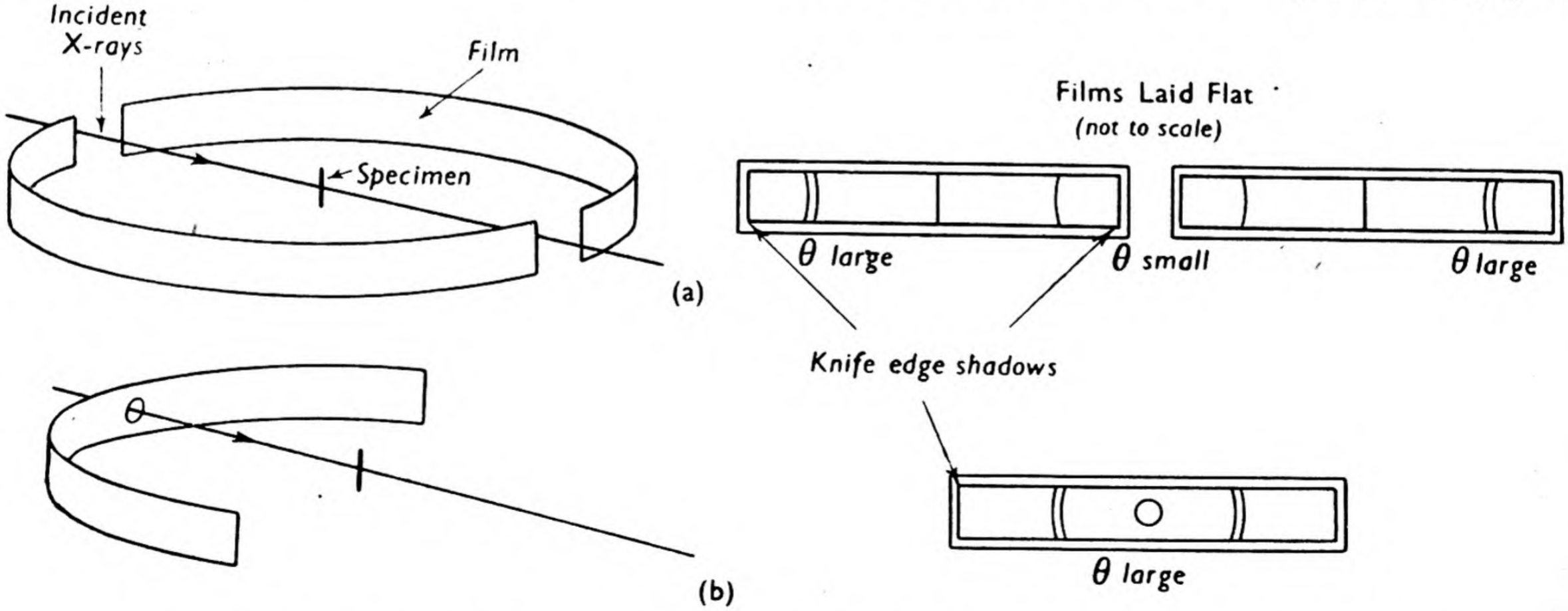

FIG. 172.2. Diagram showing two methods of mounting films in 19-cm. diameter powder cameras:
(*a*) For the complete pattern (*b*) For the high orders only

still. On the other hand, there will be more reflected rays from the middle of the specimen because it is thicker there. If the absorption is low, this latter effect will be the more important, and the recorded line, which covers the range $C_1C_2C_3$, will have a

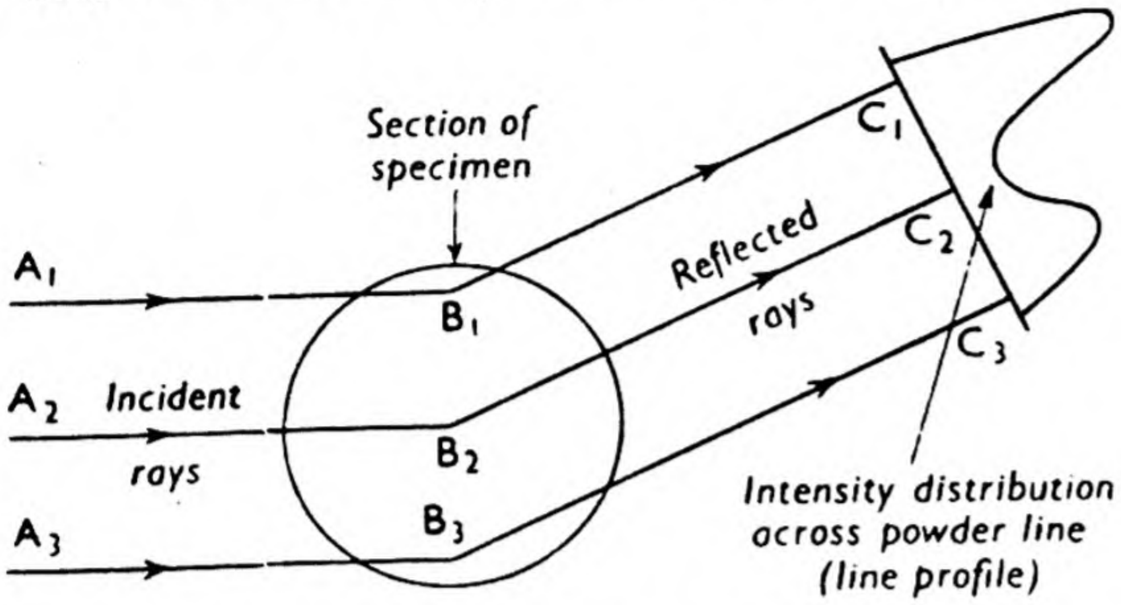

FIG. 173. Diagram showing why powder lines may appear doubled due to absorption in the specimen

maximum near the centre. If, however, the absorption effect is predominant, the total reflection from the middle of the specimen will be weaker than that from the edges. The distribution of intensity across the powder line will have the general form shown in Fig. 173; that is, to the eye the line will appear doubled.

Taylor and Sinclair (1945*a*) have considered the problem in detail and have drawn line profiles for different values of μr, where μ is the linear absorption coefficient and r is the radius of the specimen. They have shown that doubling of the lines due to reflection from the edges of the specimen, as described above, occurs only for low values of θ, and that, as θ increases, the weaker component becomes smaller and finally disappears. Only the stronger component will then be measured, and since this is at the higher angle, spacings derived from it will be low. If the value of μr for the specimens is known, the error can be calculated and so allowed for; but a more satisfactory way of making the corrections is to mix the specimen with a substance that gives reflections at known Bragg angles and to obtain the unknown ones by interpolation. For example, a curve of spacing d against S may be plotted for the lines of known spacing; and then, from the measured values of S for the unknown spacings, the values of d can be read from the curve.

4. Powder Cameras

4.1 Diameter of camera. Cameras of many different diameters are described in the literature. The smaller cameras are satisfactory for simple patterns and also for the general outlines of more complicated ones. Larger cameras give better resolution, which is useful for the measurement of cell dimensions and the detection of faint lines. The reason for this latter property is that the intensity of a line does not decrease with distance so rapidly as that of the background. The background intensity is mainly due to the white radiation scattered from the specimen, and, like all radiation from a small source, the intensity in any one direction is inversely proportional to the square of the distance. The characteristic lines, however, are confined fairly accurately to particular values of θ, and since the length of any one complete powder line (Fig. 168.1) is proportional to the distance of that line from the specimen, the intensity at any one point of the line must be inversely proportional to that distance. This fall-off in intensity is, of course, less than that of the background, and therefore the lines will be relatively stronger with respect to the background if the radius of the camera is increased.

This reasoning will not apply if the reflections are not confined accurately to particular values of θ. This will be so if the crystals are very small (**16,** 3.1) or are deformed by internal strains (**16,** 4.4); in these cases there will be no increase in contrast of the powder lines with respect to the background when the camera radius is increased.

The air in a camera produces two important effects. First, it scatters the radiation and so produces a general fogging of the film, particularly near the position of zero θ; and secondly, it absorbs the incident and the diffracted radiation. For work involving the observation of faint lines or the measurement of large spacings, it is advisable either to evacuate the camera or to fill it with hydrogen, which scatters X-rays much less than air. The absorption effect is not usually important for cameras of 9 cm. diameter or less, but for larger cameras it may be considerable, especially for the longer wavelengths. For example, in a path of 35 cm. of air, about 70 per cent of chromium $K\alpha$ radiation is absorbed.

Exposures are, of course, longer with larger cameras, but this does not matter if it is essential to obtain greater separation of the powder lines. A camera of 35 cm. diameter has been used successfully to obtain the data necessary for working out a crystal structure (Lipson and Petch, 1940); the time taken for the exposure was small compared with the total time involved in the work.

4.2 High- and low-temperature cameras. Powder cameras have also been adapted to the investigation of structures above and below room temperature (Jay, 1933; Hume-Rothery and Reynolds, 1938; Wilson, 1941; Owen, 1943; Lonsdale and Smith, 1941). No completely satisfactory design of high-temperature camera exists, because it is not always possible in

practice to satisfy simultaneously all the requirements for a particular specimen. For example, if the specimen is oxidizable at high temperatures it is necessary either to evacuate the camera, to fill it with an inert gas, or to place the specimen in a sealed enclosure. If the first method is chosen, it may be difficult to obtain a uniform temperature around the specimen, as convection is the main factor in equalizing temperatures. Moreover, if the specimen is an alloy there may be differential evaporation of the components, resulting in a change of composition. If the second method—the use of an inert gas—is chosen, the temperature within the furnace is more likely to be uniform, but differential evaporation can still take place, although it should be less then in an evacuated camera. If the third method—the sealed enclosure—is chosen, differential evaporation can be completely prevented by maintaining the enclosure at a uniform temperature; distillation cannot then take place from the hotter parts to the colder. The material of the enclosure must be amorphous and transparent to X-rays. Fused silica satisfies these conditions very well, but it reacts with many materials well below its softening point and so cannot always be used. Preliminary experiments are therefore necessary in order to find which conditions are best suited to any particular investigation.

4.3 Focusing cameras. While the ordinary type of powder camera previously described is of general utility, it sometimes involves rather long exposures. In the focusing camera (Westgren, 1931) exposures are much shorter, but this is offset by many disadvantages.

The principle of the focusing camera is illustrated in Fig. 174.1. The specimen is in the form of a thin layer of powder, *AB*, three or four centimetres long, lying on the circumference of a circle; the X-ray film, *CD*, also lies on this circle. The X-rays enter through a fine slit, *E*, and a divergent beam is used so that the whole specimen is irradiated. From the figure, it can easily be seen that rays suffering the same deviation must be 'focused' on the same point. In other words, all reflected rays with the same Bragg angle will be recorded as a single line on the film *CD*.

Since the specimen is large, exposures will be correspondingly small. The fact that the specimen has to be stationary is not a great disadvantage because, compared with the ordinary powder specimen, so many more crystals are irradiated that a larger number should be correctly oriented to produce any particular reflection; smoother lines should therefore result. The advantage of shortness of exposure time with focusing cameras is offset by the fact that with such cameras sharp lines are obtained only for reflections with high angles. Westgren has made great use of focusing cameras even with this limitation, but generally the low orders are more important than the high orders. It is true that, by the use of separate cameras for high, medium and low angles, practically the whole range of θ between 0° and 90° can be covered, but the low orders are always rather broad because, as shown in Fig. 174.2, the rays producing them strike the film very obliquely.

The symmetrical focusing camera (Gayler and Preston, 1929) is useful for accurate measurement of cell dimensions; the principle is illustrated in Fig. 175.1. It has been claimed by Cohen (1935), on theoretical grounds, that it is inherently the most accurate instrument for this purpose, but this is not borne out by results. In effect, all cameras are focusing cameras for the high orders; the ordinary focusing camera gives sharp lines

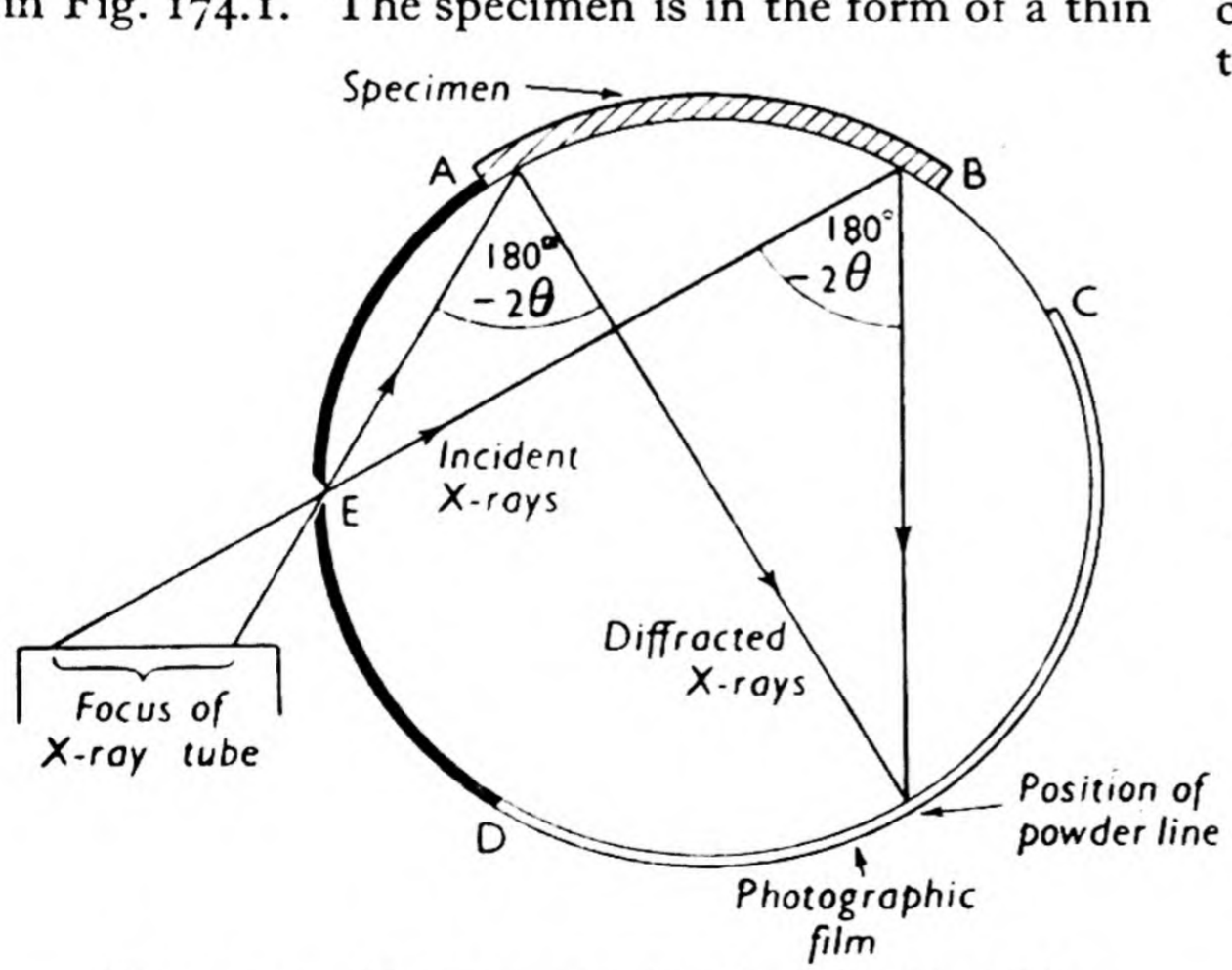

FIG. 174.1. Diagram showing the principle of the focusing camera

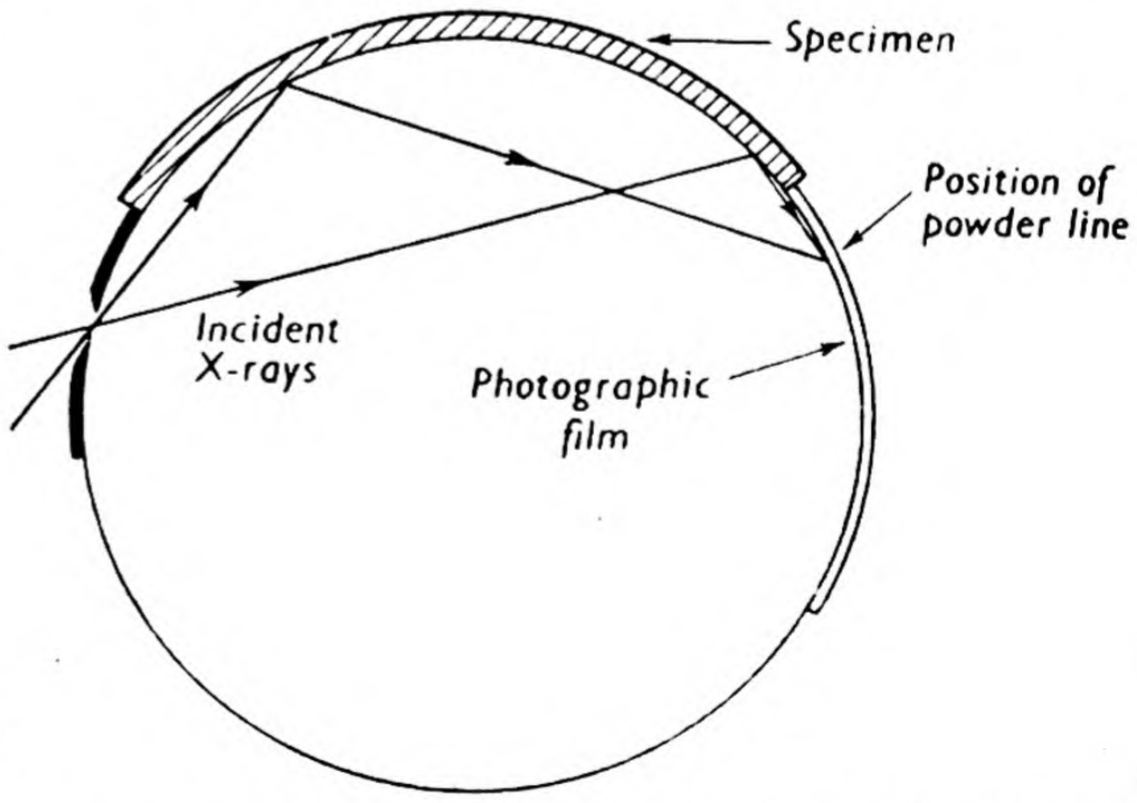

FIG. 174.2. Focusing camera for low-angle powder lines, showing the oblique incidence of the X-rays upon the photographic film

because, like a good camera lens, it has been correctly designed, whereas the ordinary powder camera gives sharp lines because the aperture is stopped down. Consequently the latter requires longer exposures, but it has the advantage over the focusing camera that *all* the lines on the film are reasonably sharp. The focusing camera, however, has

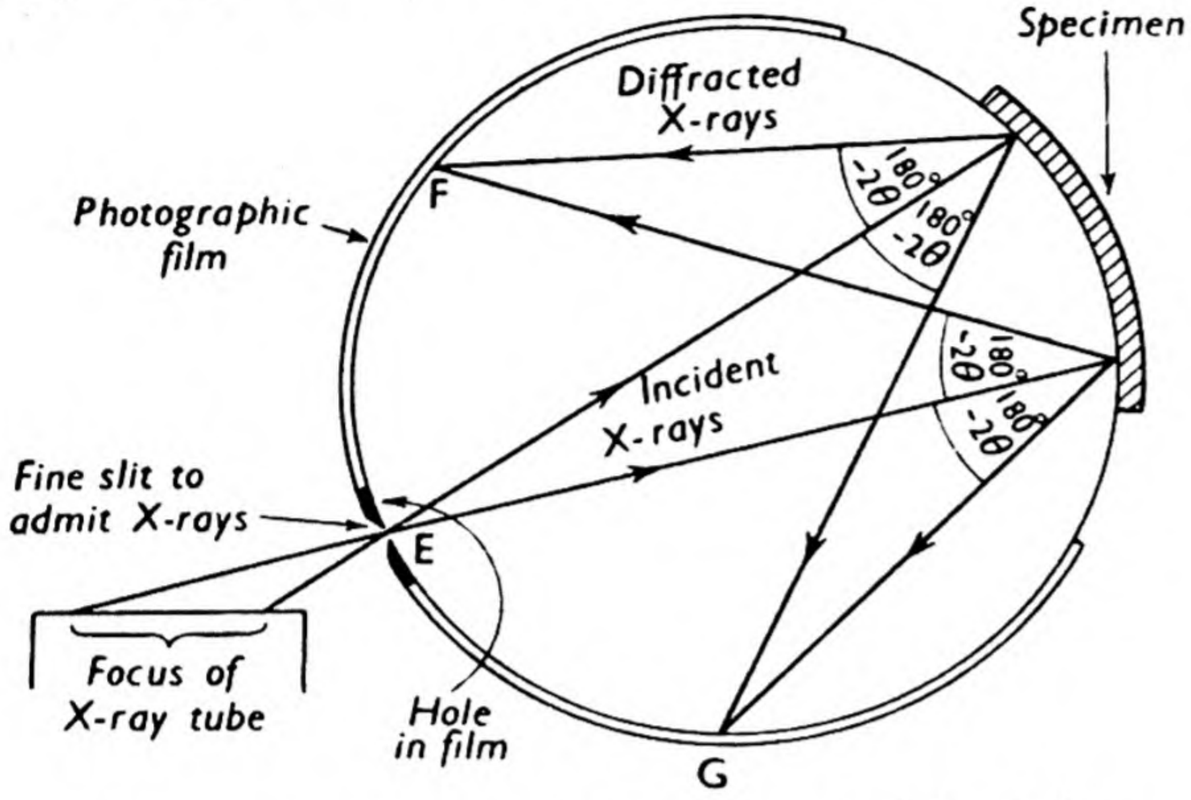

FIG. 175.1. Diagram showing the principle of the symmetrical focusing camera. F and G are the two positions of the powder lines with Bragg angles θ and are at equal distances from the entrance slit E

the advantage that the linear separation it gives for the lines is twice that given by an ordinary camera of the same diameter; but, if the latter camera is made larger to allow for this, the results it gives seem to be quite as accurate as those obtained with the focusing camera.

4.4 Cameras for block specimens. The powder method can be adapted to any polycrystalline specimen, even if it is not in the form of powder. Metals and alloys are obvious examples. X-ray photographs of materials in the condition in which they are received are often required, and, if the crystals are small, quite good 'powder' lines may be given.

The commonest type of photograph taken from a block specimen is of the *back reflection* type; the incident X-rays pass through a hole in the film, impinge on a reasonably flat part of the specimen, and are reflected back on to a film (Fig. 175.2). Some of the high-angle powder lines will be recorded, and, from the nature of these, valuable information can be obtained about the state of the specimen.

If the crystal size is large, the photograph will consist mainly of one or more Laue photographs, and so may not give the information desired. In order to give characteristic reflections, the specimen must be oscillated through a small angle (say 5°), and if it is also translated (Wainwright, 1941; Thewlis and Pollock, 1950) or rotated (Lipson, Shoenberg and Stupart, 1941) in the plane of the surface irradiated, more crystals are brought into the beam and so a more truly representative photograph is obtained.

Back-reflection methods will, of course, give only the high-angle reflections; to record the lower orders the X-rays must strike the surface at a small

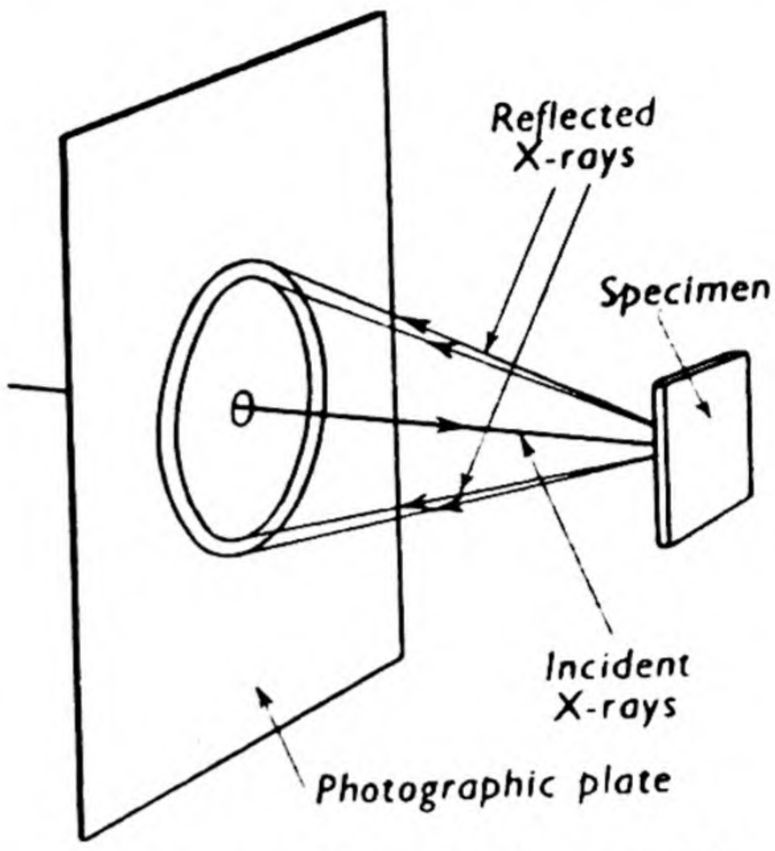

FIG. 175.2. Relative positions of photographic plate and specimen in the back-reflection method

glancing angle. Good photographs can be obtained only from specimens with reasonably flat surfaces, since, if the surface is rough, only discrete regions can contribute to the reflected beams. Even if the surface is smooth, the medium-angle reflections will be broad,

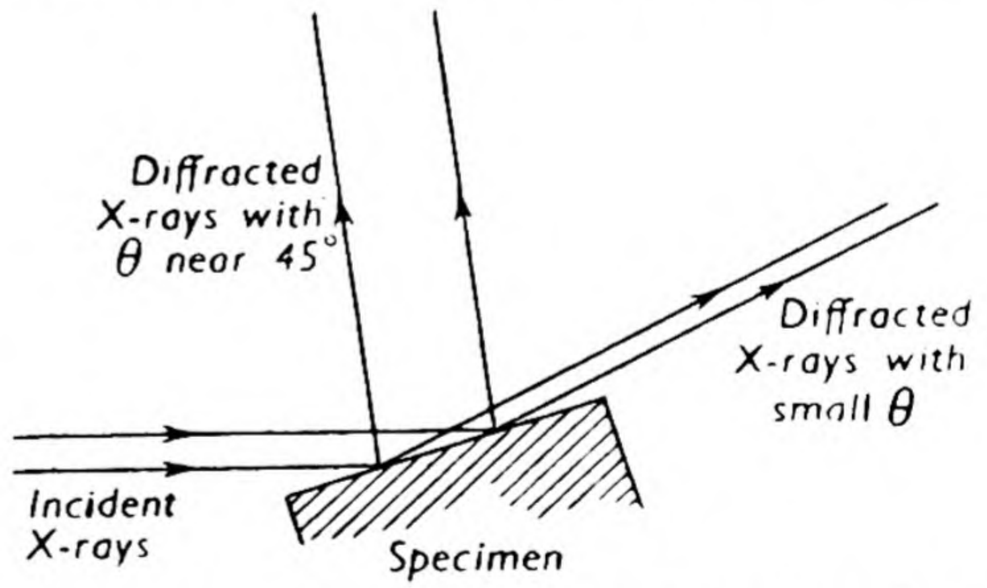

FIG. 175.3. Diagram showing why some reflections are broadened when the X-ray beam is incident at a low angle upon a large specimen

as shown in Fig. 175.3. To remedy this, the beam should be reduced in area; a narrow slit, therefore, and not a circular hole, should be used to limit the X-ray beam falling on the specimen (Jay, 1943). As was shown on p. 169, this should still result in reasonably sharp lines.

Sometimes it is necessary to correlate the structure as revealed by X-rays with other physical properties

such as micro-structure or hardness. In these cases small rods of square cross-section can be used, as they give quite good X-ray photographs if they are fine grained; the flat surfaces can be used for the observation of these properties (Lipson and Parker, 1944).

4.5 Factors affecting choice of camera. There is no one design of camera which is suitable for all types of work. For the identification of crystalline material, an ordinary camera with a diameter of about 9 cm. is suitable; either the Bradley-Jay or the van Arkel mounting can be used. If identification is to be the main work, the former mounting is preferable because it is more convenient for the rapid calculation of the Bragg angles of the low-θ lines which are most important in this connection (**17,** 2.1). The Bragg angles of these lines can be read directly by means of a scale, if values uncorrected for film shrinkage are sufficiently accurate. Some workers prefer to use a scale graduated in lattice spacings, d, but this has the disadvantage that estimated interpolation has to be made between the units on a rapidly varying scale.

The van Arkel mounting is less convenient for the rapid calculation of low values of θ from a number of films. Also, owing to the large separation of the corresponding low-θ lines, the appreciable film shrinkage renders the values obtained from a scale much less accurate than with the Bradley-Jay mounting. It should be noted that photographs taken with the van Arkel mounting can be compared directly with those taken with the Bradley-Jay mounting, provided that the same radiation and the same diameter of camera are used. For the purpose of direct comparison of photographs taken in different laboratories, the committee of the X-ray Analysis Group of the Institute of Physics (1945) has recommended that a uniform diameter of 9 cm. should be generally adopted.

If the camera is to be used for the accurate measurement of cell dimensions, the van Arkel mounting is the better of the two (**11,** 3.1). For very accurate measurements, however, it is probable that a diameter of 9 cm. is too small. It is better to use an ordinary camera of 19 cm. diameter (which is becoming standard in Great Britain), or to use a symmetrical focusing camera of about half this diameter which will give equal accuracy (**11,** 4.3). The ordinary camera has the advantage that it can also be used for general purposes where greater separation of the lines is desirable (Rooksby, 1943).

CHAPTER 12

INTERPRETATION OF POWDER PHOTOGRAPHS

1. Introduction

FROM measurement of the position of a line on a powder photograph, only one parameter can be directly derived, namely, the Bragg angle, θ, of the line. When the unit cell of the substance is known, however, indexing the lines is a straightforward matter, although the calculations are rather lengthy for the systems of lower symmetry. In this chapter special attention is paid to ways of systematising these calculations in order to reduce the amount of work involved. A semi-graphical method using the reciprocal lattice is often useful in calculating spacings in the systems of lower symmetry. When the unit cell is unknown, the problem of indexing is considerably more difficult, and trial-and-error procedures have to be used. With a simple cubic pattern, such as is given by sodium chloride for example, it is easy to index all the lines and to derive the length of the cell-side. With increase of the size of the unit cell the complexity of the pattern increases, but cubic patterns are always fairly easy to index. Patterns from substances belonging to the uniaxial systems (tetragonal, trigonal and hexagonal) are more difficult but can usually be indexed, although the trouble involved increases with increase of cell size. An orthorhombic pattern may be very troublesome to index, especially if one or more of the sides of the unit cell is large. In the monoclinic, and still more in the triclinic system, the number of variables is such that indexing is generally impossible when nothing is known about the unit cell, except perhaps when this is very small. Wholly graphical methods are often helpful in indexing, both when the cell unit is known and when it is unknown, and these are considered in a separate section.

2. Interpretation when the Unit Cell is known

When the unit cell is known, three stages in the interpretation are necessary. These stages are :

(*a*) derivation of Bragg angles ;

(*b*) calculation of Bragg angles for all possible combinations of indices *hkl* ;

(*c*) The comparison of the two sets of results.

The problems which are considered here are those that arise in the second stage. Instead, however, of calculating values of θ directly, it is better to calculate $\sin^2\theta$, since the expression for $\sin^2\theta_{hkl}$ is usually a fairly simple function of h, k and l. In order to simplify the third stage, a table of values of $\sin^2\theta$ as a function of θ is given in Table 6.

2.1 The cubic system. For the cubic system the expression for $\sin^2\theta$ can be obtained by combining Bragg's equation (**3,** 6),

$$\lambda = 2d \sin\theta$$

with the expression for d given in **1,** 3.8,

$$d = a/\sqrt{(h^2+k^2+l^2)}.$$

This gives

$$\sin^2\theta = \frac{\lambda^2}{4a^2}(h^2+k^2+l^2) \qquad (1)$$

The quantity $h^2+k^2+l^2$ is an integer, so that all that is necessary is to calculate the value of $\lambda^2/4a^2$ and to multiply it by the possible values of $h^2+k^2+l^2$, which are given in Table 5. It is not necessary to include values of $(\lambda^2/4a^2)(h^2+k^2+l^2)$ greater than unity. Values of $\sin^2\theta$ for the observed angles can be obtained by means of Table 6, and the two sets can then be compared to see which lines are actually present.

2.2 Tetragonal, hexagonal and trigonal systems. The formula for the tetragonal system is

$$\sin^2\theta_{hkl} = \frac{\lambda^2}{4a^2}(h^2+k^2) + \frac{\lambda^2}{4c^2}l^2. \qquad (2)$$

Let $\lambda^2/4a^2 = A$ and $\lambda^2/4c^2 = C$.

Then we require values of A multiplied by all possible values of h^2+k^2 (Table 5), and C multiplied by l^2. For example, if $A = 0{\cdot}10$ and $C = 0{\cdot}07$, we can draw up a table as follows :

h, k	1,0	1,1	2,0	2,1	2,2	3,0
$A(h^2+k^2)$	0·10	0·20	0·40	0·50	0·80	0·90

l	1	2	3
Cl^2	0·07	0·28	0·63

Possible values of $\sin^2\theta$ are then obtained by adding the appropriate terms in the above lists, and these are best set out in tabular form :

POSSIBLE VALUES OF $\sin^2\theta$

h,k	0,0	1,0	1,1	2,0	2,1	2,2	3,0
l = 0	0·00	0·10	0·20	0·40	0·50	0·80	0·90
l = 1	0·07	0·17	0·27	0·47	0·57	0·87	0·97
l = 2	0·28	0·38	0·48	0·68	0·78		
l = 3	0·63	0·73	0·83				

For example, the value of $\sin^2\theta_{112}$ is 0·48.

The expression corresponding to (2) for crystals based on a hexagonal lattice is :

$$\sin^2\theta_{hkl}=\frac{\lambda^2}{3a^2}(h^2+hk+k^2)+\frac{\lambda^2}{4c^2}l^2. \qquad (3)$$

This expression can also be used for those crystals of the trigonal system which are based on a rhombohedral lattice, if the indices are first transformed to those corresponding to an appropriate hexagonal unit cell. Care must be exercised in transforming indices and axes ; the procedure is discussed in **10,** 1.2. The corresponding expression for a rhombohedral lattice can, of course, be used for such crystals, but it is less convenient in form :

$$\sin^2\theta_{pqr}=\frac{\lambda^2}{4}\left[\frac{\cos^2\alpha/2}{a^2\sin\alpha/2\,.\,\sin 3\alpha/2}\right]$$
$$\times\{(p^2+q^2+r^2)-[1-\tan^2\alpha/2](pq+qr+rp)\}, \qquad (3)$$

where a is the side and α the angle between the axes of the rhombohedral unit cell, and pqr are the indices of planes referred to this unit cell. This expression can be rewritten as

$$\frac{\lambda^2}{4}\left\{\frac{(p^2+q^2+r^2)\sin^2\alpha+2(pq+qr+rp)(\cos^2\alpha-\cos\alpha)}{a^2(1-3\cos^2\alpha+2\cos^3\alpha)}\right\}.$$

2.3 Orthorhombic system. The formula for the orthorhombic system is

$$\sin^2\theta_{hkl}=\frac{\lambda^2}{4a^2}h^2+\frac{\lambda^2}{4b^2}k^2+\frac{\lambda^2}{4c^2}l^2, \qquad (4)$$

which we may write as

$$\sin^2\theta_{hkl}=Ah^2+Bk^2+Cl^2. \qquad (5)$$

A, B and C can be calculated and lists made of the quantities Ah^2, Bk^2 and Cl^2 ; sums of these quantities will then give possible values of $\sin^2\theta$.

For example, $NiAl_3$ (Bradley and Taylor, 1937) is orthorhombic with $a=6{\cdot}61$, $b=7{\cdot}36$ and $c=4{\cdot}81$ A. For cobalt $K\alpha$ radiation, $\lambda=1{\cdot}790$ A. Therefore $A=0{\cdot}01833$, $B=0{\cdot}01478$, $C=0{\cdot}0346$. Values of Ah^2, Bk^2 and Cl^2 are :

h, k or l	Ah^2	Bk^2	Cl^2
0	0·0000	0·0000	0·0000
1	0·0183	0·0148	0·0346
2	0·0733	0·0591	0·1386
3	0·1650	0·1330	0·3118
4	0·2933	0·2365	0·5544
5	0·4582	0·3695	0·8662
6	0·6599	0·5321	—
7	0·8982	0·7242	—
8	—	0·9459	—

Values of $\sin^2\theta_{hkl}$ can now be obtained by adding the quantities in the appropriate columns. For example,

$\sin^2\theta_{200}=0{\cdot}0733$

$\sin^2\theta_{210}=0{\cdot}0733+0{\cdot}0148=0{\cdot}0881$

$\sin^2\theta_{213}=0{\cdot}0733+0{\cdot}0148+0{\cdot}3118=0{\cdot}3999$

$\sin^2\theta_{543}=0{\cdot}4582+0{\cdot}2365+0{\cdot}3118=1{\cdot}0065.$

The last reflection obviously will not occur. Again the results should be set out in tabular form, but the tables will be more extensive than that in the previous section since three different indices are involved. It is necessary to calculate *all* the values of $\sin^2\theta$, since a given line may be composed of more than one set of reflections. For example, a line with $\sin^2\theta=0{\cdot}1325$ might be 030 ; actually 030 is absent and the reflection is 220 ($\sin^2\theta=0{\cdot}1324$). One must therefore not be satisfied with finding possible indices for all the lines ; one must compare all the calculated values with the observed ones.

2.4 Monoclinic and triclinic systems. For crystals in the monoclinic or triclinic systems, it is more convenient to derive the values of $\sin^2\theta_{hkl}$ directly from the reciprocal lattice, according to the formula

$$\sin^2\theta_{hkl}=\tfrac{1}{4}(\zeta^2_{hkl}+\xi^2_{hkl}).$$

The values of ξ_{hkl} are usually obtained with sufficient accuracy from a graphical plot of the reciprocal lattice, although if greater accuracy is required they can be obtained by calculation (**3**, 2.3).

3. Interpretation when the Unit Cell is unknown

When the unit cell is unknown, the assignment of indices to the lines on a powder photograph cannot be achieved by any direct method. Attempts have been made to produce direct methods, but they are of doubtful value. The most reasonable procedure is

to try to fit the powder pattern to the various crystal systems, starting with the simplest, the cubic system. If the substance does not seem to be cubic, the other systems should be tried in order of increasing complexity (Hesse, 1948). In the following sections the characteristics of cubic, tetragonal, hexagonal, trigonal, and orthorhombic powder photographs are described; systems of lower symmetry do not lend themselves to general treatment and will not be discussed here.

3.1 The cubic system. The characteristic of the cubic system is that the values of $\sin^2\theta$ have a common factor. For example, the first seven lines on a powder photograph of an oxide of cobalt and iron of the spinel type have the following values of $\sin^2\theta$:

0·0343, 0·0919, 0·1258, 0·1370, 0·1839, 0·2752, 0·3097.

By means of a slide rule, it is easily found that the first two have a common factor of about 0·0115, and if we divide all the values of $\sin^2\theta$ by 0·0115, we obtain the quantities 2·98, 7·99, 10·94, 11·91, 15·99, 23·93 and 26·93. It will be seen that these closely approximate to the values 3, 8, 11, 12, 16, 24 and 27, and the oxide is therefore cubic. The photograph was taken with Co$K\alpha$ radiation ($\lambda = 1{\cdot}790$ A.) and therefore

$$a = \lambda/2\sqrt{0{\cdot}0115} = 8{\cdot}34 \text{ A.}$$

It will be noticed that the quantities $\sin^2\theta/0{\cdot}0115$ are all slightly less than integers. This means that a slightly smaller value of the common factor would have given better results. This lower value could not have been reliably deduced from the first two lines since their accuracy is low; on the other hand, the evidence from the first two lines gave the main indication that the oxide was cubic. This illustrates a general rule: *the lower orders are essential for the correct but approximate determination of the cell dimensions; the higher orders are used for accurate determination.* Therefore, in indexing a powder photograph, one must always be prepared to modify the common factor deduced from the lower orders in order to produce better agreement with the higher orders.

After a sufficient number of lines have been indexed on a powder photograph, it is a simple matter to determine the type of lattice, and this is particularly easy for cubic substances. The rules for determining the lattice type are given in **10,** 1.5, and in the following paragraph the cubic lattices are considered in detail. Also from the indexed lines on a powder photograph of a cubic substance, it is very easy to derive the length of the unit-cell side. This is done by inserting in equation (1) values of $\sin^2\theta$ and hkl for one or more of the high-θ lines.

It is shown in **10,** 1.5, that reflections are possible from a primitive (P) lattice for all values h, k and l. Consequently the factor $(h^2+k^2+l^2)$, which we shall call N, can have as possible values every integer which can be expressed as the sum of three squares. It is obvious that the numbers 7 and 15, for example, cannot be so expressed, and we can generalise these 'forbidden numbers' in the form:

$$m^2(8n-1),$$

where m and n are integers. The five numbers below 32 which satisfy this expression are given in the accompanying table. The extension of this table up to $N = 100$ is given in Table 5, and data up to $N = 1{,}000$ can be found in the International Tables (1935).

For the all-face-centred (F) and body-centred (I) lattices there are restrictions on the possible values of h, k and l. For F, h, k and l must be either all even or all odd. For I, $h+k+l$ must be even. Some reflections may, of course, be absent for other reasons (**15,** 2.7), but here we are considering only the reflections which are always absent with these types of cubic lattice.

POSSIBLE VALUES OF N FOR CUBIC LATTICES

FORBIDDEN NUMBERS	P	F	I
	1		
	2		2
	3	3	
	4	4	4
	5		
	6		6
7			
	8	8	8
	9		
	10		10
	11	11	
	12	12	12
	13		
	14		14
15			
	16	16	16
	17		
	18		18
	19	19	
	20	20	20
	21		
	22		22
23			
	24	24	24
	25		
	26		26
	27	27	
28			
	29		
	30		30
31			
	32	32	32

As shown above, the values of N that occur on the photograph of the iron-cobalt oxide are 3, 8, 11, 12, 16, 24 and 27; that is, very few of the lines corresponding to the primitive lattice P are present. But if we compare the numbers with those possible for the face-centred lattice F, we find that they all fit in and that only three, 4, 19 and 20, are missing in the range covered. These facts are sufficient to prove that the lattice is F; the few missing lines are absent for other reasons (**15,** 2.7).

The recognition of the lattice I is not so simple, as there is a risk of error unless a sufficient number of lines is indexed. Since, for the I lattice, N must be even, the first six possible lines for I have values of N equal to 2, 4, 6, 8, 10 and 12, and these of course have the same relative value of $\sin^2\theta$ as the first six lines for the P lattice, 1, 2, 3, 4, 5, 6. The next line for I is 14, and this cannot be mistaken for the next line for P which is 8 and occurs after the gap corresponding to the forbidden number 7. If therefore we had taken the lattice to be P, the apparent existence of a line corresponding to $N=7$ would have shown the mistake. This, of course, is only one example; several other lines should also be used, if possible, to differentiate between I and P. It is important to use several lines because some can be absent for structural reasons, and it might be that line 14 for I, in a particular photograph, was missing for this reason. If indexing had continued on the assumption of a P lattice, the line for which $N=30$ in the true I lattice would have been called 15, which is a forbidden number. Just before this line was reached, however, it would have been noticed that there was no line corresponding to $N=14$ on the assumption of the P lattice; this number, 14, is not a forbidden one, but the true number, 28, of the I lattice, is a forbidden one.

It is not always possible to observe a sufficient number of lines to make a definite distinction between P and I, on the basis of the Bragg angles of the lines only. For example, there are many body-centred alloys of iron that give only four or five lines with cobalt $K\alpha$ radiation which is most suitable for such alloys (**2,** 5.3). Evidence from the intensities (Chapter 15) has then to be used, but structures that give so few lines are usually so simple that the calculations are not lengthy, and give quite definite results. Photographs can also be taken with radiations with shorter wave-lengths to provide more lines for the process of indexing.

With experience it is often possible to recognize at a glance whether a powder photograph is that of a cubic substance or not. If it is cubic, some regularity in the sequence of lines can usually be seen, as on the photograph of sodium chlorate (Fig. 180), with occasional gaps corresponding to vanishingly weak reflections and to the missing numbers given above. If the substance has a primitive lattice there must be a gap at least at every eighth line, because of the missing numbers, 7, 15, 23, 31, 39 etc.; these gaps can be seen on the photograph of sodium chlorate and they form a useful check on the indexing. If the lattice is body-centred, the sequence of lines 2, 4, 6, 8 . . ., will still be regular, but since the only even numbers in the list of forbidden values of N below 100 are 28, 60, and 92, the number of lines between the gaps can be greater than 8. The number of lines with N even between 28 and 60, and between 60 and 92, is fifteen in each case.

Interpretation based on these principles should not be attempted without experience, and conclusions should always be checked by measurement and calculation. In particular, the recognition of a face-centred cubic structure is not always easy. For example, the powder photograph of silicon (Fig. 223) is not obviously cubic because the combination of absences due to the lattice and to the structure produces a grouping of the lines which is not quite regular; nevertheless it *is* cubic.

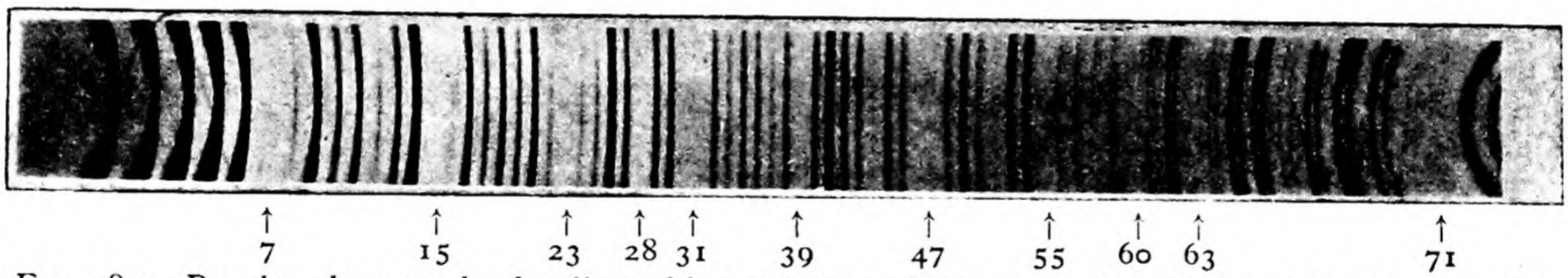

FIG. 180. Powder photograph of sodium chlorate (copper $K\alpha$ radiation). Radius of camera = 4·5 cm.

3.2 The tetragonal system. If the substance is not cubic, a more complicated pattern will be formed, and no rough survey of the photograph will give any information. The simplest procedure is to see if any relationships between the values of $\sin^2\theta$ will give an indication of the symmetry.

Suppose the substance is tetragonal. Then

$$\sin^2\theta_{hkl} = A\,(h^2+k^2) + Cl^2.$$

The problem is therefore to find values of A and C which give the observed values of $\sin^2\theta$ with integral values of h, k and l. This may seem difficult in general, but some special cases provide a certain amount of assistance. Consider the spectra with l zero;

$$\sin^2\theta_{100} = A, \quad \sin^2\theta_{110} = 2A, \quad \sin^2\theta_{200} = 4A,$$
$$\sin^2\theta_{210} = 5A, \quad \sin^2\theta_{220} = 8A, \ldots \qquad (6)$$

The occurrence of the ratio 2 is noteworthy. Except by chance, the only other system in which this ratio is found is the cubic one. If, therefore, the substance is not cubic and the $\sin^2\theta$'s of two low-angle lines are in the ratio of 2, it is probable that the substance is tetragonal and that the two lines are 100 and 110, or 110 and 200. The quantity A can be derived and the presence of other hko lines can be tested. If other lines do fit in, it is probable that the original guess is correct.

The remaining problem then is to find the value of C. A method for doing this is illustrated by the following example. The first nine lines on a powder photograph have the following values of $\sin^2\theta$:

a	0·0445	*f*	0·2204
b	0·0888	*g*	0·2245
c	0·1449	*i*	0·3117
d	0·1767	*j*	0·3554
e	0·1811		

$\sin^2\theta_b$ and $\sin^2\theta_a$ have a ratio of 2. Suppose then that the substance is tetragonal and that line *a* is 100 and line *b* 110. Take $A=0{\cdot}0444$. Then $2A=0{\cdot}0888$, $4A=0{\cdot}1776$, $5A=0{\cdot}2220$, $8A=0{\cdot}3552$. These values suggest that *d* is 200, *f* is perhaps 210 and *j* is 220. Now subtract the multiples of A from all the values of $\sin^2\theta$, even those that are thought to be indexed correctly.

Line	$\sin^2\theta$	$\sin^2\theta - A$	$\sin^2\theta - 2A$	$\sin^2\theta - 4A$	$\sin^2\theta - 5A$
a	0·0445	0·0001			
b	0·0888	0·0444	0·0000		
c	0·1449	0·1005	0·0561		
d	0·1767	0·1323	0·0879		
e	0·1811	0·1367	0·0823	0·0035	
f	0·2204	0·1760	0·1316	0·0418	
g	0·2245	0·1801	0·1357	0·0469	
i	0·3117	0·2673	0·2229	0·1341	0·0897
j	0·3554	0·3110	0·2668	0·1777	0·1334

If the original guess is correct, each horizontal line in this table of differences should contain a quantity Cl^2, and so we must look for quantities that occur frequently. The value $0{\cdot}1329 \pm 0{\cdot}0012$ occurs in the differences for lines *d*, *f*, *i* and *j*. But it does not occur for lines *c*, *e* and *g*. Suppose then that 0·1329 corresponds with $l=2$. Then $C=0{\cdot}0322$. This does not occur at all. The value $0{\cdot}1354 \pm 0{\cdot}0013$, which occurs for lines *e*, *g* and *i* is no better. We must therefore suppose that the original guess is wrong, although there has been enough success to show that it has some relation to the truth.

Suppose that line *a* is 110 and line *b* 200. Then $A=0{\cdot}0222$, and the possible multiples are 0·0444, 0·0888, 0·1110, 0·1776, 0·1998. These values may now be subtracted from the observed values of $\sin^2\theta$; the whole table should be completed, but for brevity we shall take only the first five lines.

Line	$\sin^2\theta - A$	$\sin^2\theta - 2A$	$\sin^2\theta - 4A$	$\sin^2\theta - 5A$	$\sin^2\theta - 8A$	$\sin^2\theta - 9A$
a	0·0223	0·0001				
b	0·0666	0·0444	0·0000			
c	0·1227	0·1005	0·0561	0·0339		
d	0·1545	0·1323	0·0879	0·0657	0·0035	
e	0·1589	0·1367	0·0923	0·0701	0·0418	0·0206

We now see that the value 0·0339 occurs for line *c*; this is near the value for which we were looking. Four times it is 0·1356, which is near the second value considered before. The values of the constants so derived are $A=0{\cdot}0222$, $C=0{\cdot}0339$, and it will be found possible to index all the lines on this basis. More accurate values are $A=0{\cdot}0220$ and $C=0{\cdot}0340$. From these values it will be found that *j* is 312, not 400; there are usually chance coincidences like this to trap the unwary.

The substance is $CuAl_2$ (Friauf, 1927).

3.3 The hexagonal and trigonal systems. As shown in **10,** 1.4, crystals of the hexagonal and trigonal systems can both be referred to hexagonal axes. The equation for hexagonal axes is:

$$\sin^2\theta_{hkl} = A(h^2 + hk + k^2) + Cl^2 \qquad (7)$$

where $A=\lambda^2/3a^2$ and $C=\lambda^2/4c^2$.

For the hko spectra,

$$\sin^2\theta_{100} = A,\ \sin^2\theta_{110} = 3A,\ \sin^2\theta_{200} = 4A,$$
$$\sin^2\theta_{210} = 7A,\ \sin^2\theta_{300} = 9A,\ \sin^2\theta_{220} = 12A. \qquad (8)$$

It will be seen that the most frequently occurring ratio is now 3; this cannot occur in the tetragonal system except by chance.

If a hexagonal unit cell has been successfully found by these methods, it is still possible that the true symmetry may be rhombohedral, and this will be shown by the absence of certain lines. If a rhombohedral crystal has been referred to a hexagonal unit cell, all possible reflections belong to one of two categories, depending on the relative orientation of the true rhombohedral unit cell and the hexagonal cell selected.

Case 1 $\quad -h+k+l=3n$
Case 2 $\quad h-k+l=3n$ where $n=0, 1, 2, 3$, etc.

3.4 The orthorhombic system. If the substance is orthorhombic, the problem is much more difficult; three constants have to be found and these are related to the $\sin^2\theta$'s by the equation

$$\sin^2\theta_{hkl} = Ah^2 + Bk^2 + Cl^2.$$

Some idea of the probable magnitudes of A, B and

C may be obtained from the number of lines on the photograph; the smaller these constants are, the greater the number of lines that can appear.

We have seen in **3**, 2.1 that the distance from the origin of any point hkl in reciprocal space is $2\sin\theta_{hkl}$, and therefore points with θ equal to θ_m will lie on the surface of a sphere of radius $2\sin\theta_m$. The volume of this sphere is $4\pi(2\sin\theta_m)^3/3$, and within it lie all the points with θ less than θ_m. The number of such points is given approximately by the ratio of this volume to the volume of the unit cell of the reciprocal lattice,

$$32\pi\sin^3\theta_m/3a^*b^*c^*.$$

This is not equal to the number of lines with θ less than θ_m on the powder photograph for several reasons. First, groups of reciprocal points represent planes of the same spacing; for example, the reflections hkl, $\bar{h}kl$, $h\bar{k}l$, $hk\bar{l}$, $\bar{h}\bar{k}l$, $\bar{h}k\bar{l}$, $h\bar{k}\bar{l}$ and $\bar{h}\bar{k}\bar{l}$ all give lines with the same value of θ (see table of multiplicity factors, p. 156). Thus the number of possible different values of θ is reduced to be of the order of $4\pi\sin^3\theta_m/3a^*b^*c^*$. Furthermore, some of the reflections will be of vanishingly small intensity (**15**, 2.7) and some will be absent for space-group reasons (**15**, 3.5); also some will overlap because their Bragg angles are almost identical. These effects are difficult to assess quantitatively, but it is probably fair to assume that, in all, only about half the theoretically possible number of lines will be observed. If M is the number of observed lines, then

$$M\sim 2\pi\sin^3\theta_m/3a^*b^*c^*. \qquad (9)$$

Now $A=\lambda^2/4a^2=\frac{1}{4}a^{*2}$ and therefore $a^*=2\sqrt{A}$.

Similarly $b^*=2\sqrt{B}$ and $c^*=2\sqrt{C}$.

Therefore

$$M\sim 2\pi\sin^3\theta_m/24\sqrt{ABC}\sim\sin^3\theta_m/4\sqrt{ABC},$$

or

$$\sqrt{ABC}\sim\sin^3\theta_m/4M. \qquad (10)$$

If A, B and C are of the same order of magnitude, $\sqrt{ABC}$ may be replaced by $A^{3/2}$ (or $B^{3/2}$ or $C^{3/2}$), and the approximate value of A is given by $(\sin^3\theta_m/4M)^{2/3}$.

That is, $A\sim(\frac{1}{4})^{2/3}\sin^2\theta/M^{2/3}\sim 0{\cdot}4\sin^2\theta/M^{2/3}$. (11)

For example, Bradley and Taylor (1937) found that on a powder photograph of $NiAl_3$, twenty lines occurred with values of $\sin\theta$ less than 0·5 when cobalt $K\alpha$ radiation was used. Thus we should expect that A, B and C would be about $0{\cdot}4\times 0{\cdot}25/20^{2/3}=0{\cdot}014$. Actually,

$$A=0{\cdot}0148,\quad B=0{\cdot}0346,\quad C=0{\cdot}0183.$$

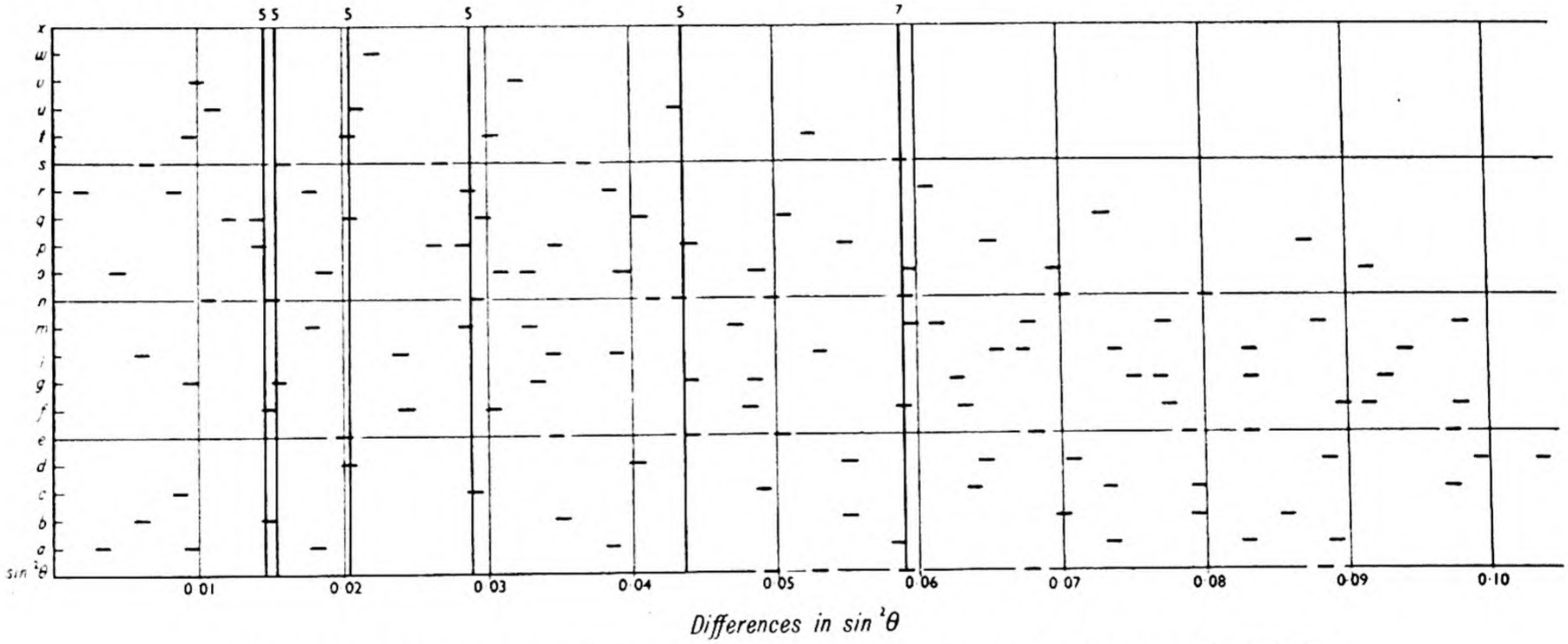

FIG. 182. Diagram of differences in $\sin^2\vartheta$ for lines on powder photograph of $NiAl_3$

It can thus be seen that the method is capable of giving the correct order of magnitude for A, B and C.

The problem is still formidable but not necessarily insoluble, as we can see by considering some simple cases.

$$\sin^2\theta_{100}=A,\quad \sin^2\theta_{010}=B,\quad \sin^2\theta_{001}=C \qquad (12)$$

$$\sin^2\theta_{011}=B+C=\sin^2\theta_{010}+\sin^2\theta_{001},$$
$$\sin^2\theta_{101}=A+C=\sin^2\theta_{100}+\sin^2\theta_{001},$$
$$\sin^2\theta_{110}=A+B=\sin^2\theta_{100}+\sin^2\theta_{010},$$
$$\sin^2\theta_{111}=A+B+C=\sin^2\theta_{100}+\sin^2\theta_{010}+\sin^2\theta_{001}. \qquad (13)$$

It might be possible to find lines whose values of $\sin^2\theta$ had this type of relation. This, however, is unlikely because the chances that 100, 010 and 001 will be absent for one or more reasons are considerable. We therefore re-write the equations in another way:

$$\begin{aligned} C=\sin^2\theta_{001}&=\sin^2\theta_{101}-\sin^2\theta_{100}\\ &=\sin^2\theta_{011}-\sin^2\theta_{010}\\ &=\sin^2\theta_{hk1}-\sin^2\theta_{hk0}, \text{ in general.} \end{aligned} \qquad (14)$$

That is, C should often occur as differences between the $\sin^2\theta$'s for two lines, and so conversely, any difference that occurs often may be tried as A, B or C.

A way of trying to find such differences is illustrated by the following analysis of $NiAl_3$. The values of $\sin^2\theta$ for the first twenty lines are given in the first column of the table below. In the succeeding columns are given the differences, up to 0·1, between the lines (lettered from a to w) shown at the heads of the columns and the lines immediately following. This table of differences may then be examined to see if any value occurs particularly frequently. One way of making this examination is to plot the differences shown in the table along horizontal lines, one for each powder line, as shown in Fig. 182. The points should be elongated to take possible errors into account; in this example the error has been taken as ±0·0005, but in general it must be found from experience with known structures.

When the diagram is complete, a vertical line is run across it and the points where several values are cut simultaneously are noted. In Fig. 182, the outstanding figure is 0·0591, which occurs seven times; 0·0437, 0·0205, 0·0153 and 0·0146 occur five times, and many values occur four times. The immediate deduction is that one of our constants, say A, is 0·0148 as this agrees both with 0·0146 and ¼ of 0·0591, and it is of the order of magnitude that we expect. We cannot yet make use of the other observations, and in any event it is better to take only one step at a time.

First we deduce that line c, $\sin^2\theta = 0{\cdot}0591$, is 200. We next note that $\sin^2\theta_b$ and $\sin^2\theta_d$ differ by 0·0148. This suggests that line b and line d have the same k and l indices and that $h = 0$ and 1 respectively. Similarly, $\sin^2\theta_f$ differs from $\sin^2\theta_g$ by 0·0148 and from $\sin^2\theta_n$ by 0·0590. This suggests that lines f, g and n have the same k and l indices and $h = 0$, 1 and 2 respectively.

It is wise not to consider more than six or eight lines to begin with; and we find that, of the first seven lines, we have indexed one completely, have some information about four, and know nothing positive about two, a and c. We may guess that line a has not a zero h index since the differences 0·0146 and 0·0591 do not occur in connection with it. It is true that 0·0586 ($\sin^2\theta_f - \sin^2\theta_a$) may possibly be 0·0591, but line f itself is supposed to have $h = 0$. If line a has not $h = 0$, then the simplest indices to try for it are 110; it cannot of course be 100; this would make $B = \sin^2\theta_a - A = 0{\cdot}0496 - 0{\cdot}0148 = 0{\cdot}0348$. This is encouraging, because 0·0350 occurs four times in the table. Also $4 \times 0{\cdot}0348 = 0{\cdot}1392$, which suggests that line m is 020.

We also note that $\sin^2\theta_e - \sin^2\theta_b = 0{\cdot}0352$. This would suggest that these lines have the same h and l indices and $k = 1$ and 0 respectively. But line b has $h = 0$ and so must be 001 or 002. This fixes C as 0·0530 or 0·0132, but both these occur only once in the table. Thus we have probably been led astray by a chance coincidence.

DIFFERENCES OF $\sin^2\theta$ VALUES ($\times 10^4$) FOR $NiAl_3$

LINE SYMBOLS

$\sin^2\theta$		*a*	*b*	*c*	*d*	*e*	*f*	*g*	*j*	*m*	*n*	*o*	*p*	*q*	*r*	*s*	*t*	*u*	*v*	*w*
a	0496																			
b	0530	034																		
c	0591	095	061																	
d	0678	182	148	087																
e	0882	386	352	291	204															
f	1082	586	552	491	404	200														
g	1230	734	700	639	552	348	148													
j	1325	829	795	734	647	443	243	095												
m	1386	890	856	795	708	504	304	156	061											
n	1565			974	887	683	483	335	240	179										
o	1672				994	790	590	442	347	286	107									
p	1716					834	634	486	391	330	151	044								
q	1858					976	776	628	533	472	293	186	142							
r	1980						898	750	655	594	415	308	264	122						
s	1999						917	769	674	613	434	327	283	141	019					
t	2063						981	833	738	677	498	391	347	205	083	064				
u	2156							926	831	770	591	484	440	298	176	157	093			
v	2266								941	880	701	594	550	408	286	267	203	110		
w	2366									980	801	694	650	508	386	367	303	210	100	
x	2587											915	871	729	607	588	524	431	321	221

The next simplest indices to try for line *b* are 011. *C* then equals $\sin^2\theta_b - 0{\cdot}0348 = 0{\cdot}0182$. This is much better, since 0·0182 occurs four times.

We are now in a position to see if our values of *A*, *B* and *C* explain all the lines. The first eight give :

	hkl	Calculated	Observed
a	110	0·0496	0·0496
b	011	0·0530	0·0530
c	200	0·0590	0·0591
d	111	0·0678	0·0678
e	102	0·0876	0·0882
f	012	0·1076	0·1082
g	112	0·1224	0·1230
j	300	0·1328	0·1325
	202	0·1318	

This is the correct solution, although the choice of axes is not the same as that used earlier in this chapter. If the axes used here are x', y' and z', their relation to the x, y and z axes in **12,** 2.3 is $x' = y$, $y' = z$, $z' = x$.

The values of *A*, *B* and *C* have to be adjusted as higher orders are taken into account. It is obvious, for example, that *C* is too low ; 0·0183 gives better agreement for the lines with $l = 2$ and will not appreciably worsen the agreement for the lines with $l = 1$.

It is possible that these methods would not work for a structure much more complicated than that of $NiAl_3$; even for this, only one of the constants is readily found, probably because it is the smallest. Nevertheless, the method does provide a way of starting on the problem and is worth trying on a photograph that does not appear to be that of a cubic, tetragonal or hexagonal substance.

4 Interpretation by Graphical Methods

4.1 The principle of graphical methods. For certain crystal systems it is possible to draw curves representing the calculated spacings, or quantities related to them, as functions of the cell dimensions. To index a given powder photograph, the spacings, or the related quantity derived from the lines on the photograph, are plotted on a diagram and compared with the curves obtained theoretically. If the cell dimensions are known, the diagram of experimental results can be placed directly on the theoretical curves and the indices read off ; if the cell dimensions are not known, the diagram has to be moved about over the curves until a fit is obtained.

In practice the method is not easily applied to systems of symmetry lower than tetragonal, hexagonal or trigonal. It is most conveniently illustrated with reference to the cubic system, in which the expression for the spacing *d* of the planes *hkl* is

$$d = a/\sqrt{h^2 + k^2 + l^2},$$

where *a* is the lattice parameter. It is, therefore, possible to calculate *d* as a function of *a* for given indices ; obviously *d* is proportional to *a*, and so the curve of *d* against *a* is a straight line passing through the origin. For each set of indices a line of different slope will be produced, as shown in Fig. 184. In

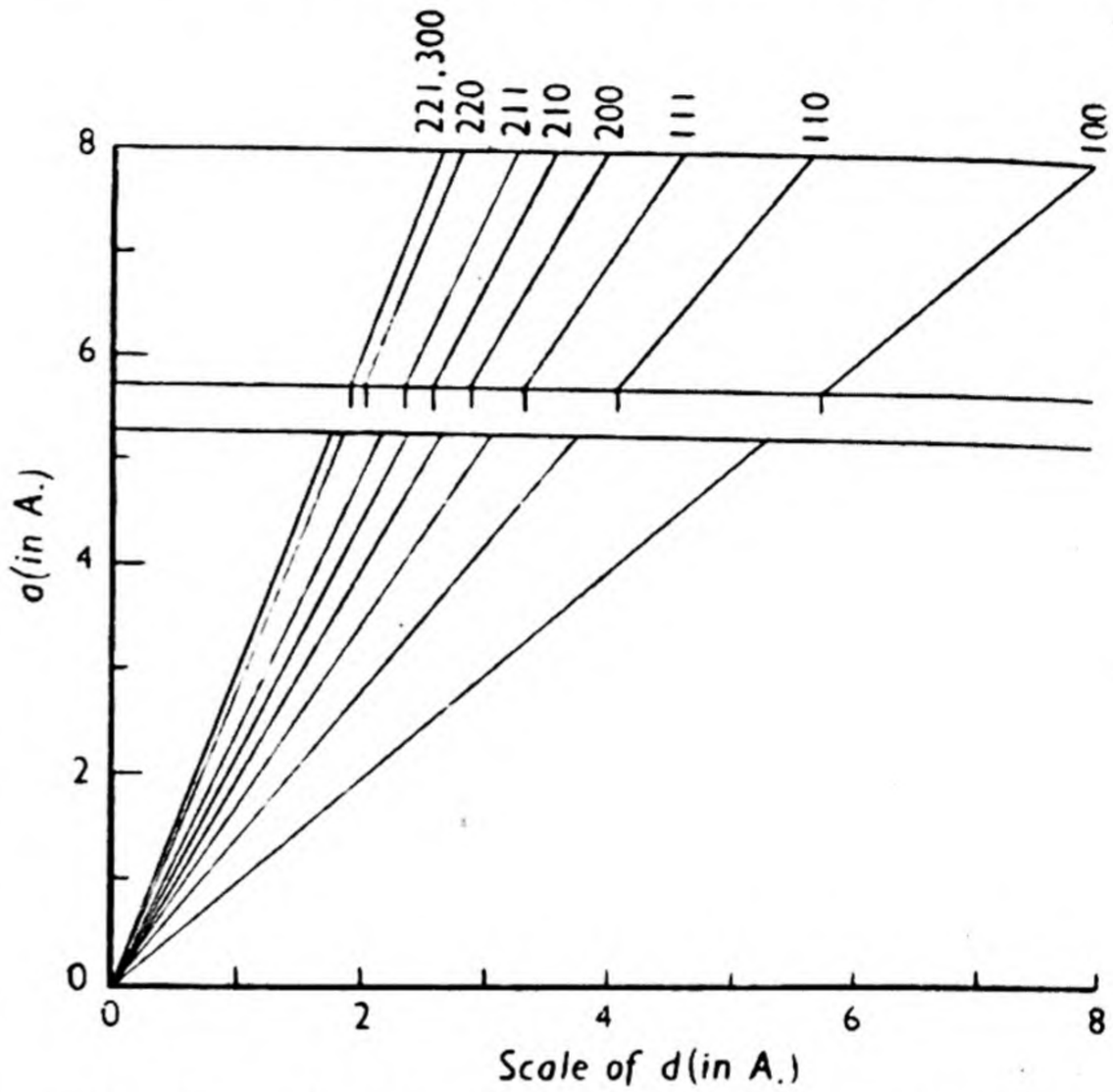

Fig. 184. Chart for indexing the powder photograph of a cubic material

order to index a photograph, all that is necessary is to mark on a strip of paper the values of the spacings ($\lambda/2 \sin\theta$) derived from the photograph and to find at which value of *a* the observed values agree with the set of theoretically derived lines, as shown in Fig. 184.

This method is described only in order to act as an introduction to the methods to be described in the following sections ; the indexing of powder photographs of cubic specimens (**12,** 3.1) is usually simple enough not to need such methods. For the tetragonal, hexagonal and trigonal systems, however, graphical methods are quite useful. In these systems there are two cell dimensions, *a* and *c*, on which the spacings depend, and thus the method as described for the cubic system cannot be used because another dimension is needed. The following methods avoid this difficulty.

4.2 Bjurström's method. The basic equation of Bjurström's method (Bjurström, 1931) for the tetragonal system is

$$\frac{1}{d^2} = \frac{1}{a^2}(h^2 + k^2) + \frac{1}{c^2} l^2. \qquad (15)$$

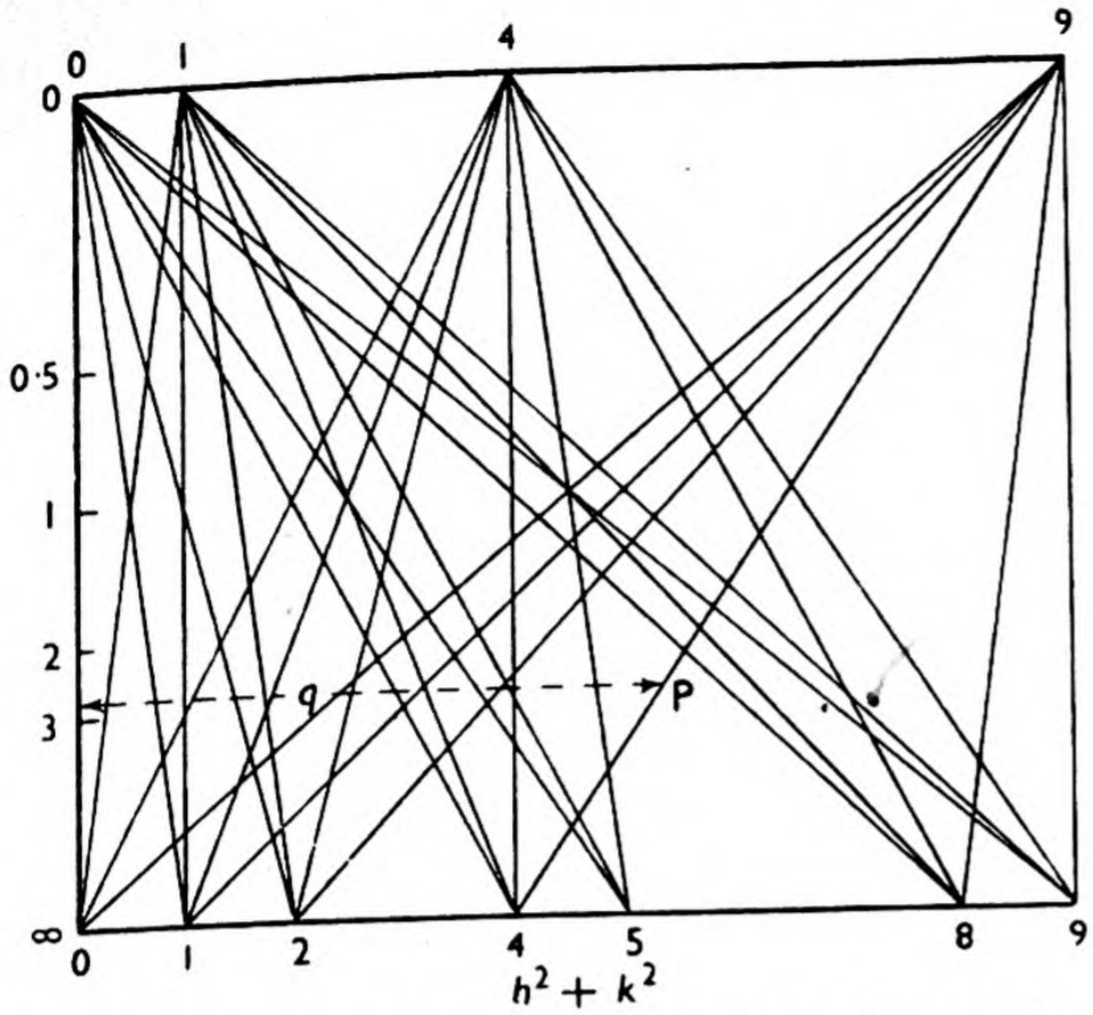

FIG. 185.1. Bjurström's chart for indexing the powder photograph of a tetragonal material

We may consider two extreme forms of equation (15); with $a = \infty$ it becomes

$$\frac{1}{d^2} = \frac{1}{c^2} l^2, \tag{16}$$

and with $c = \infty$ it becomes

$$\frac{1}{d^2} = \frac{1}{a^2}(h^2 + k^2). \tag{17}$$

If c is taken as unity, possible values of the right-hand side of equation (16) can be marked along a horizontal line, as shown at the top of Fig. 185.1; these values are, of course, the squares of the natural numbers. Similarly, possible values of $h^2 + k^2$ can also be plotted, as shown at the bottom of Fig. 185.1. These two horizontal lines may be labelled as $c/a = 0$ and $c/a = \infty$, respectively. Each point on the top line is now joined by a straight line to every point on the bottom line, and we obtain the complete diagram.

Consider a point, such as P, which lies on one of the cross-lines, at a fraction p of the distance from the top. Then the distance q from the line joining the left-hand ends of the top and bottom lines is

$$q = p(h^2 + k^2) + (1 - p) l^2, \tag{18}$$

which may be re-written as

$$q = \frac{(h^2 + k^2)}{1/p} + \frac{l^2}{1/(1-p)}.$$

By comparison of this equation with equation (15), we see that q is the value of $1/d^2$ for a tetragonal substance with $a^2 = 1/p$, $c^2 = 1/(1-p)$, and $(c/a)^2 = p/(1-p)$. Each horizontal line on Fig. 185.1 therefore represents a set of values of $1/d^2$ for a crystal with a given axial ratio, which may thus be marked on the side.

A difficulty still remains. Not only is c/a fixed as $\sqrt{p/(1-p)}$, but a is also fixed as $\sqrt{1/p}$ and c as $\sqrt{1/(1-p)}$, and another variable is needed in order to express variation in either of these axes. This is a general rule for the application of graphical methods to the uniaxial systems; two variables are always needed. In Bjurström's method the variable is obtained in the following way: the values of $1/d^2$ from the photograph to be indexed are marked along a horizontal line, and a vertical line is then drawn from the left-hand end; the values of $1/d^2$ are then joined to a fixed point on this line, and, as seen in Fig. 185.2, any horizontal section of the resulting diagram is a representation of the set of values of $1/d^2$ on a reduced scale.

The method of using the charts is then as follows. The diagram of the experimental results (Fig. 185.2) is drawn on transparent paper, and is placed on the Bjurström chart (Fig. 185.1) with the left-hand edges of both coincident, but with their relative vertical positions arbitrary. A horizontal straight edge is then moved slowly down the composite diagram. If at a certain position of the straight edge it is found that all the observed values of $1/d^2$ coincide with lines on the chart, a fit will have been found; the indices may be read off and thence c and a calculated. If a fit is not found, the scale of $1/d^2$ may be displaced vertically and the operation repeated until success is attained.

Naturally, some systematic approach must be adopted. For example, the scale of $1/d^2$ may be placed low down on the Bjurström chart and gradually moved upwards. Also it is recommended that the

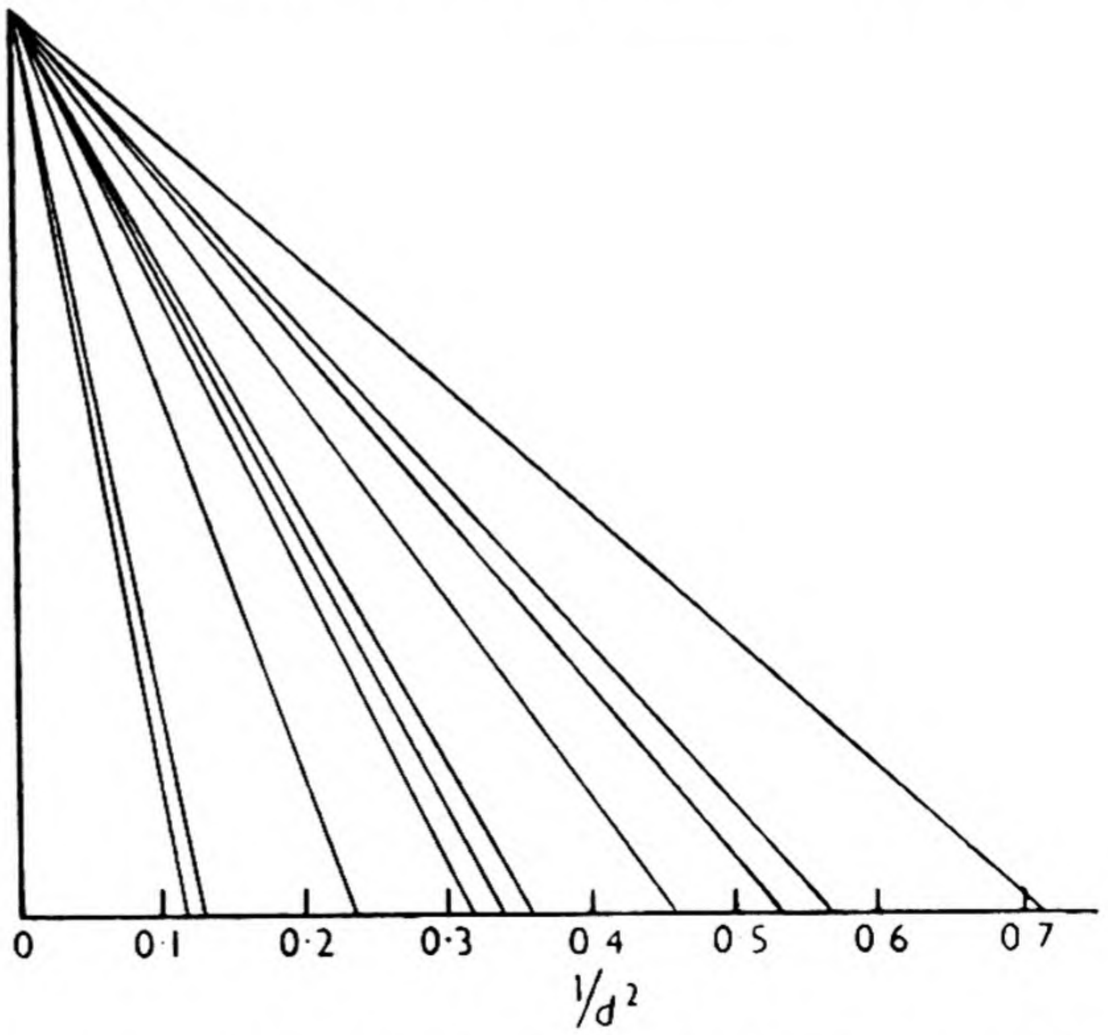

FIG. 185.2. Representation of values of $1/d^2$ on a variable scale for use with Bjurström's chart (Fig. 185.1)

lower orders should be concentrated upon first, as it is useless trying to index the higher orders unless the lower ones fit satisfactorily.

Similar methods can be used for the hexagonal system and for trigonal crystals referred to a hexagonal lattice. The equation is

$$\frac{1}{d^2} = \frac{4}{3a^2}(h^2 + hk + k^2) + \frac{1}{c^2} l^2. \qquad (20)$$

The same equation can be used for rhombohedral crystals if these are referred to hexagonal axes; in this case the lines which are absent because of the rhombohedral lattice type can be omitted from the chart.

The value of Bjurström's method is that the charts, being composed of straight lines only, are easily constructed. On the other hand, it may be found that the superposition of two sets of lines is rather confusing. Bjurström (1931) has suggested a device which overcomes this difficulty. It consists of two bars connected together so that they form two opposite sides of a parallelogram. Along these bars, points are marked at distances proportional to possible values of $h^2 + k^2$ (for the tetragonal system), and corresponding points are joined by straight wires, as shown in Fig. 186; along each wire distances are marked proportional to the squares of the natural numbers.

To use this device, a set of parallel lines is drawn at distances from a fixed line representing the values of $1/d^2$ obtained from the photograph to be analysed. The corner corresponding to $h^2 + k^2 = 0$ and $l = 0$ is placed on the line $1/d^2 = 0$. Then the apparatus is moved round until a point on it lies over each $1/d^2$ line, as shown in Fig. 186. If no such fit is found, the angle of the parallelogram is altered and the operation repeated until success is achieved.

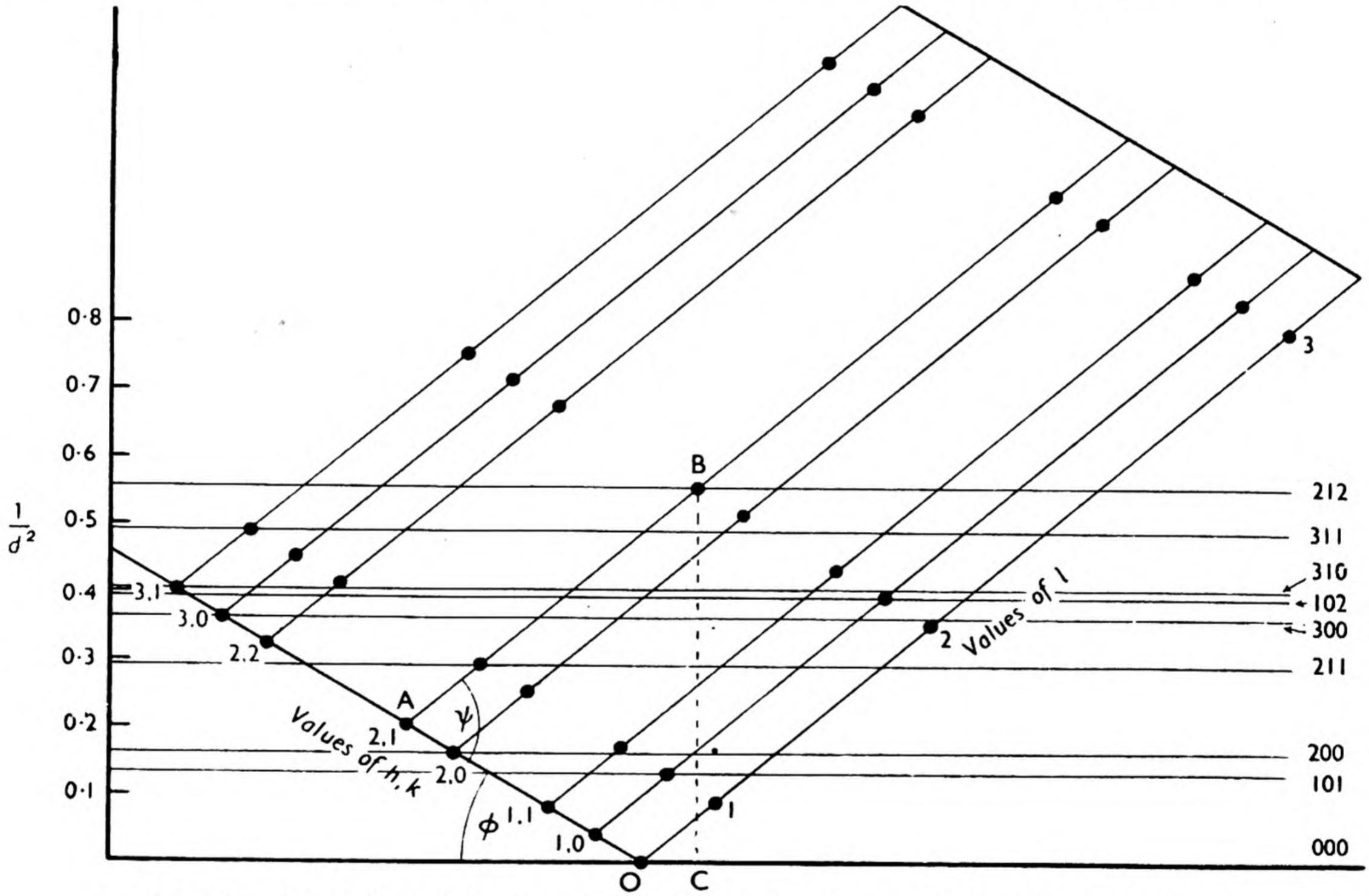

FIG. 186. Bjurström's device for indexing the powder photograph of a tetragonal material

The theory is illustrated by Fig. 186. $OA = h^2 + k^2$ and $AB = l^2$, and therefore

$$BC = (h^2 + k^2)\sin\phi + l^2 \sin(\psi - \phi) \qquad (21)$$

By comparison of this equation with equation (15), we see that BC represents $1/d^2$ if $1/a^2 = \sin\phi$ and $1/c^2 = \sin(\psi - \phi)$. Thus the different values of ϕ and ψ simulate different values of a and c.

4.3 Hull-Davey charts. If graphical methods are preferred, without the superposition of two sets of lines, the Hull-Davey (1921) charts may be used. In these charts the function log d is used. The usefulness of this function can be seen by applying it to the method described for the cubic system in **12,** 4.1.

From the equation $d = a/\sqrt{h^2+k^2+l^2}$, we have

$$\log d = \log a - \tfrac{1}{2}\log(h^2+k^2+l^2). \qquad (22)$$

For any set of indices this represents a straight line, of slope 45°, making an intercept of $-\frac{1}{2}\log(h^2+k^2+l^2)$ on the axis of d; for several sets of indices we thus obtain the diagram shown in Fig. 187. Any horizontal line such as AB or CD will represent a set of values of $\log d$ for a particular value of a. It can be seen, however, that the relative positions of the intersections of the lines on the chart with the lines AB and CD are the same; they differ only in position. Thus we can represent the complete chart by the series of points given by the intersection of a line such as AB with the lines of the chart, and we can represent different values of a by translating the line of points along its own length. Having compressed the data for the cubic system into one dimension we can now plot, at right angles, the variation in $\log d$ produced when c/a changes from unity, and so obtain charts for the tetragonal system. In a similar way charts for the hexagonal system can also be produced.

In the Hull-Davey charts, the values of $\log d$ for different values of c/a are plotted against c/a; but Bunn (1945) has shown that if another function of c/a is used, charts may be obtained which are much simpler to construct; the Institute of Physics has produced a limited number of copies of these charts.

The charts are used by plotting on a strip of paper the values of $\log d$ obtained from the photograph to be indexed. This strip of paper can be moved vertically (representing a change in a or c), or horizontally (representing a change in c/a) until a match is found as shown in Fig. 188. (It should be noted that this diagram is turned through 90°.) The scale of $\log d$ values must, of course, always be kept vertical. As in the use of the Bjurstrom method, the low orders should be concentrated upon at first.

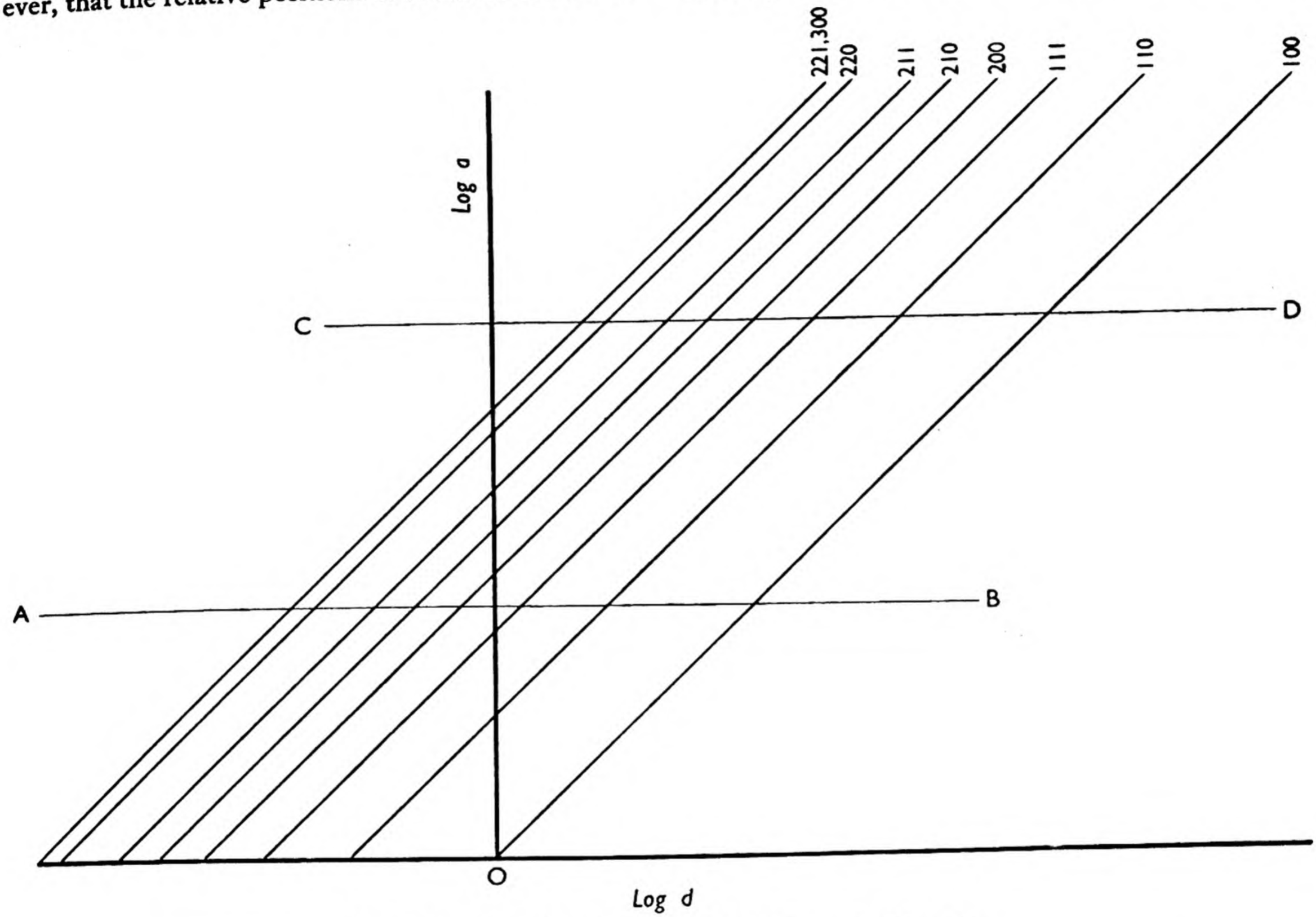

FIG. 187. Logarithmic form of chart shown in Fig. 184

5. Comparison of Analytical and Graphical Methods

The choice between graphical and analytical methods of indexing powder photographs depends to a great extent on personal preferences, but some

general advice can be given to those who have not used either method.

If the problem of indexing a powder photograph is an isolated one, and charts are not available, it is probably simpler to try the analytical methods than to construct the charts. If, however, the problem is likely to arise frequently, charts should certainly be prepared; the charts to be found in the literature are usually too small for convenient use.

If charts are available, the following procedure is recommended. From the powder photograph prepare lists of both $\sin^2\theta$ and $\log d$ (or $1/d^2$ if Bjurström's method is to be used) for all the lines. Examine the values of $\sin^2\theta$ to see if the substance is cubic (**12,** 3.1). If it appears not to be cubic, try the tetragonal and hexagonal charts. If no fit can be obtained with these, see if the values of $\sin^2\theta$ give any clues (**12,** 3.2 and **12,** 3.3), for the unit cell may be too large for the indices of the lines to be easily found graphically, particularly if many of the low orders are absent. If no solution can be found, the analytical method described in **12,** 3.4 should be tried in order to find whether the substance is orthorhombic. Graphical methods cannot be easily used for this system, although Jacob and Warren (1937) succeeded with them in finding the unit cell of uranium.

If none of these methods works, it is probable that the symmetry is lower than orthorhombic, and methods such as those suggested by Ito (1949) should be tried. Finally, if a single crystal, however small, can be obtained, it should be used in preference to a powder to find the unit cell, especially if the symmetry is lower than cubic.

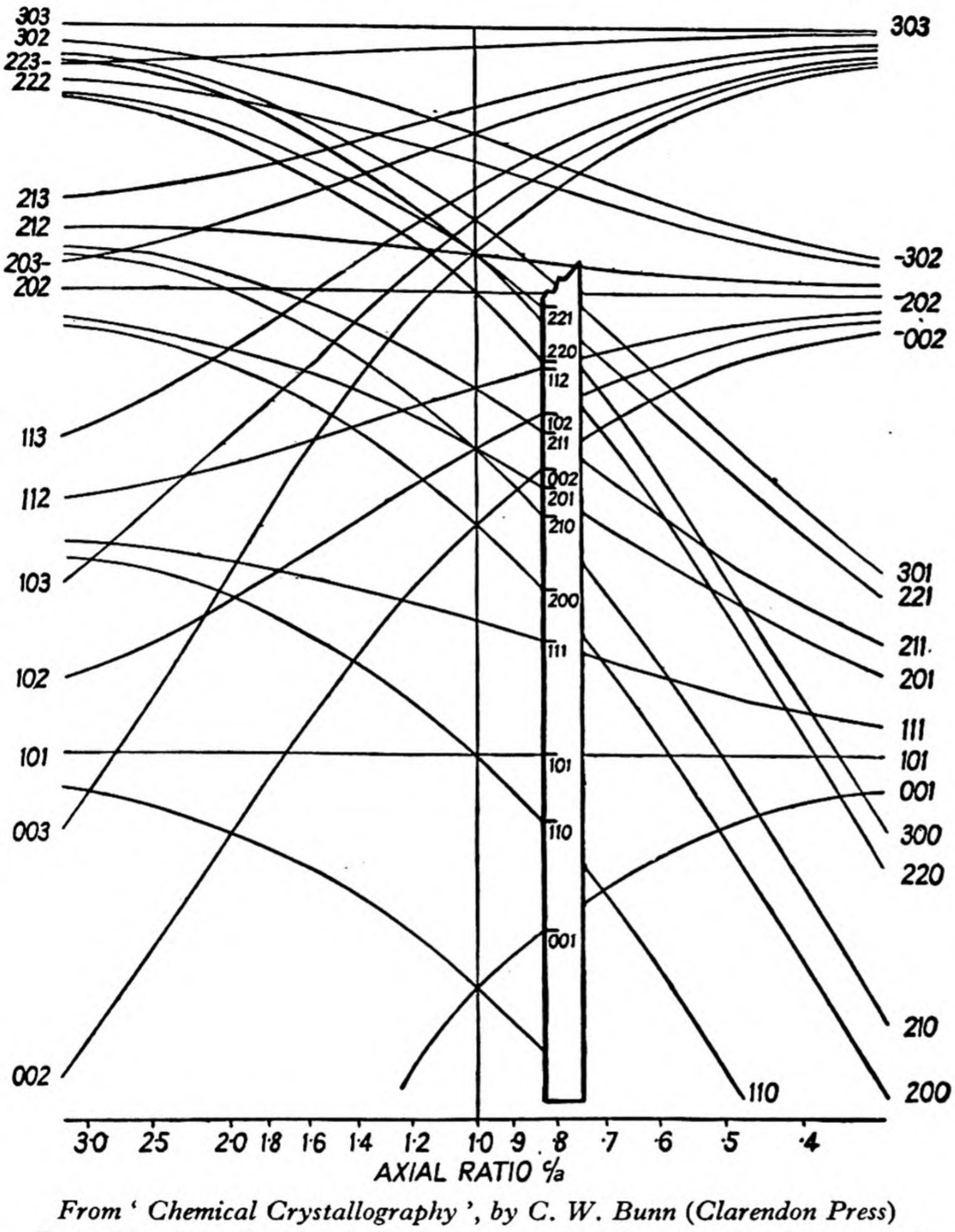

From ' Chemical Crystallography ', by C. W. Bunn (Clarendon Press)

FIG. 188. Bunn's chart for indexing powder photographs of tetragonal materials. The pattern shown is that of urea

PROBLEMS

1. Quartz has a hexagonal unit cell with dimensions

$$a = 4{\cdot}913 \text{ A.}, \quad c = 5{\cdot}405 \text{ A.}$$

The lines on a powder photograph taken with copper $K\alpha$ radiation have the following values of θ, in degrees:

a, 10·44; *b*, 13·34; *c*, 18·32; *d*, 19·78; *e*, 20·18; *f*, 21·28; *g*, 22·94; *h*, 25·15; *j*, 27·51; *k*, 27·76; *l*, 30·06; *m*, 32·12.

Find the indices of these lines.

2. The lines on a powder photograph taken with cobalt $K\alpha$ radiation have the following values of θ, in degrees:

a, 13·92; *b*, 19·24; *c*, 24·09; *d*, 27·78; *e*, 28·80; *f*, 31·65; *g*, 35·71; *h*, 41·20; *j*, 42·05; *k*, 44·53; *l*, 47·40; *m*, 50·77; *n*, 52·52; *p*, 54·65; *q*, 59·20; *r*, 61·59; *s*, 68·61; *t*, 74·05; *u*, 77·59.

Find the indices of the lines and hence find the unit-cell dimensions.

CHAPTER 13

ACCURATE DETERMINATION OF CELL DIMENSIONS

1. Introduction

THE accurate determination of cell dimensions has proved to be of great use in the study of many materials, particularly metals and alloys. Very accurate results can be obtained if measurements are made on the spectra that are reflected almost back into the incident beam, since large Bragg angles are very sensitive to small changes in cell dimensions. This can be seen by differentiating the equation $d=(\lambda \operatorname{cosec}\theta)/2$, which gives

$$\begin{aligned}\delta d &= -\lambda \operatorname{cosec}\theta \cot\theta\, \delta\theta/2 \\ &= -d\cot\theta\,\delta\theta. \end{aligned} \qquad (1)$$

Since cot θ tends to zero as θ tends to 90°, an error $\delta\theta$ in θ will result in a relatively much smaller error δd in d. Consequently, extreme precision of measurement is not called for, and high accuracy can be obtained with simple apparatus and few precautions.

The most direct way of determining cell dimensions involves the measurement of several diffraction lines on a powder photograph, and therefore a circular camera is to be preferred to a flat plate. The ordinary powder camera (**11,** 3, 1) or the symmetrical focusing camera (**11,** 4.3) may therefore be used. Lu and Chang (1941) have also recommended the use of a specimen with a flat surface at the centre of the camera. Since most thought has been devoted to the ordinary powder camera, this only will be considered in detail here, although the same general principles apply to the others.

It was recommended in **11,** 3.1, that the van Arkel method of mounting the film be used if accurate results are required; the high-angle reflections are then close together on one film and no accurate knowledge of any camera constant is needed. An approximate value of the radius may be required, but the method of derivation of the final result eliminates any error in it (Cohen, 1936). It is this fact that makes this method of mounting the film so valuable.

2. Elimination of Systematic Errors in Powder Photographs

There are several effects that cause the lines to be displaced from their true positions, so that angles measured according to the methods described in **11,** 3 will not be the true Bragg angles. But as we have seen in the previous section, a small error in θ should produce a vanishingly small error in d as θ approaches 90°; if we could determine d from a reflection with $\theta=90°$, all the systematic errors should be zero. Although this is impossible to achieve, since a Bragg angle of 90° corresponds with reflection directed back into the X-ray beam, it can be done in effect by determining d from several reflections with different θ's and extrapolating the result to $\theta=90°$.

Although any function of θ will, in theory, suffice for plotting such an extrapolation curve, it is obviously better that the curve should be linear; the finding of the correct function for this purpose involves a consideration of the various possible sources of error. These are listed below.

2.1 Non-coincidence of the axis of the camera and the rotation axis of the specimen. It can be seen from Fig. 189 that any displacement of the specimen perpendicular to the axis of the slit system will cause no error in θ; on one side of the photograph the line will be displaced to a higher value of θ and on the other side to a lower, and the average value will not be appreciably changed. On the other hand, Fig. 190 shows that a displacement along the axis will produce an error since the two lines will move nearer or further apart. Bradley and Jay (1932*b*) have shown that the error in d produced in this way is proportional to $\cos^2\theta$.

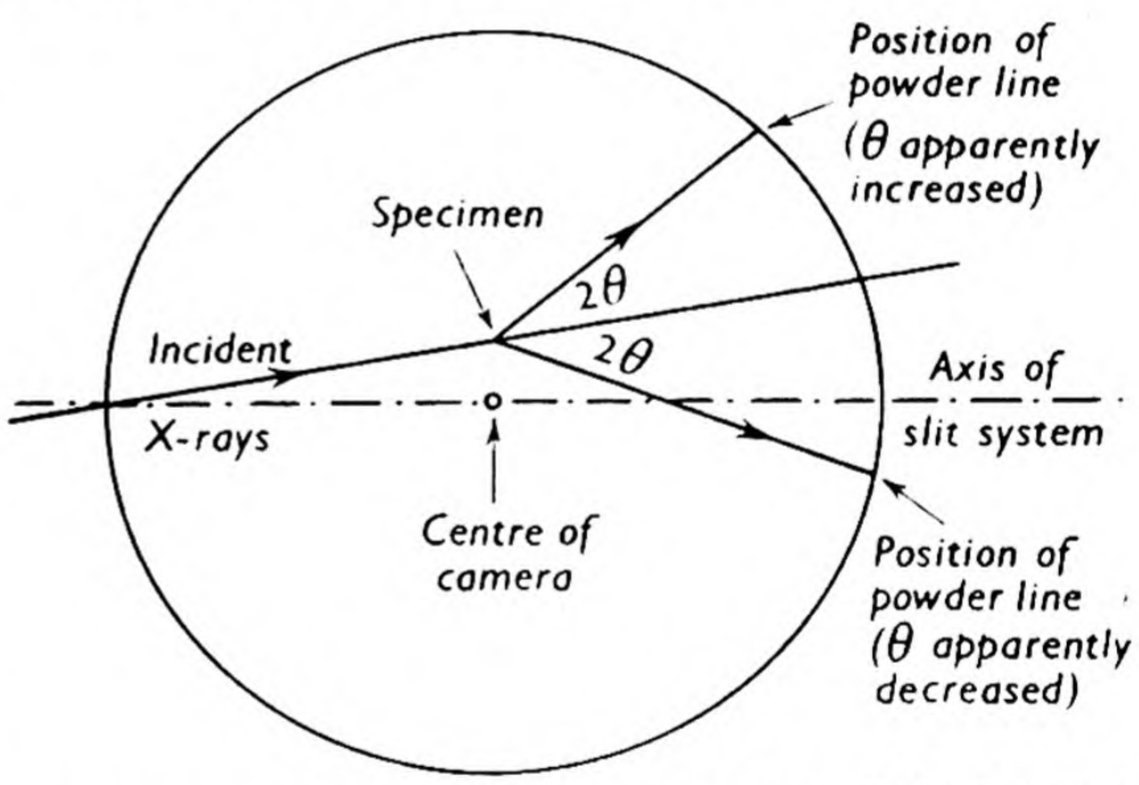

FIG. 189. Diagram showing the effect of displacement of the specimen perpendicular to the direction of the X-ray beam in a powder camera

2.2 Absorption and divergence of the X-ray beam. Although the effects of absorption in the specimen and of divergence of the X-ray beam are quite distinct from each other, it has been shown by Bradley and Jay (1932*a*) that they produce similar errors, and so are best treated together.

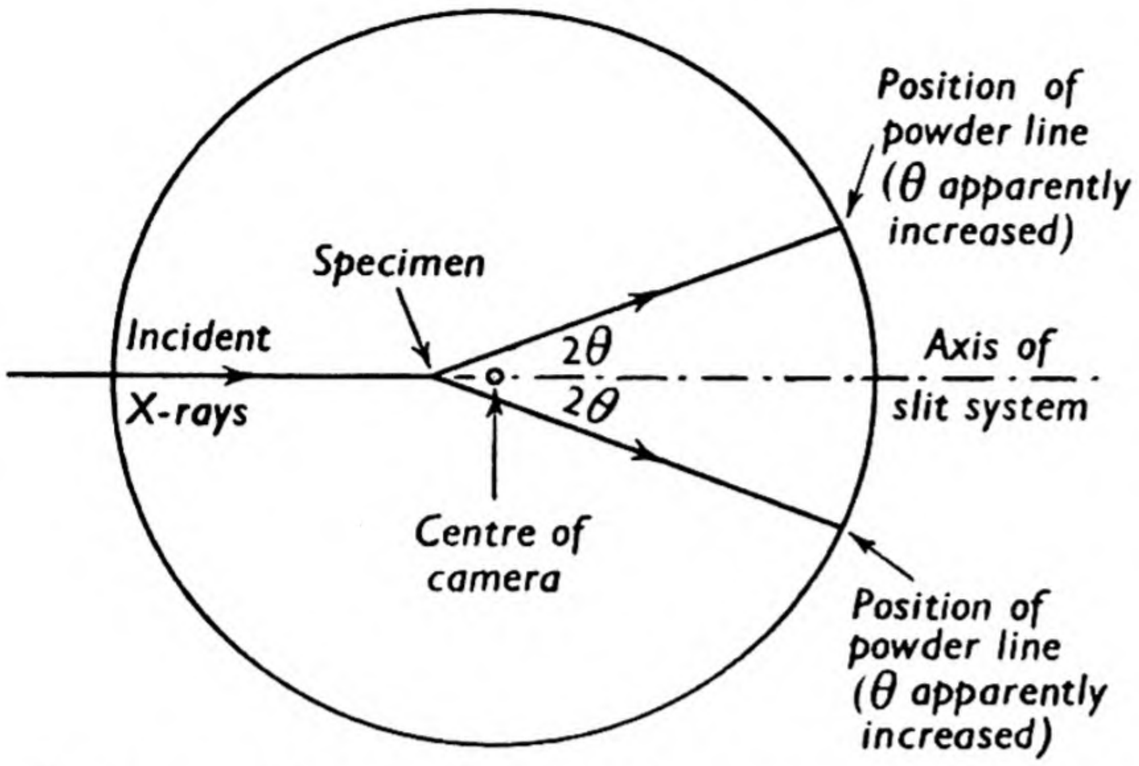

FIG. 190. Diagram showing the effect of displacement of the specimen along the direction of the X-ray beam in a powder camera

Only for a specimen in which absorption is negligible can the centres of the powder lines be taken as the correct positions. Usually the measured value of θ will be larger than the true value (**11,** 3.2), and so the calculated spacing will appear too small. A similar reasoning applies to the error produced by divergence of the X-ray beam.

The exact form of the error has not yet been found. Bradley and Jay (1932*b*) showed that it will be approximately proportional to $\cos^2\theta/\theta$; Jay (1945) suggested that it is nearer to $\cos^2\theta/\sin\theta$; Taylor and Sinclair (1945*b*) proposed the mean of these two functions. Nelson and Riley (1945*a*) showed experimentally that the mean does give better results for the specimens they have used; this function, $\frac{1}{2}(\cos^2\theta/\sin\theta+\cos^2\theta/\theta)$, is therefore recommended, and a table of its values is given in Table 10.

2.3 Finite height of the specimen. In **11,** 1 it was pointed out that each line on a powder photograph is composed of a series of overlapping lines, each component coming from a different point of the specimen. Every component except that which comes from the centre will be displaced in the same direction, so the measurement of the composite line will involve an error. On this account it has been recommended that the height of the specimen irradiated should be kept small (Buerger, 1936; Ieviņš and Straumanis, 1936). Bradley and Jay (1932*a*), however, showed that the effect is quite small, and that if the height of the irradiated part of the specimen is kept within 2 mm. in a camera of 9 cm. diameter negligible error results. Lipson and Wilson (1941) showed that the error depends also upon the shape of the focus of the X-ray tube, and that the error, for reflections with θ near 90°, probably is smaller even than Bradley and Jay claimed. In the methods described in this chapter the error is neglected.

2.4 Film shrinkage. The form of the correction for film shrinkage depends upon the type of film mounting used. It is best, however, to use a camera for which the film-shrinkage error is eliminated, as described in **11,** 3.1.

2.5 Refraction. The process of extrapolation to $\theta=90°$ does not eliminate the error due to refraction. The exact treatment of the correction for refraction is difficult except for a flat, single-crystal specimen; in practice, there is reason to suppose that the only effect of importance is the change in wave-length within the specimen (Wilson, 1940). In order to correct for refraction, the calculated cell dimensions should be divided by the refractive index n of the material. This can be found from the equation given in **2,** 4. For a cubic crystal the following expression is sometimes simpler to apply.

$$(1-n)\,a=4{\cdot}47\times10^{-6}\,(\lambda/a)^2\,\Sigma A,$$

where ΣA is the sum of the atomic numbers of the atoms in the unit cell. It will be seen that the correction is small and is rarely greater than the experimental error.

2.6 Determination of the Bragg angle of an isolated powder line. It is sometimes required to determine the spacing corresponding to a reflection that occurs by itself on a film; this problem arises, for example, in the determination of internal stresses from back-reflection photographs (**13,** 5.4). The extrapolation method cannot be used, so it is necessary to eliminate errors as completely as possible. There are two main ways of doing this.

First, the measurement of the distances is made as accurately as possible. If R is the radius of the back-reflection powder ring, and S is the distance from the specimen to the film,

$$\tan 2\theta=-R/S. \qquad (2)$$

The measurement of S involves some difficulty (Thomas, 1941), particularly if the surface of the specimen is not flat. Moreover, the film will be affected by shrinkage, and so R should not be taken as half the measured diameter of the powder halo; it is recommended that the film holder be arranged to cast shadows on the film at a known distance apart, and that R be derived from this distance by proportion.

In the second method a coating of fine annealed metal powder is deposited on the surface of the specimen (Frommer and Lloyd, 1944). A composite powder

pattern is given by the specimen and the powder and, if the angles of the latter are known, the angles of the former can be found by proportion. This method has the merit of eliminating errors automatically, but it requires longer exposures because of the absorption of the standard powder.

In dealing with lump specimens, it must be remembered that the crystal size may be large and that reflections may be of the Laue type. In order to make sure that the characteristic radiation is being used, the specimen should be oscillated through a few degrees during exposure. In order to produce continuous rings for easy measurement, it is the practice in some laboratories to rotate the film about the axis of the incident beam. This, however, is rather unsafe; if the axis of rotation does not coincide exactly with that of the X-ray beam, the lines will be broadened and so the accuracy will decrease.

2.7 Limits of accuracy. The limits of accuracy obtainable in the measurement of cell dimensions or of spacings depend greatly on the quality of the photograph measured. The highest accuracy will be obtainable from a photograph consisting of sharp, well-resolved lines, but there are factors that suggest a limit, of the order of one part in 100,000. First there is the accuracy of the wave-lengths used; the errors are probably of the order of 0·001 per cent, as evidenced by the differences between the values obtained by Siegbahn's school using photographic methods and those obtained by Bearden and Shaw using a double-crystal spectrometer (**2,** 3.1). But it is not certain that these wave-lengths should be used for the calculations from powder photographs. The emission lines are not symmetrical, and the differences between the peak positions and the centres of gravity are of the order of 0·003 per cent. For calculation of spacings from powder lines, wave-lengths corresponding to the centres of gravity may well be more significant than those corresponding to the peaks.

At the best, however, an accuracy of 0·001 per cent cannot be expected from a single photograph; the average from several photographs, taken if possible with different radiations, is necessary. For most photographs a much lower accuracy must be expected and the resolution of the $K\alpha$-doublet gives a rough idea of what can be attained. If the high-angle doublets are resolved, but are not very sharp, the accuracy should be better than 0·2 per cent and may approach 0·02 per cent. If they are not resolved one cannot expect better than 0·1 per cent accuracy. If the high orders are so blurred that they are almost invisible the low orders have to be used, and from these an accuracy of about 1 per cent can be obtained.

The high accuracy obtainable from good powder photographs is not merely of academic interest; for many applications, small changes in lattice parameter are involved, and the highest possible precision is needed to measure these changes with reasonable accuracy, as will be shown in **13,** 5·

3. Procedure for Powder Photographs of Cubic and of Uniaxial Specimens

3.1 General outline of the method for a cubic specimen. The process of derivation of cell dimensions is best described for a cubic specimen, since there is only one dimension concerned—the cell side a. Suppose that a photograph has been taken and has been measured according to the methods already described (**11,** 3.1). From the value of θ for each line a value of the cell dimension a can be derived from the relation

$$a = \tfrac{1}{2}\sqrt{N} \,.\, \lambda \operatorname{cosec} \theta, \qquad (3)$$

where $N = h^2 + k^2 + l^2$.

The value of a deduced from each measured line is then plotted against the corresponding value of $\frac{1}{2}(\cos^2\theta/\theta + \cos^2\theta/\sin\theta)$, read from Table 10. If there is no error due to eccentricity of the specimen (**13,** 2.1) the resulting points should be randomly distributed about a straight line. The point where this straight line cuts the vertical line for which $\theta = 90°$ gives the value of a which, when corrected for refraction (**2,** 4), is the value of the cell dimension at the temperature at which the photograph is taken.

Cohen (1935) recommends that analytical methods should be used in fixing the best straight line through the experimental points. There is, however, one objection to the use of these methods. The higher accuracy of the points for which θ is near 90° requires that these should be given more weight in the drawing of the line. This can be done graphically with sufficient accuracy; and analytical methods, which are rather lengthy, are unnecessary.

3.2 Methods of calculation. Since it may be necessary to evaluate the expression $\frac{1}{2}\sqrt{N}\lambda \operatorname{cosec}\theta$ for many lines, it is worth while giving some thought to the quickest way of performing the calculation.

If a large number of nearly equal values has to be determined and the same radiation is used, then the same values of N will always occur near $\theta = 90°$. Tables can therefore be drawn up relating a to θ for each line. The value of a given by a particular value of θ can then be read off directly from this table without any calculation.

If, on the other hand, many different values are required, some more general method of calculation must be used. One convenient way is to tabulate $\sqrt{N}\lambda/2$ for the different values of λ that are likely to be used; these can then be multiplied by cosec θ on a

calculating machine. The value of a calculating machine for operations such as these cannot be overestimated, but if one is not available, tables of logarithms must be used. Cosec θ and log cosec θ can be obtained from tables, but it is rather inconvenient to have to convert from minutes to decimal fractions of degrees. Mathematical tables such as those of Chappell (1944), Peters (1937, 1942) and Lohse (Neugebauer, 1935), in which the values of the functions are given at intervals of 0·01°, are therefore particularly useful.

3·3 Choice of radiation. For greatest accuracy the method requires that the extent of extrapolation should not be large; in other words, there should be at least one α-doublet with a value of θ near 90°. This can usually be arranged by suitable choice of the radiation. The tables of $\sqrt{N}.\lambda/2$ can be used to help in this choice in the following way. Find the value of $\sqrt{N}.\lambda/2$ which is nearest to, but just less than, the cell dimension. This will correspond to the last line that can appear, since $\sqrt{N}.\lambda/2 = a\sin\theta$. Repeat this for each of the radiations, and find which gives a possible value of $\sqrt{N}.\lambda/2$ nearest to a. If the value of $\sqrt{N}.\lambda/2$ is equal to a within 0·5 per cent, the corresponding line will probably not be recorded on most cameras: if the value is outside 1·5 per cent the accuracy obtainable will be reduced. These limits should, of course, be taken only as a rough guide and each case must be considered by itself.

Jette and Foote (1935) suggested the use of alloy targets which would give a number of high-angle lines and so make the extrapolation more definite. It must be borne in mind, however, that the extrapolation curves for two different radiations may not exactly coincide: absorption will be different, and as we have seen in **13,** 2.2, this is one of the most important of the factors that decide the slope of the curve. This objection may apply also to the use of α- and β-radiations from the same element.

3·4 A practical example. The various steps in the evaluation of the cell dimensions of a cubic specimen are shown in the table below. The photograph is that of aluminium at 298° C. (Wilson, 1941). The third and fourth columns in the table give the readings of the line positions, the positions of the low-angle knife edges being adjusted to readings corresponding to half the distance between them; the sum of the readings for any pair of lines then gives S, the distance between them. The values of S are given in the next column. Each reading is the mean of two or three separate ones, which for well-defined lines should agree to within 0·003 cm. (The separate values should of course be recorded in the original notes.) The values of θ are then derived from the angle ϕ_k of the camera, but this process has to be adapted to the method used for the particular photograph (see **11,** 3.1). Cosec θ is then obtained to seven significant figures; this is, of course, more than are physically significant, but it ensures that 'rounding-off' errors in the arithmetic will be small compared with the errors of observation. The product of cosec θ and $\sqrt{N}.\lambda/2$ then gives a, and this is plotted against $\frac{1}{2}(\cos^2\theta/\sin\theta + \cos^2\theta/\theta)$ (see **13,** 2.2).

CALCULATION OF LATTICE PARAMETER OF ALUMINIUM AT 298° C. FROM A POWDER PHOTOGRAPH TAKEN WITH Cu$K\alpha$ RADIATION

$h\,k\,l$	RADIATION	READINGS ON FILM in cm.		S	$\theta = S.\theta_k/S_k$	cosec θ	$\sqrt{N}\lambda/2$	a (in A.)	$\frac{1}{2}(\cos^2\theta/\theta + \cos^2\theta/\sin\theta)$
		LEFT	RIGHT						
K.E.*		(Set to	*1·433*)						
3 3 1	α_1	18·486	18·554	37·040	55·486°	1·213 610	3·357 46	4·074 64	0·360
	α_2	18·558	18·621	37·179	55·695°	1·210 582	3·365 82	4·074 59	0·356
4 2 0	α_1	19·230	19·297	38·527	57·714°	1·182 883	3·444 67	4·074 64	0·311
	α_2	19·308	19·371	38·679	57·942°	1·179 926	3·453 26	4·074 59	0·306
4 2 2	α_1	22·586	22·649	45·235	67·763°	1·080 350	3·773 46	4·076 66	0·138
	α_2	22·702	22·763	45·465	68·107°	1·077 724	3·782 86	4·076 88	0·134
3 3 3 / 5 1 1	α_1	26·324	26·388	52·712	78·963°	1·018 846	4·002 35	4·077 78	0·032
	α_2	26·575	26·643	53·218	79·721°	1·016 312	4·012 32	4·077 77	0·028
K.E.*		28·939	28·933	57·872	*86·693*				
				$(\theta_k/S_k =$	1·498 031)				

Value of a extrapolated to $\theta = 90°$ is 4·078 08 A.

Refraction correction $= 4{\cdot}47 \times 10^{-6}\left(\frac{1{\cdot}54}{4{\cdot}08}\right)^2 \times 4 \times 13{\cdot}0 = 0{\cdot}00003$ A.

$a = 4{\cdot}0781_1$ A.

* Knife edge

The best straight line is then drawn through the points as shown in Fig. 193, and the value of a at $\frac{1}{2}(\cos^2\theta/\sin\theta + \cos^2\theta/\theta) = 0$ is recorded. This, corrected for refraction, is the final result.

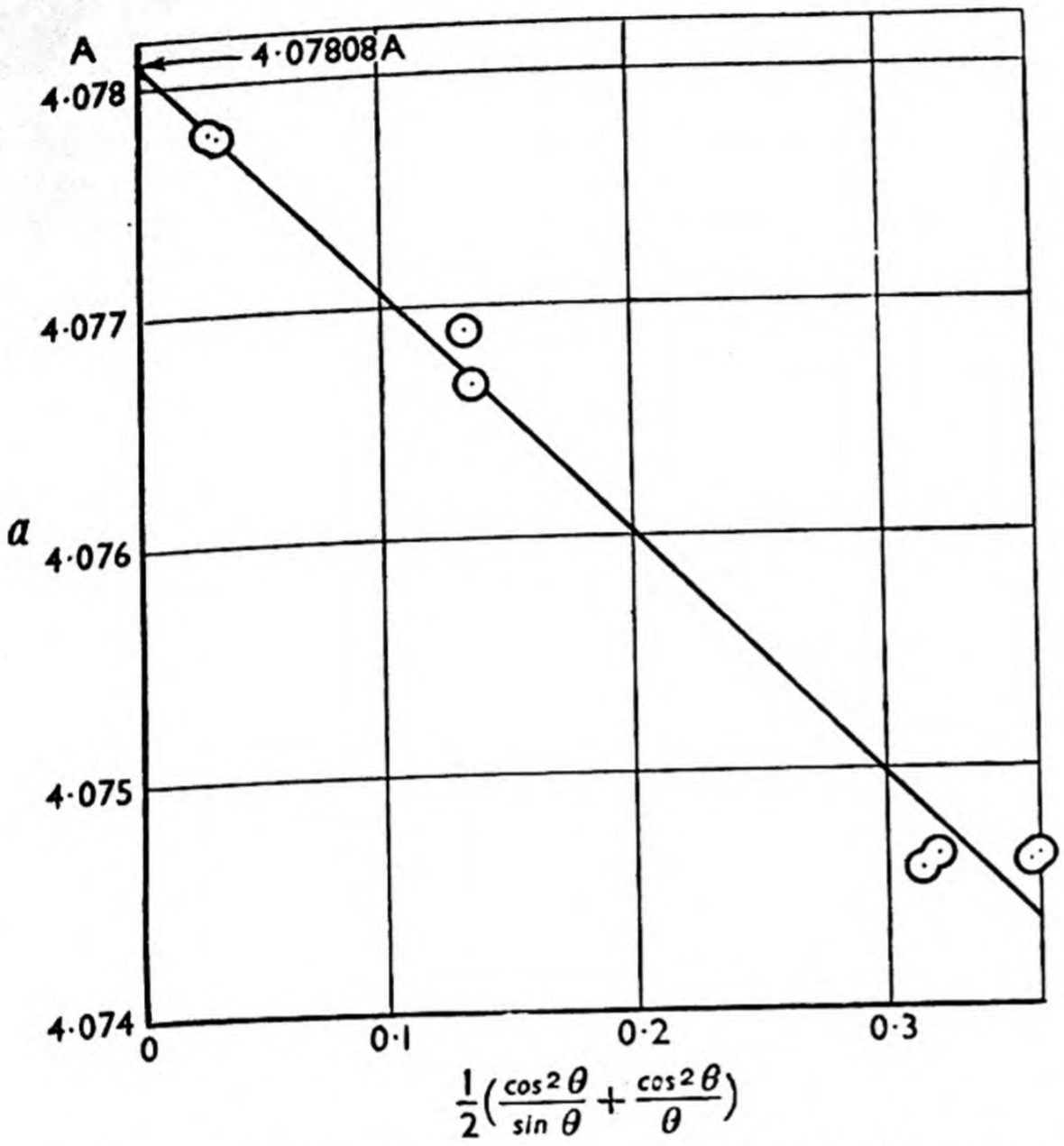

FIG. 193. Extrapolation curve for the accurate determination of the lattice parameter of aluminium at 298° C.

3.5 Method for uniaxial specimens. The graphical method described in the previous section is less easy to apply to systems other than cubic; for such systems Cohen's analytical method is of greater usefulness. Nevertheless, the graphical method is so much quicker than the analytical one that it is still often worth using.

For example, in the tetragonal system the equation relating the cell dimensions to the Bragg angle for the reflection hkl is (Appendix 2)

$$\sin^2\theta_{hkl} = \frac{\lambda^2}{4a^2}(h^2+k^2) + \frac{\lambda^2}{4c^2}l^2, \qquad (4)$$

which may be expressed as

$$\sin^2\theta_{hkl} = \frac{\lambda^2}{4a^2}\left(h^2+k^2+\frac{a^2}{c^2}l^2\right). \qquad (5)$$

Thus if the axial ratio c/a is known, the expression $h^2+k^2+(a^2/c^2)\,l^2$ can be evaluated for the measured reflections, and a can be derived in the same way as for the cubic system. If reflections for which h^2+k^2 is much greater than $(a^2/c^2)\,l^2$ are used, the error in a due to an error in a/c will be small.

Similarly, for the determination of c the equation may be written as:

$$\sin^2\theta_{hkl} = \frac{\lambda^2}{4c^2}\left\{\frac{c^2}{a^2}(h^2+k^2) + l^2\right\}, \qquad (6)$$

and c can be evaluated from reflections for which l^2 is much greater than $(c^2/a^2)\,(h^2+k^2)$.

The axial ratio can then be determined more accurately from the results and, if necessary, the calculations performed again; this usually gives satisfactory results without further refinement.

For the hexagonal system the corresponding equations are:

$$\sin^2\theta_{hkl} = \frac{\lambda^2}{3a^2}\left\{(h^2+hk+k^2) + \frac{3a^2}{4c^2}l^2\right\} \qquad (7)$$

and

$$\sin^2\theta_{hkl} = \frac{\lambda^2}{4c^2}\left\{\frac{4c^2}{3a^2}(h^2+hk+k^2) + l^2\right\}. \qquad (8)$$

The same equations can be used for rhombohedral crystals if they are referred to a hexagonal unit cell.

The choice of radiation for determining the cell dimensions of uniaxial crystals cannot be made so readily as for cubic crystals. Probably the best method is to take a photograph with a short wave-length such as copper $K\alpha$ and to find from it which wave-length will give suitable lines near $\theta = 90°$. It is possible that no single wave-length may be suitable for determining both a and c, and it may be necessary to use two different wave-lengths.

4. Procedure for Single-crystal Photographs

4.1 Introduction. Powder photographs of orthorhombic, monoclinic, and triclinic crystals in general contain too many lines for unambiguous indexing of the high orders; hence accurate values of cell dimensions cannot easily be obtained from such photographs. Accurate values can, however, be obtained from single-crystal photographs if the same general procedure as for powder photographs is applied; that is, reflections with θ near to 90° are measured and extrapolation is used to eliminate errors. The accuracy is far greater than the 1 per cent which is generally accepted as being that obtainable from layer-line measurement (**5,** 1.5). In the determination of molecular weights (**13,** 5.3), for example, an accuracy of 0·03 per cent in cell dimensions is needed to match the 0·1 per cent obtainable in density determinations, and therefore layer-line measurements are quite inadequate.

4.2 Methods for orthorhombic crystals. The accurate determination of cell dimensions from oscillation photographs is best illustrated by application of the method to an orthorhombic crystal, since only three constants a, b and c are involved.

Suppose that the crystal is set with the c-axis as

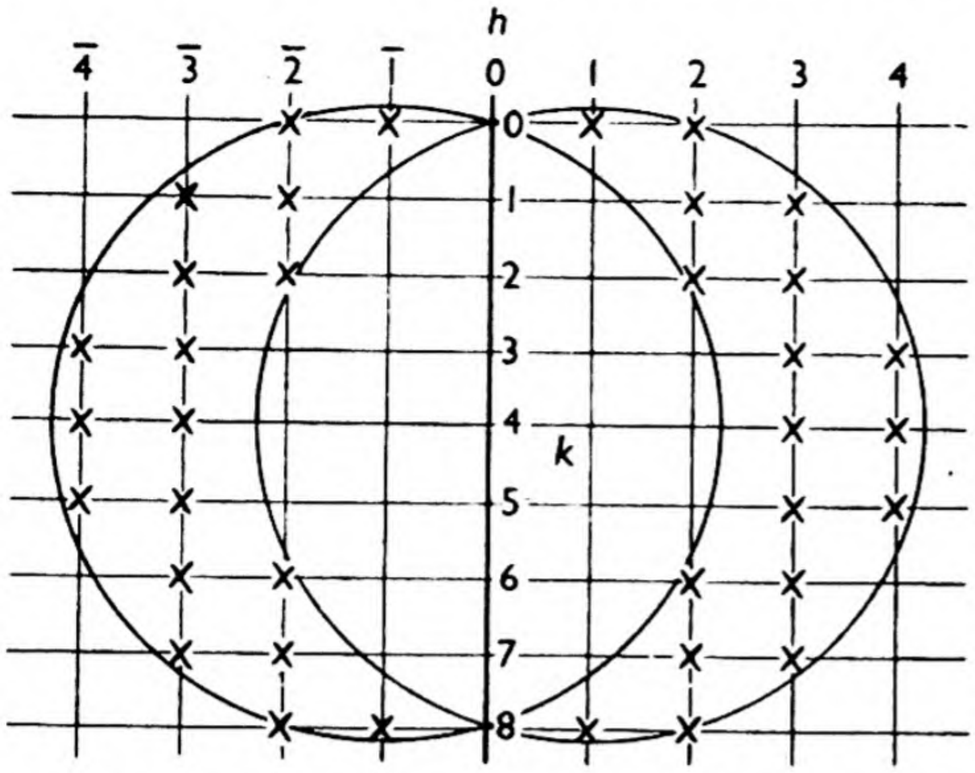

FIG. 194.1. Reciprocal lattice and reflecting circles for a symmetrical oscillation photograph. The four reflections with highest θ are 280, 180, 370, 270; measurement of these should give an accurate value of b

axis of oscillation; then the Bragg angles of spots lying on the zero layer line of the resulting photograph are given by

$$\sin^2\theta_{hk0} = \tfrac{1}{4}(h^2a^{*2} + k^2b^{*2}) \qquad (9)$$

or

$$\sin^2\theta_{hk0} = (\lambda^2/4)(h^2/a^2 + k^2/b^2). \qquad (10)$$

In order to analyse the photograph, approximate values of a and b are required. If the axial ratios are known from measurement of interfacial angles, the values of a and b can be obtained by calculation from the value of c derived from the layer lines of the oscillation photograph (**5,** 1.5); otherwise separate photographs must be taken. The reciprocal lattice can then be constructed and the photograph analysed by the usual methods (**5,** 2.5), particular attention being paid to the unambiguous indexing of spots with θ greater than 60°. In general, an oscillation photograph will not be symmetrical, and therefore the procedure for measuring θ, analogous to the measurement of a powder photograph, cannot be applied. If, however, the limits of oscillation are set to make equal angles with an axis, a symmetrical photograph will be obtained, as is shown in Fig. 194.1; this has an additional advantage, as will be shown later. The Bragg angles of the spots can then be measured in the same way as those of the lines on a powder photograph. If a special camera with calibrated knife edges is not available, the van Arkel mounting (**11,** 3.1) will be found to give a reasonable accuracy without any special precautions (Farquhar and Lipson, 1946). (It must be emphasised that this practice is recommended only for accurate measurement; for indexing, the ordinary mounting is far better.)

To determine the value of a, a photograph should be taken with the crystal oscillating so that the a-axis coincides with the direction of the X-ray beam at the middle of the oscillation; the high-angle spots will then have large h indices. The advantage of this may be seen by rewriting equation (10) as

$$\sin^2\theta_{hk0} = (\lambda/2a)^2\{h^2 + (a^2/b^2)k^2\}$$

or

$$a = \{\tfrac{\lambda}{2}\sqrt{h^2 + (a^2/b^2)k^2}\}\ \mathrm{cosec}\ \theta \qquad (11)$$

If h is large with respect to k, a small error in a/b will not greatly affect the derived value of a. Values of a can be derived from several spots and the true value determined by extrapolation against $\sin^2\theta$. This function is used in preference to $\frac{1}{2}(\cos^2\theta/\sin\theta + \cos^2\theta/\theta)$ because errors due to eccentricity of the specimen and film shrinkage are likely to be larger than those due to absorption (**13,** 2.2).

The value of b can be determined in a similar way. If the results show that b/a is considerably in error, it may be worth while repeating the calculations with the more accurate value. It is unlikely that further refinement would be necessary.

An example of the use of these methods is given in the table on p. 195 and Fig. 194.2. The upper part of the table gives the calculation of c with $c/b = 0{\cdot}7275$, as given by Groth (1906). Fig. 194.2 shows that the

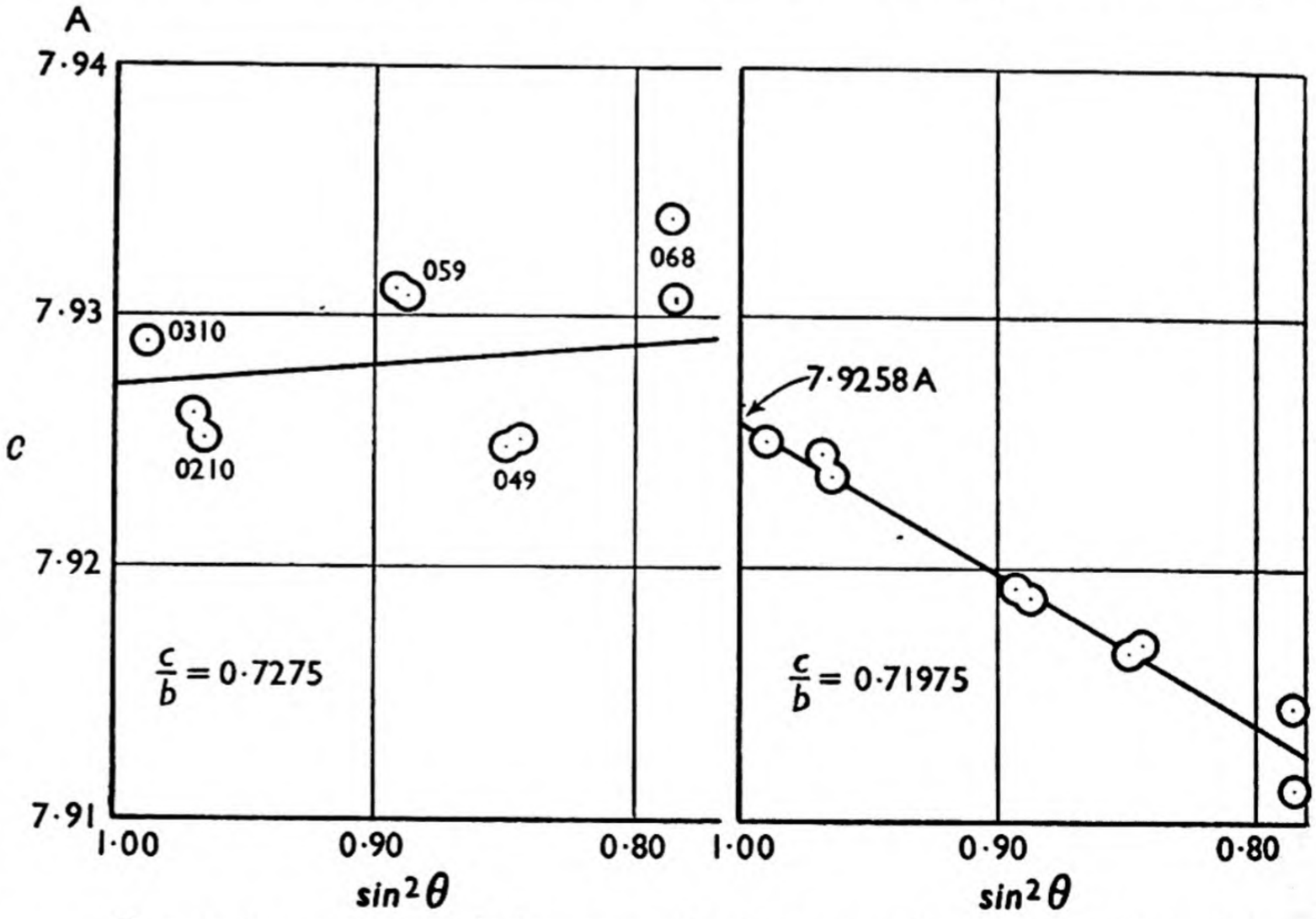

FIG. 194.2. Extrapolation curve for the accurate determination of c for thallium hydrogen tartrate, with (left) an inaccurate value of the axial ratio, and (right) an accurate value of the axial ratio

DERIVATION OF c FROM AN OSCILLATION PHOTOGRAPH OF THALLIUM HYDROGEN TARTRATE TAKEN WITH COPPER $K\alpha$ RADIATION IN A CAMERA OF RADIUS 3 CM.

$h\,k\,l$	RADIATION	θ	cosec θ	$\frac{\lambda}{2}\sqrt{\frac{c^2}{b^2}k^2+l^2}$	c (in A.)	$\sin^2\theta$
0 6 8	α_1 α_2	62·267 62·496	1·129 783 1·127 423	7·019 63 7·037 15	7·9307 7·9338	0·784 0·787
0 4 9	α_1 α_2	66·832 67·171	1·087 720 1·084 991	7·285 64 7·303 82	7·9248 7·9246	0·845 0·850
0 5 9	α_1 α_2	70·529 70·930	1·060 660 1·058 067	7·477 08 7·495 74	7·9307 7·9310	0·889 0·893
0 2 10	α_1 α_2	79·153 79·892	1·018 192 1·015 767	7·783 62 7·803 04	7·9252 7·9261	0·965 0·969
0 3 10	α_1	83·894	1·005 705	7·883 83	7·9288	0·989
0 6 8	α_1 α_2			7·002 46 7·019 94	7·9113 7·9145	0·784 0·787
0 4 9	α_1 α_2			7·278 30 7·296 46	7·9168 7·9166	0·845 0·850
0 5 9	α_1 α_2			7·465 90 7·484 54	7·9188 7·9192	0·889 0·893
0 2 10	α_1 α_2			7·781 90 7·801 33	7·9235 7·9244	0·965 0·969
0 3 10	α_1			7·880 02	7·9250	0·989

results are erratic, but they suggest that $c=7{\cdot}927\pm 0{\cdot}003$ A. In the lower part of the table the calculations are repeated with $c/b=0{\cdot}71975$, and, as shown in Fig. 194.2, the results are now consistent. Extrapolation to $\sin^2\theta=1{\cdot}0$ gives $c=7{\cdot}9258\pm 0{\cdot}0003$ A.

4.3 Procedure for monoclinic and triclinic crystals. Similar methods can be used to determine $a\sin\beta$, b, and $c\sin\beta$ for a monoclinic crystal, because if a and c are set as axes of oscillation the axes of the reciprocal lattice used for analysis are orthogonal. But in order to determine β, the crystal must have b as axis of oscillation, and the corresponding section of the reciprocal lattice is not rectangular. This results in two difficulties; first, it is not possible to obtain a symmetrical oscillation photograph; secondly, the Bragg angles depend on three quantities a^*, c^* and β^*, and so the calculation is more complicated. Various experimental means must be used to overcome the first difficulty. For example, it is possible to give the crystal several small ranges of oscillation so that chosen reflections are caused to appear first on one side of the film and then on the other. Alternatively, the crystal may be covered with a layer of powder which gives lines at known Bragg angles, the Bragg angles for the spots being obtained by interpolation. The only strictly logical method of performing the calculations is the least-squares method described by Cohen (1935); but no doubt, by suitably choosing reflections, it should be possible to devise methods similar to those described in **13**, 4.2.

Similar considerations apply to triclinic crystals, in which three constants are involved in the Bragg angles of spots on the zero layer of an oscillation photograph about *any* axis.

4.4 Choice of radiation. If the cell dimensions are large, it is unlikely that there will be no reflections with θ near 90°, whatever wave-length is used. If, however, it should happen that no such reflections

occur with a particular wave-length, another wave-length must be chosen. No general rules about the choice can be given; it will be necessary to take photographs with different wave-lengths to find which is most suitable.

5. Applications

5.1 Determination of thermal expansion coefficients. X-ray methods are well suited to the determination of coefficients of thermal expansion because the specimen, being small, can easily be kept at a uniform temperature. At one time there was some suspicion that the coefficients so measured were not identical with those for massive material, but recent work has established many cases of good agreement; Wilson (1941, 1942*b*), for example, found good agreement for various results on aluminium. X-ray methods have the additional advantage that the principal coefficients of thermal expansion of uniaxial substances can often be determined without the necessity of obtaining single crystals (Jay, 1934; Nelson and Riley, 1945*b*).

5.2 Determination of phase-boundaries in equilibrium diagrams. Suppose that the line *CD* in Fig. 196 represents the boundary between the α phase-field and the $\alpha+\beta$ phase-field in the binary

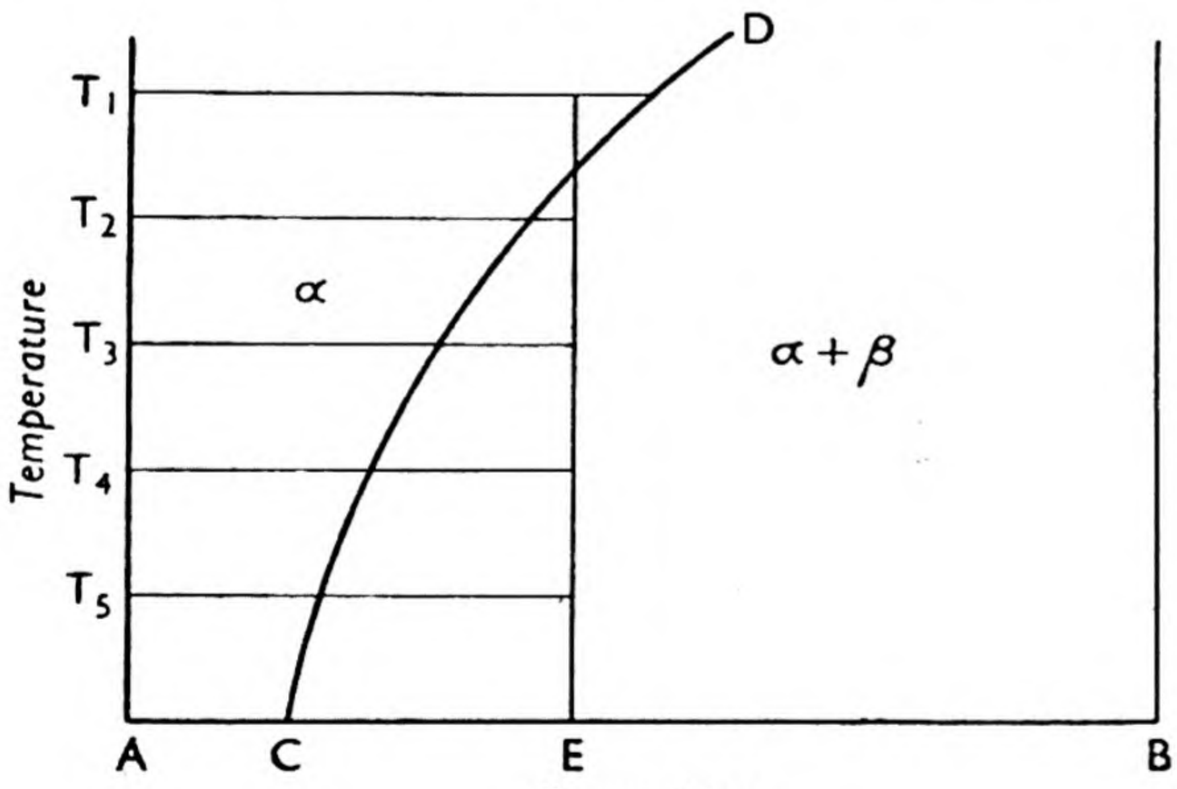

FIG. 196. The boundary between a single-phase region α and a two-phase region $\alpha+\beta$, in the phase diagram for a binary system

equilibrium diagram of the substances *A*, *B*. By quenching specimens from the temperature T_1 it may be possible to maintain them in states of solid solution, and hence to derive the curve of a cell dimension as a function of composition. If now the mixture of gross composition *E* is quenched from various temperatures T_2, T_3, T_4, ... it should always be two-phase, although the composition of the α-phase will not be constant. Measurement of the cell dimensions should enable the compositions of the α-phase to be found from the data obtained.

This method has been much used for the study of binary equilibrium diagrams of metals. It is particularly powerful because many data can be obtained from few alloys, but there are some precautions that have to be taken if dependable results are to be obtained (Hume-Rothery and Raynor, 1941). First, the initial cell dimensions must be those of alloys of which the composition is reliably known; secondly, the curve of cell dimension against composition should have an adequate number of points on it, as there may be discontinuities in slope (Bradley and Jay, 1932*a*); thirdly, the curve must not be extrapolated for data that do not lie within the range studied; and fourthly, it must be verified that there is no decomposition of the filings during quenching. The argument that the cell dimensions may be altered by the presence of internal strains (Frommer, 1943) is probably not valid for powders, since it is unlikely that such strains would have a preferred direction in the specimen; strains could, however, produce a broadening of the X-ray reflections.

5.3 Measurement of densities and molecular weights. Densities of substances can sometimes be measured most accurately by X-ray methods, the formula (Stockdale, 1940; Foote and Jette, 1940; Bragg, 1947) being

$$\rho = 1{\cdot}66020\Sigma A/V, \qquad (12)$$

where ρ is the density, ΣA is the sum of the atomic weights of the atoms in the unit cell, and V is the volume, in A.^{3}, of the unit cell.

The X-ray method can be used to determine atomic weights. Johnston and Hutchinson (1942) have in this way produced a value of the atomic weight of fluorine. Similarly, if the number of molecules in the unit cell of an organic substance is known, the molecular weight of the compound can be derived. It may happen that the space group has been determined, but the number of molecules per unit cell is not known. From the space group we can deduce the possible values of this number and hence a series of possible values of the molecular weight. As we always know the lowest possible value of the number of molecules per unit cell, this gives us the upper limit to the possible values of the molecular weight, which is often very useful information.

5.4 Measurement of internal stresses. The detection of small changes in the Bragg angles of X-ray reflections can provide useful information about the presence of internal stresses.

The principle of the method is that the change, δd, in the spacing of a set of planes in a crystal is given by the relation

$$\delta d/d = T/E, \qquad (13)$$

where E is Young's modulus and T is the applied stress, assumed to be perpendicular to the planes. If T is parallel to the planes, it will produce a Poisson contraction in the spacing, given by

$$\delta d/d = -\sigma T/E, \qquad (14)$$

where σ is Poisson's ratio. If T is not parallel to the reflecting planes, two components of the stress must be found and this can be done only by taking two or more photographs with the X-ray beam making different angles of incidence with the surface of the specimen (Thomas, 1941).

There are certain difficulties in the application of these methods which are sometimes overlooked. For example, the value of E is not necessarily that for a macroscopic polycrystalline specimen; even for a cubic crystal, the value of Young's modulus and of the rigidity modulus, upon which σ depends, are not independent of direction. This does not matter for mechanical testing, but the X-ray method selects special directions in each crystal for measurement. It seems that the most satisfactory way of finding the value of E appropriate for a given reflection is to measure the change in spacing of that reflection produced by a known stress in a similar piece of material (Frommer and Lloyd, 1944); in other words, the method is best used for *comparing* stresses.

Moreover, if the material under test is an alloy, it is always possible that changes in spacing may be due to changes in composition from point to point in the specimen; it is often difficult to produce a large casting, for example, with the same composition throughout. Nevertheless, the change of spacing produced by the solution of certain elements in others (for example, chromium in iron) is so small that differences in composition of one or two per cent are inappreciable; then changes in spacing can reasonably be attributed to the presence of internal stress. But if the change in spacing is large, as in the solution of silicon in iron (**17**, 3.2), a test for uniformity of composition must precede any determination of residual stresses from spacing measurements.

Although cell dimensions can be measured with high accuracy, it does not follow that the measurement of stress can be made with the same degree of accuracy, because only small differences are involved. X-ray reflections given by commercial materials are usually not particularly sharp, and it is probably safe to say that the accuracy in spacing measurement is not better than 0·01 per cent (**13**, 2.7). For metals, σ is usually about 0·3, so that the corresponding error in T is 0·0003 E. For steel, $E = 2 \times 10^{12}$ dynes/cm.^{2}, so that the limits of error of measurement of T will be about $\pm 6 \times 10^8$ dynes/cm.^{2} or about ± 4 tons/sq. in. Generally the accuracy will be less than this, but it may, in special cases, be greater.

PROBLEM

The following data have been obtained from a powder photograph of sodium chlorate, which is cubic:

$h^2+k^2+l^2 = N$	Radiation	θ (degrees)
72	Cu$K\alpha_1$	$83{\cdot}82_5$
70	α_2	$79{\cdot}31_8$
	α_1	$78{\cdot}58_2$
69	α_2	$77{\cdot}30_9$
	α_1	$76{\cdot}68_5$
68	α_2	$75{\cdot}56_8$
	α_1	$75{\cdot}01_7$
66	α_2	$72{\cdot}55_0$
	α_1	$72{\cdot}09_8$
65	α_2	$71{\cdot}20_7$
	α_1	$70{\cdot}79_3$

Deduce an accurate value of the lattice parameter.

CHAPTER 14

MEASUREMENT OF THE INTENSITIES OF X-RAY REFLECTIONS

1. Photographic Methods

1.1. Introduction. Most photographic records of reflections of X-ray beams from crystals are obtained as dark lines or spots on a clear background. The essential problem is the correlation of the amount of blackening with the number of X-ray quanta giving rise to it. This is not simply a problem in photographic photometry, since many factors (Chapter 15) influence the intensity, but we shall consider the problem first of how to find the number of X-ray quanta producing a given spot.

The *blackening*, D, of a photographic film suitable for X-ray crystallography is defined in terms of the intensity, I_0, of the light incident upon it and the intensity, I, transmitted through it, by the relation

$$D = \log_{10} I_0/I.$$

The quantity D has been shown to be proportional to the total number of X-ray quanta falling on unit area of the film in the region examined, provided that D is less than a certain value which varies with the film and the method of processing. Thus to obtain a measure of the number of X-ray quanta which have fallen on a film, it is necessary to find the ratio of the incident and transmitted beam after traversing a *uniformly* darkened region.

1.2 Types of photometer. The ratio of the intensity of the light incident upon the darkened photographic film to that transmitted through it may be found by means of three distinct types of photometer. The simplest is that which uses a single light source and one photocell only. The current through the photocell is registered on a meter. The deflection of the meter is observed, first without the darkened film interposed in the light beam and then with it. The ratio of these two deflections gives the value of I_0/I. The success of the measurement depends on the constancy of the light source both in position and intensity. In practice, the sagging of the light filament and fluctuations in potential across the filament are usually factors which limit the accuracy of this type of measurement.

The light-meter part of the instrument can be made more simple by equalising the intensities of the two beams. This is achieved by inserting a calibrated neutral wedge in the path of the direct beam when its strength is being determined. Such a wedge is arranged so that the density increases uniformly along its length. The method of using such a wedge is seen by the following analysis.

Suppose the distance along the wedge from the thin end to any point is d and the angle of the wedge is α. Then the corresponding thickness of absorbing material is $d\alpha$. If κ is the optical absorption coeficient, we have for the ratio of the intensities of the incident and transmitted light beams at this point of the wedge,

$$I_0/I = \text{exp. } \kappa d\alpha,$$

or

$$\log_{10} I_0/I = 0{\cdot}434\ \kappa\alpha.d.$$

The quantity $0{\cdot}434\ \kappa\alpha$ is a constant for the wedge, usually supplied by the maker, and we may replace it by the symbol q. Thus the blackening D of the wedge is given by

$$D = qd.$$

Suppose now that the number of X-ray quanta which have fallen on unit area of the spot or line (assuming it to be uniformly blackened all over) is p_1, whereas the corresponding number for the surrounding background of the spot is p_2. Then we have seen (**14,** 1.1) that

$$p_1 = cD_1, \quad p_2 = cD_2,$$

where c is a constant for the X-ray film and its conditions of processing, and D_1 and D_2 are the corresponding blackenings produced. We require to know $p_1 - p_2$.

Then $$p_1 - p_2 = c(D_1 - D_2) = cq(d_1 - d_2),$$

where d_1 and d_2 are the corresponding distances from the thin end of the optical wedge.

Thus, by the use of a calibrated wedge, the measurement of the X-ray intensity is reduced to a linear measurement of the displacement of the wedge which is required to balance the shifting of the film from ' line ' to ' background '.

The curve relating density to exposure varies for most X-ray films with the conditions of development, and from one sample of film to another. It is, therefore, essential to produce on a portion of the film which carries the photograph under examination a set of blackened steps the exposures of which are in a known ratio, or a wedge, the exposure at each point of which is known. Provided that the calibration steps cover the range of density found in the spot or line,

the blackening at any point can be converted into a quantity proportional to the X-ray exposure. One way of producing such a stepped or continuous wedge is to rotate in front of the film a wheel from which a stepped or spiral sector has been cut out. The steps on the sector are arranged so that the exposures along a radius of the rotating wheel increase in known ratios

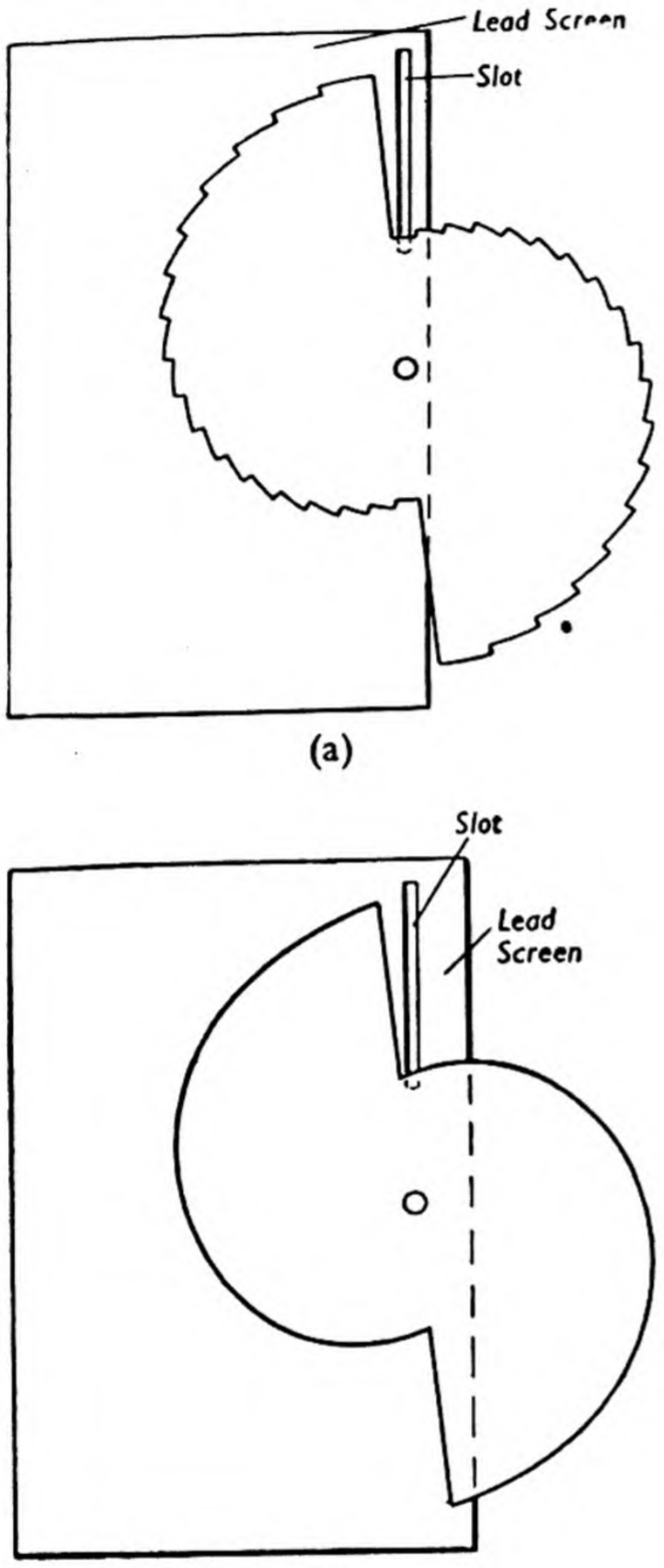

FIG. 199.1. (*a*) Stepped wheel and (*b*) spiral wheel for the derivation of the intensity-density curve of an X-ray film

in passing from one step to the next. A lead screen with a rectangular slot in it is arranged with the length of the slot parallel to the radius of the sectored wheel (Fig. 199.1). The film, after exposure to the reflections from the single crystal or powder, is placed under the lead screen so that a strip, usually near one edge, receives the imprint of the steps or wedge. To obtain a uniform intensity of the X-rays all along the length of the rectangular slot, the rotating wheel is set up several metres from the X-ray tube.

Fluctuations of the intensity of the light are usually a serious limitation in accurate photometry. If a mains supply is used to work the lamp, smoothing devices have to be introduced to keep the fluctuations of light intensity down to 1 per cent. If an accumulator is used as the source, it has to be used across a D.C. mains supply so that there is no steady fall in current during use. Finally, lamps blacken gradually and recrystallisation of the filament causes sagging

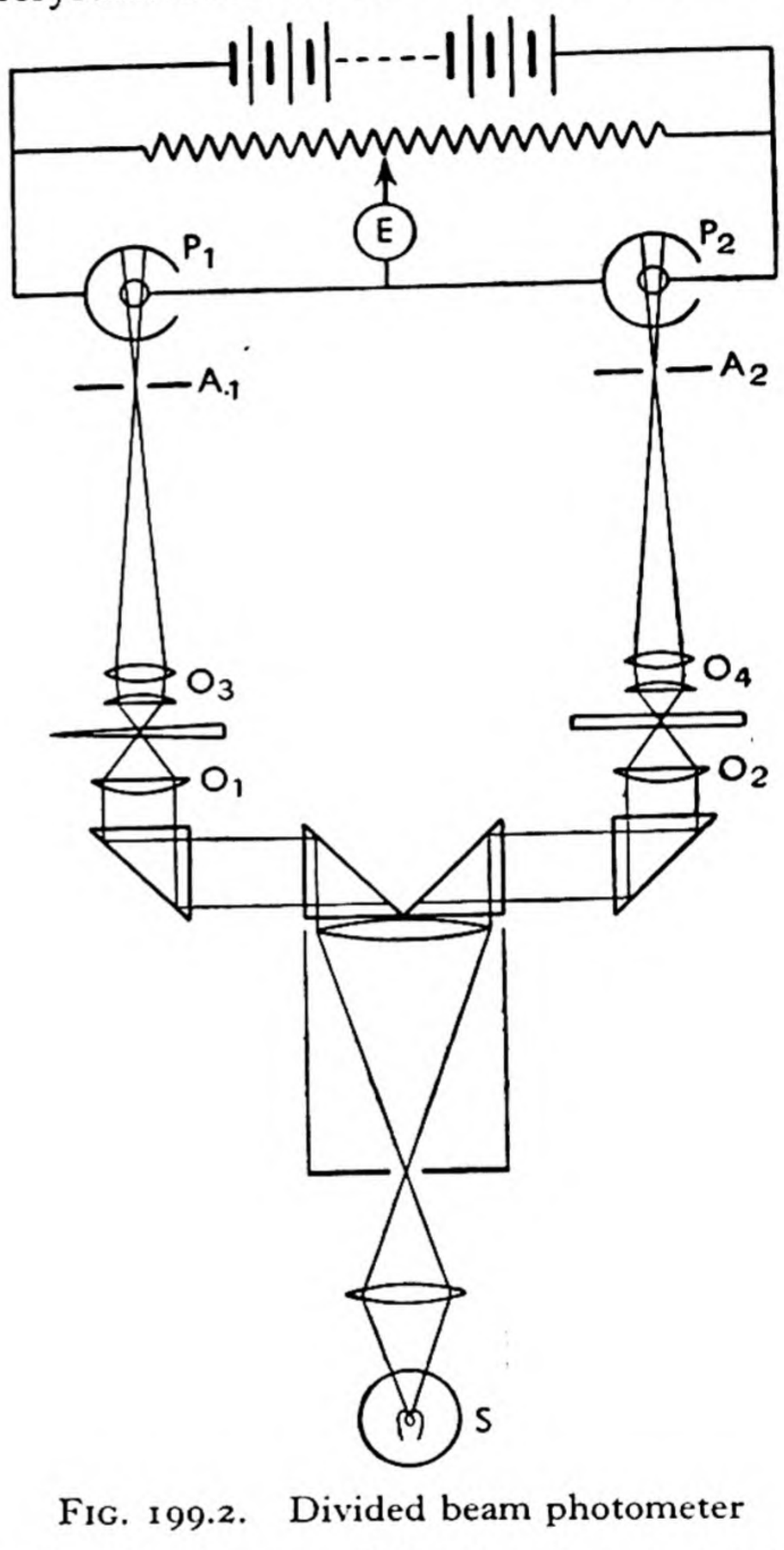

FIG. 199.2. Divided beam photometer

and drift of the image of the fiament across the slits of the photometer.

For these reasons it has become customary to employ a second type of photometer. In this instrument a light beam is divided and the intensity of light transmitted through the wedge is compared with that transmitted through the film. In Fig. 199.2 is shown the principle of the divided-beam type of photometer. The apparatus illustrated by this diagram is always used as a null instrument. The only limitationis slits by variations in the sensitivity of the photocells. The difficulty can be overcome by alternately sending the two beams leaving the objectives O_3, O_4 into the same photocell by the movement of a sliding mirror or other device.

A third type of photometer for studying lines has also been described (Williams and Hiltner, 1940); this has the advantage over the second type described above that the photometric curve is automatically traced. The light beam is divided into two parts, one part passing through the wedge and the other part passing through the X-ray film under investigation. The photographic wedge used in one of the light paths is prepared on the same film as that on which the X-ray photograph is made. This wedge is mounted on a carriage which as it moves across the first light beam causes the recording light spot to move across the photographic paper in, say, a vertical direction. The photographic line which is being photometered is made to traverse the second light beam in a horizontal direction. The movement of the photographic record is geared to the movement of the film and is also horizontal. An electro-mechanical system is used to ensure that the wedge automatically moves into such a position that the intensity of the light beam passing through it is equal to that of the beam passing through the line. In this way an automatic record giving the X-ray intensity at all points along the film is obtained.

1.3 Fundamental conditions of measurement. If the darkened area of the film under examination has a small clear space in it, more light may be transmitted through it than through all the rest of the darkened space. This difficulty may arise where there are 'pin-hole' blemishes in the photographic emulsion. The genuine photographic spots and lines due to X-ray reflections are small and vary greatly in density from the centre to the outside; areas which are uniformly black may be no more than 0·1 mm. × 0·1 mm. In order to get accurate results it may then be necessary to examine areas no larger than this at one time, since areas which are not uniformly blackened give inaccurate results. For example, suppose that in an area under examination one half had been irradiated with p X-ray quanta per unit area and the other half with $2p$. Then the number per unit area for the whole area should be $1{\cdot}5p$. Suppose that p quanta per unit area produce a blackening of unity.

Then we have

$$1 = \log_{10} I_0/I_1 = cp, \qquad I_1 = \tfrac{1}{10}\, I_0,$$
$$2 = \log_{10} I_0/I_2 = c \,.\, 2p, \quad I_2 = \tfrac{1}{100}\, I_0,$$

where I_0 is the intensity of the incident light and I_1, I_2 are the intensities of the beams transmitted through the two contiguous darkened areas. If I_3 is the transmitted light through the composite area, then

$$\frac{I_3}{I_0} = \frac{1/10 + 1/100}{2} = 0{\cdot}055.$$

Hence the corresponding darkening D_3 would be

$$D_3 = \log_{10} 1/{\cdot}055 = 1{\cdot}26.$$

Thus we should obtain a number of X-ray quanta equal to 1·26 instead of the true value 1·5.

Errors due to this cause can be decreased by using less dense spots. If, for example, within the area of the spot examined with the photometer, there are equal portions of densities 0·1 and 0·2 respectively, then the observed density would be 0·147 instead of the true value 0·15. This is not a complete solution, however, since working with weak spots increases the errors due to the uncertainties in the general background and to accidental defects due to dust and surface markings of the film. Thus the aperture limiting the light beam reaching the photocell must be small enough to keep the variations of blackening over the area examined within a prescribed range depending on the accuracy aimed at in the final result. If the aperture is reduced too far, insufficient light will reach the photocell to enable it and its recording mechanism to operate with the required accuracy.

1.4 Application to single-crystal photographs. Single-crystal photographs frequently contain small well-defined spots. To examine areas of uniform blackening within the spots, a magnified image of the spot is projected on to a small aperture and the light passing through this aperture is balanced against the light passing through a wedge, such as that described on p. 198. By fine adjustments the image of the spot can be made to traverse the fixed aperture; in this way it is divided into several hundred areas of uniform density. The area well outside the spot itself must be examined in order to obtain a reliable measure of the general background blackening. By interpolation, the X-ray exposure of the background at every point of the spot examined in the photometer is then obtained and subtracted from the observed exposure. Finally, the total number of X-ray quanta which have fallen on the film to produce the spot is obtained by simple addition of the effects of all the separate contiguous areas. An integrating photometer which enables the spot to be surveyed in a systematic manner and provides a means of determining the total X-ray flux that produced it, has been described by Robinson (1933).

1.5 Application to powder photographs. The photographic density of a line on a powder photograph varies rapidly in a direction perpendicular to the length of the line and only slowly along its length. Such lines are examined in the photometer in the same way as single-crystal spots, except that a rectangular aperture instead of a square aperture is used to limit the portion of the line under examination.

SECT. 2

The length of the aperture is, of course, arranged parallel to the length of the line, and the breadth is made so small that there is no appreciable variation of density within the rectangle under examination. The densities at a large number of points across the line are determined by the photometer and converted, by means of a calibration curve, into readings of the X-ray intensity at corresponding points. A graph is usually drawn showing the variation of the X-ray intensity across the line (Fig. 201). When the

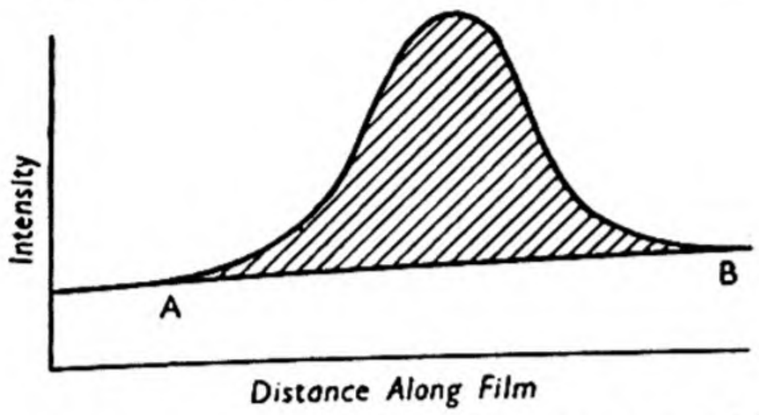

FIG. 201. Diagram showing the derivation of the total intensity of a powder line

total intensity of the reflection is required, a base line is drawn connecting the background curves on either side of the line as shown at *AB* in Fig. 201. The shaded area under the curve and above the base line is proportional to the intensity of reflection corresponding to this powder line.

1.6 Visual methods. In many single-crystal studies it is not necessary to find the intensities of the X-ray reflections with the accuracy that can be obtained by the methods described in the previous sections. Visual estimation can be used to put intensities into classes which differ by about 10 per cent, and this is often sufficient for the determination of crystal structures.

The visual method consists in matching the intensity of each spot on the film with a spot of known intensity. A series of standard spots is prepared of graduated intensities covering the range of intensities of the spots under investigation. The standard spots can be obtained with a rotating sector (**14,** 1.2), the slot in Fig. 199.1 being replaced by a series of small holes. Alternatively, the crystal itself may be made to produce the standard spots at successive points along the film. The crystal is set so that it passes through a reflecting position and exposures in the ratios of integral numbers are given.

There are two important defects of visual estimation. The first is that the eye is not sensitive to changes of intensity when the blackening is large; that is, all strong spots tend to look equally black. This difficulty can be overcome by placing several films simultaneously in the camera (Robertson, 1943). The top film will be the darkest and can be used for estimating the relative intensities of the weak and moderate spots; the films under this one can be used for the moderate and strong spots, and the results for the moderate spots can be used to put all the estimations on the same scale. The second defect is that the visual method cannot make allowance for variation in the shape of the spots. Since the shapes of the spots usually change greatly with θ, the visual method may introduce an error which is a function of θ; the possibility of such an error must always be borne in mind when interpreting the results.

1.7 Measurement of absolute intensity of reflection. When only relative measurements of the intensity of X-ray reflections are required, the methods described above are quite suitable. But to obtain absolute measurements, that is, to obtain for any plane the fraction of the incident X-ray quanta which it reflects as it passes through the reflecting position, it is necessary to employ a standard crystal with which the crystal under test may be compared. Goniometers have been devised (Robertson, 1934, Wooster and Martin, 1940) by which the crystal under investigation and the standard crystal can be brought into the X-ray beam alternately, for equal lengths of time or for times which bear a known ratio to one another. In this way there are superimposed on the same film the reflections from the two crystals. The integrated reflection of spots corresponding to both crystals is found, and thus the reflections from the crystal under test may be referred to those from the standard crystal which has been investigated with an ionisation spectrometer (**14,** 2.2).

2. Ionisation method

2.1 The ionisation spectrometer. An ionisation spectrometer resembles an optical spectrometer in that it has a collimator, a reflecting crystal surface and a recorder of the reflected beam. In this apparatus the recorder is an ionisation chamber, whereas in an optical spectrometer the reflected light is received into a telescope. The ionisation spectrometer also has two graduated scales, which give the angular setting of the crystal and of the ionisation chamber. The collimator of the X-ray beam consists of two narrow slits the length of which is vertical and parallel to the axis about which the crystal and chamber rotate.

When the instrument is used to measure the intensity of X-ray reflection from a crystal, the latter is rotated through the reflecting position, and different parts of the surface and of the interior near the surface reflect at different settings. The aperture in front of the ionisation chamber is made large enough for all these reflections to be recorded by the stationary chamber. In addition to the mechanical part of the instrument, there is also an electrical part by which the very small ionisation current (approx.

10^{-13} amp.) produced by the X-rays entering the chamber can be amplified and recorded. Details of a modern instrument are available in the literature (Wooster and Martin, 1936).

2.2 Application to single crystals. At first sight it appears that the intensity of reflection from a crystal face might be obtained by setting the crystal to the position of maximum reflection and determining with the ionisation chamber the intensity then reflected. If, now, the chamber were set to receive the direct beam, the ratio between the reflected and direct beams would apparently give the correct measure of the reflecting power of the crystal. This is true for the specular reflection of light, but it is not true for the reflection of X-rays, because there is a fundamental difference between the reflection of X-rays and that of light.

A crystal is seldom perfect, and if it be rotated uniformly through the position of maximum reflection different portions of the crystal are successively brought into the position of maximum reflection. Thus when the crystal is reflecting the greatest amount of X-rays, only a part of the crystal is in fact contributing, and in order to give every portion of the crystal a chance to contribute the crystal must be rotated through the whole reflecting position. Because of this complication, a special measure is adopted by means of which we can express the total reflection from the crystal round and about a given setting. This measure is called the *integrated reflection*, and is expressed in radians, or more usually micro-radians. It is defined as follows :

Supposing that, on rotating a crystal at a uniform angular velocity through the setting corresponding to the maximum intensity of reflection from a crystal face, the total number of X-ray quanta received in the ionisation chamber is P. We now proceed in terms of an imaginary experiment. Suppose that the crystal could be changed in such a way that it would reflect all the radiation incident upon it in every setting and that it was rotated at the same angular speed as in the previous (real) experiment. Then the integrated reflection ρ is that angle through which the crystal would rotate in the second experiment in order to produce the same number P of X-ray quanta in the ionisation chamber as in the first experiment (Fig. 202). The following alternative definition is sometimes given (Darwin, 1922). If E is the total energy reflected during a sweep at a uniform angular velocity ω through the reflecting setting, and I is the intensity of the primary beam, then the integrated reflection ρ is given by the expression $E\omega/I$. Since ω/I is the angle through which the crystal has turned during the time that unit incident X-ray energy has fallen on the crystal, $E\omega/I$ is equal to the angle through which the crystal has turned while an energy E has fallen on it, that is, $E\omega/I$ is equal to ρ.

When the atmosphere is not so damp that electric charge leaks away very rapidly or where radioactive contamination does not produce the same effect, the most convenient method of finding ρ is to allow the charge on the insulated electrode of the ionisation chamber to accumulate as the crystal rotates through the position of maximum reflection. The total charge collected is directly proportional to ρ. If now a standard crystal is substituted for the unknown and the experiment repeated, the intensity of the monochromatic component of the incident beam can be found. This ratio of integrated reflections combined with the absolute value for the standard (usually rocksalt (200), $\rho = 550 \times 10^{-6}$ for Rh$K\alpha$ (Bragg and Bragg, 1924)) determines the absolute value of the unknown ρ.

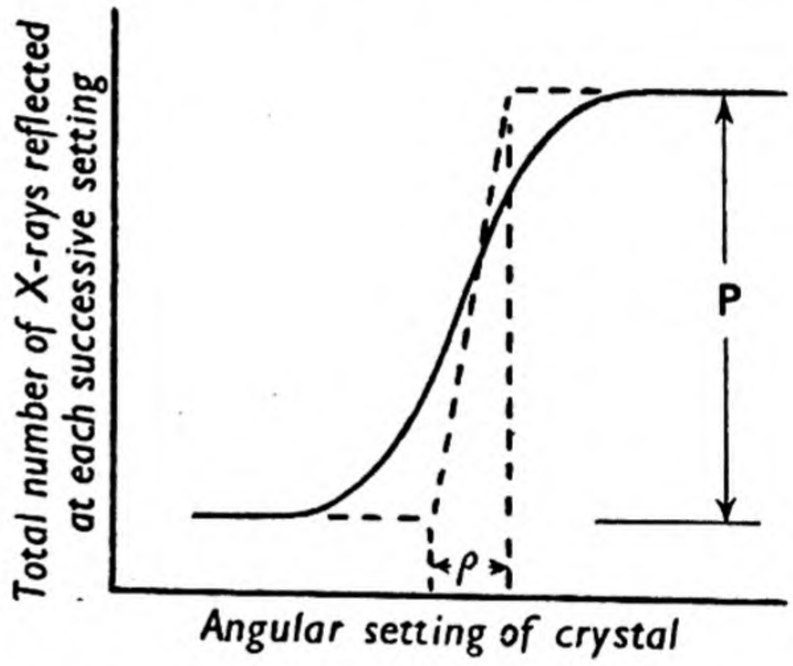

FIG. 202. Sweep curve obtained in an ionisation spectrometer when the charge is continuously accumulated on the central electrode of the ionisation chamber. The dotted curve indicates how the integrated reflection ρ is derived from the experimental (full) curve

When insulation is faulty, it may be more convenient to read the ionisation current at each separate setting of the crystal as it is rotated through the position of maximum reflection. In this case the integrated reflection is proportional to the area under the curve obtained by plotting ionisation currents as ordinates and angular settings as abscissae (Fig. 203). The value of ρ can be found as before by using a standard crystal to calibrate the intensity of the monochromatic component of the direct beam.

If it is desired to measure ρ without using an intermediate standard such as rocksalt, by sending the incident beam directly into the ionisation chamber, care must be taken to ensure that the beam is truly monochromatic. The direct beam is usually one hundred to one thousand times stronger than the reflected beam. To compare the ionisation currents produced by the direct and reflected beams, it is

necessary to reduce the intensity of the direct beam until it is about equal to that of the reflected beam. This is best done by rotating an absorbing wheel with a hole in it in the path of the beam. By making the hole of such a size that X-rays are transmitted for, say, 1/100 of a complete rotation of the wheel, the intensity of the direct beam may be reduced to this fraction of its initial value. Care must be taken to ensure that there is no synchronisation between the

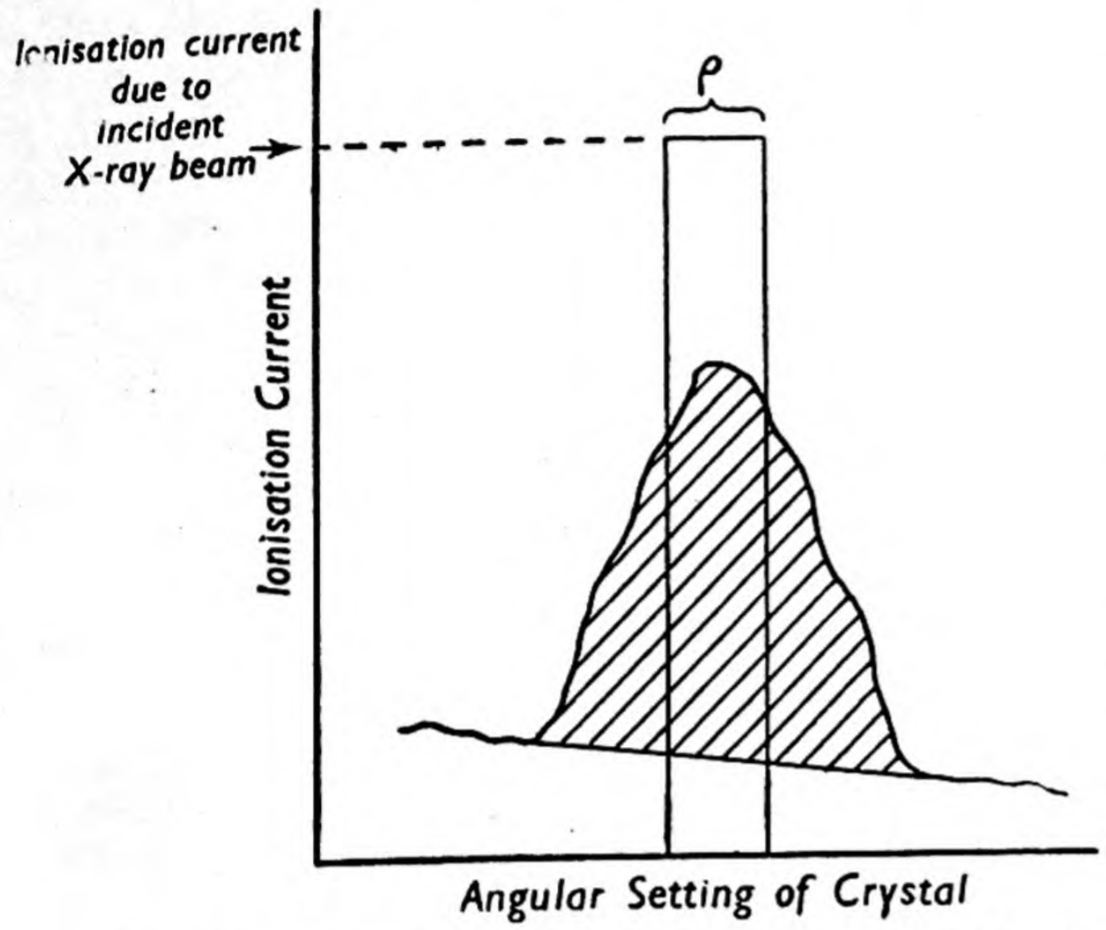

FIG. 203. Illustration of method of derivation of integrated intensity from measurements of ionisation current. The area of the rectangle equals that of the shaded part

rotation of the wheel and the pulses of X-rays coming from the tube, as quite false results may be obtained if there is. For example, if the wheel rotated 50 times per second the intensity transmitted through the wheel might be zero if the opening in the wheel happened to coincide with the path of the X-ray beam every time the potential applied to the X-ray tube was zero.

The direct beam may not be sufficiently reduced in intensity by such a wheel and then absorbing screens have to be used. The absorption coefficient varies approximately as the third power of the wave-length (**2,** 5.1) and in consequence any small admixture of short wave-length radiation will be liable to cause errors. Suppose, for example, that 5 per cent of the radiation in the direct beam is of half the wave-length of the rest—which may happen if the monochromatising crystal reflects the second order (**2,** 6). Then if the absorbing screen reduces the principal $K\alpha$ radiation to one tenth of its intensity, the radiation of half that wave-length will be reduced to about three quarters of its previous intensity. The ionisation chamber will then give readings which are not proportional to the intensity of the monochromatic radiation. This source of error can be avoided by using the 111 reflection of diamond or fluorspar for monochromatising, since the second-order reflection 222 is of zero intensity. The third and higher orders of reflection must be avoided by applying such a voltage to the X-ray tube that such short wave-lengths are not excited (**2,** 6).

2.3 Application to powders and liquids. The intensity of reflection from a powder is usually rather weak for measurement by an ionisation spectrometer, though a number of such investigations have been carried out. If a cylindrical powder specimen is used, the ionisation chamber must be provided with a narrow slit so as to give the necessary resolution. The experiment then consists in plotting the ionisation current against the angular setting of the chamber, the powder specimen remaining stationary.

A more effective way of using the apparatus may be employed if multiple slits are inserted both between the X-ray tube and the specimen, and again between the specimen and the ionisation chamber. These slits are made up of thin metal sheets arranged parallel to one another and separated by thin spacing pieces, so that a large number of narrow parallel beams pass through them. In this way a large area of the specimen can be irradiated without loss of resolving power in the study of the reflected beams. The specimen is usually a plate of suitable thickness set perpendicular to the X-ray beam. Such a method can be applied to liquids, glasses, and plastics. The thickness of the layer examined must, of course, be chosen in relation to the absorption coefficient of the material (**2,** 5.1).

As with single crystals, the measurements may be made absolute either by repeating the experiment with a standard powder or by measuring the intensity of the direct beam, using a rotating slotted wheel or an absorbing screen to reduce the intensity in the required known ratio.

CHAPTER 15

CALCULATION OF THE INTENSITIES OF X-RAY REFLECTIONS

1. Introduction

In Chapter 3 a simple construction was described for finding whether a particular X-ray reflection would occur with the crystal in a certain orientation with respect to the X-ray beam, and this construction was applied to the analysis of oscillation and Weissenberg photographs. In working out the examples given in Chapter 5, however, it will have been noticed that, although all the observed reflections can be accounted for by the construction, not all the reflections permitted by the construction are present on the photographs. Moreover, the intensities of the spots vary greatly; some spots are very intense and some are barely visible. It is obvious, therefore, that the rules expressed by the Bragg law only give the geometrical conditions that must be satisfied if a reflection is to occur; the intensity of the reflection depends on many factors, and may be zero. It is the purpose of the present chapter to enumerate these factors and to show how they may be evaluated.

2. Intensity Formulae

2.1 Expressions for relative intensities. The most important types of photograph for the estimation of intensities are the oscillation, the Weissenberg, and the powder photograph. The rotation photograph is not normally used because it often contains overlapping reflections, and the Laue photograph is not used because the spots are produced by different wave-lengths (**6,** 1.2) and, also, each spot may be composed of several orders from the same set of reflecting planes. The formulae giving the intensities of reflections are given in the International Tables (1935, p. 562), but if we wish to consider only relative values these formulae can be greatly simplified, as follows.

(i) The relative intensities I of spots on an oscillation or Weissenberg photograph are given by

$$I \propto \frac{1+\cos^2 2\theta}{\sin 2\theta} P A_s |F|^2.$$

(ii) The relative intensities I of lines on a powder photograph are given by

$$I \propto \frac{1+\cos^2 2\theta}{\sin^2\theta \cos\theta} p A_p |F|^2.$$

In these expressions, I is the integrated reflection (**14,** 2.2) of the spot or line, and θ is the Bragg angle. The other quantities that appear are as follows: P is a factor that depends upon the angle of inclination ρ of the reflecting planes to the axis of the crystal; we have therefore called it the *rho factor* (**15,** 2.3). $|F|$ is the structure amplitude, which depends upon the types of atoms in the unit cell and upon their relative positions. A_s and A_p are absorption factors (**15,** 2.4) for single crystals and powders respectively. p is a factor which takes into account the possible number of reflections from a single crystal that are superimposed to form a powder line, and is called the *multiplicity factor* (**15,** 2.6, Figs. 156, 157).

2.2 The trigonometrical factor. The expression $(1+\cos^2 2\theta)/\sin 2\theta$ takes two factors into account. The expression $(1+\cos^2 2\theta)$ allows for the partial polarization of the reflected beam; it is valid only if the incident beam is unpolarized. This is generally considered to be true for the characteristic emission from an X-ray tube; it is not true if crystal-reflected radiation (**2,** 6) is used. The expression $\sin 2\theta$ in the denominator occurs because the reciprocal points pass through the surface of the reflecting sphere (**3,** 3) at different rates. Those with θ near 0° obviously move slowly since they are near the origin of the reciprocal lattice; those with θ near 90° move along the surface of the reflecting sphere (Fig. 53). If the reciprocal lattice is rotating with an angular velocity ω, then a point P will move with a velocity $\omega.OP$, which is equal to $2\omega \sin\theta$. The component of this velocity perpendicular to the surface of the reflecting sphere is $2\omega \sin\theta.\cos\theta$, which is equal to $\omega \sin 2\theta$.

The trigonometrical factor for a powder photograph is different, for two reasons. First, the total intensity of a particular reflection is spread out along a curve and only a finite length of this curve is measured. Secondly, the probability that a particular set of planes will pass through a reflecting position is a function of θ.

Values of the two trigonometrical factors are given in Tables 8 and 9.

2.3 The rho factor. The intensity of reflection recorded on a film depends upon the rate at which the crystal planes pass through the reflecting positions. For the equatorial-layer line of a single-crystal photograph, this rate is equal to the angular velocity

of the crystal; but for other layer lines it depends upon the angle of inclination (ρ) of the planes to the axis of rotation. Cox and Shaw (1930) devised a chart which can be used to make the necessary correction for this effect. To use such a chart it should be reproduced as a transparency on a scale corresponding to the size of the camera used; it may then be laid on the photograph and the correcting factor for each spot read off. The observed intensity should then be multiplied by this factor to obtain its true value relative to the other spots on the photograph.

Cox and Shaw also give the results of an experimental investigation of the change in the blackening of the photographic emulsion when the X-rays do not strike the film perpendicularly, and so traverse a greater thickness of emulsion. This condition will obtain for all reflections recorded (*a*) on a flat plate, and (*b*) on non-zero-layer lines of an oscillation photograph taken in a cylindrical camera. For the latter type of photograph they give a correction factor expressed as a function of ζ for copper $K\alpha$ radiation.

2.4 The absorption factor. The intensity of reflection depends upon the linear absorption coefficient, μ. The calculation is simple for the reflection from a face of a single crystal, but for a cylindrical powder specimen the calculations become quite complicated. The relation between A_p and μ has been calculated by Bradley (1935) and put into a form suitable for general use. He has evaluated the quantity A_p that appears in formula (ii) (**15,** 2.1) in terms of μr, where r is the radius of the specimen. His results have been verified by graphical methods by Taylor (1945).

The value of μ to be used is that for the complete specimen and not that for the diffracting material only. If a binding agent is used, the proportion of this in the complete specimen must be known. This proportion can be found, for example, by weighing the specimen, dissolving away the binding agent with a suitable solvent, and weighing the remainder. As explained earlier (**2,** 5.1), the absorption coefficient is the product of the mean density (which can be obtained from the weight and dimensions of the specimen) and the weighted mean of the mass absorption coefficients. From the value of μr so obtained Ap can be plotted as a function of θ, and the values at any particular angle may be obtained by interpolation.

Taylor (1944*a*) and Brindley (1945) have shown that this treatment is not perfectly satisfactory unless the specimen is homogeneous. The intensities of the reflections from a particular crystal in a powder specimen depend not only on the mean value of μ but also on the value μ for the crystalline material itself. Taylor calls the latter factor the *micro-absorption factor* and gives tables of its values as a function of $(\mu - \bar{\mu})a$, where μ is the linear absorption coefficient of the diffracting material, $\bar{\mu}$ is the mean value for the specimen, and a is the effective mean radius of the particles of powder (Taylor, 1944*b*). If this last quantity cannot easily be determined, it is probably best to use Bradley's figures; the results will then be only approximately correct, but, as Taylor points out, the error is equivalent to a change in the temperature factor (**15,** 3.3) and so will not matter greatly for most work.

The absorption factor A_s for single-crystal photographs is more complicated. If the crystal is shaped into the form of a cylinder the calculations for the powder method may be used for the equatorial layer line of the photograph; if the crystal is not cylindrical, graphical methods, such as those described by Albrecht (1939), must be used. For other layer lines there is no general method of solution and it is usual to employ crystals that are so small that absorption is negligible; this, however, is not always possible.

2.5 Extinction. The accuracy of the calculation of intensities is limited also by an effect known as *extinction*; this is due to the invalidity of the underlying assumption that the incident X-ray beam is not affected by the process of diffraction; that the incident beam is so affected is shown by the following reasoning (Lonsdale, 1947*b*, 1948).

X-rays are scattered by an atom because it is set into a state of vibration by the X-rays, and each electron in it then acts as a source of radiation. The wave scattered by a plane of atoms is the resultant of waves scattered with various phase differences, the combined effect being a wave with a phase difference of 90° with respect to the incident beam. Now from Fig. 205 it can be seen that the X-rays reflected from

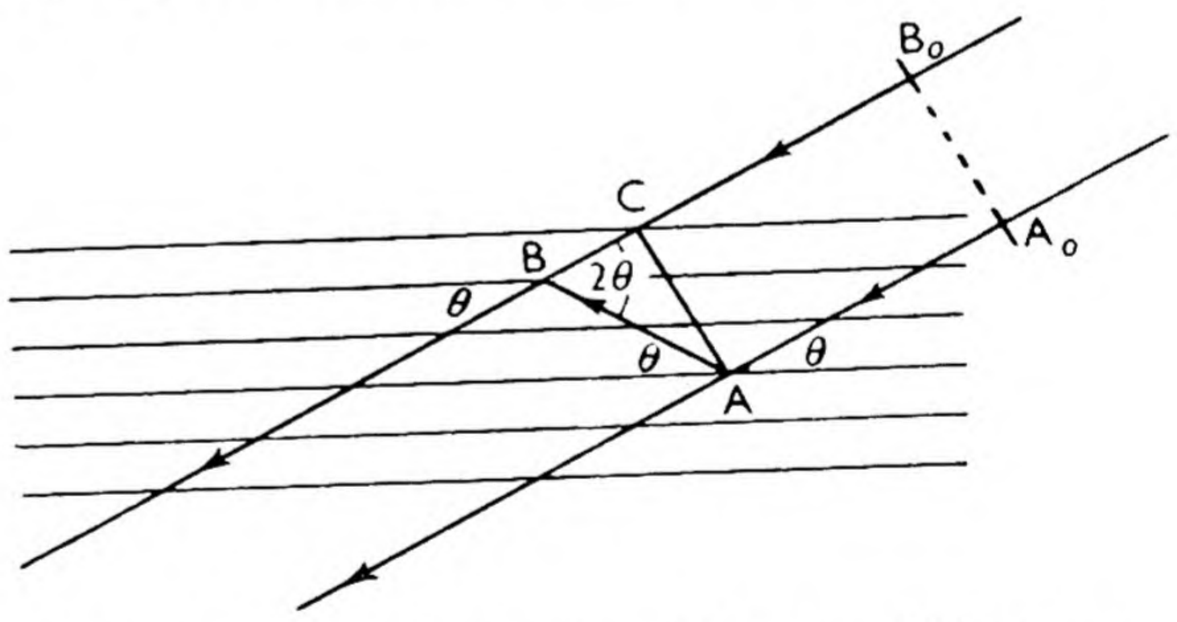

FIG. 205. Double reflection of X-rays, which causes primary extinction

a given set of lattice planes at an angle θ must also be incident at an angle θ on the other side of the same planes, and therefore reflection will again take place. At both reflections there will be a change of phase of 90°, and therefore there will be a total change of phase of 180°. In Fig. 205, A and B are two points where two such reflections have taken place. Consider

an incident ray B_0B which passes through B. If C is the foot of the perpendicular from A on to B_0B, the difference between the paths A_0AB and B_0B is $AB - CB$. This is equal to $AB(1 - \cos 2\theta)$, which equals $4d \sin \theta$ (for $AB = 2d/\sin \theta$). But $2d \sin \theta = \lambda$, and therefore, if there were no change of phase on reflection, the ray reflected at B would be in phase with the incident ray B_0B. This will be true, whatever plane B may lie upon. Since, however, there is change of phase of 180°, the twice reflected ray will be 180° out of phase with the incident ray and so will reduce its intensity. There will of course be further reflections which may reinforce the incident beam, but since the proportion of radiation reflected each time is less than unity—and usually much less than unity—the total effect is

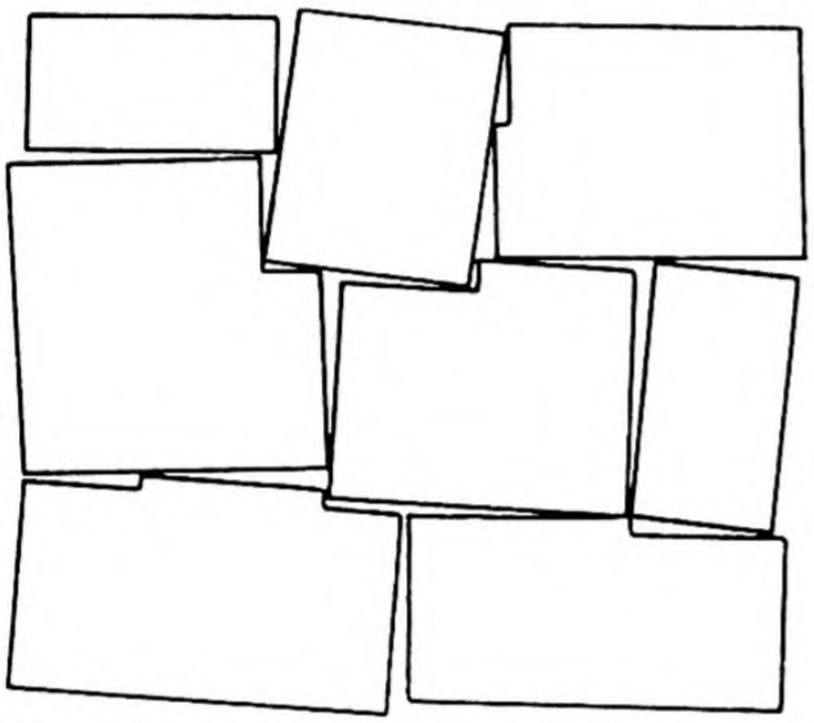

FIG. 206.1. Mosaic structure in a crystal

always a decrease in intensity. The effect will be large, however, only if the reflection is an intense one; that is, the incident beam will be reduced in intensity when it passes through the crystal at a reflecting angle. Therefore the intensity of the reflection will be reduced. This effect will occur only in regions of a crystal that are perfect; it is known as *primary extinction*.

If the crystal is not perfect, the problem is more difficult. The crystal has to be treated as if it were composed of a number of small perfect blocks slightly different in orientation, as shown in Fig. 206.1. Such a crystal is said to have a *mosaic structure*. Primary extinction in each block will cause the rays passing through it at a reflecting angle to be weakened, but such rays will not be at the correct angle for reflection by a block below; also, the rays which are reflected by the block below will not have been weakened by primary extinction in the block above. Thus the reflections from a crystal with a mosaic structure should not be greatly affected by primary extinction, if the regions which are effectively perfect are small. The formulae given in **15,** 2.1 should then be fairly accurately obeyed. Since, however, reflection from a small crystal takes place over a range of angle (**14,** 2.2), rays reflected from the lower blocks of crystal may still be affected somewhat by primary extinction in the upper blocks. This effect, the shielding of the lower blocks by the upper ones, is known as *secondary extinction*. Obviously it will be less as the imperfection of the crystal becomes greater.

One method of allowing for secondary extinction is to add to the absorption coefficient a quantity proportional to the true intensity of reflection (Bragg and West, 1929). Since the constant of proportionality is unknown and is likely to vary greatly from specimen to specimen, its determination must be carried out on the specimen for which the intensities are to be measured. The experimental work, however, is rather complicated, and it is more usual to try to select a crystal sufficiently small to render extinction negligible. While this is probably the best that can normally be done, some recent results tend to cast doubt on the validity of this procedure (Lonsdale, 1944).

Extinction is probably the most important factor limiting the accuracy of present-day measurements of intensity; it can reduce strong intensities to a tenth or even less of their theoretical values, and any quantitative work that does not take this effect into account cannot be considered as having reached the greatest possible accuracy.

2.6 The multiplicity factor. This quantity appears in the formulae for powder photographs because each line is produced by reflections from sets of planes parallel to all the faces of the same crystal form (**10,** 2.2). Each reflection on an oscillation photograph is produced by one set of parallel planes, the crystal being oscillated so that it passes through the reflecting position. Fig. 206.2 (*a*) shows a crystal

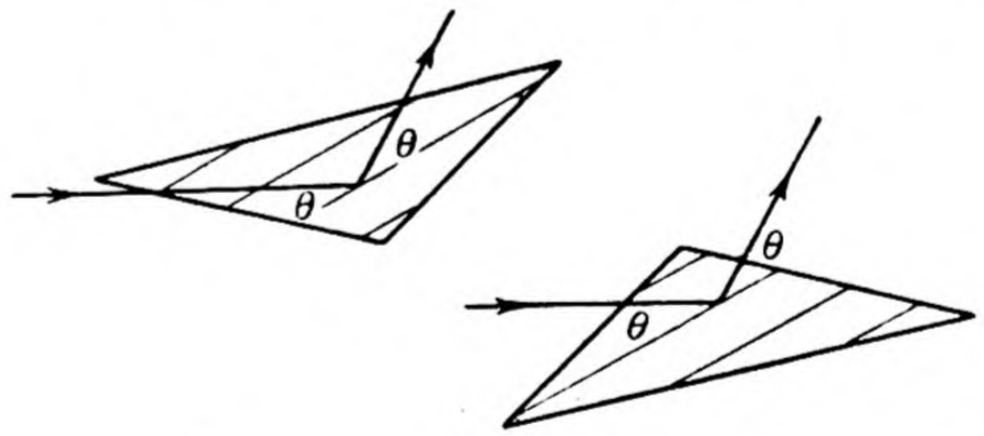

(a) (b)

FIG. 206.2. Crystal in two positions differing by 180°, reflecting X-rays from the same set of lattice planes

with one set of planes in the correct orientation to reflect the incident beam. Fig. 206.2 (*b*) shows the same crystal turned through 180°, and it will be seen that the same planes will again reflect the incident beam in the same direction. Thus if the crystal is being rotated through 360° about an axis perpendicular to the plane of the paper, the reflection in this direction will occur twice. In other words, for a single set of parallel planes the multiplicity factor for a rotation

photograph is 2. This is the simplest case. If the symmetry is high and the crystal is rotated about an axis of symmetry, several reflections of the same form will be superimposed. There is still more complication in a powder photograph, for which all reflections with the same Bragg angle, but not necessarily of the same form, are superimposed (**10,** 2.2).

The value of p depends upon the indices of the reflecting planes and on the symmetry of the crystal. For example, the reflections of the form {100} for a cubic crystal are 100, 010, 001, $\bar{1}00$, $0\bar{1}0$ and $00\bar{1}$; the multiplicity factor here is 6. The number of sets of reflecting planes is of course only 3, since the faces such as (100) and ($\bar{1}00$) are parallel. Nevertheless the multiplicity factor is 6 because, as shown in the previous paragraph, each set of planes gives two reflections. For {111} the possible arrangements are 111, $\bar{1}11$, $1\bar{1}1$, $11\bar{1}$, $1\bar{1}\bar{1}$, $\bar{1}1\bar{1}$, $\bar{1}\bar{1}1$ and $\bar{1}\bar{1}\bar{1}$; the multiplicity factor is 8. The factor is greater when indices are non-zero or unequal and reaches the value of 48 as a maximum. For crystal systems other than cubic the value of p will generally be lower. Values for all the 11 Laue symmetry groups are given in Figs. 156, 157. It should be noted that the multiplicity factor is always equal to the number of faces in the crystal form.

There is a complication in the cubic, tetragonal, hexagonal and trigonal systems: there may be two sets of reflections with identical spacing but unrelated intensity. This is denoted in the table (Figs. 156, 157) by enclosing the two multiplicity factors in a rectangle. For example, in the Laue group $m3$, the reflection 321 belongs to one set and the reflection 123 to another, each having a multiplicity factor of 24. In the Laue group $m3m$, however, both these reflections belong to the same set, or form, which thus has a multiplicity factor of 48.

In addition to this matter of complementary forms, the following point must also be noted: in the cubic system all reflections with the same value of $h^2+k^2+l^2$ have the same Bragg angle; for example, a line with $h^2+k^2+l^2=9$ may be composed of the reflections 300 (with a multiplicity factor of 6) and 221 (with a multiplicity factor of 24).

2.7 The structure factor. The term *structure factor* is used with different meanings by different workers, as will be explained in **15,** 3.1. In this book we take it to be the factor in the intensity formulae that depends upon the atomic arrangement. The structure factor is, however, more important than the other factors, and usually the other factors are evaluated only for the purpose of deriving structure factors from observed intensities. A structure factor can be zero, and it is for this reason that some of the possible spots are absent on the photographs shown in Fig. 62, for example.

The different values of the structure factor for different reflections arise in the following way. Consider a crystal which has one atom at each lattice point. Then the waves scattered from these atoms are in phase for each reflection; this is the condition for the production of a reflection. In such a crystal we could choose a unit cell which contained only one atom. In general, however, a unit cell contains many atoms; and if the waves scattered from the different atoms are not in phase with each other for a given reflection, the resultant amplitude will not be the arithmetic sum of the individual amplitudes of the waves. The phase differences for the waves depend, however, on the direction of the reflection with respect to the crystal, and so the intensity will depend on this direction, that is, on the indices *hkl*.

The structure factor involves several other factors and it is therefore necessary to devote a series of sections to its complete explanation.

3. The Structure Factor

3.1 Definition of structure amplitude. The structure amplitude is one of the quantities that is sometimes known as the structure factor, but the term *structure amplitude* is now becoming generally adopted. It is defined as the number of electrons, considered as concentrated at a single point, which would give the same intensity of scattered radiation, in the direction of the reflection considered, as is given by all the atoms in the unit cell. In order, therefore, to calculate the structure amplitude for a given reflection we need to know (i) how many electrons each atom is equivalent to; (ii) how the waves from the different atoms combine. The quantity (i) is the *atomic scattering factor*, and (ii) leads to the *geometrical structure factor*.

The geometrical structure factor is also sometimes called the structure factor and we have, therefore, thought it advisable to add the word 'geometrical' to make the term more precise. The geometrical structure factor is an expression which is characteristic of a given space group; the product of the geometrical structure factor and the atomic scattering factor of atoms of a set lying on equivalent positions in the space group gives the contribution of that set of atoms to the structure amplitude. The geometrical structure factor is in general a complex quantity, but it can be represented by two components

$$\Sigma \cos 2\pi(hx+ky+lz) \text{ and } \Sigma \sin 2\pi(hx+ky+lz)$$

where x, y and z are the co-ordinates of a set of points related by the space-group symmetry elements.

3.2 The atomic scattering factor. If atoms were merely points, their scattering factors would be equal to the number of electrons they contain, that is, to

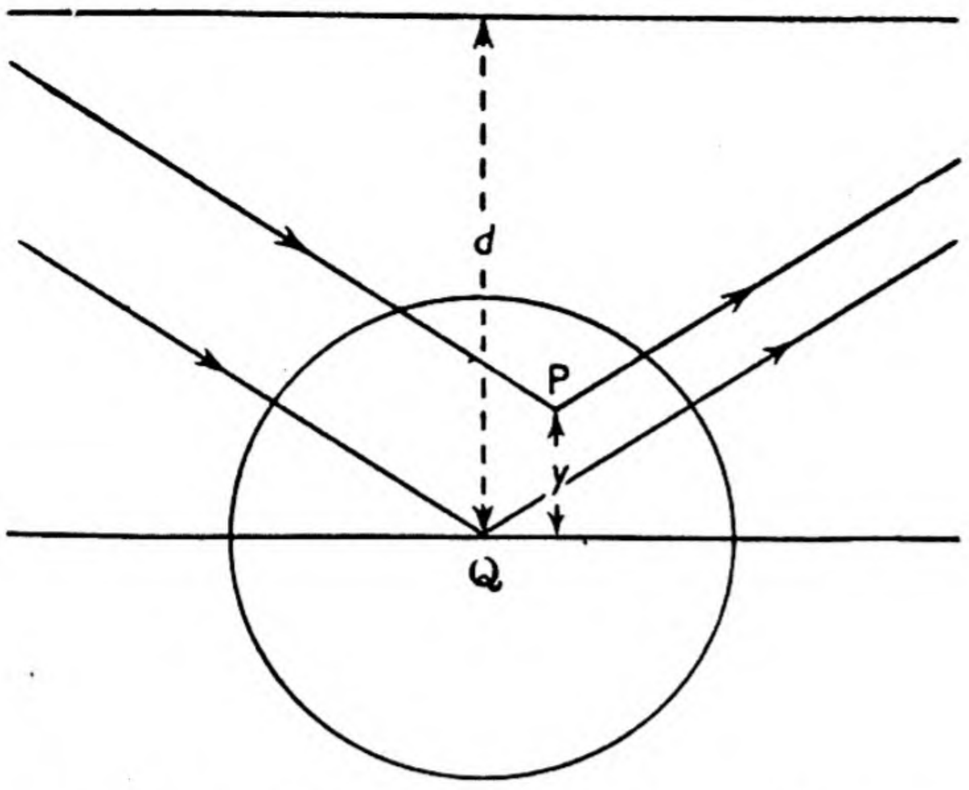

FIG. 208.1. Scattering by an atom of finite size

their atomic numbers; since they are not points, their scattering factors are less than their atomic numbers, the value depending on the spacing of the planes giving the reflection concerned; this can be seen from Fig. 208.1. The circle represents a section of an atom lying on one of a set of planes of spacing d. A ray scattered from a point such as P will have a phase difference of $2\pi y/d$ with respect to a ray scattered from a point at the centre. The total scattering from an atom of known electron density distribution can be obtained by integrating the scattering for all values of y. The calculations are difficult but it can be seen that, since the distribution of values of y is fixed for any one atom, the atomic scattering factor must be a function of d and hence o $\sin\theta/\lambda$ since $1/2d = \sin\theta/\lambda$ (James and Brindley, 1931*a*, *b*). Atomic scattering factors are usually given in tabular form, and graphical interpolation may be used to obtain the values for particular reflections (Fig. 208.2).

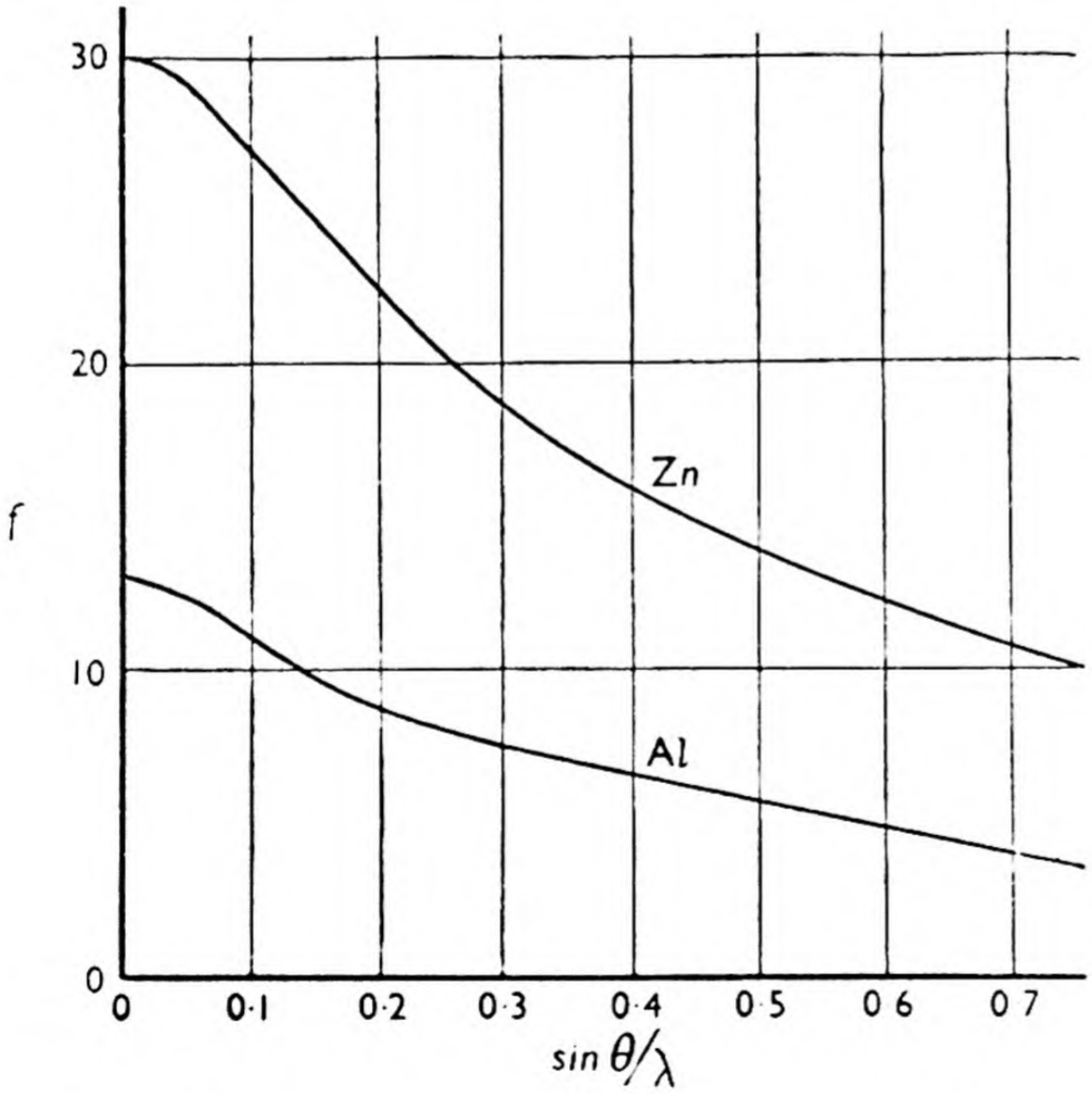

FIG. 208.2. Typical curves of atomic scattering factor

Atomic scattering factors depend primarily on $\sin\theta/\lambda$, but there are corrections due to other factors. As stated in **2**, 5.2, the scattering factor of an element will be reduced if the wave-length of the incident radiation is near an absorption edge. Theoretically the difference should be approximately constant over the whole range of θ, and so the effect is much more important at high values of $\sin\theta/\lambda$ where the scattering factor f is small.

The change, Δf_0, should, according to theory, be a function of λ/λ_k, where λ is the wave-length of the incident radiation and λ_k is that of the absorption edge.

The results of different researches are not in good agreement (Compton and Allison, 1935), but the table below gives approximate values of the averages found for Δf_0 as a function of λ/λ_k.

APPROXIMATE VALUES FOR THE DEPRESSION OF THE SCATTERING FACTOR OF AN ATOM FOR WAVE-LENGTHS IN THE PROXIMITY OF ITS *K* ABSORPTION EDGE

λ/λ_k	0·00†	0·02	0·04	0·06	0·08
0·6	0·0	0·0	0·1	0·2	0·2
0·7	0·3	0·4	0·5	0·6	0·7
0·8	0·8	1·0	1·2	1·5	1·8
0·9	2·2	2·6	3·1	3·7	4·3
1·0	4·9	3·9	3·2	2·7	2·3
1·1	2·0	1·8	1·6	1·4	1·3
1·2	1·3	1·2	1·2	1·1	1·1
1·3	1·0	1·0	0·9	0·9	0·9

† Columns 2-6 give values for additional decimal place.

This change in the value of f_0 should always be allowed for in exact work. A particular application of the change in f_0 near an absorption edge can be made in investigating the crystal structures of substances containing atoms of nearly equal atomic numbers. For example, Jones and Sykes (1937) have detected the superlattice lines (**15**, 4.2) in the alloy CuZn by the use of zinc $K\alpha$ radiation; with other radiations the difference between the scattering factors of copper and zinc is so small that the superlattice lines cannot be detected.

3.3 The temperature factor. Atomic scattering factors are derived from the electron distributions of atoms at rest. At ordinary temperatures, however, the thermal vibrations of the atoms will cause them to occupy a larger volume than they would at rest and will make the scattering still smaller. It can be shown

theoretically (Debye, 1914) that the relation between the scattering factor f of a vibrating atom to that f_0 of an atom at rest is

$$f=f_0 \exp(-B \sin^2\theta/\lambda^2). \quad (1)$$

The quantity B is not strictly a constant; it will be different for different atoms in the same crystal and will vary with direction in the crystal. Attempts to calculate B for particular cases have not led to any great degree of success, and for most work it is sufficient to regard it as a constant which can be used to make the calculated intensities of reflection agree with those observed over the complete range of θ.

3.4 The geometrical structure factor. We have already seen that the structure factor is the quantity that determines how the intensities of the reflections from a crystal depend on the atomic arrangement within the unit cell. This dependence can be calculated precisely as a function of the atomic positions and the indices of the particular reflection concerned. The general formula is:

$$|F|^2=\{\Sigma_n f_n \cos 2\pi(hx_n+ky_n+lz_n)\}^2 + \{\Sigma_n f_n \sin 2\pi(hx_n+ky_n+lz_n)\}^2 \quad (2)$$

where x_n, y_n, z_n are the co-ordinates of an atom expressed as fractional values of the cell edges, which are taken as axes of reference; and f_n is the atomic scattering factor for that atom for the value of $\sin\theta/\lambda$ associated with the indices hkl. The summation is taken over all the atoms in the unit cell. The quantities x_n, y_n, z_n, are called the *structural parameters* of the atom n.

Suppose there are two equal atoms in the unit cell, at positions $(x_1y_1z_1)$ and $(x_2y_2z_2)$. Then, since the atomic scattering factor is the same for both atoms, equation (2) reduces to

$$|F|^2=f^2[\{\cos 2\pi(hx_1+ky_1+lz_1) + \cos 2\pi(hx_2+ky_2+lz_2)\}^2 + \{\sin 2\pi(hx_1+ky_1+lz_1) + \sin 2\pi(hx_2+ky_2+lz_2)\}]^2. \quad (3)$$

As an example of such a structure, we may take that of α-iron; the co-ordinates of the atoms in this case are (000) and $(\frac{1}{2}\frac{1}{2}\frac{1}{2})$. Inserting these values in equation (3), we get:

$$|F|^2=f^2\left[\left\{1+\cos 2\pi\frac{(h+k+l)}{2}\right\}^2 + \left\{0+\sin 2\pi\frac{(h+k+l)}{2}\right\}^2\right]$$

or, since $\sin\pi(h+k+l)=0$,

$$F=f\left\{1+\cos 2\pi\frac{(h+k+l)}{2}\right\} \quad (4)$$

It can be seen that this expression is zero if $h+k+l$ is odd, so that such reflections will be absent. When $h+k+l$ is even, $F=2f$, which means that the two atoms are scattering in phase for these reflections and so the intensity is the maximum possible.

Equation (2) is often written as

$$F^2=A^2+B^2 \quad (5)$$

where $$A=\Sigma_n f_n \cos 2\pi(hx_n+ky_n+lz_n) \quad (6a)$$

and $$B=\Sigma_n f_n \sin 2\pi(hx_n+ky_n+lz_n) \quad (6b)$$

Suppose that we consider only one set of equivalent points, x, y, z, in a space group, and that we take the atomic scattering factor f as unity. Then

$$A=\Sigma \cos 2\pi(hx+ky+lz)$$

and $$B=\Sigma \sin 2\pi(hx+ky+lz), \quad (7)$$

the summations being taken over all the atoms in the set. The expressions (7) are the geometrical structure factors for the space group. Lonsdale (1936) has found it convenient to denote them by A and B, although A and B usually represent the components of the structure amplitude F, as shown in equation (5), and are therefore physical quantities, not trigonometrical expressions.

The importance of this factor is that, although it is always possible to calculate structure amplitudes by using equation (2), it is usually much simpler to collect together all the atoms related by symmetry. For example, suppose there is a centre of symmetry at the origin; that is, for an atom with co-ordinates (x, y, z), there is another with co-ordinates $(\bar{x}, \bar{y}, \bar{z})$. Then $A=2f\cos 2\pi(hx+ky+lz)$ and $B=0$. If there are several pairs of such atoms,

$$A=2\Sigma_n f_n \cos 2\pi(hx_n+ky_n+lz_n),$$

and $B=0$. This expression is much simpler than (2) and it will be seen that the presence of a centre of symmetry at the origin is a great help in simplifying the calculations. Before the advent of X-ray analysis, there was no advantage to be gained by choosing a centre of symmetry as the origin of the unit cell, and the conventional choice of origin for some of the centro-symmetrical space groups did not coincide with a centre of symmetry. While X-ray workers have attempted as far as possible to maintain the older crystallographic conventions, for these space groups it is convenient to transfer the origin to a centre of symmetry in order to make use of the fact that B is then equal to zero (Lonsdale, 1936).

If there are also other elements of symmetry, the formulae may be further simplified. For example, if there is a plane of symmetry through the origin, parallel to (010), there must be equivalent atoms at (x, y, z) and $(x, \bar{y}, z)$. The centre of symmetry will add atoms at $(\bar{x}, \bar{y}, \bar{z})$ and $(\bar{x}, y, \bar{z})$, and if we evaluate A and B for unit atoms at these points, we find that $B=0$, as before, and

$$A=2f\{\cos 2\pi(hx+ky+lz)+\cos 2\pi(hx-ky+lz)\} =4f\cos 2\pi(hx+lz)\cos 2\pi ky. \quad (8)$$

We can thus take the atoms four at a time and use only one expression for their entire contribution.

As the number of equivalent points becomes larger in space groups of higher symmetry, the geometrical structure factors also become more complicated. Expressions for these factors in the 230 space-groups are given in the International Tables, and also in a more directly usable form in *Structure Factor Tables* by Lonsdale (1936)†. It is important, however, that anyone using these should know how they are derived, in order that they may check any formulae they may use; some mistakes have been discovered and corrections have been given in the 1944 reprint of the International Tables and by Lonsdale (1950).

A slight difficulty arises in the application of these formulae when atoms lie in special positions. For example, if an atom lies on the plane of symmetry in the arrangement considered above, its position can be expressed as $(x, 0, z)$ and so it might be expected that the value of A will be obtained by putting $y=0$ in expression (7). This is not so; this expression is valid only for four atoms in general positions, and the atom on the plane of symmetry is in a special position and has only one other equivalent to it. The correct expression is therefore

$$A = 2 \cos 2\pi (hx + lz).$$

Attention must be given to this question if a crystal contains atoms in both special and general equivalent positions; a useful check is that the maximum possible value of the geometrical structure factor for any set of atoms must not be greater than the number of atoms in the unit cell, and is usually equal to this number.

3.5 Absent reflections due to lattice type. In general, one cannot easily deduce from the atomic arrangement in a crystal structure whether a particular reflection will be strong or weak. It will be strong if the contributions of the various sets of atoms, as calculated from equations 5 and 6, are large and of the same sign; and it will be small if these contributions tend to cancel each other. There are, however, some general rules connected with the lattice and with the symmetry operations of the space group, which can be used to predict the complete absence of certain reflections; and, conversely, it is often possible to determine the space group from the knowledge of the absent reflections. These absences can be recognised because they are systematic; that is, they are related in a definite way to the indices of the reflections; absences due to the smallness of the structure amplitude will not be related in any simple way to the indices.

We shall confine ourselves to the study of one example of the derivation of systematically-absent reflections—those produced by a body-centred lattice, as in **12,** 3.1. The systematically-absent reflections corresponding to the various types of centred lattices are derived by a simple method in **10,** 1.5, where the results are tabulated. The analytical method can be used as in the following example. For a body-centred lattice there will be equivalent atoms at points x_n, y_n, z_n and $\frac{1}{2}+x_n$, $\frac{1}{2}+y_n$, $\frac{1}{2}+z_n$. Substituting these values in equation (6*a*), we arrive at the expression

$$\begin{aligned} A &= \Sigma_n f_n[\cos 2\pi\{hx_n + ky_n + lz_n\} \\ &\quad + \cos 2\pi\{h(\tfrac{1}{2}+x_n) + k(\tfrac{1}{2}+y_n) + l(\tfrac{1}{2}+z_n)\}] \\ &= \Sigma_n f_n[\cos 2\pi\{hx_n + ky_n + lz_n\} \\ &\quad + \cos 2\pi\{hx_n + ky_n + lz_n + \tfrac{1}{2}(h+k+l)\}]. \end{aligned} \qquad (8)$$

If $h+k+l$ is odd, the second term will be equal and opposite to the first, and so A will be zero. It can be shown in a similar way that B is also zero when $h+k+l$ is odd, and so the intensities of the reflections with $h+k+l$ odd are zero. Similar rules governing the absence of reflection from other lattices can be worked out in a similar way, from equations (6). It must be noted that such absences are always in reflections of the general form *hkl*, and if examples of all the various types of such reflections are present, the lattice must be primitive.

Systematically-absent reflections occur also in reflections of special types, that is, in those which have one or two indices zero. These absences indicate the presence of certain symmetry elements in the space group, but discussion of this lies beyond the scope of this book. This subject is discussed in the International Tables and by Buerger (1942).

4. Applications

4.1 Structure determination. The main purpose of measurements of the intensity of X-ray reflection is the determination of crystal structures, but this subject is outside the scope of this book. Normally it is not possible to obtain much evidence about a crystal structure without a complete analysis, but occasionally it is possible to obtain some information about the structure from a knowledge of the space group and the contents of the unit cell. For example, if a monoclinic organic compound is found to give no reflections of the types *hol* with *h* odd and no reflections of the type *o*k*o* with *k* odd, the space group must be $P2_1/a$. This has four general equivalent positions; hence if the unit cell contains four molecules, these molecules may have no symmetry whatsoever. But if the unit cell contains only two molecules, then in this space group these must lie on centres of symmetry. The molecule must therefore have a centre of symmetry. Such information can be extremely useful to the chemist investigating the

† These are of course *geometrical* structure factors in the usage of this book.

constitution of an unknown compound. It is of interest to note that although, in general, the presence or absence of a centre of symmetry cannot be inferred from X-ray evidence alone, in special cases such as that just described, it can be. Glide planes and screw axes can both be found by systematic absences, and then it follows that there must also be centres of symmetry.

Sometimes it is possible to obtain further information from the shape of the unit cell. Bernal and Crowfoot (1934) and Hargreaves and Taylor (1941) have given some examples of information obtained in this way, without complete structure determination.

4.2 Study of superlattice formation in alloys. Many alloys are solid solutions of one metal in another, the different atoms being distributed at random on the available equivalent positions, and the X-ray photograph is similar to that of a pure metal of the same structure. The atomic scattering factor used in calculating the theoretical intensity of reflection would be a weighted mean of the atomic scattering factors of the atoms present. It is possible, however, that the atoms may not be distributed at random; they can still occupy the same sites, but with one type of atom in a particular position within each unit cell. For example, iron is cubic with atoms at ooo and $\frac{1}{2}\frac{1}{2}\frac{1}{2}$; that is, it has a body-centred cubic lattice. The alloy FeAl also has atoms at ooo and $\frac{1}{2}\frac{1}{2}\frac{1}{2}$, but the iron atoms tend to occupy the positions ooo and the aluminium atoms the positions $\frac{1}{2}\frac{1}{2}\frac{1}{2}$. (The structure could equally well be described as having iron atoms at $\frac{1}{2}\frac{1}{2}\frac{1}{2}$ and aluminium atoms at ooo; the difference lies only in the choice of origin, which is arbitrary.) The structure has a primitive lattice because it has unlike atoms at ooo and $\frac{1}{2}\frac{1}{2}\frac{1}{2}$; nevertheless it is usually spoken of as body-centred cubic with a *superlattice*†. If this method of description is used, it must be remembered that the presence of the superlattice means that the lattice is primitive. Another example occurs in the alloy $AuCu_3$, which is cubic with gold atoms at ooo and copper atoms at $o\frac{1}{2}\frac{1}{2}$, $\frac{1}{2}o\frac{1}{2}$, $\frac{1}{2}\frac{1}{2}o$. (Again, alternative descriptions are possible, depending upon the choice of origin.) This alloy is often described as face-centred cubic with a superlattice; the lattice is, of course, primitive.

The effect of superlattice formation on powder photographs is shown in Fig. 223, the first photograph in which is that of an ordinary body-centred cubic structure; only lines for which $h^2+k^2+l^2$ is even (**12,** 3.1) appear, since if $h^2+k^2+l^2$ is even, $h+k+l$ is also even. The second photograph, however, is that of an alloy with a superlattice; the structure is not truly body-centred, and lines with other values of $h^2+k^2+l^2$ can appear. These lines, which are fainter than the main lines, are called *superlattice lines*.

Superlattice formation is of common occurrence in alloy systems. In order to interpret any photographs showing the effect, it is necessary to be able to calculate both the positions and intensities of the superlattice lines, and for the latter purpose application of the formulae given in this chapter is essential.

4.3 Determination of proportions of constituents. It is sometimes possible to estimate the relative amounts of two or more constituents in a mixture by comparing the intensities of the lines of each pattern on a powder photograph. These intensities will, however, often depend upon factors which cannot be accurately allowed for (**15,** 2.4), and the safest way of using the method is to measure the relative intensities of lines given by a mixture of the constituents in known proportions. Occasionally, however, it may be possible to obtain absolute values of the proportions directly from the intensities. Edwards and Lipson (1943) for example, found the relative amounts of cubic and hexagonal cobalt in a solid specimen by the direct comparison of the intensities of two chosen lines.

† The use of the word ' superlattice ' is unfortunate. The original German word *Uberstruktur* conveyed perfectly the concept of a new type of ordered structure being imposed on the existing disordered phase. This has nothing to do with the type of lattice, and the word ' superlattice ' has given rise to confusion of thought.

CHAPTER 16

MEASUREMENT OF CRYSTAL GRAIN SIZE IN POLYCRYSTALLINE AGGREGATES

1. Introduction

MEASUREMENT of crystal size in polycrystalline specimens by means of X-rays is based on two quite distinct effects. First, there is the general appearance of the X-ray photographs, from which it is possible to tell immediately whether the specimen consists of large crystals or of small ones ; secondly, there is the broadening of the powder lines that is produced when the crystals become very fine indeed. The first method is difficult to apply if the crystals are less than 10^{-4} cm. in linear dimension, and the second effect becomes measurable only if the crystals are less than about 10^{-5} cm. in linear dimension. There is thus a sort of ' no-man's land ' between 10^{-4} and 10^{-5} cm., but on the whole X-ray methods cover the range of possible crystal sizes very well.

2. The " Spottiness " of Powder Photographs

2.1 Cause of spottiness. Suppose that a transmission or back-reflection photograph of a stationary polycrystalline specimen is taken with the usual mixture of characteristic and white radiations. The size of the crystals in the specimen will have a profound influence on the appearance of the photograph (**11,** 1). For example, the crystals might be so large that only one lies in the path of the beam. Since the specimen is stationary, a Laue photograph would be produced, which may or may not contain spots due to the characteristic radiations. Suppose now that several crystals are irradiated ; then the pattern will consist of several superimposed Laue photographs, a mixture easy enough to recognize but impossible to index. Spots due to the characteristic radiations are more likely to be present because there is now a greater chance that some crystals will have planes in the correct orientation to reflect these radiations. Such spots will be outstandingly strong.

As the number of crystals in the beam increases, the number of these characteristic spots increases, and they can be easily recognised because they lie on the positions of the powder lines of the substance for the particular characteristic radiation. In other words, the photograph will begin to have the appearance of a " spotty " powder photograph, but with a " spotty " background of Laue reflections. As the crystals become smaller, the spots become smaller and closer together. The characteristic powder lines become more even and the background more smooth ; and finally a perfect powder photograph results. Beyond this stage the method is not capable of distinguishing any changes in crystal size ; it is usually stated that this limit is about 10^{-4} cm.

2.2 Method of deducing grain size from spottiness. It is not easy to make quantitative deductions from the photographs. The best method, as described by Clark (1940), is to take standard photographs of specimens of which the grain size has been found by means of the microscope. Photographs of the specimen under test must then be taken with the same apparatus, and from the appearance of the photograph a fairly good idea of its grain size can be gained. This is particularly true when the specimen is such that it gives a ' spotty ' powder photograph ; the counting of the spots in a given ring then gives a quantitative index of the grain size in the specimen.

Since it is necessary to use the same apparatus for standard and test photographs, direct comparison of photographs taken in one laboratory should not be made with those taken in another. Even from photographs taken with the same apparatus, misleading results may be obtained. Clark (1940) has shown two photographs of quartz which were known to have the same average grain size ; yet one gave smoother lines than the other. The explanation was that the *distribution* of grain sizes was different ; the one that had a mixture of large and small grains gave the spottier photograph, because the reflections from the large grains were more prominent than those from the very small grains, which contributed mainly to the background.

The specimens compared must also be in the same physical condition. Internal strains, for example, will produce a spreading of the reflections (**16,** 4.4) and so the powder lines may appear continuous, simulating those from a specimen of smaller grain size.

It will be realised that with these difficulties the method has serious disadvantages as compared with the microscopic method. It is probably only of

value for specimens which cannot be examined by the microscope, and even then great care must be taken in the interpretation of the results.

3. The Broadening of Powder Lines

3.1 Cause of broadening. In order to understand the nature of the broadening of the X-ray reflections from a small crystal, we have to extend the method of deduction of Bragg's Law (**3,** 1.2) to cover the *incomplete* reinforcement of the waves scattered by successive lattice planes. Bragg's Law, $\lambda = 2d \sin \theta$, was deduced by finding the conditions under which the waves reflected from all the planes in a crystal are in phase with each other. There will, however, be an appreciable amount of radiation scattered, even if the law is not precisely obeyed, and in the following paragraph it is shown that the possible deviation from

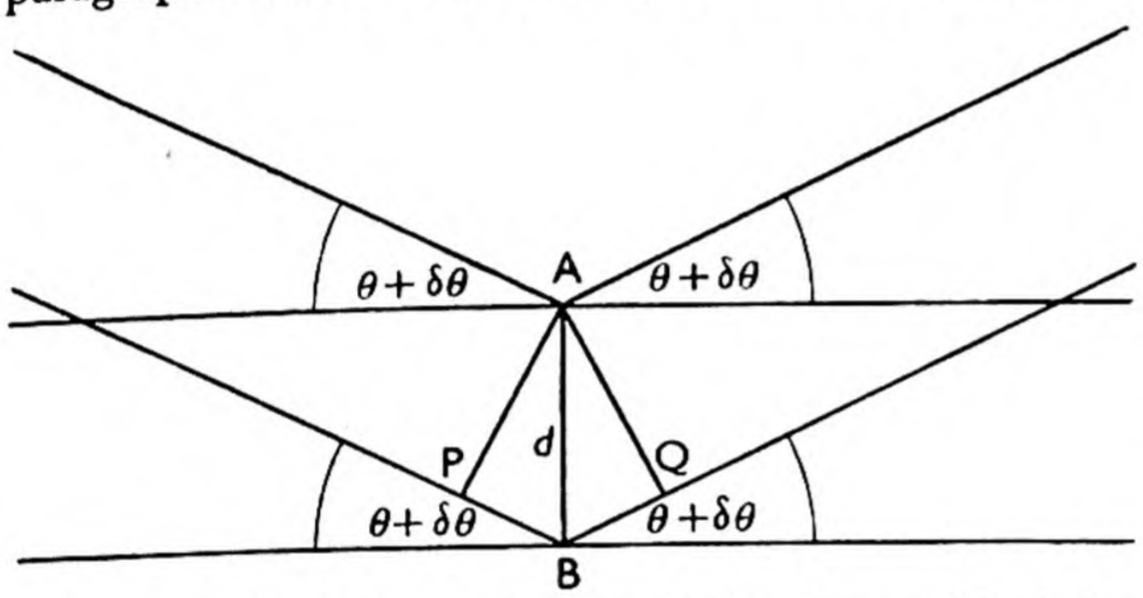

FIG. 213.1. X-rays incident upon lattice planes with slight deviation from the true Bragg angle

the law is greater the smaller the crystal. For small crystals the deviations may be quite large; the reflections appear over a range of angle and are said to be *broadened*.

The order of magnitude of the broadening can be found by a simple method due to A. R. Stokes. We consider a beam of X-rays falling upon a set of $2m$ lattice planes at an angle $\theta + \delta\theta$ and scattered at the same angle †; $\delta\theta$ is the deviation from the correct Bragg angle θ for a particular reflection from the lattice planes. As shown in Fig. 213.1, the path difference PBQ for waves scattered from successive planes is $2d \sin (\theta + \delta\theta)$. The condition for total reinforcement of the waves is of course $\lambda = 2d \sin \theta$; but suppose that $\delta\theta$ is such that the plane $m+1$ scatters 180° out of phase with the first plane; that is, that

$$2md \sin (\theta + \delta\theta) = (m + \tfrac{1}{2})\lambda \qquad (1)$$

instead of the Bragg relation

$$2md \sin \theta = m\lambda. \qquad (2)$$

If equation (1) is true for the first plane and the plane $m+1$, it will also be true for any two planes with the corresponding separation, up to the planes m and $2m$. Thus the crystal can be divided into two parts, the scattering from which will be 180° out of phase and so will cancel out exactly. The value of $\delta\theta$ given by equations (1) and (2) should therefore correspond to zero intensity of scattering.

The value of $\delta\theta$ can be found by subtracting equation (2) from equation (1). This gives

$$2md \cos \theta \, \delta\theta = \lambda/2$$

or

$$\delta\theta = \lambda/2t \cos \theta \qquad (3)$$

where t $(= 2md)$ is the thickness of the crystal. The scattering from the crystal will also be zero when $\delta\theta = -\lambda/2t \cos \theta$, and so the curve of reflected intensity against angle of scattering must be roughly like that shown in Fig. 214.1. The angular separation of the two directions in which the scattering is zero is $\lambda/t \cos \theta$. This expression cannot be expected to be precise in view of the assumptions made in its derivation. Nevertheless, it gives the same order of magnitude as expressions obtained with more rigorous assumptions (**16,** 4.1).

The broadening finds particularly simple expression in terms of the reciprocal lattice. In earlier chapters the reciprocal lattice has been regarded as an array of points. Since we are not now regarding the reflection condition as perfectly precise, the reciprocal 'points' must be considered as extended; for a spherical crystal with diameter t, each reciprocal point will be a small sphere of diameter $\delta\theta = \lambda/t \cos \theta$. Now distances from the origin in reciprocal space are equal to $\lambda/d = 2 \sin \theta$ (**3,** 2.1) and therefore the diameter of a reciprocal point, $\delta(2 \sin \theta)$, is equal to $2 \cos \theta . \delta\theta$. From the value of $\delta\theta$ given above, the diameter of each reciprocal point is

$$(\lambda/t \cos \theta) \times 2 \cos \theta = 2\lambda/t.$$

This is independent of θ and so all the reciprocal

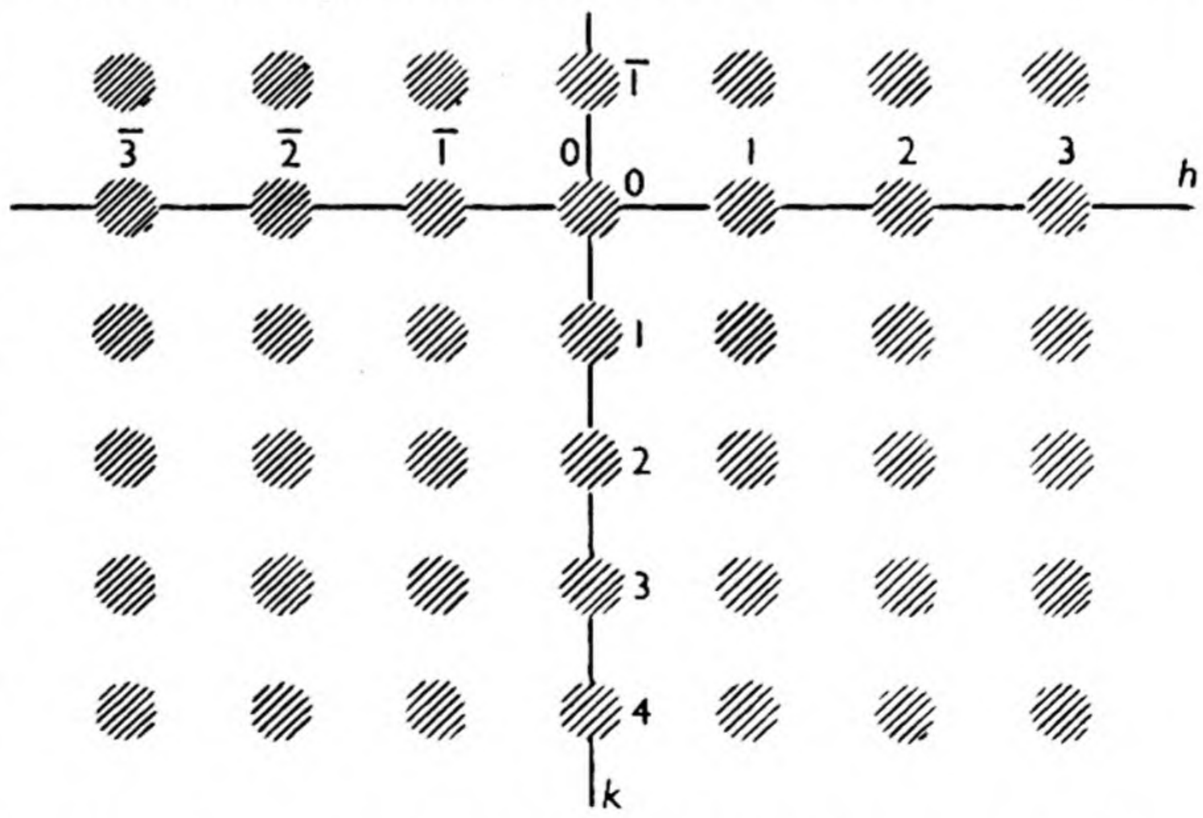

FIG. 213.2. Section of the reciprocal lattice of a small spherical crystal

† As shown in **3,** 1.2, unless this condition is obeyed no appreciable amount of radiation will be scattered from an infinitely extended plane.

points will be broadened to the same extent. A small spherical crystal would thus be represented by a reciprocal lattice of which a section is shown in Fig. 213.2; it will be noted that all the points, even the zero order 000, are broadened.

3.2 Definitions of breadths. Though broadening of X-ray lines can be obvious enough to the eye, it is less simple to describe quantitatively. The length of the base of the line is difficult to measure accurately since, as shown in Fig. 214.1, its extent is usually not clearly defined. A more useful concept is that of *half-peak breadth*, which is the distance between the two points at which the intensity is half the maximum; this is illustrated in Fig. 214.1. Although this definition

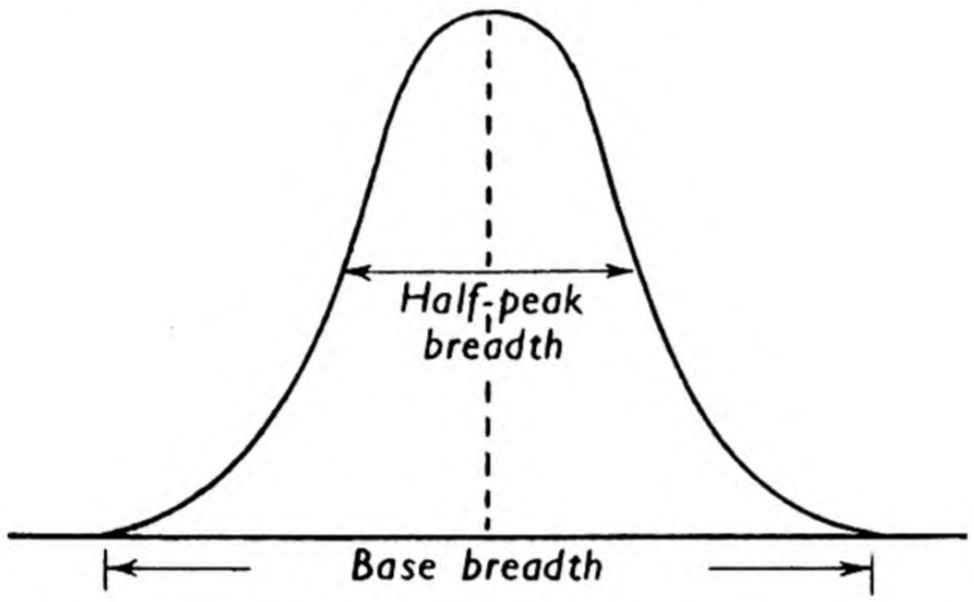

FIG. 214.1. Half-peak breadth and base-breadth for a powder line

has been much used, it suffers from the disadvantage that it does not take into account the lower part of the line profile, and Laue (1926) has proposed another concept, namely, the *integral breadth*. This is the breadth of a line with a square-topped profile of the same total area and peak height as the line profile under consideration (Fig. 214.2); it is obtained by dividing the total area by the peak intensity. This definition is used in this book, but in practice it rarely results in a quantity greatly different from the half-peak breadth.

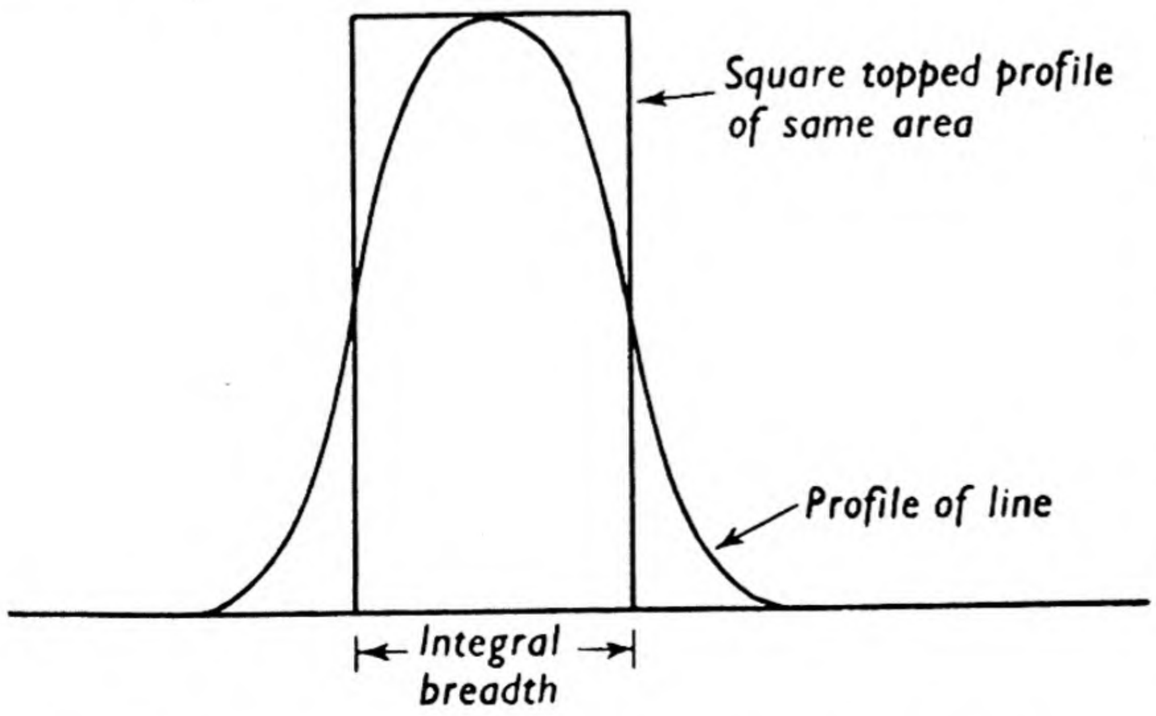

FIG. 214.2. Integral breadth of a powder line

In measuring the area of a line profile, it is necessary to decide on some convention for converting distances along the film into quantities independent of the radius of the camera. A position on the film could for example be specified by the Bragg angle θ of a reflection that would occur at that place, and this specification would have been very convenient; but it has become conventional to specify each point by the angle of deviation $\chi(=2\theta)$ (Laue, 1926). Thus equation (3), for example, could be written as

$$\tfrac{1}{2}\delta\chi = \lambda/2t\cos\theta \quad \text{or} \quad \delta\chi = \lambda/t\cos\theta. \tag{4}$$

3.3 Warren's method of measurement of broadening. It will be obvious that the broadening described in **16,** 3.1 is not obtained merely by measuring the integral breadth of the reflection; even a large perfect crystal gives reflections with a finite

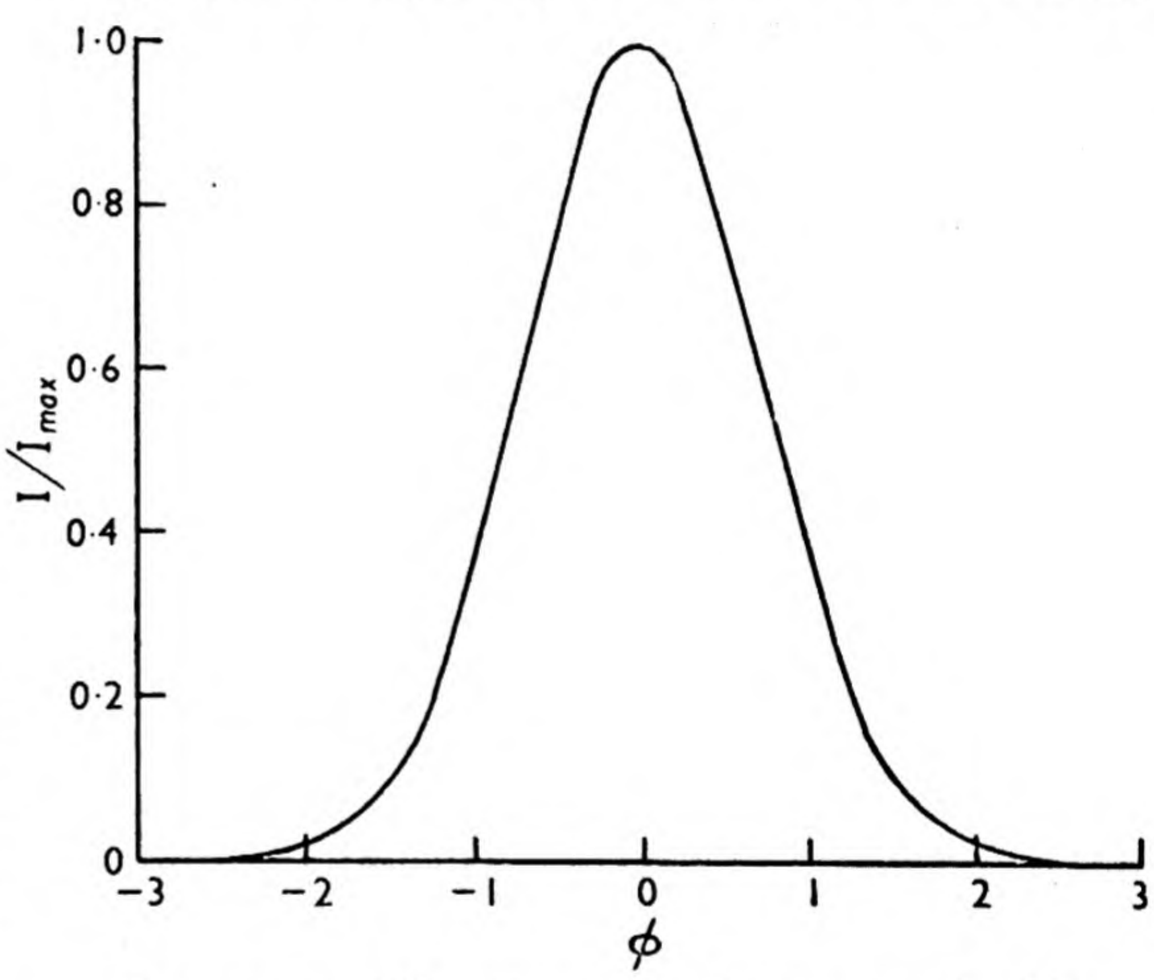

FIG. 214.3. The error curve $I = I_{max}\exp(-\phi^2)$

breadth. This is due to a number of causes: divergence of the incident beam, dimensions of the specimen, and the natural width (**2,** 3.1) of the X-ray lines themselves. In addition, the finite width of the slit of the microphotometer used will cause the measured line profiles to be slightly broader than the lines themselves. There are considerable theoretical difficulties in allowing for these factors. Warren (1941) has suggested that the squares of the elements of broadening are additive; hence if all but one are known, that one may be calculated from the others. If B_T is the total breadth of a line and B_e the broadening due to the experimental conditions mentioned above, then B_c, the broadening due to the small size of the crystals, is given by

$$B_c^2 = B_T^2 - B_e^2 \tag{5}$$

The proof of this relationship depends upon the assumption that distribution of intensity across a line

has the form $I = I_{max} \exp(-\alpha\phi^2)$ (the error curve), where I is the measured intensity at an angular deviation ϕ from the true value of θ, and α is a constant. (This function, which is illustrated in Fig. 214·3, is chosen because it has a maximum at $\phi = 0$ and falls off to zero as ϕ increases.) The proof also assumes that the elements of broadening also have this form. It is obvious, however, that the natural breadth of the emission line does not fit in with this assumption, as it contains both α_1 and α_2 peaks, and so its effects have to be allowed for separately; Smith and Stickley (1943) have described a method due to Warren for making this allowance, and the quantity B_T mentioned above must be taken as the observed breadth corrected for the presence of the $\alpha_1\alpha_2$ doublet. In practice, however, none of the elements of broadening may have the form of error curves, and so Warren's method cannot be considered to be of universal application.

3·4 Jones' method of measurement of broadening. Jones (1938) devised a more general method based on the direct comparison of broadened and sharp lines produced under the same experimental conditions. The theory is described fully by Jones and it is not proposed to give more than an outline of it here.

The sharp lines are called *s*-lines and the broadened ones, *m*-lines. The *s*-lines can be obtained in two ways: first, the specimen giving the broadened lines can be mixed with a specimen that gives ideally sharp lines; secondly, photographs of the same material in two states giving sharp and broadened lines respectively may be taken in the same camera under identical conditions. The first method is the sounder, since it does not involve the maintenance of constant conditions for two photographs, but it has three disadvantages: it involves plotting the breadths of the *s*-lines against θ and interpolating to find the corresponding breadths at the positions required; the introduction of a second substance may involve some overlapping of the lines of the two patterns; and the lines from either pattern will be weaker relatively to the background than they would be if they were recorded separately.

The integral breadths, B_0, of the *s*-lines and the *m*-lines have first to be corrected for the fact that they are produced by the α-doublet. Jones gives a curve (Fig. 215) whereby this correction can be made in terms of a/B_0, where a is the doublet separation in the same units (usually millimetres) in which B_0 is measured; a can be obtained by calculation. From this graph B/B_0 can be read off and so the required value of B obtained.

The corrected breadths of the *s*- and *m*-lines are called b and B respectively. B is the result of applying a broadening β to b; that is, each element of the sharp line is converted into an element with a breadth β,

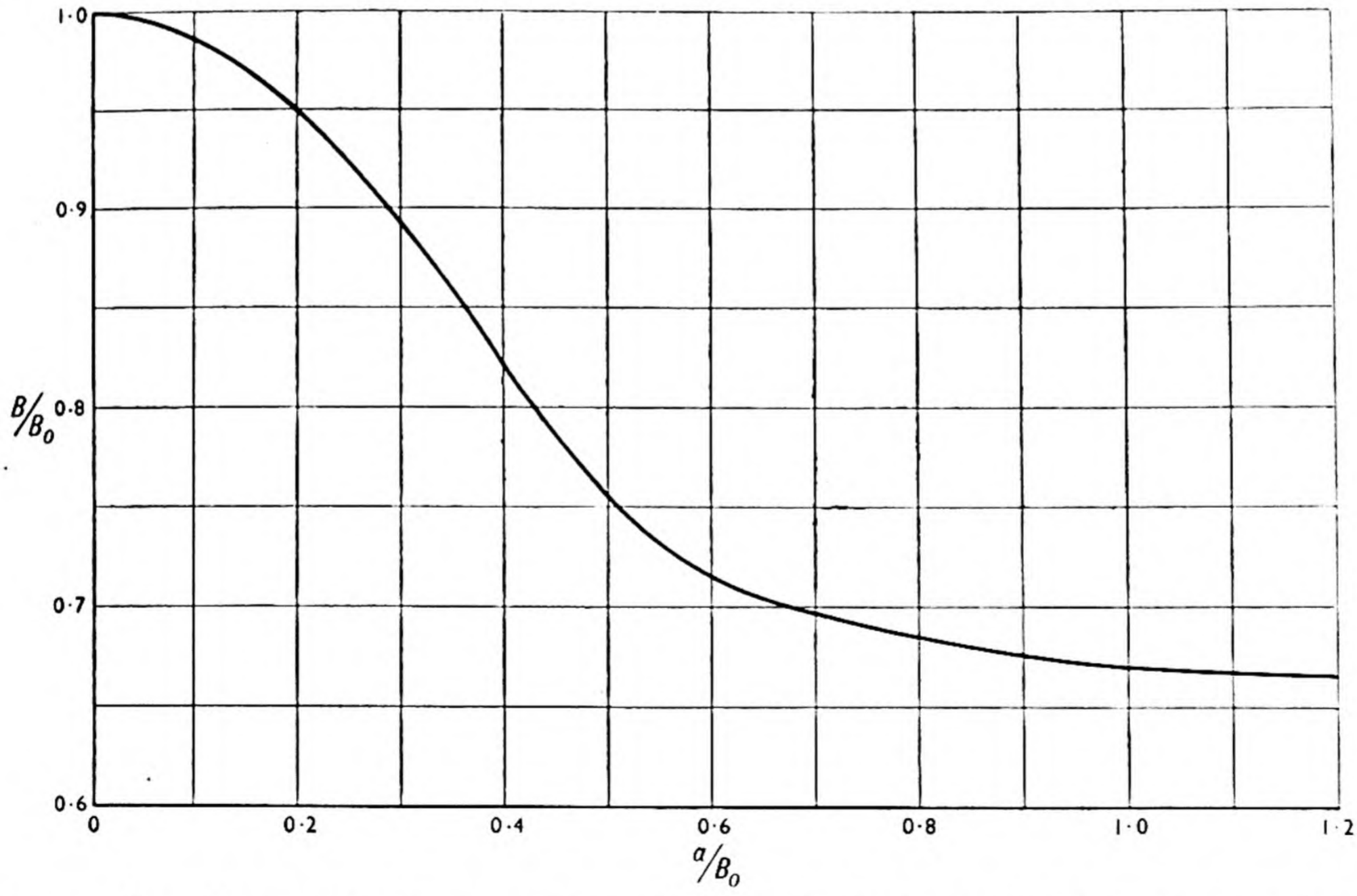

FIG. 215. Curve for correcting the observed breadth of a line for the fact that it is formed by an α-doublet

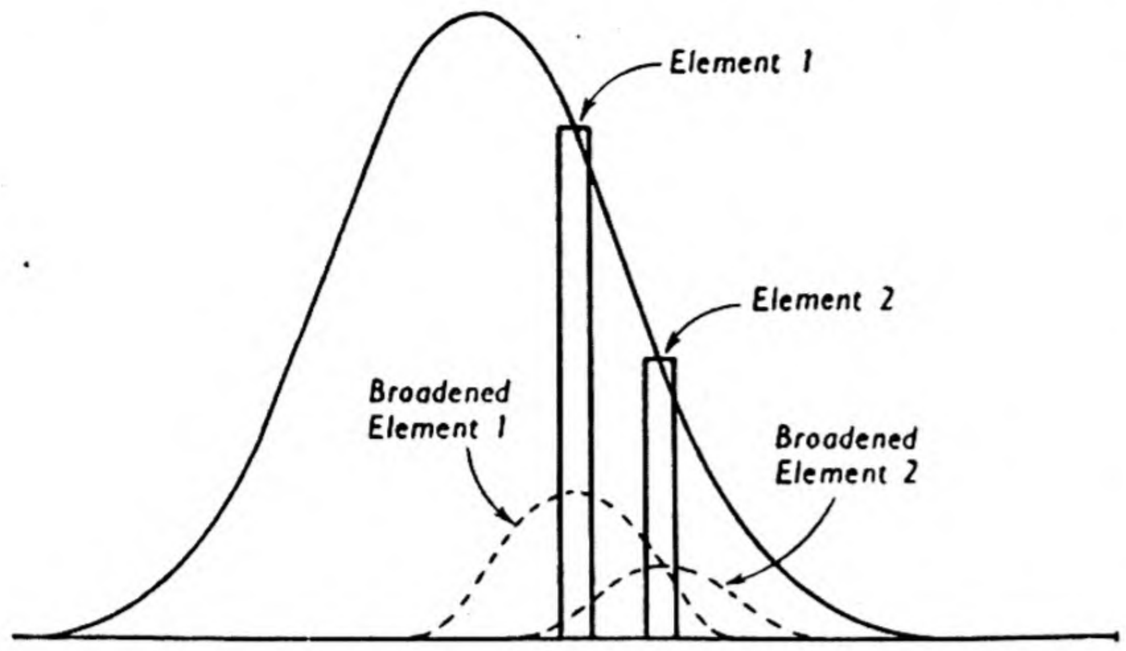

FIG. 216.1. Broadening of separate elements of powder line

as shown in Fig. 216.1, and the ordinates for all the elements are added. Jones took a typical line and found graphically the effect of operating upon it with different values of β. He expressed his results graphically in the form of a relation between b/B and β/B as shown in Fig. 216.2. In this way β can be derived from b and B.

The method has certain limitations. The exact form of the curve in Fig. 216.1 will depend upon the shape of the s-lines. Since Jones' work is based on a cylindrical camera of the type described in **11,** 3.1, his results are not necessarily applicable to the lines given by other sorts of cameras, such as the focusing camera (**11,** 4.3), or the back-reflection plate camera (**11,** 4.4). Moreover, since the line-shape will change with angle, it is not correct to use the same curve for all reflections. As Jones points out, the errors introduced in this way are likely to be less for specimens with high absorption coefficients than for those with low absorption coefficients; for the latter type, as shown in **11,** 3.2, the line-profile changes greatly with θ.

For these reasons it cannot be claimed that line broadening can be measured with any great accuracy. The measurements of breadths themselves are not likely to be more accurate than 5 per cent, even in the most favourable cases. If the broadening to be measured is large, the total error should not greatly exceed this; but if the broadening is small, so that the lower part of the curve in Fig. 216.2 has to be used, the error may be much bigger; it should be assessed separately for each individual line, and if possible the mean of several results should be used.

3.5 Stokes' method of measurement of broadening. Stokes (1948) describes a method which, although it involves a great deal of work, is of general application and requires no assumptions. The first step is to evaluate the Fourier transforms (Whittaker, 1948) of the broadened line and of the corresponding sharp line; the ratios of the ordinates of the two transforms are then found, and the transform of the resulting curve represents the pure diffraction broadening of the original line.

It will be noted that this method gives the distribution of the diffraction broadening and so is more informative than the methods of Warren and of Jones. With the advent of machines for the rapid summation of Fourier series, Stokes' method may

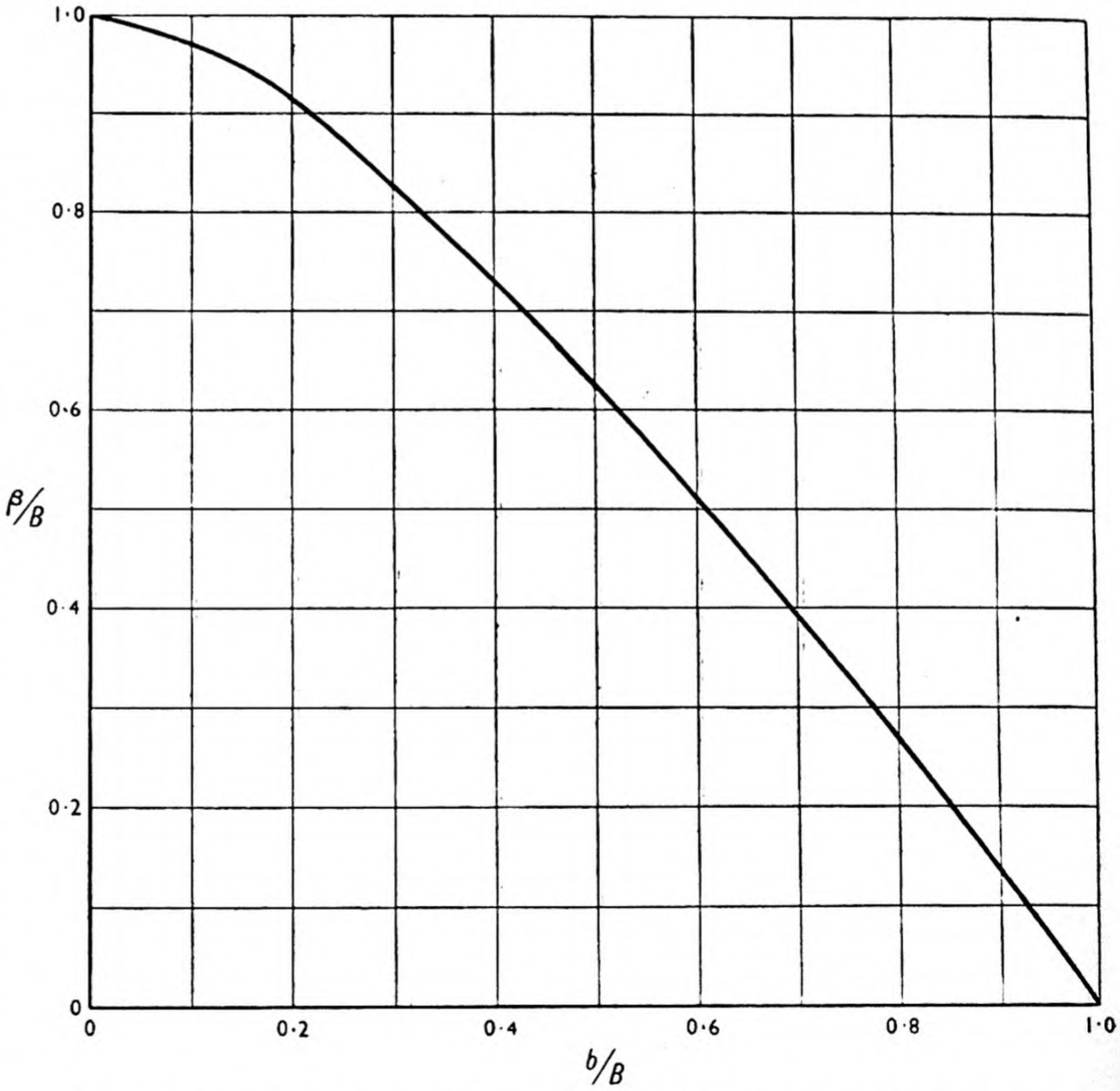

FIG. 216.2. Curve for correcting the breadth of a line for the effects of instrumental broadening

ultimately prove to be the most practicable for solving problems of this sort. It does not follow, however, that, because the method is objective, it is much more accurate than the other methods.

4. Applications

4.1 Apparent crystal size. The broadening of X-ray lines has been much used to determine the size of crystals of colloidal dimensions. It must be remembered, however, that the quantity determined is the size of *crystal* and not the size of *particle*, since a particle may contain a number of crystals.

The formula for the linear dimensions of a crystal that gives a broadening β has the form

$$t = K\lambda/\beta \cos\theta. \qquad (6)$$

The reasoning in **16,** 3.1 and 3.2 would make $K = 1{\cdot}0$ but more detailed theory gives 0·94 (Scherrer, 1920), 0·89 (Bragg, 1933), 0·92 (Seljakow, 1925) and 1·42 (Laue, 1926; Jones, 1938). Since these values are all of the order of unity, Jones (1938) has suggested that, in default of exact knowledge, the quantity t obtained from the formula $t = \lambda/\beta\cos\theta$ should be called the *apparent crystal size*.

Since 1938 the problem of the value of K has been solved (Waller, 1939; Stokes and Wilson, 1942). The value depends, however, on the quantity that is taken as the linear dimension of the crystal. Taking this as the cube root of the volume, Stokes and Wilson give $K = 1{\cdot}0747$ for spherical particles; it will have other values for other definitions of size, for other particle shapes, and for different reflections if the crystals are not spherical. For these reasons it seems desirable to retain the definition of " apparent " crystal size.

4.2 Small-angle scattering. It was pointed out in **16,** 3.1 that all the reciprocal points representing the diffraction of X-rays by a small crystal are broadened to the same extent, and that this applies even to the zero-order point 000. This, however, is true only for an isolated single crystal; it does not apply to the crystal grains in a polycrystalline mass. This can be seen by considering the reflections from a particle of matter consisting of several crystals (Fig. 217). The grain boundaries are those surfaces on either side of which there are atomic arrangements with different orientations, although there may be no actual space between grains. There will be no phase relationships between the rays scattered from different grains in a general reflection *hkl*, and so each grain will give independent reflections; and the broadenings will be characteristic of the shape and size of the crystals grains. But for the zero-order reflection 000, the atoms in *different* grains will scatter in phase, because the condition is then that the phase difference between the waves scattered by different atoms is zero; and this is so if the atoms are rigidly connected together in the same particle, whether they are in the same crystal grain or not. The whole particle will thus behave as a single crystal for this reflection, and so the broadening is a measure of the particle size.

The study of the zero-order reflection—called *small-angle scattering* or *low-angle scattering*—calls for careful work, because of the proximity of the undeviated transmitted beam. Crystal-reflected radiation (Riley, 1944; Guinier, 1945) must be used, and scattering from the air in the camera must be eliminated. Moreover, a fine beam must be used since the broadening may be small; focusing monochromators (**2,** 6) are, therefore, useful.

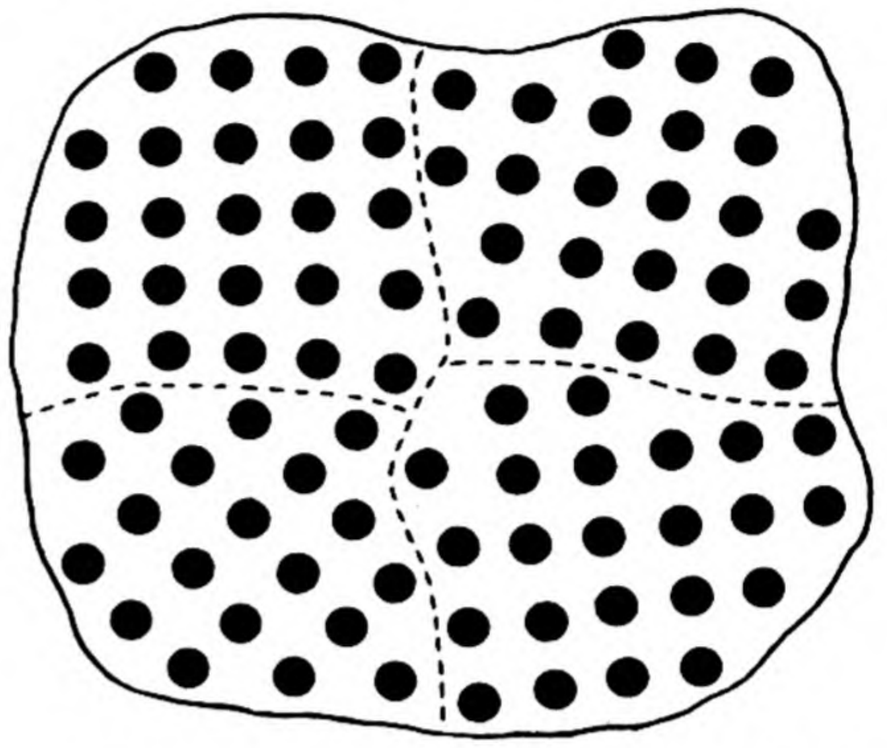

FIG. 217. Atomic positions in a particle consisting of four crystals

4.3 Structural faults. The presence of faults on the atomic scale within a crystal can lead to broadening of some of the X-ray reflections, and the measurement of the breadths of the various reflections can give information about the type of fault and its frequency of occurrence. The type of fault is illustrated by the alloy $AuCu_3$ (**15,** 4.2), which is cubic with the atoms on the points of a face-centred lattice, (000), ($0\frac{1}{2}\frac{1}{2}$), ($\frac{1}{2}0\frac{1}{2}$) and ($\frac{1}{2}\frac{1}{2}0$). At high temperatures the atoms are distributed at random and so the alloy is truly face-centred, but at low temperatures a superlattice develops; the gold atoms occupy one of the four sets of positions and the copper atoms the three others. There are thus four different ways in which the structure can form on the same lattice and, in any one crystal, regions may exist with these different positions for the gold and copper atoms. These regions are called *anti-phase nuclei*. If the nuclei are of the same order of size as the crystal in which they are formed, the superlattice lines will be as sharp as the main lines on the photograph; but if the nuclei are small, the superlattice lines will appear as if they were produced by small crystals

and so will be broadened (Jones and Sykes, 1938; Wilson, 1943*b*). The main lines, which are not affected by the re-arrangement of atoms on the lattice points, remain sharp because the lattice is perfect over the whole crystal.

Another effect of the same sort occurs in cobalt, which has a hexagonal close-packed structure. That the structure is not perfect is shown by the broadening of some of the X-ray reflections, and this broadening can be explained on the theory that there are faults that simulate the cubic close-packed structure (Edwards and Lipson, 1942; Wilson, 1942*a*). Certain reflections are common to the two structures, and these are sharp; but those that are due only to the hexagonal structure are broadened.

4.4 Distorted crystals. The measurement of the broadening of reflections is also important in the study of cold-worked metals. Although it has been suggested that the broadening is mainly due to the smallness of the crystals into which the cold-worked metal is broken down (Wood, 1941, 1943), experimental evidence suggests that it is almost entirely due to distortion of the lattice (Brindley, 1940; Stokes, Pascoe and Lipson, 1943; Smith and Stickley, 1943). Stokes and Wilson (1944) have shown that the broadening in this case is given by an equation of the form

$$\beta \cot \theta = K, \tag{7}$$

where K is a quantity that is independent of λ, but may be a function of h, k and l. This equation may be contrasted with that for small crystals:

$$\beta \cos \theta \propto \lambda.$$

Since $\cos\theta$ and $\cot\theta$ differ greatly only at small angles, the distinction between the two equations requires careful work; but this has been successfully performed, chiefly by Smith and Stickley (1943).

CHAPTER 17

IDENTIFICATION OF CRYSTALLINE MATERIALS BY MEANS OF POWDER PHOTOGRAPHS

1. Introduction

THE use of powder photographs in identification of substances is sometimes referred to as if it were a branch of chemical analysis; this is not so. The objects of the various methods of chemical analysis are the identification of each element present in the substance and also, in quantitative work, the determination of the proportion of each element present. The objects of spectrographic analysis also, employing absorption and emission spectra in the visible and the near visible, are the identification of certain elements in the substance and, in some cases, the determination of the approximate proportions of these. Emission spectra (**2**, 1.3) in the X-ray region are also employed for the same purpose, and this constitutes a branch of spectrographic analysis.

The identification of a particular crystalline substance is another matter, and this can sometimes be done without knowledge of the chemical composition of the substance. For many years the optical properties of crystalline substances have been used for the purpose of identification. Within the last twenty-five years, X-ray methods have been added to the techniques available for this purpose. Although single-crystal photographs may play a part in the identification of certain substances, the most generally applicable X-ray method is the *powder method*.

From measurements on a powder photograph, the spacings of the reflecting planes and the relative intensities of the reflections are obtained. The possible variation in these is great; and the statement can be made that, in general, *the powder pattern is uniquely characteristic of a particular crystalline substance*. (The term ' powder pattern ' is used here to denote both the relative position and the relative densities of the powder lines.) With simple substances, of course, there may be accidental similarities of powder pattern, and this emphasises the importance of independent checking in identification work. In alloys and in minerals, one type of atom is often partially replaced by another type, and this complicates the task of identification by means of powder patterns. If the variation of unit-cell dimensions with the amount of atomic replacement is known, then, by making accurate measurements of the spacings of the powder lines, we can sometimes obtain an approximate value of the relative proportions of the end members. But, if more than one type of atom replaces a given type, as is common in minerals, these proportions cannot be obtained in this way.

The powder method is invaluable when the substance occurs only in the form of a powder or of a disorientated crystalline aggregate. Since a powder specimen can with care be prepared from less than 1 mgm. of material, this method is very useful when only a very small quantity of material is available. Nevertheless, the powder method should be regarded as one method among several, although an important one. A combination of the most suitable methods is best in identification work.

In the following sections general methods of using powder patterns are discussed, along with certain difficulties which arise in practice. It is, however, when the substance belongs to a known group that the use of the powder pattern for identification is rapid and certain. When the number of possibilities is small, powder photographs should be taken of all likely substances, the same radiation and radius of camera being used. By far the most generally suitable radiation is that from a copper target, but for a particular group of substances it may be preferable to use another radiation. When such photographs have been taken, the unknown is then compared with each of them. Even if it does not fit any of them, certain possibilities can thus be eliminated, and it is usually clear what substances should next be tried. If the unknown is a mixture of two of the standard substances, some idea of the proportions in the mixture can be obtained (see **15**, 4.3).

In the comparison of powder photographs, either directly or by means of derived data, the difficulties and pitfalls discussed in **17**, 2.3 should always be kept in mind. In the last section of this chapter the application of the powder method of identification to refractories, alloys and minerals is discussed in outline. These groups of substances were chosen because they cover a large part of the field in which powder patterns are useful in identification work. They also provide examples of most of the different types of problem that occur in this work; but special difficulties may always arise in a particular investigation.

2. General Methods of Identification

2.1 Descriptions of powder photographs. When little is known of a substance, it is obviously difficult to identify it by direct comparison of its powder photograph with those of other substances, and some more general treatment is required. The method of identification must be based on the comparison of one powder photograph with a large number of others; therefore some simple way of describing a powder photograph must be devised, and this must lend itself to systematic classification. The description of any one photograph should be independent of the radiation and the size of camera with which it was taken.

The description which has been adopted in practice is that each line is defined by the spacing ($d = \lambda/2 \sin\theta$) of the planes producing it, and by its intensity expressed as a fraction of that of the strongest line of the pattern. It is perhaps unfortunate that d and not some function such as $1/d$ has been chosen, since d varies rapidly with θ at low angles and so does not lend itself to graphical methods or to interpolation in tables.

Although the interplanar spacings are independent of the radiation used to determine them, the intensities of the lines are not; the value of θ for a particular reflection depends upon λ and, as shown in **15,** 2.2, the formula for the intensity of a powder line contains a quantity which is a function of θ. It is possible to correct each individual intensity for this factor, but this is not often necessary; the trigonometrical factor (**15,** 2.2) varies rapidly only near $\theta = 0°$ and $\theta = 90°$, and in practice discrepancies are likely to arise between the intensity data obtained with different radiations only if a value of θ near 90° occurs.

The intensities of the lines should, in theory, be those determined photometrically (**14,** 1.2), but in practice it is found that visual estimation is accurate enough for most purposes. One difficulty that arises, however, is that different observers use different scales; but so long as the intensities of the lines are recorded in the correct order, it does not greatly matter whether the numbers used are proportional to the intensities or merely represent a class of intensity such as 'medium' or 'strong'.

2.2 The A.S.T.M. Index. Three indexes based on the principles outlined in the previous section have so far been produced (Hanawalt, Rinn and Frevel, 1938; Boldyrev, Mikheiev, Kovalev and Dubinina, 1939; Harcourt, 1942). The first is produced by the American Society for Testing Materials, and this promises to be the most important.† In this Index each substance is catalogued according to the values of d for the first, second and third strongest lines. Each substance has three cards, so that, since the cards are arranged in order of d, each substance will appear in three places in the index.

A typical set of cards is illustrated in Fig. 220. Only on the card which gives the strongest line first are all the available data given. The values of d and the relative intensities of the first, second and third strongest lines are given in the top left-hand corner, and below these data are quantities I which represent roughly the absolute intensities of the lines, information that may be useful when identification has been completed. Then follow the formula and

d	1.595	2.96	1.482
$\frac{I}{I_1}$	.90	1.00	.80
I			

SnO

Alpha Stannous Oxide

d	1.482	2.96	1.595
$\frac{I}{I_1}$	.80	1.00	.90
I			

SnO

Alpha Stannous Oxide

d	2.96	1.595	1.482	d in A $\lambda = .708$	$\frac{I}{I_1}$	d in A $\lambda = .708$	$\frac{I}{I_1}$
$\frac{I}{I_1}$	1.00	.90	.80	4.79	.40	1.027	.20
I				2.96	1.00	1.018	.10
				2.68	.50	0.992	.10
				2.40	.30	0.932	.10
				1.990	.40	0.900	.10
SnO				1.787	.20	0.879	.10
				1.595	.90	0.872	.10
Alpha Stannous Oxide				1.482	.80	0.860	.10
				1.369	.10	0.839	.10
				1.336	.20	0.798	.10
Tetragonal			Z =	1.220	.10	0.749	.10
				1.195	.10	0.712	.01
a. = 4.78	b. =	c. = 4.79		1.165	.30		
A =		C =		1.099	.10		
D =				1.072	.20		
n =	ω =	ε =				C.A. 27	1255

FIG. 220. A set of three cards from the A.S.T.M. index

† Copies with a first supplement can be obtained from the Society at 260 S. Broad St., Philadelphia, Pa., U.S.A.

sometimes the name of the substance, and below this is space for certain crystallographic data which is, however, rarely filled in. The right-hand side is devoted to a complete list of lines in order of spacing, together with their relative intensities; but this is included only on the cards that correspond to the strongest line (Fig. 220). The heading of the spacing column implies that the values are obtained with molybdenum $K\alpha$ radiation, but this seems unnecessary since other radiations must also have been used for some substances and the spacings should be independent of the wave-length with which they are determined. As we have seen in Chapter 15, the *intensities* vary with change of wave-length, though relative values are not usually greatly affected.

The identification of a simple compound, if it is contained in the Index, is quite easy. The values of d for all the lines are measured and that of the strongest is noted. The cards in the Index for which the strongest line has this value of d are then consulted, and it will easily be found if the pattern on one of them agrees with that of the unknown. If it is not obvious which is the strongest line, the fact that there are three cards for each substance may prove helpful.

If the substance is a mixture, it may still be possible to identify all the constituents, although the difficulties are greater; the three-card system is again particularly helpful. The exact method of use will depend both on the problem and the investigator. One way which has been found useful is to make a list of the strongest six lines and to extract from the Index any card that contains two of these six as the first, second or third strongest lines; the cards so extracted can then be examined more closely to see if all the lines on any of them are in the observed pattern. If all the stronger lines can be accounted for in this way, it will then be necessary to see if the weaker ones belong to a single pattern in the Index; success will not have been achieved until all the lines have been accounted for.

2.3 Some practical difficulties. So far we have assumed perfect accuracy both in the measurement of the powder photographs and in the spacings recorded in the Index. In practice considerable errors can occur, chiefly on account of absorption, which displaces the low-order lines (**11,** 3.2). For some of the data in the Index this error has been eliminated, either by calculation of the spacings from accurate cell dimensions, or by mixing the specimen with a substance that gives lines of accurately known spacings, which can then be used as reference lines. This, however, is not true for all the cards. The spacings of the unknown substance may also be corrected by means of a standard; but, if they are not, it is advisable to allow a fairly liberal margin of error, and to consult an extended range of cards. The range depends greatly on the spacing concerned. At about 3 A. errors of 2 per cent are possible, so that cards from 2·94 to 3·06 should be consulted. For smaller spacings the error decreases rapidly and should not be greater than 0·2 per cent at 1 A.

It may happen that certain lines recorded in the Index do not appear on a powder photograph, although it is known that the particular substance is present in the specimen. If these lines are the weakest of the pattern, it must be concluded that the details given in the Index are obtained from a better photograph than the one under consideration. This may easily be so if the substance forms only a small part of the specimen. On the other hand, certain observed lines may not be recorded in the Index. It is most likely that they are due to another constituent; but it is not impossible that they are a true part of the pattern. Many of the data in the Index were obtained with molybdenum $K\alpha$ radiation; the low values of θ which result give inaccurate values for the higher spacings, and the crowding together of the lines makes it difficult to detect weak ones. If it is suspected that some lines are omitted from the pattern recorded in the Index, the only valid test is to take a powder photograph of a pure sample of the material; this is the only satisfactory way of making sure of one's conclusions.

In general, if it is deduced that a material consists of a mixture of certain constituents in certain proportions, it is advisable to take a photograph of a similar artificial mixture. This will check whether the deduction is completely sound, and it may also show whether there are any complications such as solid solution.

Finally, the Index may contain errors. Frevel (1944) has listed a number and it is probable that there are others.

A further difficulty of a general nature also exists. The statement (**17,** 1) that the powder pattern of a substance is unique is not necessarily true; many alloys, for example, could be made that would give exactly the same powder photograph, both in the positions and in the relative intensities of the lines. This is, of course, due to the large ranges of solid solution which occur in metals; and the existence of such solid solutions is a complication that cannot be satisfactorily dealt with in the Index. Solid solution can also occur to a great extent in minerals.

Apart from this trouble, however, there is the possibility that quite different substances may have similar powder patterns. Frevel (1944) has given a list of some that have been discovered; lithium fluoride and aluminium form a striking example. This provides another reason why the Index should not be used independently of other methods, such as chemical analysis and optical investigation.

Within its limitations, the Index promises to be an extremely useful tool, and its usefulness will be increased as the number of compounds it embraces is extended from year to year, and the Index itself is freed from errors.

3. Identification within a Limited Range of Possibilities

3.1 Refractories. The application of X-ray methods to the study and classification of refractory (heat-resisting) materials has proved to be extremely useful. The number of compounds involved is not large, and it is a simple matter to make a collection of powder photographs of them. Moreover the compositions of the substances are usually fairly definite, and it is therefore not to be expected that there will be variations due to solid solution in the intensities and positions of the X-ray reflections. On the other hand, many of the substances have fairly complicated patterns, and their detection in small amounts, when with other substances, requires good photographs.

One of the most important of the refractory materials is silica, SiO_2. At ordinary temperatures this can exist in four forms, depending on the thermal history of the specimen: amorphous silica, and the low-temperature forms of quartz, tridymite and cristobalite. X-ray methods cannot be used to identify amorphous silica, although this can be easily done by a combination of optical and simple chemical methods. The powder patterns of the other three forms are, however, very distinctive; this is extremely useful because the properties of refractory materials of this kind depend greatly on the form or forms of silica present.

3.2 Alloy systems. The identification of the phases present in alloys is not always so straightforward as the identification of refractories. For example, it is not always possible to know what structures can occur in an alloy of given composition. If the compositions of possible phases are known from previous work on the equilibrium diagram, alloys of these compositions can be made and their powder patterns should then be representative of the phases that can exist in the alloys; the methods outlined in the previous sections can then be used. There are, however, some difficulties; the positions of the lines may change owing to the variation, with solid solution, of the cell dimensions, and extra lines may appear due to the formation of a superlattice (see **15,** 4.2). For these reasons the study of an unknown system should, in general, begin by finding whether any regions of solid solution exist. Next, cell dimensions are determined as functions of composition within the ranges of solid solution, and the occurrence of superlattice formation is noted. These difficulties in the study of alloys are often offset by the comparatively simple powder patterns of the structures that occur.

The general principles of the powder method applied to the study of a binary alloy system are illustrated by the set of photographs shown in Fig. 223, which are those of alloys in the iron-silicon system (Farquhar, Lipson and Weill, 1945). The photographs of the α-, η-, ϵ-, ζ- and θ-phases were obtained from alloys of the compositions given by the known equilibrium diagram (Hansen, 1936). The pure η-phase was not easily obtainable, because its composition was not accurately known, and because it does not appear to have an appreciable range of composition; in dealing with a phase of this sort, therefore, it must always be borne in mind that the photograph may show traces of neighbouring phases.

From the photographs of the single-phase alloys, the phases present in any alloy can be identified. For example, the photograph of the 30 per cent alloy obviously contains lines belonging both to the pattern of the ϵ-phase (immediately below) and to the pattern of the η-phase (immediately above). Changes due to heat treatment can also be followed. For example, the photograph of the η-phase was obtained from an alloy heated to about 900° C., and quenched in cold water; if such an alloy is annealed at about 700° it gradually dissociates into $\alpha + \epsilon$, and the change can be followed quantitatively by measuring the relative intensities of chosen lines (Lipson and Weill, 1943).

The photographs in Fig. 223 also illustrate other points. There is an extensive solution of silicon in iron, as is shown by the shifts of the lines on the first three photographs; this shift is so great that the last line, 310, does not occur on the second and third photographs, and if accurate measurements of lattice parameters are required, Co$K\alpha$ radiation should not be used (**13,** 3.3). Also a superlattice of the Fe_3Al type (Bradley and Jay, 1932*a*) develops with more than about 7 per cent silicon; this is shown by the appearance of faint extra lines on the second powder photograph.

If the equilibrium diagram of the alloy system being investigated has not previously been satisfactorily determined, the application of X-ray methods is naturally more difficult. The same general principles can be used, but a process of trial and error is needed in order to identify the single-phase alloys. No general precise principles can be given, but the change in relative intensities of the lines on a powder photograph which may result from a small change in composition often helps in deciding to which pattern certain lines belong. Obviously, as the amount of one phase increases, the intensity of all the lines of its powder pattern will increase together, and all the lines of other phases will decrease

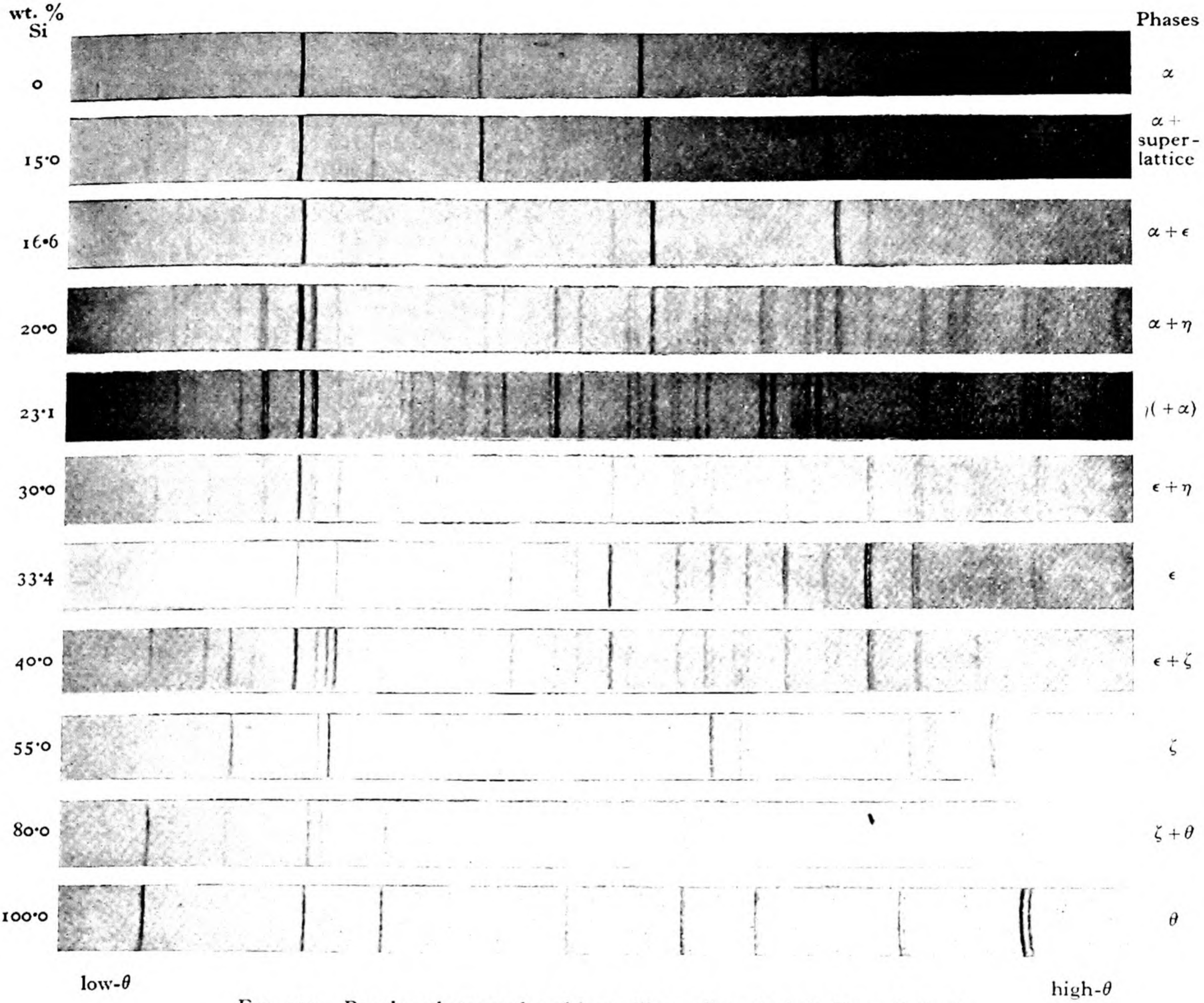

FIG. 223. Powder photographs of iron-silicon alloys (cobalt $K\alpha$ radiation) reduced from originals in which the camera radius was 9·5 cm.

in intensity. Difficulties arise, however, when a number of phases have structures which are modifications of the same structure, and so have similar powder patterns (Bradley and Lu, 1937 *a*, *b*); careful work is necessary to distinguish between them.

In a binary system use can also be made of the fact that in a two-phase region the physical properties of the two phases present are independent of the composition of the alloy; the only quantity that can change is the ratio of the quantities of the two phases. Thus the lattice parameters of the two phases will be constant in a two-phase region. The constancy in position of the lines given by different alloys is thus a useful indication that they lie in the same two-phase field.

3·3 Minerals. Powder photographs play a great part in the identification of minerals; and they are particularly helpful when the polarising microscope cannot be employed, as, for example, when the material is exceedingly fine-grained. Although reflected polarised light can be used, it is not so widely applicable in identification work as is transmitted light. Powder methods are, therefore, specially useful in the field of opaque minerals. In the identification of minerals, certain general points should be kept in mind.

(1) The material should always be examined first by means of a microscope, reflected light being used for opaque substances. This is desirable because minerals are often intergrown and frequently contain foreign inclusions. In some cases it may be necessary to use special techniques for separating the mineral constituents in a sample, or to pick out by hand a number of grains of the particular mineral being studied.

(2) The great majority of minerals belong to the systems of lower symmetry, and this results in the predominance of complex patterns in powder photographs. The chance of accidental similarities between the patterns of different minerals is consequently very much smaller than in metals or in other substances with simple structures.

(3) Atomic replacements within the same structure are very common in minerals; this results in considerable variation in the positions and relative intensities of corresponding lines in members of mineral series with the same structure. Since the shifting of the lines occurs in complicated patterns, the effect is more confusing than it is with alloys.

Although each specimen should be treated as a problem on its own, certain general points can be taken as a guide. If the substance is transparent, it should first be examined by means of the polarising microscope and its characteristic optical properties observed and measured. This is the chief method of the mineralogist, and, even when it does not give an unambiguous result, it will give clues to the nature of the most likely possibilities. The powder method can then be used, either to check the result of an identification by optical methods or to study the various possibilities suggested by it. It is not advisable to rely on the A.S.T.M. Index as the primary method of identifying a completely unknown mineral because of the difficulties discussed above. For such work it would be necessary to have a separate mineral index of powder data, in order to make provision for the extensive atomic-replacement effects. The safest way to use powder photographs in this work is in the direct comparison method, after the number of possibilities has been reduced by means of optical data or by means of simple chemical tests.

X-ray powder photographs are also becoming widely used in the study of artificial minerals. Examples of their use for this purpose are given in the *Symposium on the Chemistry of Cements* (1938), and by Bogue (1947), Chesters (1946), and Rait, Green and Goldschmidt (1942).

LIST OF APPENDIXES AND TABLES

APPENDIXES

		PAGE
Appendix 1.	Calculations for Calcite	227
Appendix 2.	Some Equations for the Various Lattices . . .	228
Appendix 3.	Instructions for Electro-plating Targets . . .	229
Appendix 4.	Solutions to Problems	230

TABLES

Table 1.	Data for X-ray Targets and Filters	233
Table 2.	Some Data for the Elements	234
Table 3.	Mass Absorption Coefficients, μ_m, for $K\alpha$-Radiations .	236
Table 4.	Gram-atomic Absorption Coefficients for $K\alpha$-Radiations .	238
Table 5.	Values of $(h^2+k^2+l^2)$, (h^2+k^2) and (h^2+hk+k^2) up to 100	240
Table 6.	Values of $\sin^2\theta$	242
Table 7.	Values of $\cos 2\pi x$ and $\sin 2\pi x$	244
Table 8.	Values of $(1+\cos^2 2\theta)/\sin 2\theta$	245
Table 9.	Values of $(1+\cos^2 2\theta)/\sin^2\theta\cos\theta$	246
Table 10.	Values of $\frac{1}{2}\left(\frac{\cos^2\theta}{\sin\theta}+\frac{\cos^2\theta}{\theta}\right)$	248

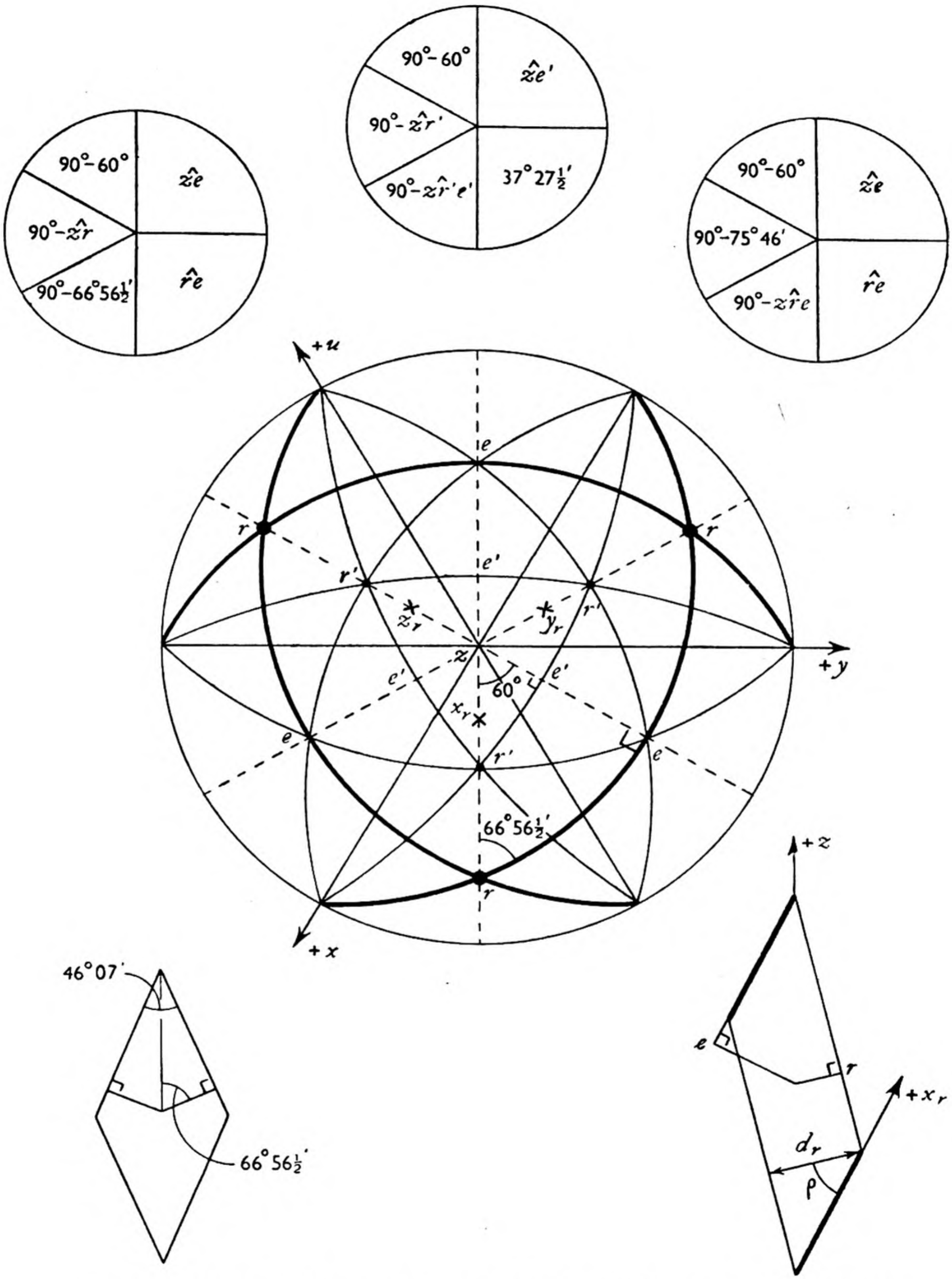

FIG. 226. (*upper*) Schemes of circular parts for solution of spherical triangles
(*middle*) Stereogram of calcite
(*lower*) Sections of the true unit rhombohedron of calcite

APPENDIX 1

Calculations for Calcite (section **10**, 3).

Note: All lengths are in kX. (kilo X-units) (section **2**, 3.2).

1. Given $a_h = 4{\cdot}98$ and $c = 17{\cdot}02$, calculate a_r and α.

$$a_r = \tfrac{1}{3}\sqrt{3a_h^2 + c^2}$$
$$= 6{\cdot}361.$$
$$\sin\frac{\alpha}{2} = \frac{3a_h}{2\sqrt{3a_h^2 + c^2}}.$$
$$\frac{\alpha}{2} = 23^\circ\ 03\tfrac{1}{2}'.$$
$$\alpha = 46^\circ\ 07'.$$

(The equations are given in Appendix 2.)

2. Given $a = 6{\cdot}361$ and $\alpha = 46^\circ\ 07'$, calculate a^* and the angle α^* between the normals to two rhombohedron faces, measured over the polar edge (Fig. 226).

From the spherical triangle zre we can calculate $\hat{zr}$, $\hat{ze}$ and $\hat{re}$, because in this right-angled triangle we are given $\hat{rze} = 60^\circ$ and $\hat{zre} = \dfrac{180^\circ - \alpha}{2} = 66^\circ\ 56\tfrac{1}{2}'$.

$$\cos\hat{zr} = \tan 30^\circ \tan 23^\circ\ 03\tfrac{1}{2}'.$$
$$\hat{zr} = 75^\circ\ 46'.$$
$$\cos 66^\circ\ 56\tfrac{1}{2}' = \cos 30^\circ \cos\hat{ze}.$$
$$\cos\hat{ze} = \frac{\cos 66^\circ\ 56\tfrac{1}{2}'}{\cos 30^\circ}.$$
$$\hat{ze} = 63^\circ\ 06\tfrac{1}{2}'.$$
$$\sin 30^\circ = \cos\hat{re}\sin 66^\circ\ 56\tfrac{1}{2}'.$$
$$\cos\hat{re} = \frac{\sin 30^\circ}{\sin 66^\circ\ 56\tfrac{1}{2}'}.$$
$$\hat{re} = 57^\circ\ 05'.$$

Since $\hat{em} = 90^\circ$, we can obtain the angle $\hat{mr}$ $(= \rho)$.

$\rho = (\hat{er} - 90^\circ) = (75^\circ\ 46' + 63^\circ\ 06\tfrac{1}{2}') - 90^\circ = 48^\circ\ 52\tfrac{1}{2}'$.

Now,

$$d_{100} = a\cos\rho_{[100]}$$
$$= 6{\cdot}361\cos 48^\circ\ 52\tfrac{1}{2}'$$
$$= 4{\cdot}183_6;$$

also,

$$a^* = \frac{\lambda}{d_{100}} = \frac{1{\cdot}539}{4{\cdot}183_6} = 0{\cdot}367_8.$$

The angle between the normals to two rhombohedron faces measured across the polar edge is the angle α^* between the vectors forming the sides of the unit cell of the reciprocal lattice; hence,

$$\alpha^* = 2\hat{re} = 114^\circ\ 10'.$$

3. Given the sides of the morphological hexagonal pseudo-cell, $a_h' = 9{\cdot}96$ and $c' = 8{\cdot}51$, calculate the elements of the corresponding rhombohedron.

By using the same equations as in (1) above, we obtain

$$a_r' = 6{\cdot}41_2 \quad \text{and} \quad \alpha' = 101^\circ\ 55'.$$

4. We can check the value of the angle α' by calculation from the angle measured on an optical goniometer between two cleavage planes, which is known to be $74^\circ\ 55'$:

$$\sin 30^\circ = \cos 37^\circ\ 27\tfrac{1}{2}'\sin\hat{zr'e'}.$$
$$\sin\hat{zr'e'} = \frac{\sin 30^\circ}{\cos 37^\circ\ 27\tfrac{1}{2}'}.$$
$$\hat{zr'e'} = 39^\circ\ 02\tfrac{1}{2}'.$$

Hence

$$\alpha' = (180 - 2\times 39^\circ\ 02\tfrac{1}{2}') = 101^\circ\ 55'.$$

We can also calculate $\hat{zr'}$.

$$\sin 37^\circ\ 27\tfrac{1}{2}' = \cos 30^\circ \sin\hat{zr'}.$$
$$\sin\hat{zr'} = \frac{\sin 37^\circ\ 27\tfrac{1}{2}'}{\cos 30^\circ}.$$
$$\hat{zr'} = 44^\circ\ 36\tfrac{1}{2}'$$

which is the angle given for 0001 : 10$\bar{1}$1 in mineralogical text-books.

5. We can solve the triangle zre as before.

$$\cos 75^\circ\ 46' = \tan 30^\circ \cot\hat{zre}.$$
$$\cot\hat{zre} = \frac{\cos 75^\circ\ 46'}{\tan 30^\circ}.$$
$$\hat{zre} = 66^\circ\ 56\tfrac{1}{2}'.$$

Hence

$$\alpha = (180 - 2\times 66^\circ\ 56\tfrac{1}{2}') = 46^\circ\ 07'.$$

APPENDIX 2

Some Equations for the Various Lattices.

In the rhombohedral lattice (R), either rhombohedral or hexagonal axes may be used (**10**.1.4) and these are related by the following equations.

Hexagonal (triple) cell

a_h = unit length on horizontal axes.

c = unit length on vertical (triad) axis.

$$a_h = 2a_r \cdot \sin\frac{\alpha}{2}.$$

$$c = 3a_r\sqrt{1 - \tfrac{4}{3}\left(\sin^2\frac{\alpha}{2}\right)}.$$

$$\frac{c}{a_h} = \sqrt{\frac{9}{4\sin^2 \alpha/2} - 3}.$$

Rhombohedral cell.

a_r = unit length along rhombohedral edge.

α = angle between polar edges.

$$a_r = \tfrac{1}{3}\sqrt{3a_h^2 + c^2}.$$

$$\sin \alpha/2 = \frac{3a_h}{2\sqrt{3a_h^2 + c^2}}.$$

$$\sin \alpha/2 = \frac{3}{2\sqrt{(c/a_h)^2 + 3}}.$$

Equations for $\sin^2\theta$.

Cubic
$$\sin^2\theta = \frac{\lambda^2}{4a^2}(h^2 + k^2 + l^2).$$

Hexagonal
$$\sin^2\theta = \frac{\lambda^2}{3a^2}(h^2 + hk + k^2) + \frac{\lambda^2}{4c^2}l^2.$$

Rhombohedral
$$\sin^2\theta = \frac{\lambda^2}{4a^2}\cdot\frac{(p^2+q^2+r^2)\sin^2\alpha + 2(pq+qr+rp)(\cos^2\alpha - \cos\alpha)}{1 + 2\cos^3\alpha - 3\cos^2\alpha}$$

Tetragonal
$$\sin^2\theta = \frac{\lambda^2}{4a^2}(h^2 + k^2) + \frac{\lambda^2}{4c^2}l^2.$$

Orthorhombic
$$\sin^2\theta = \frac{\lambda^2}{4a^2}h^2 + \frac{\lambda^2}{4b^2}k^2 + \frac{\lambda^2}{4c^2}l^2.$$

Monoclinic
$$\sin^2\theta = \frac{\lambda^2}{4a^2\sin^2\beta}h^2 - \frac{\lambda^2\cos\beta}{2ac\sin^2\beta}hl + \frac{\lambda^2}{4c^2\sin^2\beta}l^2 + \frac{\lambda^2}{4b^2}k^2.$$

Triclinic $\sin^2\theta$ is best expressed in terms of the reciprocal-lattice constants :

$$a^* = \frac{bc}{V}\sin\alpha \quad \cos\alpha^* = \frac{\cos\beta\cos\gamma - \cos\alpha}{\sin\beta\sin\gamma},$$

$$b^* = \frac{ca}{V}\sin\beta \quad \cos\beta^* = \frac{\cos\gamma\cos\alpha - \cos\beta}{\sin\gamma\sin\alpha},$$

$$c^* = \frac{ab}{V}\sin\gamma \quad \cos\gamma^* = \frac{\cos\alpha\cos\beta - \cos\gamma}{\sin\alpha\sin\beta},$$

where V, the volume of the unit cell, is equal to $abc\,(1 + 2\cos\alpha\cos\beta\cos\gamma - \cos^2\alpha - \cos^2\beta - \cos^2\gamma)^{1/2}$. Then

$$\sin^2\theta = \frac{\lambda^2}{4}[h^2a^{*2} + k^2b^{*2} + l^2c^{*2} + 2klb^*c^*\cos\alpha^* + 2lh\,c^*a^*\cos\beta^* + 2hka^*b^*\cos\gamma^*]$$

APPENDIX 3

Instructions for Electro-plating Targets.

(From *Principles of Electro-plating and Electro-forming*, by Blum and Hogaboom.)

Cleaning of targets. Remove any old plating, and polish the target on emery papers, finishing with ooo grade. Degrease the target by immersing it in hot caustic soda solution, and wash under the tap. Transfer it immediately to the plating bath.

Chromium

Bath : Chromic acid, CrO_3, 50 gm.
Sulphuric acid, H_2SO_4, 0·25–0·5 gm.
(the equivalent of chromic sulphate may be used instead of sulphuric acid)
Distilled water, 200 c.c.
Temperature : 45°–55° C.
Anode : lead.
Current : 100–300 m. amp. per sq. cm.
Note : increased temperature involves increased current.

Manganese

Bath : Manganese sulphate, $MnSO_4.H_2O$, 22 gm.
or Manganese sulphate anhydride, 15 gm.
Ammonium sulphate, $(NH_4)_2SO_4$, 26 gm.
Ammonium sulphite, $(NH_4)_2SO_3$, 0·2 gm.
Distilled water, 200 c.c.
Anode solution : strong ammonium sulphate solution in porous pot.
Temperature : room temperature.
Anode : lead.
Current : 50–70 m. amp. per sq. cm.
Note : After plating, wash quickly and dip in dilute $K_2Cr_2O_7$ solution ; then wash again.

Iron

Bath : Ferrous ammonium sulphate, 56 gm.
Ammonium chloride, 1 gm.
Distilled water, 200 c.c.
Temperature : 30° C.
Anode : iron.
Current : 6–10 m. amp. per sq. cm.

Cobalt

Bath : Boric acid, 10 gm. dissolved in 220 c.c. of boiling water.
Sodium chloride, 5 gm.
Cobalt sulphate, 144 gm.
Temperature : 34° C.
Anode : cobalt.
Current : 25 m. amp. per sq. cm.

Nickel

Bath : Nickel sulphate, $NiSO_4.7H_2O$, 21 gm.
Nickel chloride, $NiCl_2.6H_2O$, 2 gm.
Ammonium chloride, 3 gm.
Boric acid, H_3BO_3, 3 gm.
Distilled water, 200 c.c.
Temperature : 20–30° C.
Anode : nickel.
Current : 5–20 m. amp. per sq. cm.
Note : If insufficient chloride is present, the anode will not be dissolved efficiently.

Zinc

Bath : Zinc sulphate, $ZnSO_4.7H_2O$, 82 gm.
Sodium sulphate, Na_2SO_4, 15 gm.
Aluminium chloride, $AlCl_3.6H_2O$, 4 gm.
Distilled water, 200 c.c.
Small amounts of concentrated sulphuric acid should be added at intervals to maintain a low *p*H.
Temperature : room temperature.
Anode : zinc.
Current : 15–30 m. amp. per sq. cm.

Gold

Bath : Gold cyanide, AuCN, 0·45 gm.
or Gold fulminate, $2AuNH.NH_2.3H_2O$, 0·52 gm.
Potassium cyanide, 3 gm.
Sodium phosphate, $Na_2HPO_4.12H_2O$, 0·8 gm.
Distilled water, 200 c.c.
Temperature : 60°–80° C.
Anode : gold.
Current : 1–5 m. amp. per sq. cm.

Silver

Bath : Silver nitrate, 7 gm.
Potassium cyanide, 5·2 gm.
Distilled water, 100 c.c.
Method for preparing bath : Dissolve slightly more than 5·2 gm. of potassium cyanide in distilled water to make a strong solution, and add slowly to a solution of the silver nitrate until precipitation is just complete. Drain away the supernatant liquors ; and dissolve the precipitate in more cyanide solution, with warming if necessary. About 10% of the whole cyanide solution is added to form free cyanide.
Temperature : room temperature.
Anode : silver.
Current : 10–20 m. amp. per sq. cm.

APPENDIX 4

Solutions to Problems.

Chapter 5

Oscillation photographs of topaz about the *y*- and the *z*-axes (5, 2.2 to 2.5, and Figs. 63.1, 63.2). The indices are given in Figs. 230.1 and 230.2.

Chapter 7

Inclination-Weissenberg photograph of gypsum oscillated about the *y*-axis.

In the interpretation of this photograph (Fig. 93.1), use can be made of the ordinary Weissenberg chart (Fig. 91) if the derived spacings are adjusted as described below. The chart is placed on the photograph using the fiducial marks as described in 7, 2.3, and the co-ordinates are read off. These can be plotted, or indexing can be done directly on the photograph. The indexing of Fig. 231 has been done with the Wooster choice of unit cell (Fig. 138) and the values obtained from the photograph are :

unit along point row $h00 = 0{\cdot}320$,
unit along point row $00l = 0{\cdot}514$, $\beta^* = 28\frac{1}{2}°$.

But, since this is an inclination photograph and the chart is for normal-beam photographs, it is necessary to multiply the two values 0·320 and 0·514 by cos 15° (7, 3.2). When this is done we have,

$a^* = {\cdot}309$, $c^* = {\cdot}496$, and
$a = 10{\cdot}47$, $c = 6{\cdot}51$A., $\beta = 151\frac{1}{2}°$.

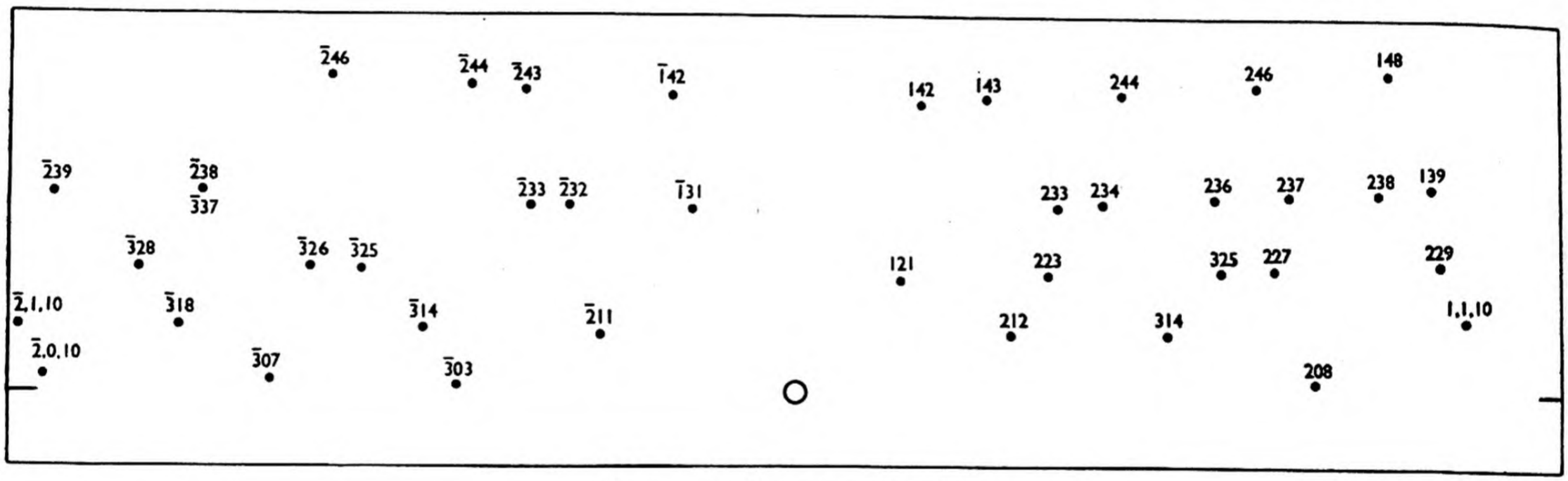

FIG. 230.1. Indexing of Fig 63.1.

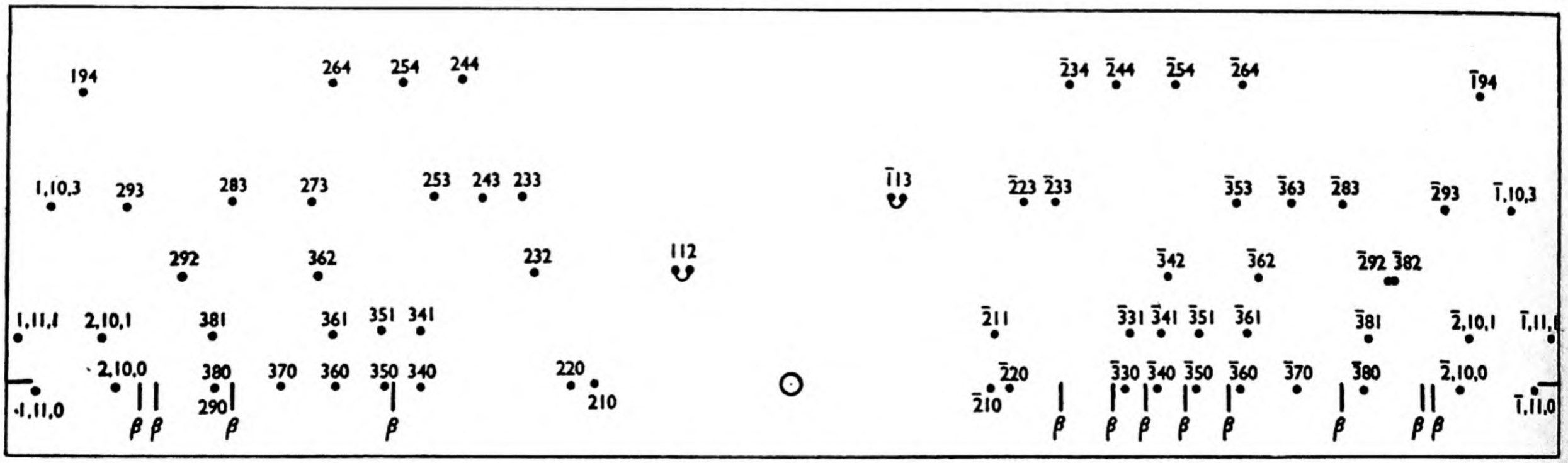

FIG. 230.2. Indexing of Fig. 63.2.

The double dots in 112 and $\bar{1}13$ are due to the use of a large specimen with considerable absorption

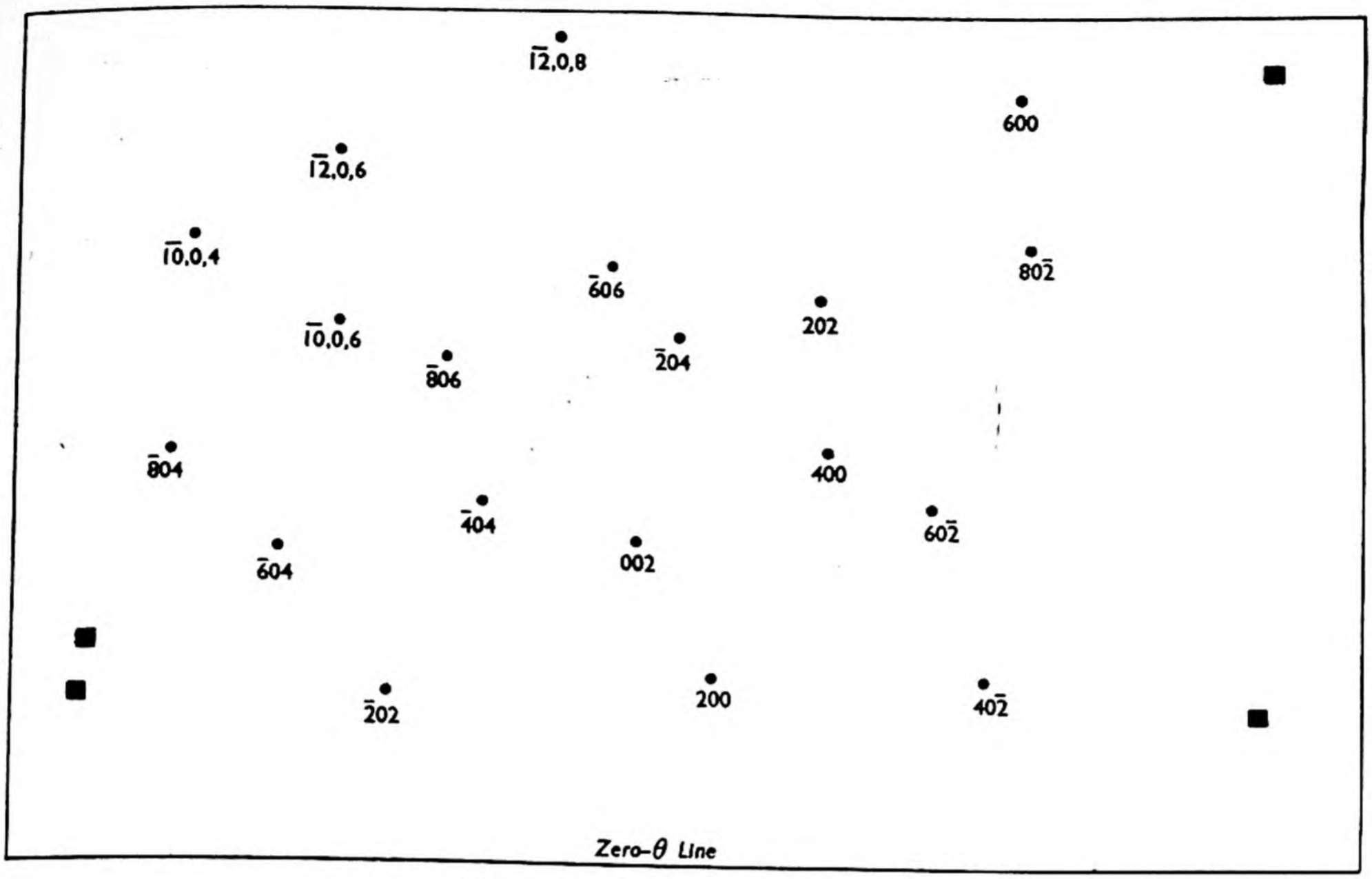

FIG. 231. Indexing of Fig. 93.1

Chapter 12, No. 1

$$A=\frac{\lambda^2}{3a^2}=0{\cdot}0328\,; \quad C=\frac{\lambda^2}{4c^2}=0{\cdot}02035.$$

The indices of the lines are :

a, 100 ; *b*, 101 ; *c*, 110 ; *d*, 102 ; *e*, 111 ; *f*, 200 ; *g*, 201 ; *h*, 112 ; *j*, 202 ; *k*, 103 ; *l*, 211 ; *m*, 113.

Chapter 12, No. 2

The values of $\sin^2\theta$ for the first six lines are :

a, 0·0579 ; *b*, 0·1086 ; *c*, 0·1666 ; *d*, 0·2173 ; *e*, 0·2321 ; *f*, 0·2754.

It will be noted that $\sin^2\theta_d$ is twice $\sin^2\theta_b$; thus the structure is probably tetragonal, with *b* as 100 and *d* as 110, and hence $A=0{\cdot}1086$. The table of differences is given opposite.

The occurence of $0{\cdot}0580 \pm 0{\cdot}0001$ suggests that $C=0{\cdot}0580$, and the first six lines can be indexed on this basis, as shown in the last column.

The remaining lines are :

g, 102 ; *h*, 200 ; *j*, 112 ; *k*, 201 ; *l*, 210 ; *m*, 211 ; *n*, 103 ; *p*, 202 ; *q*, 113 ; *r*, 212 ; *s*, 220 ; *t*, 221, 004 ; *u*, 203.

More accurate values of *A* and *C* are 0·1084 and 0·0579 respectively, giving $a=2{\cdot}72$A. and $c=3{\cdot}72$A. The material is FePt (Lipson, Shoenberg and Stupart, 1941).

Line	$\sin^2\theta$	$\sin^2\theta - 0{\cdot}1086$	$\sin^2\theta - 0{\cdot}2173$	*h*	*k*	*l*
a	0·0579			0	0	1
b	0·1086			1	0	0
c	0·1666	0·0580		1	0	1
d	0·2173	0·1087		1	1	0
e	0·2321	0·1235	0·0148	0	0	2
f	0·2754	0·1668	0·0581	1	1	1

Chapter 13

The steps in the calculation are set out opposite. The values of log a are obtained by adding $\frac{1}{2}\log N$, $\log \lambda/2$ and $\log \operatorname{cosec}\theta$; the results are plotted against the values of $f(\theta)=\frac{1}{2}\left(\frac{\cos^2\theta}{\theta}+\frac{\cos^2\theta}{\sin\theta}\right)$ shown in the last column.

The value extrapolated to $f(\theta)=0$ is $6{\cdot}5736_6$A., with an error of the order of 0·00006A. This must not be taken as a typical error; measurements were taken on a photograph (Fig. 180) with particularly sharp lines.

When the calculations are done by different people, differences of one or two units in the fifth decimal place in a, and in corresponding places in other columns in the table, may occur; this illustrates the importance of carrying out the calculations to a higher number of figures than is physically significant.

For Cu$K\alpha_1$, $\lambda/2=0{\cdot}77025$; $\log \lambda/2=\bar{1}{\cdot}886_{32}$.
For Cu$K\alpha_2$, $\lambda/2=0{\cdot}77217$; $\log \lambda/2=\bar{1}{\cdot}887_{13}$.

N	$\frac{1}{2}\log N$	$\log \sqrt{N}\frac{\lambda}{2}$	$\log\operatorname{cosec}\theta$	$\log a$	a	$f(\theta)$
72	0·928666	0·815298	0·002527	0·817825	6·57393	0·010
70	0·922549	0·810262	0·007591	853	435	30
		0·809181	0·008682	863	450	34
69	0·919425	0·807138	0·010742	880	476	43
		0·806057	0·011834	891	493	47
68	0·916254	0·803967	0·013925	892	494	55
		0·802886	0·015022	908	519	60
66	0·909772	0·797485	0·020461	946	576	83
		0·796404	0·021552	956	591	87
65	0·906457	0·794170	0·023793	963	602	97
		0·793089	0·024873	0·817962	6·57601	0·101

TABLE 1

Data for X-ray Targets and Filters

Target					β-Filter	
Element, Atomic Number	Line	Wave-length in A. units	Excitation Potential kV.	Suitable working peak kV.	Element	Thickness mm.
Ag, 47	$K\alpha_1$	0·559 41	25·5	90	Rh (or Pd)	0·079
	$K\alpha_2$	0·563 81				
	$K\beta_1$	0·497 01				
	A.E.†	0·485 5				
Pd, 46	$K\alpha_1$	0·585 45	24·4	90	Rh (or Ru)	0·073
	$K\alpha_2$	0·589 82				
	$K\beta_1$	0·520 52				
	A.E.	0·509 0				
Rh, 45	$K\alpha_1$	0·613 26	23·2	90	Ru	0·064
	$K\alpha_2$	0·617 62				
	$K\beta_1$	0·545 59				
	A.E.	0·534 1				
Mo, 42	$K\alpha_1$	0·709 26	20·0	80	Zr	0·108
	$K\alpha_2$	0·713 54				
	$K\beta_1$	0·632 25				
	A.E.	0·619 7				
Zn, 30	$K\alpha_1$	1·435 10	9·7	50	Cu	0·021
	$K\alpha_2$	1·438 94				
	$K\beta_1$	1·295 20				
	A.E.	1·283 1				
Cu, 29	$K\alpha_1$	1·540 50	9·0	50	Ni	0·021
	$K\alpha_2$	1·544 34				
	$K\beta_1$	1·392 17				
	A.E.	1·380 2				
Ni, 28	$K\alpha_1$	1·657 83	8·3	50	Co	0·018
	$K\alpha_2$	1·661 68				
	$K\beta_1$	1·500 08				
	A.E.	1·486 9				
Co, 27	$K\alpha_1$	1·788 90	7·7	45	Fe	0·018
	$K\alpha_2$	1·792 79				
	$K\beta_1$	1·620 73				
	A.E.	1·607 2				
Fe, 26	$K\alpha_1$	1·935 97	7·1	40	Mn	0·016
	$K\alpha_2$	1·939 91				
	$K\beta_1$	1·756 54				
	A.E.	1·742 9				
Mn, 25	$K\alpha_1$	2·101 74	6·5	40	Cr	0·016
	$K\alpha_2$	2·105 70				
	$K\beta_1$	1·910 16				
	A.E.	1·895 4				
Cr, 24	$K\alpha_1$	2·289 62	6·0	35	V	0·016
	$K\alpha_2$	2·293 52				
	$K\beta_1$	2·084 79				
	A.E.	2·070 1				

† A.E. = absorption edge

TABLE 2

Some Data for the Elements

Element	Symbol	Atomic number	Atomic weight	Density † (gm./c.c.)	Absorption edge (A.) ‡
Aluminium	Al	13	26·97	2·7	
Antimony	Sb	51	121·76	6·6	*2·9967*
Argon	A	18	39·944	0·0018	
Arsenic	As	33	74·91	5·7	1·0447
Barium	Ba	56	137·36	3·5	0·3314
Beryllium	Be	4	9·02	1·8	
Bismuth	Bi	83	209·00	9·8	*0·9240*
Boron	B	5	10·82	2·0	
Bromine	Br	35	79·916	0·0071	0·9200
Cadmium	Cd	48	112·41	8·6	0·4640
Caesium	Cs	55	132·91	1·9	*2·4724*
Calcium	Ca	20	40·08	1·5	3·0705
Carbon	C	6	12·01	2·3	
Cerium	Ce	58	140·13	6·9	
Chlorine	Cl	17	35·457	0·0032	
Chromium	Cr	24	52·01	7·0	2·0701
Cobalt	Co	27	58·94	8·7	1·6072
Copper	Cu	29	63·57	8·9	1·3802
Fluorine	F	9	19·00	0·0017	
Gallium	Ga	31	69·72	5·9	1·1926
Germanium	Ge	32	72·60	5·5	1·1169
Gold	Au	79	197·2	19·3	*1·0403*
Helium	He	2	4·003	0·00018	
Hydrogen	H	1	1·008	0·00009	
Indium	In	49	114·76	7·3	0·4439
Iodine	I	53	126·92	4·9	0·3742
Iridium	Ir	77	193·1	22·4	*1·1060*
Iron	Fe	26	55·85	7·9	1·7429
Krypton	Kr	36	83·7	0·0037	
Lead	Pb	82	207·21	11·3	*0·9511*
Lithium	Li	3	6·940	0·53	
Magnesium	Mg	12	24·32	1·74	
Manganese	Mn	25	54·93	7·4	1·8954
Mercury	Hg	80	200·61	13·6	1·0095
Molybdenum	Mo	42	95·95	10·1	*0·6197*

†, ‡ See p. 235 for footnotes.

TABLE 2 (*continued*)

Element	Symbol	Atomic Number	Atomic Weight	Density † (gm./c.c.)	Absorption edge (A.) ‡
Neon	Ne	10	20·183	0·00090	
Nickel	Ni	28	58·69	8·9	1·4869
Niobium	Nb (Cb)	41	92·91	8·5	0·6529
Nitrogen	N	7	14·008	0·0012	
Osmium	Os	76	190·2	22·5	*1·1413*
Oxygen	O	8	16·000	0·0014	
Palladium	Pd	46	106·7	12·0	0·5090
Phosphorus	P	15	30·98	2·0	
Platinum	Pt	78	195·23	21·5	*1·0732*
Potassium	K	19	39·096	0·86	3·4379
Radium	Ra	88	226·05	5	
Rhodium	Rh	45	102·91	12·4	0·5341
Rubidium	Rb	37	85·48	1·53	0·8157
Ruthenium	Ru	44	101·7	12·3	0·5595
Scandium	Sc	21	45·10	2·5	2·7573
Selenium	Se	34	78·96	4·5	0·9797
Silicon	Si	14	28·06	2·3	
Silver	Ag	47	107·880	10·5	0·4855
Sodium	Na	11	22·997	0·97	
Strontium	Sr	38	87·63	2·56	0·7700
Sulphur	S	16	32·06	2·0	
Tantalum	Ta	73	180·88	16·6	*1·2542*
Tellurium	Te	52	127·61	6·2	0·3901
Thallium	Tl	81	204·39	11·9	*0·9798*
Thorium	Th	90	232·12	11·3	*0·7615*
Tin	Sn	50	118·70	7·3	0·4248
Titanium	Ti	22	47·90	4·5	2·4962
Tungsten	W	74	183·92	19·3	*1·2154*
Uranium	U	92	238·07	18·7	*0·7223*
Vanadium	V	23	50·95	5·6	2·2676
Xenon	X	54	131·3	0·0058	
Yttrium	Y	39	88·92	3·8	0·7270
Zinc	Zn	30	65·38	7·1	1·2831
Zirconium	Zr	40	91·22	6·4	0·6888

† Densities are given only for the purpose of evaluating linear absorption coefficients ; for more accurate purposes standard tables should be consulted. The values given are those under ordinary laboratory conditions, but for some elements (for example, carbon) density is also dependent upon crystal structure.

‡ Wave-lengths of absorption edges are given only when they come within the range of commonly used emission wave-lengths. The *K* absorption edge is usually given, but where the L_{III} absorption edge is given the figures are italicised.

TABLE 3

Mass Absorption Coefficients, μ_m, for $K\alpha$-Radiations

Atomic No.	Element	Mo λ 0·711 A.	Zn 1·436 A.	Cu 1·542 A.	Ni 1·659 A.	Co 1·790 A.	Fe 1·937 A.	Mn 2·103 A.	Cr 2·291 A.
2	He	0·18	0·31	0·37	0·43	0·52	0·64	0·74	0·86
3	Li	0·22	0·54	0·68	0·87	1·13	1·48	1·76	2·11
4	Be	0·30	1·02	1·35	1·80	2·42	3·24	3·90	4·74
5	B	0·45	2·51	3·06	3·79	4·67	5·80	7·36	9·37
6	C	0·70	4·43	5·50	6·76	8·50	10·7	13·8	17·9
7	N	1·10	6·85	8·51	10·7	13·6	17·3	21·8	27·7
8	O	1·50	11·4	12·7	16·2	20·2	25·2	32·2	40·1
9	F	1·93	14·4	17·5	21·5	26·6	33·0	41·1	51·6
10	Ne	2·67	20·2	24·6	30·2	37·2	46·0	57·6	72·7
11	Na	3·36	25·6	30·9	37·9	46·2	56·9	72·3	92·5
12	Mg	4·38	33·0	40·6	47·9	60·0	75·7	95·2	120
13	Al	5·30	40·0	48·7	58·4	73·4	92·8	117	149
14	Si	6·70	49·5	60·3	75·8	94·1	116	146	192
15	P	7·98	59·4	73·0	90·5	113	141	177	223
16	S	10·0	75·0	91·3	112	139	175	217	273
17	Cl	11·6	85·0	103	126	158	199	245	308
18	A	12·6	93·0	113	141	174	217	270	341
19	K	16·7	119	143	179	218	269	330	425
20	Ca	19·8	142	172	210	257	317	400	508
21	Sc	21·1	153	185	222	273	338	428	545
22	Ti	23·7	167	204	247	304	377	475	603
23	V	26·5	186	227	275	339	422	530	77·3
24	Cr	30·4	213	259	316	392	490	70·5	89·9
25	Mn	33·5	234	284	348	431	63·6	79·6	99·4
26	Fe	38·3	270	324	397	59·5	72·8	90·9	115
27	Co	41·6	292	354	54·4	65·9	80·6	102	126
28	Ni	47·4	325	49·3	61·0	75·1	93·1	116	145
29	Cu	49·7	42·0	52·7	65·0	79·8	98·8	123	154
30	Zn	54·8	49·3	59·0	72·1	88·5	109	135	169
31	Ga	57·3	52·4	63·3	76·9	94·3	116	144	179
32	Ge	63·4	57·6	69·4	84·2	104	128	158	196
33	As	69·5	63·5	76·5	93·8	115	142	175	218
34	Se	74·0	69·4	82·8	101	125	152	188	235
35	Br	82·2	77·0	92·6	112	137	169	206	264

Atomic No.	Element	Mo λ 0·711 A.	Zn 1·436 A.	Cu 1·542 A.	Ni 1·659 A.	Co 1·790 A.	Fe 1·937 A.	Mn 2·103 A.	Cr 2·291 A.
36	Kr	88·1	83·0	100	122	148	182	226	285
37	Rb	94·4	91·5	109	133	161	197	246	309
38	Sr	101·2	100	119	145	176	214	266	334
39	Y	108·9	107	129	158	192	235	289	360
40	Zr	17·2	118	143	173	211	260	317	391
41	Nb	18·7	126	153	183	225	279	338	415
42	Mo	20·2	136	164	197	242	299	360	439
44	Ru	23·4	153	185	221	272	337	404	488
45	Rh	25·3	165	198	240	293	361	432	522
46	Pd	26·7	173	207	254	308	376	450	545
47	Ag	28·6	192	223	276	332	402	483	585
48	Cd	29·9	202	234	289	352	417	500	608
49	In	31·8	214	252	307	366	440	531	648
50	Sn	33·3	230	265	322	382	457	555	681
51	Sb	35·3	245	284	342	404	482	589	727
52	Te	36·1	248	289	347	410	488	598	742
53	I	39·2	269	314	375	442	527	650	808
54	Xe	41·3	283	330	392	463	552	680	852
55	Cs	43·3	298	347	410	486	579	715	844
56	Ba	45·2	307	359	423	501	599	677	819
58	Ce	52·0	358	407	476	549	636	670	235
73	Ta	101	136	164	200	246	305	364	440
74	W	105	143	171	209	258	320	380	456
76	Cs	113	152	186	226	278	346	406	480
77	Ir	118	160	194	237	292	362	422	498
78	Pt	123	172	205	248	304	376	436	518
79	Au	128	179	214	260	317	390	456	537
80	Hg	132	186	223	272	330	404	471	552
81	Tl	136	194	231	282	341	416	484	568
82	Pb	141	202	241	294	354	429	499	585
83	Bi	145	214	253	310	372	448	522	612
88	Ra	172	258	304	371	433	509	598	708
90	Th	143	286	327	399	460	536	633	755
92	U	153	310	352	423	488	566	672	805

TABLE 4

Gram-atomic Absorption Coefficients for $K\alpha$-Radiations

Atomic No.	Element	Mo	Zn	Cu	Ni	Co	Fe	Mn	Cr
2	He	0·72	1·24	1·48	1·72	2·08	2·56	2·96	3·44
3	Li	1·52	3·74	4·72	6·04	7·84	10·3	12·2	14·6
4	Be	2·71	9·20	12·2	16·2	21·8	29·2	35·2	42·8
5	B	4·87	27·2	33·1	41·0	50·5	62·8	79·6	101
6	C	8·41	53·2	66·1	81·2	102	129	165	215
7	N	15·4	96·0	119	150	191	242	305	388
8	O	24·0	182	203	259	323	403	515	642
9	F	36·7	274	332	408	505	627	781	980
10	Ne	53·8	408	497	610	751	928	1160	1470
11	Na	77·3	589	711	872	1060	1310	1660	2130
12	Mg	109	803	988	1160	1460	1840	2310	2920
13	Al	143	1080	1310	1570	1980	2500	3160	4020
14	Si	188	1390	1690	2120	2640	3260	4090	5380
15	P	247	1840	2160	2810	3500	4380	5490	6600
16	S	322	2400	2930	3580	4460	5610	6960	8750
17	Cl	412	3010	3670	4450	5600	7060	8690	10900
18	A	501	3710	4510	5630	6950	8670	10800	13600
19	K	653	4650	5590	7000	8520	10500	12900	16600
20	Ca	794	5690	6890	8420	10300	12700	16000	20400
21	Sc	952	6900	8340	10000	12300	15200	19300	24600
22	Ti	1140	8000	9770	11800	14600	18100	22800	28900
23	V	1350	9480	11600	14000	17300	21500	27000	3940
24	Cr	1580	11100	13500	16400	20400	25500	3670	4680
25	Mn	1840	12900	15600	19100	23700	3490	4370	5460
26	Fe	2140	15100	18100	22200	3320	4070	5080	6400
27	Co	2450	17200	20900	3210	3880	4750	6000	7410
28	Ni	2780	19100	2890	3580	4410	5460	6810	8510
29	Cu	3160	2670	3350	4130	5070	6280	7820	9790
30	Zn	3580	3220	3860	4710	5790	7150	8826	11000
31	Ga	3990	3650	4413	5360	6570	8120	10000	12500
32	Ge	4600	4180	5050	6110	7550	9320	11500	14200
33	As	5210	4760	5730	7030	8610	10600	13100	16300
34	Se	5840	5480	6540	7940	9870	12000	14800	18600
35	Br	6570	6150	7400	8980	10900	13500	16500	21100

Atomic No.	Element	Mo	Zn	Cu	Ni	Co	Fe	Mn	Cr
36	Kr	7370	6950	8400	10200	12400	15200	18900	23900
37	Rb	8080	7820	9330	11400	13800	16800	21000	26400
38	Sr	8870	8760	10400	12700	15400	18800	23300	29300
39	Y	9680	9510	11500	14000	17100	20900	25700	32000
40	Zr	1570	10800	13000	15800	19200	23700	28900	35700
41	Nb	1740	11700	14200	17000	20900	25900	31400	38600
42	Mo	1940	13000	15700	18900	23200	28600	34500	42100
44	Ru	2380	15600	18800	22500	27700	34300	41100	49600
45	Rh	2600	17000	20400	24700	30200	37200	44500	53700
46	Pd	2850	18500	22100	27100	32900	40200	48000	58100
47	Ag	3090	20700	24100	29800	35800	43400	52100	63100
48	Cd	3360	22700	26300	32500	39600	46900	56200	68300
49	In	3650	24600	28900	35200	42000	50500	60900	74400
50	Sn	3950	27300	31500	38200	45300	54200	65900	80800
51	Sb	4300	29800	34600	41600	49200	58700	71700	88500
52	Te	4610	31600	36900	44300	52300	62200	76300	94700
53	I	4980	34100	39900	47600	56100	66900	81600	103000
54	Xe	5420	37200	43300	51500	60800	72500	89200	112000
55	Cs	5760	39600	46100	54500	64600	77000	95000	112000
56	Ba	6210	42200	49300	58100	68800	82300	93000	112000
58	Ce	7290	50200	57000	66700	76900	89100	93900	32900
73	Ta	18200	24600	29700	36200	44500	55200	65800	79600
74	W	19400	26300	31500	38400	47500	58900	69900	83900
76	Os	21500	28900	35400	43000	52900	65800	77200	91300
77	Ir	22800	30900	37500	45800	56400	69900	81500	96200
78	Pt	24000	33600	40000	48400	59300	73400	85100	101000
79	Au	25200	35300	42200	51300	62500	76900	89900	106000
80	Hg	26500	37300	44700	54600	66200	81000	94500	111000
81	Te	27800	39700	47200	57600	69700	85000	98900	116000
82	Pb	29200	41900	49900	60900	73400	88900	103000	121000
83	Bi	30300	44700	52900	64800	77700	93600	109000	128000
88	Ra	38900	58300	68700	83900	97900	115000	135000	160000
90	Th	33200	66400	75900	92600	107000	124000	147000	175000
92	U	36400	73800	83800	101000	116000	135000	160000	192000

TABLE 5

Values of $(h^2+k^2+l^2)$, (h^2+k^2) and (h^2+hk+k^2) up to 100

N	Cubic $N=h^2+k^2+l^2$ P hkl	F hkl	I hkl	Tetragonal $N=h^2+k^2$ hk	Hexagonal $N=h^2+hk+k^2$ hk
1	100			10	10
2	110		110	11	
3	111	111			11
4	200	200	200	20	20
5	210			21	
6	211		211		
7					21
8	220	220	220	22	
9	300			30	30
9	221				
10	310		310	31	
11	311	311			
12	222	222	222		22
13	320			32	31
14	321		321		
15					
16	400	400	400	40	40
17	410			41	
17	322				
18	411		411		
18	330			33	
19	331	331			32
20	420	420	420	42	
21	421				41
22	332		332		
23					
24	422	422	422		
25	500			50	50
25	430			43	
26	510		510	51	
26	431		431		
27	511	511			33
27	333	333			
28					42
29	520			52	
29	432				
30	521		521		
31					51
32	440	440	440		
33	522			44	
33	441				

N	Cubic $N=h^2+k^2+l^2$ P hkl	F hkl	I hkl	Tetragonal $N=h^2+k^2$ hk	Hexagonal $N=h^2+hk+k^2$ hk
34	530		530	53	
34	433		433		
35	531	531			
36	600	600	600	60	60
36	442	442	442		
37	610			61	43
38	611		611		
38	532		532		
39					52
40	620	620	620	62	
41	621				
41	540			54	
41	443				
42	541		541		
43	533	533			61
44	622	622	622		
45	630			63	
45	542				
46	631		631		
47					
48	444	444	444		44
49	700			70	70
49	632				53
50	710		710	71	
50	550		550	55	
50	543		543		
51	711	711			
51	551	551			
52	640	640	640	64	62
53	720			72	
53	641				
54	721		721		
54	633		633		
54	552		552		
55					
56	642	642	642		
57	722				71
57	544				
58	730		730	73	
59	731	731			
59	553	553			

N	Cubic $N=h^2+k^2+l^2$ P hkl	F hkl	I hkl	Tetragonal $N=h^2+k^2$ hk	Hexagonal $N=h^2+hk+k^2$ hk
60					
61	650			65	54
61	643				
62	732		732		
62	651		651		
63					63
64	800	800	800	80	80
65	810			81	
65	740			74	
65	652				
66	811		811		
66	741		741		
66	554		554		
67	733	733			72
68	820	820	820	82	
68	644	644	644		
69	821				
69	742				
70	653		653		
71					
72	822	822	822		
72	660	660	660	66	
73	830			83	81
73	661				
74	831		831		
74	750		750	75	
74	743		743		
75	751	751			55
75	555	555			
76	662	662	662		64
77	832				
77	654				
78	752		752		
79					73
80	840	840	840	84	
81	900			90	90
81	841				
81	744				
81	663				

N	Cubic $N=h^2+k^2+l^2$ P hkl	F hkl	I hkl	Tetragonal $N=h^2+k^2$ hk	Hexagonal $N=h^2+hk+k^2$ hk
82	910		910	91	
82	833		833		
83	911	911			
83	753	753			
84	842	842	842		82
85	920			92	
85	760			76	
86	921		921		
86	761		761		
86	655		655		
87					
88	664	664	664		
89	922			85	
89	850				
89	843				
89	762				
90	930		930	93	
90	851		851		
90	754		754		
91	931	931			65
91					91
92					
93	852				74
94	932		932		
94	763		763		
95					
96	844	844	844		
97	940			94	83
97	665				
98	941		941		
98	853		853		
98	770		770	77	
99	933	933			
99	771	771			
99	755	755			
100	10,00	10,00	10,00	10,0	10,0
100	860	860	860	86	

TABLE 6

Values of $\sin^2\theta$

(The decimal point has been omitted)

$\theta°$	·0	·1	·2	·3	·4	·5	·6	·7	·8	·9	Differences ·01	·02	·03	·04	·05
00	0000	0000	0000	0000	0000	0001	0001	0001	0002	0002					
1	0003	0004	0004	0005	0006	0007	0008	0009	0010	0011					
2	0012	0013	0015	0016	0018	0019	0021	0022	0024	0026					
3	0027	0029	0031	0033	0035	0037	0039	0042	0044	0046					
4	0049	0051	0054	0056	0059	0062	0064	0067	0070	0073					
5	0076	0079	0082	0085	0089	0092	0095	0099	0102	0106	Interpolate				
6	0109	0113	0117	0120	0124	0128	0132	0136	0140	0144					
7	0149	0153	0157	0161	0166	0170	0175	0180	0184	0189					
8	0194	0199	0203	0208	0213	0218	0224	0229	0234	0239					
9	0245	0250	0256	0261	0267	0272	0278	0284	0290	0296					
10	0302	0308	0314	0320	0326	0332	0338	0345	0351	0358	1	1	2	2	3
1	0364	0371	0377	0384	0391	0397	0404	0411	0418	0425	1	1	2	3	3
2	0432	0439	0447	0454	0461	0468	0476	0483	0491	0498	1	1	2	3	4
3	0506	0514	0521	0529	0537	0545	0553	0561	0569	0577	1	2	2	3	4
4	0585	0593	0602	0610	0618	0627	0635	0644	0653	0661	1	2	3	3	4
15	0670	0679	0687	0696	0705	0714	0723	0732	0741	0751	1	2	3	4	4
6	0760	0769	0778	0788	0797	0807	0816	0826	0835	0845	1	2	3	4	5
7	0855	0865	0874	0884	0894	0904	0914	0924	0934	0945	1	2	3	4	5
8	0955	0965	0976	0986	0996	1007	1017	1028	1039	1049	1	2	3	4	5
9	1060	1071	1082	1092	1103	1114	1125	1136	1147	1159	1	2	3	4	6
20	1170	1181	1192	1204	1215	1226	1238	1249	1261	1273	1	2	3	5	6
1	1284	1296	1308	1320	1331	1343	1355	1367	1379	1391	1	2	4	5	6
2	1403	1415	1428	1440	1452	1464	1477	1489	1502	1514	1	2	4	5	6
3	1527	1539	1552	1565	1577	1590	1603	1616	1628	1641	1	3	4	5	6
4	1654	1667	1680	1693	1707	1720	1733	1746	1759	1773	1	3	4	5	7
25	1786	1799	1813	1826	1840	1853	1867	1881	1894	1908	1	3	4	5	7
6	1922	1935	1949	1963	1977	1991	2005	2019	2033	2047	1	3	4	6	7
7	2061	2075	2089	2104	2118	2132	2146	2161	2175	2190	1	3	4	6	7
8	2204	2219	2233	2248	2262	2277	2291	2306	2321	2336	1	3	4	6	7
9	2350	2365	2380	2395	2410	2425	2440	2455	2470	2485	2	3	5	6	8
30	2500	2515	2530	2545	2561	2576	2591	2607	2622	2637	2	3	5	6	8
1	2653	2668	2684	2699	2715	2730	2746	2761	2777	2792	2	3	5	6	8
2	2808	2824	2840	2855	2871	2887	2903	2919	2934	2950	2	3	5	6	8
3	2966	2982	2998	3014	3030	3046	3062	3079	3095	3111	2	3	5	6	8
4	3127	3143	3159	3176	3192	3208	3224	3241	3257	3274	2	3	5	7	8
35	3290	3306	3323	3339	3356	3372	3389	3405	3422	3438	2	3	5	7	8
6	3455	3472	3488	3505	3521	3538	3555	3572	3588	3605	2	3	5	7	8
7	3622	3639	3655	3672	3689	3706	3723	3740	3757	3773	2	3	5	7	8
8	3790	3807	3824	3841	3858	3875	3892	3909	3926	3943	2	3	5	7	8
9	3960	3978	3995	4012	4029	4046	4063	4080	4097	4115	2	3	5	7	9
40	4132	4149	4166	4183	4201	4218	4235	4252	4270	4287	2	3	5	7	9
1	4304	4321	4339	4356	4373	4391	4408	4425	4443	4460	2	3	5	7	9
2	4477	4495	4512	4529	4547	4564	4582	4599	4616	4634	2	3	5	7	9
3	4651	4669	4686	4703	4721	4738	4756	4773	4791	4808	2	3	5	7	9
4	4826	4843	4860	4878	4895	4913	4930	4948	4965	4983	2	3	5	7	9

θ°	·0	·1	·2	·3	·4	·5	·6	·7	·8	·9	Differences ·01	·02	·03	·04	·05
45	5000	5017	5035	5052	5070	5087	5105	5122	5140	5157	2	3	5	7	9
6	5174	5192	5209	5227	5244	5262	5279	5297	5314	5331	2	3	5	7	9
7	5349	5366	5384	5401	5418	5436	5453	5471	5488	5505	2	3	5	7	9
8	5523	5540	5557	5575	5592	5609	5627	5644	5661	5679	2	3	5	7	9
9	5696	5713	5730	5748	5765	5782	5799	5817	5834	5851	2	3	5	7	9
50	5868	5885	5903	5920	5937	5954	5971	5988	6005	6022	2	3	5	7	9
1	6040	6057	6074	6091	6108	6125	6142	6159	6176	6193	2	3	5	7	9
2	6210	6227	6243	6260	6277	6294	6311	6328	6345	6361	2	3	5	7	8
3	6378	6395	6412	6428	6445	6462	6479	6495	6512	6528	2	3	5	7	8
4	6545	6562	6578	6595	6611	6628	6644	6661	6677	6694	2	3	5	7	8
55	6710	6726	6743	6759	6776	6792	6808	6824	6841	6857	2	3	5	7	8
6	6873	6889	6905	6921	6938	6954	6970	6986	7002	7018	2	3	5	7	8
7	7034	7050	7066	7081	7097	7113	7129	7145	7160	7176	2	3	5	6	8
8	7192	7208	7223	7239	7254	7270	7285	7301	7316	7332	2	3	5	6	8
9	7347	7363	7378	7393	7409	7424	7439	7455	7470	7485	2	3	5	6	8
60	7500	7515	7530	7545	7560	7575	7590	7605	7620	7635	2	3	5	6	8
1	7650	7664	7679	7694	7709	7723	7738	7752	7767	7781	2	3	5	6	8
2	7796	7810	7825	7839	7854	7868	7882	7896	7911	7925	1	3	4	6	7
3	7939	7953	7967	7981	7995	8009	8023	8037	8051	8065	1	3	4	6	7
4	8078	8092	8106	8119	8133	8147	8160	8174	8187	8201	1	3	4	6	7
65	8214	8227	8241	8254	8267	8280	8293	8307	8320	8333	1	3	4	5	7
6	8346	8359	8372	8384	8397	8410	8423	8435	8448	8461	1	3	4	5	7
7	8473	8486	8498	8511	8523	8536	8548	8560	8572	8585	1	3	4	5	6
8	8597	8609	8621	8633	8645	8657	8669	8680	8692	8704	1	2	4	5	6
9	8716	8727	8739	8751	8762	8774	8785	8796	8808	8819	1	2	4	5	6
70	8830	8841	8853	8864	8875	8886	8897	8908	8918	8929	1	2	3	5	6
1	8940	8951	8961	8972	8983	8993	9004	9014	9024	9035	1	2	3	4	6
2	9045	9055	9066	9076	9086	9096	9106	9116	9126	9135	1	2	3	4	5
3	9145	9155	9165	9174	9184	9193	9203	9212	9222	9231	1	2	3	4	5
4	9240	9249	9259	9268	9277	9286	9295	9304	9313	9321	1	2	3	4	5
75	9330	9339	9347	9356	9365	9373	9382	9390	9398	9407	1	2	3	4	4
6	9415	9423	9431	9439	9447	9455	9463	9471	9479	9486	1	2	3	3	4
7	9494	9502	9509	9517	9524	9532	9539	9546	9553	9561	1	2	2	3	4
8	9568	9575	9582	9589	9596	9603	9609	9616	9623	9629	1	1	2	3	4
9	9636	9642	9649	9655	9662	9668	9674	9680	9686	9692	1	1	2	3	3
80	9698	9704	9710	9716	9722	9728	9733	9739	9744	9750	1	1	2	2	3
1	9755	9761	9766	9771	9776	9782	9787	9792	9797	9801					
2	9806	9811	9816	9820	9825	9830	9834	9839	9843	9847					
3	9851	9856	9860	9864	9868	9872	9876	9880	9883	9887					
4	9891	9894	9898	9901	9905	9908	9911	9915	9918	9921					
85	9924	9927	9930	9933	9936	9938	9941	9944	9946	9949	Interpolate				
6	9951	9954	9956	9958	9961	9963	9965	9967	9969	9971					
7	9973	9974	9976	9978	9979	9981	9982	9984	9985	9987					
8	9988	9989	9990	9991	9992	9993	9994	9995	9996	9996					
9	9997	9998	9998	9999	9999	9999	1.00	1·00	1·00	1·00					

TABLE 7

Values of cos $2\pi x$ and sin $2\pi x$

Argument for cosines x		cos $2\pi x$ or sin $2\pi x$	Argument for sines x	
0·00	0·00	1·000	0·25	0·25
0·01	0·99	0·998	0·24	0·26
0·02	0·98	0·992	0·23	0·27
0·03	0·97	0·982	0·22	0·28
0·04	0·96	0·969	0·21	0·29
0·05	0·95	0·951	0·20	0·30
0·06	0·94	0·930	0·19	0·31
0·07	0·93	0·905	0·18	0·32
0·08	0·92	0·876	0·17	0·33
0·09	0·91	0·844	0·16	0·34
0·10	0·90	0·809	0·15	0·35
0·11	0·89	0·771	0·14	0·36
0·12	0·88	0·729	0·13	0·37
0·13	0·87	0·685	0·12	0·38
0·14	0·86	0·637	0·11	0·39
0·15	0·85	0·588	0·10	0·40
0·16	0·84	0·536	0·09	0·41
0·17	0·83	0·482	0·08	0·42
0·18	0·82	0·426	0·07	0·43
0·19	0·81	0·368	0·06	0·44
0·20	0·80	0·309	0·05	0·45
0·21	0·79	0·249	0·04	0·46
0·22	0·78	0·187	0·03	0·47
0·23	0·77	0·125	0·02	0·48
0·24	0·76	0·063	0·01	0·49
0·25	0·75	0·000	0·00	0·50
0·26	0·74	−0·063	0·99	0·51
0·27	0·73	−0·125	0·98	0·52
0·28	0·72	−0·187	0·97	0·53
0·29	0·71	−0·249	0·96	0·54
0·30	0·70	−0·309	0·95	0·55
0·31	0·69	−0·368	0·94	0·56
0·32	0·68	−0·426	0·93	0·57
0·33	0·67	−0·482	0·92	0·58
0·34	0·66	−0·536	0·91	0·59
0·35	0·65	−0·588	0·90	0·60
0·36	0·64	−0·637	0·89	0·61
0·37	0·63	−0·685	0·88	0·62
0·38	0·62	−0·729	0·87	0·63
0·39	0·61	−0·771	0·86	0·64
0·40	0·60	−0·809	0·85	0·65
0·41	0·59	−0·844	0·84	0·66
0·42	0·58	−0·876	0·83	0·67
0·43	0·57	−0·905	0·82	0·68
0·44	0·56	−0·930	·081	0·69
0·45	0·55	−0·951	0·80	0·70
0·46	0·54	−0·969	0·79	0·71
0·47	0·53	−0·982	0·78	0·72
0·48	0·52	−0·992	0·77	0·73
0·49	0·51	−0·998	0·76	0·74
0·50	0·50	−1·000	0·75	0·75

TABLE 8

Values of $(1+\cos^2 2\theta)/\sin 2\theta$

$\theta°$	·0	·1	·2	·3	·4	·5	·6	·7	·8	·9	·0	$\theta°$
2	28·60	27·23	25·99	24·86	23·82	22·86	21·98	21·16	20·40	19·69	19·03	87
3	19·03	18·41	17·83	17·28	16·77	16·29	15·83	15·40	14·99	14·60	14·23	86
4	14·23	13·88	13·54	13·22	12·92	12·63	12·35	12·08	11·82	11·58	11·34	85
5	11·34	11·12	10·90	10·69	10·49	10·29	10·10	9·921	9·745	9·576	9·412	84
6	9·412	9·253	9·099	8·950	8·806	8·666	8·530	8·398	8·270	8·146	8·025	83
7	8·025	7·908	7·794	7·682	7·574	7·468	7·366	7·266	7·168	7·073	6·980	82
8	6·980	6·890	6·801	6·715	6·631	6·548	6·468	6·389	6·312	6·237	6·163	81
9	6·163	6·091	6·021	5·952	5·884	5·818	5·753	5·689	5·627	5·566	5·506	80
10	5·506	5·447	5·389	5·332	5·277	5·222	5·169	5·116	5·065	5·014	4·964	79
11	4·964	4·915	4·867	4·820	4·773	4·728	4·683	4·639	4·595	4·553	4·510	78
12	4·510	4·469	4·428	4·388	4·349	4·310	4·271	4·234	4·197	4·160	4·124	77
13	4·124	4·088	4·053	4·019	3·985	3·951	3·918	3·886	3·854	3·822	3·791	76
14	3·791	3·760	3·729	3·700	3·670	3·641	3·612	3·583	3·555	3·527	3·500	75
15	3·500	3·473	3·446	3·420	3·394	3·368	3·343	3·318	3·293	3·268	3·244	74
16	3·244	3·220	3·197	3·173	3·150	3·128	3·105	3·083	3·061	3·039	3·017	73
17	3·017	2·996	2·975	2·954	2·934	2·913	2·893	2·873	2·854	2·834	2·815	72
18	2·815	2·796	2·777	2·758	2·740	2·722	2·703	2·686	2·668	2·650	2·633	71
19	2·633	2·616	2·599	2·582	2·565	2·549	2·532	2·516	2·500	2·484	2·469	70
20	2·469	2·453	2·438	2·422	2·407	2·392	2·378	2·363	2·348	2·334	2·320	69
21	2·320	2·306	2·292	2·278	2·264	2·251	2·237	2·224	2·210	2·197	2·184	68
22	2·184	2·172	2·159	2·146	2·134	2·121	2·109	2·097	2·085	2·073	2·061	67
23	2·061	2·049	2·038	2·026	2·015	2·003	1·992	1·981	1·970	1·959	1·948	66
24	1·948	1·937	1·927	1·916	1·906	1·895	1·885	1·875	1·865	1·855	1·845	65
25	1·845	1·835	1·825	1·816	1·806	1·796	1·787	1·778	1·768	1·759	1·750	64
26	1·750	1·741	1·732	1·723	1·714	1·706	1·697	1·688	1·680	1·672	1·663	63
27	1·663	1·655	1·647	1·638	1·630	1·622	1·614	1·606	1·599	1·591	1·583	62
28	1·583	1·576	1·568	1·561	1·553	1·546	1·539	1·532	1·524	1·517	1·510	61
29	1·510	1·503	1·496	1·490	1·483	1·476	1·470	1·463	1·456	1·450	1·443	60
30	1·443	1·437	1·431	1·424	1·418	1·412	1·406	1·400	1·394	1·388	1·382	59
31	1·382	1·376	1·371	1·365	1·359	1·354	1·348	1·343	1·337	1·332	1·326	58
32	1·326	1·321	1·316	1·311	1·306	1·300	1·295	1·290	1·285	1·280	1·276	57
33	1·276	1·271	1·266	1·262	1·257	1·252	1·248	1·243	1·239	1·234	1·230	56
34	1·230	1·226	1·221	1·217	1·213	1·209	1·205	1·201	1·196	1·192	1·189	55
35	1·189	1·185	1·181	1·177	1·174	1·170	1·166	1·162	1·159	1·155	1·152	54
36	1·152	1·148	1·145	1·142	1·138	1·135	1·132	1·129	1·126	1·122	1·119	53
37	1·119	1·116	1·113	1·110	1·107	1·105	1·102	1·099	1·096	1·094	1·091	52
38	1·091	1·088	1·086	1·083	1·081	1·078	1·076	1·073	1·071	1·069	1·066	51
39	1·066	1·064	1·062	1·060	1·058	1·056	1·054	1·052	1·050	1·048	1·046	50
40	1·046	1·044	1·042	1·041	1·039	1·037	1·036	1·034	1·032	1·031	1·029	49
41	1·029	1·028	1·026	1·025	1·024	1·022	1·021	1·020	1·019	1·018	1·016	48
42	1·016	1·015	1·014	1·013	1·012	1·012	1·011	1·010	1·009	1·008	1·007	47
43	1·007	1·007	1·006	1·005	1·005	1·004	1·004	1·003	1·003	1·002	1·002	46
44	1·002	1·002	1·001	1·001	1·001	1·000	1·000	1·000	1·000	1·000	1·000	45
°	·0	·9	·8	·7	·6	·5	·4	·3	·2	·1	·0	$\theta°$

Values of the function for angles less than 45° are obtained for the degree values at the left and at the top of the table; those for angles greater than 45°, from the values in the right and at the bottom.

TABLE 9

Values of $(1 + \cos^2 2\theta)/\sin^2 \theta \cos \theta$

$\theta°$	·0	·1	·2	·3	·4	·5	·6	·7	·8	·9
2	1639	1486	1354	1239	1138	1048	968·9	898·3	835·1	778·4
3	727·2	680·9	638·8	600·5	565·6	533·6	504·3	477·3	452·3	429·3
4	408·0	388·2	369·9	352·7	336·8	321·9	308·0	294·9	282·6	271·1
5	260·3	250·1	240·5	231·4	222·9	214·7	207·1	199·8	192·9	186·3
6	180·1	174·2	168·5	163·1	158·0	153·1	148·4	144·0	139·7	135·6
7	131·7	128·0	124·4	120·9	117·6	114·4	111·4	108·5	105·6	102·9
8	100·3	97·80	95·37	93·03	90·78	88·60	86·51	84·48	82·52	80·63
9	78·79	77·02	75·31	73·66	72·05	70·49	68·99	67·53	66·12	64·74
10	63·41	62·12	60·87	59·65	58·46	57·32	56·20	55·11	54·06	53·03
11	52·04	51·06	50·12	49·19	48·30	47·43	46·58	45·75	44·94	44·16
12	43·39	42·64	41·91	41·20	40·50	39·82	39·16	38·51	37·88	37·27
13	36·67	36·08	35·50	34·94	34·39	33·85	33·33	32·81	32·31	31·82
14	31·34	30·87	30·41	29·96	29·51	29·08	28·66	28·24	27·83	27·44
15	27·05	26·66	26·29	25·92	25·56	25·21	24·86	24·52	24·19	23·86
16	23·54	23·23	22·92	22·61	22·32	22·02	21·74	21·46	21·18	20·91
17	20·64	20·38	20·12	19·87	19·62	19·38	19·14	18·90	18·67	18·44
18	18·22	18·00	17·78	17·57	17·36	17·15	16·95	16·75	16·56	16·36
19	16·17	15·99	15·80	15·62	15·45	15·27	15·10	14·93	14·76	14·60
20	14·44	14·28	14·12	13·97	13·81	13·66	13·52	13·37	13·23	13·09
21	12·95	12·81	12·68	12·54	12·41	12·28	12·15	12·03	11·91	11·78
22	11·66	11·54	11·43	11·31	11·20	11·09	10·98	10·87	10·76	10·65
23	10·55	10·45	10·35	10·24	10·15	10·05	9·951	9·857	9·763	9·671
24	9·579	9·489	9·400	9·313	9·226	9·141	9·057	8·973	8·891	8·810
25	8·730	8·651	8·573	8·496	8·420	8·345	8·271	8·198	8·126	8·054
26	7·984	7·915	7·846	7·778	7·711	7·645	7·580	7·515	7·452	7·389
27	7·327	7·266	7·205	7·145	7·086	7·027	6·969	6·912	6·856	6·800
28	6·745	6·692	6·637	6·584	6·532	6·480	6·429	6·379	6·329	6·279
29	6·230	6·183	6·135	6·088	6·042	5·995	5·950	5·905	5·861	5·817
30	5·774	5·731	5·688	5·647	5·605	5·564	5·524	5·484	5·445	5·406
31	5·367	5·329	5·292	5·254	5·218	5·181	5·145	5·110	5·075	5·040
32	5·006	4·972	4·939	4·906	4·873	4·841	4·809	4·777	4·746	4·715
33	4·685	4·655	4·625	4·595	4·566	4·538	4·509	4·481	4·453	4·426
34	4·399	4·372	4·346	4·320	4·294	4·268	4·243	4·218	4·193	4·169
35	4·145	4·121	4·097	4·074	4·052	4·029	4·006	3·984	3·962	3·941
36	3·919	3·898	3·877	3·857	3·836	3·816	3·797	3·777	3·758	3·739
37	3·720	3·701	3·683	3·665	3·647	3·629	3·612	3·594	3·577	3·561
38	3·544	3·527	3·513	3·497	3·481	3·465	3·449	3·434	3·419	3·404
39	3·389	3·375	3·361	3·347	3·333	3·320	3·306	3·293	3·280	3·268
40	3·255	3·242	3·230	3·218	3·206	3·194	3·183	3·171	3·160	3·149
41	3·138	3·127	3·117	3·106	3·096	3·086	3·076	3·067	3·057	3·048
42	3·038	3·029	3·020	3·012	3·003	2·994	2·986	2·978	2·970	2·962
43	2·954	2·946	2·939	2·932	2·925	2·918	2·911	2·904	2·897	2·891
44	2·884	2·878	2·872	2·866	2·860	2·855	2·849	2·844	2·838	2·833

θ°	·0	·1	·2	·3	·4	·5	·6	·7	·8	·9
45	2·828	2·824	2·819	2·814	2·810	2·805	2·801	2·797	2·793	2·789
46	2·785	2·782	2·778	2·775	2·772	2·769	2·766	2·763	2·760	2·757
47	2·755	2·752	2·750	2·748	2·746	2·744	2·742	2·740	2·738	2·737
48	2·736	2·735	2·733	2·732	2·731	2·730	2·730	2·729	2·729	2·728
49	2·728	2·728	2·728	2·728	2·728	2·728	2·729	2·729	2·730	2·730
50	2·731	2·732	2·733	2·734	2·735	2·737	2·738	2·740	2·741	2·743
51	2·745	2·747	2·749	2·751	2·753	2·755	2·758	2·760	2·763	2·766
52	2·769	2·772	2·775	2·778	2·782	2·785	2·788	2·792	2·795	2·799
53	2·803	2·807	2·811	2·815	2·820	2·824	2·828	2·833	2·838	2·843
54	2·848	2·853	2·858	2·863	2·868	2·874	2·879	2·885	2·890	2·896
55	2·902	2·908	2·914	2·921	2·927	2·933	2·940	2·946	2·953	2·960
56	2·967	2·974	2·981	2·988	2·996	3·004	3·011	3·019	3·026	3·034
57	3·042	3·050	3·059	3·067	3·075	3·084	3·092	3·101	3·110	3·119
58	3·128	3·137	3·147	3·156	3·166	3·175	3·185	3·195	3·205	3·215
59	3·225	3·235	3·246	3·256	3·267	3·278	3·289	3·300	3·311	3·322
60	3·333	3·345	3·356	3·368	3·380	3·392	3·404	3·416	3·429	3·441
61	3·454	3·466	3·479	3·492	3·505	3·518	3·532	3·545	3·559	3·573
62	3·587	3·601	3·615	3·629	3·643	3·658	3·673	3·688	3·703	3·718
63	3·733	3·749	3·764	3·780	3·796	3·812	3·828	3·844	3·861	3·878
64	3·894	3·911	3·928	3·946	3·963	3·980	3·998	4·016	4·034	4·052
65	4·071	4·090	4·108	4·127	4·147	4·166	4·185	4·205	4·225	4·245
66	4·265	4·285	4·306	4·327	4·348	4·369	4·390	4·412	4·434	4·456
67	4·478	4·500	4·523	4·546	4·569	4·592	4·616	4·640	4·664	4·688
68	4·712	4·737	4·762	4·787	4·812	4·838	4·864	4·890	4·916	4·943
69	4·970	4·997	5·024	5·052	5·080	5·109	5·137	5·166	5·195	5·224
70	5·254	5·284	5·315	5·345	5·376	5·408	5·440	5·471	5·504	5·536
71	5·569	5·602	5·636	5·670	5·705	5·740	5·775	5·810	5·846	5·883
72	5·919	5·956	5·994	6·032	6·071	6·109	6·149	6·189	6·229	6·270
73	6·311	6·352	6·394	6·437	6·480	6·524	6·568	6·613	6·658	6·703
74	6·750	6·797	6·844	6·892	6·941	6·991	7·041	7·091	7·142	7·194
75	7·247	7·300	7·354	7·409	7·465	7·521	7·578	7·636	7·694	7·753
76	7·813	7·874	7·936	7·999	8·063	8·128	8·193	8·259	8·327	8·395
77	8·465	8·536	8·607	8·680	8·754	8·829	8·905	8·982	9·061	9·142
78	9·223	9·305	9·389	9·474	9·561	9·649	9·739	9·831	9·924	10·02
79	10·12	10·21	10·31	10·41	10·52	10·62	10·73	10·84	10·95	11·06
80	11·18	11·30	11·42	11·54	11·67	11·80	11·93	12·06	12·20	12·34
81	12·48	12·63	12·78	12·93	13·08	13·24	13·40	13·57	13·74	13·92
82	14·10	14·28	14·47	14·66	14·86	15·07	15·28	15·49	15·71	15·94
83	16·17	16·41	16·66	16·91	17·17	17·44	17·72	18·01	18·31	18·61
84	18·93	19·25	19·59	19·94	20·30	20·68	21·07	21·47	21·89	22·32
85	22·77	23·24	23·73	24·24	24·78	25·34	25·92	26·52	27·16	27·83
86	28·53	29·27	30·04	30·86	31·73	32·64	33·60	34·63	35·72	36·88
87	38·11	39·43	40·84	42·36	44·00	45·76	47·68	49·76	52·02	54·50

TABLE 10

Values of $\frac{1}{2}\left(\frac{\cos^2\theta}{\sin\theta}+\frac{\cos^2\theta}{\theta}\right)$

θ°	·0	·1	·2	·3	·4	·5	·6	·7	·8	·9
10	5·572	5·513	5·456	5·400	5·345	5·291	5·237	5·185	5·134	5·084
11	5·034	4·986	4·939	4·892	4·846	4·800	4·756	4·712	4·669	4·627
12	4·585	4·544	4·504	4·464	4·425	4·386	4·348	4·311	4·274	4·238
13	4·202	4·167	4·133	4·098	4·065	4·032	3·999	3·967	3·935	3·903
14	3·872	3·842	3·812	3·782	3·753	3·724	3·695	3·667	3·639	3·612
15	3·584	3·558	3·531	3·505	3·479	3·454	3·429	3·404	3·379	3·355
16	3·331	3·307	3·284	3·260	3·237	3·215	3·192	3·170	3·148	3·127
17	3·105	3·084	3·063	3·042	3·022	3·001	2·981	2·962	2·942	2·922
18	2·903	2·884	2·865	2·847	2·828	2·810	2·792	2·774	2·756	2·738
19	2·721	2·704	2·687	2·670	2·653	2·636	2·620	2·604	2·588	2·572
20	2·556	2·540	2·525	2·509	2·494	2·479	2·464	2·449	2·434	2·420
21	2·405	2·391	2·376	2·362	2·348	2·335	2·321	2·307	2·294	2·280
22	2·267	2·254	2·241	2·228	2·215	2·202	2·189	2·177	2·164	2·152
23	2·140	2·128	2·116	2·104	2·092	2·080	2·068	2·056	2·045	2·034
24	2·022	2·011	2·000	1·989	1·978	1·967	1·956	1·945	1·934	1·924
25	1·913	1·903	1·892	1·882	1·872	1·861	1·851	1·841	1·831	1·821
26	1·812	1·802	1·792	1·782	1·773	1·763	1·754	1·745	1·735	1·726
27	1·717	1·708	1·699	1·690	1·681	1·672	1·663	1·654	1·645	1·637
28	1·628	1·619	1·611	1·602	1·594	1·586	1·577	1·569	1·561	1·553
29	1·545	1·537	1·529	1·521	1·513	1·505	1·497	1·489	1·482	1·474
30	1·466	1·459	1·451	1·444	1·436	1·429	1·421	1·414	1·407	1·400
31	1·392	1·385	1·378	1·371	1·364	1·357	1·350	1·343	1·336	1·329
32	1·323	1·316	1·309	1·302	1·296	1·289	1·282	1·276	1·269	1·263
33	1·256	1·250	1·244	1·237	1·231	1·225	1·218	1·212	1·206	1·200
34	1·194	1·188	1·182	1·176	1·170	1·164	1·158	1·152	1·146	1·140
35	1·134	1·128	1·123	1·117	1·111	1·106	1·100	1·094	1·088	1·083
36	1·078	1·072	1·067	1·061	1·056	1·050	1·045	1·040	1·034	1·029
37	1·024	1·019	1·013	1·008	1·003	0·998	0·993	0·988	0·982	0·977
38	0·972	0·967	0·962	0·958	0·953	0·948	0·943	0·938	0·933	0·928
39	0·924	0·919	0·914	0·909	0·905	0·900	0·895	0·891	0·886	0·881
40	0·877	0·872	·0868	0·863	0·859	0·854	0·850	0·845	0·841	0·837
41	0·832	·0828	0·823	0·819	0·815	0·810	0·806	0·802	0·798	0·794
42	0·789	0·785	0·781	0·777	0·773	0·769	0·765	0·761	0·757	0·753
43	0·749	0·745	0·741	0·737	0·733	0·729	0·725	0·721	0·717	0·713
44	0·709	0·706	0·702	0·698	0·694	0·690	0·687	0·683	0·679	0·676
45	0·672	0·668	0·665	0·661	0·657	0·654	0·650	0·647	0·643	0·640
46	0·636	0·632	0·629	0·625	0·622	0·619	0·615	0·612	0·608	0·605
47	0·602	0·598	0·595	0·591	0·588	0·585	0·582	0·578	0·575	0·572
48	0·569	0·565	0·562	0·559	0·556	0·553	0·549	0·546	0·543	0·540
49	0·537	0·534	0·531	0·528	0·525	0·522	0·518	0·515	0·512	0·509

TABLE 10 (*continued*)

$\theta°$	·0	·1	·2	·3	·4	·5	·6	·7	·8	·9
50	0·506	0·504	0·501	0·498	0·495	0·492	0·489	0·486	0·483	0·480
51	0·477	0·474	0·472	0·469	0·466	0·463	0·460	0·458	0·455	0·452
52	0·449	0·447	0·444	0·441	0·439	0·436	0·433	0·430	0·428	0·425
53	0·423	0·420	0·417	0·415	0·412	0·410	0·407	0·404	0·402	0·399
54	0·397	0·394	0·392	0·389	0·387	0·384	0·382	0·379	0·377	0·375
55	0·372	0·370	0·367	0·365	0·363	0·360	0·358	0·356	0·353	0·351
56	0·349	0·346	0·344	0·342	0·339	0·337	0·335	0·333	0·330	0·328
57	0·326	0·324	0·322	0·319	0·317	0·315	0·313	0·311	0·309	0·306
58	0·304	0·302	0·300	0·298	0·296	0·294	0·292	0·290	0·288	0·286
59	0·284	0·282	0·280	0·278	0·276	0·274	0·272	0·270	0·268	0·266
60	0·264	0·262	0·260	0·258	0·256	0·254	0·252	0·250	0·249	0·247
61	0·245	0·243	0·241	0·239	0·237	0·236	0·234	0·232	0·230	0·229
62	0·227	0·225	0·223	0·221	0·220	0·218	0·216	0·215	0·213	0·211
63	0·209	0·208	0·206	0·204	0·203	0·201	0·199	0·198	0·196	0·195
64	0·193	0·191	0·190	0·188	0·187	0·185	0·184	0·182	0·180	0·179
65	0·177	0·176	0·174	0·173	0·171	0·170	0·168	0·167	0·165	0·164
66	0·162	0·161	0·160	0·158	0·157	0·155	0·154	0·152	0·151	0·150
67	0·148	0·147	0·146	0·144	0·143	0·141	0·140	0·139	0·138	0·136
68	0·135	0·134	0·132	0·131	0·130	0·128	0·127	0·126	0·125	0·123
69	0·122	0·121	0·120	0·119	0·117	0·116	0·115	0·114	0·112	0·111
70	0·110	0·109	0·108	0·107	0·106	0·104	0·103	0·102	0·101	0·100
71	0·099	0·098	0·097	0·096	0·095	0·094	0·092	0·091	0·090	0·089
72	0·088	0·087	0·086	0·085	0·084	0·083	0·082	0·081	0·080	0·079
73	0·078	0·077	0·076	0·075	0·075	0·074	0·073	0·072	0·071	0·070
74	0·069	0·068	0·067	0·066	0·065	0·065	0·064	0·063	0·062	0·061
75	0·060	0·059	0·059	0·058	0·057	0·056	0·055	0·055	0·054	0·053
76	0·052	0·052	0·051	0·050	0·049	0·048	0·048	0·047	0·046	0·045
77	0·045	0·044	0·043	0·043	0·042	0·041	0·041	0·040	0·039	0·039
78	0·038	0·037	0·037	0·036	0·035	0·035	0·034	0·034	0·033	0·032
79	0·032	0·031	0·031	0·030	0·029	0·029	0·028	0·028	0·027	0·027
80	0·026	0·026	0·025	0·025	0·024	0·023	0·023	0·023	0·022	0·022
81	0·021	0·021	0·020	0·020	0·019	0·019	0·018	0·018	0·017	0·017
82	0·017	0·016	0·016	0·015	0·015	0·015	0·014	0·014	0·013	0·013
83	0·013	0·012	0·012	0·012	0·011	0·011	0·010	0·010	0·010	0·010
84	0·009	0·009	0·009	0·008	0·008	0·008	0·007	0·007	0·007	0·007
85	0·006	0·006	0·006	0·006	0·005	0·005	0·005	0·005	0·005	0·004
86	0·004	0·004	0·004	0·003	0·003	0·003	0·003	0·003	0·003	0·002
87	0·002	0·002	0·002	0·002	0·002	0·002	0·001	0·001	0·001	0·001
88	0·001	0·001	0·001	0·001	0·001	0·001	0·001	0·000	0·000	0·000

Reprinted by permission of the Physical Society and the authors, Nelson and Riley (1945*a*)

SUBJECT INDEX

Where a main reference exists under a heading, it is printed in bold type

Greek letters
- α, β } angles of tilt, 102
- α, β, γ } interaxial angles, 8
- α, β } radiations, 26
- ζ, 39
- η, 96
- θ, 36
- λ, 25
- μ, absorption coefficient, 30
- μ, angular displacement of layer line, 93
- ν, 49
- ξ, 39
- ρ, density, 29
- ρ, polar co-ordinate, 39
- ϕ, angle of powder camera, 171
- ϕ, cylindrical co-ordinate, 39
- ψ, angle of powder camera, 171
- ψ, polar co-ordinate, 39

Absent reflections, 100, 210
Absolute intensities, 201
Absorbing wheel, 203
Absorption coefficients, 29, 30, 97
- edges, 30, 31
- error in powder lines, **171**, 190, 221
- factor, 204, 205
- in air in powder camera, 173
- in powder specimens, 171

Accuracy of lattice-parameter measurements, 191
Alloy targets, 192
Alloys, 222
Alpha (α) doublet, 28, 57, 191
Aluminium, 86, 196, 221
Angström unit (A.), 25, **29**
Anticathode, 27
Anti-phase nuclei, 217
Apparent crystal size, 217
Aragonite, 17
A.S.T.M. index, **220**, 224
Asymmetric lines on powder photographs, 169
Asymmetric method for powder photographs, 171
Atomic absorption coefficient, 30
Atomic scattering factors, 207
$AuCu_3$, 211, 217
Avogadro's number, 29, 30
Axial ratio (*see also* Unit cell), 7, **10**, 118, 163, 165

Background on powder photographs, 169, 201
Back-reflection cameras, **175**, 190
Back-reflection Laue photograph, 41, 81-84
Base breadth of powder lines, 214
Bernal chart, **50** ff., 58, 62, 64, 131
Beryl, 13
Bjurström charts, 184 ff.
Block specimens, 175
Borosilicate glass, 170
Bragg law, 34 ff., 40
Bravais lattice, 11 ff., 37 ff., 49, 52, 53, 62, **132** ff.
Breadths of powder lines, 214
Broadening of powder lines, 212, **213**
Buerger (Precession) method, 45
Bunn charts, 187, **188**

Calcite, 29, 32, 163 ff.
Calculation of lattice parameters, 192
Cams, 46, 47
Canada balsam, 170
Central point row, 89
Centro-symmetry, 3, 6, 161
Characteristic radiation, **26**, 55, 57, 58, 113
Charts, Bernal (ξ–ζ), 50 ff.
- Bunn, 188
- rho-phi (ρ-ϕ), 108
- theta (θ), 108
- Weissenberg, 89, **91**
- Wooster, 94, **95**

Chemical analysis, 219
Choice of radiation, 192, 195
Choice of size of powder camera, 176
Clinographic projection, 18, 24
Cobalt, 211, 218
Collimator for powder cameras, 169
Collimators, 46
Complementary forms, 153, 207
Constancy of angle, Law of, 15
Continuous radiation, 25, 55, 57
Co-ordinates, Crystallographic, 39, 103 ff.
Cristobalite, 222
Crystal classes, 7, 9, **146** ff., 150–151
Crystal constants, 13 ff.
Crystal faces, 5, 158
- forms, 5
- lattices, 9, 11 ff.

Crystal-lattice constants, 13
Crystal optics, 101, 219
Crystal-reflected radiation, **32**, 55, 57, 204
Crystal systems, 7 ff.
Crystallographic axes, 4 ff.
$CuAl_2$, 181
CuZn, 208
Cylindrical co-ordinates, 39, 51
- screen, 43, 89

d-values (*see* Spacing of lattice planes)
De Jong-Bouman Method, 44, 45
Density, 196
Depression of scattering factors, 208
Description of powder photographs, 220
Diameters of powder cameras, 173, 176
Diamond, 15, 32, 55–61, 110–120, 203
Dibromocholesteryl chloride, 88
Displacement of powder specimens, 189
Distortion, 218
Divergence of X-ray beams, 190
Divergent-beam photograph, **42**
Divided-beam photometer, 199
Double-crystal Weissenberg goniometer, 96, 97
Doublets, 191

Electron orbits, 26, 31
Ellipsoid axes, 5
Enantiomorphism, 5, 6, 161, 162
Equations to the normal, 16
Equatorial inclination–Weissenberg photograph, 93
Equal-area (Lambert's) projection, 22, 24
Equi-inclination Weissenberg photograph, 99
Equivalent positions, 209
Error curve, 214, 215
Errors in powder lines, 189, 190
Etch figures, 101, 102, **158**
Excitation voltage, 27, 32
Extinction, 205
Extrapolation for elimination of errors, 189 ff.

Face symmetry, 158, 160
Faults in crystal structure, 217
FeAl, 211
Fe_3Al, 222
Fe-Si, 222, 223
Felspar, 16, 121
Fibre photographs, 41, 42, 45, 122 ff., 130, 131
  texture, 122
Fibres, 122
  organic, 130
Film shrinkage, 190
Filters, 31, 32, 55, 58
Fluorescent radiation, 29, 31, 32
Fluorite, 32
Fluorspar, 203
Focus of X-ray tube, 27, 169
Focusing cameras, 174
' Forbidden ' numbers of powder lines, 179
Forms of faces and zone axes, 5, 149, 152 ff.
Fourier transform, 216
Friedel law, 36

Gas X-ray tube, 27
Geometrical structure factor, 207, **209**
Glancing-angle cameras, 175
Glide planes, 211
Glide twinning, 17
Gnomonic projection, 21 ff., 24, 74, 75, 84
  net, 21, 85
Goniometer, Optical, 101
  X-ray,
    Laue, 71
Goniometer,
  X-ray,
    Oscillation, 48
    Weissenberg, 43, 87
      Two-crystal Weissenberg, 96, 97, 99
Grain size in metals, 212
Gram-atomic absorption coefficient, 30
Graphical methods for indexing powder photographs, 184
Gypsum, 16, 32, 66, 68, 70, 80, 81, 93, 98, 119 ff., 138 ff.
  twin, 120
Guttapercha, 131

Half-peak breadth, 214
Harmful effects of X-rays, 33
Harmonics (of characteristic radiation), 32
Height of powder specimen, 190
Hexagonal axes, 10, 119, 141
High-temperature powder cameras, 173
Hot-cathode tube, 27
Hull-Davey charts, 186

Identity period, 52
Inclination angle (μ), 93
Indices (plane, face, Miller), **4**, 34, 35
  Zone, 6, 15, 141
Integral breadth, 214
Integrated reflection, **202**, 204
Integrating photometer, 200
Intensity formulae, 204
Intensity of reflection, 152, 204 ff.
Inter-axial angles, 8, 10
Internal strains, 173, **196**, 212
Interplanar spacing, 35, 36
Ionisation spectrometer, 115 ff., 201
Iron, 86
Iron-cobalt oxide, 179
Iron pyrites, 75 ff.

Kα doublet, 28
Kilo-X units (kX.), 29
Knife edges, 170

Lattice, Bravais, 132 ff., 137
  constants, 13
  Hexagonal and Rhombohedral, 141 ff., 153
  parameters, 10, 189 ff., 223
  planes, 14, 15
  Reciprocal, 37
Laue goniometer, 71
  -oscillation photographs, 112, 113
  photographs, 41, 42, **71** ff., 107ff., 117, 120, 161
    (back-reflection), 41
    standard sets of, 86
    symmetry of, 41
    transmission, 41
  symmetry, 58, **160** ff.
  symmetry groups, 9
Layer lines, **49**, 51, 58, 62, 67
LiF, 221
Limiting sphere, 48
Linear absorption coefficient, 30
Low-angle scattering, 217

Low-temperature camera, 173
Lunes, 54, 58, 60, 66

Magnification for measurement of powder photographs, 171
Mass-absorption coefficient, 30
Mathematical tables, 192
Matrices (*see* Transformation of axes and indices)
Maximum speed of crystal rotation, 47
Measurement of powder photographs, 171
Metal wires, 122, 123
  sheets, 122, 125
Mica, 14
Micro absorption factor, 205
Miller indices (or symbols), **4**, 34, 35, 142, 143, 153, 163
  -Bravais indices, 142, 143, 153, 163
Minerals, 122, 224
Mixtures of powders, 221
Molybdenum, 126 ff.
Molybdenum trioxide, 79
Morphology of crystals, 3
Morphological constants, 13
Mosaic crystal, 97
Mosaic structure, 206
Moving-film methods, **43**, 44, 45, **87** ff., 109, 126, 129
  Buerger (precession), 45
  for fibre specimens, 42
  De Jong-Bouman, 44
  Schiebold-Sauter, 44
  Weissenberg, 43, **87** ff.
Multiple films, 201
Multiplicity, 182, 204, **206**
Multiplicity factors, 153 ff., 156–157
Muscovite mica, 14

$NiAl_3$, 178, 182–184
Normal-beam Weissenberg photograph, 92, 94

Optical activity, 6, 161, 162
  goniometry, 101
Optical properties of crystals, 219, 224
Orders of reflection, 36
Orientation of crystals, 101 ff.
  by X-ray methods, 107 ff.
Orthographic projections, 18, 24
Oscillating, Methods of, 46, 47
Oscillation photograph, 41 ff., **48** ff., 102, 103, 109, 117, 161 ff.
  symmetry of, 58

Particle size, 217
Perfect crystals, 97
Phase boundaries, 196
Phase change on scattering, 205
Photocell, 198
Photographic blackening, 198
Photometers, 198
Physical properties of crystals, 9
Pentaerythritol, 32
Piezoelectricity, 160
Pin-hole blemishes in film, 200
Plane spacings, **35**, 152, 153, 167
Point groups, 7, 147, 148, 150, 151
Poisson's ratio, 197
Polar directions, 102, 158, 159, 160, 164
Polarization, 204
Polarizing microscope, 224
Pole figures, 23, 123, 128, 129
Powder photographs, 41, 42, 152, **168** ff.
  lines and background, 201
Polycrystalline aggregates, 16, 122, 123
Precession (Buerger) method, 45
Preferred orientation, 122 ff.
Primary extinction, 206
Profiles of powder lines, **173**, 214, 216
Projections, 17 ff.
Pyroelectricity, 102, 160 ff.

Quartz, 16, 17, 32, 81–84, 161, 163, 188, 212, 222

Radiation, Characteristic, 26, 28
  Crystal-reflected, 32
  Fluorescent, 31, 32
  Harmful, 33
  White, 25, 48
Rational indices, Law of, 15
Reciprocal lattice, 37 ff., 48 ff., 74, 120
Reflecting circle, **40**, 54, 58, 60, 65
Reflecting sphere, **40**, 48, 49
Refraction of X-rays, 29, 190
Refractive index, 29, 190
Refractories, 222
Relative intensities, 97, 204
Repeat distance, 52
Representation surface, 9
Resolution of powder lines, 173
Rho (ρ) factor, 204
Rocksalt, 32
Rotation of film for back-reflection photographs, 191
Rotation of plane of projection, 111
Rotation photograph, 41, 42, 43, 53, 109
Rounding-off errors, 192
Row lines, 49
Rubber, 130, 131

Scheelite, 13
Schiebold method, 45
Schiebold-Sauter method, 43, 44, 45
Screen (absorption), 31, 32
Screw axis, 211
Secondary extinction, 206
Sector, 199
Setting of crystals, 102 ff.
Shapes of spots, 201
Silicon, 180, 223
Single-crystal photographs, 41 ff.
Small-angle scattering, 217
Sodium chlorate, 180, 197
Solid solution, **196**, 221, 222
Space groups, 143, 163, 164, 210
Spacing of lattice planes, 35, 36, 220
  Effective, 29
Specimen, size and shape, 45

Specimens for powder photographs, 170
Spectrographic analysis, 219
Spinel, 117
Spottiness of powder lines, 168, **212**
Standard crystal for absolute intensities, 201, **202**
Standard powder, 191
Standard spots for visual estimations, 201
Stannous oxide, 220
Stereographic projection, **19** ff., 24, 111 ff., 123 ff. 147, 148
Strains, 173
Streaks, 55, 57, 113
Structural parameters, 209
Structure amplitude, **207**
Structure factor, 207
Superlattice, **211**, 217, 222
Symmetry elements, 3 ff., 10, 146 ff., 158
Synchronisation, 47, 203
Systematically-absent reflections, 145, 146, 163, 164, 210
Systems of crystallographic axes, 132 ff., 141 ff., 153

Target, 27
Temperature factor, 208
Thallium hydrogen tartrate, 195
Thermal expansion, 196
Tilted-crystal method, 42, 43
Tilted layer lines, 102, 103, 119
Topaz, 62 ff.
Transformation of axes and indices, 137 ff., 141, 144, 165 ff., 178
Transmission Laue photographs, 41
Tridymite, 222
Trigonal crystals, 161 ff.
Trigonometrical factor, 204
Tungsten, 123, 124
Tungsten *L* radiation, 57
Twin crystals, 16, 17, 116 ff.

Uniformity of speed of rotation, 46, 47
Unit cell, 11 ff.
  Dimensions of, 13, 51, 52, 62, 100, 189 ff.
  Volume of, 163 ff.
Uniterminal axes (*see* Polar directions)
Units of length, 25, **29**
Urea nitrate, 32

Visual methods of estimating intensity, 201

Wave-length of X-rays, 25, 28, 29
  Effects of different, 55
Wedge, 198
Weissenberg chart, 89
  goniometer, 87, 89, 97
  method, 42 ff., 87 ff.
Widmanstätten figures, 23
Wooster chart, 94

X-ray photographs, 41 ff.
  tubes, 27, 28, 33
X-rays, Absorption of, 29, 30
  Characteristic, 26
  Crystal-reflected, 32
  Diffraction of, 34 ff.
  Fluorescent, 29
  Harmful effects of, 33
  Harmonics of, 32
  Optimum voltage of, 27
  Reflection of, 35 ff.
  Refraction of, 29
  Scattering of, 29, 31
  Wave-lengths of, 25, 28
  White, 25, 32, 55 ff.
X-units, 29

Young's Modulus, 197

REFERENCES AND NAME INDEX

PAGE

Albrecht, G., 1939, *Rev. Sci. Instr.*, **10**, 221 . 205
Allison, S. K., *See* Compton, A. H.
American Society for Testing Materials (A.S.T.M.) 220, 224
American Society for X-Ray and Electron Diffraction (ASXRED). *See* Buerger, M. J.
Arkel, A. E. van 176, 194
1926, *Physica*, **6**, 64 171

Bearden, J. A. 191
1941, *J. App. Phys.*, **12**, 395 . . . 29
and Shaw, C. H., 1935, *Phys. Rev.*, **48**, 18 28
Bernal, J. D. 49-52, 58, 62, 131
Bernal, J. D. and Crowfoot, D. M., 1934, *Annual Reports of the Chemical Society*, **30**,, 423 211
Birge, R. T., 1941, *Reports of Progress in Physics*, **8**, 90 29
Bjurström, T. 185–188
1931, *Z. Phys.*, **69**, 346 . . . . 184, 186
Bogue, R. H., 1947, Book : *The Chemistry of Portland Cement*, New York : Reinhold Pub. Corp. 224
Boldyrev, A. K., Mikhiev, V. I., Kovalev, G. A. and Dubinina, V. N., 1939, *Ann. Inst. Mines, Leningrad*, **13**, 1 220
Bouman, J. *See* Jong, W. F. de
Bozorth, R. M., and Haworth, F. E., 1938, *Phys. Rev.*, **53**, 538 32
Bradley, A. J. 171, 172, 176
1935, *Proc. Phys. Soc.*, **47**, 879 . . . 205
and Jay, A. H., 1932 *a*, *Proc. Roy. Soc.*, A, **136**, 210 . . . . . 196, 222
and Jay, A. H., 1932 *b*, *Proc. Phys. Soc.*, **44**, 563 . . . . . 170, 189, 190
Lipson, H., and Petch, N. J., 1941, *J. Sci. Instr.*, **18**, 216 169
and Lu, S. S., 1937 *a*, *Z. Krist.*, **96**, 20 . 223
and Lu, S. S., 1937 *b*, *J. Inst. Metals*, **60**, 319 223
and Taylor, A., 1937, *Phil. Mag.*, (7) **23**, 1049 . . . . . 178, 182
Bragg, W. H., and Bragg, W. L., 1924, Book : *X-rays and Crystal Structure*, London : Bell 202
Bragg, W. L.
34–36, 39–41, 48, 78, 116, 120, 129, 137–140, 170, 171, 173, 177, 180, 189, 194, 195, 204, 213
1933, Book : *Crystalline State*, Vol. I. London, Bell 29, 217
1937, Book : *Atomic Structure of Minerals*, Ithaca, N. Y. : Cornell Univ. Press, London : Oxford Univ. Press . 64, 137

PAGE

Bragg, W. L.
1947, *J. Sci. Instr.*, **24**, 27 196
and Lipson, H., 1938, *Nature*, **141**, 367 . 168
and West, J., 1929, *Z. Krist.*, **69**, 118 . 206
See also Bragg, W. H.
Bravais, A. 8–11, 37–39, 49, 52, 62, 72, 83, 102, 132, 135, 137, 142–145, 148, 153
Brindley, G. W., 1940, *Proc. Phys. Soc.*, **52**, 117 218
1945, *Phil. Mag.*, **36**, 347, ... 205
See also James, R. W.
British X-ray and Radium Protection Committee, 1943 33
Buerger, M. J., 1936, *Amer. Mineralogist*, **21**, 11 170, 190
1942, Book : *X-ray Crystallography*, New York : John Wiley . . 45, 139, 210
1944, Book : *The Photography of the Reciprocal lattice*. ASXRED Monograph No. 1 45
Bunn, C. W. 188
1942, *Proc. Roy. Soc. A.*, **180**, 40 . . 131
1945, Book : *Chemical Crystallography*, Oxford : Clarendon Press 187
Peiser, H. S. and Turner-Jones, A., 1944, *J. Sci. Instr.*, **21**, 10 43

Carlisle, C. H., and Dornberger, K., 1948, *Acta Cryst.*, **1**, 194 48
Cauchois, Y., and Hulubei, H., 1947, Book : *Longuers d'onde des Emissions X et des Discontinuités d'absorption X*, Paris : Hermann 27
Chang, Y. L. *See* Lu, S. S.
Chappell, 1944, Book : in *Five-figure Logarithm Tables*, London : H.M. Stationery Office 192
Chesters, A. H., 1946, Book : *Steel Refractories*, London : Percy Lund, Humphries . 224
Clark, G. L., 1940, Book : *Applied X-rays*, New York : McGraw-Hill 212
Cohen, M. U., 1935, *Rev. Sci. Instr.*, **6**, 68 174, 191, 195
1936, *Z. Krist.*, **94**, 288 . . . 171, 189
Compton, A. H., and Allison, S. K., 1935, Book : *X-rays in Theory and Experiment*, New York : Van Nostrand . . 46, 208
Coster, D., Knol, K. S., and Prins, J. A., 1930, *Z. Phys.*, **63**, 345 . . . . 36, 160
Cox, E. G., and Shaw, W. F. B., 1930, *Proc. Roy. Soc.*, A, **127**, 71 205
Crowfoot, D. M. *See* Bernal, J. D.

Dana, E. S., 1898, Book : *Textbook of Mineralogy*, New York : John Wiley . 81, 163, 165
Darwin, C. G., 1922, *Phil. Mag.*, **43**, 808 . . 202

PAGE

Davey, W. P. 187
1934, Book : *A Study of Crystal Structure and its Applications*, New York : McGraw-Hill 109
See also Hull, A. W.
Dawson, W. E., 1928, *Phil. Mag.*, **5**, 756 . . 109
Debye, P., 1914, *Ann. der Phys.*, **43**, 49 . . 209
Donnay, J. D. H. 144
Donnay, J. D. H., 1934, *Amer. Min.*, **19**, 593 . 16
Dornberger, K. *See* Carlisle, C. H.
Dubinina, V. N. *See* Boldyrev, B. K.

Edwards, O. S., and Lipson, H., 1942, *Proc. Roy. Soc.*, A, **180**, 268 218
and Lipson, H., 1943, *J. Inst. Metals*, **69**, 177 211
Ekstein, H., and Fahrenhorst, W., 1934, *Z. Krist.*, **89**, 525 109

Fahrenhorst, W. *See* Ekstein, H.
Fairbairn, H. W., 1949, Book : *Structural Petrology of Deformed Rocks*, Cambridge, Mass : Addison-Wesley Press . . 122
Fankuchen, I. 65
Farquhar, M. C. M., and Lipson, H., 1946, *Proc. Phys. Soc.*, **58**, 200 194
Lipson, H., and Weill, A. R., 1945, *J. Iron Steel Inst.*, **11**, 457 222
Foote, F., and Jette, E. R., 1940, *Phys. Rev.*, **58**, 81 196
Fourier, J. B. J. 216
Frevel, L. K., 1944, *Indust. and Eng. Chem., Anal. Edit.*, **16**, 209 221
See also Hanawalt, J. D.
Friauf, J. B., 1927, *J. Amer. Chem. Soc.*, **49**, 3107 181
Friedel, G. 36, 160
Frommer, L., 1943, *J. Inst. Metals*, **69**, 26 . 196
and Lloyd, E. H., 1944, *J. Inst. Metals*, **70**, 91 . . . . . 190, 197

Gayler, M. L. V., and Preston, G. D., 1929, *J. Inst. Metals*, **41**, 211 . . . 174
Goldschmidt, H. J. *See* Rait, J. R.
Green, A. T. *See* Rait, J. R.
Greninger, A. B., 1935, *Z. Krist.*, **91**, 424 . . 109
Gross, R., 1920, *Zbl. Min. Geol. Palaeont.*, **52** . 109
Groth, P., 1906, Book : *Chemische Krystallographie*, **3**, 322, Leipzig : Engelmann . 194
Guinier, A., 1945, Book : *Radiocristallographie*, Paris : Dunod 217

Hanawalt, J. D., Rinn, H. W., and Frevel, L. K., 1938, *Indust. and Eng. Chem., Anal. Edit.*, **10**, 457 220
Handbook of Industrial Radiology, 1949, 2nd edition, London : Arnold 33
Hansen, M., 1936, Book : *Der Aufbau der Zweistofflegierungen*, Berlin : Springer . 222
Harcourt, G. A., 1942, *Amer. Mineralogist*, **27**, 63 220
Hargreaves, A., and Taylor, W. H., 1941, *J. Sci. Instr.*, **18**, 138 211
Harker, D. 144

PAGE

Hartshorne, N. H., and Stuart, A., 1950, Book : *Crystals and the Polarising Microscope* (2nd edit.), London : Arnold . . . 101
Haworth, F. E., 1940, *Rev. Sci. Instr.*, **11**, 88 . 109
See also Bozorth, R. M.
Hesse, R., 1948, *Acta Cryst.*, **1**, 200 . . . 179
Hiltner, W. A. *See* Williams, R. C.
Honess, A. P., 1927, Book : *The Nature, Origin and Interpretation of Etch Figures on Crystals*, New York : John Wiley . 102
Hull, A. W. 187
and Davey, W. P., 1921, *Phys. Rev.*, **17**, 549 186
Hume-Rothery, W. and Raynor, G. V., 1941, *J. Sci. Instr.*, **18**, 74 196
and Reynolds, P. W., 1938, *Proc. Roy. Soc.*, A, **167**, 25 173
Hutchinson, D. A. *See* Johnston, H. L.

Ievinš, I., and Straumanis, M., 1936, *Z. Phys. Chem.*, B, **33**, 165 . . . . . 171, 190
International Tables, 1935, *Internationale Tabellen zur Bestimming von Kristallstrukturen*, Berlin : Borntraeger (Revised edit., 1944) . . 30, 107, 145, 149, 204, 210
Ito, T., 1939, *Z. Krist.*, **100**, 297 . . . 121
Ito, T., 1949, *Nature*, **164**, 755. 1950. A Method of Indexing the Powder Photograph of a Crystal regardless of its Symmetry. Article in *X-ray Studies on Polymorphism*, Tokyo : Maruzen Co., Ltd. . 188

Jacob, C. W., and Warren, B. E., 1937, *J. Amer. Chem. Soc.*, **59**, 2588 188
Jackson, W. W., and West, J., 1931, *Z. Krist.*, **76**, 211 14
James, R. W., and Brindley, G. W., 1931 *a*, *Phil. Mag.*, **12**, 81 208
and Brindley, G. W., 1931 *b*, *Z. Krist.*, **78**, 470 208
Jay, A. H. 171, 176
1933, *Z. Krist.*, **86**, 106 173
1934, *Z. Krist.*, **89**, 282 196
1943, *J. Inst. Metals*, **69**, 22 . . . 175
1945 (private communication) . . . 190
See also Bradley, A. J.
Jeffrey, J. W., 1949, *Acta Cryst.*, **2**, 15 . . 102
Jette, E. R., and Foote, F., 1935, *J. Chem. Phys.*, **3**, 605 192
See also Foote, F.
Johansson, T., 1933, *Z. Phys.*, **82**, 507 . . 32
Johnston, H. L., and Hutchinson, D. A., 1942, *Phys. Rev.*, **62**, 32 196
Jones, F. W. 216
1938, *Proc. Roy. Soc.*, A, **166**, 16 . 215, 217
and Sykes, C., 1937, *Proc. Roy. Soc.*, A, **161**, 440 208
and Sykes, C., 1938, *Proc. Roy. Soc.*, A, **166**, 376 218
Jong, W. F. de, and Bouman, J., 1938, *Z. Krist.*, **98**, 456 ; *Physica*, **5**, 220 . . . 44

Knol, K. S. *See* Coster, D.

PAGE

Kovalev, G. A. *See* Boldyrev, A. K.
Kratky, O., 1930, *Z. Krist.*, **72**, 529 . . . 129

Laue, M. von
9, 41, 42, 46, 58, 71–86, 102, 107–114, 117, 120, 121, 153, 155, 160–165, 168, 169, 175, 191, 204, 207, 212
1926, *Z. Krist.*, **64**, 115 . . . 214, 217
Lipson, H., 1942, *J. Sci. Instr.*, **19**, 63 . . 171
Nelson, J. B., and Riley, D. P., 1945, *J. Sci. Instr.*, **22**, 184 32
and Parker, A. M. B., 1944, *J. Iron Steel Inst.*, **1**, 123 176
and Petch, N. J., 1940, *J. Iron Steel Inst.*, **142**, 95 173
and Riley, D. P., 1943, *Nature*, **151**, 250 . 29
and Rogers, L. E. R., 1944, *Phil. Mag.* (7), **35**, 544 171
Shoenberg, D. and Stupart, G. V., 1941, *J. Inst. Metals*, **67**, 333 . . . 175
and Weill, A. R., 1943, *Trans. Faraday Soc.*, **39**, 13 222
and Wilson, A. J. C., 1941, *J. Sci. Instr.*, **18**, 144 190
See also Bradley, A. J., Bragg, W. L., Edwards, O. S., Farquhar, M. C. M., and Stokes, A. R.
Lohse, O., 1935, *Tafeln für numerisches Rechnen mit Maschinen.* (Engelmann, Leipzig, 2nd edition). 192
Lonsdale, K., 1936, Book: *Structure Factor Tables*, London: Bell . . 209, 210
1944, *Nature*, **153**, 433 . . . 42, 206
1947, *Phil. Trans.*, A, **240** (No. 817), 219 . 42
1948, Book: *Crystals and X-rays*, London: Bell 205
Lonsdale, K., and Smith, H., 1941, *J. Sci. Instr.*, **18**, 133 . . . . . 170, 173
Lu, S. S., and Chang, Y. L., 1941, *Proc. Phys. Soc.*, **53**, 517 189
See also Bradley, A. J.
Lukesh, J. S., 1940, *Rev. Sci. Instr.*, **11**, 200 . 170

Majima, M., and Togino, S., 1927, *Sci. Pap. Inst. Phys. Chem. Res., Tokyo*, **7**, 75, 259 86, 109
Martin, A. J. P., 1931, *Min. Mag.*, **22**, 519 . 102
See also Wooster, W. A.
Mikhiev, V. I. *See* Boldyrev, A. K.
Miller, W. H., 4, 5, 35, 37, 83, 142–145, 153, 163, 166
Müller, A., 1924, *Proc. Roy. Soc.*, A, **105**, 500 . 109

Nelson, J. B., and Riley, D. P., 1945*a*, *Proc. Phys. Soc.*, **57**, 160 190
1945*b*, *Proc. Phys. Soc.*, **57**, 477 . . . 196
Neugebauer, P. V., 1935, Book: *Lohse Tafeln*, Leipzig: Engelmann 192

Orowan, E., 1942, *Nature*, **149**, 355 . . . 109
Owen, E. A., 1943, *J. Sci. Instr.*, **20**, 190 . . 173

Parker, A. M. B. *See* Lipson, H.

PAGE

Peiser, H. S. *See* Bunn, C. W.
Petch, N. J. *See* Bradley, A. J., and Lipson, H.
Peters, J., 1937, Book: *Kreis und Evolventen-Funktionen*, Leipzig: Kollmann-Werke, A.G. 192
1942, Book: *Seven-Place Values of Trigonometric Functions*, New York: Van Nostrand; London: Macmillan . . 192
Phillips, F. C., 1946, Book: *An Introduction to Crystallography*, London: Longmans Green . . .16 ff., 101, 144, 149, 152
Preston, G. D. *See* Gayler, M. L. V.
Prins, J. A. *See* Coster, D.
Pollock, A. R. *See* Thewlis, J.

Rait, J. R., Green, A. T., and Goldschmidt, H. J., 1942, Second Report on Refractory Minerals, London: Iron and Steel Institute 224
Recommendations of the British X-ray and Radium Protection Committee, 1948: National Physical Laboratory, Teddington 33
Reynolds, P. W. *See* Hume-Rothery, W.
Riley, D. P. (editor), 1944, Proceedings of a Conference on the ultra-fine structure of coals and cokes, London: B.C.U.R.A. 217
See Lipson, H., and Nelson, J. B.
Rinn, H. W. *See* Hanawalt, J. D.
Rinne, F., 1922, Book: *Kristallographische Formenlehre und Anleitung zu kristallographische-optischen sowie röntgenographischen Untersuchungen*, Leipzig: Jänecke 109
Robertson, J. M., 1934, *Phil. Mag.*, **18**, 729 . 97
1943, *J. Sci. Instr.*, **20**, 175 . . . 201
Robinson, B. W., 1933, *J. Sci. Instr.*, **10**, 233 . 200
Rogers, L. E. R. *See* Lipson, H.
Rooksby, H. P., 1943, *Nature*, **152**, 304 . . 176

Sachs, G. *See* Schiebold, E.
Sauter, E. 43–45
Scherrer, P., 1920, Book: *Zsigmondy Kolloidchemie*, 3rd edit., p. 387 . . . 217
Schiebold, E. 43–45
Schiebold, E., and Sachs, G., 1926, *Z. Krist.*, **63**, 34 109
Schleede, A., and Wellmann, M., 1932, *Z. Krist.*, **83**, 148 170
Schmidt, B., 1929, *Z. Physik*, **58**, 577 . . 109
Sears, J. E., and Turner, A., 1941, *J. Sci. Instr.*, **18**, 17 171
Seljakow, N., 1925, *Z. Phys.*, **31**, 439 . . 217
Shaw, C. H. 191
See Bearden, J. A.
Shaw, W. F. B. *See* Cox, E. G.
Shoenberg, D. *See* Lipson, H.
Siegbahn, M. 191
1925, Book: *The Spectroscopy of X-rays*, London: Oxford Univ. Press . 28, 29
Sinclair, H. B. *See* Taylor, A.

PAGE

Smith, C. S., and Stickley, E. E., 1943, *Phys. Rev.*, **64,** 191 . . . . 215, 218
Smith, H. *See* Lonsdale, K.
Spencer, R. C., 1931, *Phys. Rev.*, **38,** 630 . . 28
Steers, J. A., 1942, Book : *An Introduction to the Study of Map Projections*, London : Univ. of London Press 22
Stickley, E. E. *See* Smith, C. S.
Stockdale, D., 1940, *J. Inst. Metals*, **66,** 287 . 196
Stokes, A. R. 213
1948, *Proc. Phys. Soc.*, **61,** 382 . . . 216
Pascoe, K. J., and Lipson, H., 1943, *Nature*, **151,** 137 218
and Wilson, A. J. C., 1942, *Proc. Camb. Phil. Soc.*, **38,** 313 217
and Wilson, A. J. C., 1944, *Proc. Phys. Soc.*, **56,** 174 218
Straumanis, M. *See* Ievinš, I.
Stuart, A. *See* Hartshorne, N. H.
Stupart, G. V. *See* Lipson, H.
Sykes, C. *See* Jones, F. W.
Symposium on the Chemistry of Cements, 1938, Stockholm : Ingeniörsvetenskapsakademien 224

Taylor, A., 1944 *a*, *Phil. Mag.*, **35,** 215 . . 205
1944 *b*, *Phil. Mag.*, **35,** 640 . . . 205
1945, Book : *Introduction to X-ray Metallography*, London : Chapman & Hall 170, 205
and Sinclair, H. B., 1945 *a*, *Proc. Phys. Soc.*, **57,** 108 173
and Sinclair, H. B., 1945 *b*, *Proc. Phys. Soc.*, **57,** 126 190
Taylor, W. H. *See* Hargreaves, A.
Thewlis, J., 1933, *Z. Krist.*, **85,** 74 (Summarised in *J. Sci. Instr.*, 1941, **18**) . . . 109
Thewlis, J., and Pollock, A. R., 1950, *J. Sci. Instr.*, **27,** 172 175
Thomas, D. E., 1941, *J. Sci. Instr.*, **18,** 135 . 190, 197
Togino, S. *See* Majima, M.
Turner, A. *See* Sears, J. E.
Turner-Jones, A. *See* Bunn, C. W.
Tutton, A. E. H., 1922, Book : *Crystallography and Practical Crystal Measurement*, London : Macmillan 145

Ulrey, C. T., 1918, *Phys. Rev.*, **11,** 401 . 25, 26

Wahlstrom, E. E., 1943, Book : *Optical Crystallography*, New York : Wiley . . . 101
Wainwright, C., 1941, *J. Sci. Instr.*, **18,** 203 . 175
Waller, I., 1939, *Proc. Roy. Soc. Sci., Upsala*, **2,** No. 7, 3 217
Warren, B. E. 215, 216
1941, *J. App. Phys.*, **12,** 375 . . . 214
See also Jacob, C. W.
Weill, A. R. *See* Farquhar, M. C. M., and Lipson, H.
Weissenberg, K. . . 43–45, 70, 87–100, 109, 204
Weissenberg, K., 1924, *Z. Phys.*, **23,** 229 . . 43
Wellmann, M. *See* Schleede, A.
West, J. *See* Bragg, W. L., and Jackson, W. W.
Westgren, A., 1931, *Trans. Amer. Inst. Min. Met. Eng., Inst. Metals Div.*, 13 . . . 174
Whittaker, E. J. W., 1948, *Acta Cryst.*, **1,** 165 . 216
Williams, R. C., and Hiltner, W. A., 1940, *Pub. Observ. Univ. Michigan*, **8,** 45 . . 200
Winchell, A. N., 1937, Book : *Elements of Optical Mineralogy*, Part I, *Principles and Methods*, New York : John Wiley . 101
Wilson, A. J. C., 1940, *Proc. Camb. Phil. Soc.*, **36,** 485 190
1941, *Proc. Phys. Soc.*, **53,** 235 . 173, 19 196
1942 *a*, *Proc. Roy. Soc.*, A, **180,** 277 , 218
1942 *b*, *Proc. Phys. Soc.*, **54,** 487 . . 196
1943 *a*, *Nature*, **151,** 562 29
1943 *b*, *Proc. Roy. Soc.*, A, **181,** 360 . . 218
See also Lipson, H., and Stokes, A. R.
Wood, W. A., 1941, *J. Sci. Instr.*, **18,** 153 . 218
1943, *Nature*, **151,** 585 218
Wooster, W. A. 95, 96, 120, 137-140
Wooster, N., and Wooster, W. A., 1947, *Phil. Mag.*, **37,** 262 109
Wooster, W. A., 1936, *Z. Krist.*, **94,** 375 . . 137
1938, Book : *A Textbook on Crystal Physics* (reprinted 1949), Cambridge : Univ. Press 17, 161
1946, *Phil. Mag.*, **37,** 262 109
1948, *J. Sci. Instr.*, **25,** 129 . . . 129
and Martin, A. J. P., 1936, *Proc. Roy. Soc.*, A, **155,** 150 . . . . 201, 202
and Martin, A. J. P., 1940, *J. Sci. Instr.*, **17,** 83 97
and Wooster, N., 1933, *Z. Krist.*, **84,** 327 94
See also Wooster, N.
Wyckoff, R. W. G., 1931 145

X-ray Analysis Group of the Institute of Physics, 1945, *J. Sci. Instr.*, **22,** 57 . . . 176

Yu, S. H., 1937, *Z. Krist.*, **96,** 1 . . . 47

JAMMU & KASHMIR UNIVERSITY
LIBRARY
No. 14398
Date 31.3.56
SRINAGAR

ALLAMA IQBAL LIBRARY
14398

PRINTED IN GREAT BRITAIN BY ROBERT MACLEHOSE AND CO. LTD.
THE UNIVERSITY PRESS, GLASGOW